# AN ABSTRACT OF THE DISSERTATION OF

Benjamin A. Flugstad for the degree of Doctor of Philosophy in Biological and Ecological Engineering presented on June 10, 2013.

Title: Water Content and Electrical Conductivity Profile Measurements for Dispersive Media using Enhanced Time Domain and Frequency Domain Models

Abstract approved:

_____

John S. Selker

Water conservation and water quality are rapidly increasing in importance in all areas of the world. The ability to accurately measure soil water content and salinity, over a wide variety of conditions, is key to meeting this need. A set of forward prediction models and waveform interpretation algorithms to extract Volumetric Water Content (WC) and Electrical Conductivity (EC) profiles vs. position and time for electrically lossy and dispersive geophysical and biological media are presented. These are applicable to both Time Domain and Frequency Domain Electromagnetic Wave Propagation Transmission and Reflection measurements. These forward prediction models are developed using physically based First Principles models from the Theory of Electromagnetics together with Scattering (S) Parameter and Transmission (T) Parameter network modeling techniques applied to wave propagation in various media with cascaded domains of different properties. The interpretation algorithms fit the pre-derived Forward Prediction models to the measurement data via lookup tables, interpolation and optimization methods. Presented applications include the transmission line methods of Time Domain Reflectometry, Time Domain Transmission, Frequency Domain Reflectometry and Frequency Domain Transmission including high dynamic range Frequency Domain Vector Network Analysis. Other applications include Ground Penetrating Radar and Microwave Remote Sensing. The models account for temporal and spatial heterogeneity to obtain WC and EC vs. time and position. Models are introduced for composite media with multiple constituents of varying Ohmic (EC) and dielectric (electric permittivity) properties accounting for dispersive frequency dependence and loss. These models interpolate between the physical upper and lower bounds of parallel and serial influences of each of the capacitive and conductive constituents. New models are also introduced accounting for charged interfaces and resulting bound and semi-bound water constituents within the pore spaces of soils containing clay or organic matter fractions resulting in a transition zone from bound to free water (via a semi-bound water zone) impacting the frequency dependence on electric permittivity. Validations of the models are presented via comparisons to actual measured data over wide ranges of water content, electrical conductivity and soil types.

# Water Content and Electrical Conductivity Profile Measurements for Dispersive Media using Enhanced Time Domain and Frequency Domain Models

by
Benjamin A. Flugstad

A DISSERTATION

submitted to

Oregon State University

in partial fulfillment of
the requirements for the
degree of

Doctor of Philosophy

Presented June 10, 2013
Commencement: June 2014

Doctor of Philosophy dissertation of Benjamin A. Flugstad presented on June 10, 2013

APPROVED:

---

Major Professor, representing Biological and Ecological Engineering

---

Head of the Department of Biological and Ecological Engineering

---

Dean of the Graduate School

I understand that my dissertation will become part of the permanent collection of Oregon State University libraries. My signature below authorizes release of my dissertation to any reader upon request.

---

Benjamin A. Flugstad, Author

ACKNOWLEDGEMENTS

I (Benjamin A. Flugstad) dedicate this dissertation to my wife Becky who gave me the motivation to complete this after seeing the faith, fight, endurance and willpower she has exhibited as she faced incredible life challenges one after the other. Her positive spirit though what she has faced is testimony to her character. Thanks Becky!

I also want to thank both of my parents for their dedication in teaching me via examples the values of hard work, excellence, commitment, service to others and faith in God. They provided these examples and life lessons under the most difficult of circumstances and I am forever grateful to them.

I also want to sincerely thank my major professor, Dr. John S. Selker for the many years of dedicated support and collaboration through this research project. John and his team have played a huge role in the success of this project and all predecessors of it. Thanks, John, for sticking with me over the years when personal challenges caused delays in the program. I also want to sincerely thank my minor professor Dr. Andreas Weisshaar for his excellent insights and contributions to this program especially serving as my electromagnetics advisor through this process. I also want to acknowledge Dr. Vijai K. Tripathi for serving earlier on as my minor professor and also providing excellent insights and contributions in the area of electromagnetics to the program despite facing immense difficult personal challenges. His wisdom, grace and selfless attitude exhibited despite his own difficult circumstances will impact me for my entire life. I also want to thank Drs. Richard Cuenca and Marshall English for their excellent contributions both serving on my committee and in several other collaborations over the years extending even to our cranberry farm for experimental methods. I have learned so much from all of you. I also want to thank Dr. Michael Borman for serving as my representative to the Graduate

School Council and for helping me through several process hurdles along the way. I also want to thank Sandia Laboratories as well as the Small Business Innovation Research (SBIR) program for providing funding during a portion of this project. In addition, I want to thank Stan Kaveckis of Tektronix, Inc. of Beaverton, OR for opening up his lab and making available test equipment for this project. I also want to thank Dr. Shaun Kelly for assistance in early data collection and processing. Finally I want to thank everyone for the many years of patience in waiting for this Dissertation and sticking with me through the whole process.

# CONTRIBUTION OF AUTHORS

Dr. John S. Selker was a key collaborator/advisor in both the development of the forward prediction models and developing the experimental methods for validation of the forward prediction models. He also contributed to the actual validation testing and processing of a portion of the results. Drs. Richard Cuenca, Marshall English, Andreas Weisshaar and Vijai Tripathi also provided key contributions to the model developments and experimental validations over the years. Dr. Shaun Kelly also assisted in early field TDR data collection, and comparison Neutron Probe and Gravimetric data collection.

# TABLE OF CONTENTS

Page

TABLE OF CONTENTS (Continued)

Page

TABLE OF CONTENTS (Continued)

Page

LIST OF FIGURES

Figure Page

Figure Page

Figure Page

Figure Page

Figure Page

Figure Page

Figure Page

Figure Page

LIST OF FIGURES (Continued)

Figure Page

Figure Page

Figure Page

LIST OF TABLES

Table Page

**Water Content and Electrical Conductivity Profile Measurements for Dispersive Media using Enhanced Time Domain and Frequency Domain Models**

# Chapter 1: Introduction:

## Overview:

Water conservation and water quality management have both become key items of importance, in recent decades, in all areas of the world. Both the quanity and quality of the water must be optimized, carefully managed and delicately balanced across competing economic, social and environmental needs. This requires use of methods to accurately measure different parameters in different use models of water that correlate to either the quantity and/or quality of the water. An example of a measured parameter correlating to water quantity would be the volumetric water content in different media containing water. An example of a measured parameter correlating to water quality would be the electrical conductivity of different media containing water which can be correlated to the salt content or salinity of the water if the volumetric water content is also measured. Examples of media could include foods, soils, plants/organic material, wood, biological tissues, hazardous waste materials and other biological and/or geophysical media. The ability to accurately measure volumetric water content and electrical conductivity, over a wide range of these parameters, for all of these types of media is therefore of great value.

Irrigated agriculture is one area where accurate water content measurement (in this case in soils) is of great value. The ability to accurately schedule irrigation based on accurate measurements of how much and where the water is in the soil or crop root zone will save on water and energy costs and optimize crop yields. One of the typical problems encountered in irrigated agriculture (especially in semi-arid and arid climates such as the Imperial Valley of California) is the problem of salinity in the soil after irrigating for several years. Salts from the irrigation water are deposited in the soil and build up over years due to the absence of alot of winter rains or sufficient irrigation to leach the salts. Therefore, accurate methods of measuring soil water content in the presence of salinity would be of great value. Also the ability to measure the salinity itself, accurately, would be of great value in terms of assessing water quality. Finally methods that make these measurements with a minimum amount of soil disturbance or even make the measurements non-invasively would also be of great value.

In support of these needs, A set of forward prediction models and waveform interpretation algorithms to extract Volumetric Water Content (WC) and Electrical Conductivity (EC) profiles vs. position and time for electrically lossy and dispersive geophysical and biological media are presented. These are applicable to both Time Domain and Frequency Domain Electromagnetic Wave Propagation Transmission and Reflection measurements. These forward prediction models are developed using physically based First Principles models from the Theory of Electromagnetics together with Scattering (S) Parameter network modeling techniques applied to wave propagation in various media with cascaded domains of different properties. The algorithms fit the pre-derived Forward Prediction models to the measurement data via lookup tables, interpolation and optimization methods. Initial presented applications include the guided cascaded transmission line techniques of Time Domain Reflectometry (TDR), Time Domain Transmission (TDT), Frequency Domain Reflectometry (FDR) and Frequency Domain Transmission (FDT). Other applications include non-invasive electromagnetic wave propagation techniques such as Ground Penetrating Radar (GPR) and Microwave Remote Sensing. The forward prediction models are established for different media types including soils and foods accounting for temporal and spatial variable heterogeneity to obtain WC and EC vs. time and position. The models are developed in both the time and frequency domains utilizing Fast Fourier Transform (FFT) and Inverse Fast Fourier Transform (IFFT) algorithms. Mixing Models are introduced for composite media with multiple constituents of varying Ohmic (EC) and dielectric (electric permittivity) properties accounting for dispersive frequency dependence and loss. These composite dielectric/Ohmic mixing models interpolate between the physical upper and lower bounds of parallel and serial influences of each of the capacitive and conductive constituents. New models are also introduced accounting for charged interfaces and resulting bound and semi-bound water constituents within the pore spaces of soils containing clay or organic matter fractions. A new model accounting for a gradual transition from bound to free water (via a semi-bound water zone) and subsequent influences on the frequency dependence on electric permittivity is also presented.

## Statement of Need:

There is an increasing need in science and industry to develop methods of accurately measuring the volumetric water content (WC) and/or electrical conductivity (EC) and other properties/parameters vs. position and time in various Geophysical and Biological media. A key area where this need arises is in agriculture where there are increasing demands on limiting irrigation water use while also minimizing any impacts to water quality. Irrigation is used in agriculture everywhere from arid and semi-arid zones such as shown in figure 1.1 in western Nebraska (where an irrigated crop is in the background and the natural vegetation – sagebrush is in the foreground) to areas of high but seasonal rainfall such as the cranberry farm in Bandon Oregon shown in figures 1.2 – 1.5. Each of these farm types has a large dependence on water and any methods to help conserve the water use while maintaining crop yields would be of huge value. The ability to image the wetting front of infiltrating irrigation water would be of great value in balancing the demands of the crop against the need to conserve water. This could all be integrated into a closed loop feedback control system fully automating irrigation scheduling and helping the farmer to save significantly on both energy and water costs. The ability to also measure electrical conductivity and to therefore be able to assess salinity will also assist the farmer and irrigation districts in managing water quality.

Figure 1.1: Irrigated Farm in Western Nebraska in Semi-Arid Climate Zone

Figure 1.2: Cranberry Bog near Bandon, Oregon

Figure 1.3: Flooded Cranberry Bog with Berries Ready for Corraling and Harvest
Note: Storms and high winds blew some of the berries to one corner of the bog

Figure 1.4: Elevator and Booms for Removing Cranberries from Flooded Bog

Figure 1.5: Irrigation Reservoir and Pump House for Cranberry Farm

Note: Cranberry farms require significant water use from spring until fall (harvest)

There is therefore again an increasing need in science and industry to develop methods of accurately measuring the volumetric water content (WC) and/or electrical conductivity (EC) and other properties/parameters vs. position and time in various Geophysical and Biological media. To enable this there is in more general terms a need to extract profiling information on the location and properties of both spatially and time varying domains within media as well as the boundaries developed between those domains.

Examples of Geophysical media on a smaller localized or even microscopic scale include the inorganic fractions of soils made up of water or other liquids, air or other gases, discrete coarse rocks or gravel, progressively finer sand, silt and/or very fine clay particles as well as embedded minerals and/or salts. Salts will always be in solution in the liquids in the presence of geological materials resulting in electrically lossy media that can influence propagation characteristics of electromagnetic waves for example. The water fraction (even without salts) can influence electromagnetic wave propagation at higher frequencies (> 1 GHz) as it becomes dispersive and lossy from a dielectric (electric permittivity) standpoint. The impact of this can extend down to lower radio frequencies (1 - 100 MHz) for the case of bound and semi-bound water in a medium (water molecules close to a charged surface or boundary). Subsurface terrain on a localized scale (top few meters) can include natural soils of all types with various layering/strata/heterogeneity. Alternatively, it could include man-made structures such as hazardous waste sites, reservoir liners or concrete structures possibly in different layers in combination with soil layers. On a more macroscopic scale where simple location of coarse domain boundaries (on their top or bottom) may be the focus, examples of geophysical media include oceans, lakes, rivers, surface terrain such as mountains, valleys or other surface topographical features/boundaries as well as coarse deeper sub-surface terrain potentially containing aquifers, oil reserves, open caverns or other layered strata creating deep internal boundaries between these domains. In all these cases identification and characterization of boundaries and domains is of interest and lossy/dispersive constituents must be accounted for.

Examples of Biological media include the organic fractions of soils as well as foods, wood and physiological/biomedical media such as skin, muscles, organs and other soft tissues as well as cartilage, ligaments and bones where again both boundary and domain locations and properties are of interest and where electrically lossy/dispersive constituents must also be accounted for.

The ability to form an image or profile picture of WC and EC in a medium would be of great use in numerous applications where knowledge of those profiles are of interest. An example would include the location of a wetting front in the context of the depth of the root zone of various crops in agriculture. Another example could include the water content vs. position in food or wood/lumber products to assess degree of drying in a drying process. Still another could be the characterization of both the water content and salt content vs. position in a food during a food processing application.

This dissertation presents a new set of measurement methods and associated algorithms to address these types of profiling measurement needs. The presented approaches utilize electromagnetic wave propagation measurement methods and algorithms applied to media with cascaded domains or zones of different properties including lossy/dispersive properties. The key goal is to extract the profiles of WC and EC vs. position and time in various media that may contain several cascaded variable domains. These domains may have properties that are driven by fixed spatial heterogeneity (e.g. natural soil structure and strata/layering) or temporal heterogeneity (e.g. wetting fronts of changing WC or alternatively changing EC due to fertilization schedules). Accounting for lossy/dispersive media is also a key feature as this can result in the distortion and attenuation of propagating electromagnetic waves. This profiling measurement could be an excellent companion technology with other measurement techniques such as pressure or tension infiltrometry to gain a full 3D perspective of a wetting front into a soil vs. position and time.

The algorithms make use of fitted forward prediction models to the measurement data using physically-based models derived from the theory of electromagnetics and scattering (S) parameter network theory. They are applied to media with cascaded domains of varying properties including lossy/dispersive constituents. The initial evaluation test methods presented include the invasive guided transmission line technologies of Time Domain Reflectometry (TDR) and Time Domain Transmission (TDT). The evaluation test media includes soils of different WC and EC profiles. Soils represent many of the measurement challenges common to all geophysical and biological media and therefore serve as good evaluation test media. The techniques presented in this dissertation are again also applicable to non-invasive techniques such as GPR and Remote Sensing and other electromagnetic waveguide / antenna reflection/transmission measurements. In

addition they are also applicable to many other types of geophysical and biological media far beyond soils. These additional applications will be the focus of future ongoing research.

**Rationale:**

The accurate measurement of WC and EC in soils over wide ranges of those parameters vs. position and time is of great importance to a number of fields such as agriculture, environmental engineering, water resources engineering and others. Water content (WC) measurement techniques have historically been divided into two categories:

1.) Direct Methods: Where WC is measured directly via Gravimetric Analysis
2.) Indirect Methods: Where some other Parameter is measured and correlated to WC.

The direct method of Gravimetric analysis involves a slow invasive and labor intensive technique where a soil core sample is required along with an oven dryer and a 24 hour drying period. This direct method therefore does not provide real time feedback on WC, and can't be repeated in time for a given location. However it is very accurate and does not require expensive instrumentation.

In comparison, some of the initial historical indirect methods involved expensive and sometimes cumbersome techniques. One example includes the Neutron Probe which correlates the hydrogen content to WC, requiring calibration to identify water content, but also involves radioactive materials presenting serious usability and environmental hurdles [103], [109]. Another family of inexpensive methods correlates directly or indirectly the measured soil water potential to volumetric water content (with accuracy significantly limited by soil-dependent relationship which isn't a consistent function due to the hysteretic relationship of water content to water potential) [103]. Another developed indirect method includes correlating the heat capacity or specific heat to WC (Thermal Methods) [103], [109]. These methods have various accuracy limitations including those due to required calibration and do not measure the electrical conductivity of the soil. In addition, many of these earlier indirect methods involved a tremendous amount of site specific calibration and post processing and so don't provide a real-time measurement [103]. Measurement of water content for foods has also historically been done by variations of gravimetric analysis. In addition, real time measurement of the WC and EC of foods has historically not been widely implemented in food processing facilities.

There is therefore a need in both the agriculture and food industries for fast, accurate, inexpensive and easy to use methods of measuring WC and EC of soils and foods where calibration is not required for real time decision making (e.g. irrigation scheduling decisions for farms, and industrial mixing of ingredients for various food processing applications).

In the last 30 years a number of other indirect methods have been developed to improve in part on these limitations (more so in the soils area). A popular category of newer indirect methods includes various electromagnetic methods such as resistance probes, induction methods, capacitance probes and wave propagation techniques [103], [109]. These techniques involve measurement of either the electrical resistance or alternatively the electric permittivity to correlate to EC or WC. The more popular approach recently has been the choice of correlating the relative electric permittivity or dielectric constant to WC. Examples of applications of this category include lower to moderate frequency lumped element electrical circuit methods such as capacitance probes and higher frequency distributed element (wave propagation) electromagnetic methods such as TDR/TDT and GPR). Other electromagnetic-based indirect methods include Nuclear Magnetic Resonance (NMR). However, NMR currently presents significant cost barriers to widespread use but can be considered in the future for non-invasive measurements of WC in applications that might be less cost sensitive. Several of the electromagnetic methods still can present accuracy problems (e.g. the lower to moderate frequency lumped circuit element electromagnetic methods such as resistance probes, capacitance probes and induction methods). Therefore, in recent decades, higher frequency distributed element wave propagation electromagnetic methods such as the guided wave transmission line methods of TDR and TDT have gained great popularity in that they have the potential of measuring both water content and electrical conductivity in a fast, accurate and automated fashion without any hazardous materials. However, these transmission line methods still have the limitation of being invasive to the soils. Therefore other non-guided wave propagation technologies such as Ground Penetrating Radar (GPR) and Remote Sensing (RF, Microwave and up through Infrared) and NMR have been developed which offer even further advantages as they are non-invasive to the soils under test.

However, these electromagnetic wave propagation methods have to date largely been applied to bulk overall average measurements along a probe length or large domain space. In addition, they also run into accuracy and resolution issues in lossy/dispersive media. The new

models presented in this dissertation are designed to overcome these limitations and provide a profiling algorithm for WC and EC vs. position and time and also account for and characterize the presence of lossy/dispersive constituents or domains. The concepts presented in this dissertation will be applicable to all of these electromagnetic methods involving either invasive guided cascaded transmission line probes (TDR/TDT) or non-invasive non-guided cascade domain techniques such as GPR or Remote Sensing. A complete review of the various competing technologies and citations are covered in the literature review chapter and associated appendix.

## Overview of Dissertation Chapters:

In this dissertation a set of measurement algorithms are developed initially for TDR and TDT systems, but which may well have applicability to GPR and Remote Sensing Technologies and other non-invasive electromagnetic waveguide or antenna reflection/transmission technologies. The measurement procedure utilizes both a forward prediction model together with an inverse solving algorithm (the latter to fit measured data to the appropriate form of the forward prediction model via lookup tables together with an optimization procedure) to extract the desired parameters of WC and EC vs. position and time. This introduction chapter provides a top level brief overview of the algorithms and models and overall measurement approach. The dissertation proceeds with chapter 2 devoted to a comprehensive review of the recent literature relevant to this research (including Appendix C supplementing the literature review chapter) to give a snapshot of the state of the art currently in place in this field.

Subsequent chapters in the dissertation describe the new algorithms developed by the research of the author to build on the previous pioneering work already provided by earlier researchers, scientists and engineers. A family of forward prediction models specific to simulating TDR and TDT waveforms in soils vs. WC and EC profiles are introduced in the forward prediction modeling chapter 3 of this dissertation with the underlying background theory covered in more depth in the several associated appendices for that chapter. The forward prediction models were developed for soils of different types and degrees of heterogeneity with a wide range of WC and EC values. An inverse algorithm utilizes lookup tables together with an optimization procedure to fit the correct form of the forward prediction model to a specific soil type and soil heterogeneity to account for the “fixed” (non-varying) parameters of that specific soil and therefore allow for robustness in measuring the variable or “temporal” parameters of that soil (such as WC and EC varying with time and position). Also presented in this dissertation is a Finite Element Method approach applied to the models by dividing the transmission lines into fine mesh boundaries and domains and solving for the S-Parameters at each of the internal and external boundaries. The models are developed in Matlab. The appendices for the Forward Prediction Model chapter cover background information such as Scattering (S) Parameters applied to the cascaded transmission line TDR/TDT models, the dielectric mixing models of composite media and the bound and semi-bound water models and other background theory.

The validation of the forward prediction models against the actual data-sets are presented in a subsequent chapter of the dissertation. Multiple methods of validation are included involving both actual measurement data in various soils in the field as well as the laboratory and also comparison simulation data with other software tools and programs. Field validation included soils of different types such as sand, silt/loam and clay on different test farms. Laboratory validations included fixtures of various soils with artificially constructed/developed layered media synthesizing different accurately calibrated values of WC and EC vs. position. Finally, an additional validation method for the models included RF/Microwave circuit boards of cascaded transmission line sections of known values of varying impedance and lengths. Limitations of the models including challenges with uniqueness of solutions along with a sensitivity analysis of the models are presented in the Results and Discussion section of the validation chapter.

These forward prediction models are used in combination with an inverse solving algorithm to fit new measured data to the models and extract the water content and electrical conductivity vs. position and time in a medium under test. This inverse solving algorithm and associated optimization fitting procedure is presented in introductory fashion in this dissertation and will be the focus on follow-on research and publications. The new proposed algorithms fit these models to actual measurements via the combination of optimization methods along with the utilization of lookup tables and interpolation. The dissertation concludes with a summary/conclusion chapter to pull all these elements together and to discuss opportunities for future ongoing research and new potential applications.

## Parametric Measurement Techniques in Biological and Geophysical Media

In a general sense with biological and geophysical media, the measurement of the parameters can be obtained through either passive (non-stimulated) or active (stimulated) means. A passive measurement would involve the measurement of some parameter associated with a signal that is emitted naturally from a media without stimulation. Examples of passive means could include the measurement of an Electrocardiogram (ECG) of a patient via various electrodes attached to the patient's chest and in turn connected to a multi-channel highly sensitive analog front end data acquisition circuit to measure the very low level ECG waveforms between various electrodes as emitted naturally from the patient. Another example of a passive measurement would be the remote sensing of naturally emitted infrared radiation from the canopy of vegetation (such as an orchard) and subsequent correlation of that information to vegetation vigor vs. spatial position within the orchard. In contrast, an active measurement would involve the measurement of some parameter associated with a signal that is emitted from a media in response to a stimulation signal. Examples of active (stimulated) measurements include the broad category of measurements termed "Scattering" measurements where the measured scattered signals can be complex combinations of both transmitted and reflected signals about a medium that are all responses from a stimulus signal to the medium. Examples of active stimulated scattering measurements can include electromagnetic methods (e.g. Radar, X-Ray, Nuclear Magnetic Resonance (NMR), Time Domain Reflectometry (TDR), Time Domain Transmission (TDT), Ground Penetrating Radar (GPR), Microwave Remote Sensing, etc.) or alternatively non-electromagnetic methods (e.g. Seismic, Ultrasound, Acoustic, etc.). The overall description and review of the state of the art of these technologies and many others (both electromagnetic and non-electromagnetic) are covered in the literature review (chapter 2) and referenced in Appendix C. The focus of this present research was on active scattering electromagnetic methods due to the strong interaction of WC (correlated to electric permittivity) as well as electrical conductivity on propagating electromagnetic waves. This presents many opportunities for correlating scattered reflected and transmitted electromagnetic waves to WC and EC in a medium.

## Review of Electromagnetic Methods

The electromagnetic methods can be grouped into two major categories: Lumped and Distributed. Lumped circuit element methods combine lower measurement frequencies and/or smaller sample geometries to insure that the sample under test is small compared to the wavelength of measurement. Distributed element methods involve a sample under test that is comparable or even large compared to the wavelength of measurement and so transmission line and other electromagnetic wave propagation effects must be accounted for.

Lumped element methods can further be divided into electric field and magnetic field approaches: Electric field methods such as capacitance, resistance and/or impedance probes measure the electric permittivity and/or electrical conductivity. Magnetic field methods such as induction probes measure the magnetic permeability and sometimes indirectly the electrical conductivity (via eddy currents induced by magnetic fields).

Similarly, distributed element methods can also be further divided into the sub-categories of guided wave techniques (e.g. transmission lines and/or waveguides using Time Domain Reflectometry (TDR), Time Domain Transmission (TDT) and various Frequency Domain techniques); Free space or non-guided wave techniques (RF Ground Penetrating Radar and Microwave Remote Sensing); and combination wave propagation and nuclear magnetic spin resonance: (NMR)

This dissertation will focus on wave propagation based electromagnetic methods applied initially to soil volumetric water content and electrical conductivity measurements vs. position and time. The technologies and associated algorithms presented in this dissertation will focus on a few key wave propagation based electromagnetic methods involving scattering measurements. The measured scattered signals or first level measured parameters are in turn are used to derive the subsequent intermediate levels of parameters and ultimately arrive at the final desired level target parameters of volumetric water content and electrical conductivity vs. position and time in soils as described in this dissertation.

The work presented in this dissertation involves “guided” wave propagation methods such as TDR and TDT but the algorithms developed offer application to non-guided wave

propagation methods such as Ground Penetrating Radar (GPR) and Microwave Remote Sensing. This is important as the guided wave methods often require the insertion of a measurement probe invasively into a medium such as a soil whereas the non-guided methods offer the opportunity for non-invasive measurements. Therefore a promising future avenue of research will be in the application of these algorithms to non-invasive and non-guided electromagnetic methods.

## Statement of Problem:

There are a number of key parameters that are important as candidate measurements in various biological and geophysical media. Often the determination of these parameters includes the measurement of more readily obtained "first level" parameters that correlate to the target or desired "ultimate" parameters of interest. An example of a "first level" parameter is the electromagnetic parameter electric permittivity (ε) that in turn can correlate to the desired parameter of interest: volumetric water content (θ) via various regression or other models (described throughout this dissertation). Another example of a first level parameter would be the measurement of another electromagnetic property: the bulk electrical conductivity (σ) which can correlate to other material parameters of interest such as the salinity or salt content and other constituent information or properties of the media. In actuality, combining existing technologies of measurement systems together with complex geophysical or biological media can often lead to the need to progressively sort through multiple levels of obtained parameters to finally arrive at the target or desired parameters of interest in a fashion analogous to the peeling off of different layers of an onion. In this case the first level "measured" parameters may be used to obtain subsequent multiple intermediate levels of "derived" parameters through various algorithmic iterations until the "ultimate" or "desired" parameters can be obtained with a sufficient level of certainty. With our example of volumetric water content and salinity the prerequisite parameters one level up (electric permittivity and electrical conductivity) may in turn require other preceding first level measured and intermediate level derived parameters that must be measured and determined first. The "first level" measurement could be in the form of a measured or scattered signal and the subsequent levels of "derived" parameters could involve calculated network or system parameters initially at higher levels and progressively moving to lower parametric levels to converge on the localized parameters of interest. In addition, for a specific example such as soils, the parameters may be functions of both position and time as influenced by spatial heterogeneity and temporal non-deterministic measurement noise and/or trend-able deterministic temporal parameters such as temperature and/or rainfall/irrigation.

All of these add to measurement complexity and are typical of measurements of biological and geophysical media. In general the following are some common hurdles that must

be overcome and accounted for properly in electromagnetic measurements of biological and geophysical media:

1.) Dynamic Range: Influenced by the noise floor for low level signals and linearity issues for high level signals. Wider band time domain systems such as TDR and TDT typically have higher noise floors and lower Dynamic range vs. narrowband swept frequency domain methods such as Frequency Domain Reflectometry (FDR) and Frequency Domain Transmission (FDT).

2.) Imaging Geometry / Spatial Resolution: This is a tradeoff between the scale of an area that needs to be measured vs. the precision that is needed for finer/smaller feature reproduction. This typically influences the spectrum or frequency range of various technologies. Fine resolution or smaller resolved dimensions require higher frequencies whereas coarse resolution and larger dimensions and deeper penetration point towards lower frequencies.

3.) Propagation Loss & Dispersion Mechanisms. These are evidenced when a propagating wave of multiple frequency components has frequency dependence on either the amplitude (attenuation/loss) or velocity/speed (dispersion) of the individual spectral components. Examples of parameters that influence this include the following:

   a. Electrical conductivity ($\sigma$): Dispersion at lower frequencies and Attenuation at higher frequencies.

   b. Loss component of electric permittivity ($\varepsilon''$) or dielectric loss mechanisms:

      i. Free Water: Dispersion and Attenuation at higher frequencies > 1 GHz.

      ii. Bound and Semi-Bound Water: Interfacial mechanisms at clay and organic matter charged surfaces: Dispersion and Attenuation at intermediate frequencies > 10 MHz.

4.) Spatial Heterogeneity: These are associated with target parameters being a function of position and ultimately functions of the constituents which vary vs. position.

a. Ordered: This could include a well-defined Layering profile in a medium that could include significantly different materials in each layer as well as complex interfacial / boundary mechanisms. An example of this could be a soil with a sandy loam upper layer and then an impermeable clay layer or vein below it.

b. Random/Stochastic: This would include random spatial distributions of various constituents. This can lead to the need to develop complex parametric mixing models as well as stochastic models of various media. An example could include a dielectric mixing model for a soil with multiple significant constituents (air, free water, bound water, semi-bound water, non-clay mineral solids, clay solids, organic matter solids).

5.) Multiple Confounding Variables:

a. Underdetermined Systems: This is where there are more unknowns than independent equations or measurement parameters. Either more measurement parameters must be added (multiple parameters) or other assumptions made to extract all of the desired unknowns.

b. Dominant Undesired Variables: This would be where the influence of an undesired variable or parameter dominates over the desired measured parameter or variable. An example of this could include electrical conductivity mechanisms dominating over dielectric mechanisms at lower frequencies, greatly attenuating the desired measurement signal. Methods for removing the effects of dominant variables to be able to extract other lesser variables/parameters must often be developed.

c. Uniqueness of Solutions: For higher order systems of multiple variables there can be more than one combination of solutions for a particular measured waveform which is the converse of the “Underdetermined Systems” described above. Determining which solution is the correct one can be a key challenge and require additional measurement information and/or recent historical knowledge of the parametric trends in the medium.

6.) Environmental Dependencies: An example could include strong temperature dependence.

7.) Temporal Variation: This is associated with target parameters being functions of time. These variations can be due to following mechanisms:

   a. Non-Deterministic Temporal Disturbances: Random Noise or alternatively Electromagnetic Interference (EMI), etc. Mitigations might include averaging measurements (noise) or insuring distance from interfering sources (EMI) or even shielding/guarding where practical/feasible.

   b. Deterministic Temporal Variations: This could include both of the following:

      i. "True" desirable changes of the parameter (e.g. water contents of soils changing with time due to irrigation or rainfall). Trending of certain parameters vs. time is often a key measurement goal to track desirable temporal variations.

      ii. "Disguised" non-desirable "non-true" variations of the parameter (e.g. diurnal temperature variations changing the first level measurements leading to errors in the calculated targeted parameter). This could be mitigated by simultaneously monitoring temperature and compensating for it in the measurement algorithms and also by using signal processing filtering techniques.

8.) Limitations of Measurement System: This could include limitations of both the measurement instrumentation and measurement probes. Examples include bandwidth and dynamic range limitations as well as geometry limitations of the probes. Another limitation could be the requirement for invasive placement of the probes in a medium vs. non-invasive capability.

In summary all of the above issues can arise in measurements of biological and geophysical media. They show the need for obtaining measurements of the desired target parameters vs. position (due to spatial heterogeneity) and time (due to temporal variations). They also show the need for extensive signal processing techniques to mitigate many of the other issues. These confounding issues when combined with the earlier discussions on multiple level algorithms (obtaining first level measurements of other parameters to correlate to the ultimate desired parameters) and finally combining this with multiple variable / multiple target parameter algorithms can lead to much complexity in measurement algorithms associated with biological and geophysical media. The larger the number of first level measurements and intermediate levels of derived parameters that must be determined first before obtaining the target parameters under interest, the larger the number of potential sources of error that will exist. This is due to the fact that each level has its own amount of uncertainty or precision limitations. In addition, for multiple target parameter algorithms, the larger the number of variables or parameters that must be simultaneously determined at a particular level, the larger the number of independent parametric measurements that must be obtained at all levels to obtain enough measurement and derived parameters to solve for the number of target unknowns. Geophysical and Biological media often present all of these types of measurement challenges, leading to the need for some A-priori assumptions of the measurement media and system to allow for convergence on a solution. Presentation of a few novel examples of these types of multi-level complex algorithms describing their capabilities along with their limitations and potential mitigations will be presented in introductory fashion in this dissertation. Algorithms associated with soil volumetric water content and electrical conductivity measurements vs. position and time will be the initial case studies presented in this dissertation. A summary of what is possible in terms of these types of measurements will be given along with the necessary assumptions that must be made on both the media and measurement structures to make these measurements possible and reliable with acceptable certainty. Finally, expanding these algorithms to other applications will also be addressed briefly to show possible roadmaps to further research.

**Statement of Opportunity:**

The above discussion clearly shows the complexity of parametric measurements associated with biological and geophysical media. It also shows the need or opportunity for new research into measurement algorithms and solutions/systems for these applications. It is clear, after giving consideration to these challenges, that not all measurements are possible. The capabilities of measurements will depend on the specific measurement system as well as measurement media. This dissertation is therefore going to address the following three key research questions or goals:

1.) Given different types of assumptions on measurement systems and media under test, what parameters can be reliably extracted and what are the conditions for assuring those reliable measurements using data from electromagnetic measurements?

2.) To what extent can development of a family of forward prediction models based on physically-based electromagnetic and geophysical models accounting for both the measurement structures/devices and measurement media be extended to address all of these sources of variation?

3.) Given the forward prediction models, to what extent can an inverse solving algorithm be developed based on an optimization procedure and lookup tables to fit the measurements to the appropriate form of the forward prediction model to reliably extract the target parameters given these sources of variation?

A test scenario of soil water content and electrical conductivity measurements vs. position and time with various soil conditions (both laboratory and field) will be used to answer the above questions. The initial measurement system will assume a multiple cascaded section transmission line probe configured for Time Domain Reflectometry (TDR) and Time Domain Transmission (TDT) measurements. Information in both the frequency domain and time domain will be utilized by the algorithms. A brief high level outline for the algorithm approach is given next and the full details of the algorithms will be developed in later chapters of this dissertation.

## Overview/Outline of Algorithm:

The following is a brief high-level outline of the elements of the forward prediction and inverse solving algorithms associated with the presented technology. The full details of these algorithms will be developed and presented in later chapters of this dissertation:

## Forward Prediction Model:

Initial assumptions for modeling can be enumerated as:

a.) The transmission line is of known geometry and length (accounted for in prediction model).

b.) The transmission line probe can be divided into multiple cascaded sections of various lengths (partitioning of the transmission line).

c.) The feeding cable and interconnections to the transmission line probe are modeled as additional transmission line sections.

d.) The soil solids fraction and air filled porosity are accounted for vs. position, section or layer in the soil. This includes the solids type (e.g. clay vs. silt vs. sand vs. organic matter). Models for Permittivity and Conductivity of the Solids Fraction vs. Position are included. This is considered a fixed component of the soil structure and is obtained in initial actual measurements via a learned optimization procedure (to fit the appropriate forward prediction model type to the specific soil type and heterogeneity). A-Priori knowledge of this structure can also be provided as fixed inputs to the models.

e.) The configuration can be taken to be either as a Time Domain Reflectometry Probe (Open Circuited Transmission Line) or a Time Domain Transmission Probe (50 Ohm Terminations).

Model Variable Inputs:

1.) Ultimate Target Predicted Parameters (Inputs for the forward prediction model):

a.) Volumetric Water Content vs. Position (Entered Directly for Each Section)

b.) Bulk Electrical Conductivity vs. Position (Actually Calculated from Supporting Input Parameters & Intermediate Level Parameters Below)

2.) Supporting Input Parameters (Obtained from the Fixed Inputs above):

a.) Soil Solid Constituents (Relative Percentages) vs. Position (Each Section)

b.) Soil Solid Constituents (Electromagnetic Models vs. Constituents)

c.) Air-Filled Porosity vs. Position (for Each Section)

d.) Electrical Conductivity of Water vs. Position (for Each Section)

e.) Electrical Conductivity of Solids vs. Position (for Each Section)

f.) Dielectric Models of Water for each Section

- Free vs. bound vs. semi-bound water (different dielectric/Debye models)

Simulated and Calculated Intermediate Level Parameters:

1.) Dielectric & Ohmic Parametric Composite Mixing Models (Two Major Categories).

a.) Parametric Level (permittivity, permeability & conductivity)

- 8 Different Mixing Models (described later in this dissertation)

b.) Network Level (phase constant and impedance)

- 7 Different Mixing Models (described later in this dissertation)

2.) Frequency Domain Electromagnetic Propagation Models for Each Transmission Line Section.

a.) Complex Propagation Constant within Each Section

b.) Complex Characteristic Impedance of Each Section

c.) Complex Reflection Coefficient at Each Section Boundary

3.) Frequency Domain Scattering (S) Parameter Network Models for Each Transmission Line Section: S11 (input reflection coefficient) and S21 (forward transmission coefficient) for each section.

4.) Frequency Domain Scattering Parameter Cascaded Network Models for Entire Transmission Line: Progressive Development of an Effective overall S11 Model for the Entire Network.

5.) Simulated Frequency Domain Representation of the Stimulus TDR/TDT Pulse/Step.
6.) Product of #4 and #5 to give a Frequency Domain Representation for a TDR/TDT Waveform
7.) Optional Simulated Additive Noise (Frequency Domain Representation) added to #6 to give a Noisy Realistic Frequency Domain Representation of the TDR/TDT Waveform.

Model Variable Outputs:

1.) Simulated First Level Measurements
    a. TDR and TDT Waveforms (IFFT on #7 from Previous Steps)
2.) Tabulation of All Calculated Intermediate Level Parameters
3.) Tabulation of All Entered Inputs

## Inverse Solving Algorithm:

The inverse solving algorithm is based on fitting first level measurements (e.g. a TDR and/or TDT waveform) to the appropriate forward prediction model and also involves other elements. A very high-level outline of the general flow is outlined below and described in additional detail throughout the dissertation:

Initial Assumed Inputs (Fixed Components or Fixed Inputs of Model – Same as Forward Prediction):

a.) Transmission Line of Specific Geometry & Length (all accounted for in prediction model).
b.) Multiple Cascaded Sections of Various Lengths (Partitioning of the Transmission Line).
c.) Models for Feeding Cable and Interconnections to Probe (Modeled as Additional Transmission Line Sections).
d.) Configuration as Time Domain Reflectometry (TDR) Probe (Open Circuited Transmission Line) or Time Domain Transmission (TDT) Probe (50 Ohm Termination).

Other Assumed Fixed Inputs:

e.) Varying Levels of A-priori knowledge of the Soil Type and Constituents and Relative Volumetric Percentages (Either from a Calibration for the required soil specific model inputs or from Prior Soil Assessments).

Measured First Level Inputs:

1.) TDR and TDT Waveforms (Voltage vs. Time).

2.) Temperature (Incorporated as a Variable in the Algorithms for Future Use but Assumed to be constant at 10°C for this Dissertation). Use of this would require a soil temperature measurement as part of the overall instrumentation.

Calculated Intermediate Level Parameters/Items & Algorithm Procedure:

1.) Frequency Domain Representation of TDR/TDT Waveforms (from FFT of Measured Waveform).

2.) Removal of TDR Stimulus Product (Using FFT of TDR/TDT Pulse from Forward Prediction Model along with A-Priori Knowledge of Pulse/Step) to Obtain Frequency Domain Representation of S11 of Entire Probe.

3.) Determine Initial Starting Value of Bulk Electrical Conductivity from Low Frequency Portion of Spectrum of S11 (Cross-checked with the ending long time value of the time domain waveform). This value is initially used for each section in the transmission line.

4.) Determine Initial Starting Value of Electric Permittivity (and ultimately Water Content) for the first Section utilizing the high frequency portion of the spectrum of S11 (along with cross checking on the first returned reflected pulse in the time domain waveform). This is indirectly obtained via determination initially of the characteristic impedance of the first section (from the first step reflection coefficient) along with knowledge of the electrical conductivity value from #3 and assumptions made on all the other non-dielectric electromagnetic parameters (e.g. magnetic permeability of media, series resistivity of probe conductors).

5.) If the conductivity is very low then develop a first coarse approximation of the impedance profile and subsequent electric permittivity and ultimately subsequent water content vs. position along the probe using a time domain de-convolution

procedure such as the “Layer Peeling” algorithm described later in this dissertation. If the conductivity is significant then use the first section value for the electric permittivity and ultimately water content for the starting value for each section in the transmission line (skip the time domain de-convolution step).

6.) With the initial values of the parameters for each section placed into the forward prediction model then initiate a Global Optimization procedure using simulated annealing where the various parameters (water content and electrical conductivity) are perturbed and the forward prediction model result (simulated time domain waveform) is compared to the actual measured time domain waveform and assessed for goodness of fit (using a method similar to the sum of squared errors). The perturbation step for each parameter is determined via a stochastic “temperature” value as determined from the simulated annealing procedure (described in detail later in this dissertation). This method or step can be implemented with either lookup tables of pre-run forward prediction model runs (requiring also interpolation) or with the forward prediction model actually activated real time (better resolution but slower measurement speed for the latter).

7.) If the goodness of fit has converged to an acceptable level then perform a better fine tune fit of the model to the data again using either time domain de-convolution or frequency domain de-embedding methods together with interpolation (if lookup tables were used for the forward prediction model).

8.) As a final fine tune fit perform a localized optimization procedure (First Derivative (Gradient)/ Second Derivative (Hessian) Newton Based method). Note: This final step only works if the above steps can obtain a fit that is acceptably close to a true minimal solution.

9.) Generate a report of all the simulated output parameters (water content and electrical conductivity vs. position) along with all of the intermediate level calculated parameters.

10.) If the algorithm fails to converge on an acceptable solution then report the results of the last closest iteration based on the goodness of fit measurements (the algorithm will abort if acceptable convergence is not detected within a certain number of iterations).

As implied by the earlier discussions and stated research questions there are limitations to the above approach and under certain conditions it may not converge to a solution. This dissertation will give an assessment of the limitations of this algorithmic approach to describe the conditions, assumptions or boundaries within which the algorithm will perform successfully and the conditions where it may not converge.

## Overview of Results:

The forward prediction models and algorithms have been initially validated with guided wave electromagnetic methods (Wideband Time Domain TDR and TDT along with higher dynamic range Frequency Domain FDR and FDT methods in a geophysical media (soils)). The algorithms have application to other electromagnetic methods including non-guided and non-invasive methods such as ground penetrating radar and microwave remote sensing. In addition the algorithms have application to other biological media such as foods, wood, biomedical/physiological tissues as well as other geophysical media such as deeper subsurface terrain and aquifers as well as atmospheric or even ocean and river surface current measurements. The extension of these models to the other electromagnetic methods and other types of media will be the subject of future follow-on research.

# Chapter 2: Literature Review

## Overview:

This chapter provides a literature review of parametric sensing and imaging technologies involving inverse scattering processing algorithms. Background literature for the proposed water content and electrical conductivity measurements/algorithms in layered, heterogeneous and lossy soils and other media is presented.

The processing and interpretation of complex measured scattering signals and waveforms is a common requirement in most parametric sensing and imaging measurement systems. Imaging technologies ranging from medical ultrasound, Positron Emission Tomography and X-Rays to geophysical microwave remote sensing or even seismic methods must all process a set of scattered signals or complex combination of reflected and/or transmitted signals. Various inverse or de-convolution algorithms must be utilized to extract the necessary parametric information vs. position and time to create the various temporal images or profiles of the target medium. This literature review chapter (along with Appendix C) will review the recent literature and state of the art on a representative subset of these parametric sensing, imaging and profiling technologies involving the solving of inverse scattering problems. This will serve as background information for the proposed Soil Water Content and Electrical Conductivity Measurement Algorithms and Models presented in this dissertation.

## Introduction:

There are numerous needs over a wide range of applications in society where various parameters must be identified via various measurement means. A very common class of measurements involves sensing, imaging and profiling various parameters vs. position and time. In everyday life everyone is constantly faced with sensing, imaging and profiling problems. As we walk or drive or even sit we are continuously processing our surroundings visually via scanning with our eyes as well as utilization of our other senses and assessing what is around us

vs. position and time to allow for making decisions on every step of our daily lives. Our brains process multi-parameter algorithms involving the utilization of all of our senses simultaneously to assess our immediate environment. We can even trend these measurements vs. time to anticipate what may be to come and influence our next actions (e.g. watching the progression of a car to see if it will stop before an intersection that we are also approaching or hearing the sound of a siren on an emergency vehicle or whistle on a train before we see it and trending the level of sound vs. time). Therefore often the utilization of multiple simultaneous sensing technologies using multiple parameters adds target parameter detection power and dynamic range (or sensitivity for a binary classification test) and certainty/accuracy/selectivity (or specificity for a binary classification test) to a measurement. In every arena of life there are various sensing, imaging and profiling measurement needs and there is a continual progression of technological developments to allow for making those measurements and processing the results. The processed results can then be used to enable decision making that can occur either manually or in automated fashion based on the processed measurements.

A common element of these sensing, imaging and profiling technologies involve measuring and processing a received signal or set of different signals that emanate from the imaging zone or medium under test. These signals can come either from passive means (signals naturally radiating or emanating from the measurement zone – e.g. infrared thermal radiation) or alternatively actively via the scattering (complex combination of reflected and transmitted signals/waveforms) about various media as a result of a sourced signal or signals from a measurement system (e.g. RADAR, ultrasound, X-Ray's, depth soundings, microwave remote sensing, Time Domain Reflectometry, etc.). There can even be combinations of both passive and active signals. An example of this includes Magnetic Resonance Imaging where a very strong external DC magnetic field aligns the nuclear magnetic dipoles of all atoms of a measurement medium in a common fashion and an actively induced RF signal then disturbs specific nuclear magnetic dipoles (e.g. Hydrogen atom nuclei) and then subsequently a passive RF signal at that same nuclear magnetic resonant frequency is emanated as those dipoles re-align with the external magnetic field. The subsequent signal processing and image processing of those emanated passive RF signals vs. position/direction allows for imaging of soft tissue (containing Hydrogen atoms) in a medium or patient.

This paper will focus on reviewing the current literature and state of the art of existing sensing, imaging and profiling measurement technologies utilizing actively induced signals resulting in scattering signal processing problems and associated algorithms. In all of these cases a set of inverse or de-convolution problems must be solved to extract the desired parameters from the measured scattered or received signals. Wave propagation of some form are common to all of these technologies with the frequencies sufficiently high and wavelengths small or comparable (for at least a significant portion of the spectrum) compared with the geometries of measured media such that wave propagation and scattering modeling techniques can be utilized.

A wide range of wave propagation scattering technologies have been developed in science and industry and they can be divided into two major categories as follows (along with examples of each):

A.) Electromagnetic Wave Propagation Methods
    a. Non-Guided:
        i. Microwave Remote Sensing
        ii. Microwave RADAR
        iii. Ground Penetrating RADAR
    b. Guided / Bounded:
        i. RF / Microwave Transmission Lines
        ii. RF / Microwave Waveguides

B.) Non-Electromagnetic Wave Propagation Methods
    a. Positron Emission Tomoagraphy
    b. Acoustic
    c. Ultrasound
    d. Seismic

This review will focus on the first category (electromagnetic methods) but the techniques are applicable to a broad range of fields outside of electromagnetics. For each of these technologies there are some common hurdles that must be overcome and accounted for properly. These include the following:

1.) Dynamic Range: Influenced by the noise floor for low level signals and linearity issues for high level signals.

2.) Imaging Geometry / Spatial Resolution: This typically influences the spectrum or frequency range of various technologies. Fine resolution or smaller resolved dimensions require higher frequencies whereas coarse resolution and larger dimensions and deeper penetration point towards lower frequencies.

3.) Propagation Loss & Dispersion Mechanisms. An example includes electrical conductivity for electromagnetic methods which limits penetration depth and leads to wave propagation attenuation especially for higher frequencies along with dispersion / wave retardation at lower frequencies. Another would be dielectric loss mechanisms which can cause both attenuation and dispersion at lower frequencies (clay interfacial mechanism) or higher frequencies (water).

4.) Spatial Heterogeneity:
    a. Ordered: This could include a well-defined Layering profile in a medium that could include significantly different materials in each layer as well as complex interfacial / boundary mechanisms. An example of this could be a soil with a sandy loam upper layer and then an impermeable clay layer or vein below it (soil profile typical of Bandon, Oregon). The clay layer can also contain complex interfacial or boundary mechanisms such as charged layers that influence electromagnetic wave propagation.
    b. Random/Stochastic: This would include random spatial distributions of various constituents. This can lead to the need for complex parametric mixing models as well as stochastic models of various media. An example could include a dielectric mixing model for a soil with four significant constituents (air, water, mineral solids, organic matter).

5.) Multiple Confounding Variables:
    a. Underdetermined Systems: This is where there are more unknowns than independent equations or measurement parameters. Either more measurement parameters must be added (multiple parameters) or other assumptions need to be made to extract all of the desired unknowns.

b. Dominant Undesired Variables: This would be where the influence of an undesired variable or parameter dominates over the desired measured parameter or variable. An example of this could include electrical conductivity mechanisms dominating over dielectric mechanisms at lower frequencies and swamping or greatly attenuating the desired measurement signal. Methods for removing the effects of dominant variables to be able to extract other lesser variables/parameters must often be developed.

c. Uniqueness of Solutions: For higher order systems of multiple variables there can be more than one combination of solutions for a particular measured waveform. Determining which solution is the correct one can sometimes be a key challenge and require additional measurement information and/or a-priori or recent historical knowledge of the parametric trends in the medium.

6.) Environmental Dependencies: An example could include the strong temperature dependencies of parameters that influence wave propagation in both electromagnetics and acoustics.

7.) Temporal Variation: This is associated with various parameters changing with time. Trending of certain parameters vs. time is often a key measurement goal.

## Review of Methodologies:

This review chapter will summarize the existing literature and state of the art of technologies within the category of electromagnetics methods that also make use of inverse scattering algorithms as a part of parametric sensing, imaging and profiling measurement systems. These methods have far broader applications beyond electromagnetics but this review will focus on the electromagnetics methods.

A common modeling technique used by both electromagnetic and non-electromagnetic scattering algorithms involves the utilization of Scattering (S) Parameters and Transmission (T) parameters (background theory developed in [1] through [18] and summarized in Appendix B). The underlying theory for S-parameters and T-Parameters has its roots in classical linear matrix algebra and scattering particle physics dating back to the later $19^{th}$ century and early $20^{th}$ century.

One of the earliest references to the application of S-parameters to an engineering problem is in the work by Campbell and Foster (1920) [1] in applying these techniques to the modeling of networks associated with telephone substation and switching/repeater circuits. However, the widespread utilization of S-parameters and T-Parameters in the context of modeling engineering problems did not occur until the post World War II period with the pioneering modeling work at the Massachusetts Institute of Technology (MIT) beginning with the work of Montgomery et al (1948) [2]. This continued on into the next decade with the early pioneering work on signal flow graphs by Dr. Samuel .J. Mason also of MIT with his two landmark publications in 1953 [3] and 1956 [4] where his theory on modeling cascaded networks ("Mason's Non-Touching Loop Rule) was presented. That same year (1956) also saw several publications on S-parameters in a special issue of the Transactions of International Radio Engineers (IRE) Journal devoted to this topic including [5] and [6]. A good review of the use of signal flow graphs together with S-parameters was presented by Hunton in 1960 [7]. The practical use of S-Parameters in actual measurements was made possible with the invention and release of the first commercially available network analyzer (Hewlett Packard 8410) in the later 1960's corresponding with the 1967 HP Journal Article: "S-Parameter Theory and Application" [8] and referenced in [9] and [10]. Scattering (S) parameter and Transmission (T) Parameter modeling can be applied to all branches of science where scattering phenomena exist and are even used in non-science disciplines. The background theory for S-Parameters and T-Parameters is again given in Appendix B.

## Electromagnetic Methods:

Electromagnetic methods include all measurement technologies that extract parameters or dependent variables that either directly or indirectly correlate to or are functions of readily measure-able independent fundamental electromagnetic parameters or variables. The underlying background theory for these fundamental electromagnetic parameters and variables is developed in Appendix A. Electromagnetic methods can be further divided into subcategories as follows:

A.) Static Methods: This includes methods where the electromagnetic field parameters (electric or magnetic field) are neither functions of position or time (i.e. DC fields). An example of this includes a direct Ohmic measurement of electrical resistance of a

medium using a 4-electrode (4-wire) system with DC voltage and current measurements [103], [109].

B.) Quasi-Static Methods: This includes methods where the fields still approximate as not being functions of position but may be strong functions of time. An example of this would be a capacitance probe [103] where there are time varying electric fields but at any given moment of time the electric fields can be approximated as being constant over the entire sample volume. This approximation can hold well into the RF (several hundred MHz) range if the sample geometry is still small compared to the wavelength of the measurement signal. Lower to Moderate Frequency (e.g. several kHz to low MHz) AC resistance measurements [103] would also fall into this category as would inductive (induced magnetic fields) methods [103] at lower to moderate frequencies.

C.) Wave Propagation Methods: With these methods the electromagnetic parameters are strong functions of both position and time. An example of this could be the transmission line based technology of time domain reflectometry [19] where waves propagate down a transmission line probe or alternatively within a waveguide and reflect at impedance discontinuities and return to the source. Transit times are determined to deduce dielectric parametric information on the medium within the transmission line or waveguide. Another example would include Ground Penetrating RADAR where a wave (typically in the middle RF Range) is transmitted via a source antenna into a soil or other medium and reflections caused by subsurface layering boundaries (such as aquifers) are measured at a receive antenna located strategically based on the angles of incidence and reflection. A third method would include microwave remote sensing of the upper surfaces of a soil over a wide area via aircraft.

This literature review chapter will be focusing primarily on this latter third category of wave propagation methods in the context of electromagnetic methods. However an actual Time Domain Reflectometry (TDR) or Time Domain Transmission (TDT) measurement system (as covered in this dissertation) contains elements of both the second and third categories of electromagnetic methods as the waveforms are broadband in nature and the wavelengths of the

lower frequency components of the waveforms are long compared with the probe dimensions and the wavelengths of the higher frequency components are comparable or short compared with the dimensions of the probes. However, it is the third category (wave propagation methods) of electromagnetic methods where scattering problems arise due to the complex combination of reflected and transmitted signals about a medium or region under test. It is in this category where S-Parameters or other wave propagation modeling techniques are often employed and sophisticated inverse scattering algorithms are utilized. The literature on these electromagnetic wave propagation methods and inverse scattering algorithms will be summarized in the sections to follow. Electromagnetic wave propagation methods will be explored from several disciplines or measurement applications ranging from electrical engineering problems to soil science problems and several other disciplines to give a broad snapshot of how these algorithms are being used and applied today.

A forward prediction model will be presented in this dissertation utilizing new models for handling complex composite media with mixtures of various constituents that make up the various sections in the network and using both S-Parameters and T-Parameters. In addition a new set of techniques/algorithms for solving subsequent inverse scattering problems for such networks will also be presented in this dissertation.

With the forward prediction models the equations and modeling techniques given in Appendix A and Appendix B can be used to develop either S-Parameters and/or T-Parameters for an entire network based on knowledge of the electromagnetic parameters or properties of each section within the network. However, in the solving of the inverse scattering problem the reverse path must be followed. The elements inside the network are considered as unknowns and often the only piece of information is the measured external scattered signal exiting the input port (for the case of the transmission line for the above example). Or more generally if there are multiple ports (i.e. more complex structures) the measured scattered signals at each port must be utilized to ascertain information about the internal parameters or properties of the medium. Varying amounts of a-priori knowledge about the medium itself can sometimes be utilized if available to supplement the information from the measured external scattered signals to help reduce the number of variables or unknowns and simplify the inverse scattering problem. An example of this would be knowledge in advance that the system or medium can be approximated as being lossless (i.e. the loss tangent of each sub-section or the entire medium is sufficiently low where

the energy storage term (real component of permittivity) dominates over the energy loss terms (imaginary component of permittivity and/or electrical conductivity) as described in Appendix A). Another example might be knowledge that the entire medium is homogeneous with no cascaded boundaries or sub-sections of changing properties. This type of information can be very useful if available to simplify the inverse scattering problem.

An example of an inverse scattering algorithm that is applicable for the case of lossless networks but still can accommodate a cascaded series of subsections within a network was introduced in the landmark work by Bruckstein and Kailath (1987) [20]. In their work they introduced two different methods of solving an inverse scattering problem for lossless but cascaded multi-section networks. Their approaches are applicable to a wide variety of inverse scattering problems in all branches of science and have been utilized by many researchers and have also been leveraged by commercial simulation tools in industry. The two approaches introduced were entitled the "Layer Peeling" and "Layer Adjoining Methods". The techniques were introduced initially in the context of transmission (T) parameters ((B-17) in Appendix B) but the concepts can easily be extended to S-Parameters per the conversions of equations (B-18) and (B-19) in Appendix B (also touched upon in [20]). These approaches are summarized briefly as follows and the full derivations can be found in [20].

## General Inverse Problem:

Assumptions: The overall system is both a causal system and a lossless system over the entire network:

Given a stimulus signal at a particular port "1" in a network (modeled by $a_1(0,t)$) and a measured scattered signal at that same port (modeled by $b_1(0,t)$) where "0" represents the index for first cascaded section in the sequence of sections as you propagate into the network from port "1" and "t" represents time (assuming a time domain representation) determine the properties and associated parameters of each section in a network.

Procedures for the Inverse Algorithms [20]:

A.) Layer Peeling Method:

a.) Assume knowledge of the stimulus and scattered signals ($a_1(n,t)$, $b_1(n,t)$) at the input of section n (where n = 0 (the input at port 1) initially and incremented in subsequent iterations).

b.) Determine the T-Parameters (or alternatively S-Parameters and converting to T-Parameters) (as defined in Appendix B) of the first section initially or nth cascaded section in subsequent iterations via identification of the first non-zero scattered terms that appear in the scattered signal ($b_1(n,t)$) due to the causality assumption – i.e. $b_1(n,t)$) can't appear at the input of section "n" until after $a_1(n,t)$ has traveled to the boundary of the next section "n+1" and reflected and returned.

c.) Propagate through to determine the left and right propagating signals at the input boundary of the next cascaded section (modeled by $a_1(1,t)$ and $b_1(1,t)$ for the first iteration and $a_1(n+1,t)$ and $b_1(n+1,t)$ in subsequent iterations). Multiply the signals at the input of section "n" by the inverse of the T-Matrix of section "n" to give the signals at the input of section "n+1" (per (B-17) in Appendix B but inverting the equation/matrix to make the outputs a function of the inputs). Note that these terms at this next boundary of the n+1 section are now "synthesized or simulated signals" and are no longer directly measured signals.

d.) Peel off this nth layer to enable calculations of the parameters for the next section or layer (section n+1). This "peeling" can be accomplished by multiplying the overall network T-Parameter matrix looking into the "nth" section by the inverse of the T-matrix specific to section "n" (as determined in step b) to remove (or de-embed) it from the overall T-Matrix to now give a new overall T-Matrix looking into the input of the next section (n+1).

Increment "n" by 1 and repeat steps a-d for subsequent sections in a recursive manner ("Layer Peeling") until the parameters have been determined for the entire network.

B.) Layer Adjoining Method:

a. Begin again with the knowledge of the stimulus and scattered signals at the input of port 1 and section 0. But for this method the same signals (n=0 or $a_1(0,t)$, $b_1(0,t)$) will be used for each iteration.

b. Determine the transmission T-Matrix of section n (or section 0 for the first iteration) with a procedure similar to step "b" in the Layer Peeling method.

c. Determine the signals at the boundary of the next section (n+1) by multiplying the input signals by the inverse of the T-Matrix for section n (similar to step "c" in the Layer Peeling method).

d. Adjoin the T-Matrix of this section "n" to the chain of T-Matrices already Identified for Previous sections (n-1, n-2 … 1, 0) to create an overall transfer function from the input of the network (Port 1) up to this point (section n).

e. Increment "n" and repeat steps a-d but utilize the original input signals (n=0) for step "a" along with the progressively developing transfer function (of cascaded T-Matrices) from steps b-d to determine the signals at the n+1 section as a function of the original signals at the n=0 section (input at port 1 to the overall network).

The Layer Peeling method is actually analogous to the utilization of difference equations (subtracting out successive influences of each section to solve for the properties of the subsequent section based on the properties and signals associated with the immediate preceding section) whereas the Layer Adjoining Method is analogous to the use of integral equations (convolution or building up of the network and successively accumulating the influences of each block to solve for a signal internal to the network based on the external scattered signals and entire convolved path of transfer matrices between the external port and the desired signal of interest within the network). Both methods eventually arrive at the same pieces of information and so are essentially equivalent.

Again, the Layer Peeling and Layer Adjoining algorithm procedures originally assumed both lossless and causal systems. Later on in this review techniques for handling lossy media will be covered (including again those with multiple cascaded sections).

In summary very complex networks of multiple ports as well as multiple cascaded sections between the ports each including impedance discontinuities, delay and loss terms can be modeled via S-Parameters or T-Parameters. It is these more complex networks that are typically associated with real world systems. These systems can be both electromagnetic and non-electromagnetic with the electromagnetic methods covered in this review. We will begin with the discussion of electromagnetic inverse scattering problems in the next section starting with a popular technology (TDR) to illustrate many aspects of inverse scattering problems that can arise even with simplified structures or measurement systems. There are several applications of dielectric based measurements for agriculture [102].

## Electromagnetic Inverse Scattering Problems:

### An Initial Example: Transmission Line Method: Time Domain Reflectometry

There are a number of measurement technologies that make use of transmission line probes and which can be modeled as either single or dual port networks with the models shown in figures B.2 to B.4 in Appendix B. In all cases the measured signal is some form of "scattered" signal composed of some combination of reflected and transmitted signals about that probe. The appropriate parameter(s) of interest must be extracted from those measured scattered signals.

An initial example, Time Domain Reflectometry (TDR), which makes use of an electromagnetic transmission line probe will be covered in this section to illustrate many of the typical challenges that are found in inverse scattering problems. Various embodiments of this technology can be modeled by either a basic single port network (for the case of TDR) or a two port network (for the case of Time Domain Transmission (TDT)). Even though TDR is modeled as a single port technology it will be shown that there are still many complexities that need to be addressed with the associated inverse scattering algorithms.

A good introductory overview of TDR is given in [19] and covered also in Appendix B. As indicated TDR can be modeled as a single port network where the end of the probe is an open circuit and a stimulus signal is propagated down the probe and the entire signal is reflected at the open circuit termination and eventually returns towards the source (although potentially with various amounts of loss depending on the dielectric media within the transmission line and also potentially with multiple reflections if there are multiple cascaded sections of different properties along the path).

TDR is used for a wide variety of applications ranging from characterizing printed circuit board traces and interconnects (and even internal structures of Integrated Circuits (IC's) to geophysical applications such as soil water content measurements and various industrial applications such as liquid level sensors in tanks and trending the curing of concrete and finally food processing applications. In the next section a sampling of literature will be covered on TDR beginning with soil water content measurements and subsequently moving on to other applications of TDR.

## TDR Soil Water Content Measurements

The early classical embodiments of TDR soil water content measurement systems related water content to some other measurable parameter such as the soil dielectric constant or relative permittivity $\varepsilon_r$, TDR transit time or the phase velocity of the TDR waves via empirical regression models. Two of the more popular earlier classical models (shown below) are the Topp equation (relating water content to the dielectric constant (Topp et al., 1980) [21]) and the index of refraction equation (relating water content to the ratio of the phase velocity of waves in free space to the phase velocity of waves in the soil (Herkelrath, 1991) [22]). It was in Dr. Topp's classical landmark 1980 paper [21] that TDR was first introduced to the application of soil water content measurements.

Topp Equation:

$$\theta = A_0 + A_1 \varepsilon_r + A_2 \varepsilon_r^2 + A_3 \varepsilon_r^3 \qquad (2\text{-}1)$$

where

$$\varepsilon_r = \left( \frac{t}{2L_P \sqrt{\mu_0 \varepsilon_0}} \right)^2 = \left( \frac{c\,t}{2L_p} \right)^2 \qquad (2\text{-}2)$$

t = Transit Time (of traveling wave down and back the length of the probe).

$L_P$ = Length of Probe

c = Speed of Light in Free Space

Index of Refraction Equation:

$$\theta = K_1 + \frac{K_2}{V_{p_T}} \qquad (2\text{-}3)$$

$A_0$ - $A_3$ (2-1) are empirically derived constants (from linear regression) and $\varepsilon_r$ is the real portion of the dielectric constant or relative permittivity (equivalent to $\varepsilon_r'$ from (A-11) in Appendix A). $K_1$ and $K_2$ (2-3) are constants that can either be empirically derived (linear regression on field data) as utilized in [22] or exactly derived from electromagnetic theory (using (A-9) to (A-23) in Appendix A) and composite soil models (the latter approach utilized by the author in the accompanying forward modeling and inverse scattering papers). $K_2$ is typically close to the phase velocity of waves in free space, and $V_{p_T}$ is the effective phase velocity of the transmission line in an overall soil mix of the three phases of solids, water and air (see (A-18) of Appendix A). The ratio of $K_2 / V_{p_T}$ is termed the index of refraction and for those subset of cases where the soil or media can assumed to be lossless this ratio is functionally equivalent to the square root of the dielectric constant or relative permittivity (A-9, A-10 and A-18 of Appendix A) assuming also that the relative magnetic permeability is approximately equal to one – a good assumption in most soils).

The relative electric permittivity or dielectric constant (for use in (2-1)) and phase velocity (for use in (2-2)) can (assuming lossless media in section 2 in figures B.2 and B.4 of Appendix B) be determined by a very simple measurement of the total transit time of a propagating pulse as it travels initially forward about the probe through section 2 and then reflects the open circuit termination and returns to the input at the boundary between section 1 and 2 (figures B.2 and B.4 of Appendix B). Both of these methods represent very simplified inverse scattering problems and both assume that the network is essentially lossless to allow for the accurate determination of the transit time and subsequent calculation of the dielectric constant (for (2-1) or determination of the phase velocity (for (2-2). Therefore, these empirical regression models work best in soils where the electrical conductivity and other loss mechanisms are relatively low.

In the presence of high salinity or electrical conductivity σ (which dominates at lower frequencies per (A-10) of Appendix A and/or dielectric loss mechanisms due to ε" (which dominate at higher frequencies especially for the case of water again per (A-10) it can become difficult if not impossible to determine transit time and phase velocity from a TDR trace. This is due to the second reflection disappearing due to high attenuation of the propagating wave or spreading out due to high dispersion (frequency dependence of the phase velocity) as can be seen by close examination of equations (A-9) to (A-23) of Appendix A when the loss tangent ((A-10) is finite or large. Also, in the presence of high conductivity σ, the TDR trace can decay exponentially or show a downward slope or ramp due to frequency dependent reflections caused by a drop-off in the characteristic impedance with decreasing frequency (in the lower frequency portion of the spectrum) of the transmission line that makes up the TDR probe (equations (A-21) and (A-22) of Appendix A when $\sigma >> \omega\varepsilon''$ and $\sigma >> \omega\varepsilon'$).

Another limitation can be if there are charged interfaces in the soil due to clay constituents or organic matter constituents or alternatively Maxwell Wagner charged interfaces at water/soil boundaries [35, 36] all of which can lead to a lower limit on water content due to bound water mechanisms. In addition, these methods assume only one homogeneous section within the transmission line probe whereas in reality there can be profiling in the soils or other test media utilizing TDR. Therefore, there were several limitations to these original classical embodiments of TDR soil water content measurement technologies although they still have value over a reasonable range of applications.

Other techniques have been developed to account for and accommodate lossy media, bound water / charged interfaces as well as cascaded sections and samplings of the current literature on these improved techniques will be covered in this review as well as alternative methods covered in the accompanying papers by the author.

In two papers, Arcone (1986) [23, 24] investigated the limits of single reflection TDR in the presence of high electrical conductivity σ [23] as well as frequency dependent dielectric loss mechanisms or the presence of the loss component (imaginary) component of the electric permittivity (ε'') due to dielectric relaxation phenomena [24]. In [23] it was shown that electrical conductivity if significant will dominate over the dielectric influences at lower frequencies and that crossover frequency will rise as conductivity increases (consistent with (A-10) of Appendix A). It was shown that for an electrical conductivity value of 0.1 S/m that the conductivity effects dominated over the dielectric effects at frequencies below 300 MHz for a particular mid-range value of water content or dielectric constant. The crossover frequency dropped to 100 MHz for a conductivity value of 0.01 S/m consistent with the square root functions of equations (A-9) to (A-23) of Appendix A. Therefore higher frequencies are needed to determine the dielectric constant when electrical conductivity is present. However, there is also greater attenuation at higher frequencies when either electrical conductivity or dielectric loss mechanisms are present and so there is a point where the TDR trace will not be usable for determining dielectric properties and water content from a reflected signal at the end of the probe. However, a "first reflection" at the input to the probe can still be utilized to determine water content even in the presence of very high conductivity (via utilizing the high frequency information in the signal) although the zone of measurement is greatly reduced.

In [24] numerical simulations were utilized and parameters such as time alignment, waveform truncation and noise were simulated as functions of different values of both the real and imaginary component of the permittivity to simulate different media. It was found that significant errors could occur if the frequency components of the traveling pulse approach the dielectric relaxation frequencies of any of the dielectric constituents. This could be applied to a wide variety of media and not just soils/water. The relaxation frequency of water is up at ~17 GHz however its influences can show up at much lower frequency (~ 1GHz). From close inspection of equations (A-9) to (A-23) of Appendix A it can be shown that when the dielectric

loss mechanisms due to ε" become significant that all the key electromagnetic parameters become functions of frequency. Dielectric loss mechanisms (for the case of water) therefore dominate at higher frequencies in contrast to the effects of electrical conductivity which generally dominate at lower frequencies (although σ does influence high frequency attenuation).

Therefore at the lower end of the spectrum (lower frequencies) the effect of electrical conductivity σ is predominant. There have been a number of studies to characterize the effects of electrical conductivity on TDR systems and the influences on dielectric measurements in general. One such study by Campbell (1990) [25] characterized the impacts of electrical conductivity on dielectric property measurements from 1 – 50 MHz and it was found that it can have significant impact in this frequency range (as expected from equations (A-9) to (A-23) of Appendix A when electrical conductivity dominates over the dielectric loss mechanisms). Again, close inspection of equations (A-9) to (A-23) of Appendix A show that as electrical conductivity continues to rise it will eventually get to the level where it dominates over all dielectric phenomena at lower frequencies (including the real component of the permittivity which drops out of the equations for very large σ). In those cases the classical utilization of TDR or any other wave propagation technology breaks down if a transit time or wave phase velocity based algorithm is used in attempt to correlate that to the dielectric constant to obtain water content. Alternative algorithms and approaches must be utilized and they will be explored later in this review focusing on the latest research on inverse scattering algorithms in lossy media. Alternative approaches will also be presented in later chapters of this dissertation.

Researchers at the US Salinity Lab in California have conducted extensive research into the impacts of electrical conductivity on TDR measurements. A key outcome was actually taking advantage of this low frequency dependence on σ to aid in the development of methodologies to simultaneously measure electrical conductivity and water content within certain constraints. In a series of landmark papers by Dr. Frank Dalton and several key collaborators [26 – 30] a methodology was developed to measure the electrical conductivity with TDR using the low frequency or long time (eventually settling point on a TDR trace) to measure σ. This relationship is given in the following expression:

$$\sigma = \frac{G_f}{Z_0}\left(\frac{1-S11_{LT}}{1+S11_{LT}}\right) = \frac{G_f}{Z_0}\left(\frac{1-\Gamma_{LT}}{1-\Gamma_{LT}}\right) \quad (2\text{-}4)$$

Where

$G_f$ = Geometrical Factors for the Specific Probe

$Z_0$ = Characteristic Impedance of Driving Cable (Typically 50 Ω)

In the time domain the "LT" suffix represents long time (final settled value) measurement for S11 or Γ (reflection coefficient) of the TDR waveform. Alternatively for a frequency domain representation the DC or low frequency values of S11 or Γ would be utilized.

As long as the electrical conductivity is within modest ranges the water content (function of the dielectric parameters) can also still be simultaneously measured with the same TDR trace. There are again limitations to the range that this can be successful although new algorithms (including those by the author) offer the potential of extending this range. There are several other papers by other researchers covering this topic including Topp et al. [31] and Kelly et al. [32]. In this latter work [32] short length TDR probes were explored as a mitigation for conductivity and its associated attenuation influences on the propagating waves. The short probes also allowed for higher fine resolution spatial measurements especially if higher frequencies are also employed. Another mitigation for conductivity explored in this study [32] was the use of insulated or coated probes utilizing Teflon and it was found that could extend the use of TDR probes to regions of higher conductivity although would require a new calibration curve.

Returning back to the higher end of the TDR spectrum where dielectric loss mechanisms dominate (at least those of water): Heimovaara in a multi-part series of publications (1994) [33], [34] modeled the dielectric relaxation of water utilizing the classical Cole-Cole model as part of a development of overall models for the complex permittivity of a composite mixture of solids, water and air that make up soils. The Cole-Cole model for the permittivity is shown as follows:

$$\varepsilon_r^* = \left[ \varepsilon_\infty + \frac{\varepsilon_s - \varepsilon_\infty}{1 + j\omega\tau^{(1-\beta)}} \right] \tag{2-5}$$

where

$\varepsilon_s$ = Low frequency dielectric constant

$\varepsilon_\infty$ = High frequency dielectric constant

$\tau$ = Relaxation time of the polar water molecule $H_2O$.

β = A Parameter to account for spread in the resonance and is between 0 and 1.

If β = 0 (2-5) reduces to the more classical representation of relaxation or the Debye relaxation model covered in [36]. For the case of the Debye relaxation models the expressions for the real and imaginary components of the permittivity can be shown to be the following:

$$\varepsilon' = \varepsilon_0 \left[ \varepsilon_\infty + \frac{\varepsilon_s - \varepsilon_\infty}{1 + \omega^2\tau^2} \right] \tag{2-6}$$

$$\varepsilon'' = \frac{\omega \varepsilon_0 \tau (\varepsilon_s - \varepsilon_\infty)}{1 + \omega^2\tau^2} \tag{2-7}$$

These models can be plugged into (A-10) for the loss tangent and subsequently into equations (A-9) to (A-23) of Appendix A for all of the other electromagnetic parameters and it can be readily seen that the wave propagation parameters and characteristic impedance become very complex especially above 1 GHz where the loss component of permittivity becomes more significant due to the dielectric relaxation phenomena as modeled by either the above Cole-Cole or Debye models. Therefore very high bandwidth TDR systems run into limitations at the high end of frequency due to the dispersion and attenuation due to the dielectric loss mechanisms of water.

Heimovaara et al. [35] also compared time domain to frequency domain measurements of permittivity from 300 kHz – 1 GHz using time domain reflectometry and a vector network analyzer (VNA) respectively. He found that the VNA provided much cleaner measurements due to the wider dynamic range and swept narrowband measurements of the VNA. There are many tradeoffs between time domain and frequency domain measurements and both have their

advantages. One of the advantages of the time domain measurement is measurement speed (although at the expense of noise and dynamic range).

Petropoulos [36] characterized the time domain impulse response of dielectrics modeled by both the Debye relaxation model ($\beta=0$ in (2-5) and the Cole-Cole relaxation model (finite $\beta < 1$ in (2-5). The impulse response was generally smoothed for the Cole-Cole responses and sharper for the Debye responses. The responses were distinct enough that it was concluded that they could be distinguished from each other in a real world measurement (in terms of media following one model vs. the other). However, it is believed that water follows closer to the Cole-Cole model and therefore has a wider spread in the dielectric relaxation resonance and therefore more dispersion in the waveform further away from the center frequency (down as low as 1 GHz even though the relaxation resonance for water is up at ~17 GHz). This is important for TDR soil water content measurements and must be accounted for.

As indicated earlier, in addition to the effects of electrical conductivity $\sigma$ and the dielectric loss mechanisms due to $\varepsilon$" of water, there is another set of mechanisms that can impact the performance of TDR soil water content measurements. These fall in the category of bound water mechanisms or alternatively charged interfacial mechanisms such as those due to clay interfaces, organic matter interfaces and other charged interfaces between solid constituents and water as well as ions in solution (e.g. Maxwell Wagner effect). Several of these mechanisms can be modeled by relaxation models (analogous to water) but the time constants and associated physical mechanisms and processes are much slower than that of free water and so result in lower to medium frequency influences (often superimposed on the impacts of electrical conductivity but moving up to higher frequencies as well). Curtis (2001) [37] developed a durable laboratory fixture for measuring the dielectric properties of both sandy and clay soils using Vector Network Analysis (VNA) which can measure the S-Parameters of a fixture with a particular medium within. He verified initially the spectrum of the relaxation resonance for free water (Debye or Cole-Cole resonance at ~17 GHz) and also observed that propagating signals had completly disappeared above 10 GHz even with the dynamic range of the VNA due to attenuation from the lower tail of that relaxation resonance. In addition he characterized sets of both sand and clay soils of various water contents and observed additional significant relaxation loss mechanisms below 1 GHz in the clay soils due likely to relaxation phenomena associated with charged interfaces (e.g. Maxwell Wagner interactions) evidenced by the rise of the loss component of

permittivity with decreasing frequency in those clay soils (a portion of this could have been potentially caused by finite electrical conductivity as well which dominates at lower frequencies). Kelleners et al. (2005) [38] characterized the real and imaginary components of permittivity of bentonite vs. frequency and also found a strong dependence the dielectric properties on frequency below 500 MHz. They also compared capacitance probes to TDR and found significant errors in the capacitance probes for measuring water content in the presence of clay soils due to the lower RF frequency operation of the those probes (falling into regions where both the dispersion from the bentonite frequency dependence of the dielectric properties as well as the influences from electrical conductivity were both dominating and masking the effects of the permittivity of water). It was again recommended that frequencies above 500 MHz be utilized (consistent with the upper spectrum of TDR systems).

TDR has been applied to identifying the properties of other media besides water. Robinson [39] utilized TDR to measure the permittivity of clay and other minerals using a number of different immersion fluids to fill the Pores in the medium. These fluids are themselves also dielectrics. It was found that within certain conditions that the base permittivity of various clays and minerals could be determined but that this relies on the utilization of accurate dielectric mixing models. For the case of swelling clays and other phenomena it was determined that the dielectric mixing models can break down. The exploration of recent literature on dielectric mixing models will be covered in depth later in this review and also in later chapters of this dissertation including the forward Prediction models as well as in Appendix C.

Chen et Or (2006) [40] examined the temperature dependence on all three of the key mechanisms covered above (Low Frequency electrical conductivity $\sigma$, Low to Moderate Frequency Maxwell Wagner influences on permittivity influenced by charged interfaces such as in clay constituents, and High Frequency permittivity influenced primarily by free water molecules). It was found (as expected) that the low frequency conductivity increases with temperature. In contrast it was also found that the permittivity at high frequencies due to free water exhibited decreases with temperature (also as expected). However, in the low to middle ranges of frequency where Maxwell Wagner influences can be predominant due to charged interfaces such as clay/water boundaries it was found that there was a complex interplay with conductivity $\sigma$ on influencing the dependencies of the permittivity with temperature. It was found that both the real and loss components of permittivity due to Maxwell Wagner influences

increased with both temperature as well as with conductivity (implying a nonlinear cross-dependency with conductivity). A further complication is that as these Maxwell-Wagner influences on the loss component of permittivity increased it also pushed up to higher frequencies where the cross-over was to where the free water took over in terms of the primary influence on the bulk permittivity. From their specific study it appeared that the dominant ranges of the Maxwell Wagner influences were primarily under 100 MHz. In their study they also found that these M-W influences did not have significant effects on the TDR transit time in the time domain as long as the other accompanying parameter (electrical conductivity) was low enough to be able to identify a definable transit time from the TDR trace. This would imply that in their setup the bulk of the dominant portion of the spectrum for the TDR pulse was > 100 MHz. All of these findings do show that temperature is a factor and it likely will be a good companion measurement parameter to be used with a TDR measurement system and associated algorithms.

In addition to the limitations associated with loss mechanisms and dispersive mechanisms as described above, there are other potential confounding factors on TDR soil water content measurements that have led to other studies. Knight [41] studied the spatial sensitivity of TDR probes of two geometries (coaxial probe and a parallel wire probe). For both cases the electromagnetic Laplace's equation (2-8) was used to solve for the electric potential and subsequently the electric field **E** via (2-10) both as a function of position between the probes to assess the sensitivity of the probe to changing water content at different distances away from the probe conductors.

Laplace's Equation (Electromagnetics): $$\nabla^2 \Phi = 0 \qquad (2\text{-}8)$$

Poisson's Equation: $$\nabla^2 \Phi = -\frac{\rho}{\varepsilon} \qquad (2\text{-}9)$$

Expression for Electric Field: $$\mathrm{E} = -\nabla \Phi \qquad (2\text{-}10)$$

Where $\Phi$ = Potential (Volts)

$\rho$ = Charge Density

E = Electric Field Intensity (Gradient of Voltage or Potential) (V/m)

Laplace's equation is for charge free regions (or charge neutral regions where no net charge exists in the medium). Poisson's equation is for regions containing net charge which intuitively one might initially believe could be the case for a soil/water mixture with free ions in solution and the

overall medium. However, the assumption is made on charge neutrality in the medium (same number of positive and negative ions) which allows for Laplace's equation to be used. It was found in [41] that most of the sensitivity was near the vicinity of the probe wires especially if they were very thin (leading to strong electric fields in those locations). The same was true with the coaxial probe if the center conductor was very thin (the fields were strongest near those thin wires and hence most of the stored energy and sensitivity to changing soil properties would be in the regions near the probe wires). Therefore if air gaps were present near those wires then there was the potential for errors in determining the water content.

Note: Hypothetically, if there was net charge (non-charge neutrality) out in the medium and Poisson's equation was utilized, the findings [41] could potentially be mitigated somewhat (although certainly not completely) due to the extension of the electric field and potential functions deeper in the medium (via inspection of (2-9) and (2-10) where the electric field function would be an integral of the net charge density distribution and the potential function would in turn be the integral of the electric field). But again it is assumed that there is charge neutrality and no net charge in the medium and so Laplace's equation is applicable. In addition, the high dielectric constant of water and the wet soils due to polar molecules would have the opposite effect and reduce the electric field for a given amount of free charge (from again inspection of (2-9)). However, despite the lower electric field in a dielectric for a given amount of charge that same polar dielectric behavior allows for more energy to be stored for a given electric field and subsequent potential (as a high dielectric medium along with a particular probe geometry forms a capacitor with a certain capacitance per unit length). If an air gap was present near the wire surface (with dielectric constant = 1) compared with wet soil everywhere else (with perhaps an effective dielectric constant as high as 20 with the water constituent having a dielectric constant of 78) significant energy could still potentially be stored in the dielectric region even though the field strength is higher in the air gap and falling off somewhat moving away from the probe wires. This would (at least in theory) tend to extend the zone of influence further out from the probe wires in terms of where the energy is stored. This mitigation would only work to a point as the energy stored per unit volume of the dielectric will drop off as the square of the voltage and subsequently the electric field (or gradient of voltage) whereas would only increase linearly with the dielectric constant. The field mapping of the medium within a transmission line probe should be studied more and other articles related to this will be covered

later in this review especially in the context of fields within a composite dielectric material made up of several constituents in a heterogeneous mixture.

A more recent study was conducted by Hinnell et al (2006) [42] to assess the impact of rod diameters and potential disruptions to water flow around the rods in TDR systems on the accuracy of the water content measurement as well as the disturbance on the actual water content profile by the probes. It was found that there was some impact but that the errors on measured permittivity and subsequent water content measurements were very small due to these air gaps and flow disruptions and considered insignificant compared to other sources of error in the TDR system.

The sources of potential errors due to the invasive nature of the TDR probes have led to the exploration of non-invasive soil water content measurements. Selker et al. [43] investigated the potential of developing a non-invasive TDR measurement system that would be placed on the surface of the soil or other media. In this study it was found that reasonable sensitivity and accuracy could still be obtained by simply developing a new calibration curve. This type of measurement would be sensitive to the moisture content only near the soil surface. Alternative non-invasive wave propagation technologies have also been developed including ground penetrating radar as well as microwave remote sensing. The frequency ranges that are used with the technologies dictate how deep the penetration influence will be. These alternative non-invasive technologies will be covered later in this review. Nuclear Magnetic Resonance has also been explored as a non-invasive measurement technology for soil water content, soil porosity and even concrete moisture content [43], [44] and [45]. Even a portable tractor or truck/trailer mounted versions were produced for soil measurements and bridge deck concrete measurements respectively [43]. They operated on the principal that Hydrogen (and thus water) could be detected in the media via its Nuclear Magnetic Resonance in the RF frequency range (the frequency of which would depend on the strength of the accompanying applied DC magnetic field). The DC field would align all of the nuclear magnetic spin orientations and then a coupled RF signal at the Hydrogen NMR frequency would disrupt the nuclear spins of those atoms and then as they re-align with the external DC magnetic field RF radiation at that same NMR frequency would be released from the media and a particular inverse scattering algorithm would detect that and assess the presence, amount and position of water in the soil or alternatively in

concrete. This was a potentially powerful 3-D non-invasive imaging technology with the main downside being cost.

Back on the topic of TDR: Another limitation of the original two wire TDR probe was the fact that it was a balanced line of very high characteristic impedance (> 200 Ohms when air filled or with very dry soil) whereas the driving signal was typically sourced via an unbalanced coaxial transmission line of lower characteristic impedance (typically near 50 Ohms). The result was that a 4:1 balun typically had to be placed between the driving coax and TDR probe (both to translate between the unbalanced and balanced lines as well as to attempt to partially match to the much higher impedance of the TDR transmission line). However, the latter item (impedance matching) was of lesser concern as the first reflection could be distinguished from the second reflection in a TDR trace. Of greater concern was the potential distortion of the waveform especially at higher frequencies as it passed through that balun. To address this TDR probes have been developed that have multiple conductors in an attempt to emulate the unbalanced feeding coax. Multi-wire probes were investigated (Zegelin et al. [47]) without baluns and found to provide cleaner signals. Therefore today multi-wire probes (three or more electrodes) have become the standard for TDR measurements and two-wire probes are rarely used.

In a more recent study Ball [48] provided both analytical and computer numerical determinations of the actual characteristic impedance in open air of a variety of modern multi-wire TDR probe configurations. He utilized conformal mapping or transformation techniques to map the solution for a two wire probe into multiwire configurations. He also used direct numerical simulations using the Method of Moments to solve for the potential functions and charge functions about the probe to determine the capacitance C per unit length of a TDR transmission line probe to aid in calculating the characteristic impedance of the probe in open air via utilization of a simplification of (A-22) in Appendix A (assuming loss tangent = 0 and free space permeability and permittivity for open air) shown as follows:

$$Z_{\mathrm{OpenAir}} = f(G)\sqrt{\frac{\mu_0}{\varepsilon_0}} = f(G)\eta_{OpenAir} = \sqrt{\frac{L}{C}} \qquad (2\text{-}11)$$

He then utilized various assumptions to rearrange and simplify the equation to the following to allow for calculating the characteristic impedance of the probe in open air as a function of the derived Capacitance per unit length:

$$Z_{OpenAir} = f(G)\sqrt{\frac{\mu_0 \varepsilon_0}{{\varepsilon_0}^2}} = \frac{f(G)}{\varepsilon_0 c} = \frac{1}{cC} \tag{2-12}$$

Where

c = Velocity of Waves in Free Space

and all other parameters are as previously defined.

He used this calculation to validate the results from the conformal transformations. This result was also used to provide specific probe calibration information to allow for exact measurement of the low frequency electrical conductivity σ that is determined from the long time (final settling value) of the TDR trace together with the geometry calibration for the specific probe (using (2-4)).

Improved field based measurement techniques have also been investigated including an improved Access Tube design with surface mount electrodes [107] shown to be effective over a wide range of soil types and test media although with increased dispersion (decreased waveform slopes) under the presence of dielectric loss. The impacts of bound water and temperature and its impact on dispersion must also be accounted for and have been investigated in several studies [106], [115], [116] and [120]. The electric permittivity (real and imaginary components) and relaxation behavior of bound water has been found to have a strong temperature dependence. Free (unbounded) water has a moderate temperature dependence on its dielectric properties. Therefore, temperature must be accounted for in all dielectric models of soil (especially in the context of water). Additional studies on the dielectric relaxation and complex permittivity of soils included [110] to [113] and [115] to [119] accounting also for multi-constituents.

**TDR Measurement in Layered Soils:**

As discussed in earlier sections one of the challenges with inverse scattering problems is when there are multiple cascaded sections between one port and another which can result in much complexity in the scattered signals. This situation can also occur with TDR soil water content measurements. There have been a number of studies to assess the performance of TDR measurements in layered soils or with other varying profiles of water content vs. depth. This is closely related to dielectric / permittivity mixing composite media problems but at a more macroscopic scale. The background research for these types of dielectric mixing and layered media models/problems are covered in depth in Appendix C. A summary sampling of this work will also be covered in this section specific to the application of TDR.

Souza et al. (2001) [49] developed and evaluated a technique using multi-wire TDR probes with built in discontinuities or segments in the probe (segments with different rod diameters and spacing's) in an attempt to be able to signature or de-convolve those built in discontinuities and use them as spatial markers to assess water content profiles or water content values vs. depth. They found some success under limited conditions in the laboratory but also found limitations in terms of the range of impedances that can be detected as well as the depth that the probes could be useful for (i.e. the complex scattered signals when combined with other confounding elements such as loss led to limits on how many reflected elements could be handled). They suggested and planned more research on other probe geometries and followed up in 2004 [131] with a variable volume TDR multi-rod probe design for assessing water content over a large volume via volume averaging.

Ferre et al (2002) [50] combined TDR water content measurement problems with soil water infiltration problems. The goal was to assess the water content profile vs. depth to identify the wetting front and use this info to cross validate the infiltration models to allow for extracting soil hydraulic parameters such as the soil hydraulic conductivity from the infiltration models. They characterized the potential errors that could occur in the calculation of the hydraulic conductivity due to incorrect identification of the wetting or infiltration front due to the effects of different TDR probe geometries. These errors could occur from either inaccuracies in the water content measurement itself (i.e. the spacial sensitivities of the probes) or alternatively disruptions

to the wetting front and breakthrough curves due to the invasive probe rods themselves. It was found that probes with wider spacings had less disruption to the wetting front but also had a smoothing effect on the detection of the wetting front due to wider spatial sensitivity limitations. They also experimented with the orientation of the probes (vertical and horizontal) and found that the best sensitivity to detecting of the wetting fronts was with horizontally placed probes at various depths (a non-surprising result). Vertically placed probes (although less invasive) have several additional challenges in their inverse scattering problems due to the need to "de-convolve" the wetting front profile vs. time. Horizontal probes still have limitations as well if the wetting front is non-uniform (e.g. fingered flow) [51]. Fingered flow could actually lead to the need of profiling measurements in the horizontal axis as well (and interesting research opportunity) that could be combined with vertical profiling for a powerful soil water content imaging tool (i.e. a 2-D or even 3-D imaging need instead of the largely 1-D TDR method) although bringing up again the question and need for non-invasive imaging techniques. More research is planned on this measurement need and it shows the great value of combining accurate water content profiling measurement technologies with other companion technologies such as infiltrometers that are used to determine the soil hydraulic properties. Combining these two areas of technologies is one of the research interests/focuses of this author.

Schaap et al. [52] analyzed the performance of TDR soil water content measurements in layered media of multiple layers of different thicknesses and properties and even orientations (both parallel and orthogonal layer orientations relative to the probe). They assessed the influences of these layers to the overall TDR measurement as if the layered media was one composite block (i.e. there was no attempt to de-convolve or identify the specific layers individually from the TDR measurement). Their findings included that if there are a small number of larger sections of which the probe penetrates that the effective overall permittivity of the composite dielectric mixture follows a classical relation referred to as refractive averaging and given by the following equation (for two sections):

Refractive Averaging Model:
$$\varepsilon_{eff} = \left( \frac{L_1\sqrt{\varepsilon_1} + L_2\sqrt{\varepsilon_2}}{L_{Tot}} \right)^2 \qquad (2\text{-}13)$$

Where $\varepsilon_{eff}$ = Effective Overall Permittivity of the Composite Mixture

$\varepsilon_1$ = Permittivity of Medium in Section 1

$\varepsilon_2$ = Permittivity of Medium in Section 2

$L_1$ = Length of Probe in Section 1

$L_2$ = Length of Probe in Section 2

$L_{Tot}$ = Total Length of the Probe = $L_1 + L_2$

As a further finding of the above it was found that a "thick" layer is defined as a layer that is greater than one quarter of a wavelength of the frequency of measurement. Therefore this refractive mixing model is frequency dependent and the spectrum of the TDR signal would need to be closely evaluated. Higher frequencies would lead to smaller/thinner limits of the thicknesses above which would satisfy the above relation. It was also found that if there were a large number of closely spaced thin layers and the layers were thinner than a quarter wavelength of the frequency of measurement that the mixing model switched to following a simple arithmetic mean model as follows:

Arithmetic Mean Model: $$\varepsilon_{eff} = \frac{\varepsilon_1 L_1 + \varepsilon_2 L_2}{L_{Tot}} \quad (2\text{-}14)$$

It was also found that if layers were oriented parallel to the probe that the resulting overall permittivity tended to follow the arithmetic mean. Finally it was found that for broadband methods such as TDR that the mixing models tended to follow one or the other mixing models (which would imply that the layering is either predominately large compared to a quarter wavelength or small compared to a quarter wavelength to the majority of the frequency components or spectrum in the TDR pulse). However for narrowband single frequency measurements much more frequency dependence was shown. This should be studied more and additional papers on dielectric mixing models and layered media will be covered later in this review.

Robinson et al. [53] confirmed an earlier calibration method originally developed by Heimovaara [33] which identified definable start and end times of TDR waveforms via the drawing of tangents along the rise/fall times of the various edges. The calibrations also were

conducted in both air and water to obtain a precise calibration for a particular sensor or probe. In this method the delay associated with the sensor head (or transition/connectors into the probe) can be removed or zeroed out and a true representation of the actual effective probe length and associated delay or transit time can result. In this work [53] a three section cascaded transmission line model to model the driving cable, sensor head and resulting TDR probe length (all with different impedances) was developed. This latter simulation was conducted in the frequency domain with the scattering parameters defined for each section and convolved together and then an IFFT conducted to provide a simulated time domain representation. These simulations showed good agreement with actual TDR measurements of this specific setup. They also extended the simulation to layered soil dielectrics and found again that for thicker layer dimensions that the refractive mixing model of (2-13) can be followed (but again only if the dimensions of the layer are large compared to a quarter wavelength of the highest significant frequency component in the TDR pulse).

Yu in 2005 [54] provided a comparison analysis of frequency domain and time domain methodologies for the non-uniform case of TDR measurements of various construction materials including soils of different types and layers. Numerical simulations were provided and the Finite Difference Time Domain (FDTD) method was utilized for the time domain simulations and the frequency domain model was developed as a multi-section cascaded non-uniform network problem. In the frequency domain progressive Impedance transformations were conducted/simulated moving one section at a time back from the load to determine the characteristic impedance looking into each section after the non-uniform TDR transmission line network was initially divided into multiple sections (each of uniform permittivity and conductivity values) (see (2-15) which is for the impedance transformation looking into a network at various lengths back from the load and also for the general case of lossy transmission lines [12]). This method of partitioning and impedance transformation made the system compatible with utilize the Layer Peeling method described earlier in this review [20] to de-convolve or de-embed the various sections as part of an inverse solving algorithm (although the Layer Peeling algorithm again holds the assumption of a lossless network and the impedance transformations used in this work [54] was for the general case of networks with loss. The expression for impedance transformations that was utilized was as follows and is leveraged directly from electromagnetic theory [12]:

Progressive Impedance Transformation Procedure: Beginning from the Load End and Moving Away from the Load One Section at a Time:

First Step: $Z_{in}(n) = Z_L$

All Subsequent Steps:
$$Z_{in}(n-1) = \frac{Z_{in}(n) + Z_c(n)\left(\tanh\left(\gamma_n L_n\right)\right)}{Z_c(n) + Z_{in}(n)\left(\tanh\left(\gamma_n L_n\right)\right)} \qquad (2\text{-}15)$$

Where

$Z_{in}(n)$ = Impedance looking into the input of the nth section.

$Z_c(n)$ = Characteristic Impedance of the nth section.

$Z_L$ = Load Impedance at the end of the network.

$\gamma_n$ = Propagation Constant of section n per (A-9) and (A-23), (Appendix A)

$L_n$ = Length of section n.

Again, this procedure continues until the whole network back to the input is created (analogous to the progressive network building method with S-Parameters via (B-28). The researches indicated that this procedure can be reversed using techniques similar to the peeling method of [20]. However the layer peeling method assumes a lossless network and (2-15) above is for the general case of a network with loss. It was indicated that this research was still in progress.

Robinson et al (2003) [55] provided a comprehensive summary paper of the recent advances over the past two decades in TDR Soil Water Content and Electrical Conductivity measurements. They reviewed the basic principles of TDR and then covered all of the above challenges in TDR and how they have been handled. The reiterated the problem of dielectric relaxation in soils. It was pointed out that air is non-dispersive and water is only dispersive above 1 GHz as it approaches its relaxation frequency of 17 GHz. However there are many other constituents in soils that can be dispersive in the main spectrum of TDR (1 MHz – 2 GHz). Soils with charged boundaries can again lead to Maxwell Wagner interfacial mechanisms that can restrict the flow or movement of water and lead to slower relaxation time constants dropping these mechanisms into the main RF band covered by TDR (< 1 GHz). These relaxation resonances again lead to frequency dependence of the electric permittivity which leads to dispersion (frequency dependent phase velocity ((A-18)) as well as frequency dependent

reflection coefficients due to frequency dependent characteristic impedance ((A-21) and finally frequency dependent attenuation (equations (A-9) and (A-16) of Appendix A) all of which can lead to errors in the identification of the permittivity contribution from water leading to errors in the water content measurement. Various alcohols can also have relaxation resonances well down into the RF range and impact TDR measurements. To address this, an equation was developed to model an apparent permittivity that can be derived directly from (A-18). However, as can be seen from (A-18) this is a complex frequency dependent equation and TDR is a broadband system. In this work they compared time domain to frequency domain analysis. In the time domain they reviewed again the potential for modeling the TDR probe as a multi-section probe as well as assessing info on dispersion by looking at the spread of edges of reflected waveforms via an inverse scattering model. In the frequency domain they revisited the earlier Cole-Cole and Debye relaxation models and discussed the challenges associated with extracting permittivity in the presence of relaxation mechanisms in the RF bands (leading to frequency dependent dispersion, attenuation and reflections as can again be seen from equations (A-9) to (A-23) of Appendix A). The concept of an "effective frequency" was reviewed and defined as the frequency of a broadband TDR system where the majority of the energy is located. A companion definition would be that of a maximum frequency which represents the frequency above which there is significant rolloff of the spectrum and which can typically be obtained from the rise/fall times of the edges. If the effective frequency and maximum frequencies are swamped by dielectric relaxation phenomena then there is great potential for errors in the measurement. In contrast if they are above the Maxwell Wagner type relaxation mechanisms as well as above the frequency of influence by electrical conductivity mechanisms then there is still the opportunity for accurate measurements.

This leads to the concept of an optimal frequency range defined as follows:

Low Frequency Error Zone ($\sigma$, Maxwell Wagner $\varepsilon$") $<$ **f** $<$ High Frequency Error Zone ($\varepsilon$" of water)

If the low frequency error zone overlaps the high frequency error zone then it will be difficult to obtain an accurate TDR soil water content measurement. The frequency range of 500 MHz to 1 GHz appears to be the most optimal "safe" zone based on a review of most of the literature. This paper also reviewed again the issues associated with probe geometry and the spatial sensitivities

and confirmed earlier results of the largest sensitivity of the probes near the probe locations if thin wires or rods are utilized. However, much better uniformity of the electric fields between the electrodes was found if flat blades were used instead of round rods for the electrodes. Much additional research needs to be conducted on optimal probe geometries. This comprehensive review presented three key outcomes or needs for future research:

a. Improved modeling and inversion of the TDR waveform to extract information on the permittivity and relaxation behavior of the constituents: This would allow for the characterization of dispersive materials and potentially lead to a better understanding of the behavior of porous media and bound water mechanisms (in clay soils) and how that impacts TDR measurements.

b. A method to allow for characterizing the real and imaginary components of the permittivity vs. frequency for soils over wide conditions would be of much value to aid in developing models that can be utilized by TDR or other electromagnetic systems to separate out those influences from the influences due directly to free water.

c. Present probe designs and measurement algorithms limit the use of TDR soil water content measurements to largely non-saline conditions. However, much of the irrigated land in the world (including the desert SW of the USA) is in regions of high salinity. There is a great need to develop water content measurements that can be used in regions of high salinity or electrical conductivity.

In a more recent publication and presentation given at the TDR 2006 conference at Purdue University in September of 2006 Huisman et al [56] also provided a review of current TDR technologies and algorithms used for soil water content. They indicated that before a successful inverse modeling technique can be employed that all of the following aspects of a TDR soil water content measurement system must be defined:

1.) Forward Model Type/Approach
2.) Input or Stimulus Signal
3.) Optimization Strategy
4.) Measurement Device / Technology
5.) Probe Type / Geometry

For the forward model they reviewed both the time domain and frequency domain analysis approach but focused especially on the frequency domain approach and acknowledged that they are equivalent in terms of outcome and readily interchangeable via Fast Fourier Transform (FFT) and Inverse Fast Fourier Transform (IFFT) algorithms. In this work S-Parameters were utilized and an equation equivalent to (B-28 above was used to lay the foundation for a forward prediction model accounting for multiple cascaded sections. They also reviewed the past literature on methods to define the input or stimulus signal and also account for the feeding cable and sensor head connection (interface to the probe). They reviewed the past calibration methods developed again by Heimovaara [33] and reviewed by Robinson [55]. It was suggested in this work that temperature dependence be added to the models to account for variations in the permittivity of the feeding cable and sensor heads as functions of temperature to be able to accurately define the position in both space and time of the input stimulus (required for an accurate TDR measurement). This would be needed before any automated testing with the probes can be utilized vs. time. A temperature sensor would also have to accommodate this system to provide info to the calibration model. Optimization methods were also reviewed in this paper to fit the measured inverse scattering data to the forward prediction models. It was cited that most modern methods utilize some form of genetic algorithm or utilize the Shuffled Complex Evolution Metropolis algorithm both of which find a global minimum of the objective function in the presence of a complex error landscape. They reviewed the constraints for these types of optimization problems citing the sheer complexity if there are many layers in the profiles to be de-convolved via genetic based optimization or fitting algorithms. They suggested a flexible 4-

parameter functional to describe each layer to provide a simplified optimization problem. An appropriate objective function for the optimization problem is also a key need. This is where the ability to switch between the frequency and time domains is of great value. Sensitivity to some parameters are higher in the frequency domain and to others in the time domain. Both domains therefore offer great value. The frequency dependence on the permittivity is an example of an item better characterized in the frequency domain and therefore better optimized in that domain. They offered an approach where the time domain is used initially to identify in coarse fashion the system (e.g. the permittivity profile vs. depth in a soil) and then fine tune optimization could occur in the frequency domain. The choice of domains is also dictated by the available measurement devices (e.g. Vector Network Analyzer for the frequency domain and a TDR system for the time domain). Vector Network Analyzers have much better dynamic range and lower noise due to the ability to provide swept narrowband measurements. However, this comes at the sacrifice of measurement time which is a key advantage of the time domain measurement approach. Choice of probe type was also covered in this review paper. They reviewed 2-wire, 3-wire and 7-wire probes. They generally found better performance and agreement with forward prediction models with the 7-wire probe.

Additional work on the application of TDR or transmission line techniques to Layered media included [121], [122] and [131]. These studies all showed the need to account for frequency dependence on the dielectric properties as well as other loss mechanisms such as that due to electrical conductivity due to ionic behavior and the challenges that presents to trying to extract a layered profile via an inversion algorithm. There is a direct tradeoff between spatial resolution and frequency/bandwidth of the systems but in the presence of either dielectric or ionic loss mechanisms this is confounded via dispersion and attenuation. Accounting for all of these mechanisms is at the center of the proposed forward prediction algorithms presented in this dissertation.

## Other Applications of TDR:

### Concrete:

TDR transmission line methods are used in many other applications. One such application is the assessment of the properties of concrete. Qiwei et al. [57] utilized a 3-wire TDR probe to track and trend both the dielectric constant (relative permittivity $\varepsilon_r$) and electrical conductivity $\sigma$ of three different formulations of concrete vs. time as it was going through its curing process (using (2-2) and (2-4)). They found that both the permittivity and conductivity dropped steadily during the curing process and eventually leveled off as the curing process neared completion. This example shows the value of using TDR or other inverse scattering measurement technologies to "trend" properties vs. time. That would also be of value in the soil water content technologies covered above as well as in the industrial liquid level sensor technologies covered next.

### TDR Industrial Liquid Level Sensors:

TDR can also be used to detect the level of one or more fluids in a tank. Nemarich [58] described a TDR system that senses the levels of two fluids in a tank (using the equations for lossless TDR operation from above – e.g. (2-4) where transit time now would be the travel time between the top and bottom fluid interfaces and back). This could include a fuel along with some other backfilling or compensating fluid to insure the tank is always full and doesn't have significant air volumes that could form a volatile mixture with the fuel. For best performance and sensitivity with the TDR the upper fluid needed to have low conductivity (to prevent attenuation of the propagating wave to the lower fluid interface) as well as a lower dielectric constant than the fluid below it (to insure a well definable reflection of the TDR pulse at the interface to the lower fluid). This work leveraged approaches that were developed previously by the US Navy in the 1980's.

Cataldo et al. (2006) [59] perform a series of experiments on TDR liquid level sensors with high replication to assess the precision and uncertainty of these types of measurements. They performed this evaluation with four different types of fluids: Diesel Oil, Fuel, Acetone and De-ionized water. They assessed uncertainty in the measurements of the permittivity as well as the

level of the fluid. They found that the uncertainties on the measured relative permittivity's were approximately 2% or less with all of the fluids and the uncertainties on the measured level of the fluids were 1% or less with all the fluids indicating good performance. The fluids ranged from low permittivity's (Diesel Oil and Fuel – both around 2.2) to medium permittivity (Acetone – 21.7) and finally high permittivity (De-Ionized Water – 79). The tests were performed using a graduated cylinder filled with one of the fluids at a time and the probe fully submerged. The level measurement was defined by the ability to measure accurately the full length of submerged probe via the extracted measured TDR signal for the four different dielectrics (four different wave velocities - analogous to the problem when a TDR probe would penetrate one fluid to the boundary of a fluid below it – the effective length through the first fluid must be accurately determined).

Gerding et al. (2006) [60] developed an improved TDR system for industrial liquid level measurement that had faster and narrower pulses to allow for detecting thinner layers of fluids. The faster pulses were generated using a comb generator made up of four stages: 1.) Fast logic circuitry to generate an initial pulse of modest speed and rise/fall time, 2.) Bipolar transistor stage driven hard into saturation operating as a switch to speed up the trailing edge of the pulse, 3.) Differentiator circuit (high pass filter) that results in two spikes (derivatives of both edges of the previous pulse with the trailing edge spike more pronounced and faster) and 4.) Schottky diode wired in such a way to serve as a limiter to clip off the lesser spike or pulse and preserve the more pronounced and faster pulse. On the receiver end of this TDR system they also developed samplers that operated with "interleaving" by having two sampling clocks that were offset very slightly in frequency and both of very high stability. This is analogous to using a strobe lights of two slightly different rates that will wander through a high speed rotating shaft to eventually obtain a snapshot of every portion of a revolution (or cycle) even though the shaft is rotating at much higher speed. This allows for the reproduction of much higher speed signals with moderate speed sampling circuits and therefore utilization of standard Analog to Digital Converters in the data acquisition system. This was accomplished via a special Phase Locked Loop (PLL) design and other hardware and software. The PLL allowed for very low phase noise and very high stability on the sampling signals.

## Time Domain (TDR) and Frequency Domain (VNA) in Electrical Engineering Applications

TDR was actually originally invented by electrical engineers for use in identifying and locating cable faults by sending the TDR signal down the cable and looking for reflections that would occur at the fault locations. TDR has since found its way into numerous other applications both within and outside of Electrical Engineering (some of the latter examples covered in the previous sections). Within electrical engineering one of the most common applications is the characterizations of the signal paths in printed circuit boards, hybrid microcircuits and even within the packages and chips of integrated circuits (IC's). Characterizing the RF signal integrity of signals traveling through various cables, interconnects , circuit traces, packaging leads, and terminations at IC's (and even into the internal routing of IC's themselves) is of great importance in understanding the performance of the circuits from both their intended use perspective as well as in the context of EMC (electromagnetic compatibility). The former can shed insights as to whether the signals will operate properly at the frequencies and pulse edges that are needed (as high speed digital circuits are now essentially RF circuits that must be modeled as transmission lines). If there isn't a proper termination or approximate match at the ends of the traces (which themselves are often transmission lines at today's frequencies of digital circuits) then there can be bad reflections and ringing which can degrade the performance of the circuitry's intended functions. In addition, these reflections or ringing together with a bad layout that can serve as antennas can lead to radiated emissions which not only exceed the EMC standards by the regulatory/agency bodies (especially IEC/EN which cover Europe and many other countries and which are typically the most stringent standards in the world) but also create havoc in interfering with other equipment.

Therefore there is a need to characterize these signal paths in situ in the various circuitry. This can (and should) be done initially before design and layout via simulations with RF/microwave simulation tools if available. But after initial design and layout is completed there is the need to characterize and measure these circuits directly. This can present other challenges as well as there may be complex fixturing paths that must be created to get the measurement signals down to the "circuit under test". This is where frequency domain vector network analyzers (VNA's) with S-Parameter measurement capability along with de-embedding techniques and software become powerful measurement tools [11]. The identification of S-Parameters of the fixtures and subsequent conversion to T-Parameters per (B-18) from Appendix

B allows for a very straight forward way to de-embed the effects of fixtures. In addition, port extension calibrations that remove the effects of delay and loss of feeding cables are also readily obtained with modern VNA's via either single port or two port calibrations using shorts, opens, known loads and thru measurements (e.g. SOLT) calibrations or alternatively utilizing TRL calibrations (Thru-Reflect-Line) the latter of which does not rely on the need for known matched loads as the SOLT relies on [11], [13]. However, the SOLT method is broadband and the TRL method is narrowband. All of these calibration methods can move the measurement plane of reference closer to the actual intended circuit under test to create a cleaner/simpler measurement that is easier to interpret. So there is much power in the use of frequency domain VNA measurements to characterize electronic circuits.

There is also much value in being able to characterize these circuits in the time domain. Time domain characterizations are often more intuitive to interpret in the context of trying to understand and characterize how a particular circuit and layout will impact the integrity of a digital signal which is often a broadband signal of multiple harmonics. Therefore TDR offers great value to these types of measurement problems. In fact most VNA's have an available option that allows for providing IFFT (Inverse Fast Fourier Transform) software to generate a time domain signal from the measured frequency domain S-Parameters. The key advantage of VNA's is their narrowband sweep capability (over a wide frequency range) which allows for better dynamic range and lower noise as well as the ability to characterize the frequency dependence on items such as the permittivity. However, the major disadvantage of a VNA is the measurement time and that is where dedicated TDR systems (utilizing a scope with a fast rise time pulse source/stimulus and then fast samplers to detect the measured response) are of great value. They offer much faster measurement speed and often are sufficient in terms of signal to noise ratio as again the key often in electrical engineering is looking at the integrity of the signal (often a digital signal) as it travels down a signal path. If the goal is characterizing the signal integrity of those digital/pulse waveforms then TDR is the measurement of choice. If the goal is characterizing the frequency dependence of the permittivity or propagation and/or impedance parameters of a particular RF structure then a VNA would be the measurement of choice. So as was the case before there are advantages of both the time domain and frequency domain measurement methods.

There is a wealth of literature on the use of TDR in electronic packaging, printed circuit boards, IC's, etc. This literature review will touch on only a key subset of those articles to again give examples of the types of inverse scattering problems that are faced with these measurements and the types of solutions that have been developed to address those needs.

Jong, Tripathi and Janko [61] modeled various interconnects typically found in connectors or other attachments to circuit boards or lead-frame interconnects to IC packages in both the time domain and frequency domain. In this work these connectors, lead-frames or interconnects were broken down into multiple sections and modeled as cascaded transmission lines using T-Parameters. The effects of impedance discontinuities and delays of each sub-segment in the connectors were separated out into two separate T-matrices for each sub-segment. This led to a T-Matrix covering the transfer of signal across an impedance discontinuity as well as a separate "Delay Matrix" or T-Matrix covering the delays. As was covered earlier in this review the T-Parameters are especially useful for modeling cascaded transmission lines as the matrices can simply be multiplied together to form the overall T-Matrix of a network (or in this case a connector or packaging interconnect). They are also especially useful in de-embedding or de-convolving per algorithms such as the Layer Peeling algorithm covered earlier [20] or other de-embedding procedures [11] as individual segments can be de-embedded by multiplying the overall T-Matrix of the network by the inverse of the T-Matrix for the first segment or section to remove its contribution. In this work [61] the inverse matrices for both the delay T-matrix and impedance boundary T-Matrix for the section to be de-embedded would be multiplied by the overall T-Matrix of the network looking into the point of where the de-embedding is occurring (depending on far the layer peeling steps have proceeded into the network) to de-embed or peel off that particular segment. The researchers modeled a typical interconnect by a series of right angle bends and modeled the overall interconnect as a distributed model of cascaded transmission line segments as noted with impedance discontinuities at the bends and delay elements in between the bends. They also generated a hybrid model which contained some lumped elements (shunt capacitors and series inductors) mixed amongst the distributed cascaded sections. The hybrid model can be advantageous if computer calculation speed is critical. In this work they also simulated and evaluated a "Tee Junction" that is common in VLSI clocks within IC's. In this latter model there are both cascaded sections as well as a split in the paths due to the TEE and the two subsequent paths are modeled as stubs with a discontinuity at the entrance (due to the right

angle change). In all of these cases actual TDR measurements were made and compared to the simulations with good agreement.

Schuster et al. [62] also studied and modeled circuit paths and interconnects as cascaded sections of transmission lines and compared two inversion algorithms: Numerical FDTD as well as the Layer Peeling Method [20]. They also presented a method of combining these two methods to offer a simple and efficient method of analyzing linear and lossless 1-port or 2-port networks. The analyzed networks or circuits included a microstrip feeding transmission line on a printed circuit board assembly (PCBA) with FR4 dielectric connecting to a bonding wire connection to a semiconductor device (IGBT – Insulated Gate Bipolar Transistor). In the FDTD method a voltage stimulus is simulated and propagated down the path and simulations of reflected and transmitted waveforms are made at each subsequent boundary. They are obtained by performing 2-D calculations of the electric field at each incremental FDTD step using Laplace's equation ((2-8) and subsequently (2-10) in two dimensions). The simulated voltages of the propagating pulses are obtained by integrated the fields along the path as the wave is propagated. At the boundary of the bond wire it is partially transmitted and reflected and all of that is simulated and the impedance can be calculated at each FDTD step/location. Once the FDTD time domain simulation is completed (the waveform has been fully propagated down through the bond wire and all reflections returned to the source) then the Layer Peeling method can be utilized to obtain an impedance profile vs. time and subsequently vs. position along the signal path (as again the causal, linear and lossless network assumptions apply which allow for the application of the Layer Peeling method as covered earlier in this review [20]). The original FDTD time domain simulation can also be used directly to ascertain information about signal integrity such as propagation delay, signal distortion and reflection (or ringing). The procedure presented in this work was conducted entirely in the time domain and therefore did not rely on FFT calculations.

A study involving the de-embedding of packaging interconnects involving ABCD or Transmission (T-Matrix) parameters and conversions to S-Parameters involved the work in [132]. Another study [133] investigated the use of Cascaded S-Parameters to the measurement and simulation of multilayer PCB's. The applications of T-Parameters as well as S-Parameters are essential components of the algorithms presented in this dissertation and are covered in Appendix B.

Pannala et al. [63] performed network analysis in the time domain (TDNA) to extract the S-Parameters of both TDR (reflection) and TDT (transmission) systems utilizing models of transient signals represented by rational functions as follows (shown for both the time and frequency domain representations):

Time Domain: $$y_n = \sum_{k=1}^{M} a_k e^{s_k n \delta t} \tag{2-16}$$

Frequency Domain: $$Y(\omega) = \sum_{k=1}^{M} \frac{a_k}{j\omega - s_k} \tag{2-17}$$

Where the complex poles $s_k$ are obtained from the measured TDR and/or TDT signals using a procedure entitled the "Generalized Pencil of Function" method (GPOF) and the residues or coefficients $a_k$ are computed using a recursive de-convolution procedure (in their case solving the inverse matrix equations by the method of least squares). So there are three steps as follows:

1.) Obtain the TDR/TDT measurements w/Time Windowing or Time Referencing
2.) Obtain the Complex Poles of the Modeled Transients Function via the GPOF method
3.) Obtain the Residues of the Modeled Transients Function via Recursive De-Convolution

With these three steps the system under test can be characterized. The GPOF method utilizes a technique whereby the generalized eigenvalues of a matrix pencil (defined as a $j^{th}$ order polynomial of "j" matrices ($A_j$) with scale functions or coefficients $\lambda_j$ given as follows):

$$L(\lambda) = \sum_{i=1}^{j} A_i \lambda_i \tag{2-18}$$

The roots or eigenvalues of this polynomial of matrix equations (matrix pencil) used to represent the modeled transients function are then used to determine the complex poles of the system. They applied these techniques to the inverse problems of extracting parameters associated with various PCBA traces as well as an array of vias in a thin film hybrid circuit structure. The results were used to generate S-Parameters in the time domain which were in turn converted to the

frequency domain via FFT's and compared to actual VNA measurements of the S-Parameters directly in the frequency domain. Good agreement was found between both for all the simulated cases (errors < 3%).

Ong et al. (2003) [64] presented a simplified de-embedding calibration technique using only a symmetric "thru" calibration standard or connection. This is an approximate technique that was compared to the classical calibration techniques of Short/Open/Load/Thru (SOLT) and Thru/Reflect/Line (TRL) calibrations discussed earlier and described in [13] and several of the other references. In their method they also applied the Layer Peeling de-convolution algorithms discussed earlier [20] to construct a model of half or the thru connection (based on symmetry) utilizing cascaded transmission line sections and measured TDR signals on the thru connection. They then performed mathematical conversions to "synthesize" models for the short, open and matched load that would be needed if a full SOLT cal was performed. Therefore using measured signals and developed models with just a thru measurement they were able to emulate a full SOLT cal. They demonstrated that the method performed comparably with the TRL calibration method up to 7 GHz. They suggested that this method would be a good calibration alternative to PCBA's with SMA connectors where other reasonable calibration standards or reference structures are not available.

Antonini et al. (2005) [65] reviewed methods to extract equivalent circuit models of various PCBA structures. By extracting and modeling complex geometrical PCBA structures, features and signal paths with equivalent circuit elements (such as lumped resistors (R's), inductors (L's) and capacitors (C's)) via inverse solving algorithms the resulting models an be used to predict and model signal integrity performance with reduced computer computational requirements. The extracted models can even be compatible with classical simulation tools such as Spice including the development of H-Spice models that are often used today in performing simulations of structures within IC's during IC and ASIC (Application Specific IC) design. They then validated this procedure by comparing to actual results in both the frequency domain (via VNA measurements) and the time domain (via TDR measurements). The structure under test that was used was for this study was a set of plated through holes (PTH) vias along with feeding circuit traces. To obtain the circuit element models they first obtained the S-Parameters for the networks and then converted them to Y-Parameters or admittance parameters as described in several of the references (e.g. [12], [13]). They then used a vector fitting procedure to develop

rational functions for each of the admittance parameters in analogous fashion to how the s-parameters and transients functions were fitted with rational function expressions in the previous covered reference above [64]. However, in this case it was the Y-Parameter coefficients that were fitted with rational functions with both residue and pole information in the frequency domain. Once these rational functions were acquired for the various coefficients they can be modeled with equivalent passive lumped circuit elements (various networks of R's, L's, and/or C's). An assumption for this procedure was therefore that these networks were passive networks and not active networks (which is a valid assumption if simulating PCBA traces, vias and other passive structures). They then validated this method with a specific test board containing a variety of different feeding microstrip transmission line traces that would start on one layer or the board (typically the top layer) and then go through a PTH or via and finish on another layer (typically the bottom). They compared their simulations and extracted models with actual VNA (frequency domain) and TDR (time domain) measurements and found that good agreement could be obtained if sufficient sample points were used as well as time windowing or gating was employed (to remove unwanted reflections beyond the area of interest). In the time domain they also used another popular technique common to modern microwave and optical digital transmission instrumentation characterization entitled "eye diagrams". For this latter case a pseudo-random bit sequence (PRBS) is sent (pulse stream or sequence of pseudo random 1's and 0's) is generated (often with a Bit Error Rate Tester (BERT) such as [66]) and the transmitted time domain signal is measured with a high speed oscilloscope with high persistence (included within the BERT) that can create a picture of how the time synchronization of the edges of these pulses are performing. If there is much jitter than the "eye" will close on the diagram (see reference [65] and [66]). Again, the ultimate goal of these researchers [65] was to show that lumped element models could be used to accurately model these PCBA structures which reduces computational requirements for subsequent signal integrity simulations and creates compatibility with popular simulation tools (SPICE).

Aksen et al. in an earlier study [67] presented a procedure that allowed for modeling lossless two-ports with mixed lumped and distributed elements in cascaded fashion. They also utilized various techniques to model the parameters of a system with various polynomials which in turn can be converted to lumped element models (similar to the above approach in [65]). However, in this earlier study they used the transfer or transmission matrix (T-Parameters) as well as S-Parameters (with conversions back and forth per equations (B-17) to (B-19) of

Appendix B and the final models were actually composed of both distributed models (T-matrices) and lumped elements between them such as shunt capacitors and series inductors. An application of their technique was for analyzing matching and equalizing networks (including broadband equalizers). They used a simulated ladder or low pass structure in their models.

Sun et al. (2006) [68] presented a technique of modeling various circuit interconnects found typically on chip with RF mixed signal ASIC's and other IC's with wideband lumped element models. The models also accounted for loss mechanisms in the various substrate materials (silicon and various dopents) as well in the metal structures of the transmission lines that can lead to frequency dependence in the parameters of the models. The techniques were applied up to 40 GHz via scaling from lumped models generated at 10 GHz. Additional lumped elements were added to the network models (extra R's, L's and C's) to account for the frequency dependence. S-Parameters of the networks were initially generated via a full-wave electromagnetic simulator using FDTD methodologies and solving for the field quantities. Then the equivalent lumped element models were extracted from those S-Parameters with some lumped elements modeling the behavior at higher frequencies and others to account for the lower frequency (lower microwave) portion of the structure. Various filter models were then constructed to model that frequency dependence. They compared the simulated results with actual S-Parameter measurements on test circuits to emulate the interconnects and found good agreement up to 40 GHz (< 3% errors). The values of these lumped element equivalents is again to allow for utilization in circuit simulation packages such as SPICE or ADS (Agilent) in RF mixed mode ASIC or other IC designs.

Kim et al. (2005) [69] presented a new method to simulate and characterize the frequency dependent characteristic impedance ((A-22) and propagation constant (equations (A-9) and (A-23) of Appendix A) of circuit based transmission lines via single port TDR measurements and the creation of non-physical RLGC models for the transmission lines. The classical physically based parameters of Series Resistance R, Series Inductance L, Shunt Conductance G and Shunt Capacitance C (all per unit length) for a transmission line model are shown in equations (A-20) and (A-21) of Appendix A in terms of their influences on the propagation constant and characteristic impedance respectively of a transmission line. These parameters in the classical literature have all been physically based in that they were functions of the geometry of the physical structure of the transmission line. However in this work [69] non-physical RLGC models

are derived based on the measurements of a single port TDR signal and subsequent inverse algorithms. Coplanar waveguide transmission line structures were utilized. In addition, time windowing was performed on the TDR trace to separate the first reflection $\Gamma_1$ from the second reflection (possible only if the propagation time of the transmission line is long compared to the rise and fall times of the pulse). This allowed for separate measurements of the frequency dependent characteristic impedance ((A-21 and A-22) and the frequency dependent propagation constant (equations A-20 and A-23) of Appendix A). This can be shown from (2-19) and (2-20) that are simplifications of (B-16) of Appendix B and readily seen from the signal flow graph in figure B.4 of Appendix B considering only the first and second reflection terms for a 2 section network.

First Reflection (Time or Frequency Domain):

$$\text{S11\_Input}(1^{st}\ \text{Ref}) \quad = \quad \Gamma_1 = \frac{Z_2 - Z_1}{Z_2 + Z_1} \tag{2-19}$$

Second Reflection (Frequency Domain):

$$\text{S11\_Input}(2^{nd}\ \text{Ref}) \quad = \quad \left(1-\Gamma_1^2\right)\Gamma_L e^{-2\gamma_2 L_2} = \left(1-\Gamma_1^2\right)\Gamma_L e^{-2(\alpha_2+j\beta_2)L_2} \tag{2-20}$$

Assuming the driving cable in section 1 (figures B.2 and B.4 of Appendix B) is 50 Ω and any other imperfections associated with it are de-embedded via one-port SOL calibrations then the characteristic impedance of the transmission line under test in section 2 ($Z_2$) can be readily calculated from the first reflection using (2-19) and when utilized in the frequency domain (via an FFT) the frequency dependence of the characteristic impedance can be determined and modeled. They further observed that the phase shift to the characteristic impedance (found readily from the phase shift of the intrinsic impedance η portion of the expression or (A-19) was typically very small for these transmission lines (< 0.6º) due to relatively small loss tangents (< 0.05) ((A-10) and therefore the impedance can still be modeled as being approximately real (although the real part still having frequency dependence). The physical interpretation for this being that for an approximate TEM wave structure in the dielectric that the electric field and magnetic fields are transverse (orthogonal) to each other and hence the same is true for the current density and electric field and so minimal energy should be dissipated in the conductors. In addition any series loss components due to the series R component will not show up until the second reflection term

(propagation term) as propagation down the line is required to induce any losses from the induced currents in the metallic conductors. Therefore the only losses showing up in the first reflection are the dielectric losses which although finite were found to be reasonably small to allow for the real approximation for the characteristic impedance. This therefore allowed for determining the frequency dependent characteristic impedance (dominated by the dielectric parameters) via an FFT of the first reflection (after time windowing) and utilization of (2-19) and solving for $Z_2$. The extraction of the non-physical models for the shunt G and C components.

Then the propagation constant was solved for from time windowing of the second reflection and conducting of an FFT to obtain (2-20) and via knowledge of $\Gamma_1$ from (2-19) and the first reflection measurement from step 1. The problem that remained is that there were two remaining unknowns in (2-20) ($\Gamma_L$ and $\gamma_2$) (assuming the length is known) with only one equation to solve for them. The authors addressed this by measuring two identical coplanar waveguide transmission lines with identical load terminations but of different lengths. This allowed for them to develop two simultaneous equations of the form of (2-20) (with only the length terms different and known) and allowed for them to extract the frequency dependent propagation constant from two successive TDR measurements of different length lines with the time windowing on the second reflection for each. Finally, with frequency domain plots of both the frequency dependent characteristic impedance (first reflection) and frequency dependent propagation constant (second reflection) expressions were used to derive the non-physical models for R, L, G and C. This was done by deriving a series shunt per unit length model based on the propagation constant and characteristic impedance functions and subsequent derived voltage and current terms along an incremental section of the transmission line. The equivalent series impedance and shunt admittance per unit length terms were given as follows:

Series Impedance per Unit Length: $$X = Z_2\gamma_2 = R + j\omega L \tag{2-21}$$

Shunt Admittance per Unit Length: $$Y = \frac{\gamma_2}{Z_2} = G + j\omega C \tag{2-22}$$

It is actually readily seen that these equations can be obtained via algebraic manipulation of equations (A-20) and (A-21). Those equations also allow for the modeling of the frequency

dependence of both the propagation constant and characteristic impedance. Upon obtaining (2-21) and (2-22) the individual R, L, G and C terms are determined as follows:

$$R = \text{Real}(X) \qquad L = \text{Imag}(X) / \omega$$
$$G = \text{Real}(Y) \qquad C = \text{Imag}(Y) / \omega$$

Again, these are non-physical models derived directly from time windowed TDR measurements and subsequent FFT's. This procedure can be applied to microstrip, stripline and coupled transmission lines. This allows for the determination of all four key elements (R, L, G and C) with a single port TDR measurement. Therefore an accompanying TDT measurement is not needed. One advantage of time domain TDR measurements over frequency domain VNA measurements pointed out in this paper (and well known in the industry) is that TDR measures both the transient response and the steady state response of a network whereas a VNA measures only the steady state response at one frequency at a time (via swept measurements). This allows for TDR to characterize the broadband frequency performance and response of a system with a much faster measurement time as compared with VNA where sweeps over the lower frequency portions of the spectrum require long times (and contribute to most of the measurement time limitations of the frequency domain VNA approach).

Kao et al. (2006) [70] modeled high speed but also high density interconnects and presented an inverse algorithm / procedure to extract the impedance profiles of interconnects via TDR. Coupling or crosstalk between lines was also simulated (and which can be modeled by multi-port and mixed-mode S-Parameters). They also used multi-segment cascaded transmission line models for each interconnect path. They utilized Digital Visual Interface (DVI) and Peripheral Component Interconnection (PCI) Express type interconnections for their simulations and evaluations. DVI interfaces are typically used between a notebook PC and an LCD display with bandwidths up to 2.2 GHz. The PCI Express connector has an effective bandwidth up to 6.25 GHz. The parameter extraction was done utilizing even and odd mode analysis where the even and odd mode impedances are defined as follows for two coupled lines:

Even Mode Impedance:

This is the characteristic impedance of one particular line of a coupled pair when both lines are excited by a common mode signal (i.e. same amplitude and same polarity of signal applied to both coupled lines relative to a common ground). By definition and convention it is equal to 2 times the common mode impedance with expressions given by (2-23). The even mode impedance will always be equal to or greater than the single ended (uncoupled) impedance (equal only for the uncoupled case).

Odd Mode Impedance:

This is the characteristic impedance of one particular line of a coupled pair when both lines are excited in a differential manner (signal of one line equal in amplitude but opposite in polarity to the other line). By definition and convention it is equal to ½ of the differential mode impedance with the expressions given in (2-23). The odd mode impedance will always be equal to or less than the uncoupled single ended impedance. They are equal for the uncoupled case (lines far apart).

If both of the transmission lines were far apart and no coupling occurred then their "single ended" characteristic impedance values would be derived as per earlier formulations in this review. However, when coupling occurs it impacts the effective impedance. If it was assumed that two identical geometry transmission lines (with uncoupled characteristic impedance = Zo) are adjacent and coupled (such as a USB connection with parallel stripline transmission lines) then the even and odd mode impedances would be given as follows:

Common Mode Coupling: $$Z_e = 2Z_{cm} = \frac{V_1 + V_2}{I_1 - I_2} = \frac{2V_{cm}}{I_{cm}} \qquad (2\text{-}23)$$

Differential Mode Coupling: $$Z_o = \frac{Z_{dm}}{2} = \frac{V_1 - V_2}{I_1 - I_2} = \frac{V_{dm}}{2I_{dm}} \qquad (2\text{-}24)$$

Where

$Z_e$ = Even Mode Impedance $Z_o$ = Odd Mode Impedance

$Z_{cm}$ = Common Mode Impedance $Z_{dm}$ = Differential Mode Impedance

And $V_1$, $V_2$, $I_1$ and $I_2$ are the voltages and currents into ports 1 and 2 respectively.
Again by definition and convention (and independent of geometry) the single ended characteristic impedance for a line is equal to the following:

$$Z_{SI\_uncoupled} = \sqrt{Z_o Z_e} \tag{2-25}$$

Where $$Z_o \leq Z_{SI\_uncoupled} \leq Z_e \tag{2-26}$$

Again all of these impedances in (2-25) and (2-26) would only be equal for the uncoupled case. The physical interpretation of (2-26) would be that for the common mode case the common signal from an adjacent line adds a mutual inductive coupling element to the series inductance which increases the impedance relative to the single ended case. Therefore the even mode impedance will be greater than or equal to the uncoupled impedance. In contrast for the differential mode case there is an extra shunt capacitive coupling term (as the voltages are different between ports 1 and 2) and the mutual series inductive term is actually subtracted from the series inductance due to the opposite sign of the currents between the two ports. Therefore the odd mode impedance will be less than or equal to the uncoupled impedance.

The measurement of these parameters can be accomplished with a multi-port network analyzer with mixed mode S-Parameter measurement mode capability. Such a network analyzer is shown in the reference [72]. The definitions for the Mixed Mode S-Parameters are derived and presented by Bockelman et al. [71] for a four port network which can be used to model two coupled transmission lines per the above conventions. This results in a 4x4 S-Parameter matrix giving S-Parameters to cover common mode, differential mode as well as cross terms (conversions from common mode to differential mode and vice versa) scattering coefficients/parameters. This is diagramed by the following with the full derivations given in [71]:

$$\begin{bmatrix} b_{dm1} \\ b_{dm2} \\ b_{cm1} \\ b_{cm2} \end{bmatrix} = \begin{bmatrix} s_{11} & s_{12} & s_{13} & s_{14} \\ s_{21} & s_{22} & s_{23} & s_{24} \\ s_{31} & s_{32} & s_{33} & s_{34} \\ s_{41} & s_{42} & s_{43} & s_{44} \end{bmatrix} \begin{bmatrix} a_{dm1} \\ a_{dm2} \\ a_{cm1} \\ a_{cm2} \end{bmatrix} = \begin{bmatrix} S_{dd} & S_{dc} \\ S_{cd} & S_{cc} \end{bmatrix} \begin{bmatrix} a_{dm1} \\ a_{dm2} \\ a_{cm1} \\ a_{cm2} \end{bmatrix} \quad (2\text{-}27)$$

The “b” terms are the scattered response signals to the stimulus “a” terms consistent with earlier definitions. These terms are again normalized to impedance per the earlier conventions of S-Parameters (equations (B-2) to (B-5)) of Appendix B. The above is a specific case for the general case of (B-1) of Appendix B where here there are four ports and they are used for assessing the response of coupled lines to both common mode and differential mode stimuli. Common mode, differential mode and cross conversion terms (common mode to differential mode conversion and differential mode to common mode conversion) are covered by the above. The upper left quadrant of the S-Matrix covers the differential mode response to differential mode stimuli s-parameters. The lower right quadrant covers the common mode response to common mode stimuli s-parameters. The other two quadrants cover the cross conversion between modes S-Parameters as diagrammed in (2-27).

Therefore, Kao et al. [70] used TDR to obtain information about both the odd mode and even mode impedances and developed and presented models for the mutual coupling series inductance and shunt capacitance terms based on these models. To accomplish this both the even mode and odd mode impedance profiles must be extracted via TDR and inverse solving algorithms. This can be accomplished using a differential TDR measurement system with two ports. The procedure for obtaining the even mode and odd mode impedance profiles is covered in [73] which is an application note by Agilent Technologies for making these types of measurements with their high speed scopes and dual-port TDR modules. Upon obtaining the even mode and odd mode impedance profiles the authors [70] modeled each coupled path as a series of cascaded elements and performed their own proprietary de-convolution procedure (LUMP.CIR Matlab program) for each coupled path and reconstructed the impedance profiles. This allowed for developing distributed models for each of the coupling elements (mutual inductances and mutual capacitances) to model each section in the cascaded transmission lines that made up both coupled lines. They called this modeling approach the “segmented-distributed-coupled” model as it combined multiple inverse solving problems (cascaded sections / multiple reflections, coupled lines with mutual inductances and capacitances and resulting crosstalk to model high speed and

high density connectors). Their simulation results compared favorably with actual measurements using the Agilent differential TDR system for both the DVI and PCI Express connector systems. However, their simulations for this problem assumed a lossless system (acceptable for these particular simulation and inverse problems).

Pro et al. (2006) [74] utilized both the 4-Port Vector Network Analyzer (frequency domain) from Agilent Technologies and dual port TDR / High Speed Scope (time domain) from Tektronix to characterize high speed interconnects in disk drive circuits. They utilized the mixed mode S-Parameter representations as described in the previous sections to model these interconnects and to assess crosstalk/coupling, loss/bandwidth and other signal integrity issues. The utilized mixed-mode scattering parameters in both the frequency and time domains (utilizing IFFT's to convert from the frequency domain to the time domain) to compare to the mixed mode VNA and TDR measurements. They developed test coupons of PCBA traces of several different widths to emulate different levels of characteristic impedances. They assessed the tradeoffs between impedance and transmission bandwidths. They also looked at limitations caused by different amounts of windowing (apertures in the metallization back planes) and found more coupling and lower bandwidth depending on how much windowing was in place. They proposed a copper backplane or overlay which in their evaluations showed superior performance.

Guo et al. (2006) [75] evaluated both single ended and differential delay lines routed in both serpentine and flat spiral fashion for crosstalk (between switchbacks or loops in the patterns) and other signal integrity degradations. They utilized TDR and TDT measurements and generated eye diagrams as well [66]. Crosstalk between sections in the delay line patterns leads to noise and edge jitter and subsequently a "closing" of the eye diagrams. With the serpentine patterns there can be crosstalk on the near end that eventually couples from input to output and leads to a ladder type noise waveform that will appear at the output before the desired signal. They found that a flat spiral pattern mitigates for this. They also found that the combination of differential signaling together with the utilization of the flat spiral pattern led to greatly reduced crosstalk. They developed models for the mutual coupling capacitive and inductive terms for adjacent lines (both within the same pattern at different locations as well as between differential pairs) to create matrices of coupling terms for four effective lines.

**Other Modeling Techniques for Electrical Engineering Inverse Scattering Problems:**

Sadiku et al. [76] provided derivations for the S-Parameters for the case of three and four section networks of a cascaded network and presented those formulas. They utilized techniques discussed earlier including utilizing signal flow graphs and models [3], [4] as well as utilizing Transmission T-Parameters and associated conversions to S-Parameters ((B-17) – (B-19) in Appendix B) to initially determine the T-Parameters of the overall network or cascaded sections and then convert back to S-Parameters to obtain the final results. These models are directly applicable to transmission line applications such as TDR but could be extended to a number of applications inside and outside of electrical engineering.

Rahman et al. [77] modeled asymmetric multilayer coplanar waveguide (CPW) transmission lines with various numbers of step discontinuities (e.g. step changes in the width of the center conductor leading to step changes in impedance). These types of CPW lines are common in Monolithic Microwave Integrated Circuits (MMIC's). They calculated and modeled the S-Parameters initially of a single step discontinuity and then generalized the approach to a cascaded transmission line model where multiple discontinuities could occur along the line. They utilized complex mode-matching techniques to model the excitation of 3 different wave propagation modes (CPW, slot line and parallel plate modes) that could occur due to discontinuities in the CPW center conductor, slots between the conductors and finally the outer ground connections). They found good agreement between their results for asymmetric CPW step discontinuities with other results published in the literature for symmetric CPW step discontinuities.

Simpson [78] in an earlier study provided a generalized methodology for modeling n-Port networks (e.g. (B-1) but with cascade connections between them (i.e. multiple n-port networks in cascade). The techniques covered above in this review to this point described cases where within a single network of multiple ports where there could be cascaded paths between the various ports within that network (e.g. S-Parameters of standard multi-segment cascaded sections between two particular ports – (B-1 together with (B-28) or even coupling between paths to different ports (mixed mode S-Parameters and cascaded connections between multiple ports within a single multi-port network (2-27). However, in this earlier work [78] a generalized methodology for

solving for the overall S-Parameters of multiple n-port networks with various cascade connections between them was developed. Methodologies to reduce the multiple cascaded n-port networks to a single multiple-port network with associated overall S-Parameters were provided. These techniques would have applications to a wide variety of scattering problems both within and outside of electrical engineering.

Cho et al (2005) [79] presented a general 3-Port S-Parameter de-embedding technique to remove the effects of on-wafer probing structures for characterizing three terminal devices such as MOSFET transistors in RF and Microwave IC's / wafers. The test structures employ shielded wafer probes modeled themselves as transmission lines. Therefore the inverse problem involves three ports each of which contain a cascaded network of initially one of the wafer probe paths and associated metallic interconnects and finally the particular connection to the intrinsic device (i.e. source, drain or gate of a MOSFET). 3-Port S-Parameters and associated conversions to 3 Port T-Parameters were utilized to model the three ports (each of which had the cascaded sections leading to the particular connection on the MOSFET). They provided calibration methodologies to de-embed the wafer probe and interconnects for each port using T-Parameter methodologies similar to those described in [11] for standard two ports but in this case for 3-Ports. In addition, "Short" and "Load" calibration standards are impractical for wafer probe calibrations and so various "dummy thru" standards along with "open" connections and finally the device under test overall S-Parameter measurements were used together with T-Matrix procedures similar to [11] and an approach similar (but not exactly the same) as the TRL methods [13]. Since there is shielding on each wafer tip connection the 3 ports can be modeled as isolated and so standard S-Parameters can be employed (i.e. no cross coupling and therefore no mixed mode S-Parameter modeling needs). They found good performance with their 3-Port de-embedding methodologies compared with classical two-port de-embedding methods.

There have been a number of more recent studies associated with solving generalized inverse scattering problems in lossy media for electrical engineering as well as non electrical engineering electromagnetic applications. Frolik and Yagle [80] developed general models for forward and inverse scattering problems in discrete (layered) and lossy media. Their work was motivated by geophysical measurement needs such as radio-glaciology (radar propagation through glaciers) and radar reflections from other stratified dielectrics. In addition, their work was also motivated by the need within electrical engineering for modeling techniques for interchip

communication with lossy transmission lines as well as the design of optical waveguide gratings. They modeled the systems as discrete time systems ((B-34) from Appendix B) as opposed to continuous systems ((B-33) from Appendix B) and made use of discrete Fourier transform as well as Z-transform techniques as well as discrete matrix Green's function (the latter for modeling lossy media). They developed a forward (transmission) scattering model via the development of forward propagation matrices for each discrete segment or layer (similar to transmission matrices or T-Parameters [11] and (B-17) but utilizing z-transforms instead of FFT's for the frequency domain representation of the signals and parameters in the matrix due to the discrete time representation in the time domain. The overall product of each propagation (or segment transmission matrix) makes up what they term the transition matrix (again all in the z-domain). For each segment there is further division into a transfer matrix (at the impedance boundary of each segment) and a time-delay matrix (for transmission through each segment – accounting for phase delay and attenuation effects). These two matrices are multiplied together to form the layer propagation matrix for each segment. They also described the system in terms of a scattering matrix (S-parameters) again in the z-domain but favored the propagation or transmission matrix as the total transition matrix can be developed as a simple product of the individual propagation matrices of each segment and then the overall result can be converted back the scattering matrix at the end of the process (using the conversions of equations (B-18) and (B-19) of Appendix B). The transition matrix also acts as the z-transform of the discrete matrix Green's function for the medium. They also develop a recursive expression for relating the n+1 transmission parameters as a function of the nth transmission parameters to allow for identifying and de-convolving each layer (somewhat analogous to the layer peeling and layer adjoining methods [20] but in this case for lossy media). They also developed the layer propagation matrices in the discrete Fourier domain accounting for phase and attenuation components within a segment and impedance discontinuities at the boundaries (again in the form of transmission matrices). Finally they develop an inverse algorithm utilizing a set of discretized integral equations (matrix of summation equations) called an asymmetric Toeplitz system of equations. The problem is applied to a standard RLCG model for a transmission line through layered media. An assumption was made that dispersion was negligible but loss/attenuation was not which further reduced the set of inverse variables (defines RC = LG for each transmission line segment cutting in half the number of inverse variables). A numerical algorithm was developed to solve the set of simultaneous discretized integral equations (matrix of summation equations) using recursive solving algorithms (Levinson and Schur). The Toeplitz/Levinson approach (integral equations) is analogous the layer

adjoining method [20] but in this case for lossy media and the Schur method (which utilizes difference equations) is analogous to the layer peeling method [20] but again in this case for lossy media.

Numerous other studies have investigated inverse scattering problems in electrical engineering applications. Wu et al. [81] presented a novel approach entitled Space –Spectral Domain Approach (SSDA) to calculate S-Parameters and field/current distributions for three dimensional discontinuity problems in MMIC applications. The SSDA approach combined two earlier modeling and inverse solving approaches (The spectral domain approach (SDA) and method of lines (MOL) approach) and attempted to utilize the strengths of each while eliminated the weaknesses of each. The MOL approach models the circuit path in the 1-D direction parallel with the target wave propagation direction and the SDA approach modeled the plane that is transverse or orthogonal to the wave propagation direction (successive 1-D orthogonal transects). Therefore, combining both approaches allowed for a 3-D modeling approach. They were able to model various discontinuities along microstrip transmission lines such as progressive tapers or other discontinuities and structures commonly found in MMIC's with this approach. Their approach was validated via good agreement with other approaches in the literature.

Cwik et al. [82] developed models to represent the cascaded connection of planar periodic surfaces separated by homogeneous but lossy layers of dielectrics. These periodic screens are often used in wave propagation systems as filters. They can be free standing patches or alternatively periodic apertures in metallic structures or other arrays sandwiched between dielectric layers. They developed the general set of scattering parameters and also utilized what are termed "Floquet Harmonics". These latter "Floquet" models are utilized as the scattered fields can be modeled by or expanded into "Floquet modes" which are discrete spatial harmonics or spatially periodic propagating waves of both directions (reflected and transmitted waves about that surface). They incorporated these Floquet models into the composite S-Parameters developed for the entire cascaded network utilizing cascaded section S-Parameter construction techniques similar to (B-28) and others cited in the literature [3], [4] and [5]. They also utilized "building blocks" in that they developed S-parameter and Floquet models for arrays of a smaller number of sections and then utilized those to scale up to or develop expressions for larger cascaded periodic structures built up with those individual building blocks. They found this approach to be efficient as it allowed for analyzing individual sections to simplify the analysis as

opposed to simulating the entire structure. However, they indicated that accurate identification of the S-parameters for the individual sections are required for this approach to truly be advantageous.

Wang, Xia and Zhou (2005) [83] presented a solving engine involving a single integral equation (SIE) for a 3D arbitrarily shaped combined conducting and dielectric body illuminated by a propagating plane wave. They showed that this technique (which solves for the effective electric current on the surface) results in computational efficiency relative to the coupled integral equation method (standard within the classical Method of Moments method) that solves for both the electric field and magnetic field induced currents on the surface. The SIE method results in fewer unknowns to solve on the integrating solving surface. They further utilized the Fast Multipole Method (FMM) to reduce computing complexity and memory requirements for numerical solutions. Scattering waves from this surface (propagating waves in the air region away from the surface) can then be readily derived from these solutions for the effective surface current distributions on the combined dielectric / conductive body.

## Non-Invasive Geophysical Electromagnetic Methods:

We will now revisit a class of inverse scattering problems discussed earlier (Geophysical methods including Soil Water content measurements). In this section the focus will be on non-invasive geophysical electromagnetic methods. As indicated during the section on TDR soil water content measurements the TDR probes are typically quite invasive to the soil and so there is desire to develop non-invasive methods to assess the properties of soil and other geophysical media. One set of non-invasive methods touched on earlier was in the area of Nuclear Magnetic Resonance (NMR) [44], [45] and [46]. Those technologies were demonstrated to be viable for identifying water at modest depths but come at fairly high cost and have not made it into the widespread commercial arena (although probably deserving of more research). Two very popular non-invasive technologies that have gained wider use in the last two decades are Ground Penetrating Radar (GPR) and Microwave Remote Sensing. Both operate on somewhat similar principles in that electromagnetic waves of particular frequencies are transmitted down into the soil and the waves reflect at various interfaces and the return scattered waves are utilized via inverse scattering algorithms to ascertain different properties concerning the soil. The frequency

of operation also dictates the depth to which the soil properties or boundaries can be identified. Higher frequencies give finer spatial resolution information but at the expense of penetrating to shallower depths. Microwave remote sensing often falls into this category and the measurements typically are scans of the surface or near surface moisture content of the soils and in other cases are utilized to ascertain information about surface vegetation (sometimes using even higher frequencies – e.g. infrared to correlate thermal activity to vigor in plants). But in the context of soil moisture contents the frequencies of use range from higher RF (several hundred MHz) to low microwave (10's of GHz). For the case of GPR lower frequencies are often employed (e.g perhaps 25 MHz up to 1.5 GHz) to allow for deeper penetration imaging of the soil such as identifying aquifers at deeper depths. We will touch on these two distinct technologies briefly in this section of this review. In GPR both transmission measurements and reflection measurement approaches are used (different transmit and receive antenna at different locations for the former and one common transmit/receive antenna for the latter). For the case of microwave remote sensing reflection measurements are the only mode with the transmit and receive antennas located in an aircraft or even a satellite. GPR antennas can be ground mounted or on trailers and sometimes are airborne. GPR measurements typically make use of the measurement of the propagation parameters (equations B-15 and A-9) and (2-2 – the latter for lossless cases) but for these technologies there isn't a transmission line structure but instead unbounded waves propagating into the soils although with a directional pattern focused on the soil (therefore the RLGC models for transmission lines are not applicable to GPR). Microwave remote sensing technologies use the reflection information at the soil surface and so are dominated more by the impedance at that surface (A-19) although again there is no transmission line and the waves are again radiating and propagating in unbounded form (although in a directional path or pattern) (therefore the RLGC models of transmission lines are not applicable in these analyses). The unbounded wave equations for propagation (A-9) and for the impedance/reflection (A-19) again show the potential for lossy media due either to complex permittivity and/or electrical conductivity and both can influence the performance of the GPR and Microwave Remote Sensing measurements and must be accounted for.

## Ground Penetrating Radar:

Ground Penetrating RADAR (GPR) involves similar scattering problems involved with TDR (involving reflections at impedance discontinuities/boundaries) but with the important difference of being a non-guided system (no transmission lines). GPR works best in cases where there are layered media or major material constituent changes such as at aquifer boundaries. Therefore, the physics associated with wave propagation in layered media apply here as well. Again, several of the models associated with layered media and reflections at interfaces are covered in the Appendicies (especially Appendix C which involves a detailed review of the literature for dielectric mixing models and layered media models). A few of these will be discussed here in the specific context of the applications to GPR.

There have been a number of recent studies on GPR and a few will be touched on here [84], [85], [86], [87], [129] and [130]. Serbin et al. [84] evaluated GPR towards the upper end of its typical range (1 GHz) to assess near surface water content measurements. Their system employed a horn antenna that served as both the transmit and receive antenna. The employed both surface reflection (SR) and propagation time (PT) measurements (the SR measurement influenced by (A-19) along with (B-11 (reflection coefficient) and the PT measurement influenced by (A-9) along with (2-2 (transit time) – the latter for a lossless condition). A PT measurement is only possible if there is a pre-determined dominant discontinuity such as a layer profile in the soil at a particular known depth that a secondary reflection can be keyed off of to measure the transit or propagation time. They had the ability to move their antenna gradually along the soil surface (i.e. scanning vs. position). They compared their results with TDR. They found that the SR measurements were limited to the top 2 cm of soil and missed information from deeper critical moisture content depths (i.e. throughout the root zone). They also found that the SR measurement were biased by the presence of different crop canopies. Therefore there was much variability in the SR measurements. However, they found good performance with the PT portion of the measurement as reflections from the surface canopy and soil surface could be separated out (or de-embedded or de-convolved) from the reflections at the deeper soil depths to allow for a reasonable PT calculation. They also found strong temperature dependencies and found a diurnal variation pattern correlating night and day cycles and so indicated a temperature correction calibration is needed on all the measured parameters (both SR and PT). They also

indicated that this higher frequency embodiment of GPR could be used to validate measurements from microwave remote sensing and would be much more convenient to use than invasive TDR and very invasive gravimetric analysis that are presently used for validation of microwave remote sensing.

Other recent supporting studies on GPR have also been conducted. Martinez et al [85] characterized and modeled the dielectric constant values of various Geologic materials to aid in the calibration and inverse measurement algorithms for a GPR system. They modeled three different rock types with variable mineralogy, porosity and saturation. They reviewed and evaluated different types of dielectric mixing models and chose the "Time-Propagation" mixing model shown as follows:

Time Propagation (Refractive) Mixing Model: $$\varepsilon_r = \left[\sum \mathrm{V_i} \left(\varepsilon_n\right)^{0.5}\right]^2 \qquad (2\text{-}28)$$

This expression comes from a more classical "Power Law" mixing model (Lichtenecker-Rother equation cited by the authors in [85] and covered later in [97], [99]):

Generalized Power Law Mixing Model: $$\varepsilon_r = \left[\sum \mathrm{V_i} \left(\varepsilon_n\right)^{\alpha}\right]^{1/\alpha} \qquad (2\text{-}29)$$

Therefore in this study [85] the empirical parameter $\alpha$ was set to 0.5. Close inspection of (2-28) (where $\alpha = 0.5$) shows that it is equivalent to the refractive mixing model of (2-13). Therefore the Time-Propagation and Refractive mixing models are equivalent. Since the permittivity can be a function of frequency (2-28) and (2-13) are functions of frequency and therefore need to be modeled or characterized at several frequencies for the media of interest. Also, these dielectric mixing models do not account for the effects of loss and are therefore only valid for lower loss media ($\sigma <$ mS/m) and are also only valid for non-magnetic materials (i.e. $\mu_r$ must equal one). They conducted simulations from 50 MHz to 450 MHz or over a reasonable portion of the typical GPR range. They validated their simulations with actual measurements on sandstone and limestone using two way travel times through the test media. They found good correlations with the actual measurements. The power of this simulation tool is that it lays the ground work for an inverse algorithm to identify the properties of rocks and soils via measured scattered signals from a GPR system (i.e. two way travel time).

Grote et al [86] performed GPR evaluations at two frequencies (450 MHz and 900 MHz) to evaluate upper soil (top 10 cm) soil water content in a vineyard in California. The results were compared to gravimetric analysis, TDR as well as soil texture measurements. They found good agreement with the ultimate gold standard (gravimetric) and also good agreement with TDR. There were slight differences between the 450 MHz and 900 MHz data with slightly higher measured values of moisture content for the lower frequency and slightly different spatial differences. They reasoned that the lower frequency had a larger zone of influence (as expected) leading to the slightly different values. They concluded that more research should be conducted on multiple frequency GPR systems to allow for ascertaining data on the soil properties over different spheres of influence (again lower frequencies allowing for a larger spatial sensitivity and the higher frequencies allowing for finer spatial resolution – although limited to regions near the soil surface for the higher frequencies).

Lambot et al. (2006) [87] evaluated air-launched GPR measurement systems to measure the soil surface content. In this particular work a full wave analysis was employed within a particular time window (as opposed to simply identifying a single echo and calculating a dominant propagation time). They utilized both the surface reflection (SR) and full-wave analysis methods. With the full wave approach the entire waveform can be examined and time windows employed to analyze separately various reflections (e.g. the surface reflection vs. other reflections vs. depth). The performance of the system was evaluated against various levels of conductivity as well as complex multiple layers in the soil. For conductivity it was found that significant errors occurred at 1 – 2 GHz if the conductivity was greater than 0.1 S/m. The sensitivity to conductivity increased as frequency was decreased (a finding that is again consistent with equations (A-9) to (A-19) of Appendix A and when examining the loss tangent (A-10) which show that conductivity is more dominant at lower frequencies – although it can impact all frequencies if high enough due to attenuation of the waves and swamping of the signature second reflection wave necessary to calculate propagation times). Similar findings were also noted in the TDR soil water content studies discussed earlier. They did find that the time windowing and de-convolving of the first reflection from the full wave method is much less prone to errors than the surface reflection (SR) measurement approach. The full wave method also allows for removing the effects of the antenna via models of that antenna. The full wave method does not require a-priori knowledge of the height of the antenna above the ground as that portion of the wave (i.e.

the transit time from the antenna to the first reflection and back) can be de-convolved from the full measurement via inverse algorithms on the full scattered waveform. In contrast the SR measurement method is very sensitive to antenna height estimation errors as it needs that distance as part of its calibration. In terms of layering impacts of the soil they recommended that the soil be relatively smooth until a depth representing ½ of the wavelength of the GPR frequency. They indicated that with the full wave inversion methodology that there are very good research opportunities for enhancing the inverse algorithms to account for soil layering and conductivity (research areas that are already under way for TDR). Their overall conclusion is that the full wave inversion method be used in the future to replace the surface reflection SR technique.

Other studies have been conducted using technologies similar to GPR to either reconstruct or identify the locations of objects buried in soils or other layered media. Song et al. (2005) [88] presented a fully 3D inverse scattering solving technique compatible with GPR measurements to identify inhomogeneous objects in various layers within a medium. They utilized the contrast source inversion (CSI) technique together with various integral equation formulations utilizing the dyadic Green's functions for layered lossy media to solve for scattered field quantities at a particular buried layer based on the known stimulus field quantities on a plane external or at the surface of the multilayer medium. The CSI method has been used with success in other nonlinear electromagnetic inversion techniques. It involves stimulating the medium with another sequence of sources described by a complex functional and works in conjunction with the dyadic Green's functions and integral equations to solve for the fields at various solution surfaces or planes within the medium. Both the forward and adjoint versions of the Green's function operators are utilized in the integral equations to propagate the solution over the entire medium. The adjoint operators are utilized in the integral equations to back-propagate the wave solution as part of the inverse algorithm (to create an image of the constituents of the medium via scattered signals returning out of the medium). This approach can be used with GPR.

Cui et al. (2005) [89] presented a 3D electromagnetic inverse scattering technique that can be utilized to identify buried objects in a medium such as landmines or unexploded ordinance. They utilized the extended Born approximations that are often utilized in inverse solving or imaging problems when the contrast of the target medium is small relative to its surroundings. In this procedure the inverse scattering problem is handled as a linear inverse problem. If the contrast is higher then higher order solutions or models can be utilized that handle

better the multiple scattering components that could be present. They also employed the use of Green's functions in an integral equation methodology to solve for the magnetic field quantities at various surfaces to progressively create a 3-D image. They account for conductivity σ in their object function but neglect the loss component of permittivity by conducting the simulation at a low enough frequency where conductivity dominates (i.e. per inspection of (A-10). The integral equations can be nonlinear as the electric field is a function of the conductivity object function and the overall integral to solve for the magnetic field includes both the electric field and conductivity operator in the integrand operation. They therefore provided ranges of assumptions and subsequent techniques (e.g. extended Born approximations) where the integral equations can be linearized. The overall goal again is to construct an image of the medium and provide a methodology whereby a scattered signal such as measured from a technology similar to GPR (but at lower frequencies) can be used as part of an inverse scattering algorithm to image the object inside the medium. They tested the procedure with and electromagnetic wave propagation setup with separate transmit and receive antenna located 1m apart and with a buried object under test (2m on each dimension) and buried just over 2m down. They tested at ten very low frequencies from 0.25 MHz to 4.75 MHz (much lower than the typical range of most GPR systems). They found that the contrast was very high for the buried medium and so the extended Born approximations broke down and they instead found better accuracy with the high order systems and the full nonlinear integral equations.

Karlovsek et al (2012) [129] investigated the challenges of frequency dependent dielectric behavior on GPR performance for steel fiber reinforced concrete. They showed the need for comprehensive characterization of the dielectric properties vs. frequency (1 MHz – 5 GHz) and the need for developing enhanced models. They also utilized PET/CT scans for validating images of the concrete and also utilized transmission line methods for assessing the frequency dependence of the dielectric properties with and without the steel fibers in the concrete. Future research will include High Frequency Structure Simulation (HFSS) methods to conduct full 3D electromagnetic simulations to validate the models. In a separate study, Karlovsek et al (2012) [130] also investigated the use of GPR for identifying the locations of cavities or voids around tunnels as a non-invasive alternative to drilled boreholes. This technique can be used to assess the quality of the grout around tunnels as it cures/settles potentially being utilized real time during the grouting process.

**Microwave Remote Sensing:**

Microwave remote sensing has also seen a number of recent studies. Kuo and Moghaddam (2007) [90] addressed the scattering problems of multilayer rough surfaces with arbitrary inhomogeneous dielectric layers in between the surfaces or boundaries. This was in the context of Radar remote sensing of moisture contents over terrestrial surfaces that contain layers with rough interfaces separated by inhomogeneous dielectric layers of varying moisture contents. They presented a technique to solve for the scattering fields at a particular surface or boundary distinct from the surface of the incident waves utilizing the extended boundary condition method (EBCM) together with developing the overall scattering matrix for the composite layered medium with rough interfaces. Utilization of the EBCM technique is in contrast to utilizing the method of moments (MoM) the latter of which would solve a set of matrix (discretized integral) equations where the basis functions reside on the same surface as the incident fields or scatterer. With EBCM the testing/solving surface can be conveniently chosen such that the scattered fields can be modeled by or expanded into "Floquet modes" which are discrete spatial harmonics or spatially periodic propagating waves of both directions (reflected and transmitted waves about that surface). In other words this assumes that the rough surface can be modeled by an extended boundary that is spatially periodic in nature with a fixed period. Transmission and Reflection coefficients and subsequent matrices can be formed based on the scattering of the propagating Floquet modes at that periodic surface (to model the rough surface). These in turn can be used to generate the scattering matrix at that interface. In addition, the inhomogeneous dielectric layer beneath the rough interface can in turn be modeled as a set of piecewise homogeneous thin sub-layers each of which are also small compared to a wavelength. The overall scattering matrix of that layer composed of the cascaded sub-layers can then be developed via the recursive progression of generating the scattering matrix first for the bottom layer and then progressing upward layer by layer to build the overall scattering matrix for the composite layer (made up of those piecewise homogeneous sub-layers). The scattering matrix of that inhomogeneous layer can then be combined with the scattering matrix of the rough interface to develop the overall scattering matrix looking into the rough surface (scattering coefficients for the entire medium – rough interface combined with the inhomogeneous dielectric layer below it). This technique leads to less unknowns and coefficients to solve for as compared to the Method of Moments. The technique (ECBM) was validated for a medium with two rough surfaces and a four-layer

piecewise dielectric profile between the rough surfaces by comparing to simulations involving the analytical small perturbation method (SPM) as well as the Method of Moments (MoM). Good agreement was found between all three methods. Finally they also performed some sensitivity experiments of the scattering coefficients to various frequencies in a field setting. They utilized three frequencies (137 MHz, 435 MHz and 1 GHz) the lower of which was better suited for deeper penetration and the latter two (higher frequencies) more suited to assessing the moisture content variations near the surface (validated by the sensitivity of the different frequencies to different depths of changing moisture content and those effects on the subsequent scattering coefficients). The authors also indicated that their technique can be expanded to model 3-D scattering from a 2-D rough surface.

Zhang et al. [91] examined the use of microwave remote sensing for detecting the freezing and thawing of the soil surface. This is based on the theory that the dielectric constant is much lower for frozen (tightly constrained water molecules) than it is for liquid (free water molecules). They developed an empirical dielectric mixing model to accommodate the air, soil, liquid water and frozen water (ice) constituents. The starting point for their model was identical in form to (2-29) with assumption on volume fractions and real values for the permittivity's of the four constituents of air, soil, free water and bound water. They adapted this mixing model in empirical fashion to add temperature functions and other functions related directly to the bound water (or frozen water constituents). They also added parameters to adapt the bound water function / fraction to account for clay constituents. Finally they added factors that relate how the soil bulk density as well as the density of the solid fraction influences the freezing process and hence the dielectric mixing models. Their empirical expression for the dielectric mixing model with all of these added factors can be found in the reference [91] and an updated variation of it will be presented in [96] covered in a moment. They suggested that this model could be utilized with microwave remote sensing to identify transitions between freezing and thawing soils.

Gorrite et al. (2005) [92] presented a new tool for accurate permittivity reconstruction utilizing a coaxial probe that can be filled with various constituents (such as soil). Accurate knowledge of the permittivity would then be applicable to microwave remote sensing properties of the earth's subsurface such as soil water content. They utilized both S-Parameters and T-Parameters and utilized a multi-segment cascaded transmission line model with different dielectrics (with loss components) to model their coaxial probe. They developed forward models

for the cascaded sections with S-Parameter and T-Parameter methods similar to those discussed earlier in this review and in the previously cited literature for cascaded lines. They then utilized inversion algorithms to de-embed the feeding sections to the portion of the probe under test again utilizing transmission line de-embedding and inversion methods similar to those described previously in the literature [11], [20]. They validated their models using test media of air, Teflon, and ethanol in their coaxial probe/fixture with measurements from 300 kHz – 3 GHz (consistent with the range of the Agilent Technologies 8753 Vector Network Analyzer). They reported errors on permittivity measurements on the order of 0.1 – 1%. Utilization of this coaxial measurement fixture could therefore be used to assess the dielectric properties of a variety of soils directly via transmission VNA measurements and those results utilized to aid future remote sensing technologies, algorithms and calibrations.

Ball et al. [93] had earlier conducted a similar study utilizing waveguide cells and transmission methods with a VNA. They filled a waveguide with a particular medium under test and then sealed it off with two Teflon barriers. They tested cheese curd and de-ionized water. The goal of their study was an attempt to develop a simplified procedure with frequencies that are harmonics of the quarter wavelength frequency for the waveguide to attempt to extract data without resorting to multiple cascaded transmission lines and associated S-Parameters. In essence they were simply looking for half-wave resonances of the waveguide and using those measured resonant frequencies as part of an inverse algorithm to ascertain properties of the permittivity of the medium. They used three successive harmonics all at half wave resonances to accurately determine the resonances (via resonance spacing algorithms).

In recent years there have been many applications and studies involving microwave remote sensing at different bands to assess surface zone moisture content over very large areas (states, countries and even continents). Examples of these studies include [108], [114], [123], [126] and [128]. Additional studies [124] and [125] have been conducted to improve the processing of backscattering signals over non-uniform surfaces such as furrowing and other surface roughness features.

The key features of GPR and Microwave Remote Sensing are being non-invasive. Other investigations into comparing non-invasive methods to other methods include [127] which compared complex imaging methods to transmission line methods. The algorithms presented in

this dissertation will have applications to both non-invasive GPR and Remote Sensing applications as well as invasive Transmission Line (e.g. TDR/TDT) methods.

**Dielectric/Permittivity Mixing Models:**

This literature review for this topic is covered in more depth in Appendix C and has also been touched on in several earlier sections of this literature review chapter leading to equations 2-13 & 2-28 (Refractive Mixing Models), (2-14 (arithmetic mean model) and (2-29 (which is actually a generalized power law mixing model that will discussed again in a moment). In this section we will cover briefly a number of other recent articles on modeling the permittivity of a medium that is applicable to many branches of inverse scattering problems.

To start this process the assumption for all of the previous equations in this review must be stated. That is that for all of the previous equations the permittivity is assumed to be homogeneous and isotropic within the zone or volume that it is being modeled for. If there is heterogeneity in the permittivity within a medium then that medium is divided into multiple sections each containing a homogeneous value for the permittivity. Models for cascaded networks are then developed to handle these cascaded sections. The other assumption of isotropic materials implies that the permittivity is the same value in all three axis. There are some materials for which this is not true (e.g. sapphire substrates in hybrid microcircuits). For the case of anisotropic media the permittivity is actually represented by a tensor in 3 dimensions [12] where the permittivity will have different values in different dimensions as well as cross coupling terms. Omar [94] presented a technique whereby an inhomogeneous media filled within a waveguide could get excited by stimulus waves from multiple directions (modeled as an n-port network with appropriate scattering parameters). This technique would allow for reconstructing the permittivity tensor as well as other information about the inhomogeneous mixture via the solving of an inverse algorithm based on the measured scattered signals from these multiple measurement ports (excitation points) in the cavity.

Mironov et al [95] applied the generalized refractive mixing dielectric model (GRMDM) (equations 2-13 and 2-28) to a soil containing also a humus component (organic matter). They found that this model could be utilized for organic matter constituents and adapted the model

accordingly. In a follow-up paper Mironov et al. [96] presented an updated version of the generalized refractive mixing dielectric model with a number of the improvements that had been incorporated specific to soils (e.g. the above reference [95] for organic matter and reference [91] for frozen water and other bound water mechanisms (e.g. clay), and other recent adaptations including accounting for Debye and Cole/Cole models for dielectric loss). The updated generalized refractive mixing dielectric model is given as follows where the square root of the overall permittivity (accounting for all terms including loss terms) is defined as the complex refractive index (CRI) or n* and given as follows:

Complex Refractive Index n*:

$$n^* = \sqrt{\varepsilon_T} = 1 + (\sqrt{\varepsilon_{Solids}} - 1)W_{Solids} + \sqrt{\varepsilon_{Air}}W_{Air} + \sqrt{\varepsilon_{B\_Water}}W_{B\_Water} + \sqrt{\varepsilon_{F\_Water}}W_{F\_Water}$$

$$n^* = n + j\kappa \tag{2-30}$$

Where

n = Refractive Index (real/energy storage terms)

κ = Normalized Attenuation Coefficient (imaginary/loss terms)

The "W" terms represent the respective volumetric fractions of the various constituents for solids, air, bound water (B_Water) and free water (F_Water) and the permittivity terms are for those respective constituents and all are given by complex values. For the case of the solids fraction the volumetric fraction can be further defined as follows:

$$W_{Solids} = \frac{\rho_d}{\rho_m} \tag{2-31}$$

(2-31) therefore relates the solids fraction to the ratio of the bulk density of the dry soil to the specific density of the soil solids. The solid components of mineral constituents (standard minerals and swelling clays) as well as organic constituents are modeled under this formula for the solids. In addition, the real and imaginary terms of the permittivity can be modeled in to (2-30) (as a function of frequency) based on the following relations:

$$n = \sqrt{\frac{\left(\sqrt{(\varepsilon')^2 + (\varepsilon'')^2}\right) + \varepsilon'}{2}} \tag{2-32}$$

$$\kappa = \sqrt{\frac{\left(\sqrt{(\varepsilon')^2 + (\varepsilon'')^2}\right) - \varepsilon'}{2}} \tag{2-33}$$

Equations 2-32 and 2-33 can be derived for a particular medium by utilizing equations A-9, A-16 and A-17. (2-32) can be obtained by dividing (A-17) (phase constant) by the special case of (A-9) for free space. (2-33) can be obtained by dividing (A-16) (attenuation constant) by the special case of (A-9) (again for free space). In both of these cases the conductivity is either embedded into the loss component of permittivity (by dividing by angular frequency) or alternatively set to zero.

Again equations (2-30) to (2-33) are all functions of frequency to model the frequency dependence of the permittivity terms (both the real and imaginary/loss terms). This general model has been applied to a number of soils over a wide variety of conditions with good performance. Much more research is needed in this area of dielectric mixing models including better determination of how physical scale (microscopic vs. macroscopic) impacts these models. Mironov et al. [116] – [119] has since provided enhanced versions of these GRMDM and other models including the development of the Mineralogy-based soil dielectric model (MBSDM) that can account for multiple frequency dependent relaxation models. An additional study [112] investigated applying the combination of both TDR (Time Domain Reflectometry) and FDR (Frequency Domain Reflectometry) to assess the dielectric properties of the soil including the frequency dependence. In complex dielectric mixing models this frequency dependence becomes a challenging parameter as it will depend on moisture content and constituent makeup in the soil.

Serdyuk et al. [97] compared 7 different popular dielectric mixing models as follows (with all the formulations and models left to the reference):

1.) Maxwell-Garnett (Spherical Inclusions)

2.) Bruggeman Effective Medium Approximation

3.) Coherent Potential Function

4.) Power Law Models ((2-29) and the basis for the refractive mixing models)

5.) Odelevski's Model

6.) Arithmetic Mean ((2-14))

7.) Geometric Mean (Square Root of the Product for a Two Component Mixture)

In their study they found that the Bruggeman, Power Law (within certain ranges of the parameter $\alpha$ in (2-29) and Geometric Mean models could be applied with reasonable accuracy. They conducted numerical simulations of a stochastic two component mixture at very low frequencies (1 mHz to 1 kHz) or essentially a DC analysis of dielectric mixing models. Again, more research is needed on this (as well as how well these other models translate to RF frequencies).

Jylha et al. (2005) [98] analyzed numerically various disordered 3D mixtures of substances assuming spherical inclusions of equal volumes distributed throughout the volume of a background or substrate material. An additional assumption is that the spheres did not touch each other. They utilized the Maxwell Garnett, Bruggeman and Coherent Potential models for dielectric mixing (all covered also in the previous reference [97]). They provided a uniform model with a particular parameter that could be used to reduce the general model to any of those three specific dielectric mixing models (please refer to [98] for the exact formulation). They confirmed the findings in the previous work [97] that the Bruggeman model provided a reasonable estimate of the effective permittivity. They concluded this via numerical simulations and actual measurements on a swiss cheese sample. They also presented some techniques to reduce computational time on the solving algorithms.

Todd et al. [99] evaluated the power law mixing models to model the complex permittivity of composite systems. They utilized a model that was very similar in form to (2-29) presented earlier. They modeled the system accounting for interphase relationships between the constituents and properties of the general connecting matrix. They adapted the model with particular values of the parameters and termed the adapted model the "interphase power law" (IPL) model and found reasonable agreement between simulations and actual measurements with a particular polymer and filler material (resulting in a complex mixture with interphase relationships). They also compared the results to the Bruggeman model and other models from the studies cited above and found that those other models overestimated the permittivity of these particular mixtures whereas the IPL model showed better agreement.

Broveli et al. (2005) [100] modeled the electrical properties of partially saturated sandstones. They developed pore-scale models based on grain size distribution and porosity to allow for computing the effective electrical conductivity and effective permittivity of partially saturated media. They accomplished this via the following steps:

1.) Generate/Simulate a closely packed system utilizing the grain size distribution and porosity
2.) Simulate the primary drainage paths to obtain the phase distributions over several levels of water contents or degrees of saturation.
3.) Compute the electromagnetic parameters via solving of the basic governing partial differential equations (via FDTD methods) for the potential and electric field (e.g. Laplace's equation from (2-8) for the potential and (2-10) for the electric field). The current density J and the Displacement current/flux density D can then be calculated as follows for both Ohmic and Dielectric mechanisms respectively:

$$J = \sigma E = -\sigma \nabla \Phi \tag{2-34}$$

$$D = \varepsilon E = -\varepsilon \nabla \Phi \tag{2-35}$$

They then developed three different approaches to modeling the conductivity:

1.) Hypothetical Conductivity Directly Through the Solid Fractions.
2.) Two Resistors in Parallel: Aqueous Solution and the Matrix-Water Interface
3.) Joint Volume and Surface Contributions to Conductivity.

They also modeled the electric permittivity vs. frequency and water content utilizing a similar FDTD numerical simulation approach and considering the overall bulk structure and porosity (i.e. no surface effects for the permittivity). The overall results of this study showed that the two resistors in parallel model gave the best agreement with actual experiment results for conductivity. They also found the models with permittivity based on the overall bulk soil volume agreed well with experimental results over a wide range of water contents. They found that the effects of clay constituents (coating the sandstone particles) influenced the permittivity below 350 MHz due to Maxwell-Wagner interfacial processes resulting in frequency dependence on the

permittivity below that point and thus dispersion. But above that frequency and up to 1 GHz there was little or no frequency dependence and therefore no dispersion.

Chen et al. (2006) [101] examined geometrical factors and interfacial processes and assessed their impacts on the complex permittivity of partially saturated porous media. They evaluated in depth the Maxwell-Wagner interfacial processes that can occur at charged clay/water interfaces. They also modeled the impacts of conductivity as well as frequency. They are in process of adding temperature dependence to their models. They emphasized the frequency range < 500 MHz where Maxwell-Wagner effects are dominant (as well as lower frequency conductivity which interplays with the M-W interfacial processes). They incorporated the "Maxwell-Wagner-Bruggeman-Hanai (MWBH) form of mixing model that accounts for the roles of phase configuration, inclusion shape, electrical conductivity and frequency. Their findings showed that significant errors can occur with the classical Topp Model below 100 MHz when these complex interfacial M-W processes are present.

This dissertation will present enhanced models and algorithms to address these and several of the other limitations of the models described in this literature review chapters as well as in Appendix C.

## Global Optimization Methods Applied to Inverse Scattering Problems:

Often times due to the sheer number of unknowns and the complexity of various scattering problems the measured scattered results must be fitted to pre-determined solutions or forward prediction models or object signal representations via global optimization methods. There are a number of different optimization techniques employed today. Simulated annealing and genetic algorithms are two such popular approaches. Two studies utilizing genetic algorithms applied to inverse scattering problems are briefly covered as follows:

Zhang et al. (2006) [104] applied the use of Genetic algorithms to the inverse scattering problem of extraction of dispersive material properties from vector network analyzer S-Parameter measurements. They employed a Debye relaxation model (similar to equations 2-6 and 2-7) and also embedded the conductivity into the expression via division by angular frequency. They

initially utilized two case studies of a parallel plate transmission line and then a microstrip transmission line and later added a third case for a stripline transmission line. Determination of the total attenuation constant and phase constant (equations A-16 and A-17) as functions of frequency with embedded Debye models for the loss components of permittivity (and embedded conductivity divided by angular frequency) were the goals of the optimization problem utilizing the measured S-Parameter data. They developed a genetic algorithm to perform this algorithm. Interim values for the attenuation constant and phase constant vs. frequency (with the embedded Debye models) would be generated at each "generation" in the genetic algorithm. A fitness index is assigned to each of the offspring to assess goodness of fit (and to insure selection of the best offspring for propagating to the next generation). The overall results from the genetic algorithm optimization methods were compared to rigorous numerical simulations via full-wave FDTD methods and good agreement was found.

Qing (2006) [105] developed a dynamic differential evolution strategy for solving electromagnetic inverse scattering problems. The difference in their approach is that the population is updated dynamically as opposed to waiting to the next generation which results in a larger virtual population and faster convergence to a solution. They utilized several test cases including minimization problems where the minimization function can have numerous parameters. They then applied the approach to a sample electromagnetic inverse problem involving multiple perfectly conducting cylinders within a domain where fields or scattering signals can therefore be measured in various measurement locations and the inverse problem is reconstruction of the actual locations and geometries of the cylinders. They conduct the simulations at 300 MHz. They found that this approach was indeed much faster and more efficient than the classical genetic algorithms which use standard differential evolution strategies. The author [105] indicated that additional research is proceeding with these approaches and more work is needed.

## Conclusion:

There is a wealth of information on different inverse scattering problems over a wide variety of fields of disciplines. Much can be learned by exploring the techniques employed across these disciplines to find better overall methods to solve inverse scattering problems. This is an exciting area of research especially in the realms of non-invasive methodologies (both electromagnetic and non-electromagnetic). Research is still in its infancy for many of these technologies and the decades ahead should be fruitful in the provision of measurement solutions that benefit society and improve the quality of life and productivity of all.

The enhanced models and algorithms presented in this dissertation will provide the next step in enhancing these inverse scattering problems applied to the cases of lossy and heterogeneous media such as soils and foods. Applications to both non-invasive (e.g. GPR and Microwave Remote Sensing) as well as invasive (e.g. Transmission Line based TDR and TDT) methods will be presented.

## References:

[1] G.A. Campbell, R.M. Foster, "Maximum Output Networks for Telephone Substation and Repeater Circuits", *Trans of the AIEE,* v39, pp 231-280, 1920.

[2] C. Montgomery, R.H. Dicke, E.M. Purcell, *Principles of Microwave Circuits,* New York, McGraw-Hill Book Co., Inc., 1948.

[3] S.J. Mason, "Feedback Theory – Some Principles of Signal Flow Graphs", Proc IRE, v41, pp 1144 – 1156, Sept. 1953.

[4] S.J. Mason, "Feedback Theory – Further Principles of Signal Flow Graphs", Proc IRE, v44, pp 920-926, July 1956.

[5] H. Carlin, "The Scattering Matrix in Network Theory", *IRE Trans on Circuit Theory",* v3, no. 2, pp 88-97, Jun 1956.

[6] V. Belevitch, "Elementary Applications of the Scattering Formalism in Network Design", *IRE Trans on Circuit Theory",* v3, No. 2, pp 97-104, Jun 1956.

[7] J.K. Hunton, "Analysis of Microwave Measurements by Means of Signal Flow Graphs" IRE/IEEE Transactions on Microwave Theory and Techniques (MTT), v8, no.2, pp 206-212, Mar 1960.

[8] R.W. Anderson, "S-Parameters Theory and Application", 1967 HP Journal, Hewlett Packard Company, v18, no. 6, Feb 1967.

[9] R.W. Anderson, L. Smith, J. Gruszynski, "S-Parameter Techniques for Faster, more Accurate Network Design", HP Test and Measurement Application Note 95-1, P/N 5952-1130, Hewlett Packard Company, 79 pp. Nov. 1996.

[10] "S-Parameter Design" Agilent AN 154 Application Note, P/N 5952-1087, Agilent Technologies, Inc., 44 pp, Latest Revision reprinted Jun 2006.

[11] "De-embedding and Embedding S-Parameter Networks Using a Vector Network Analyzer", Application Note 1364-1, P/N 5980-2784EN, Agilent Technologies, Inc., 24 pp, May 2004

[12] S. Ramo, J. Whinnery, T. Van Duzer, *Fields and Waves in Communication Electronics,* 3rd Edition, John Wiley & Sons, Inc., 844pp, 1994.

[13] D. Pozar, *Microwave Engineering,* 2nd Edition, John Wiley & Sons, 1998.

[14] P.C. Magnusson, G.C. Alexander, and V.K. Tripathi, *Transmission Lines and Wave Propagation,* 3rd edition, CRC Press, 460 pages, 1992.

[15] N.N. Rao, *Elements of Engineering Electromagnetics,* Prentice-Hall, Englewood Cliffs, New Jersey, 1977.

[16] A.E. Bailey, *Microwave Measurements,* 2nd Addition, Peter Peregrinus Ltd, p28-73, 1989.

[17] L. Eyges, *The Classical Electromagnetic Field*, Dover Publications, Inc., NY, 413 pp, 1972.

[18] J. Helszajn, *Passive and Active Microwave Circuits*, John Wiley & Sons, p1-23, 1978.

[19] "Time Domain Reflectometry Theory", Application Note 1304-2, P/N 5966-4855, Agilent Technologies, Inc., 16 pages, Latest Revision reprinted May 2006.

[20] A. Bruckstein, T. Kailath, "An Inverse Scattering Framework for Several Problems in Signal Processing", *ASSP Magazine, IEEE,* vol. 4, no. 1, Part: 1, pp 6-20, Jan 1987.

[21] G.C. Topp, J.L. Davis, and A.P. Annan, "Electromagnetic Determination of Soil Water Content: Measurements in Coaxial Transmission Lines", *Water Resources Research,* vol. 16, no. 3, pp 574-582, 1980.

[22] W.N. Herkelrath, S.P. Hamburg, F. Murphy, "Automatic, Real Time Monitoring of Soil Moisture in a Remote Field Area with Time Domain Reflectometry", *Water Resources Research,* vol. 27, no.5, pp 857-864, 1991.

[23] S. Arcone, "Conductivity Limitations in Single-Reflection Time-Domain Reflectometry", *J. Phys. E: Sci. Instrum*, v19, pp 1067-1069, May 1986.

[24] S. Arcone, "A Numerical Study of Dielectric Measurements using single-reflection time-domain reflectometry", *J. Phys. E: Sci. Instrum*, v19, no.6, pp 448-454, Jun. 1986.

[25] J.E. Campbell, "Dielectric Properties and Influence of Conductivity in Soils at One to Fifty Megahertz", *Soil Sci. Soc. Am. J*, v54, pp332-341, 1990.

[26] F.N. Dalton, W.N. Herkelrath, D.S. Rawlins, and J.D. Rhoades, "Time Domain Reflectometry: Simultaneous Measurement of Soil Water Content and Electrical Conductivity with a Single Probe, *Science* (Washington) v224, pp 989-990, 1984.

[27] S. Dasberg, F.N. Dalton, "Time Domain Reflectometry Field Measurements of Soil Water Content and Electrical Conductivity", *Soil Sci. Soc. Am. J,* v49, pp 293-297, 1985.

[28] F.N. Dalton, M.Th. Van Genuchten, "The Time-Domain Reflectometry Method for Measuring Soil Water Content and Salinity", *Geoderma,* v38, pp237-250, 1986.

[29] F.N. Dalton, J.A. Poss, "Soil Water Content and Salinity Assessment for Irrigation Scheduling using Time Domain Reflectometry: Principles and Applications", *Acta Hort,* v278, no.1, pp 381-393, 1990.

[30] F.N. Dalton, "Development of Time-Domain Reflectometry for Measuring Soil Water Content and Bulk Soil Electrical Conductivity", *Soil Science* sp. pub.# 30, pp 143-167, 1992.

[31] G.C. Topp, M. Yanuka, W.D. Zebchuk, S. Zegelin, "Determination of Electrical Conductivity Using Time Domain Reflectometry: Soil and Water Experiments in Coaxial Lines", *Water Resources Research*, v24, no. 7, pp 945-952. 1988.

[32] S.F. Kelly, J.S. Selker, J.L. Green, "Short High Resolution TDR Probes to Measure Water Content in High Salinity Soils", Tech. note subm. to *Soil Science Society of America Journal*, Jan 1994.

[33] T.J. Heimovaara, "Frequency Domain Analysis of Time Domain Reflectometry Waveforms: 1. Measurement of the complex Dielectric Permittivity of Soils", *Water Resources Research*, v30, no. 2, pp 189-199, 1994.

[34] T.J. Heimovaara, "Frequency Domain Analysis of Time Domain Reflectometry Waveforms: 2. A Four-Component Complex Dielectric Mixing Model for Soils", *Water Resources Research*, 1994.

[35] T.J. Heimovaara, E.J.G. de Winter, W.K.P. Van Loon, D.C. Esveld, "Frequency-Dependent Dielectric Permittivity from 0 to 1 GHz: Time Domain Reflectometry Measurements compared with Frequency Domain Network Analyzer Measurements", *Water Resources Research,* v32, no.12, pp 3603-3610, Dec 1996.

[36] P.G. Petropoulos, "On the Time-Domain Response of Cole-Cole Dielectrics", *IEEE Trans on Antennas and Propagation*, vol. 53, no. 11, pp 3741-3746, Nov. 2005.

[37] J. O. Curtis, "A Durable Laboratory Apparatus for the Measurement of Soil Dielectric Properties", *IEEE Trans on Instrumentation and Measurement,* vol. 50, no. 5, pp 1364-1369, Oct. 2001.

[38] T.J. Kelleners, D.A. Robinson, P.J. Shouse, J.E. Ayars, T.H. Skaggs, "Frequency Dependence of the Complex Permittivity and its Impact on Dielectric Sensor Calibration in Soils", *Soil Science Soc Am J,* v69, p 67-76, 2005.

[39] D.A. Robinson, "Measurement of the Solid Dielectric Permittivity of Clay Minerals and Granular Samples Using a Time Domain Reflectometry Immersion Method", *Vadose Zone Journal*, v3, pp 705-713, 2004.

[40] Y. Chen, "Effects of Maxwell-Wagner Polarization on Soil Complex Dielectric Permittivity under Variable Temperature and Electrical Conductivity", *Water Resources Research,* v42, W0624, 14pp, Jun 2006.

[41] J.H. Knight, "Sensitivity of Time Domain Reflectometry Measurements to Lateral Variations in Soil Water Content", *Water Resources Research,* v28, no.9, pp 2345-2352, 1992.

[42] A.C. Hinnell, T.P.A. Ferre, A.W. Warrick, "The Influence of Time Domain Reflectometry Rod Induced Flow Disruption on Measured Water Content during Steady State Unit Gradient Flow", *Water Resources Research,* v42, W08420, 8pp, 2006.

[43] Selker, J.S., L.Graff, and T. Steenhuis. 1993. *Noninvasive Time Domain Reflectometry Moisture Measurement Probe.* Soil Sci. Soc. of Amer. Journ. v57. no. 4 pp 934-936.

[44] B.J. Hogan "One-Sided NMR Sensor System Measures Soil/Concrete Moisture", *Design News*, pp 108-111, May 1986.

[45] R.F. Paetzold, A. De Los Santos, G.A. Matzkanin, "Pulsed Nuclear Magnetic Resonance Instrument for Soil-Water Content Measurement: Sensor Configuration", *Soil Science Soc Am J,* v51, pp 287-290, 1987.

[46] Z.R. Hinedi, Z.J. Kabala, T.H. Skaags, D.B. Borchardt, R.W.K. Lee, A.C. Chang, "Probing Soil and Aquifer Material Porosity with Nuclear Magnetic Resonance", *Water Resources Research,* v29, no. 12, pp 3861-3866, Dec 1993.

[47] S.J. Zegelin, I. White and D.R. Jenkins, "Improved Field Probes for Soil Water Content and Electrical Conductivity Measurement Using Time Domain Reflectometry", *Water Resources Research,* vol. 25, no.11, pp 2367-2376, 1989.

[48] J.A.R. Ball, "Characteristic Impedance of Unbalanced TDR Probes", *IEEE Trans on Instrumentation and Measurement,* v51, no. 3, pp 532-536, Jun 2002.

[49] C.F. Souza, E.E. Matsura, R. Testezlaf, "Electromagnetic Determination of Water Content: Measurements in Multi-Wire Probes with Electrical Impedance Discontinuities", *Proceedings of the 2001 Microwave and Optoelectronics Conference,* vol. 1, pp 133-136, 2001.

[50] T.P.A. Ferre, H. **H. Nissen, J. Simunek,** "The Effect of the Spatial Sensitivity of TDR on Inferring Soil Hydraulic Properties from Water Content Measurements Made during the Advance of a Wetting Front", *Vadose Zone Journal,* v1, pp281-288, 2002.

[51] J.S. Selker, C.K. Keller, J.T. McCord, *Vadose Zone Processes,* Lewis Publishers, NY, CRC Press, LLC, pp 140 – 141, 1999.

[52] M.G. Schaap, D.A. Robinson, S.P. Friedman, A. Lazar, "Measurement and Modeling of the TDR Signal Propagation through Layered Dielectric Media", *Soil Sci Soc Am J,* v67, pp 1113 - 1121, 2003.

[53] D.A. Robinson, M. Schaap, S.B. Jones, S.P. Friedman, C.M.K. Gardner, "Considerations for Improving the Accuracy of Permittivity Measurements using Time Domain Reflectometry: Air-Water Calibration, Effects and Cable Length", *Soil Sci Soc Am J.,* v67, pp 62-70, 2003.

[54] X. Yu, "Frequency versus Time Domain Simulation of Non-uniform TDR System", *Proc of 2005 European Microwave Conference,* v2, 3pp, Oct 2005.

[55] D.A. Robinson, S.B. Jones, J.M. Wraith, D. Or, S.P. Friedman, "A Review of Advances in Dielectric and Electrical Conductivity Measurements in Soils Using Time Domain Reflectometry", *Vadose Zone Journal,* v2, pp 444-475, 2003.

[56] J.A. Huisman, S. Lambot, H. Vareecken, "Determining Soil Water Content Variation along the TDR Probe with Inverse Modeling: Theory, Practice and Challenges", *Proc TDR 2006,* Purdue University, Paper ID 28, 10pp, Sep 2006.

[57] X. Qiwei, S. Lihua, G. Cheng, "Measurements of the Electromagnetic Constants of Concrete Materials by Time-Domain Reflectometry", *Proceedings of the 3rd International Symposium on Electromagnetic Compatibility, 2002,* pp 230-233, May 2002.

[58] C.P. Nemarich, "Time Domain Reflectometry Liquid Level Sensors", *IEEE Instrumentation and Measurement Magazine",* vol. 4, no. 4, pp 40-44, Dec 2001.

[59] A. Cataldo, L. Tarricone, M. Vallone, F. Attivissimo, A. Trotta, "An Assessment on the Accuracy of Time-Domain Reflectometry for Measuring Level and Permittivity of Liquids", *Proceedings of the 23rd IEEE Instrumentation and Measurement Technology Conference, 2006,* pp 2332-2337, 2006.

[60] M. Gerding, T. Musch, B. Schiek, "A Novel Approach for a High-Precision Multitarget-Level Measurement System Based on Time-Domain Reflectometry", *IEEE Trans on Microwave Theory and Techniques",* v54, no. 6, pp 2768 – 2773, Jun 2006.

[61] J.M. Jong, V.K. Tripathi, B. Janko, "Equivalent Circuit Modeling of Interconnects from Time Domain Measurements", *Proceedings, 42nd Electronic Components and Technology Conference, 1992,* pp 730-735, May 1992.

[62] C. Schuster, W. Fichtner, "Signal Integrity Analysis of Interconnects Using the FDTD Method and Layer Peeling Technique", *IEEE Trans on Electromagnetic Compatibility,* v42, no. 2, May 2000.

[63] S. Pannala, M. Swaminathan, "Extraction of S-Parameters from TDR/TDT Measurements using Rational Fractions", Special Publication: Packaging Research Center, Georgia Institute of Technology & Sun Microsystems, 26pp, 2002.

[64] C.J. Ong, A. Tripathi, D. Miller, L. Tsang, "De-embedding a Device-Under-Test (DUT) using Thru' Measurements", *Proceedings of Electrical Performance of Electronic Packaging Conference, 2003,* pp 89-92, Oct 2003.

[65] G. Antonini, A. C. Scogna, A. Orlandi, V. Ricchiuti, G. Selli, S.Luan, J.L. Drewniak, "Validation of Circuit Extraction Procedure by Means of Frequency and Time Domain Measurement", *Proceedings of the 2005 International Symposium on Electromagnetic Compatibility,* vol. 1, pp 45-50, Aug. 2005.

[66] Agilent Technologies Data Sheet: "Agilent J-BERT N4903A High Performance Serial BERT with Complete Jitter Tolerance Testing" Agilent Technologies, Publication Number: 5989-2899EN, Jan 2007.

[67] A. Aksen, B.S. Yarman, "A Semi-Analytical Procedure to Describe Lossless Two-Ports with Mixed Lumped and Distributed Elements", *IEEE International Symposium on Circuits and Systems 1994,* vol. 5, pp 205-208, Jun 1994.

[68] S. Sun, R. Kumar, S.C. Rustagi, K. Mouthaan, T.K.S. Wong, "Wideband Lumped Element Model for On-Chip Interconnects on Lossy Silicon Substrate", *2006 IEEE Symposium on Radio Frequency Integrated Circuits,* 4 pp, Jun 2006.

[69] W. Kim, M. Swaminathan, "Simulation of Lossy Package Transmission Lines using Extracted Data from One-Port TDR Measurements and Non-Physical RLGC Models", *IEEE Trans on Advanced Packaging,* v28, no. 4, pp 736-744, Nov 2005.

[70] C.H. Kao, C.C. Tseng, F.M. Lee, M.F. Lai, "A Better Technique Using Multisegment Modeling and Analysis of High-Density and High-Speed Connectors", *IEEE Trans on Advanced Packaging,* vol. 29, no. 1, pp 140-148, Feb. 2006.

[71] D.E. Bockelman, W.R. Eisenstadt, "Combined Differential and Common-Mode Scattering Parameters: Theory and Simulation", *IEEE Trans on Microwave Theory and Techniques,* v43, no.7, pp 1530-1539, Jul 1995.

[72] Agilent Technologies Brochure: "Agilent PNA Microwave Network Analyzers" , Agilent Technologies, Publication Number: 5989-6014EN, Feb 2007.

[73] E. Bogatin, M. Resso, "Differential Impedance Measurement with Time Domain Reflectometry", Agilent Technologies, Application Note: 1382-5, Publication Number: 5988-4796EN, May 2002.

[74] J.D. Pro, M.E. Roen, "Characteristic Impedance and Signal Loss Measurements of Head-to-Preamplifier Interconnects", *IEEE trans on Magnetics,* vol. 42, no. 2, Part 1. pp 261-265, Feb. 2006.

[75] W.D. Guo, G.H. Shiue, C.M. Lin, R.B. Wu, "Comparisons Between Serpentine and Flat Spiral Delay Lines on Transient Reflection/Transmission Waveforms and Eye Diagrams", *IEEE Trans on Microwave Theory and Techniques,* v54, no. 4, pp 1379 - 1387, Apr 2006.

[76] M.N.O. Sadiku, C.M. Akujuobi, "S-Parameters for Three and Four Cascaded Two-Ports", *IEEE Proceedings: SoutheastCon, 2004*. pp 410-412. 2004.

[77] K.M. Rahman, C. Nguyen, "Analysis of Cascaded Asymmetric Coplanar Waveguide Step Discontinuities", *IEEE 1997 Digest: Antennas and Propagation Society International Symposium,* vol. 4, pp 2522-2525, Jul 1997.

[78] G.R. Simpson, "A Generalized n-Port Cascade Connection" *Microwave Symposium Digest, MTT-S International,* vol. 81, no. 1, pp 507-509, Jun 1981.

[79] M. H. Cho, G. W. Huang, L. K. Wu, C.S. Chiu, Y.H. Wang, K.M. Chen, H.C. Tseng, T.L. Hsu, "A Shield-Based Three-Port De-Embedding Method for Microwave On-Wafer Characterization of Deep-Submicrometer Silicon MOSFETs", *IEEE Trans on Microwave Theory and Techniques,* v53, no. 9, pp 2926 – 2934, Sep 2005.

[80] J.L. Frolik, A.E. Yagle, "Forward and Inverse Scattering for Discrete Layered Lossy and Absorbing Media", *IEEE Trans on Circuits and Systems II: Analog and Digital Signal Processing,* vol. 44, no. 9, pp 710-722, Sep 1997.

[81] K. Wu, M. Yu, R. Vahldieck, "Rigorous Analysis of 3-D Planar Circuit Discontinuities Using the Space-Spectral Domain Approach (SSDA)", *IEEE Trans on Microwave Theory and Techniques,* v40, no. 7, pp 1475 - 1483, Jul 1992.

[82] T. Cwik, R. Mittra, "The Cascade Connection of Planar Periodic Surfaces and Lossy Dielectric Layers to Form an Arbitrary Periodic Screen", *IEEE Trans on Antennas and Propagation,* vol. 35, no. 12, pp 1397-1405, Dec. 1987.

[83] P. Wang, M. Xia, L. Zhou, "Analysis of Scattering by Combined Conducting and Dielectric Bodies using Single Integral Equation Method and Fast Multipole Method", Microwave Conference Proceedings, 2005, Asia-Pacific Conference, vol. 5, 4 pp, Dec. 2005.

[84] G. Serbin, D. Or, "Near Surface Soil Water Content Measurements Using Horn Antenna Radar: Methodology and Overview", *Vadose Zone Journal,* v2, pp 500-510, Nov. 2003.

[85] A. Martinez, A.P. Byrnes, "Modeling Dielectric-Constant Values of Geologic Materials: An Aid to Ground-Penetrating RADAR Data Collection and Interpretation", *Current Research in Earth Sciences, Bulletin 247, part 1,* Kansas Geological Survey, 2001.

[86] K. Grote, S. Hubbard, Y. Rubin, "Field-Scale Estimation of Volumetric Water Content Using Ground-Penetrating Radar Ground Wave Techniques", *Water Resources Research,* v39, no.11, 14pp, Nov. 2003.

[87] S. Lambot, L. Weihermuller, J. A. Huisman, H. Vereecken, M. Vanclooster, E.C. Slob, "Analysis of Air-Launched Ground-Penetrating RADAR Techniques to Measure Soil Surface Water Content", *Water Resources Research,* v.42, W11403, 12 pages, Nov 2006.

[88] L.P. Song, Q.H. Liu, F. Li, Z.Q. Zhang, "Reconstruction of Three-Dimensional Objects in Layered Media: Numerical Experiments", *IEEE Trans on Antennas and Propagation,* vol. 53, no. 4, pp 1556-1561, Apr 2005.

[89] T.J. Cui, Y. Qin, Y. Ye, J. Wu, G.L. Wang, W.C. Chew, "High-Order Inversion Formulas for 3D Buried Dielectric Objects", *Proc 2005 IEEE Antennas and Propagation Society International Symposium,* v2A, pp 131-134, July 2005.

[90] C.H. Kuo, M. Moghaddam, "Electromagetic Scattering from Multilayer Rough Surfaces With Arbitrary Dielectric Profiles for Remote Sensing of Subsurface Soil Moisture", *IEEE Transactions on Geoscience and Remote Sensing"* vol 45, no. 2, pp 349 – 366, Feb. 2007.

[91] L. Zhang, J. shi, Z. Zhang, K. Zhao, "The Estimation of Dielectric Constant of Frozen Soil-Water Mixture at Microwave Bands", Proceedings: IEEE International Geoscience and Remote Sensing Symposium 2003, vol. 4, pp 2903-2905, July 2003.

[92] A.G. Gorriti, E.C. Slob, "A New Tool for Accurate S-Parameters Measurement and Permittivity Reconstruction", *IEEE Trans on Geoscience and Remote Sensing,* vol. 43, no. 8, pp 1727-1735, Aug. 2005.

[93] J.A.R. Ball, B. Horsfield, "Resolving Ambiguity in Broadband Waveguide Permittivity Measurements on Moist Materials", *IEEE Trans on Instrumentation and Measurement,* vol 47, no. 2, pp 390-392, Apr 1998.

[94] A.S. Omar, "Reconstruction of the Dyadic Dielectric Constant Profile of Anisotropic Inhomogeneous Media", *Proceedings of the 16th National Radio Science Conference, NRSC 1999,* pp INV5/1 – INV5/7.

[95] V.L. Mironov, P.P. Bobrov, "Soil Dielectric Spectroscopic Parameters Dependence on Humus Content", *IEEE International Symposium Proceedings: Geoscience and Remote Sensing Symposium 2003,* vol. 2, pp 1106-1108, July 2003.

[96] V.L. Mironov, M.C. Dobson, V.H. Kaupp, S.A. Komarov, V.N. Kleshchenko, "Generalized Refractive Mixing Dielectric Model for Moist Soils", *IEEE Trans on Geoscience and Remote Sensing,* vol. 42, no. 4, pp 773-785, Apr 2004.

[97] Y.V. Serdyuk, A.D. Podoltsev, S.M. Gubanski, "Numerical Simulations and Experimental Study of Frequency-Dependent Dielectric Properties of Composite Material with Stochastic Structure", *IEEE Trans on Dielectrics and Electrical Insulation,* vol. 11, no. 3, pp 379-392, Jun 2004.

[98] L. Jylha, A.H. Sihvola, "Numerical Modeling of Disordered Mixture Using Pseudorandom Simulations", *IEEE Trans on Geoscience and Remote Sensing,* vol. 43, no. 1, pp 59-64, Jan. 2005.

[99] M.G. Todd, F.G. Shi, "Complex Permittivity of Composite Systems: A Comprehensive Interphase Approach", *IEEE Trans on Dielectrics and Electrical Insulation,* vol. 12, no. 3, pp 601-611, Jun 2005.

[100] A. Broveli, G. Cassiani, E. Dalla, F. Bergamini, D. Pitea, A.M. Binley "Electrical Properties of Partially Saturated Sandstones", *Water Resources Research,* v41, W08411, 12pp, Aug 2005.

[101] Y. Chen, D. Or, "Geometrical Factors and Interfacial Processes Affecting Complex Dielectric Permittivity of Partially Saturated Porous Media", *Water Resources Research,* v42, W06423, 9pp, Jun 2006.

[102] Nelson, Stuart O., "Agricultural Applications of Dielectric Measurements". *IEEE Trans on Dielectrics and Electrical Insulation.* vol 13, no. 4: pp 688-702. 2006

[103] Klute A., *Methods of Soil Analysis Part 1 – Physical and Mineralogical Methods*. American Society of Agronomy, Soil Science Society of America 2nd Edition. 1188p. 1994

[104] J. Zhang, M. Y. Koledintseva, D.P. Pommerenke, J.L. Drewniak, "Extraction of Dispersive Material Parameters Using Vector Network Analyzers and Genetic Algorithms", *Proceedings of the 23rd IEEE Instrumentation and Measurement Technology Conference, 2006,* pp 462 – 467, Apr 2006.

[105] A. Qing, "Dynamic Differential Evolution Strategy and Applications in Electromagnetic Inverse Scattering Problems", *IEEE Trans on Geoscience and Remote Sensing,* vol. 44, no. 1. pp 116-125, Jan. 2006.

[106] Escorihuela, M.J., Y.H. Kerr, J.C. Calvet, "Influence of Bound-Water Relaxation Frequency on Soil Moisture Measurements", *IEEE Transactions on Geoscience and Remote Sensing,* vol.45, no.12, pp4067-4076, Dec 2007

[107] Casanova J.J., S.R. Evett, R.C. Schwartz, "Design of Access-Tube TDR Sensor for Soil Water Content: Testing", *IEEE Sensors Journal,* vol.12, no. 6, pp 2064-2070, June 2012

[108] Aubert, M., N.N. Baghdadi, M. Zribi, K. Ose, M.E. Hajj, E. Vaudour, E.G. Sosa "Toward an Operational Bare Soil Moisture Mapping Using TerraSAR-X Data Acquired Over Agricultural Areas", *IEEE Journal of Selected Topics in Applied Earth Observations and Remote Sensing,* pp 1-17, 2013 Approved for Future Publication

[109] Henry Z. A., G.C. Zoerb, G.S. Birth, *Instrumentation and Measurement for Environmental Sciences,* American Society of Agricultural Engineers. 3rd Edition.pp7-01 to 7-10, 1991

[110] Sarri A. M. Batisti, MM. Bientinesi, "Measurements of Complex Permittivity of Geological Materials Mixtures at RF Frequencies", 6th European Conference on Antennas and Propagation. P2109-2113, March 2012

[111] Mohammed H.U.R., M. Dawood, A.V. Alejos, "Experimental Detection and Characterization of Brillouin Precurser Through Loamy Soil at Microwave Frequencies", *IEEE Transactions on Geoscience and Remote Sensing",* vol.50, no. 2, pp 436 – 445, Feb 2012

[112] Umenyiora C.A., R.L. Druce, R.D. Curry, P.Norgard, T. McKee, J.J. Bowders, and D.A. Bryan, "Dielectric Constant of Sand Using TDR and FDR Measurements and Prediction Models". *IEEE Transactions on Plasma Science",* vol. 40. no. 10. pp2408-2415, Oct 2012

[113] Wagner N., K. Lauer, "Simultaneous Determination of the Dielectric Relaxation Behavior and Soil Water Characteristic Curve of Undisturbed Soil Samples". IEEE International Geoscience and Remote Sensing Symposium pp3202-3205, 2012

[114] Rautiainen, K, J. Lemmetyinen, J. Pulliainen, J. Vehvilainen, M. Drusch, A. Kontu, J. Kainulainen, J. Seppanen, "L-Band Radiometer Observations of Soil Processes in Boreal and Subartic Environments". *IEEE Transactions on Geoscience and Remote Sensing",* vol. 50. no. 5. pp1483-1497, May 2012

[115] M. Valery, K. Yann, W. Jean-Pierre, K. Liudmila, D. Francois, "Temperature and Texture Dependent Dielectric Model of Moist Soils at the SMOS Frequency". IEEE International Geoscience and Remote Sensing Symposium. pp1127-1130, 2012

[116] Mironov, V.L., Y. Kerr, J.P. Wigneron, L. Kosolapova, F. Demontoux, "Temperature and Texture Dependent Dielectric Model for Moist Soils at the 1.4 GHz". IEEE Geoscience and Remote Sensing Letters. pp419-423, May 2013

[117] Mironov, V.L., P.P. Bobrov, S.V. Fomin, "Multi-Relaxation Generalized Refractive Mixing Dielectric Model of Moist Soils". IEEE International Geoscience and Remote Sensing Symposium. pp 5177-5179, 2012

[118] Mironov, V.L., P.P. Bobrov, S.V. Fomin, "Multi-Relaxation Generalized Refractive Mixing Dielectric Model of Moist Soils". IEEE Geoscience and Remote Sensing Letters. pp 603-606, May 2013

[119] Mironov, V.L., L.G.Kosolapova, S.V. Fomin, "Physically and Mineralogically Based Spectroscopic Dielectric Model for Moist Soils" *IEEE Trans on Geoscience and Remote Sensing*, vol. 47, no. 7, pp 2059 – 2070, July 2009

[120] Wigneron, J.P. A. Chanzy, P. de Rosnay, C. Rudiger, J.C. Calvet, "Estimating the Effective Soil Temperature at L-Band as a Function of Soil Properties", *IEEE Trans on Geoscience and Remote Sensing*, vol. 46, no. 3, pp 797-807, March 2008

[121] Becker, R."Spatial Time Domain Reflectometry for Monitoring Transient Soil Moisture Profiles" PhD Dissertation, Institut für Wasser und Gewässerentwicklung Universität Karlsruhe, 230p, 2004

[122] Nussberger, M., "Soil moisture Determination with TDR:Single-Rod Probes and Profile Reconstruction Algorithms", PhD Dissertation, Swiss Federal Institute of Technology Zurich, 110p, 2005

[123] Srivastava, H.S. P. Patel, Y. Sharma, R.R. Navalgund "Large-Area Soil Moisture Estimation Using Multi-Incidence-Angle RADARSAT-1 SAR Data", *IEEE Trans on Geoscience and Remote Sensing*, vol. 47, no. 8, pp 2528-2535, Aug 2009

[124] Volksch, I., M. Schwank, C. Matzier, "L-Band Reflectivity of a Furrowed Soil Surface". *IEEE Trans on Geoscience and Remote Sensing*, vol. 49, no. 6, pp 1957-1966, June 2011

[125] Song K., X. Zhou, Y. Fan, "Empirically Adopted IEM for Retrieval of Soil Moisture From Radar Backscattering Coefficients". *IEEE Trans on Geoscience and Remote Sensing*, vol. 47, no. 6, pp 1662-1672, June 2009

[126] Pathe C., W. Wagner, D. Sabel, M. Doubkova, J.B. Basara, "Using ENVISAT ASAR Global Mode Data for Surface Soil Moisture Retrieval Over Oklahoma, USA". *IEEE Trans on Geoscience and Remote Sensing*, vol. 47, no. 2, pp 468-480, Feb 2009

[127] Arnautovski-Toseva, V., K.E.K. Drissi, C. Faure, C. Pasquier, K. Kerroum, "TM Plane Wave Coupling to Wire Conductors above Homogeneous Soil: Comparison between Complex Image and Transmission Line Approach", 20th International Conference on Software, Telecommunications and Computer Networks (SoftCOM), pp 1-5, 2012

[128] Mecklenburg, S., M. Drusch, Y.H. Kerr, J. Font, M. Martin-Neira, S. Delwart, G. Buenadicha, N. Reul, E. Daganzo-Eusebio, R. Oliva, R. Crapolicchio, "ESA's Soil Moisture and Ocean Salinity Mission: Mission Performance and Operations", *IEEE Trans on Geoscience and Remote Sensing*, vol. 50, no. 5, pp 1354-1366, May 2012

[129] Karlovsek, J., N. Wagner, A. Scheuermann, "Frequency-Dependent Dielectric Parameters of Steel Fiber Reinforced Concrete", 14th International Conference on Ground Penetrating Radar (GPR), pp 510-516, 2012

[130] Karlovsek J., A. Scheuermann, D.J. Willimas,, "Investigation of Voids and Cavities in Bored Tunnels using GPR", 14th International Conference on Ground Penetrating Radar (GPR), pp 496-501, 2012

[131] Souza C.F.,D. Or, and E. E. Matsura, "A Variable-Volume TDR Probe for Measuring Water Content in Large Soil Volumes", *Soil Science Soc. Am J*, vol. 68, pp 25-31, 2004

[132] Chang Y.C., I. Shawn, S. H. Hsu, "A De-embedding Method for Extracting S-Parameters of Vertical Interconnect in Advanced Packaging" IEEE 20th Conference on Electrical Performance of Electronic Packaging and Systems, pp219-222 Oct 2011

[133] Paulis, F.D., Y.J. Zhang, J. Fan, "Signal/Power Integrity Analysis for Multilayer Printed Circuit Boards Using Cascaded S-Parameters" *IEEE Trans on Electromagnetic Compatibility*, vol. 52, no. 4, pp 1008 – 1018, Nov. 2010

[134] I. Daubechies, "The Wavelet Transform, Time-Frequency Localization and Signal Analysis", *IEEE Trans on Information Theory*, v36, no. 5, pp 961-1005, Sept 1990.

[135] D. Gabor, "The Theory of Communications", *J. Inst. Elect. Eng.* v93, no. 3, pp 429-457, 1946.

[136] J.Yao, P. Krolak, C. Steele, "The Generalized Gabor Transform", IEEE Trans. on Image Processing, v4, no.7, pp 978 – 988, July, 1995.

[137] J.C. van den Berg, *Wavelets in Physics*, Cambridge University Press, 2004.

[138] Matlab version R2012a, Mathworks Corporation, 2012.

[139] Microwave Design Computations: MWI.exe: Software for Determination of Characteristic Impedance of Microstrip and Stripline Transmission Lines. Rogers Corporation, Chandler, AZ.

# Chapter 3: Forward Prediction Models

## Overview of Models:

A set of Forward Prediction models to simulate electromagnetic wave propagation based Volumetric Water Content (WC) and Electrical Conductivity (EC) measurements for geophysical and biological media are presented in this chapter. The initial simulated structures and validation methods included the guided cascaded transmission line techniques of Time Domain Reflectometry (TDR) and Time Domain Transmission (TDT) methods [19]. However, the models are also directly applicable to non-invasive non-guided cascaded domain electromagnetic wave propagation techniques such as Ground Penetrating Radar (GPR) [85], Microwave Remote Sensing [87] and other antenna-based transmission/reflection measurements. The initial simulation and validation media included soils of different types with a wide range of WC and EC values. Simulation of WC and EC profiles vs. position within the media is included in the forward prediction models to model spatial heterogeneity and resulting impacts on TDR/TDT waveforms utilizing cascaded transmission line models. The prediction models are developed in both the time and frequency domains utilizing physically based models from the theory of electromagnetics and Scattering (S) Parameter network modeling techniques along with Fast Fourier Transform (FFT) and Inverse Fast Fourier Transform (IFFT) algorithms [1-18]. New models are introduced for composite media of multiple dielectric constituents each with frequency dependence on the real (energy storage) and imaginary (energy loss) components of permittivity, and Ohmic loss constituents (with various values of electrical conductivity). These composite dielectric/Ohmic mixing models interpolate in different fashion between the physically driven upper and lower bounds of parallel and serial influences of each of the capacitive and conductive constituents. New models are also introduced accounting for charged interfaces and resulting bound and semi-bound water constituents within the pore spaces of soils containing clay or organic matter fractions. A new model accounting for a continuous but gradual transition from bound to free water and subsequent influences on the frequency dependence on permittivity is also presented. The focus of this chapter will be on the underlying theory and components of the forward prediction models supported also by appendices A-D giving additional technical background information. The forward prediction models introduced in this chapter are applicable to all types of media including those with lossy constituents such as soils with high salinity (high EC). The models also account for the dispersive and lossy effects of the permittivity of water at high frequencies (> 1 GHz).

## Background:

TDR involves the generation and propagation of a high speed pulse down a particular transmission line embedded in a medium under test and terminated with a reflecting load (typically an open circuit but could alternatively be a short circuit). The TDR procedure in its conventional historical form involves measuring the total transit time of the reflected pulse in returning to the input and correlating that transit time to electromagnetic properties of the medium. This includes the electric permittivity which in turn can be correlated to other physical properties of the medium such as WC. TDT involves the propagation of a similar high speed pulse down again a transmission line embedded in a medium under test but this time connected to a measurement receiver on the opposite end to measure the transmitted signal through the medium. A reflected signal at the input (due to internal partial reflections in the medium under test) can still also be measured with a TDT system and combined with the transmission measurement to give extra measurement information over and above what would be provided by a simple TDR system. This will be shown to be important given the number of measurement variables or unknowns that can be present in a soil WC and EC measurement. The models also have good portability and applicability to the non-invasive wave propagation measurement methods such as Ground Penetrating Radar (GPR) and Remote Sensing (RS) providing alternatives to the invasive TDR and TDT systems. Examples of TDR and TDT waveforms for a sandy soil vs WC and EC are given in Appendix D.

Soils represent most of the key challenges typically found with geophysical and biological media. These challenges can include the following:

1.) Multiple constituents: Soils can contain gases (e.g. air), liquids (e.g. water) as well as solids fractions. Within the solids fractions soils can contain anywhere from coarse down to fine particle sizes such as sand, silt and clay and also can contain organic matter fractions. These constituents can have stochastically based relative and absolute fractions from macroscopic all the way down to microscopic scales. Various zones of particular scales can either be considered homogeneous or heterogeneous based on the following distinctions:

a. Spatial Homogeneity: This describes a zone of a particular scale/size where the stochastic constituent distributions remain consistent throughout that zone. In that case that zone can still be deemed homogeneous despite the complex makeup.

b. Spatial heterogeneity: In this case the constituent fractions or stochastic constituent distributions are functions of position on macroscopic scales so that the media can no longer be deemed homogeneous. This could include layered media or other spatial heterogeneity.

2.) Significant simultaneous presence of both electric permittivity (dielectric) and electrical conductivity (Ohmic) influences. These electromagnetic properties could also be functions of position and are influenced largely by the volumetric water contents and salt contents or concentrations vs. position. This requires a broad range of frequencies in an electromagnetic based measurement system as lower frequencies are needed to identify the EC (Ohmic) influences and higher frequencies are needed for the WC (dielectric or permittivity) influences.

3.) Frequency dependence on the dielectric properties of some of the constituents (including different dependencies for different constituents: e.g. bound, semi-bound and free water constituents). This also requires the use of a broad range of frequencies to separately identify these constituents as well as distinct models to represent those differing constituents.

4.) Temporal variation of some of the constituents (e.g. changing WC and/or salt content vs. time).

5.) Temperature dependence of the electromagnetic properties of the constituents.

6.) Measurement Noise: Both in terms of the measurement system (noise floor) and of the external environment (e.g. interference, etc.) due to the field nature of these measurements.

7.) Dynamic Range on Spatial Resolution: The ability to simultaneously identify fine features vs. position (with higher frequencies) vs. coarse spatial variation (with lower frequencies). This is influenced by the bandwidth of the measurement system with a wider bandwidth allowing for a wider range of spatial resolutions but often at the sacrifice of higher noise.

8.) Dynamic Range on Parametric (Property) Measurements: The range of variations detectable on a particular target parameter such as WC or EC. This is limited at the fine resolution ("small signal") by noise and on the high ("large signal") end by linearity limitations such as clipping or headroom in the measurement system. A narrow bandwidth would provide higher dynamic range (by lowering noise) but at the sacrifice of lower measurement speed due to the requirement of a swept measurement over wide ranges of frequency to cover the other issues above.

9.) Uniqueness of Solutions: A desired measurement situation where all relevant combinations of target parameters each result in their own unique measurement waveform.

Multiple variables leading to complex measurement needs can therefore result from the consideration of all of the above challenges. Larger numbers of variables or unknowns leads to a larger number of independent measurements that must be made to solve for all these unknowns. There are therefore limitations as to what measurements are possible given all of the above challenges. However, the greater amount of information that can be obtained via a series of measurements, the higher the probability of success in extracting the desired parameters such as WC and EC vs. position and time. Combining both a reflection and transmission measurement (e.g. TDR and TDT) together with utilizing info in both the time and frequency domains can provide a large amount of measurement info to resolve many variables. The measurement systems need to cover a wide range of frequencies from lower RF (lower MHz ranges) up to lower Microwave (several GHz) to individually resolve all of the frequency dependency issues.

A wide frequency range or wide bandwidth is one of the advantages of a measurement system such as TDR or TDT as it involves a fast rise time pulse (to give high frequency content) as well as moderate pulse widths and repetition rates (to give lower and moderate frequency content). However, as indicated, the wider bandwidth can lead to other limitations such as higher noise. Therefore post-processing in the frequency domain can provide additional benefits via the utilization of Digital Filtering to home in on performance in a narrower frequency band.

In addition, these measurements often include the need to profile the WC and EC or other relevant properties vs. position within the media (due to spatial heterogeneity) as well as trend these parameters vs. time (due to temporal variations). To identify and characterize the spatial heterogeneity requires partitioning the medium into smaller sub-regions (cascaded domains) to create finite elements on a mesh scale that permits the homogeneity assumption within those individual mesh elements concerning the stochastic constituent distributions or fractions. Spatial heterogeneity on larger macroscopic scales is then modeled by having different relative constituent fractions or distributions in different mesh elements or sub-regions. Trending these measurements vs. time for each element then provides the latter (temporal) component of the measurement.

In similar fashion, for guided electromagnetic methods such as TDR and TDT systems based on transmission lines, the line must be divided into these smaller cascaded segments or finite elements at a mesh scale to satisfy the assumptions of homogeneity at the individual element level while still allowing for heterogeneity at the overall system or cascaded transmission line level. A successful measurement algorithm will then be able to individually de-convolve (time domain) or de-embed (frequency domain) those internal elements based on external system boundary measurements (in both the time and frequency domains) to extract the relevant parameters for each individual internal element. The external system boundary measurements would be at the input of a cascaded transmission line for a TDR system and at both the input and output of a cascaded transmission line network for a TDT system (with more information thus available with the latter system). A schematic 1D network representation of this type of cascaded transmission line partitioned into finite elements is shown in the following figure:

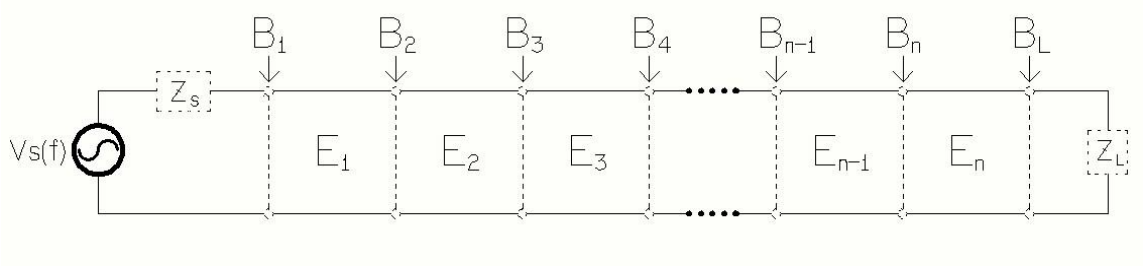


Figure 3.1: Finite Element Representation of a Cascaded Transmission Line

Where

$Vs(f)$ = Input AC Source (Broadband Multiple Frequency Source for TDR & TDT)

$Z_S$ = Source Impedance (Typically near 50 Ohms)

$Z_L$ = Load Impedance (Typically near 50 Ohms for TDT and Open Circuit for TDR)

$E_n$ = Element n (with Homogeneous Electromagnetic Property Distributions across the Element)

$B_n$ = Boundary between Element "n" and Element "n-1"

$B_L$ = Boundary between Last Element "n" and the Load Impedance

Again, the assumption is that each finite mesh element has consistent stochastic distributions of its constituents (e.g. Water Content, Solids Content, etc.) across the element and thus can be considered to be homogeneous from an electromagnetic perspective over that element. By cascading elements of different properties the heterogeneity of the entire line can be modeled. The overall transmission line of multiple elements is modeled utilizing Scattering (S) Parameters and Transmission (T) Parameters [8] the details of which are described in Appendix B.

The forward prediction models utilize physically based electromagnetic wave propagation models at both the individual element level as well as at the overall (macroscopic) cascaded transmission line system level (see figure 3.1). The following are examples of the types of models developed at each level:

1.) Models Developed at the Individual Element or Transmission Line Segment Level:

- Identification of All Constituents within a Particular Element (each $E_n$ as shown in figure 3.1):
    - Gases (Typically Air for Soils although other gases could be modeled)
    - Solids
        - Minimally to Non-Charged Interfaces & Coarser Sized Particles: Sand
        - Minimally Charged Interfaces & Intermediate Sized Particles: Silt
        - Moderately Charged Interfaces & Intermediate Sized Particles: Organic Matter
        - Highly Charged Interfaces & Very Fine Particles: Clay
    - Liquids: Primarily Water (Although other non-Water Liquids could also be modeled)
        - Bound Water (at Charged Interfaces)
        - Semi-Bound Water (Distribution rolling off with Distance from Charged Interfaces)
        - Free Water (Sufficiently Far from Charged Interfaces)
- Electrical Conductivity of Each Constituent
- Frequency Domain Models of Electric Permittivity of Each Constituent.
- Stochastic Volumetric Fractions or Distributions of Constituents within a Given Element $E_n$
    - Porosity and Solids Stochastic Fractions: Treated as Constants vs. Time.
    - Volumetric Fractions of Water Constituents and Air Constituent: Treated as Variables.
- Composite Mixing Models for both the Electrical Conductivity and Electric Permittivity
    - Different Stochastic Models between Bounds of Parallel & Serial Constituent Models all in the Frequency Domain.
- Frequency Domain Electromagnetic Wave Propagation Constant $\gamma$ (function of medium properties & probe geometry)
- Frequency Domain Electromagnetic Characteristic Impedance Z (function of medium properties & probe geometry)
- Physical Length of Each Element

2.) Models Developed at the Overall Cascaded Transmission Line System Level:

- Identification of an Impedance Boundary / Interface between Each Element for the Entire Network (at each $B_n$ as shown in figure 3.1).
- Identification of a Propagation / Transmission Term to Model Propagation and Loss within Each Element $E_n$ for the Entire Network (each a function of the specific propagation constant $\gamma$ and element length L for each independent element).
- Frequency Domain Reflection Coefficient $\Gamma$ at each Impedance Boundary $B_n$ between the Elements $E_n$ (Function of Impedance Discontinuities between Elements).
- Development of the Scattering (S) Parameters and Transmission (T) Parameters [8] in Frequency Domain for each Impedance Boundary/Interface $B_n$ between Each Element (Both Reflection and Transmission Terms).
    - S11, S21, S12 & S22 at Each Boundary (S-Parameters Defined in Appendix B)
    - T11, T21, T12 & T22 at Each Boundary (T-Parameters Defined in Appendix B)
- Development of the Scattering (S) Parameters and Transmission (T) Parameters in Frequency Domain for each Element ($E_n$) Propagation Term (within the Actual Element) (Forward and Reverse Transmission Terms Only).
    - S21 & S12 within Each Element (Again S-Parameters Defined in Appendix B)
    - T11 & T22 within Each Element (Again T-Parameters Defined in Appendix B)
- Development of Overall Cascaded Transmission Line Models for the Entire Network in the Frequency Domain using three different methods:
    - Equivalent Overall S-Parameters from Mason's Non-Touching Loop Rule
    - Equivalent Overall T-Parameters from Matrix Multiplication
        - Conversions between T-Parameters and S-Parameters
    - Nested Construction Method (Simplified Alternative for S11 and S22 Only)
- Generation of Frequency Domain Representation of the Time Domain Stimulus (Pulse) via a Fast Fourier Transform (FFT) on the Pulse Waveform.
- Multiplication of the Frequency Domain Representation of the Pulse with the Frequency Domain Representation of the Overall S-Parameters to Give a Frequency Domain Representation of the Reflected Signal at the Input (TDR and TDT) and Transmitted Signal at the Output (TDT).

– Perform an IFFT on these two Frequency Domain Representations to Obtain a Simulation of the Reflected Time Domain Signal (TDR and TDT) and Transmitted Time Domain Signal (TDT).

Scattering (S) Parameter along with Mason's Non-Touching Loop rule and Transmission (T) Parameter network theory and finally the Nested Construction Method are all utilized to construct the overall network from the individual elements or cascaded segments (cascading all the individual elements together to form the overall transmission line models). These modeling techniques are described in detail in Appendix B.

As indicated earlier a wide frequency range or wide bandwidth is one of the advantages of a measurement system such as TDR or TDT as it involves a fast rise time pulse (to give high frequency content) as well as moderate pulse widths and repetition rates (to give lower and moderate frequency content). The wide bandwidth is necessary to account for the frequency dependence of the constituents in each element $E_n$ as well as to allow for resolving the fine element geometries. However, this presents other measurement challenges as a wider bandwidth system typically has higher noise and lower dynamic range vs. a narrow band measurement system such as a Vector Network Analyzer (VNA). Another challenge (although not necessarily a disadvantage) is that a wide bandwidth system such as TDR and TDT when combined with a shorter to moderate length transmission line probe is essentially the combination of a lumped element and distributed element (wave propagation) measurement system. A purely lumped element system is where the wavelengths of the particular frequency components are long compared with the dimensions of the transmission line probe ($\lambda_S > 10L$) where $\lambda_S$ is the shortest wavelength (due to the highest frequency) in the measurement system and L is the length of the probe. In contrast a purely distributed element system is where the dimensions of the transmission line probe are significant in comparison to even the longest wavelength $\lambda_L$ (of the lowest frequency) in a measurement system ($L > 0.1\lambda_L$) and potentially very long compared to the shorter wavelengths (higher frequencies) in a particular measurement system ($L >> \lambda_S$). A TDR or TDT system is actually a varying degree hybrid of both a lumped element and distributed element system depending on the particular frequency range and the specific probe geometry.

The frequency range of a TDR or TDT system can be divided into the following zones as shown in table 3.1 when considering also the frequency dependence of the constituents of soils:

**Table 3.1: Different Frequency Zones/Ranges in a TDR/TDT System**

| Zone | Equivalent Probe Model | Primary Sensitivity (Lossy Media) | Primary Sensitivity (Low Loss Media) | Frequency Range & Criteria |
|---|---|---|---|---|
| Zone 1 | Lumped Element (Entire Probe) | Electrical Conductivity $\sigma$ (Bulk Equivalent for Entire Probe) | Ending Termination TDR: ~ Open Circuit TDT: ~ 50 Ohms | Lowest Frequencies $F < \sigma/(2\pi\lvert\varepsilon^*\rvert)$ |
| Zone 2 | Lumped Element (Entire Probe) | Electric Permittivity Real Term ($\varepsilon'$) & Imaginary (Loss) Term ($\varepsilon''$) (Bulk Equivalent for Entire Probe) | Electric Permittivity Real Term ($\varepsilon'$) (Bulk Equivalent for Entire Probe) Together with Ending Termination if TDT | Moderate Frequencies $F \geq \sigma/(2\pi\lvert\varepsilon^*\rvert)$ but Still Satisfies Lumped Element Model |
| Zone 3a | Distributed Element (Overall Probe Length) | Electric Permittivity Real Term ($\varepsilon'$) & Imaginary (Loss) Term ($\varepsilon''$) (Equivalent Distributed Model for Entire Probe) | Electric Permittivity Real Term ($\varepsilon'$) (Equivalent Distributed Model for Entire Probe) | Higher Frequencies $F \geq 0.1\ (V_{PP}/L_P)$ Transmission Line Effects Apply |
| Zone 3b | Distributed Element (Even At $E_n$ Lengths) | Electric Permittivity Real Term ($\varepsilon_n'$) & Imaginary (Loss) Term ($\varepsilon_n''$) (Equivalent Distributed Models for each specific $E_n$) | Same as Lossy Media for Zone 3b (Generally All Geophysical and Biological Media Exhibit some Loss by these Frequencies) | Highest Frequencies $F \geq 0.1\ (V_{PEn}/L_{En})$ Transmission Line Effects Apply even Within each $E_n$ |

Where $\sigma$ = Electrical Conductivity

$\varepsilon'$ = Real or Energy Storage Term of Electric Permittivity

$\varepsilon''$ = Imaginary or Loss Term of Electric Permittivity

$|\varepsilon^*|$ = Magnitude of the Complex Permittivity ($|\varepsilon^*| = |\varepsilon' - j\varepsilon''|$

where $j = \sqrt{-1}$ )

$V_{PP}$ = Equivalent Phase Velocity of Waves along Entire Probe (Zone 3a)

$V_{PEn}$ = Equivalent Phase Velocity of Waves within a Particular Element $E_n$

$L_P$ = Length of Entire Probe (TDR or TDT)

$L_{En}$ = Length of an Individual Mesh Element $E_n$

F = Frequency

1.) Zone 1: Lower Frequency Zone/Range: The lower frequency portion of the TDR or TDT spectrum actually sees the entire probe simultaneously as a single “Lumped Element” due to the long wavelengths compared to the probe length. Zone 1 frequencies are sensitive mainly to the lumped impedance contribution from the electrical conductivity influencing a lumped shunt (electrode to electrode) conductance term for the probe model for a lossy medium with moderate to higher conductivity. The boundary between Zone 1 and Zone 2 in frequency depends on the level of conductivity relative to the permittivity components (real and loss terms of the permittivity) (higher conductivity means a higher frequency transition from Zone 1 to Zone 2). Note: if conductivity is zero then the Zone 1 frequencies are sensitive only to the ending termination (open circuit for TDR & 50 Ohms for TDT). This can be seen in figures D.1 – D.4 in Appendix D in examining the longer time settled values.

Zone 2: Medium Frequency Zone/Range: This frequency range still sees the entire probe as a single “Lumped Element” (i.e. the geometry of the probe is still small compared to the wavelengths of the propagating signals in this frequency range) but in this range the lumped impedance is sensitive to mainly the permittivity terms (i.e. as frequency increases in Zone 2 the conductivity eventually is much lower than the magnitude of either the loss (imaginary) components or storage (real) components of the permittivity multiplied by angular frequency (i.e. $\omega\varepsilon'' = 2\pi F\varepsilon'' >> \sigma$, and/or $\omega\varepsilon' = 2\pi F\varepsilon' >> \sigma \rightarrow F \geq \sigma/(2\pi|\varepsilon^*|)$ ) .

Zone 3: Higher Frequency Zone/Range: In this zone the probe geometry becomes significant with the wavelengths of the signals in this frequency range and the probe must be considered as a transmission line with distributed elements. As frequencies proceed further up in Zone 3 they become independently sensitive to finer geometries and features within the probe in terms of impedance changes and therefore can resolve those finer impedance changes vs. position (Initially the entire probe (Zone 3a) and eventually the individual elements $E_n$ (Zone 3b)). The actual transition frequency between Zone 2 and Zone 3 depends on the geometry or length of the probe. Zone 3 frequencies are primarily sensitive to the permittivity (both real (storage) and imaginary (loss)) terms in a medium.

Note that Zone 3 is divided into two separate sub-zones (lower and higher frequency ranges within Zone 3). It is important to note that if Zone 3b frequencies were not present in a TDR/TDT spectrum then it would be impossible to resolve the probe/media properties at the individual finer

(finite mesh element $E_n$) level. Therefore, the dimensions of the mesh elements must be chosen based on the higher frequency components or bandwidth limitations of the TDR and TDT systems to insure that those individual elements are resolvable. These types of tradeoffs will be discussed further in the later chapter describing limitations associated with these types of measurement systems and associated algorithms. Another item that comes into play is the cost of a system that will clearly go up as the bandwidth of the system goes up.

Various implementations of electromagnetic wave propagation measurement methods such as TDR, TDT, waveguides, Ground Penetrating Radar (GPR) and Microwave Remote Sensing are gradually gaining acceptance as the methods of choice for measuring WC and/or EC in soils and other geophysical and biological media. However, early implementations of these technologies have still relied on a great amount of site specific calibration and/or empirical regression equations and only limited attention has been focused on using physically based electromagnetic wave propagation models. Therefore, there are many limitations or bounds on the existing implementations of these methods including limitations on WC measurement accuracy when EC and/or the dielectric loss component of the permittivity is high leading to frequency dependent dispersion and attenuation effects on the propagating waves. Also there is great variation on geometrical zone of influence of these measured parameters (based on the various frequency ranges of the techniques). Lower frequencies favor deeper penetration but at the cost of coarser resolution and higher frequencies favor finer resolution but at the cost of lesser penetration depth.

In addition there is currently not a good solution for measuring the parameters vs. position especially in lossy media (i.e. most of the current methods perform an overall average measurement of the parameters and don't profile them vs. position). Finally, some of the methods (especially solely lumped element methods such as capacitance probes) don't use frequencies high enough to insure that only water is influencing the electric permittivity measurement. This becomes an issue in the case of high EC where there may not be sufficient phase shift in the measurement to extract out the capacitive component to measure the permittivity and therefore water content accurately (i.e. they end up with only Zone 1 frequencies). Therefore, there is a great need to provide improved measurement interpretation algorithms that incorporate physically based models accounting for all the electromagnetic parameters and minimizing the reliance on empirical regression equations and site-specific calibration.

This project has therefore focused on providing such a physically based set of forward based prediction models and inverse interpretation algorithms for the various implementations of electromagnetic WC and EC measurement systems. One goal was investigating the feasibility of developing a TDR or TDT WC and EC measurement system for soils (and applicable to other media such as foods) that is accurate even at high levels of EC. Another goal was investigating the feasibility of developing a profiling algorithm to measure the WC vs. position along a transmission line probe for low to moderate values of EC.

The high frequency portion of the frequency domain information (Zone 3) is key to being able to extract water content from the data when electrical conductivity is high and/or charged interfacial mechanisms are present (e.g. clay) and is also important for being able to resolve finer mesh elements $E_n$ when accounting for spatial heterogeneity (i.e. profiling). The medium frequency portion (Zone 2) is important in determining water content at lower to moderate levels of conductivity and/or separately identifying influences of charged interfacial processes such as those associated with Clay. Finally the low frequency information (Zone 1) is key to determining the electrical conductivity itself. Also, the time domain information can be used to extract the water content profile vs. position when EC is low to moderate.

An important note is that since Zone 2 and Zone 1 frequencies are normally associated with the "lumped element" portion of the TDR/TDT system spectrum it would normally not be possible to profile those specific parameters identified solely in those zones vs. depth. For example an overall average electrical conductivity for the entire probe can normally be all that is expected for that parameter and a fine resolution profile of EC vs. depth is typically not possible (especially with a TDR system). However, a TDT system can provide more information to allow for some level of profiling of EC vs. position (as there are now two different locations where EC can be measured). In addition, other assumptions associated specific to a particular soil can be made to indirectly correlate EC to Water Content (for example assuming salt concentrations or salinities of the water are inversely proportional to water content – an assumption that is only valid if the salts inherent in the soil are large in content compared to the externally applied salts coming in from either irrigation water or rainfall). This can lead indirectly to an EC profile vs. position based on the WC profile vs. position and the two EC measurements at both boundaries (in a TDT system). However, this assumption would only be valid if the EC is dominated by the

salts in the water solution and the solids fraction do not contribute significantly to the EC (typically valid for most soils although not all soils).

In contrast, both the real (storage) and imaginary (loss) components of the electric permittivity associated with free water can be profiled vs. position as it shows up in the higher frequency portion of the spectrum (Zone 3). Therefore the WC associated with free water can be profiled vs. position even in the presence of higher EC. However, variation of the frequency dependence of permittivity as free water transitions to semi-bound water and eventually to fully bound water brings the functions down into Zone 2 frequencies and so there can be limitations at to how well bound and semi-bound water can be profiled vs. position along the probes. All of this is addressed in this dissertation in the chapters to come. There are certainly limitations as to what is possible with these types of measurements and that analysis will be provided fully in a later chapter but touched on briefly in this chapter as well in appropriate locations where different aspects of the models are developed and described.

TDR and TDT data was collected over a wide range of soil conditions, water contents and electrical conductivities to aid in the development and validation of the forward prediction models and inverse algorithm and finally to conclude on the commercial and technical feasibility of the proposed TDR and TDT systems. In response to these objectives TDR data was obtained in the field (several soil types and conditions) and both TDR and TDT data was collected in the laboratory using different types of measurement instrumentation and TDR/TDT probes/fixtures over a wide range of water contents and electrical conductivities. In parallel with this the software algorithm was developed and enhanced and simulation runs were generated and compared to the actual data in both the frequency and time domains using Fast Fourier Transform (FFT) and Inverse Fast Fourier Transform (IFFT) algorithms. These comparisons are presented in the next chapter on validation of the forward prediction models. This chapter will focus on the underlying theory and components of the forward prediction model.

**Forward Prediction Model Background Theory:**

Existing TDR water content measurement systems relate the volumetric water content (WC) to some other measurable parameter such as the soil dielectric constant, TDR transit time or the phase velocity of the TDR waves via empirical regression models. Two of the more popular historical models (shown below) are the Topp equation [21] (relating water content to the dielectric constant) and the index of refraction equation [22] (relating water content to the ratio of the phase velocity of waves in free space to the phase velocity of waves in the soil).

The following mathematical models are utilized to relate water content to measured electromagnetic parameters in existing TDR instrumentation:

Topp Equation:

$$\theta = A_0 + A_1 \varepsilon_r + A_2 \varepsilon_r^2 + A_3 \varepsilon_r^3 \quad (3\text{-}1)$$

(Empirical Linear Regression - Multi-Point Calibration)

Index of Refraction Equation:

$$\theta = K_1 + \frac{K_2}{V_{p_T}} \quad (3\text{-}2)$$

(Partially Physically Based - Two-Point Calibration)

Where:

$\theta$ = Volumetric Water Content

$\varepsilon_r$ = Relative Electric Permittivity or Dielectric Constant

$A_0 \rightarrow A_3 =$ Empirical Regression Coefficients

$V_{PT}$ = Equivalent Phase Velocity in Composite Soil Mix

$\frac{K_2}{V_{PT}} \cong \sqrt{\frac{\varepsilon_r \varepsilon_0}{\varepsilon_0}} = \sqrt{\varepsilon_r}$ = Index of Refraction

$K_1, K_2$ = Coefficients either Physically Derived from Electromagnetic Models or Fitted by Regression

($K_2 \cong$ Phase Velocity in Free Space)

As indicated $A_0$ through $A_3$ are empirically derived constants (via linear regression) and $\varepsilon_r$ is the real portion of the dielectric constant and where $K_1$ and $K_2$ are constants that can either be empirically derived (linear regression on field data) or exactly derived from electromagnetic theory and composite soil models. $K_2$ is typically close to the phase velocity of waves in free space and $V_{p_T}$ is the effective phase velocity of the transmission line in an overall soil mix of the three phases of solids, water and air. The ratio of $K_2 / V_{p_T}$ is the index of refraction.

Both of these models are largely dependent on empirical regression data in their present use (although the index of refraction model can be approximately derived from electromagnetic models per Appendix A and the Literature Review Chapter) and also are largely dependent on the accurate determination of either TDR transit time and/or phase velocity. In the presence of high salinity or electrical conductivity it becomes difficult if not impossible to determine transit time and phase velocity from a TDR trace in that the second reflection disappears due to high attenuation or is spread out due to high dispersion. Also, in the presence of high conductivity, the time domain trace decays exponentially (figure D.3 in Appendix D) due to frequency dependent reflections due to variations in the characteristic impedance with frequency of the transmission line that makes up the TDR probe (Lower impedance with lower frequency as will be shown later when the mathematical models are developed). Therefore new enhanced physically based models based on the theory of electromagnetics to address these issues are presented in this dissertation.

## Forward Prediction Model:

There are two basic versions or complexity levels for the TDR/TDT Forward Prediction Models:

- Simplified (Base) Version for WC & EC that Predicts TDR and TDT Waveforms as a Function only of the Shunt (Between Electrodes) Terms ($\sigma$, $\varepsilon'$, and $\varepsilon''$) for Various Probe Geometries.

- General Purpose Version for Predicting TDR Waveform as a Function of Impedance Z and all its constituents ($\sigma$, $\varepsilon'$, $\varepsilon''$, $\mu'$, $\mu''$ and Rs, accounting for all series (along electrode) and shunt (between electrodes) terms) vs. position along the probe for Different Probe Geometries (w/terms defined later in this section).

Assumptions behind Forward Prediction Model for Soils:

Here we assume:

- That the soils is a homogenous but stochastic mixture of solids, water and air in the soil specific to each element (at the finite element mesh level $E_n$).
- That the permittivity (real and imaginary) terms of solid components are constant with frequency.
- That the permittivity (real and imaginary) terms of free water component varies with frequency due to a dielectric relaxation resonance as predicted by the Debye model including also temperature dependence.
- That the permittivity (real and imaginary) terms of semi-bound water components varies with frequency due to a stochastic distribution and summation of Debye models with progressively lower dielectric relaxation resonances as the semi-bound water approaches fully bound water (i.e. as the charged interfaces of the solids are approached).
- That the permittivity (real and imaginary) terms of fully-bound water components are significantly lower than free water and are almost independent of frequency (very slight/mild relaxation resonances near or below 10 MHz).
- That the electrical conductivity $\sigma$ is constant and independent for each solid component in the mixture and equal to zero for the air component. Electrical conductivity $\sigma$ is only a variable for the liquid water component of the mixture.
- That the system consists of non-magnetic soil/food components/constituents (e.g. $\mu'/\mu o = 1$, $\mu'' = 0$).
- That the TEM wave propagation mode down a transmission line is in a linear isotropic media from an electromagnetics standpoint (e.g. permittivity and electrical conductivity are not anisotropic tensors).
- That there is no significant radiative loss component.
- That non-ideal connectors can be accounted for as additional cascaded sections to the transmission line.

Inputs to Optimize Water Content/EC Prediction Model for Foods and Soils

In order to fully describe the conditions effecting propagation the following four sets of soil based Calibration Constants which embody all the information required (for each transmission line cascaded element $E_n$) must be identified. These are the:

- Air Filled Porosity $\phi$ (Pore Volume Fractions when Empty: WC = 0).
- Solid Component(s)/Constituent(s) Complex Dielectric Constant(s).
- Solid Component(s)/Constituent(s) DC Electrical Conductivity(s).
- A-priori information on Macroscopic Spatial Heterogeneity Associated with the Soil Structure

Similarly, the following five parameters will be assumed sufficient to serve as Calibration constants for the probe. These are the:

- Transmission Line Geometry Factors (A scale factor that is a function of the specific probe geometry impacting characteristic impedance of the probe transmission line).
- Connector Geometry Factor (A scale factor that is a function of the specific connector geometry or interfacing interconnection geometry impacting characteristic impedance of the connector).
- Connector Dielectric Constant
- Connector Electrical Conductivity.
- Termination Impedance (Approximate Open Circuit for TDR and near 50 Ohms for TDT).

The following are the Input Variables for the forward prediction models:

- Electrical Conductivity of Water Component: $\sigma_w$
- Volumetric Water Content for each Finite Element ($E_n$): $\theta_n$
- Bulk Electrical Conductivity of each Finite Element ($E_n$): $\sigma_n$

(Derived from $\theta_n$, $\sigma_w$ and Electromagnetic Mixing Models presented in this dissertation)

- Frequency: f

The following are the Outputs of the forward prediction models:

- Frequency Domain S-Parameters:

  S11 = Input Net Reflection Coefficient of Overall Network (TDR & TDT)

  = $f1\ (\theta_n, \sigma_w, f)$

  S21 = Forward Net Transmission Coefficient of Overall Network (TDT)

  = $f2\ ((\theta_n, \sigma_w, f)$

- Time Domain Prediction of TDR and TDT traces:
  - TDR: Inverse Fast Fourier Transform (IFFT) on the product of S11 (in the frequency domain) and the FFT of a step or pulse.
  - TDT: IFFT on the product of S21 (frequency domain) and the FFT of a step or pulse.

Note: The above frequency domain S-Parameters and time domain TDR/TDT predictions will in a real world measurement system be functions of time on a very coarse scale (as wetting fronts / infiltration proceeds into the soil over hours and days). Therefore, any final instrumentation containing algorithms based on these models should sample at a rate that will capture all important temporal changes. But this is again a very coarse long time scale (perhaps sampling at several minute intervals to capture temporal changes measured over hours and days). In contrast, the measurement time lengths of the TDR/TDT waveforms are measured in microseconds, nanoseconds and picoseconds (so tiny fractions of a second). In addition, the models divide the probe into several cascaded elements ($E_n$) but the measured outputs are only available at the probe terminations (Inputs/Outputs). Therefore, all information about how the parameters vary along the probe must be extracted out of the terminal measurements. Methods on how to accomplish this will be presented in this dissertation.

In summary there are a modest number of calibration constants that must be identified for the specific probe types and soil types to enable the forward prediction models. The outputs of the forward prediction models then simply become functions of the water content of each element ($\theta_n$) as well as the electrical conductivity of the water ($\sigma_w$ and resulting bulk $\sigma_n$) and finally are also a function of frequency. A measurement system inverse algorithm will then perform the reverse operation in extracting the water content and bulk electrical conductivity profiles by fitting the measured data to pre-run predictions from the forward prediction models (involving lookup tables and optimization/fitting algorithms).

## Guided / Bounded Waves in a Lossy Homogeneous Medium: Transmission Lines.

TDR and TDT systems fall under the category of guided or bounded electromagnetic wave propagation technologies and more specifically transmission lines where two or more conductors are used to "guide" the waves in a particular direction or path [12-17]. Two examples of guided transmission lines are shown in the following figures for 2-wire and 3-wire TDR probes respectively (also showing a wetting front in the soil showing the importance of profiling vs. depth).

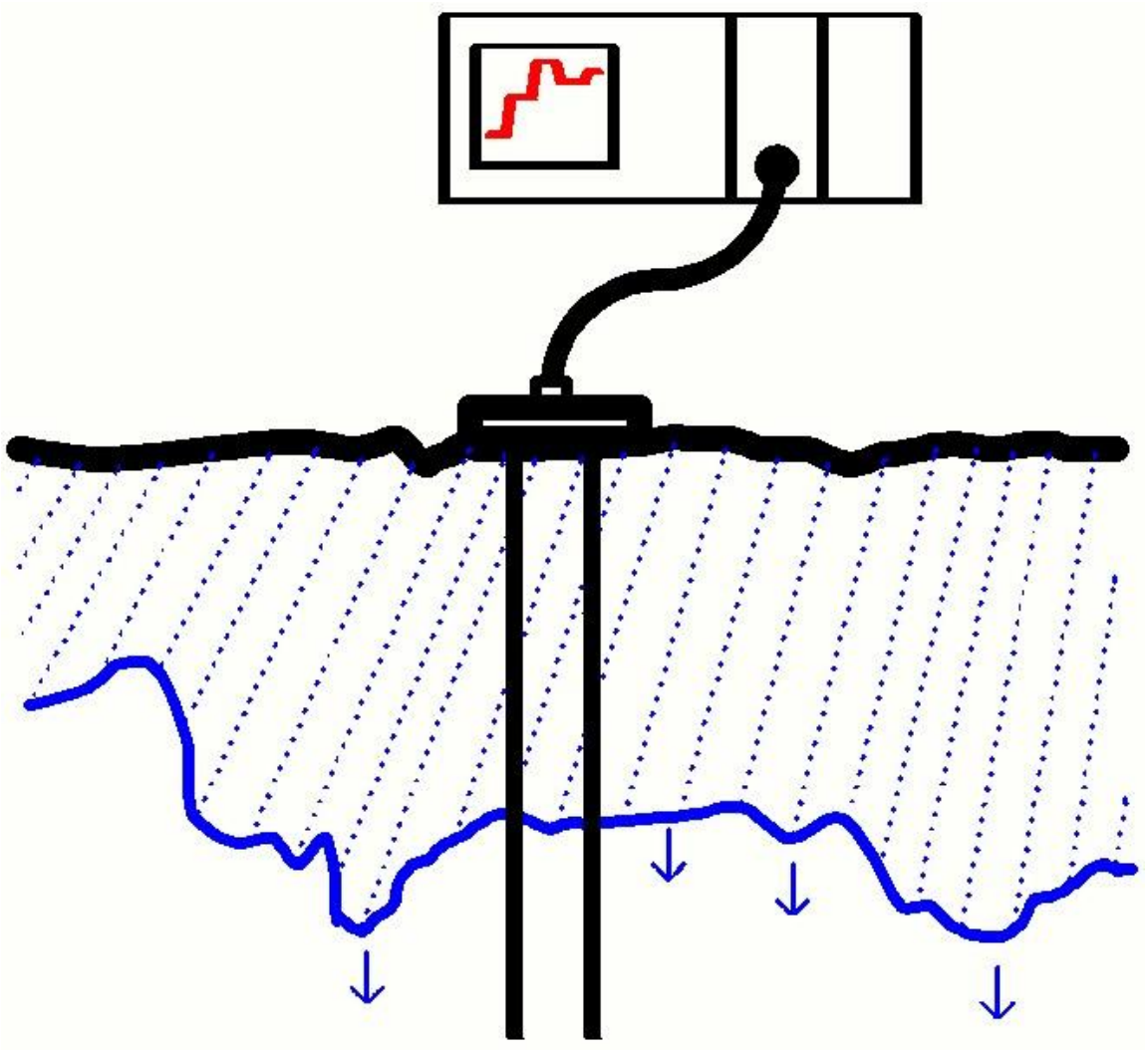

Figure 3.2a: 2 Wire TDR Probe in a Soil with a Wetting Front

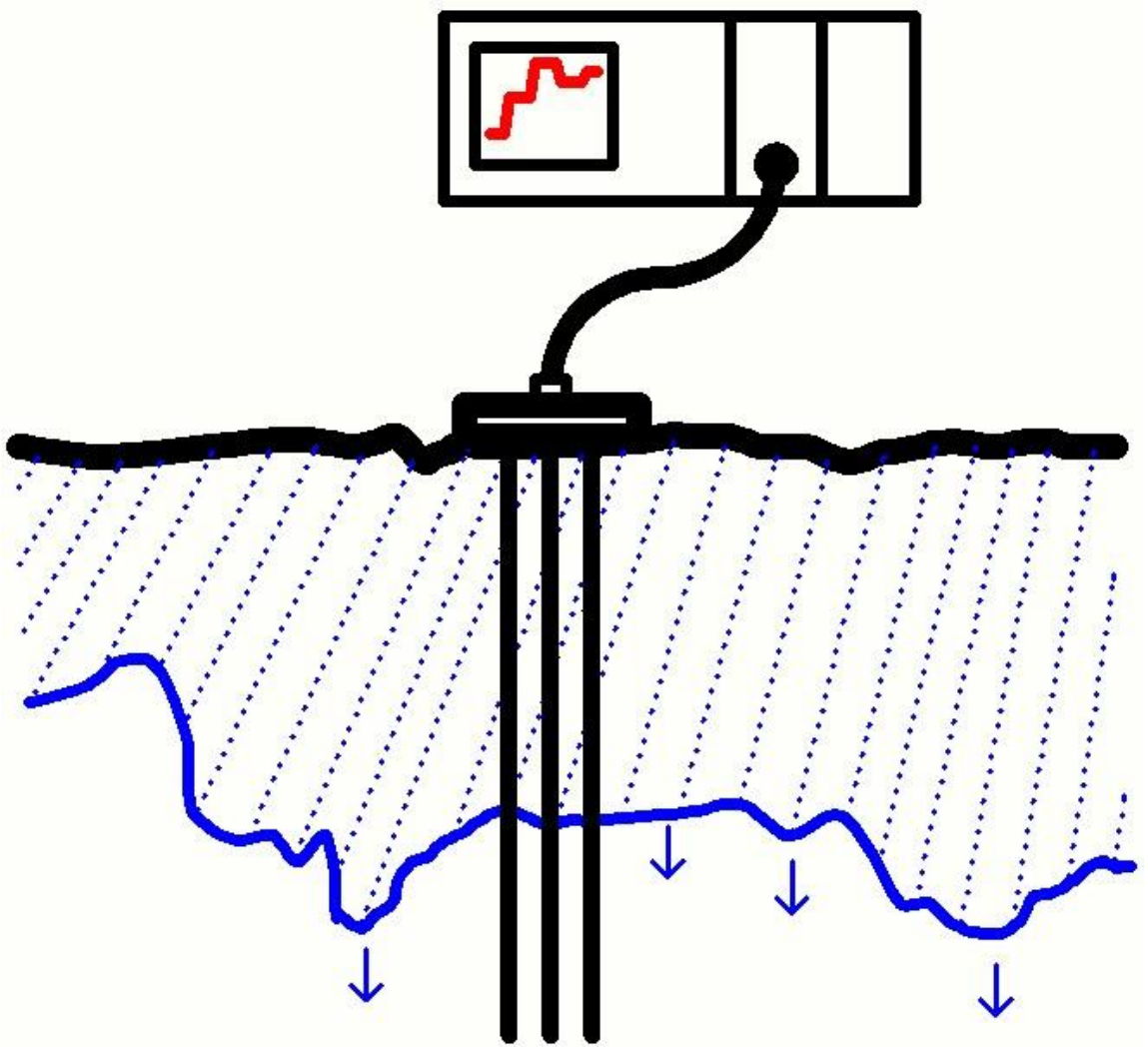

Figure 3.2b: 3-Wire TDR Probe in a Soil with a Wetting Front

Models from the theory of electromagnetics for the propagation and reflection of waves along various types of transmission lines are shown in Appendix A. One particular important parameter that influences the propagation and characteristic impedance of the waves is the loss tangent. The loss tangent (as defined in Appendix A (A-10)) is important in that when it is greater than one the loss terms are dominating and when it is less than one the dielectric or storage terms are dominating in terms of influencing the electromagnetic propagation and impedance functions. As will be shown later, this fact is fundamental in being able to separate out water content from electrical conductivity when conductivity is high. The measured scattering S-parameter information (described in Appendix B) must be examined at frequencies above where the loss

tangent drops below 1 (excluding complex permittivity) to be able to extract the dielectric information and water content values from the data (Zone 2 and Zone 3 frequencies in a TDR/TDT system). In contrast the value of electrical conductivity can be extracted from low frequency information (Zone 1 frequencies in a TDR/TDT system) where the loss tangent becomes greater than one (if conductivity is non-zero).

This use of different portions of the frequency domain information to extract water content and electrical conductivity is one of the key approaches used by the algorithms presented in this dissertation. This can be illustrated by taking equations A-31 and A-32 (Appendix A) and derive expressions for the phase velocity, transmission coefficient and characteristic impedance vs. frequency (developing expressions similar to the earlier equations in (A-7 to A-10, A-16 to A-19 in Appendix A) but for the parallel wire geometry transmission line):

Transmission Coefficient (2-Wire Probe - Forward Propagation Only – Neglecting End Reflections):

$$T_{2WP} = e^{-\gamma_T L_T} = e^{-(\alpha_T + j\beta_T)L_T} \tag{3-3}$$

Where

$T_{2WP}$ = Transmission Coefficient

$L_T$ = Length of the Probe (meters)

$\gamma_T$ = Equivalent Propagation Constant (from equation (A-31))

$\alpha_T$ = Equivalent Attenuation Constant = real($\gamma_T$)

$\beta_T$ = Equivalent Phase Constant = imag($\gamma_T$)

From the above the phase velocity can be derived as follows:

$$V_{P_T} = \frac{\omega}{\beta_T} = \frac{\omega}{\text{imag}(\gamma_T)} \tag{3-4}$$

Where

$V_{P_T}$ = Phase Velocity along the 2-Wire Probe Inserted in a Particular Medium

Examples of information that can be extracted at different portions of the spectrum are illustrated in the following plots (which utilize equations A-31 and A-32 (Appendix A) and 3-3 and 3-4) applied to a special case where the parallel wire is inserted into a liquid (free (unbounded) water of different values of electrical conductivity)).

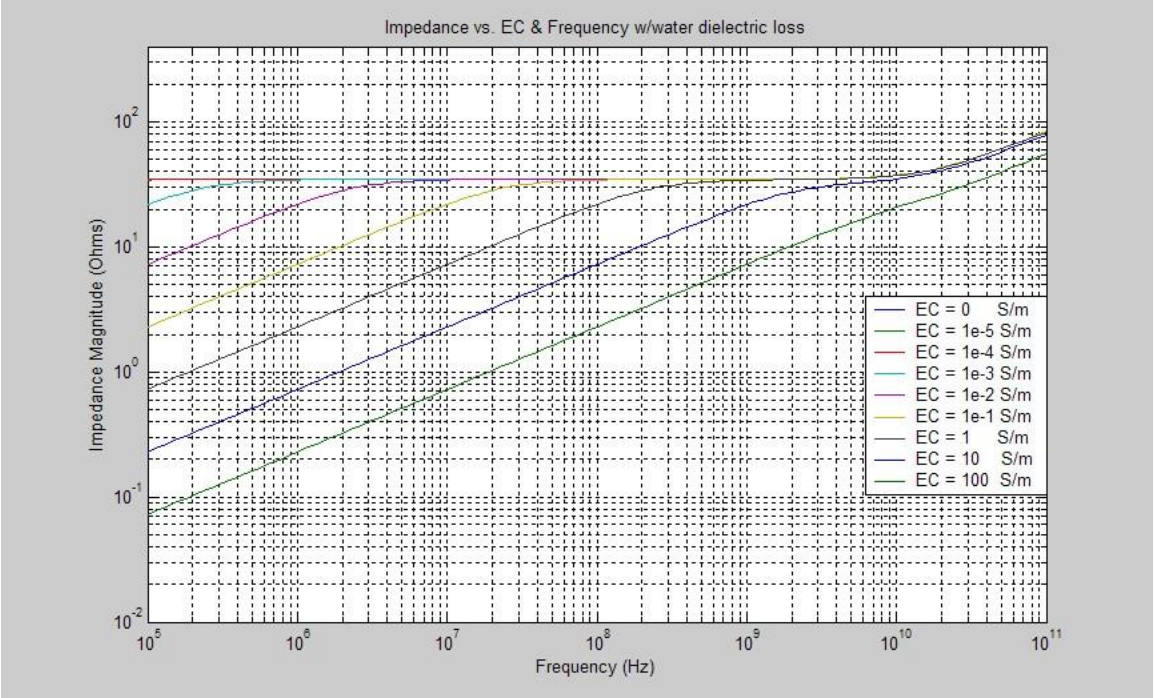


Figure 3.3: Characteristic Impedance (equation (A-32)) vs. EC &Frequency (2-Wire Probe in Water)

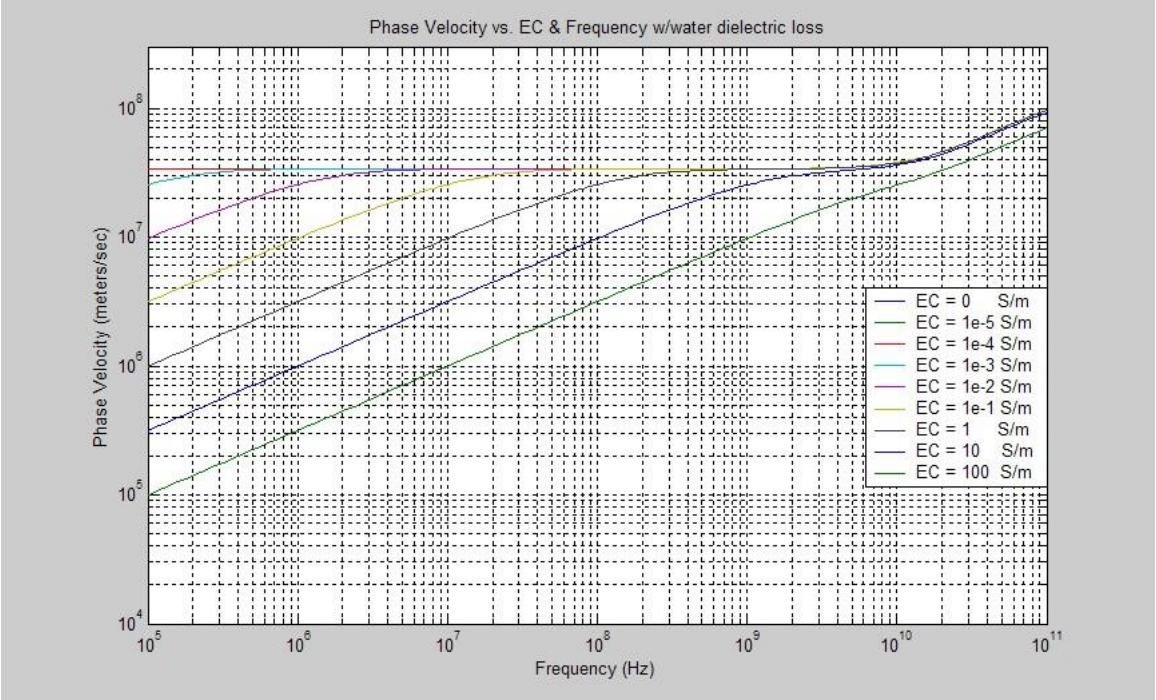


Figure 3.4: Phase Velocity (equation (3-4)) vs. EC & Frequency (2-Wire Probe in Water)

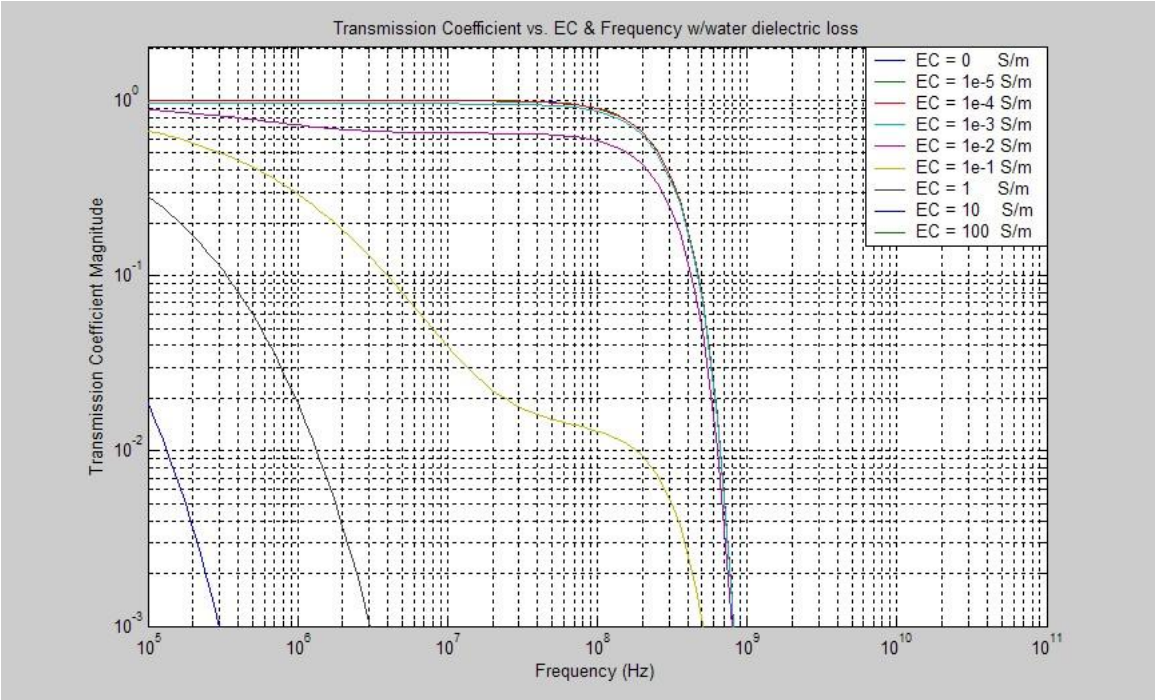


Figure 3.5: Transmission Coefficient (equation (3-3)) vs. EC & Frequency (1m long 2-Wire Probe in Water)

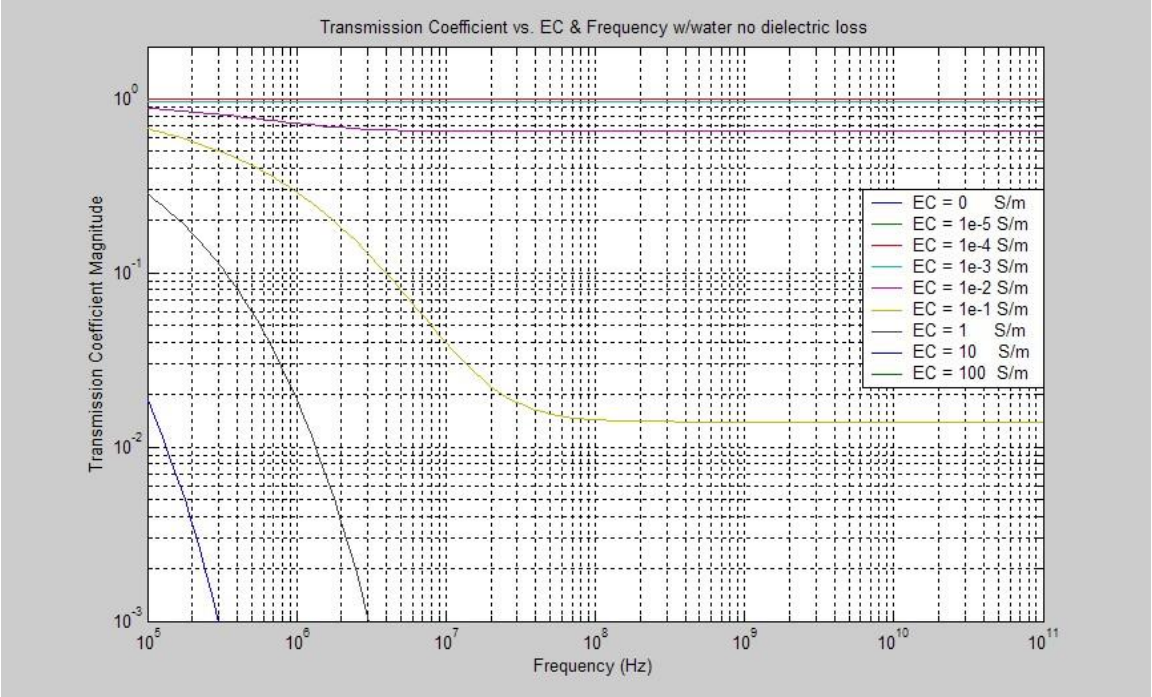


Figure 3.6: Transmission Coefficient vs. EC & Frequency (2-Wire Probe in Water but Dielectric Loss (ε") Removed from Expression – to illustrate contributions to lower frequency loss from EC alone).

These figures show the following:

1.) Low Frequency (~Zone 1) Effects dominated by Electrical Conductivity (EC):

   a. The characteristic impedance (figure 3.3) drops off with decreasing frequency with the corner frequency increasing with increasing EC.

   b. The phase velocity (figure 3.4) also drops off (retards) with decreasing frequency again with the corner frequency increasing with increasing EC. This results in low frequency dispersion.

   c. The transmission coefficient has loss initiating even at very low frequencies in the presence of moderate to high conductivity.

2.) Moderate (Mid-Range) Frequencies (~Zone 2) Dominated by Permittivity of Water (Real Portion)

   a. There is a plateau in the characteristic impedance (figure 3.3) in mid-range frequencies where the effects of permittivity dominate over the EC. The lower corner frequency is dependent on EC.

b. There is a plateau in the phase velocity (figure 3.4) in mid-range frequencies where again the effects of permittivity dominate over the EC. The lower corner frequency is again dependent on EC.

c. There is a bench that is visible (for low to moderate EC values) in the transmission coefficient (figures 3.5 and 3.6) where attenuation ceases to increase due solely to the effects of EC. This corresponds to the frequency where permittivity dominates over EC. However, the attenuation already occurring at lower frequencies is preserved to higher frequencies (along that bench) and if the EC is very high the attenuation swamps all but the lowest frequencies in a signal.

3.) Very High Frequencies (~Zone 3) Dominated by Both Permittivity Terms of Water (Real & Imaginary Portion) and Dielectric Relaxation Phenomena.

a. The characteristic impedance (figure 3.3) rises from the Zone 2 plateau at very high frequencies due to the influences of dielectric relaxation of water (permittivity drops and impedance rises).

b. The Phase velocity (figure 3.4) also rises at very high frequencies due to dielectric relaxation resulting in dispersion of high frequency components when water is present.

c. The transmission coefficient (figure 3.5) shows significant loss at higher frequencies due to the increasing presence of dielectric loss (ε”) due to the onset of the dielectric relaxation effects (significantly below the actual Debye resonance). By comparing figures 3.5 and 3.6 one can see the influence on transmission loss due solely to the dielectric loss due to relaxation effects. In actual soils the solids mitigate this somewhat and push the dielectric loss to higher frequencies (fig 4d in Appendix D) as water makes up only a fraction of the volume but the loss is still significant as will be shown. This also applies to the phase velocity (influencing dispersion) and impedance (influencing reflections).

## Cascaded Transmission Line Models:

In soils and other complex geophysical and biological media there is typically heterogeneity that prevents the use of a single model that is valid over the entire length of the transmission line. However, typically it is possible to divide the transmission line into sub-sections in a finite element mesh arrangement where each of the sections or elements themselves can be considered homogeneous with consistent electromagnetic properties over the length of that element $E_n$. This approach is followed with the forward prediction models (as shown schematically earlier in figure 3.1 and in the following figure):

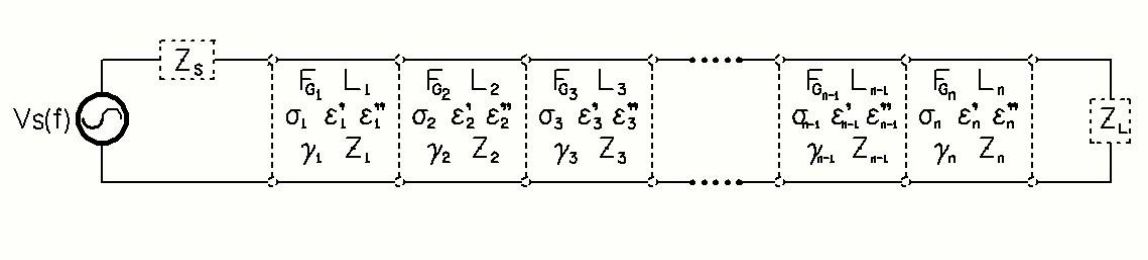


Figure 3.7: Heterogeneous Cascaded Transmission Line Divided into Homogeneous Elements

Where

$F_{Gn}$ = Probe Geometry Factor for Transmission Line Cascaded Element n.

$L_n$ = Length of Transmission Line Cascaded Element n.

$\sigma_n$ = Bulk Equivalent Electrical Conductivity of Cascaded Element n.

$\varepsilon_n'$ = Bulk Equivalent Electric Permittivity Real (Storage) Term of Cascaded Element n.

$\varepsilon_n''$ = Bulk Equivalent Electric Permittivity Imaginary (Loss) Term of Cascaded Element n.

$\gamma_n$ = Equivalent Propagation Constant for Transmission Line Cascaded Element n.

$Z_n$ = Equivalent Characteristic Impedance of Transmission Line Cascaded Element n.

Each transmission line sub-section or cascaded element also employs a distributed circuit model with a series Resistance per unit length (R), series Inductance per unit length (L), shunt Conductance per unit length (G) and shunt Capacitance per unit length (C) as shown in figure 3.8. The series terms represent model elements (R and L) along the length of the transmission line electrodes and Shunt terms represent model elements (G and C) between the electrodes. The

distributed element transmission line models must be identified for each element n. The model showing two sections or elements (n-1 and n) is shown in the following figure:

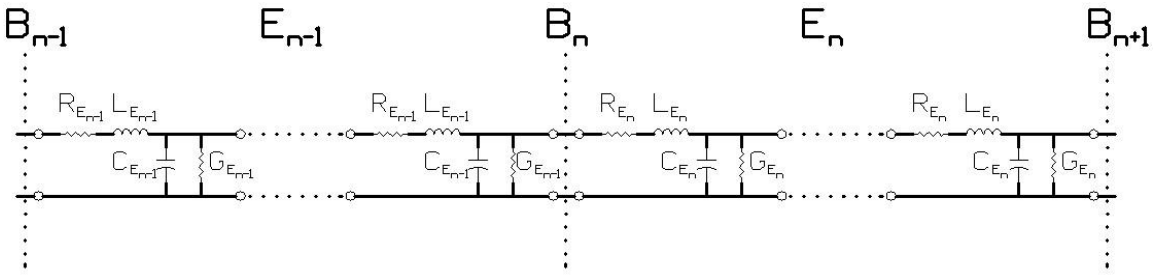


Figure 3.8: Distributed Transmission Line Model for Two Cascaded Sections

Models must then be developed for all the electromagnetic parameters for each finite element or cascaded subsection ($E_n$). This must be conducted at multiple levels within each element $E_n$ beginning with developing models for the base parameters ($\sigma_n$, $\varepsilon_n$', and $\varepsilon_n$") and then the transmission line distributed parameters ($R_n$, $L_n$, $G_n$, $C_n$) and finally the propagation and characteristic impedance expressions ($\gamma_n$, $Z_n$) all for each finite element $E_n$. As will be described in the next section on modeling composite media the base parameters ($\sigma_n$, $\varepsilon_n$', and $\varepsilon_n$") are equivalent bulk parameters for section/element $E_n$ and are themselves complex stochastic functions of the distributions of micro-constituents in that particular section or element $E_n$. These constituents can include liquids (typically water for soils including fully bound, semi-bound and free-water molecules), as well as solids (both mineral and organic constituents), and gases (typically air for soils). These constituents are all distributed in stochastic fashion within a soil (depending on the particular soil type and particle size distribution and porosity). The development of these models for the base parameters for a particular element will be developed fully in the section on composite dielectric mixing models later in this chapter.

**Reflection at an Impedance Boundary $B_n$:**

As shown in figures 3.1, 3.7, and 3.8 there can be boundaries ($B_n$) between different cascaded elements of different electromagnetic properties in a transmission line. When there is a boundary between two different impedance's (figure 3.9) then boundary constraints on electric

and magnetic fields will dictate that there will be reflected and transmitted traveling wave components at that boundary. Such a boundary is shown in the following figure for a simple network of two distinct characteristic impedance levels $Z_1$ and $Z_2$ representing two cascaded elements in a transmission line.

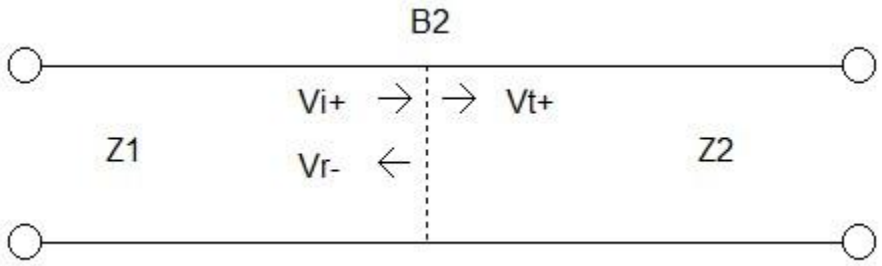


Figure 3.9: Impedance Discontinuity on a Transmission Line

Where

Vi+ = Amplitude of the Incident Voltage Waveform in Section 1 Approaching Boundary B2.

Vr- = Amplitude of the Reflected Voltage Waveform in Section 1 Returning from Boundary B2.

Vt+ = Amplitude of the Transmitted Voltage Waveform in Section 2 Just Beyond Boundary B2.

The reflection coefficient $\Gamma_2$ at boundary $B_2$ is defined as the ratio of the reflected wave amplitude to the incident wave amplitude at impedance boundary $B_2$ and is given by the following expression (3-5):

$$\Gamma_2 = \frac{Z_2 - Z_1}{Z_2 + Z_1} \qquad (3\text{-}5)$$

Where:

$Z_1$ = Characteristic Impedance of Section 1.

$Z_2$ = Characteristic Impedance of Section 2.

The voltage transmission coefficient* simply across boundary $B_2$ is then given as follows:

$$T_2 = 1 + \Gamma_2 \quad (3\text{-}6)$$

This transmission coefficient is associated solely with the boundary and is not the transmission coefficient across the length of the line within a given impedance section (equation 3-3). Therefore there are two transmission coefficients for each section (one for the boundary and one for the length of the section).

*Note: As will be shown in Appendix B the Forward Transmission Coefficient in S-Parameters (S21) is actually equal to the above expression (3-6) multiplied by the square root of the ratio of the magnitude of $Z_1/Z_2$ or in other words the voltage transmission coefficient normalized to the square root of impedance ratio. This is due to the fact that S-Parameters are defined by the square root of power of signals whereas (3-6) above is simply a ratio of voltages (not accounting for power or energy). Equation 3-6 arises simply due to the fact that the voltage must be consistent across a boundary from Kirchoff's Voltage Law and therefore the transmitted voltage just beyond the boundary in section 2 is equal to the sum of the incident and reflected voltages on the section 1 side of the boundary. However, the reflection coefficient (3-5) is exactly equal to the expression for S11 in S-Parameters as both the incident and reflected signals are in the same impedance section and so the normalization ratio is equal to 1. All of this will be discussed further in Appendix B where the expressions for S-Parameters will be defined and applied to the models in this dissertation. The forward prediction models in this dissertation make extensive use of S-Parameter modeling techniques to model the cascaded transmission line sections.

Equation A-32 (Appendix A) becomes a complex number in the presence of electrical conductivity and/or complex permittivity and therefore so does the reflection and transmission coefficients in equation 3-5 and 3-6 respectively. This is included in the computer models that generated the predictions for this report. Applying our earlier example of a 2-wire probe inserted into water of different EC values the following figures illustrate the magnitude and phase of the reflection coefficient vs. frequency at a boundary between a 50 Ohm transmission line and the 2-wire probe (the latter inserted into water).

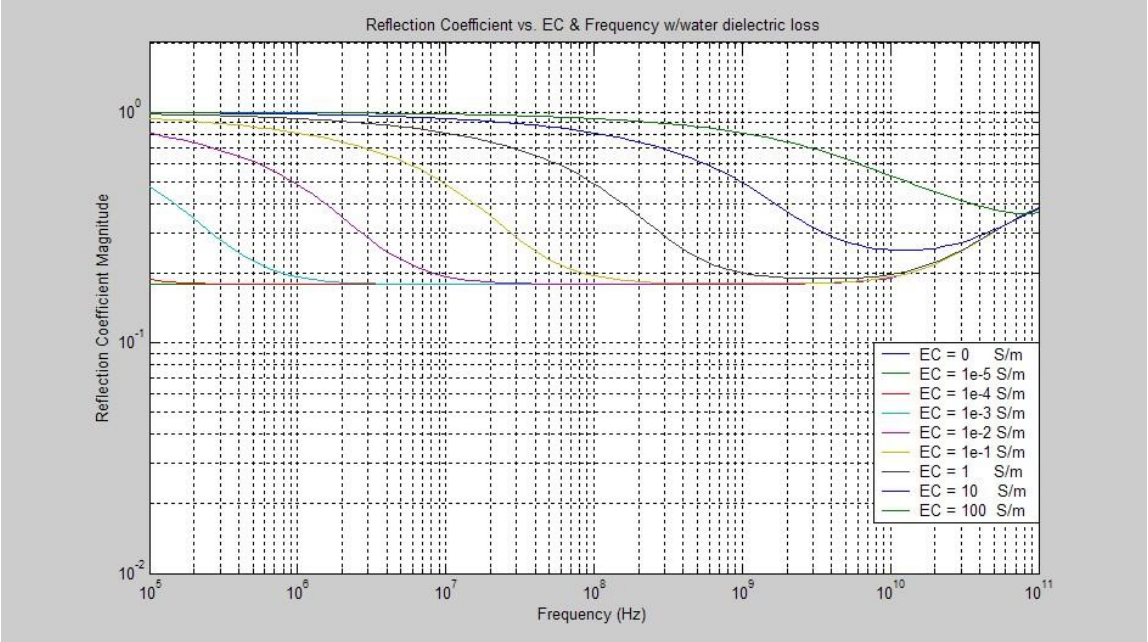


Figure 3.10: Reflection Coefficient vs. EC & Frequency (Boundary with 50Ω & 2-Wire Probe in Water)

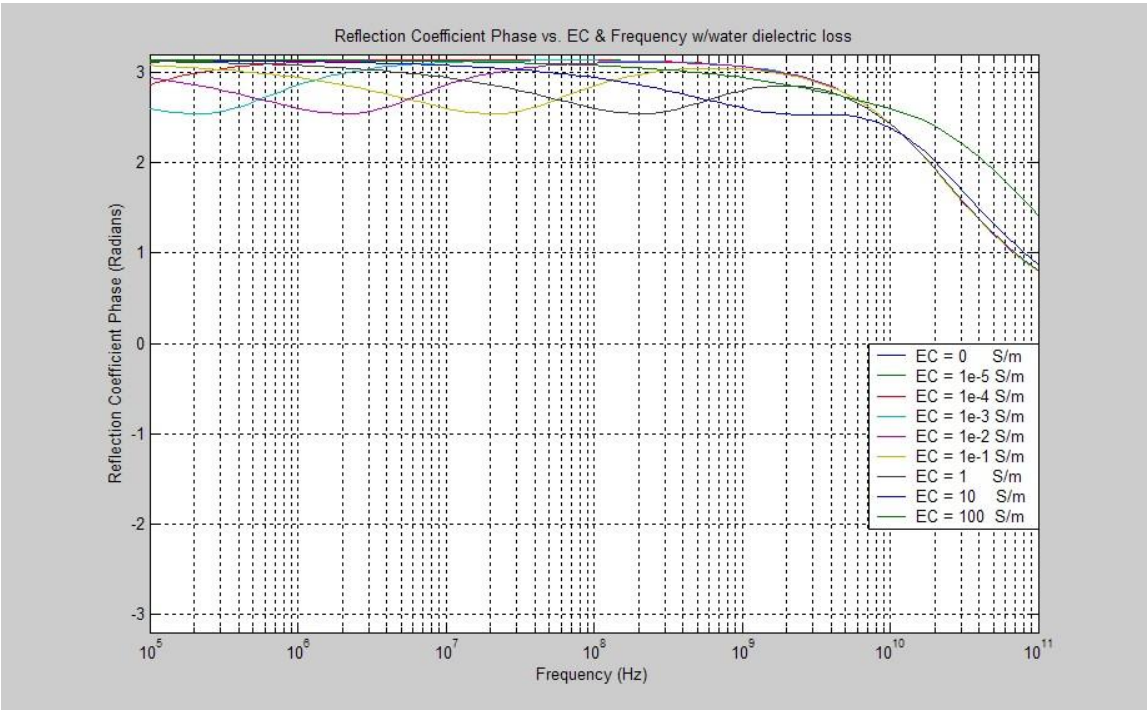


Figure 3.11: Reflection Coefficient Phase vs. EC & Frequency (Boundary: 50 Ω & 2-Wire Probe in Water)

In both figure 3.10 and figure 3.11 we can again see the same three different frequency ranges as seen earlier in figures 3.3 – 3.5. At low frequencies the impedance (A-32 – Appendix A) and therefore the reflection coefficient (3-5) are both dominated by electrical conductivity (~Zone 1 frequencies per the earlier definitions). In this region the reflection coefficient approaches -1 (magnitude of 1 and a phase of 180 degrees or $\pi$ radians) as seen in figures 3.10 and 3.11 due to the fact that the impedance drops to very low levels at low frequencies in the presence of EC (figure 3.3). Then at mid-range frequencies (~ Zone 2 with the lower corner frequency dependent on EC) we enter a range where the permittivity dominates over EC. In this region the reflection coefficient translates to a value of approximately -0.18 or a magnitude of 0.18 and a phase of 180 degrees or $\pi$ radians (due to the fact that the impedance is near 35 Ohms in this range (probe geometry and water combo)). There is a small blip or dip in phase during this transition visible in figure 3.11. Finally at higher frequencies (~ Zone 3) the reflection coefficient rises to a positive number (and lower phase) due to the drop off in permittivity (and therefore increase in impedance) due to dielectric relaxation phenomena. Figures 3.10 and 3.11 again show the utility of using the frequency domain to extract different parametric information.

Extending equation 3-5 to the overall multiple section cascaded line of figures 3.1 and 3.7 results in individual reflection coefficients at each boundary as shown in the following figure:

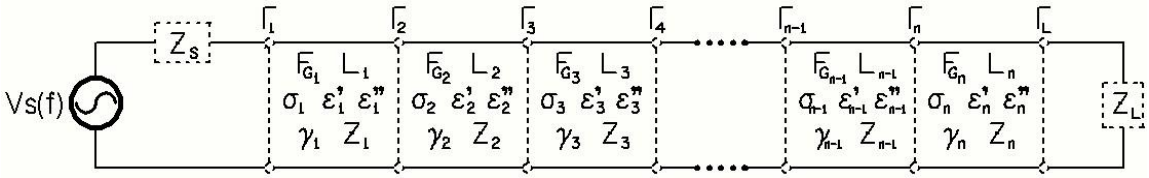

Figure 3.12: Cascaded Transmission Line Showing Reflection Coefficients at Each Boundary

The next section will focus on developing models for the individual parameters in each particular element $E_n$. Complex parametric mixing models involving contributions from multiple stochastically distributed micro-constituents making up the composite media will be developed. Later on, Appendix B will then describe the S-Parameter and T-Parameter models to globally model the overall transmission line accounting for all of the multiple reflection and transmission coefficients at each boundary to simulate the TDR and TDT signals in both the time domain and frequency domain.

## Composite Media:

The earlier expressions (equations A-5 to A-32 in Appendix A) give the electromagnetic propagation and characteristic impedance functions based on the two simplified cases of uniform plane waves and guided TEM waves (transmission lines) with a homogeneous medium. The expressions assumed a medium with an effective overall magnetic permeability $\mu$, electrical conductivity $\sigma$, and electrical permittivity $\varepsilon$ (both storage and loss terms) as if those parameters were homogeneously distributed within the medium. (Note: different EC or $\sigma$ values were used for the example illustrated in figures 3.3-3.6 and figures 3.10-3.11). For heterogeneous composite media such as soils and other geophysical or biological media these expressions are too simplified. Expressions for the overall propagation constant and characteristic impedance must be developed based on the relative percentages and spatial distributions of all the significant sub-constituents within a soil. In a soil these sub-constituents can include the following:

1.) Gases
    a. Primarily Air for Soils
2.) Solids
    a. Lesser Charged & Coarse Geometry Mineral Solids (Sand)
    b. Highly Charged & Fine Geometry Mineral Solids (Clay)
    c. Moderately Charged & Moderate Geometry Mineral Solids (Silt)
    d. Moderately Charged & Moderate Geometry Organic Matter
3.) Liquids
    a. Primarily Water for Soils
        i. Free Water (Regions outside the influence of a Charged Interface)
        ii. Semi-Bound Water (Regions approaching a Charged Interface)
        iii. Fully Bound Water (Directly Adjacent to a Charged Interface)

Before developing electromagnetic models for the composite mixture or overall heterogeneity which combine the influences of all of these constituents we must first develop base electromagnetic models for each of these major constituents individually. For the forward prediction models presented in this dissertation the following models are utilized for the various individual constituents:

Air:

With air the electromagnetic properties are assumed to follow those of free space. The electromagnetic parameters are therefore given as follows:

$\varepsilon_{air} = \varepsilon'_{air} = \varepsilon_o$ = 8.854e-12 Farads/Meter (or $\varepsilon_{r\_air}$ = relative permittivity = dielectric constant = 1)

$\varepsilon''_{air}$ = 0 (no dielectric losses with air)

$\mu_{air} = \mu_o$ = 12.6e-7 Henries/Meter

$\sigma_{air}$ = 0

Solids:

For each solid constituent (various mineral constituents and organic matter) there are unique values for the electromagnetic parameters. The forward prediction models are equipped to enter values for the electrical conductivity as well as real and imaginary portion of the permittivity (including frequency dependence) for each individual solid constituent. However, for the purposes of validating the forward prediction models with soils the solid components are all assumed to be non-magnetic, non-conductive as well as having only minimal dielectric losses (maximum loss tangent of 0.01) with no frequency dependence. However, indirectly certain types of solid components (those with significant charged interfaces) can contribute heavily to frequency dependent and lossy dielectric processes as they interact with water. However, those frequency dependent permittivity models for charged interfaces (such as are present with clay and organic matter) are incorporated into the models for bound and semi-bound water and not incorporated into the models for the solid constituents themselves. Therefore the electromagnetic parameters for the solid constituents themselves for the specific case soils are assumed to be the following:

$\varepsilon'_{solid\_n} = \varepsilon'_{r\_solid\_n}\ \varepsilon_o$ (where $\varepsilon'_{r\_solid\_n}$ = dielectric constant for the particular "nth" solid constituent)

$\varepsilon''_{solid\_n} / \varepsilon'_{solid\_n}$ = Loss Tangent for the "nth" solid constituent <= 0.01 for all frequencies.

$\mu_{solid\_n} = \mu_o$ = 12.6e-7 Henries/Meter (all solid constituents are non-magnetic)

$\sigma_{solid\_n}$ = 0 (all solid constituents are assumed to be non-conductive)

Again there are provisions in the forward prediction models to assign higher dielectric losses (and frequency dependence) as well as electrical conductivity values and even magnetic properties to each individual solid constituent (potentially needed for other geophysical and biological media). However, for the specific validations with soils the above assumptions were followed for the electromagnetic parameters for the solid constituents. The dielectric constant varies depending on the specific solid constituent (an example is 3.8 for the dielectric constant for quartz or silicon dioxide used in the models for sand).

Liquids:

As indicated the primary liquid in soils is water. For the purposes of the forward prediction models presented in this dissertation the water constituent is divided into three sub-components depending on proximity to charged interfaces:

- Free Water: Outside the influence of Charged Interfaces
- Semi-Bound Water: Inside the influence of Charged Interfaces but not Directly Adjacent
- Fully Bound Water: Directly Adjacent to the Charged Interfaces

A very simplified diagram to show the concept of fully bound water is shown in figure 3.13. The figure which follows (figure 3.14) then shows how all three of these constituents of water may be distributed in a particular pore relative to one edge or charged interface of the pore:

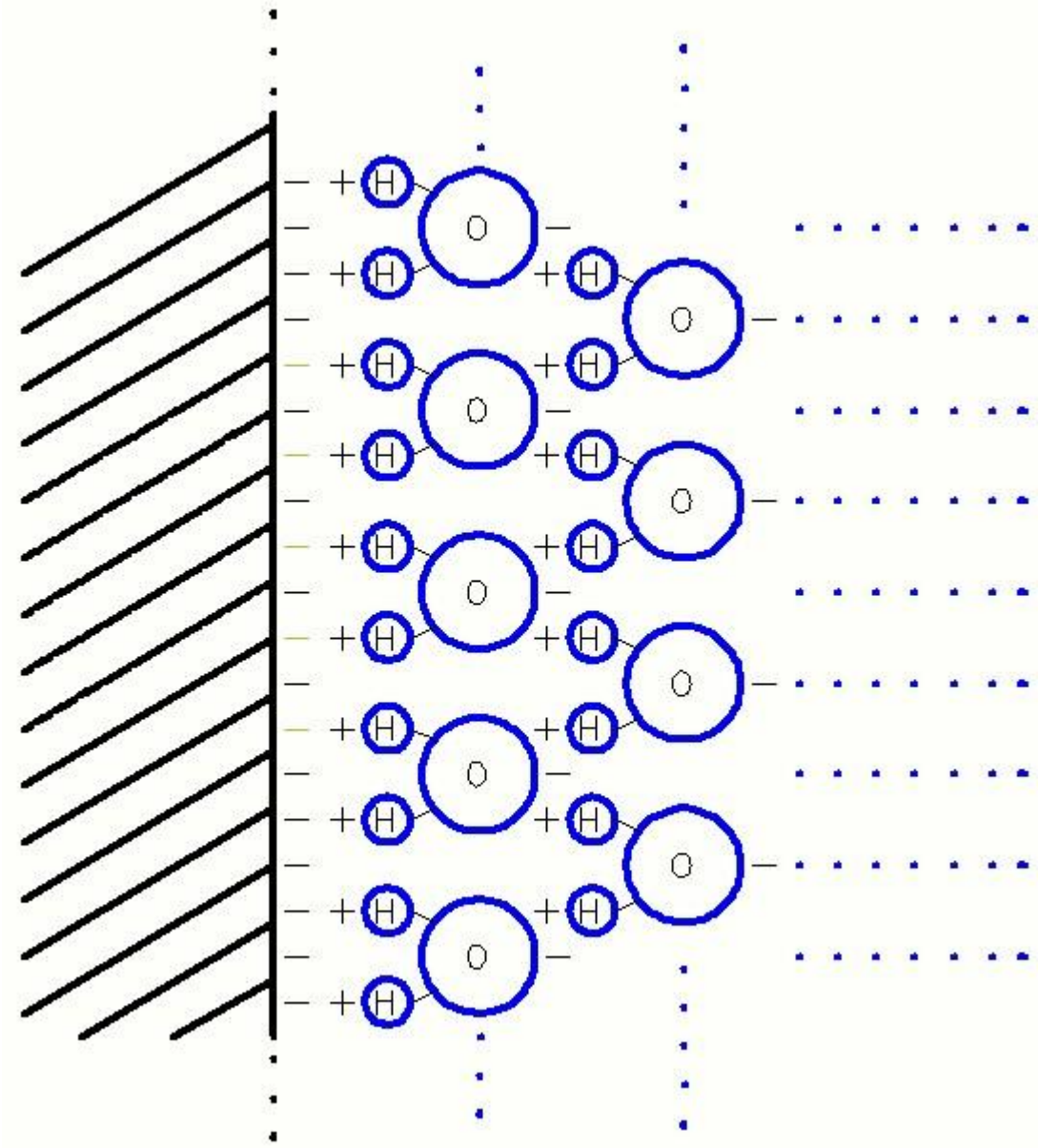


Figure 3.13: Negatively Charged Interface on Soil Solids Resulting in Fully Bound Water Zone

In reality the molecular make-up near the charged interface is much more complicated than what figure 3.13 shows (often involving other cations such as Sodium, Calcium, Magnesium, etc. in combination with water molecules). However the figure simply illustrates the concept of a negatively charged interface (of which could be present on clay surfaces as well as organic matter surfaces and even to a small extent on all surfaces) and how it will attract and constrain the water molecules due to their polar behavior .

As we move away from the negatively charged interface the water molecules are influenced less and less by that charged interface. Therefore, there is a transition from fully bound water through semi-bound water and eventually arriving at the zone where the polar water molecules are fully free of the influence of the charged interfaces. The following (again very simplified conceptualization) (figure 3.14) shows how the three constituents of fully bound water, semi-bound water and fully free water might be distributed within a particular pore moving away from one boundary of the pore which contains a negatively charged interface:

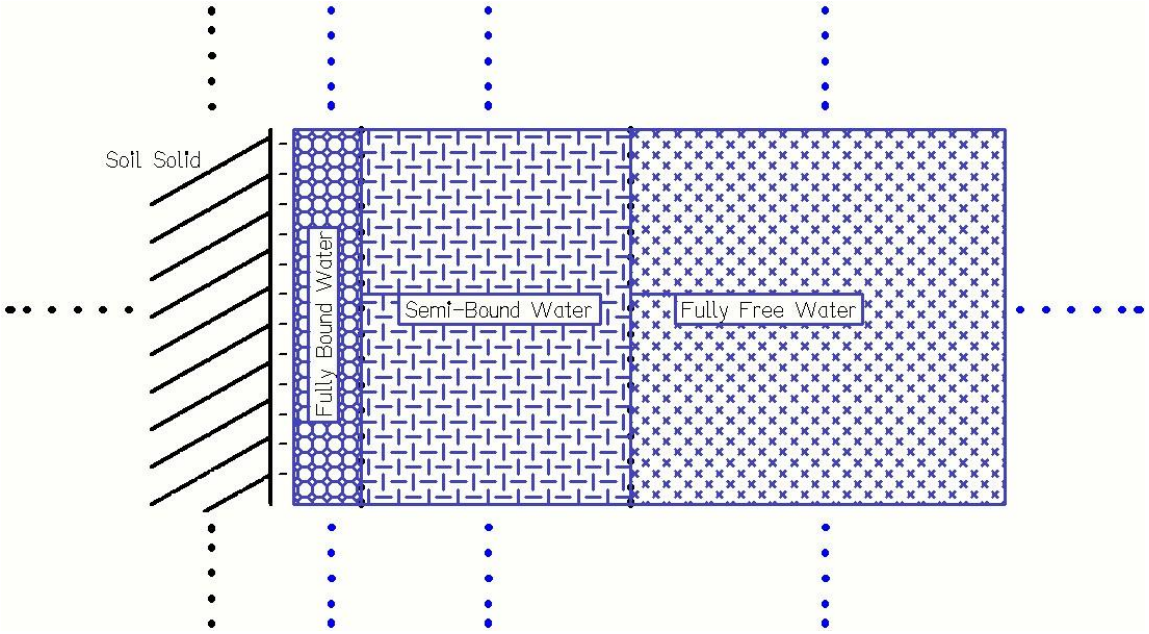


Figure 3.14: Zones of Fully Bound, Semi-Bound and Fully Free Water near a Charged Interface in a Pore

The following are the models and assumptions for the electromagnetic parameters for each of these sub-constituents for water:

**Free Water:**

For this type of water the individual water molecules are unconstrained from any charged interfaces and are fully mobile and free to respond to any external applied AC electric field such as would be present in a propagating electromagnetic wave propagating through the medium containing the free water. For larger pores that are filled (under wet conditions) free water is the

largest constituent of water (of the three sub-constituents). For small fine pores the bound and semi-bound water is of much more significant fractions compared to the free water

The permittivity models for free water are assumed to follow the Debye models of (A-13) and (A-14) in Appendix A ($\kappa = 0$ in (A-12)). It is assumed that the dielectric relaxation resonance frequency is at ~17 GHz which results in the following simplifications to (A-13) and (A-14):

$$\varepsilon'_{FW} = \varepsilon_0 \left[ \varepsilon_\infty + \frac{\varepsilon_s - \varepsilon_\infty}{1 + \left( \frac{f}{f_{rel}} \right)^2} \right] = \varepsilon_0 \left[ \varepsilon_\infty + \frac{\varepsilon_s - \varepsilon_\infty}{1 + \left( \frac{f}{1.7e10} \right)^2} \right] \tag{3-7}$$

$$\varepsilon''_{FW} = \frac{\left( \frac{f}{f_{rel}} \right) \varepsilon_0 (\varepsilon_s - \varepsilon_\infty)}{1 + \left( \frac{f}{f_{rel}} \right)^2} = \frac{\left( \frac{f}{1.7e10} \right) \varepsilon_0 (\varepsilon_s - \varepsilon_\infty)}{1 + \left( \frac{f}{1.7e10} \right)^2} \tag{3-8}$$

where $\varepsilon_s$ = Low frequency dielectric constant

$\varepsilon_\infty$ = High frequency dielectric constant

f = frequency (Hz)

$\tau$ = Relaxation time of the polar water molecule $H_2O$.

$f_{rel}$ = Relaxation resonance of water = $\frac{1}{2\pi\tau}$

**Semi-Bound Water:**

By examining figure 3.14 it is seen that there is a transition zone from free water down to fully bound water as distance from a charged interface decreases. In the forward prediction models presented in this dissertation this transition zone is modeled as an exponential change in permittivity properties between the free water models (3-7) and (3-8) and the fully bound water models (described in the next section). The model involves an exponential reduction in the dielectric relaxation resonance as distance is decreased from the charged interface. In addition the low frequency permittivity (or low frequency dielectric constant) (the value significantly below the Debye resonance) also decreases exponentially with decreasing distance from the charged

interface (approaching the value for bound water). These models are given as follows for a parallel combination of the individual transects of the semi-bound water zone:

$$\varepsilon'_{SBW_{TP}}(f) = \sum_{n=1}^{N} \varepsilon_0 \left[ \varepsilon_\infty + \left( \frac{\left(\varepsilon_{S\_SBW}(n) - \varepsilon_\infty\right)}{1 + \left( \frac{f}{f_{rel\_SBW}(n)} \right)^2} \right) \right] \Delta n \qquad (3\text{-}9)$$

= Total Real Component of Permittivity in Semi-Bound Water vs. Normalized Position & Frequency

$$\varepsilon''_{SBW_{TP}}(f) = \sum_{n=1}^{N} \varepsilon_0 \left(\varepsilon_{S\_SBW}(n) - \varepsilon_\infty\right) \left( \frac{\left( \frac{f}{f_{rel\_SBW}(n)} \right)}{1 + \left( \frac{f}{f_{rel\_SBW}(n)} \right)^2} \right) \Delta n \qquad (3\text{-}10)$$

= Total Imaginary Comp of Permittivity in Semi-Bound Water vs. Normalized Position & Frequency

$$f_{rel\_SBW}(n) = f_{rel\_FW} \left( a_1 e^{-(K-n)/b_1} \right) \qquad 1 < n < K\text{-}1 \qquad (3\text{-}11)$$

$$f_{rel\_SBW}(n) = f_{rel\_FW} \left( 1 - a_2 e^{-(K-n)/b_2} \right) \qquad K < n < N \qquad (3\text{-}12)$$

$$\varepsilon_{S\_SBW}(n) = \varepsilon_{S\_FW} \left( c_1 e^{-(K-n)/d_1} \right) \qquad 1 < n < K\text{-}1 \qquad (3\text{-}13)$$

$$\varepsilon_{S\_SBW}(n) = \varepsilon_{S\_FW} \left( 1 - c_2 e^{-(K-n)/d_2} \right) \qquad K < n < N \qquad (3\text{-}14)$$

Where

$\varepsilon_{S\_SBW}(n)$ = Low Frequency Permittivity of Semi-Bound Water at Normalized Distance n

$f_{rel\_SBW}(n)$ = Dielectric Relaxation (Debye) Resonance of Semi-Bound Water at Normalized Distance n

$a_1, a_2, b_1, b_2, c_1, c_2, d_1, d_1$ = Shape Coefficients for Semi-Bound Water Permittivity Functions

$\varepsilon_{S\_FW}$ = Low Frequency Permittivity of Free Water

$f_{rel\_FW}$ = Dielectric Relaxation (Debye) Resonance of Free Water (~17 GHz)

$n = \Delta n$ = Normalized Distance Increment within Semi-Bound Water Zone

N = Normalized Total Distance/Width of Semi-Bound Water Zone

K = Normalized Distance to Exponential Inflection Point of Semi-Bound Water Permittivity Model

These models for the individual transects within the semi-bound water zone are illustrated in the following figures (3.15-3.18):

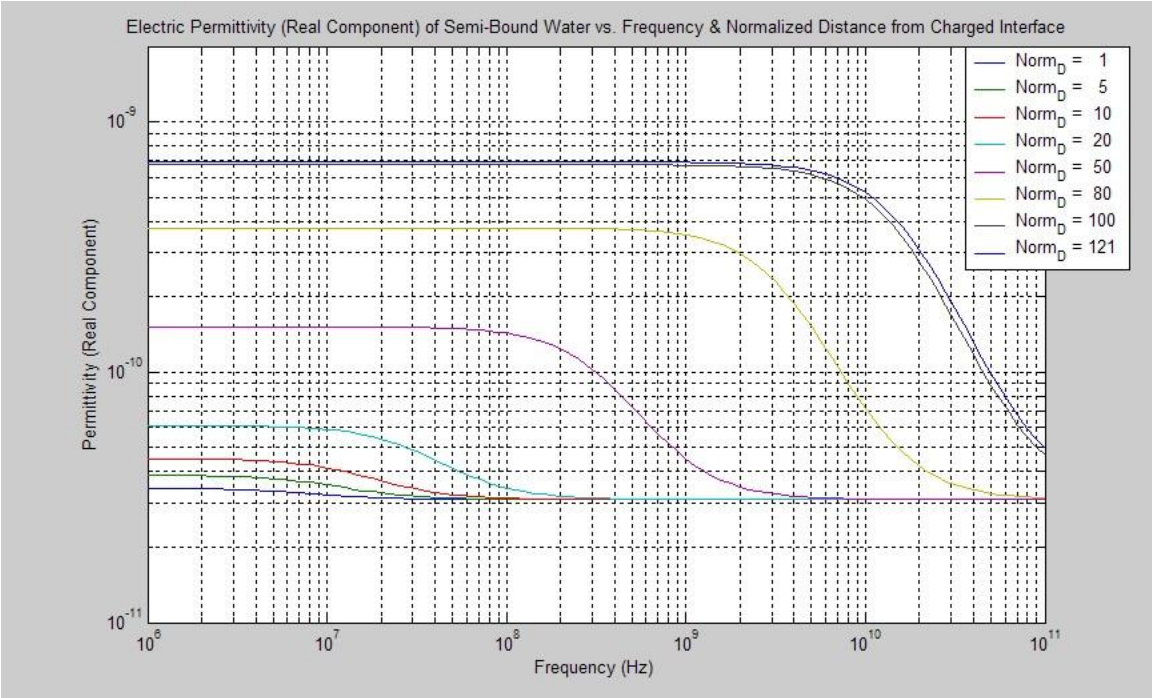


Figure 3.15: Real Component of Permittivity of Semi Bound Water vs. Normalized Distance (from a Charged Interface) and vs. Frequency

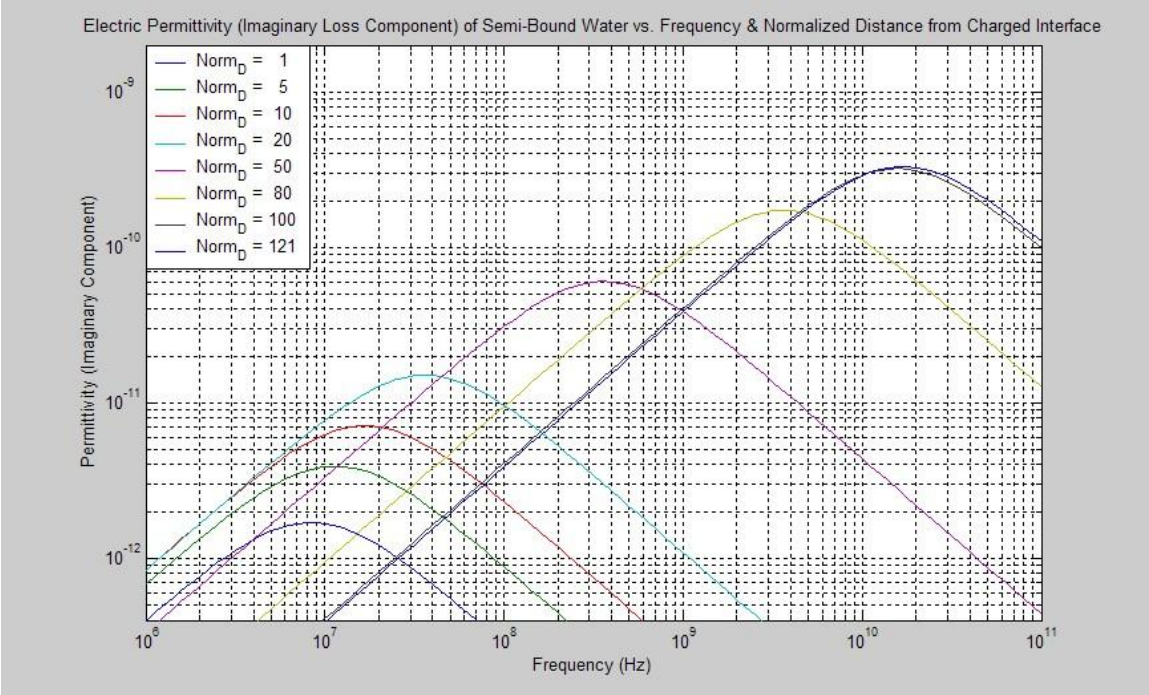


Figure 3.16: Loss Component of Permittivity for Semi-Bound Water vs. Normalized Position and Frequency

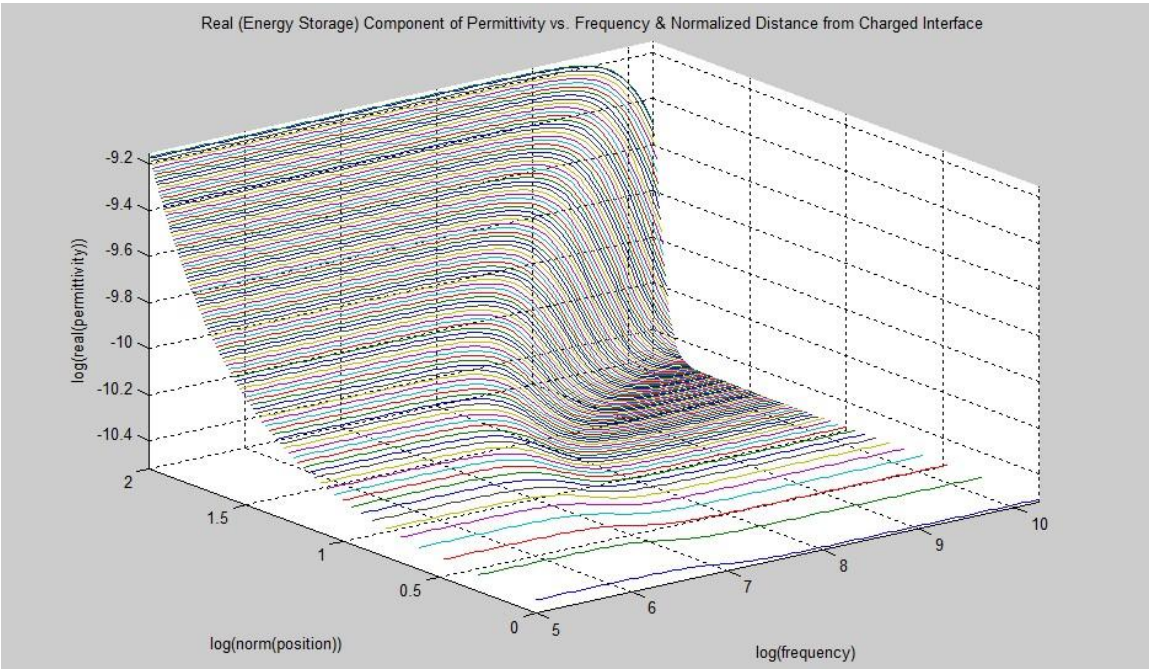


Figure 3.17: Real Component of Permittivity (ε') of Semi Bound Water vs. Normalized Distance (from a Charged Interface) and vs. Frequency

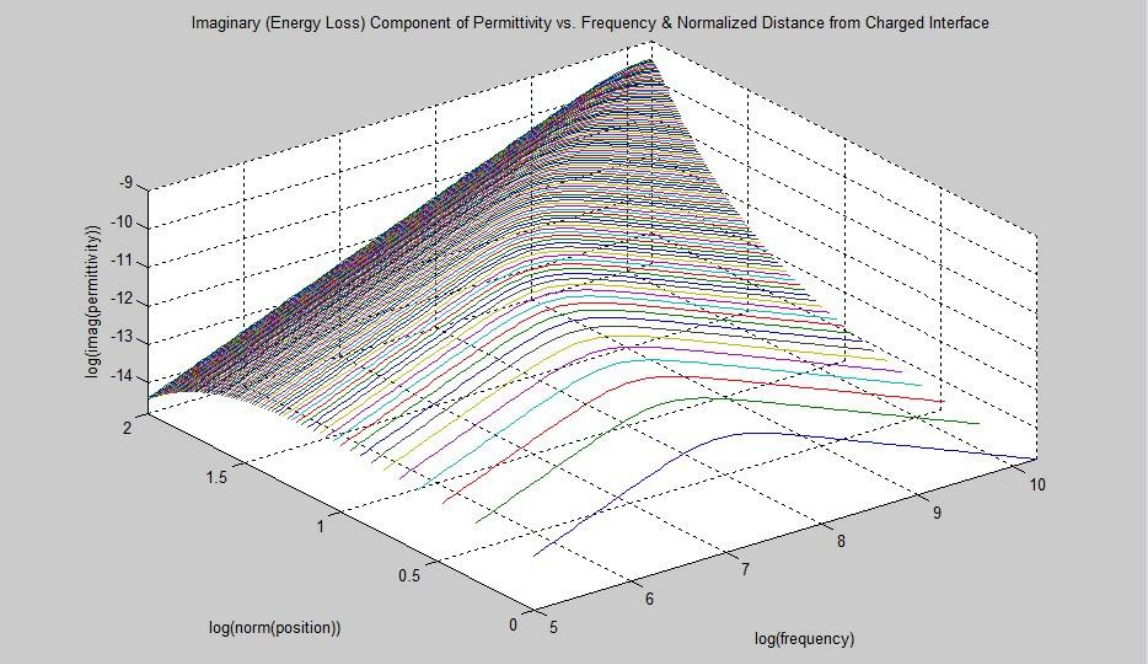


Figure 3.18: Loss Component of Permittivity (ε") of Semi Bound Water vs. Normalized Distance (from a Charged Interface) and vs. Frequency

Changing the shape coefficients can move the location of the inflection point and change the exponential rate of change of all the various parameters in the semi-bound water zone. The forward prediction model has capability to change these coefficients. The volume fraction of semi-bound water is then partitioned up with all of these individual incremental transects of different permittivity values. For the case of a parallel combination of the individual transects the overall permittivity components for the semi-bound zone can be approximated by the summations of (3-9) and (3-10) as if the individual transects are all in parallel (a theoretical upper bound to the permittivity components that will become important later when we discuss the overall composite dielectric mixing models for the entire soil).

In contrast to the parallel model, for a series model or combination of the semi-bound water transects the equivalent total real and imaginary components of permittivity are described by the following alternative expressions:

$$\varepsilon'_{SBW_{TS}}(f) = \frac{1}{\left[\sum_{n=1}^{N} \frac{\Delta n}{\varepsilon_0 \left[\varepsilon_\infty + \left(\frac{\left(\varepsilon_{S\_SBW}(n) - \varepsilon_\infty\right)}{1 + \left(\frac{f}{f_{rel\_SBW}(n)}\right)^2}\right)\right]}\right]} \tag{3-15}$$

= Total Real Component of Permittivity in Semi-Bound Water vs. Normalized Position & Frequency for a Series Combination of the Semi-Bound Water Transects.

$$\varepsilon''_{SBW_{TS}}(f) = \frac{1}{\left[\sum_{n=1}^{N} \frac{\Delta n}{\varepsilon_0\left(\varepsilon_{S\_SBW}(n) - \varepsilon_\infty\right)\left(\frac{\left(\frac{f}{f_{rel\_SBW}(n)}\right)}{1+\left(\frac{f}{f_{rel\_SBW}(n)}\right)^2}\right)}\right]} \quad (3\text{-}16)$$

= Total Imaginary Comp of Permittivity in Semi-Bound Water vs. Normalized Position & Frequency for the Series Model of the Semi-Bound Water Transects.

**Fully Bound Water:**

In this zone the low frequency permittivity is a very low value (equal to the low end of the semi-bound water zone) and the relaxation effects are greatly reduced (although not zero). This is due to the constrained forces on the water molecules in this zone due to the proximity of the negatively charged interface (figure 3.13). The Relaxation resonance for the fully bound water (and hence the lower limit of the semi-bound water limit) is currently set to just under 10 MHz in consistent fashion with current literature on Maxwell Wagner effects [106]. The forward prediction models have capability of changing the location of this resonance. The curves for the real and imaginary portion of the permittivity vs. frequency for the fully bound element can be seen in figures 3.15 and 3.16 respectively for the Normalized Distance = 1 values. The approached value for the bound water curves for the permittivity (real and imaginary terms) can also be seen in figures 3.17 and 3.18 as the log of normalized distance approaches 0.

## Composite Models Accounting for Heterogeneity:

In a soil there is typically a heterogeneous combination of all of the above constituents of air, soil solids (various minerals and organic matter) and water (free water, semi-bound water and fully bound water). There are different levels of heterogeneity leading to multiple aspects of composite dielectric modeling. These levels are shown as follows in table 3.2 with discussion following:

**Table 3.2: Levels of Heterogeneity and Resolving Requirements**

| Level | Heterogeneity Type | Required Frequency Zones for Resolving Heterogeneity | Resolving Method | A-Priori and/or Learned Site Calibration & Analysis/ID Requirements |
|---|---|---|---|---|
| Level 1 | Macroscopic Soil Structure & Soil Type Changes vs. Position | Zone 3a and Zone 3b Frequencies | Zone 3a: Refractive Dielectric/Cascade Propagation Model (Coarse Macroscopic Mixing Model at Entire Probe Dimensions)<br><br>Zone 3b: S-Parameters (Individually Resolve Heterogeneity to $E_n$ Dimensions) New Models | A-Priori Identification of Soil Type vs. Depth at Site. Learned Calibration for Specific Soil Structure (Layers) & Soil Type vs. Depth. |
| Level 2 | Macroscopic Soil Variables (Water Content & Electrical Conductivity) Changes vs. Position | Zone 1, Zone 3a and Zone 3b Frequencies | Zone 1: Coarse Electrical Conductivity Over Entire Probe (Lumped Element)<br><br>Zone 3a: Coarse Water Content Value: Refractive Dielectric/Cascade Propagation Model (Coarse Macroscopic Mixing Model at Entire Probe Dimensions)<br><br>Zone 3b: S-Parameters (Individually Resolve Water Content Profiles to $E_n$ Dimensions) New Models | No Incremental Calibration Required Assuming Level 1 Calibration Already Conducted |
| Level 3a | Microscopic Heterogeneity w/non-Consistent Stochastic Distributions at scales smaller than $E_n$ | Non-Resolvable | Non-Resolvable | Non-Resolvable |
| Level 3b | Microscopic Heterogeneity with Stochastic Distributions Consistent or Homogeneous over a Limited Dimension or Scale ($E_n$) | Non-Resolvable at Microscopic (Sub $E_n$) Scale but Utilize Zone 3b Frequencies to Resolve to $E_n$ Scale | Non-Resolvable at Microscopic Scale but Utilize Zone 3b Frequencies to Resolve to $E_n$ Scale assuming Micro-constituent Stochastic Distributions are Homogeneous over $E_n$. New Mixing Models | a.) A-Priori Analysis/ID of Soil Types at each $E_n$<br><br>b.) Learned Calibration of Stochastic Distributions of Micro-constituents |

1.) Level 1 Heterogeneity: Macroscopic Spatial Heterogeneity on Soil Structure: This could include major veins or layering in a soil or even aquifer boundaries. The layers could even be different soils types. It could also include larger cracks or animal burrows or rocks or other major boundaries or interruptions in a soil. The dimensions of these spatial zones are typically large enough that the Zone 3 frequencies in a TDR/TDT system could independently identify and resolve them with appropriate measurement algorithms and models. However, this type of heterogeneity clearly complicates and confounds the measurement of the target variables (such as profiling the target heterogeneity of changing water content vs. position) as covered in #2 and #3 below. Some A-priori knowledge of this type of heterogeneity will be required to be able to independently extract it from the macroscopic spatial heterogeneity of #2 below. As described in prior literature in Appendix C along with the literature review chapter and expanded further upon in this chapter and later chapters of the dissertation it can be shown that the "refractive" dielectric mixing models or the (essentially equivalent) "cascaded" composite propagation constant models offer promise for modeling wave propagation through this type of macroscopic heterogeneity as they model the propagation as if it travels through each major spatial zone or layer in succession (certainly valid at Zone 3 frequencies). However, the refractive dielectric mixing / cascade propagation model applies to Zone 3a frequencies and represents an overall equivalent model for the entire probe (and therefore does not allow for profiling). New models presented in this dissertation (involving S-Parameters and cascaded transmission line models to break the probe up into multiple finite element $E_n$ sections) allow for using Zone 3b frequencies to profile the heterogeneity into segments. But since the overall goal is to measure WC and EC and not the soil structure heterogeneity (which itself is largely fixed) the goal for level 1 heterogeneity is to identify it via A-priori and learned calibrations to eventually remove those features as unknowns and incorporate them instead into the "fixed" portions of the models so that WC and EC can be accurately measured as variables vs. position without any additional confounding unknowns.

2.) Level 2 Heterogeneity: Macroscopic Spatial Heterogeneity on Target Soil Variables: This is the more relevant form of heterogeneity where the key variables of volumetric water content and bulk electrical conductivity are changing over macroscopic dimensions in the soil (dimensions large enough where Zone 3 frequencies in the TDR/TDT systems can detect and resolve at least the water content profiles). In this case the soil structure / soil type is either assumed to be uniform or homogeneous over the measurement zone or alternatively has been calibrated out via the above Level 1 calibration. Level 2 heterogeneity could include a wetting front (figure 3.2 or other water content profiles). Zone 1 frequencies are required to identify and extract electrical conductivity and therefore EC normally can't (without other assumptions and measurements) be profiled vs. position (although again other techniques are described in this dissertation to give some information on EC profiles). The specific geometries of the water content profile zones will dictate whether the "refractive dielectric" / "cascaded propagation constant" mixing models described in #1 can still apply or whether new models (presented in this dissertation and based on cascaded sections based on the assumption of #3b below) will apply. Describing the conditions which dictate where different models apply will be one of the key goals of this dissertation.

3.) Microscopic Localized Heterogeneity: On a smaller scale there can still be significant heterogeneity with constituent makeup and properties being functions of position within a soil. However, in this case the geometrical dimensions associated with these changes are small compared with all wavelengths in a TDR / TDT signal (including Zone 3a and 3b frequencies). Therefore these changes or microscopic constituent distributions can not be independently identified or resolved. However, each of these micro-constituents acting together with the other micro-constituents still significantly influence propagation and impact all frequencies in a TDR / TDT system (Zone 1, 2 and 3 frequencies) and therefore must be accounted for. It is at this level that the typical porosity and stochastic pore size distributions for most soils fall into. Therefore this level of micro-heterogeneity is really the key level for understanding and modeling volumetric water content and its influence on the electromagnetic properties of a soil. As will be shown from both the data and the forward prediction model analysis the refractive dielectric mixing model (or alternatively the equivalent cascaded propagation constant mixing model) can not properly model this type of micro-heterogeneity as these constituents simultaneously influence the same portion of the traveling wave (making up a localized "lumped element" model). Therefore new dielectric

and propagation constant mixing models must be developed to account for the effects of this heterogeneity. Therefore, several new dielectric mixing and propagation constant mixing models are introduced and evaluated in this dissertation to account for this type of micro-heterogeneity. This type of micro-heterogeneity can be further divided into the following two sub-categories:

a. Stochastically spatially distributed micro-constituents but with the distributions non-consistent or essentially changing with position at all measurable scales even at sub-element ($E_n$) scales (and also changing in time). This lack of consistency in the stochastic spatial distributions would prevent the use of a single model to represent even sub-elements of a transmission line probe inserted into such a medium.

b. Stochastically spatially distributed micro-constituents with the stochastic distributions consistent over some limited spatial dimension (large enough to be detectable by Zone 3b frequencies at individual finite element $E_n$ type scales or dimensions). This allows for a homogeneity assumption over that spatial zone or element (creating the potential for developing dielectric mixing, propagation constant mixing and other electromagnetic parameter mixing models for that zone or element). The relative distributions of the constituents can have temporal (time) dependencies (i.e. water content changing with time) but at any particular time snapshot the relative spatial distributions are still consistent over that entire element $E_n$ (again satisfying the homogeneous assumption). This assumption allows for the construction of a cascaded transmission line model for an entire TDR/TDT probe made up of these types of micro-homogeneous elements to model macro heterogeneity (figures 3.1, 3.7 and 3.8).

The forward prediction models presented in this dissertation assume and account for levels 1, 2 and 3b of heterogeneity. It is believed that most soils can satisfy assumption 3b to some extent with the bandwidths and geometries of today's TDR and TDT systems. However, it is also acknowledged that this assumption does not always hold given real world media and this will be discussed further in the chapter on limitations and assumptions associated with the models.

Accounting for level 1 and level 2 macroscopic heterogeneity can be accomplished by applying cascaded transmission line models including the use of Scattering (S) parameters and Transmission (T) parameters as described in Appendix B along with Zone 3b frequencies. Alternatively if an overall approximation of the heterogeneity at the full probe length dimensions is sufficient then Zone 3a frequencies along with the refractive dielectric or cascaded propagation constant electromagnetic mixing models (discussed later in this section) can be applied to model for level 1 and/or level 2 macroscopic heterogeneity to essentially model the TDR probe as embedded in an equivalent single medium. Each of these approaches will be presented and described in this dissertation. The latter approach (refractive model) has been applied and evaluated extensively in the literature (see literature review chapter along with Appendix C). There are many assumptions behind the refractive model (or equivalent cascaded propagation constant model) but again the largest assumption is that the waves successively propagate through the different zones (in independent cascaded fashion) due to the geometries of the zones significant or large compared with the wavelength. Again, this depends on the actual dimensions of those zones and is typically best paired with the Zone 3a frequencies in a TDR/TDT waveform. This dissertation will again describe where the refractive dielectric / cascaded propagation constant models can still be successfully applied as well as where other models (introduced in this dissertation) are better suited.

There are certainly limits to how much level-1 heterogeneity can be tolerated to allow for successful calibration for it and the subsequent successful profiling (spatial dependence) and trending (temporal/time dependence) of the volumetric water content (level 2 and level 3 heterogeneity). The forward prediction models presented in this dissertation assume that the level 1 heterogeneity can be accounted for and incorporated in to a fixed calibration for the cascaded sections in the models based on the combination of A-priori knowledge of the soil measurement site together with learned calibrations with the measurement system at the actual site. It is important to state that there are not sufficient measurement parameters with a TDR or even a TDT system to guarantee extracting all the measurement unknowns if both the level 1 and level 2 macroscopic heterogeneity categories are both fully unknowns. The uniqueness assumption for the waveforms can also not be guaranteed to be satisfied if both level 1 and level 2 heterogeneities are simultaneously measurement unknowns. Therefore some level of site calibration must be assumed to minimize the unknown nature of the level 1 heterogeneity.

**New Composite Dielectric Mixing and Propagation Constant Mixing Models:**

The new dielectric mixing and propagation constant mixing models developed and presented in this dissertation beginning with this section of this chapter build on earlier composite mixing models covered in the literature. A summary of the most popular existing models in literature is provided in Appendix C. The full comprehensive coverage on the literature covering existing composite mixing models is provided in the literature review chapter. The new models developed in this dissertation and covered next again build on those earlier models covered in the literature.

Simplifying assumptions concerning the heterogeneity types of Table 3.2 can be made where valid to allow for derivable mathematical models at both the overall probe as well as finite element $E_n$ levels. The most powerful models make use of stochastic models for both the percentages (by volume) and spatial distributions of all the sub-constituents within a soil. The models presented in this dissertation assume that a soil can initially be divided into a 1-D finite element set of cascaded elements along the probe axial direction (i.e. $E_n$). Then, in turn, equivalent electromagnetic models at each individual $E_n$ must be developed for the base electromagnetic parameters (figure 3.7), as well as the equivalent impedance elements per unit length (figure 3.8) and ultimately the characteristic impedance $Z_n$ and propagation constant $\gamma_n$ for each element $E_n$.

To develop the models for the individual parameters per unit length within a given $E_n$, a further sub-division of the network must be made within each $E_n$. These are at finer partitions that are short compared with even the shortest Zone 3b wavelengths (i.e. far finer dimensions than $E_n$) at a 1-D level that we will term $dX_i$ where all $dX_i$ "micro-elements" are assumed consistent in terms of stochastic distributions of micro-constituents within them across the entire element $E_n$. These fine partitioned micro-elements $dX_i$ are then actually divided down one level further to into a 2-D finite-element type grid that segments that micro-element $dX_i$ into a j x k array of micro-constituent cells each with individual values for the electromagnetic parameters as shown in figure 3.19. The third dimension (orthogonal to direction of TDR probe and to the micro-element $dX_i$) is assumed homogeneous within each segment over the length of influence from the probe. The values for these parameters at this micro-constituent level are determined by stochastic functions based on the soil type and values for the bulk volumetric water content and electrical

conductivity at the $E_n$ level or resolution. The intent is to develop models for the individual electromagnetic parameters $\sigma_n$, $\varepsilon_n$', $\varepsilon_n$'', $R_n$, $L_n$, $G_n$ and $C_n$, and ultimately $Z_n$ and $\gamma_n$ that are valid over the individual homogeneous element $E_n$ as shown in figures 3.7 and 3.8. However, these models are actually derived at the $dX_i$ micro-element level creating distributed models at the $E_n$ element level by cascading several $dX_i$ that in turn each act as lumped models at the micro-element $dX_i$ level based on the j x k array of stochastically distributed micro-constituent cells in that micro-element $dX_i$. A further assumption on this is that each jk cell has only one constituent (whether it be water (bound, semi-bound or free water), organic solids, mineral solids, or air). There are again stochastic functions to identify the probability of each jk cell being a particular micro-constituent type. Then, electromagnetic properties for each of these individual micro-constituents are paired with the constituent type and plugged into the particular jk cell depending on the probabilistic constituent type. Once the stochastic distributions are established the key next step in the modeling process is to assess how these micro-constituents are connected throughout the array. There are two theoretical bounds to how they can be connected in how they impact the property ranges and ultimately the impedance and propagation term ranges. These theoretical bounds are whether the cells are connected in parallel vs. in series. All mixing arrangements and models fall between these theoretical bounds or limits.

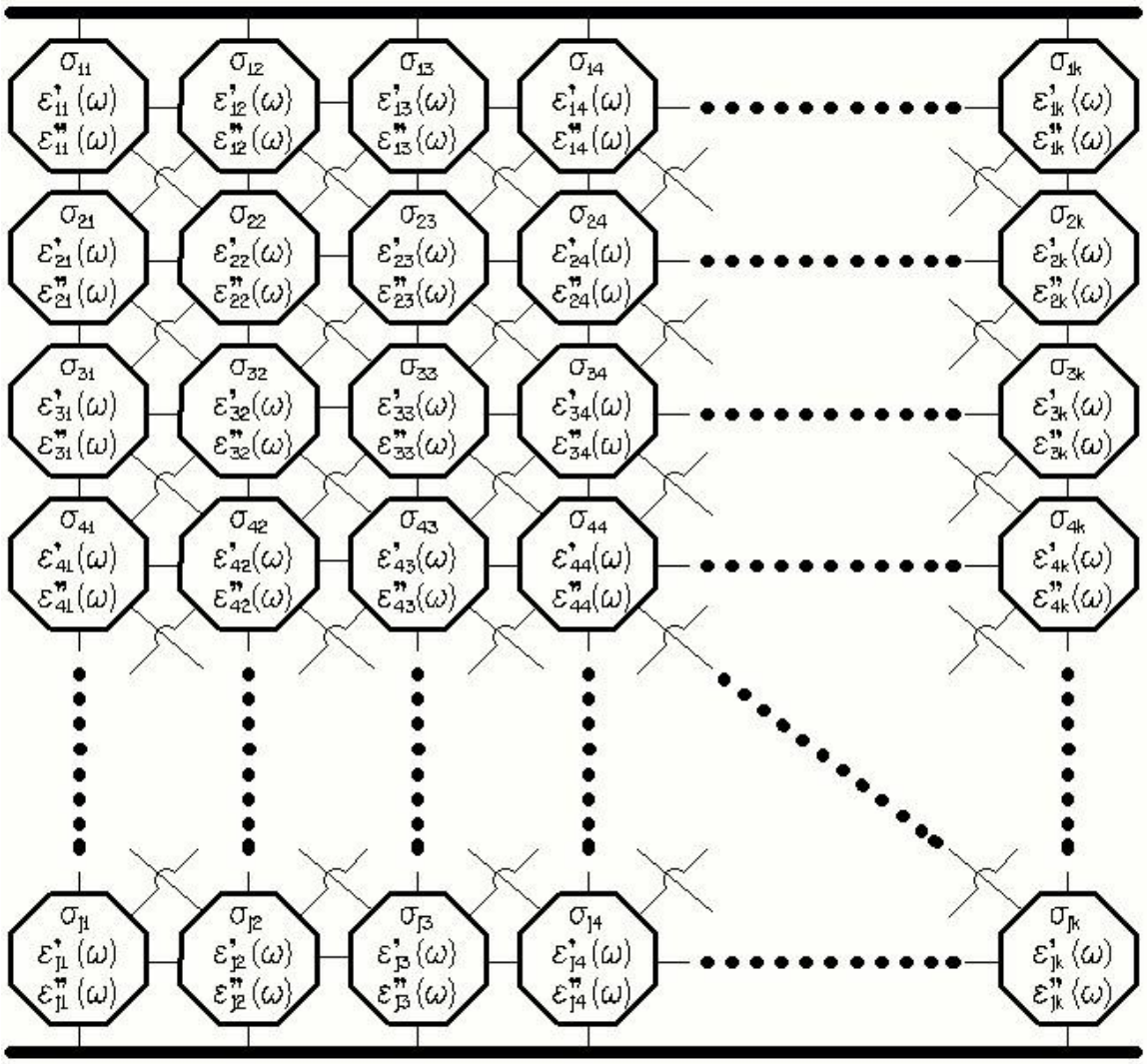


Figure 3.19: j x k Cell Array of Micro-constituents forming Micro-Element $dX_i$ as a Shunt (Electrode to Electrode) Electromagnetic Model.

These dXi form the Shunt Component Models per unit Length ($G_n$ & $C_n$) Distributed in Cascaded but Homogeneous Fashion over the Length of a Transmission Line Finite Element $E_n$ per Figure 3.8.

## Theoretical Bounds:

There are two theoretical bounds that govern all dielectric mixing models given as follows:

A. Parallel Model:
    a. All Micro-Constituents (jk Cells) in a Micro Element $dX_i$ are connected in Parallel Fashion.
    b. Lower Limit for Characteristic Impedance
    c. Lower Limit for Phase Velocity
    d. Upper Limit for Propagation Constant

B. Series Model:
    a. All Micro-Constituents (jk Cells) in a Micro Element $dX_i$ are connected in Series Fashion.
    b. Upper Limit for Characteristic Impedance
    c. Upper Limit for Phase Velocity
    d. Lower Limit for Propagation Constant

## Parallel Model:

In the parallel model theoretical boundary all micro-constituents (jk Cells) of equal type are assumed to be arranged or ordered vertically as shunt paths (between transmission line electrodes) in figure 3.19 so that the water portion, solids portion and air portion can be considered to be individual sets of vertical columns fully in parallel within $dX_i$ as shown diagrammatically as follows in figure 3.20:

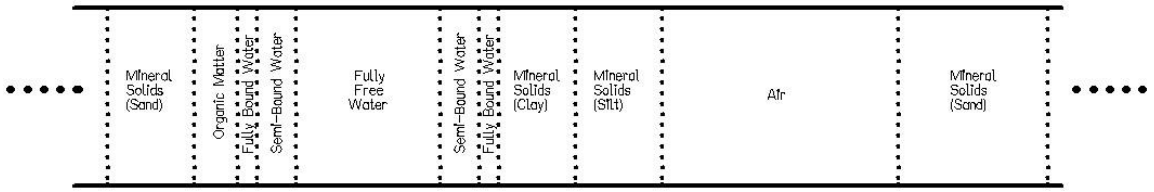


Figure 3.20: Shunt Micro-Element $dX_i$ reduced to Parallel Model for jk Cells (All micro-constituents of Common Types Ordered in Vertical Shunt (Electrode to Electrode) Columns)

where each of the micro-constituents are biased by their volumetric contents or fractions and in this model all contribute to the same location in the wave (as opposed to the cascade propagation constant or refractive dielectric mixing models where they influence the propagating wave in succession).

Upper "Parallel Model" Model for Permittivity (real component):

$$\varepsilon_U' = \varepsilon'_{Parallel} = (1-\phi)\varepsilon'_{S_{TP}} + \theta_{FW}\varepsilon'_{FW} + \theta_{SBW}\varepsilon'_{SBW} + \theta_{BW}\varepsilon'_{BW} + (\phi-\theta)\varepsilon'_{A} \quad (3\text{-}17)$$

Where

$$\varepsilon'_{S_{TP}} = F_O\varepsilon'_O + F_C\varepsilon'_C + F_{St}\varepsilon'_{St} + F_{Sd}\varepsilon'_{Sd} \quad (3\text{-}18)$$

Similarly the upper parallel model limit for the imaginary component of the permittivity is as follows:

$$\varepsilon_U'' = \varepsilon''_{Parallel} = (1-\phi)\varepsilon''_{S_{TP}} + \theta_{FW}\varepsilon''_{FW} + \theta_{SBW}\varepsilon''_{SBW} + \theta_{BW}\varepsilon''_{BW} + (\phi-\theta)\varepsilon''_{A} \quad (3\text{-}19)$$

Where

$$\varepsilon''_{S_{TP}} = F_O\varepsilon''_O + F_C\varepsilon''_C + F_{St}\varepsilon''_{St} + F_{Sd}\varepsilon''_{Sd} \quad (3\text{-}20)$$

And finally the upper parallel model limit for the electrical conductivity is as follows:

$$\sigma_U = \sigma_{Parallel} = (1-\phi)\sigma_{S_{TP}} + \theta_{FW}\sigma_{FW} + \theta_{SBW}\sigma_{SBW} + \theta_{BW}\sigma_{BW} + (\phi-\theta)\sigma_{A} \quad (3\text{-}21)$$

Where

$$\sigma_{S_{TP}} = F_O\sigma_O + F_C\sigma_C + F_{St}\sigma_{St} + F_{Sd}\sigma_{Sd} \quad (3\text{-}22)$$

$\theta$ = Total Volumetric Water Content or Water Fraction of the Soil and is made up of the three Sub-Constituents of water given as follows:

$$\theta = \theta_{FW} + \theta_{SBW} + \theta_{BW} \quad (3\text{-}23)$$

Where $\theta_{FW}$ = Volumetric Content or Fraction of Free Water

$\theta_{SBW}$ = Volumetric Content or Fraction of Semi-Bound Water

$\theta_{BW}$ = Volumetric Content or Fraction of Fully Bound Water

The other parameters in (3-17) to (3-22) are defined as follows:

$\phi$ = Porosity of Soil

$F_O$ = Volumetric Content or Fraction of Organic Matter

$F_C$ = Volumetric Content or Fraction of Clay

$F_{St}$ = Volumetric Content or Fraction of Silt

$F_{Sd}$ = Volumetric Content or Fraction of Sand

And for all of the electromagnetic parameters the suffixes are defined in general as follows:

FW: Denotes Value of Particular Parameter in Free Water

SBW: Denotes Value of Particular Parameter in Semi-Bound Water

BW: Denotes Value of Particular Parameter in Fully Bound Water

$S_{TP}$: Denotes Value of Particular Parameter in the Parallel Combination of all Solid Constituents

O: Denotes Value of Particular Parameter in Organic Matter Solids

C: Denotes Value of Particular Parameter in Clay Solids

St: Denotes Value of Particular Parameter in Silt Solids

Sd: Denotes Value of Particular Parameter in Sand Solids

A: Denotes Value of Particular Parameter in Air

The forward prediction models have provisions for all of the above parameters but in the actual validations for soils several of the parameters were assumed either small or alternatively equal to zero (e.g. EC or $\sigma$ equals zero in air as well as very small in the solids and $\varepsilon'' = 0$ in air and is assumed small and not frequency dependent in the solid constituents). In contrast, for other constituents the models become quite complex as with the three water components which employ (3-7 to 3-14) (for the parallel model) incorporated into (3-17) and (3-19).

The upper or parallel model can also be defined at the propagation constant level:

Upper “Parallel Model” propagation constant (or factor) limit:

$$\gamma_U = \gamma_{Parallel} = \sqrt{(1-\phi)\gamma_{S_{TP}}^2 + \theta_{FW}\gamma_{FW}^2 + \theta_{SBW}\gamma_{SBW}^2 + \theta_{BW}\gamma_{BW}^2 + (\phi-\theta)\gamma_A^2} \quad (3\text{-}24)$$

Where

$$\gamma_{S_{TP}} = \sqrt{F_O\gamma_O^2 + F_C\gamma_C^2 + F_{St}\gamma_{St}^2 + F_{Sd}\gamma_{Sd}^2} \quad (3\text{-}25)$$

Where: all the subscripts and volumetric fractions are defined the same as for the individual permittivity and conductivity parallel models further above. In the case of these propagation constant models the propagation constant in a particular constituent (say free water) is based on the permittivity (real and imaginary terms) and conductivity for the free water component alone (using equations similar to (A-9) or (A-31) in Appendix A). Similar models for the propagation constant terms of the other constituents can also be developed based on the electromagnetic parameters of those specific constituents. Therefore it can be shown that (3-24) and (3-25) can be derived from (3-17) to (3-22). It can therefore be shown that these upper limit "parallel" models for the propagation constant yield identical results to those for based on the parallel limits for the individual parameters (permittivity and conductivity).

The "parallel model" bound represents the upper limit for the equivalent propagation constant as well as the equivalent electromagnetic parameters (permittivity and electrical conductivity) for micro-element $dX_i$ which in turn means that the parallel model represents the lower limit or lower bound of the equivalent characteristic impedance and phase velocity for micro-element $dX_i$.

**Series Model:**

On the other end or boundary for wave propagation models we have the series model. In the series model theoretical boundary all micro-constituents (jk Cells) of equal type are assumed to be arranged or ordered horizontally in figure 3.19 so that the water portion, solids portion and air portion can be considered to be individual sets of horizontal rows fully in series vertically within the shunt (electrode to electrode) micro-element $dX_i$ as shown diagrammatically as follows in figure 3.21:

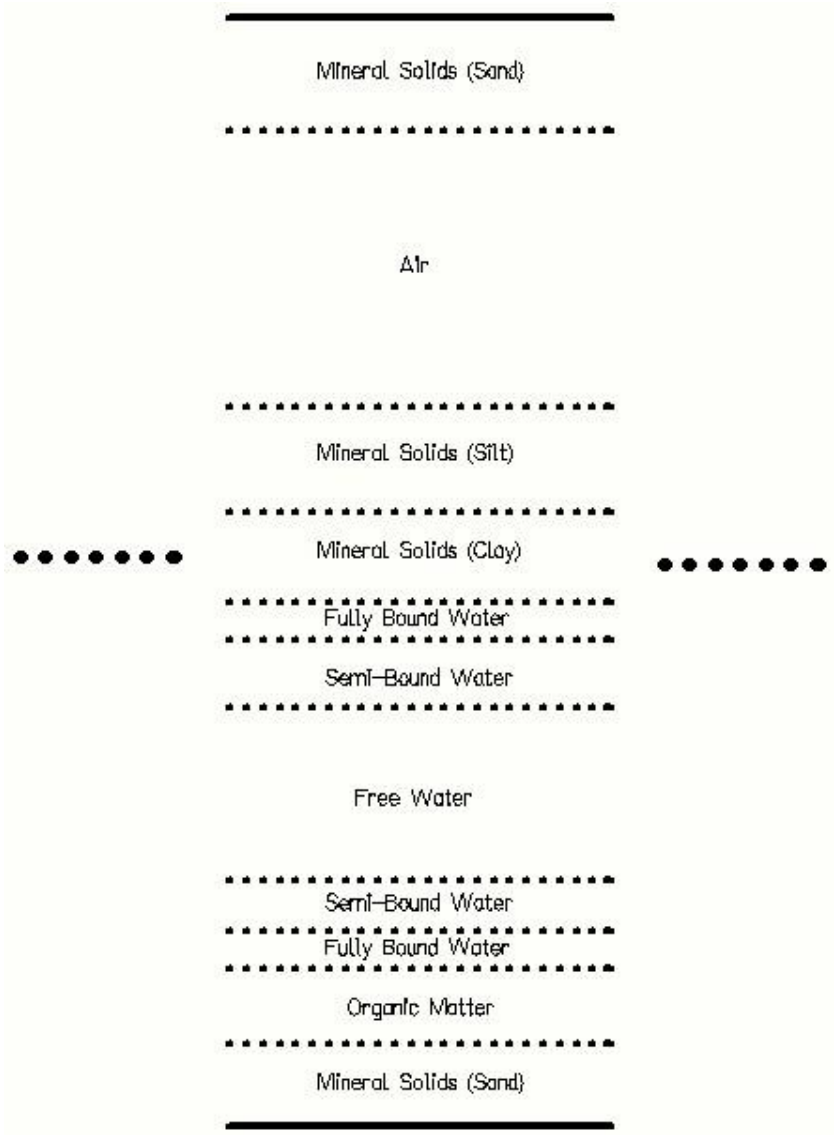


Figure 3.21: Shunt (Electrode to Electrode) Micro-element $dX_i$ with series model for jk Cells (All micro-constituents of Common Types Ordered in Horizontal Rows)

The series model represents the lower theoretical limit of the equivalent propagation constant as well as equivalent electromagnetic parameters of micro-element $dX_i$. This implies that the series model also represents the upper limit for the equivalent characteristic impedance and phase velocity for micro-element $dX_i$.

The series composite models based on the individual electromagnetic parameters are given as follows:

Lower "Series Model" Limit of Permittivity (real component):

$$\varepsilon'_{L} = \varepsilon'_{Series} = \frac{1}{\frac{1-\phi}{\varepsilon'_{S_{TS}}} + \frac{\theta_{FW}}{\varepsilon'_{FW}} + \frac{\theta_{SBW}}{\varepsilon'_{SBW}} + \frac{\theta_{BW}}{\varepsilon'_{BW}} + \frac{\phi-\theta}{\varepsilon'_{A}}} \tag{3-26}$$

Where

$$\varepsilon'_{S_{TS}} = \frac{1}{\frac{F_O}{\varepsilon'_{O}} + \frac{F_C}{\varepsilon'_{C}} + \frac{F_{St}}{\varepsilon'_{St}} + \frac{F_{Sd}}{\varepsilon'_{Sd}}} \tag{3-27}$$

Similarly the lower "series model" limit for the imaginary component of permittivity is given as follows:

$$\varepsilon''_{L} = \varepsilon''_{Series} = \frac{1}{\frac{1-\phi}{\varepsilon''_{S_{TS}}} + \frac{\theta_{FW}}{\varepsilon''_{FW}} + \frac{\theta_{SBW}}{\varepsilon''_{SBW}} + \frac{\theta_{BW}}{\varepsilon''_{BW}} + \frac{\phi-\theta}{\varepsilon''_{A}}} \tag{3-28}$$

Where

$$\varepsilon''_{S_{TS}} = \frac{1}{\frac{F_O}{\varepsilon''_{O}} + \frac{F_C}{\varepsilon''_{C}} + \frac{F_{St}}{\varepsilon''_{St}} + \frac{F_{Sd}}{\varepsilon''_{Sd}}} \tag{3-29}$$

Finally the lower "series model" limit for the electrical conductivity is given as follows:

$$\sigma_L = \sigma_{Series} = \frac{1}{\frac{1-\phi}{\sigma_{S_{TS}}} + \frac{\theta_{FW}}{\sigma_{FW}} + \frac{\theta_{SBW}}{\sigma_{SBW}} + \frac{\theta_{BW}}{\sigma_{BW}} + \frac{\phi-\theta}{\sigma_A}} \tag{3-30}$$

Where

$$\sigma_{S_{TS}} = \frac{1}{\frac{F_O}{\sigma_O} + \frac{F_C}{\sigma_C} + \frac{F_{St}}{\sigma_{St}} + \frac{F_{Sd}}{\sigma_{Sd}}} \tag{3-31}$$

And in similar fashion to the parallel model the series model can be applied to the propagation constant level as well:

Lower propagation constant (or factor) limit:

$$\gamma_L = \gamma_{Series} = \frac{1}{\sqrt{\frac{1-\phi}{\gamma_{S_{TS}}^2} + \frac{\theta_{FW}}{\gamma_{FW}^2} + \frac{\theta_{SBW}}{\gamma_{SBW}^2} + \frac{\theta_{BW}}{\gamma_{BW}^2} + \frac{\phi-\theta}{\gamma_A^2}}} \tag{3-32}$$

Where

$$\gamma_{S_{TS}} = \frac{1}{\sqrt{\frac{F_O}{\gamma_O^2} + \frac{F_C}{\gamma_C^2} + \frac{F_{St}}{\gamma_{St}^2} + \frac{F_{Sd}}{\gamma_{Sd}^2}}} \tag{3-33}$$

All of the volumetric contents or fractions along with the various suffixes in (3-26) to (3-33) are defined the same as in the parallel model with the exception of the following:

$S_{TS}$: Denotes the value of a particular parameter in the series combination of the solid constituents.

As was the case with the parallel model, for the specific case of the validation with soils some of the parameters in the series model are assumed equal to zero or alternatively very small (e.g. the electrical conductivity is assumed to be zero in both the solids and air fractions and the permittivity loss component is zero in air and assumed small and non-frequency dependent in the solids fraction). However, the water components again lead to very complex models with this

time (for the series model) equations 3-7, 3-8, 3-11 to 3-14 and 3-15 to 3-16 being applied to equations 3-26, 3-28 and indirectly to 3-32.

As indicated the parallel and series models represent the theoretical limits or bounds for the shunt components in a transmission line model and hence provide the theoretical limiting bounds for the electromagnetic wave propagation and impedance terms. All dielectric and ohmic mixing models governing wave propagation and impedance terms fall within these two theoretical bounds. Each micro-element $dX_i$ (figure 3.19) would have its own set of values for the parallel and series model theoretical bounds (equations 3-18 to 3-32). It is then assumed that these values and hence the stochastic distributions as modeled in $dX_i$ are then homogeneous or uniform across the entire finite element $E_n$ (figures 3.1, 3.7 and 3.8) allowing for a particular set of models for each $E_n$. Again, at the $dX_i$ resolution the distances are tiny compared to the shortest wavelength in a TDR or TDT waveform spectrum but at the $E_n$ resolution the distances are significant to the wavelengths of the Zone 3b frequencies in a TDR or TDT waveform. This allows for the detection of changes along a transmission line at the $E_n$ spatial resolution and hence the desire to find a resolution that allows for the homogeneity assumption within that element while still being large enough to be resolvable by Zone 3b frequencies in the TDR/TDT waveform.

The segmenting of this transmission line probe over its length into different $E_n$ elements is made possible by the use of scattering (S) parameter models of cascaded networks (described in Appendix B) in the frequency domain and represents one of the novel approaches used by the forward prediction models and algorithms presented in this dissertation. This allows for the algorithm to determine water content vs. depth along a probe and not just an overall average of water content which is the basis of most existing TDR measurement systems (see literature review chapter).

Within each of the segments or cascaded stages expressions need to be derived for propagation constant and characteristic impedance. These then serve as the fundamental expressions from which boundary reflection coefficients (at segment boundaries), boundary transmission coefficients (across segment boundaries) and segment transmission coefficients / propagation or phase shift terms (over the length of each segment) can be derived. These in turn are the necessary input parameters for the S-parameter models of cascaded networks. These

models must be derived as some form of weighted stochastic interpolation model between the theoretical bounds of the parallel and series models for each element $E_n$ (based on the models for the micro-elements $dX_i$ that are assumed homogeneous over the element $E_n$). Several of these stochastic weighting interpolation models are presented as follows:

## Stochastic Interpolation Models:

It is desired to develop models that make use of all the boundary constraints available to allow for the development of a physically based model that has a minimum dependence on empirical fitting or linear and nonlinear regression fitting. As indicated above there are two very dominant boundary conditions that constrain or give theoretical upper and lower boundaries to all the electromagnetic propagation constant and impedance ranges. These two boundaries are based on two opposite limits on how the physical sub-constituents are arranged within a micro-element $dX_i$ within the medium (figure 3.19) namely the parallel model (figure 3.20 and equations (3-17) to (3-25)) and the series model (figure 3.21 and equations (3-26) to (3-33)). These are physically based models that can be exactly derived from the two bounding distributed circuit models for a transmission line (components modeled as being either in series or in parallel within the shunt network). All other derived or empirical models for propagation constant and impedance must reside between these theoretical limits to be physically based models.

The task then is to find models for propagation constant and impedance that fit the data and reside between these two theoretical limits and still are based as much as possible on physical and not empirical models. One such interpolating model is the cascade model (or equivalent refractive dielectric mixing model) given in simplified fashion in equations (C-1), (C-2), (C-12 to C-14), (C-16) and (C-18) in Appendix C. The cascade or refractive mixing models resides between the theoretical limits of the parallel and series models. It is the simplest form of interpolating models but (as discussed) is only a good fit to the data over limited regions of water content and electrical conductivity combinations. The cascade or refractive model is one of many models included in the suite of models with the forward prediction models. The particular form of the cascade/refractive models utilized in the forward prediction models are given as follows for the propagation constant and permittivity terms:

**Cascade/ Refractive Model:**

$$\gamma_T = \gamma_{S_{cc}}(1-\phi) + \gamma_{FW}\theta_{FW} + \gamma_{SBW}\theta_{SBW} + \gamma_{BW}\theta_{BW} + \gamma_A(\phi-\theta) = \alpha_T + j\beta_T \quad (3\text{-}34)$$

Where

$$\gamma_{S_{CC}} = \gamma_O F_O + \gamma_C F_C + \gamma_{St} F_{St} + \gamma_{Sd} F_{Sd} \quad (3\text{-}35)$$

$$\sqrt{\varepsilon'_T} = \sqrt{\varepsilon'_{S_{CC}}}(1-\phi) + \sqrt{\varepsilon'_{FW}}\theta_{FW} + \sqrt{\varepsilon'_{SBW}}\theta_{SBW} + \sqrt{\varepsilon'_{BW}}\theta_{BW} + \sqrt{\varepsilon'_A}(\phi-\theta) \quad (3\text{-}36)$$

Where

$$\sqrt{\varepsilon'_{S_{CC}}} = F_O\sqrt{\varepsilon'_O} + F_C\sqrt{\varepsilon'_C} + F_{St}\sqrt{\varepsilon'_{St}} + F_{Sd}\sqrt{\varepsilon'_{Sd}} \quad (3\text{-}37)$$

$$\sqrt{\varepsilon''_T} = \sqrt{\varepsilon''_{S_{CC}}}(1-\phi) + \sqrt{\varepsilon''_{FW}}\theta_{FW} + \sqrt{\varepsilon''_{SBW}}\theta_{SBW} + \sqrt{\varepsilon''_{BW}}\theta_{BW} + \sqrt{\varepsilon''_A}(\phi-\theta) \quad (3\text{-}38)$$

Where

$$\sqrt{\varepsilon''_{S_{CC}}} = F_O\sqrt{\varepsilon''_O} + F_C\sqrt{\varepsilon''_C} + F_{St}\sqrt{\varepsilon''_{St}} + F_{Sd}\sqrt{\varepsilon''_{Sd}} \quad (3\text{-}39)$$

$$\sqrt{\sigma_T} = \sqrt{\sigma_{S_{CC}}}(1-\phi) + \sqrt{\sigma_{FW}}\theta_{FW} + \sqrt{\sigma_{SBW}}\theta_{SBW} + \sqrt{\sigma_{BW}}\theta_{BW} + \sqrt{\sigma_A}(\phi-\theta) \quad (3\text{-}40)$$

Where

$$\sqrt{\sigma_{S_{CC}}} = F_O\sqrt{\sigma_O} + F_C\sqrt{\sigma_C} + F_{St}\sqrt{\sigma_{St}} + F_{Sd}\sqrt{\sigma_{Sd}} \quad (3\text{-}41)$$

Where all parameters and subscripts are as previously defined.

Again it can be shown that these models result in values for the propagation constant, characteristic impedance and electromagnetic parameters (permittivity terms and electrical conductivity) between the limits of the parallel and series model. There are limited regions where the cascade / refractive models fit to actual soil datasets and those cases are described in the validation chapter.

Several additional stochastic interpolating models between the limits of the parallel and series models have been investigated by the research covered in this dissertation. Interpolation models acting at both the propagation constant level as well as the individual electromagnetic parameters level (permittivity and conductivity) have been developed. A few examples of these models are given next (with several others also evaluated). Methodologies of interpolation incorporated include the following: Rectangular Mean Model, Geometric Mean Model, Inverse Mean Model and Arithmetic Mean Model with various weighting coefficients. These interpolation methods were incorporated at both the propagation constant level as well as the individual electromagnetic parameter level (with different physical interpretations for each). The interpolation methods are paired together where physical interpretations are equivalent. These are described as follows:

1.) Rectangular Mean Interpolation Model on Propagation Constant and Arithmetic Mean Interpolation Model on the Electromagnetic Parameters (Permittivity and Conductivity):

With these models it is assumed that a weighted stochastic distribution of the shunt components at both the series and parallel theoretical limits are actually connected in parallel in the distributed transmission line model. These relative stochastic weighting fractions or constants are determined based on assumptions about the soil makeup and it is at this level where some empirical fitting to data has been conducted. These models are shown as follows:

**Rectangular Mean Interpolation Model**

(for Propagation Constant):

$$\gamma_T = \gamma_{Rectangular} = \sqrt{\frac{(1+K_1)\gamma_L^{\,2} + K_2\gamma_U^{\,2}}{1+K_1+K_2}} \qquad (3\text{-}42)$$

**Arithmetic Mean Interpolation Model**

(for Electromagnetic Parameters of Permittivity and Conductivity):

$$\varepsilon'_T = \varepsilon'_{Arithmetic} = \frac{(1+A_1)\varepsilon'_L + A_2\varepsilon'_U}{1 + A_1 + A_2} \quad (3\text{-}43)$$

$$\varepsilon''_T = \varepsilon''_{Arithmetic} = \frac{(1+A_1)\varepsilon''_L + A_2\varepsilon''_U}{1 + A_1 + A_2} \quad (3\text{-}44)$$

$$\sigma_T = \sigma_{Arithmetic} = \frac{(1+A_1)\sigma_L + A_2\sigma_U}{1 + A_1 + A_2} \quad (3\text{-}45)$$

**Other Interpolation Models:**

2.) Inverse Rectangular Mean Interpolation Model on Propagation Constant and Direct Inverse Mean Interpolation Model on Electromagnetic Parameters (Permittivity Terms and Conductivity):

With these models it is assumed that a weighted stochastic distribution of the shunt components at both the series and parallel theoretical limits are actually connected in series in the distributed transmission line model. These relative stochastic weighting fractions or constants are determined based on assumptions about the soil makeup and again at this level some amount of empirical fitting to data has been conducted. These models are shown as follows:

Inverse Rectangular Mean Interpolation Model for Propagation Constant:

$$\gamma_T = \gamma_{Inverse} = \sqrt{\frac{1 + J_1 + J_2}{\left(\frac{1+J_1}{\gamma_L^{\,2}}\right) + \left(\frac{J_2}{\gamma_U^{\,2}}\right)}} \quad (3\text{-}46)$$

Inverse Mean Interpolation Model for Permittivity and Conductivity:

$$\varepsilon'_T = \varepsilon'_{Inverse} = \frac{1 + J_3 + J_4}{\left(\frac{1+J_3}{\varepsilon'_L}\right) + \left(\frac{J_4}{\varepsilon'_U}\right)} \quad (3\text{-}47)$$

$$\varepsilon''_{T} = \varepsilon''_{Inverse} = \frac{1 + J_3 + J_4}{\left(\frac{1+J_3}{\varepsilon''_{L}}\right) + \left(\frac{J_4}{\varepsilon''_{U}}\right)} \tag{3-48}$$

$$\sigma_{T} = \sigma_{Inverse} = \frac{1 + J_3 + J_4}{\left(\frac{1+J_3}{\sigma_{L}}\right) + \left(\frac{J_4}{\sigma_{U}}\right)} \tag{3-49}$$

3.) Arithmetic Mean (Cascade) Interpolation Model on Propagation Constant Bounds and Refractive Interpolation Model on Electromagnetic Parameter Bounds.

With these models it is assumed that a weighted stochastic distribution of the shunt components at both the series and parallel theoretical limits are actually connected in cascade in the distributed transmission line model. These relative stochastic weighting fractions or constants are determined based on assumptions about the soil makeup and again at this level some amount of empirical fitting to data has been conducted. The difference between a parallel type of representation and a cascade type of representation is that the parallel model assumes that all the sub-components simultaneously influence the same location of the propagating wave whereas in the cascade model each sub-component influences a given location in the propagating wave in succession as if the wave propagates through the constituents one at a time. These models are shown as follows:

Arithmetic Mean (Cascade Interpolation) Model for Propagation Constant:

$$\gamma_{T} = \gamma_{Arithmetic} = \frac{(1+B_1)\gamma_{L} + B_2\gamma_{U}}{1 + B_1 + B_2} \tag{3-50}$$

Refractive Interpolation Model for Permittivity Terms and Conductivity:

$$\sqrt{\varepsilon'_{T}} = \sqrt{\varepsilon'_{Refractive}} = \frac{(1+B_1)\sqrt{\varepsilon'_{L}} + B_2\sqrt{\varepsilon'_{U}}}{1 + B_1 + B_2} \tag{3-51}$$

$$\sqrt{\varepsilon''_{T}} = \sqrt{\varepsilon''_{Refractive}} = \frac{(1+B_1)\sqrt{\varepsilon''_{L}} + B_2\sqrt{\varepsilon''_{U}}}{1 + B_1 + B_2} \quad (3\text{-}52)$$

$$\sqrt{\sigma_{T}} = \sqrt{\sigma_{Refractive}} = \frac{(1+B_1)\sqrt{\sigma_{L}} + B_2\sqrt{\sigma_{U}}}{1 + B_1 + B_2} \quad (3\text{-}53)$$

4.) Geometric Mean Interpolation Model for Propagation Constant and Electromagnetic Parameters

Finally the geometric mean model assumes that the actual propagation constant and electromagnetic parameters reside logarithmically between the series and parallel theoretical limits with the weighting factors again dependent on soil assumptions or some degree of empirical fitting. In contrast to the above sets of interpolation models the geometric mean model has a different physical interpretation when applied to the propagation constant vs. the individual limits of the electromagnetic parameters of permittivity and conductivity. The models are given as follows:

Geometric Mean Interpolation Model for Propagation Constant:

$$\gamma_T = \gamma_{Geometric} = \sqrt{\gamma_L{}^{a}\gamma_U{}^{(2-a)}} \quad (3\text{-}54)$$

where 0 <= a <= 2.

Geometric Mean Interpolation Model for Permittivity and Conductivity:

$$\varepsilon'_T = \varepsilon'_{Geometric} = \sqrt{\varepsilon'_L{}^{b}\,\varepsilon'_U{}^{(2-b)}} \quad (3\text{-}55)$$

$$\varepsilon''_T = \varepsilon''_{Geometric} = \sqrt{\varepsilon''_L{}^{b}\,\varepsilon''_U{}^{(2-b)}} \quad (3\text{-}56)$$

$$\sigma_T = \sigma_{Geometric} = \sqrt{\sigma_L{}^{b}\sigma_U{}^{(2-b)}} \quad (3\text{-}57)$$

where 0 <= b <= 2.

In all of these stochastic interpolation models for the propagation constant and electromagnetic parameters (permittivity and conductivity) the weighting constants are arranged so as the upper and lower limit boundary condition constraints are not violated as well as these models set up so as to insure that the units come out correctly (another physical constraint). In the above models $K_1$, $K_2$, $J_1$, $J_2$, $J_3$, $J_4$, $A_1$, $A_2$, $B_1$, $B_2$, a and b are all weighting constants or parameters based on assumptions about the soil. They are also arranged based on the constraints that the propagation constants and electromagnetic parameters must end up being between the theoretical boundaries of the parallel and series model. In essence those weighting constants or parameters are essentially functions of the soil type, soil porosity ($\phi$), and overall soil water content ($\theta$) the latter of which insures that the above interpolation models are all nonlinear with water content (i.e. the weighting constants change with water content).

The full results of comparing the performance of these different models to the actual datasets for various soils are covered in the next chapter on validation (including precise derivations of the weighting constants or functions). An example snapshot of some observed trends are given here to show how it influences the selections and functions for deriving the weighting constants. It was found from examination of the laboratory data for sandy soils that the following trends were followed:

Trends for Sandy Soil for All Tested Ranges of Electrical Conductivities:

Very Low Water Contents (WC< 0.05): Strong Weighting towards Parallel Model

Low-Medium Water Contents (0.05 < WC < 0.15): Equal Weighting of Series & Parallel Model

Medium Water Contents (0.15 < WC < 0.30): Slight to Moderate Weighting towards Series Model

High Water Contents (WC > 0.30): Strong Weighting towards Parallel Model

One potential physical interpretation of these trends (upon examining figures 3.19, 3.20 and 3.21) could be that as a particular soil region approaches a two component model (i.e. either air and

solids or water and solids but not all three simultaneously at significant fractions) then there can be conceived of or hypothesized continuous through paths between the two transmission line conductors (oriented in vertical or semi vertical tortuous paths) that would support biasing towards a parallel model. In contrast, when there are significant simultaneous percentages of all three of the major constituents (solids, air and water) then it can be conceived of or hypothesized that there would be interruptions or discontinuities in any vertical column path that would then support some mix of the series and parallel models or even slight biasing towards the series model. In the independent domain model for soils there can be narrow pores and wide pores (or wide cells or compartments) in series with each other. They can also be independent of other paths (uncoupled) and at intermediate water contents (depending on whether we are on a wetting or drying cycle and depending on the history of the wetting/drying cycles). The smaller pores could be full and the wider pores or compartments empty. The data appears to support these types of trends/interpretations although more research will be needed to fully validate or prove those types of models. This is illustrated in very simplified fashion in the following figures:

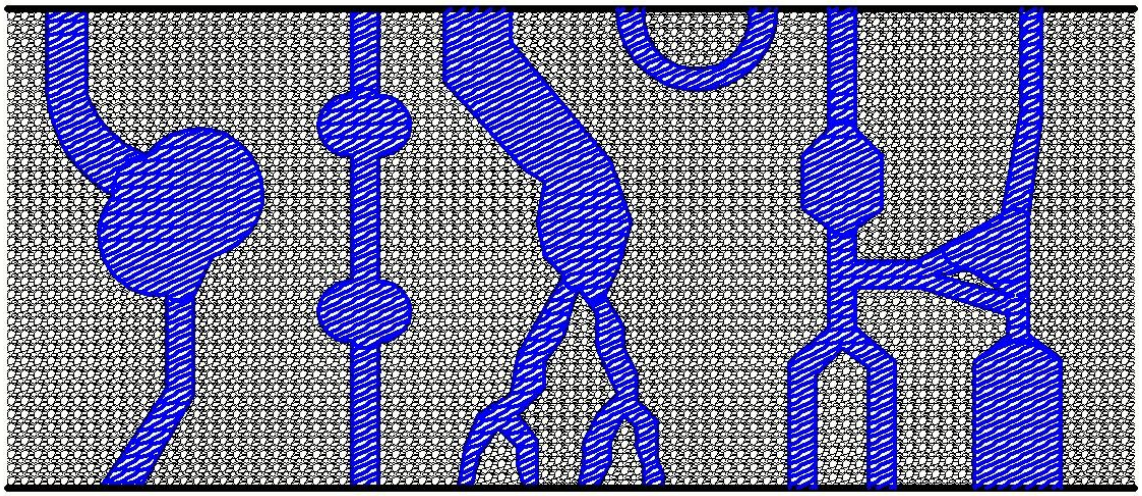

Figure 3.22: Saturated Soil Element between Two Transmission Line Conductors

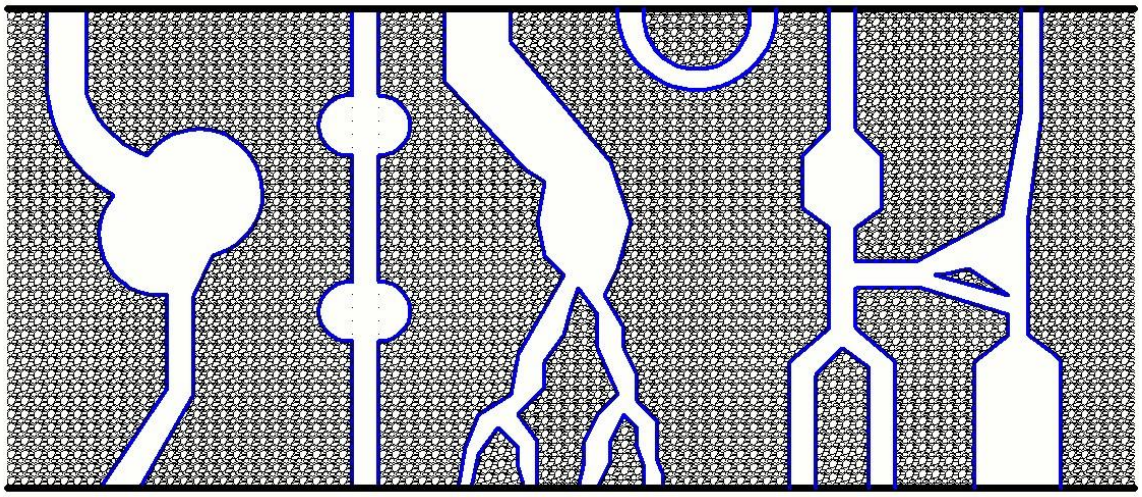

Figure 3.23: Dry Soil Element between Two Transmission Line Conductors

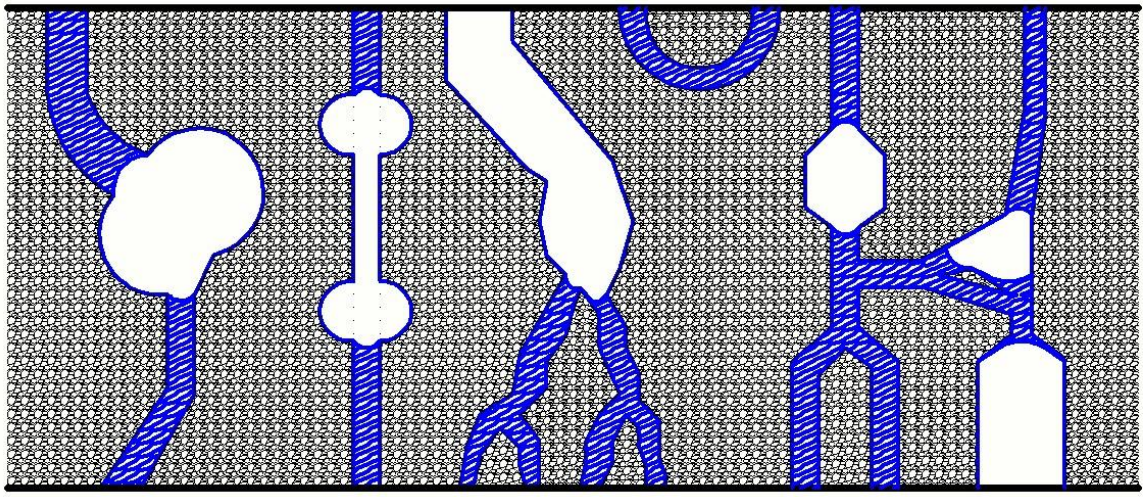

Figure 3.24: Intermediate Water Content Soil Element between Two Transmission Line Conductors

In reviewing figures 3.22 – 3.24 one can envision that the two extreme cases (saturated soil – figure 3.22 and dry soil – figure 3.23) approximate the parallel model as there is a large stochastic probability that a "thru" path can be found in the majority of pore paths between the conductors for either air (fully dry soil) or water (fully saturated soil). Both of these extremes approximate a two component model. In contrast in reviewing figure 3.24 for the intermediate water content one can envision a reasonable stochastic probability of obstructions that would prevent fully "thru" paths. This would tend to lean towards the series model although there is a probability of finer paths/pores making it all the way through (if there are no large compartments in series) and so one can envision that some intermediate model between the extremes of the

parallel and series model could be appropriate here. Obviously these models are not perfect as there are infinite different stochastic distributions of tortuous pore paths and sizes. But the data for many of the soils tested in this research tend to point towards the parallel model being the appropriate model at the extremes of very wet or very dry soils and an intermediate model between the parallel and series models appropriate for mid-range water contents. Several different trial functions/models for the weighting coefficients of the above interpolation models have been evaluated against large numbers of datasets in both laboratory and field settings. Those results and final chosen models (for the coefficients) are presented in the next chapter on validation of the models although one example of a final model is given further below in (3-58) through (3-61).

All of the above interpolation models can (to different degrees) be made to accurately model the electromagnetic propagation constant and electromagnetic parameters vs. frequency for changing water content and electrical conductivity. This is accomplished by the proper selection or derivation of the weighting factors $K_1$, $K_2$, $J_1$, $J_2$, $J_3$, $J_4$, $A_1$, $A_2$, $B_1$, $B_2$, a and b to support or model the above biasing trends of the parallel model at the extremes of very dry or very wet soil and an intermediate model (between the series and parallel models) for intermediate water contents. For sand this means that the interpolation models need to trend towards the parallel model at both extremes of water contents (very wet and very dry) as a two compartment model of soils is approached. In intermediate water contents the model must then move somewhere between these model extremes. In general the above advanced interpolation models with the above weighting trends were found to be the best fitting models to actual data. For the sub-case of high electrical conductivities the simpler cascade model (from which classical equations such as the index of refraction equation used in existing TDR systems can be derived) was still found to be an acceptable fit but it was a poorer fit in medium to higher water contents with lower conductivity. Therefore, the basis of the new algorithm will be these interpolation models since good fit is required for all values of electrical conductivity and water content.

One example of an attempt to incorporate the above biasing or weighting trends into the interpolation algorithms is given below for a special variation of the geometric mean model where the weighting parameters have been made functions of the water content, air content and porosity.

Enhanced Geometric Mean Model with Weighting Functions Incorporated:

In this case the weighting constants "a" and "b" are set up in the geometric mean model as follows to give more weighting to the parallel model at higher water contents as well as very low water contents and progressively more equal billing to the series model for intermediate water contents:

$$\gamma_T = \gamma_{GeometricFT} = \sqrt{\gamma_L^{((\frac{\theta(\phi-\theta)}{0.25\phi^2})+.15)}\gamma_U^{((1-(\frac{\theta(\phi-\theta)}{0.25\phi^2}))+.85)}} \quad (3\text{-}58)$$

$$\varepsilon'_T = \varepsilon'_{GeometricFT} = \sqrt{\varepsilon'^{((\frac{\theta(\phi-\theta)}{0.25\phi^2})+.15)}_L \varepsilon'^{((1-(\frac{\theta(\phi-\theta)}{0.25\phi^2}))+.85)}_U} \quad (3\text{-}59)$$

$$\varepsilon''_T = \varepsilon''_{GeometricFT} = \sqrt{\varepsilon''^{((\frac{\theta(\phi-\theta)}{0.25\phi^2})+.15)}_L \varepsilon''^{((1-(\frac{\theta(\phi-\theta)}{0.25\phi^2}))+.85)}_U} \quad (3\text{-}60)$$

$$\sigma_T = \sigma_{GeometricFT} = \sqrt{\sigma_L^{((\frac{\theta(\phi-\theta)}{0.25\phi^2})+.15)}\sigma_U^{((1-(\frac{\theta(\phi-\theta)}{0.25\phi^2}))+.85)}} \quad (3\text{-}61)$$

Similar weighting functions could be incorporated into the other three interpolation models that are functions of the water and air contents (functions of water content and porosity). Examples of these final models (in terms of functions for the coefficients) will be shown in the next chapter on model validation. In the inverse solving measurement algorithm in its present state (presented in the later chapter on the inverse algorithms), the lookup table for water content was generated with the rectangular mean interpolation model for propagation constant and the largely equivalent arithmetic mean interpolation model for the permittivity and conductivity models with functions derived to give best fit weighting parameters as presented in the next chapter on validation. These specific coefficients $K_1$, $K_2$, $A_1$, $A_2$ for these models are set up as functions of water content $\theta$ and porosity $\phi$ (and hence indirectly also the air content) to arrive at overall interpolation models for (3-42) to (3-45). Again, these final chosen models will be presented in the next chapter on validation and compared against the numerous datasets. There is not one unique model that covers all soils and so the individual models for the different soil types will be presented in the

validation chapter but again they will be in the form of the above interpolation models with special functions derived for the coefficients as functions of water content $\theta$ and porosity $\phi$ (and hence again indirectly also the air content).

## Non-Invasive Circuit Board Based Measurement Systems:

There is one final item in the context of dielectric or electromagnetic mixing models related to the research presented in this dissertation. On a couple of the laboratory datasets a special fixture was developed (shown in the methods/validation chapter) that allowed for inserting a transmission line through the soil as well as sandwiching two RF/microwave (RT/Duroid dielectric) Printed Circuit Board Assemblies with various transmission line patterns on the top and bottom of the fixture containing a soil. Both TDR (open circuit termination on the far ends of the lines) as well as TDT (50 Ohm termination on the far end and capability for both transmission and reflection measurements) were possible with all three transmission lines associated with these fixtures. There were different transmission line patterns evaluated on the PCBA's and they were all oriented orthogonal to the parallel wire transmission line that went through the center of the fixture (again all shown in various figures in the next chapter on methods/validation). One of the transmission line patterns on the PCBA's that showed the best performance was a coplanar waveguide transmission line pattern (three-conductor). Another transmission line pattern tested was coplanar strips (two conductors). Data will be presented in the next chapter to show the performance of one pattern against another as well as against final models chosen. These PCBA's allowed for non-invasive measurements of the water content in the soil fixture and were compared against the internal transmission line measurements. Again, both TDR and TDT measurements were possible with these fixtures.

Non-Invasive Propagation Constant:

A set of models were developed for the propagation constant of the PCB adjoined to the soil. The model is analogous to the rectangular mean interpolation model of (3-42) but in this case we are one level higher up where the interpolation is between the models for the soil propagation constant and the PCB propagation constant. The weighting functions were initially assigned as equal as shown in (3-62).

$$\gamma_{\mathrm{TCB}} = \sqrt{\frac{(\gamma_{\mathrm{T\_Soils}})^2 + (\gamma_{\mathrm{PCB}})^2}{2}} = \alpha_{\mathrm{TCB}} + \mathrm{j}\beta_{\mathrm{TCB}} \tag{3-62}$$

Similar interpolation models were derived for the permittivity and conductivity using models similar in form to the arithmetic mean interpolation models of (3-43) to (3-45) only in this case the interpolation is between the PCB parameters and the soil as if they are influencing the transmission line shunt components in parallel (a reasonable assumption since both dielectrics are directly adjoined to the transmission line conductors although from opposite sides).

For the special simplified cases where losses are lower (and the RT Duriod dielectric on one side of the PCB conductors does mitigate the losses from the soil somewhat) the following can be extracted for a first order approximation of some of the key electromagnetic parameters:

Effective Phase Velocity:

$$\mathrm{V}_{\mathrm{P_{TCB}}} = \frac{\omega}{\beta_{\mathrm{TCB}}} \tag{3-63}$$

Effective Dielectric Constant:

$$\varepsilon_{eff_{\mathrm{TCB}}} = \left( \frac{1}{\mathrm{V}_{\mathrm{P_{TCB}}} \sqrt{\mu_r \mu_0 \varepsilon_0}} \right) \tag{3-64}$$

Non-Invasive Intrinsic Impedance:

$$\eta_{\mathrm{TCB}} = \frac{\mathrm{j}\omega\mu}{\gamma_{\mathrm{TCB}}} \tag{3-65}$$

Non-Invasive (3-conductor) Coplanar Waveguide Impedance [12]:

$$Z_{\mathrm{TCB}} = \left(\frac{1}{\pi}\right)\left[\ln\left(2\sqrt{\frac{a}{w}}\right)\right]\eta_{TCB} \tag{3-66}$$

Non-Invasive (2-conductor) Coplanar Strips Impedance:

$$Z_{TCB} = \left(\frac{1}{\pi}\right)\left[\cosh^{-1}\left(\frac{a}{d}\right)\right]\eta_{TCB} \qquad (3\text{-}67)$$

where

a = spacing between outer two traces on 3-trace non-invasive probe.

d = spacing between two traces on 2-trace non-invasive probe.

w = width of center trace on 3-trace non-invasive probe
or width of each trace on 2-trace non-invasive probe.

$\gamma_{T\_Soils}$ = Overall Electromagnetic Propagation Constant of Composite Soil

$\gamma_{CB}$ = Propagation Constant in Circuit Board (RT-Duroid)

$\gamma_{TCB}$ = Overall Propagation Constant of Overall Circuit Board-Soil Mix

$\eta_{TCB}$ = Intrinsic Impedance of overall circuit board-soil mix.

$\eta_0$ = Intrinsic Impedance of free space.

$Z_{TCB}$ = Characteristic Impedance of overall circuit board / soil transmission line

$V_{PTCB}$ = Effective Phase Velocity of Circuit Board / Soil Composite Transmission Line

$\varepsilon_{effTCB}$ = Effective relative permittivity or dielectric constant

and all the other parameters are as defined earlier. Models for this circuit board / soil composite are evaluated in the next chapter on model validation.

## Conclusions on Composite Mixing Models:

All of the various models presented for composite media utilizing figures 3.19 – 3.24 and equations (3-7 to 3-16) and (3-17 to 3-67) would form the basis for models for each element $E_n$ in a cascaded transmission line (per figures 3.1, 3.7 and 3.8). Scattering S-parameter models are then used to model the overall cascaded transmission line (Appendix B). These cascaded segments can be used to model TDR or TDT transmission line systems in soils. Each segment or element $E_n$ on the transmission line would have its own expression for propagation constant and characteristic impedance which are functions of frequency and all the electromagnetic parameters (Appendix A). Each segment/element would also have a corresponding physical length $L_n$. Boundaries $B_n$ between these segments/elements $E_n$ can be modeled by reflection coefficients and transmission coefficients as described in Appendix B covering S-parameter network theory.

## Example Plots from Forward Prediction Models

Several examples of predictions from the forward prediction models are given in figures 3.25 – 3.88. These figures give predictions for the following utilizing the reflection/transmission TDR/TDT/FDR/FDT fixtures of Laboratory Validation method #2 (figures 4.3a-c):

TDR Waveforms
TDT Waveforms
FDR (S11) Spectra
FDT (S21) Spectra
50Ω End Terminations (TDR/FDR/TDT/FDT) vs. Open Circuit Terminations (TDR/FDR Only)
Open Air
Dry Soil: WC = 0
Intermediate Water Content: WC = 0.15
Wet Soil: WC = 0.33
Saline Soil: WC = 0.33, EC = 1.2 S/m
Parallel Model vs. Series Model: Extremes of Limits per Physics/Electromagnetics
Mason's Non-Touching Loop Rule vs. T-Parameter Methods

As can be seen from figures 3.25 – 3.36 the techinques of T-Parameters vs. Mason's Non-Touching Loop Rule arrive at the same result. As will be shown in the Validation results chapter the same is true for the Nested Construction Method. Therefore all three methods can be used to cross check each other including serving as aids in optimization fitting algorithms coming at the same solution from different directions. Figures 3.25 – 3.36 also show that the Parallel model and Series model are equivalent for the special case of only one constituent (in this case the probe in open air for those subset of figures). However, as can be seen from figures 3.37 – 3.88 the Parallel and Series models progressively deviate away from each other as multiple constituents are added (soil, water) and especially as the WC increases and EC increases. As will be shown in the validation results chapter the actual data resides somewhere between the two theoretical limits of the Parallel and Series models for most conditions. However, at the extremes of WC (very dry and very wet) the Parallel model will be shown to be a good approximate fit. Again, for a one constituent model (e.g. open air) the parallel and series models are equivalent. At all intermediate water contents interpolation models between the Parallel and Series models such as those

presented in this chapter are required for the best fit. Those results are all given in the validation results chapter for a wide variety of laboratory and field test conditions.

Extensive comparisons between actual data and simulated data including both time and frequency domain plots for TDR/FDR and TDT/FDT systems using all the models developed in this chapter including the composite models (including bound and semi-bound water models) are given in the validation chapter as well as Appendix D of this dissertation. The specific examples given in the validation chapter and Appendix D include very dry soils, very wet soils, very saline soils, intermediate water contents, intermediate EC's (over wide ranges of each) as well as cascaded sections of different water contents. As will be shown in those chapters the parallel model was found to be a good fit at the extremes of water content (either very dry or very wet or cascades of very dry sections and very wet sections). In constrast for intermediate water contents various interpolation models are required. It will be shown that the rectangular mean model provided very good fits at all intermediate water contents (with different relative interpolation scalings between the Series and Parallel models). The other interpolation models work in similar fashion. In the next two chapters (Validation Methods and Results) the different models will be evaluated against several datasets through all ranges of values for water contents and electrical conductivities typically found in the field. Different soil types are also evaluated. The Validation Results chapter along with Appendix D shows the capabilities of the forward prediction models with comparisons to actual data across all conditions that can be found in the field.

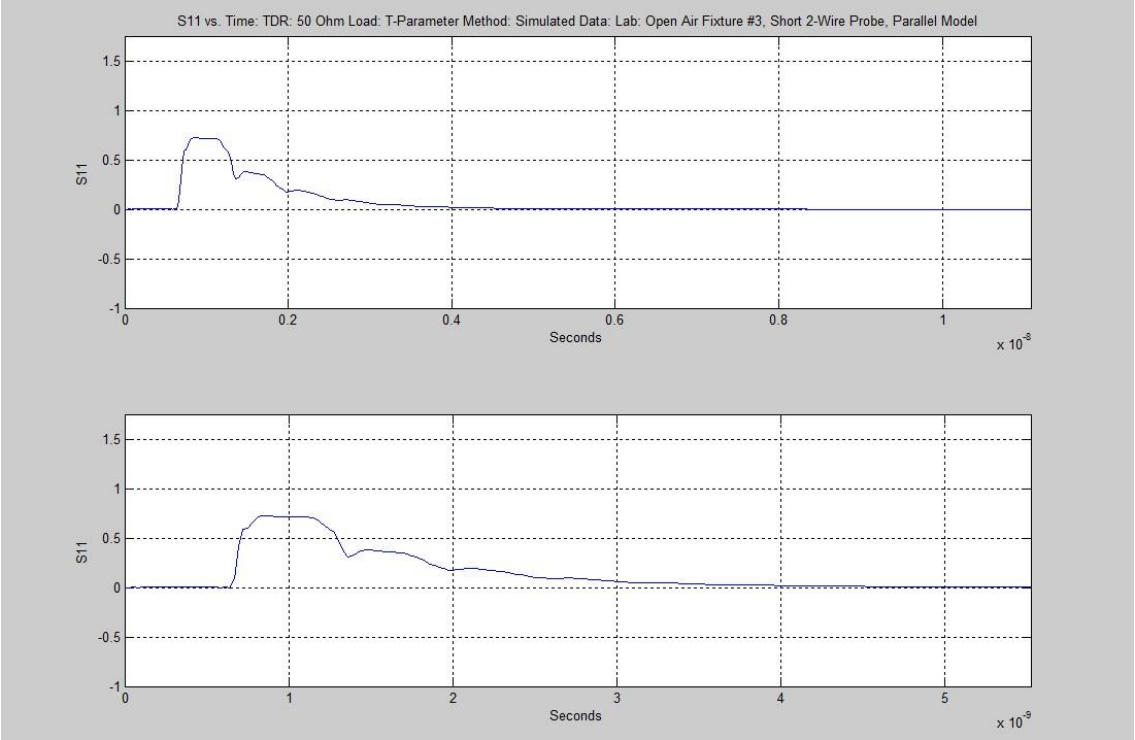


Figure 3.25: 2-Wire Probe: Open Air: TDR Pred.: 50Ω Term: T-Parameter Method: Parallel Model

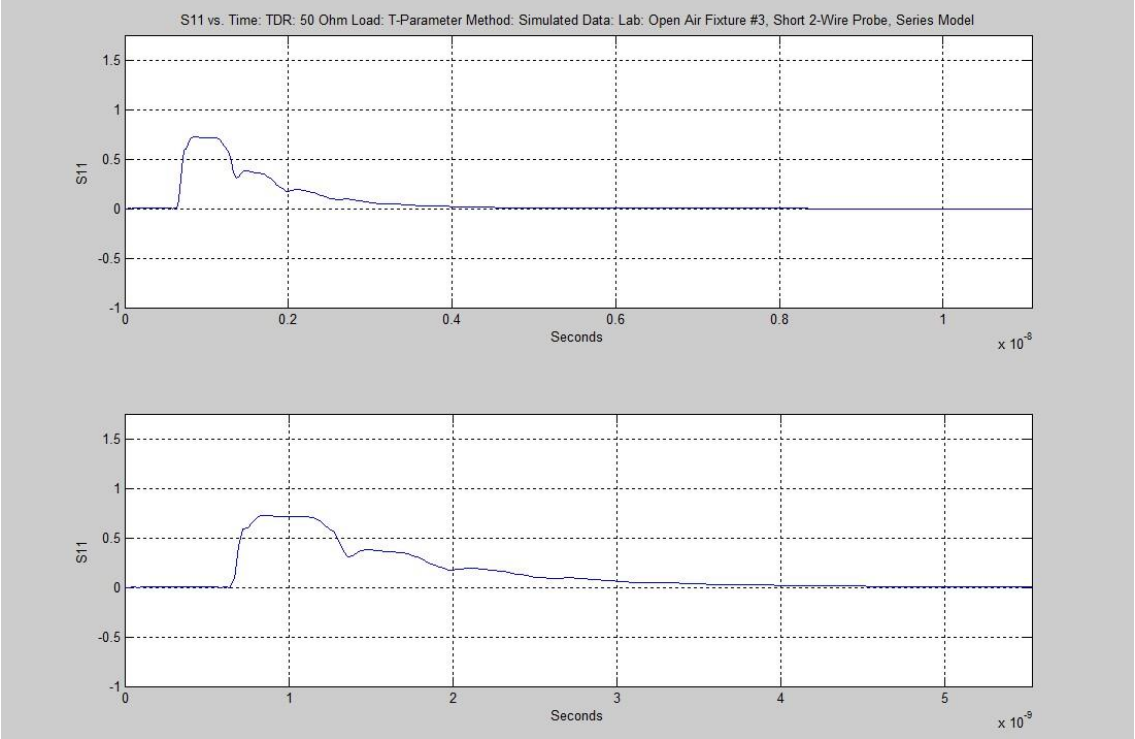


Figure 3.26: 2-Wire Probe: Open Air: TDR Pred.: 50Ω Term: T-Parameter Method: Series Model

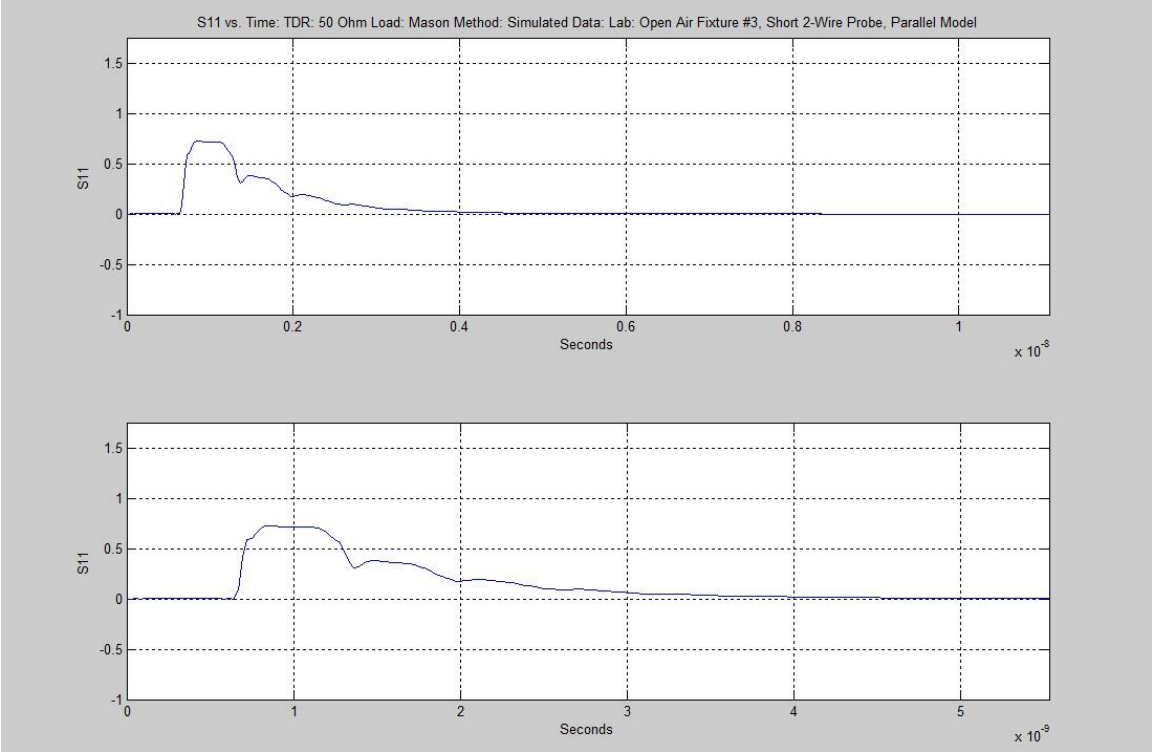


Figure 3.27: 2-Wire Probe: Open Air: TDR Pred.: 50Ω Term: Mason Method: Parallel Model

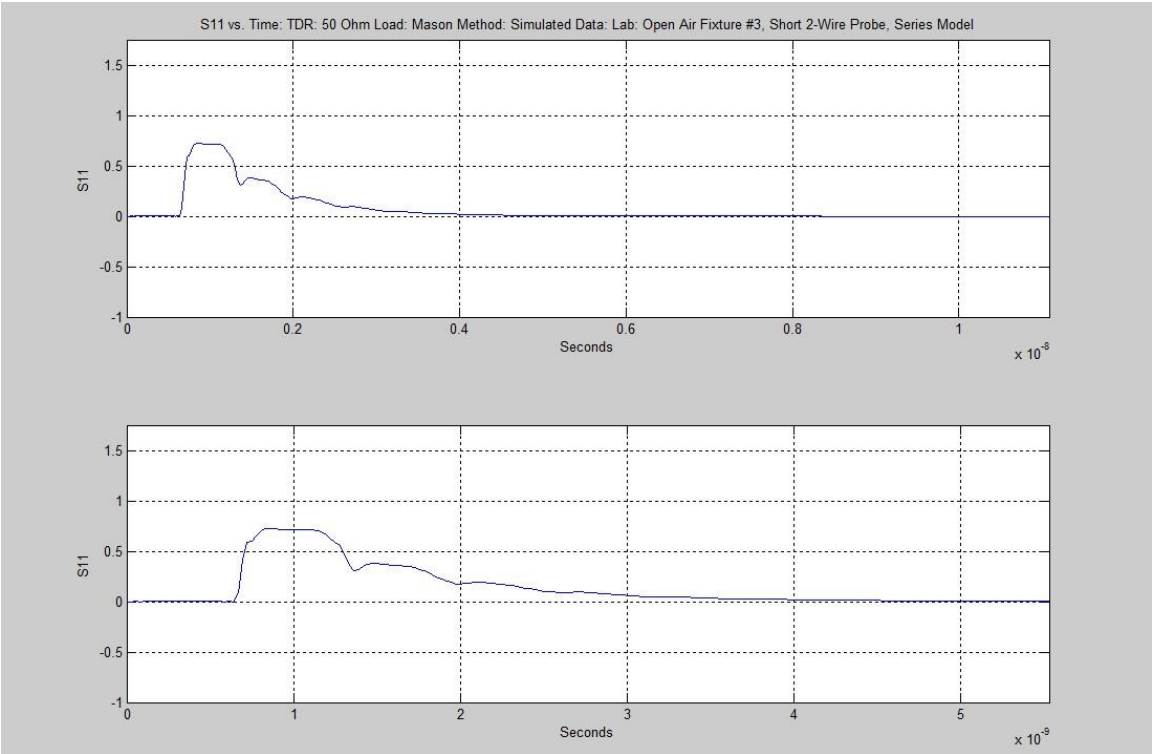


Figure 3.28: 2-Wire Probe: Open Air: TDR Pred.: 50Ω Term: Mason Method: Series Model

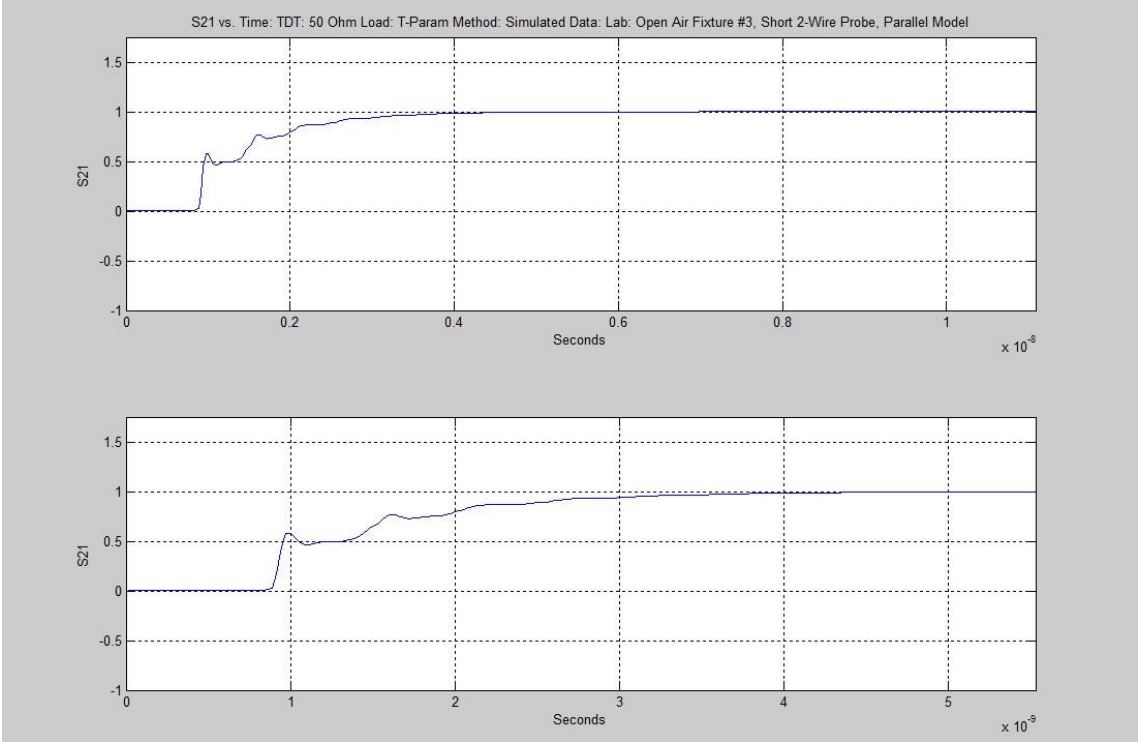


Figure 3.29: 2-Wire Probe: Open Air: TDT Pred.: 50Ω Term: T-Parameter Method: Parallel Model

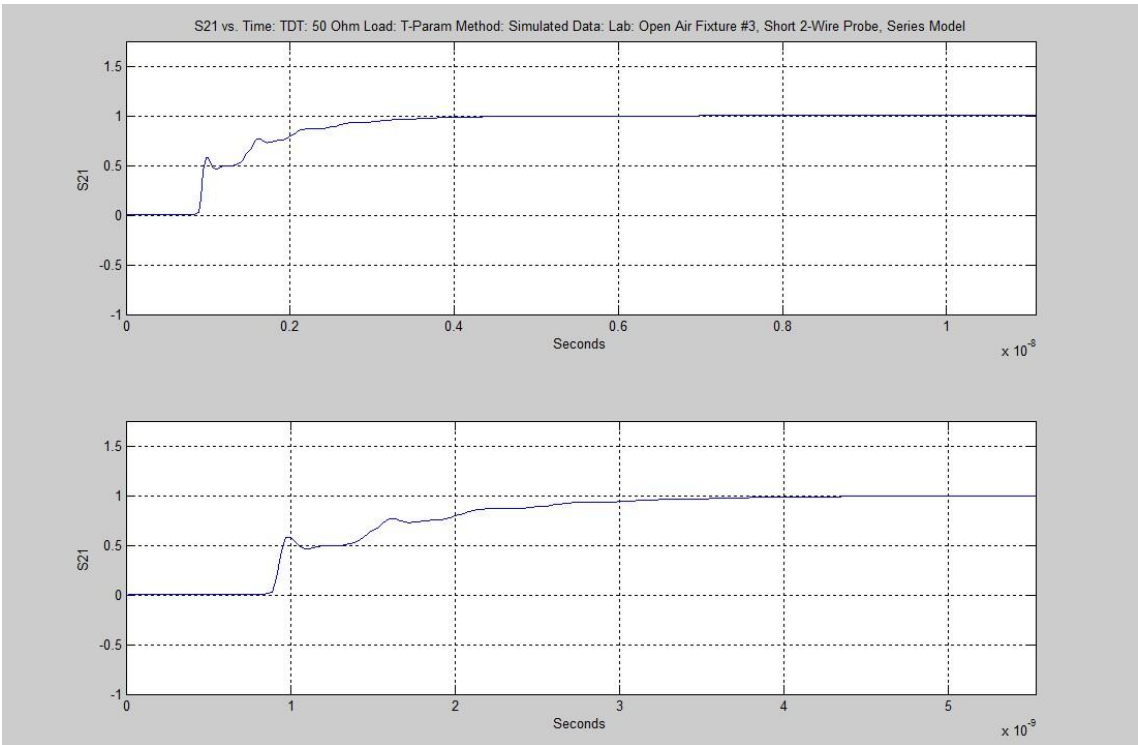


Figure 3.30: 2-Wire Probe: Open Air: TDT Pred.: 50Ω Term: T-Parameter Method: Series Model

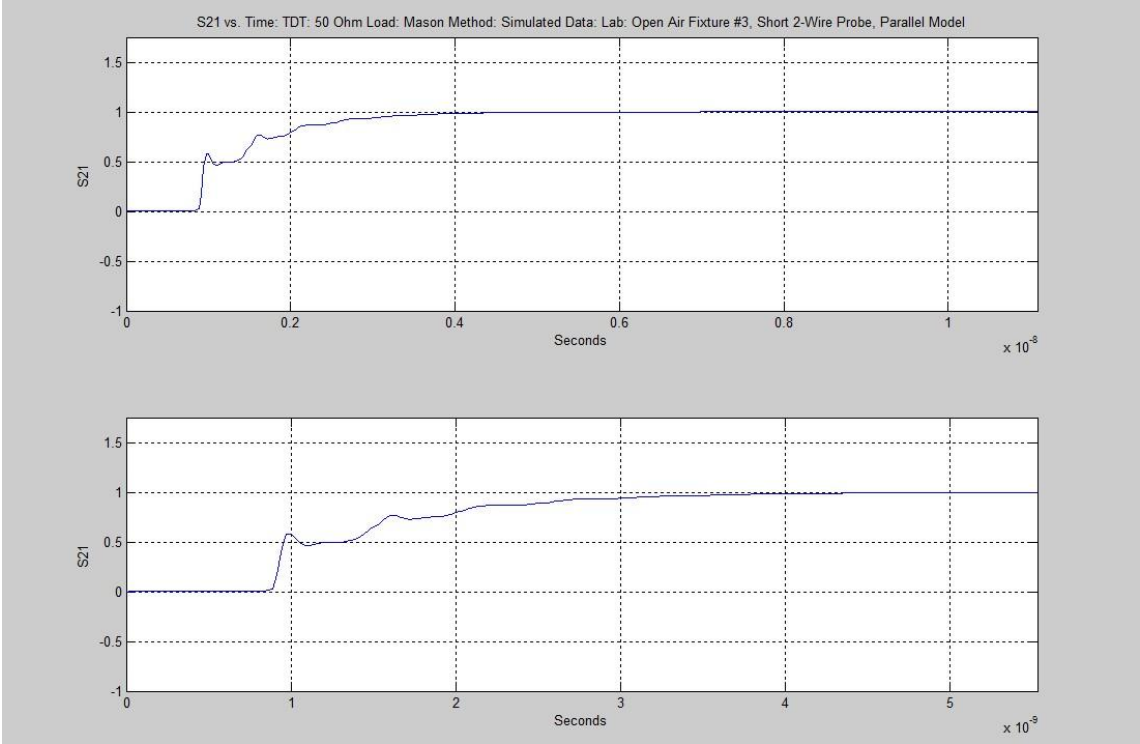


Figure 3.31: 2-Wire Probe: Open Air: TDT Pred.: 50Ω Term: Mason Method: Parallel Model

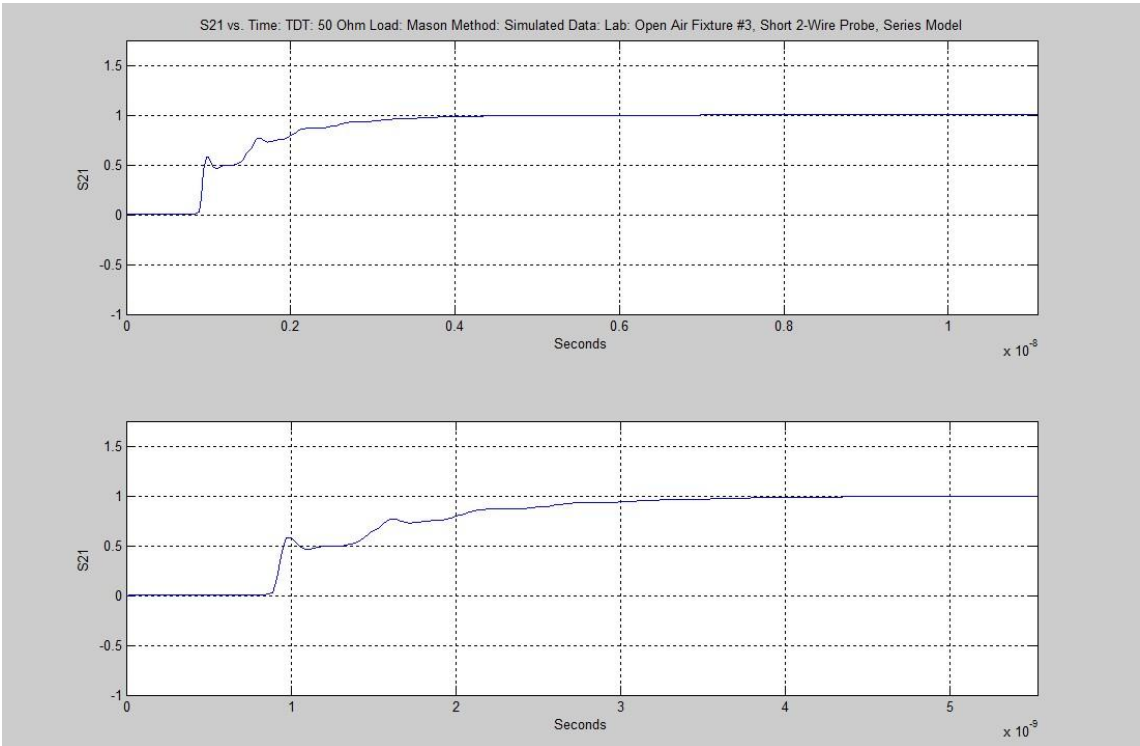


Figure 3.32: 2-Wire Probe: Open Air: TDT Pred.: 50Ω Term: Mason Method: Series Model

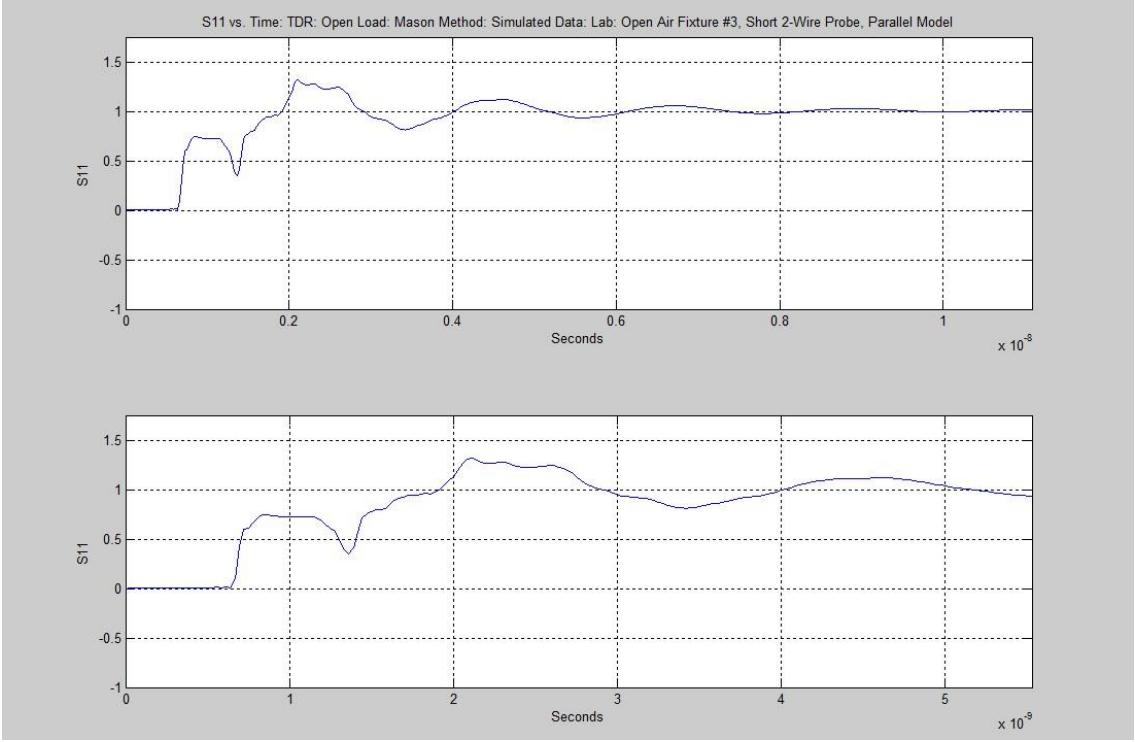


Figure 3.33: 2-Wire Probe: Open Air: TDR Pred.: Open Term: Mason Method: Parallel Model

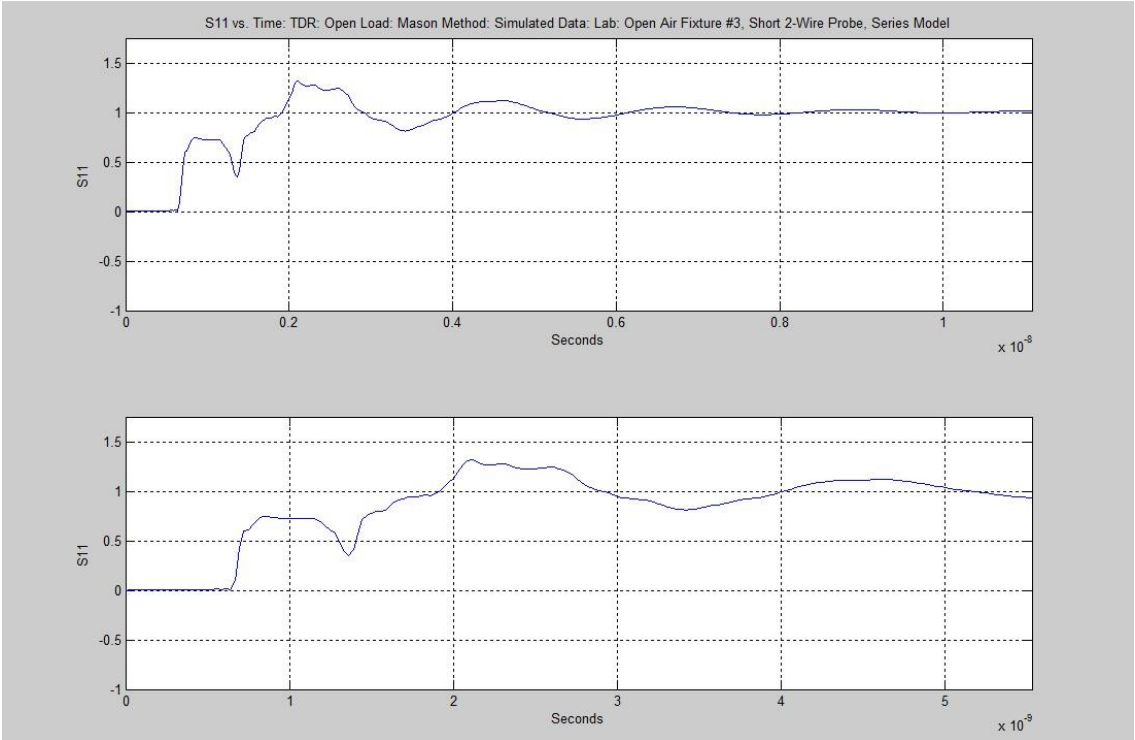


Figure 3.34: 2-Wire Probe: Open Air: TDR Pred.: 50Ω Term: Mason Method: Series Model

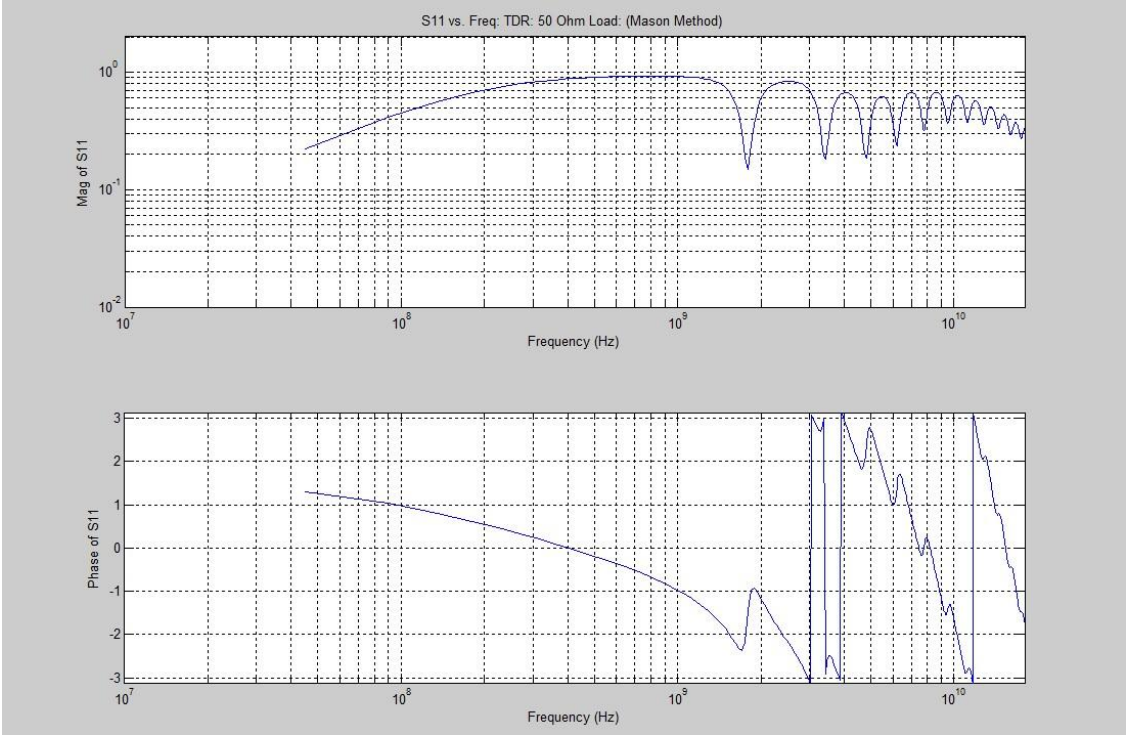


Figure 3.35: 2-Wire Probe: Open Air: FDR Pred.: 50Ω Term: T-Parameter Method: Parallel Model

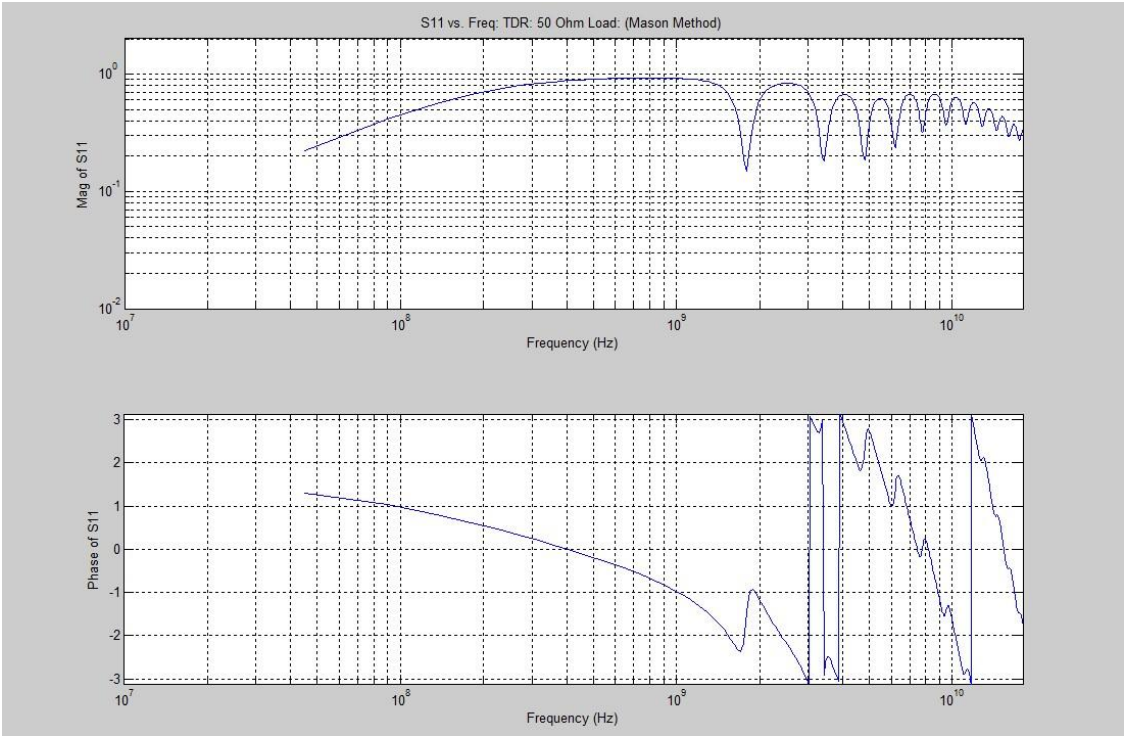


Figure 3.36: 2-Wire Probe: Open Air: FDR Pred.: 50Ω Term: T-Parameter Method: Series Model

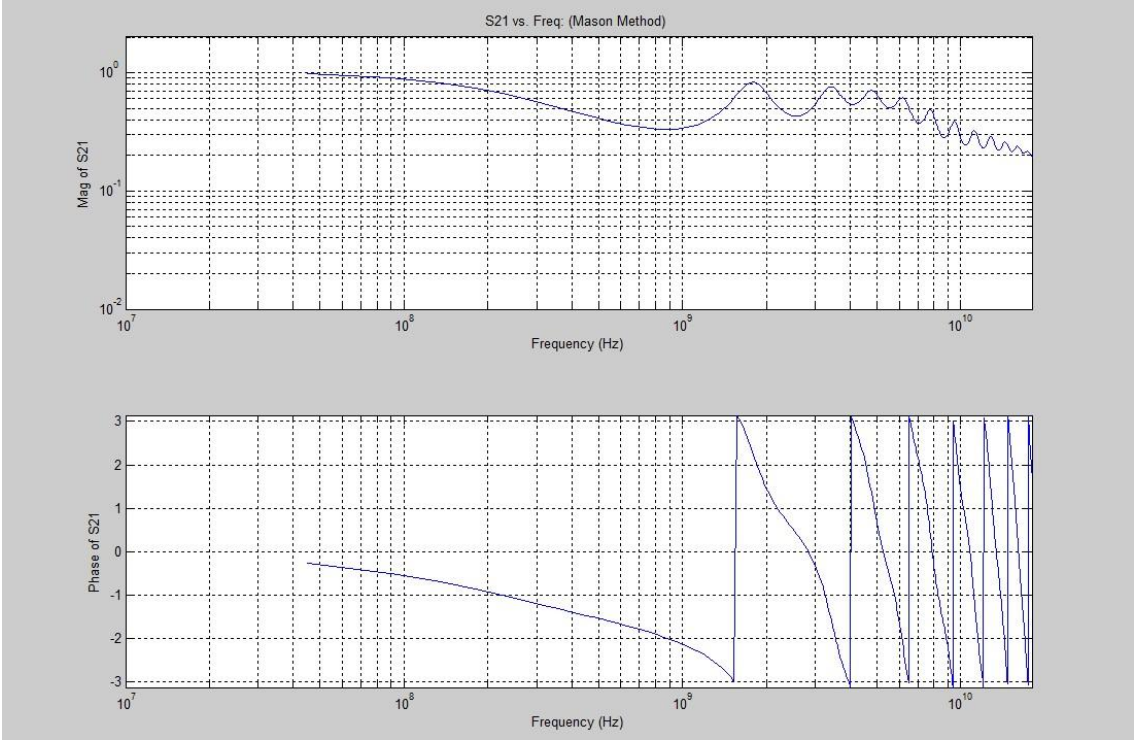


Figure 3.37: 2-Wire Probe: Open Air: FDT Pred.: 50Ω Term: Mason Method: Parallel Model

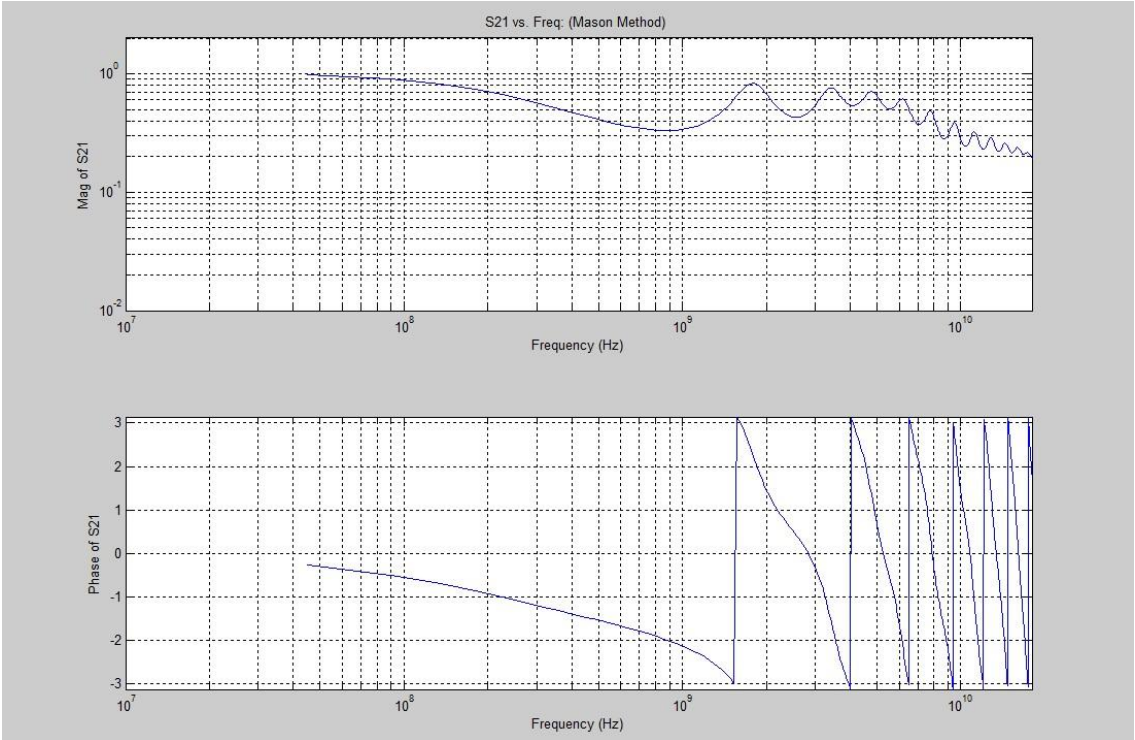


Figure 3.38: 2-Wire Probe: Open Air: FDT Pred.: 50Ω Term: Mason Method: Series Model

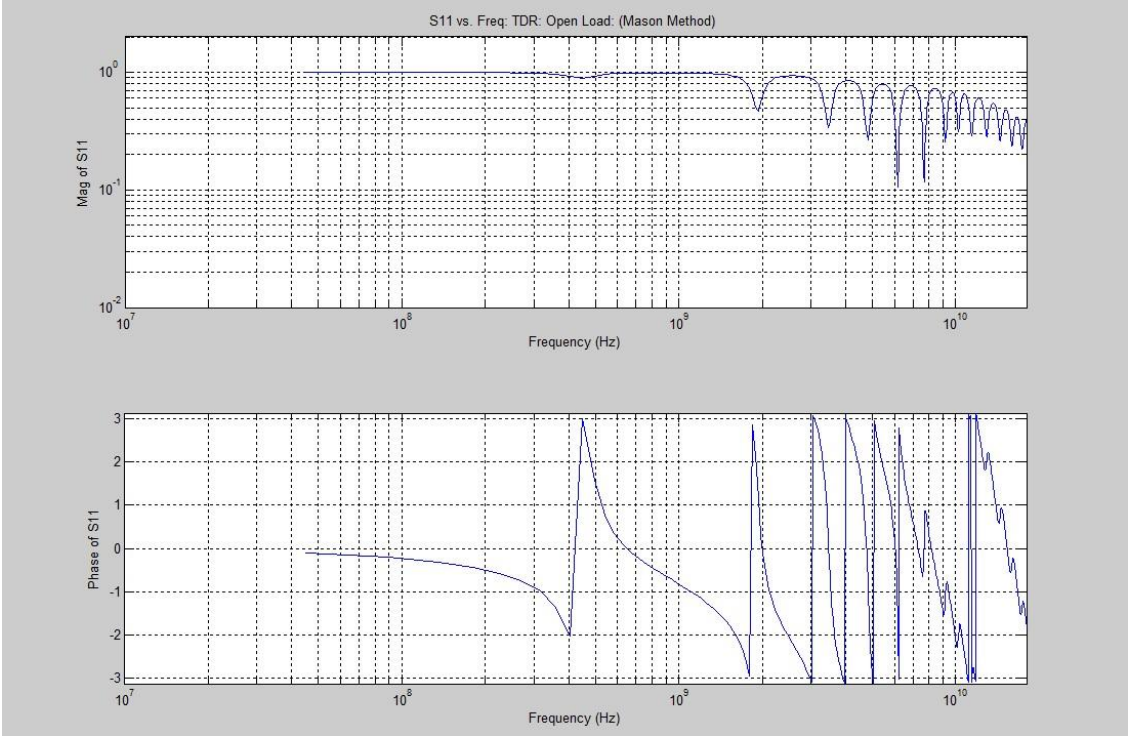


Figure 3.39: 2-Wire Probe: Open Air: FDR Pred.: Open Term: Mason Method: Parallel Model

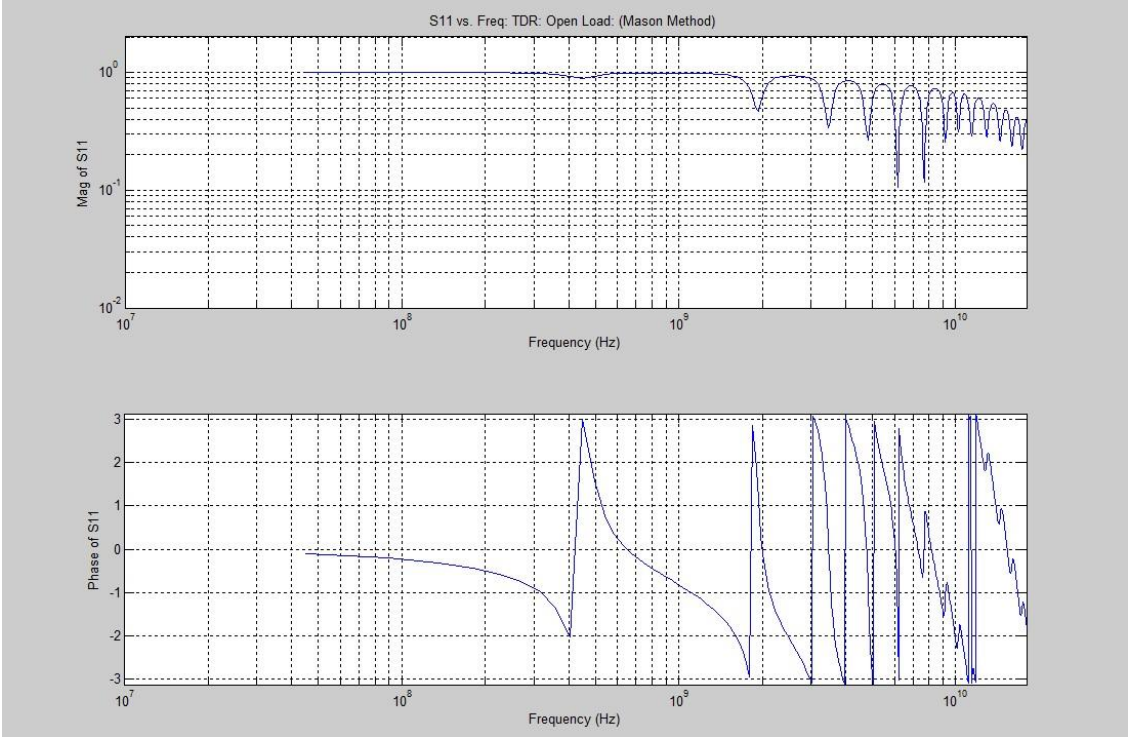


Figure 3.40: 2-Wire Probe: Open Air: FDR Pred.: Open Term: Mason Method: Series Model

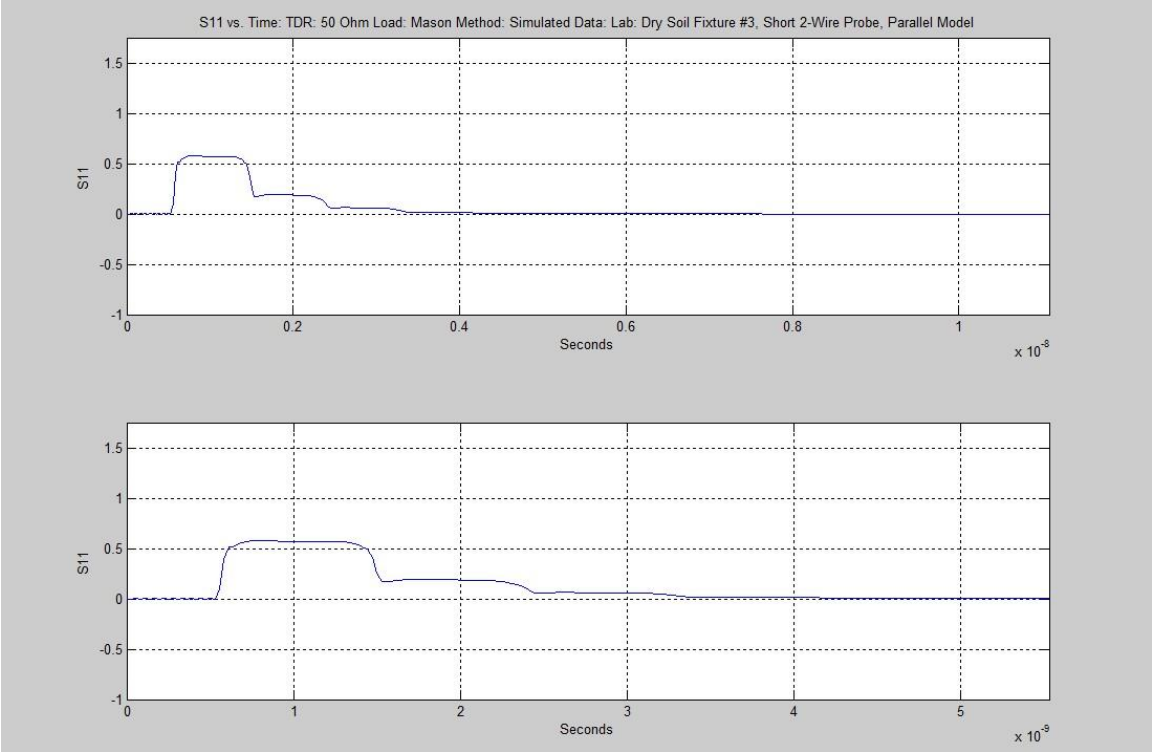


Figure 3.41: 2-Wire Probe: Dry Soil: TDR Prediction: 50Ω Termination: Mason Method: Parallel Model

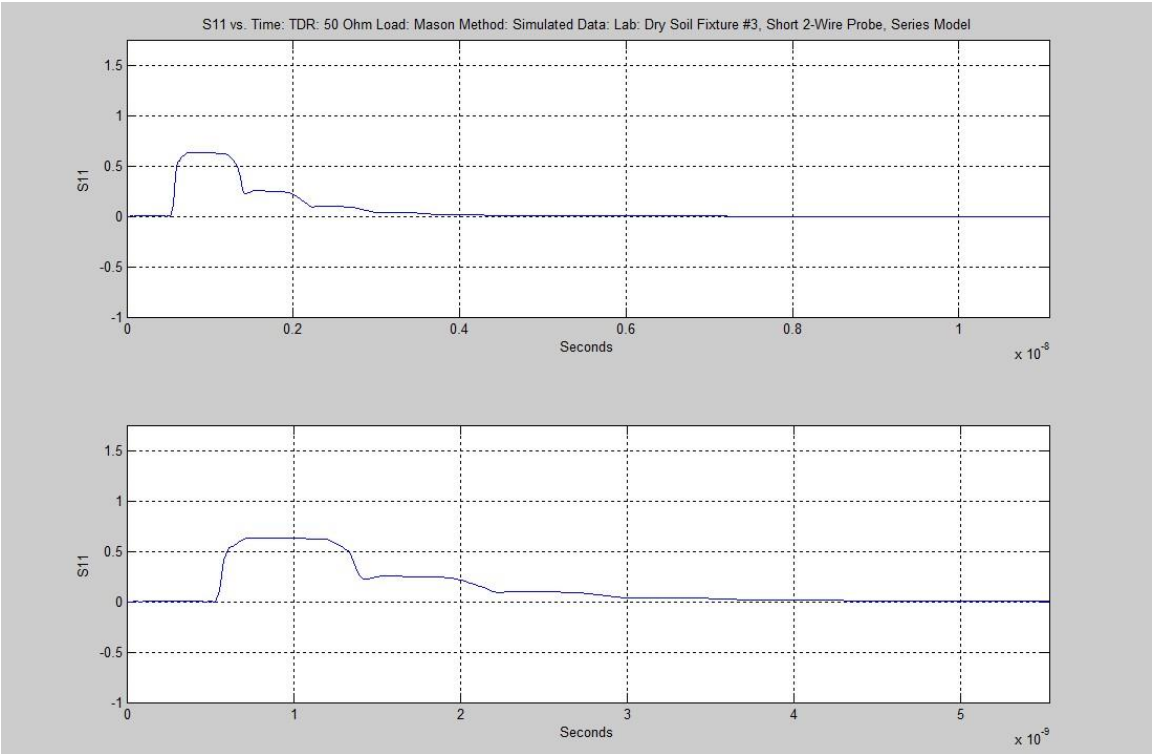


Figure 3.42: 2-Wire Probe: Dry Soil: TDR Prediction: 50Ω Termination: Mason Method: Series Model

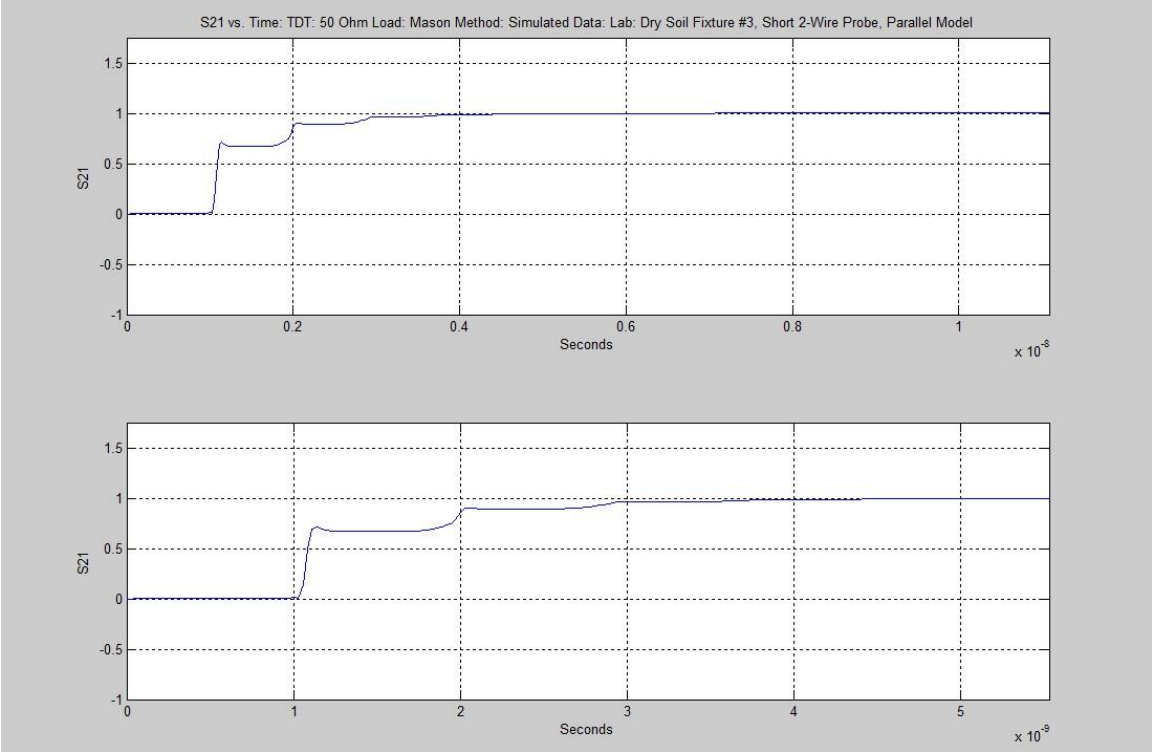


Figure 3.43: 2-Wire Probe: Dry Soil: TDT Prediction: 50Ω Termination: Mason Method: Parallel Model

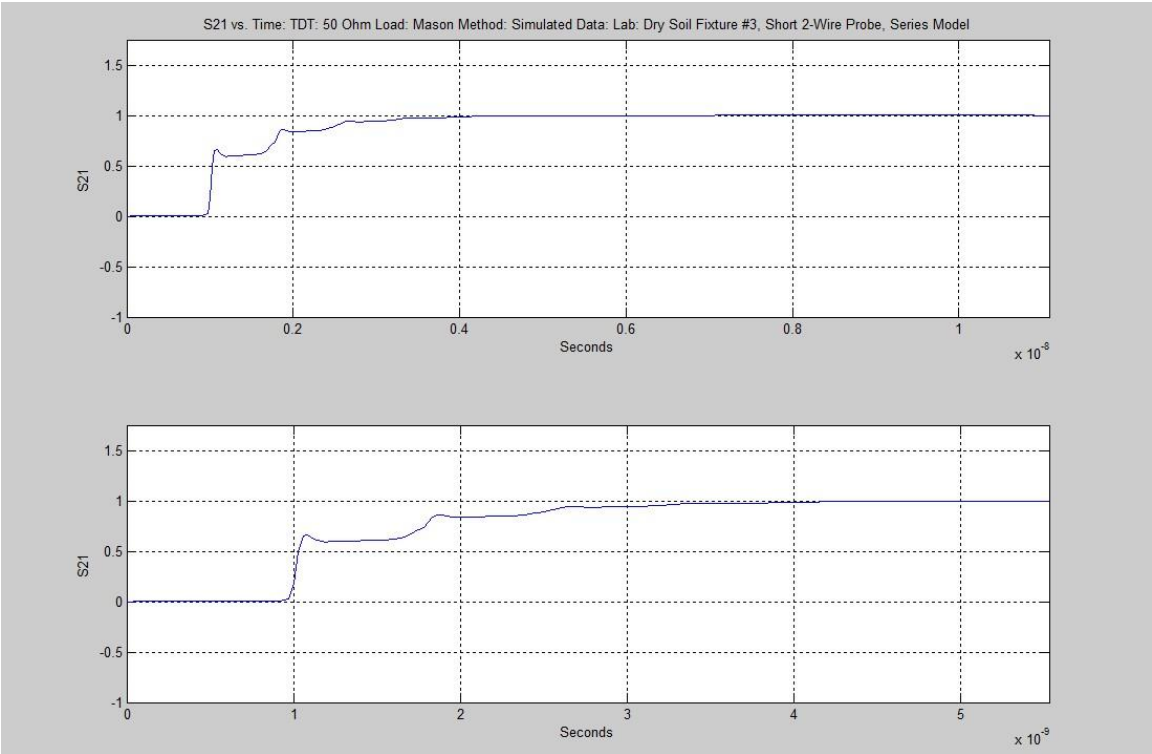


Figure 3.44: 2-Wire Probe: Dry Soil: TDT Prediction: 50Ω Termination: Mason Method: Series Model

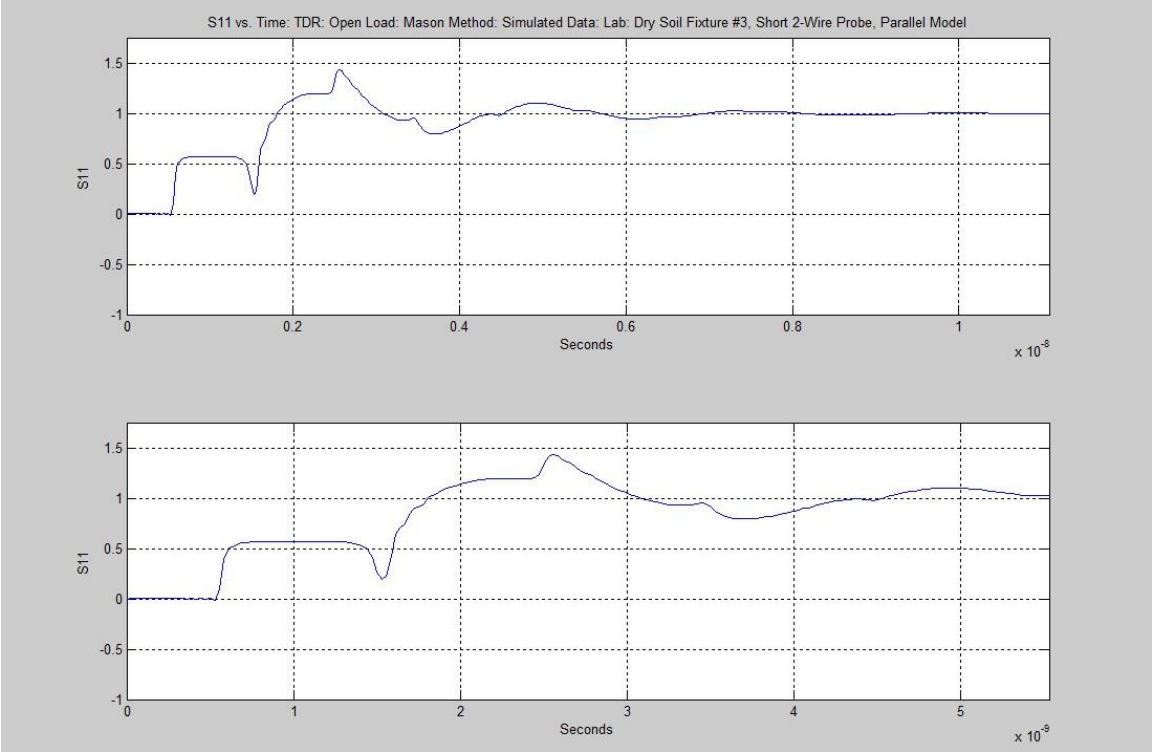


Figure 3.45: 2-Wire Probe: Dry Soil: TDR Prediction: Open Termination: Mason Method: Parallel Model

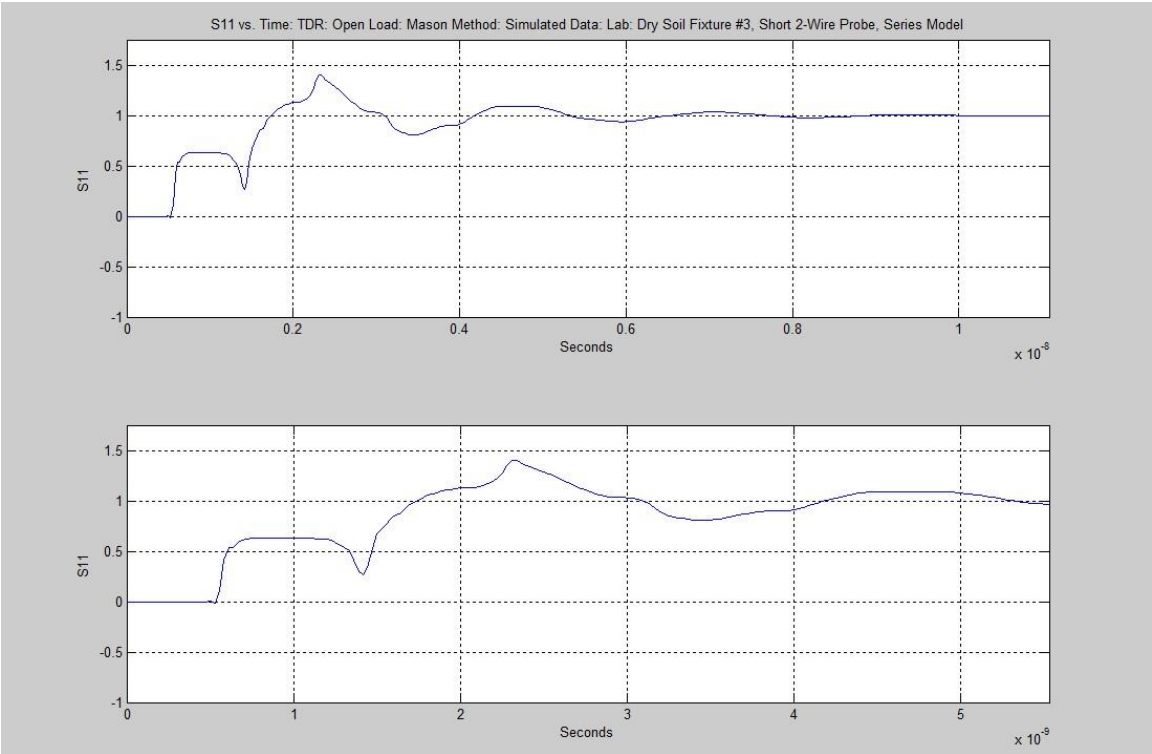


Figure 3.46: 2-Wire Probe: Dry Soil: TDR Prediction: Open Termination: Mason Method: Series Model

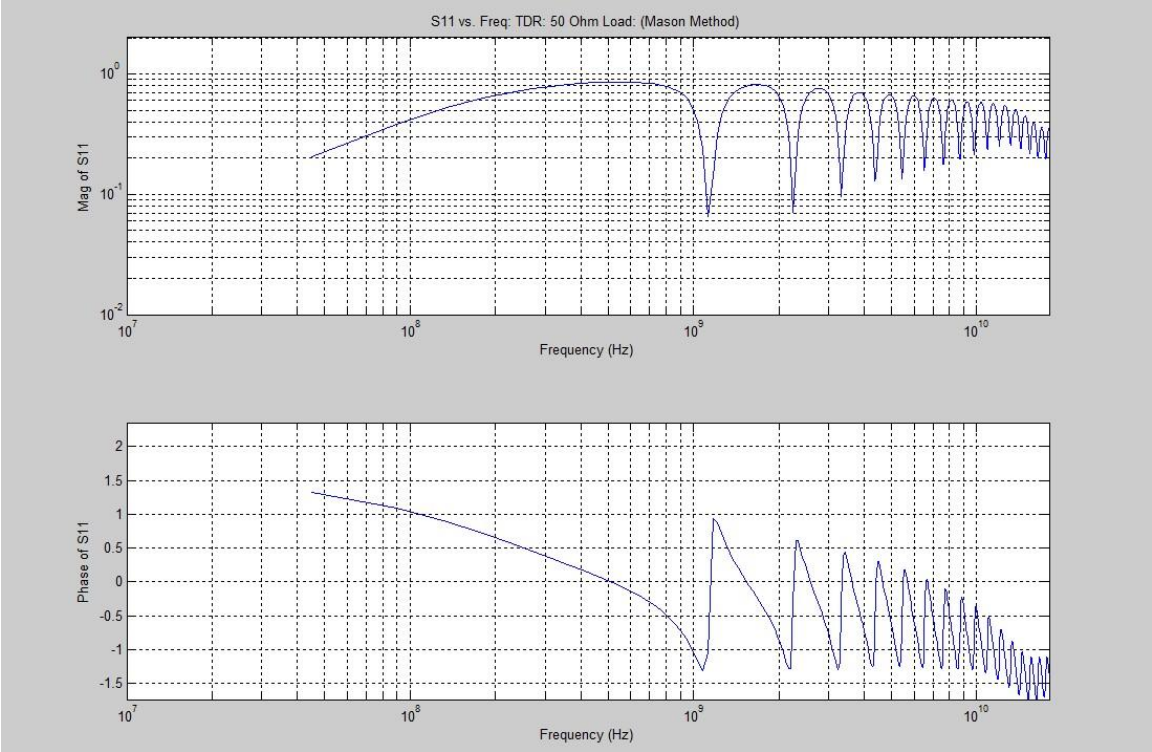


Figure 3.47: 2-Wire Probe: Dry Soil: FDR Prediction: 50Ω Termination: Mason Method: Parallel Model

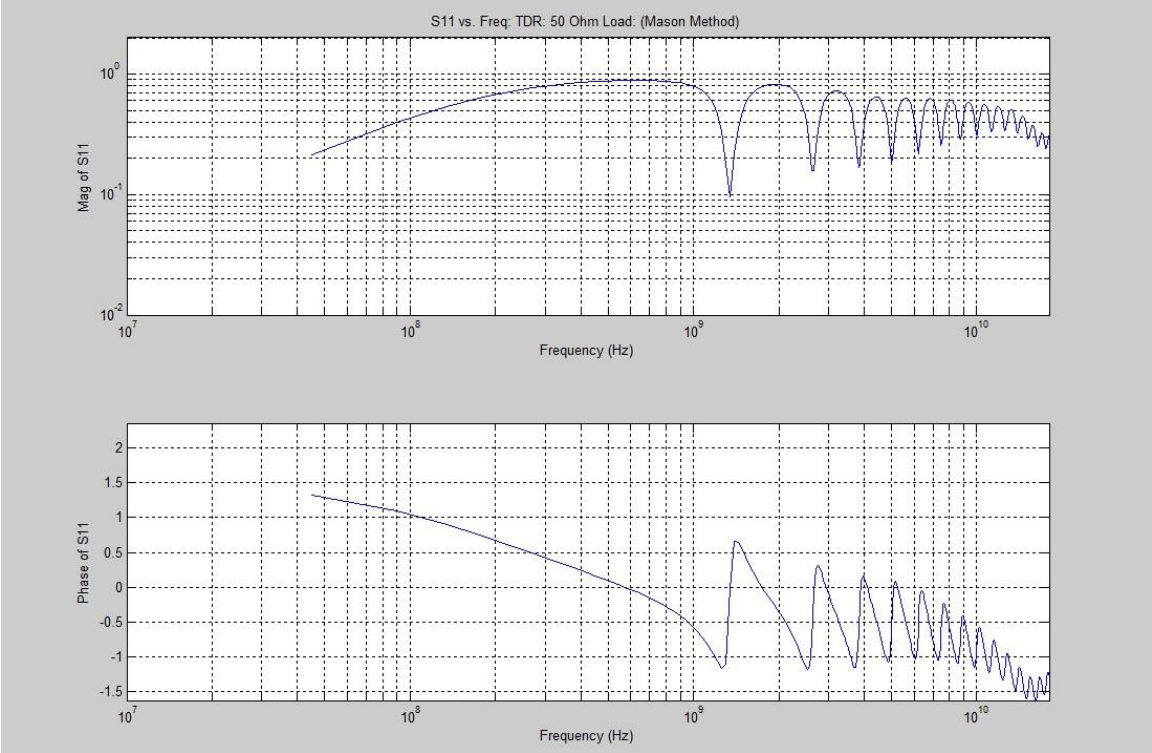


Figure 3.48: 2-Wire Probe: Dry Soil: FDR Prediction: 50Ω Termination: Mason Method: Series Model

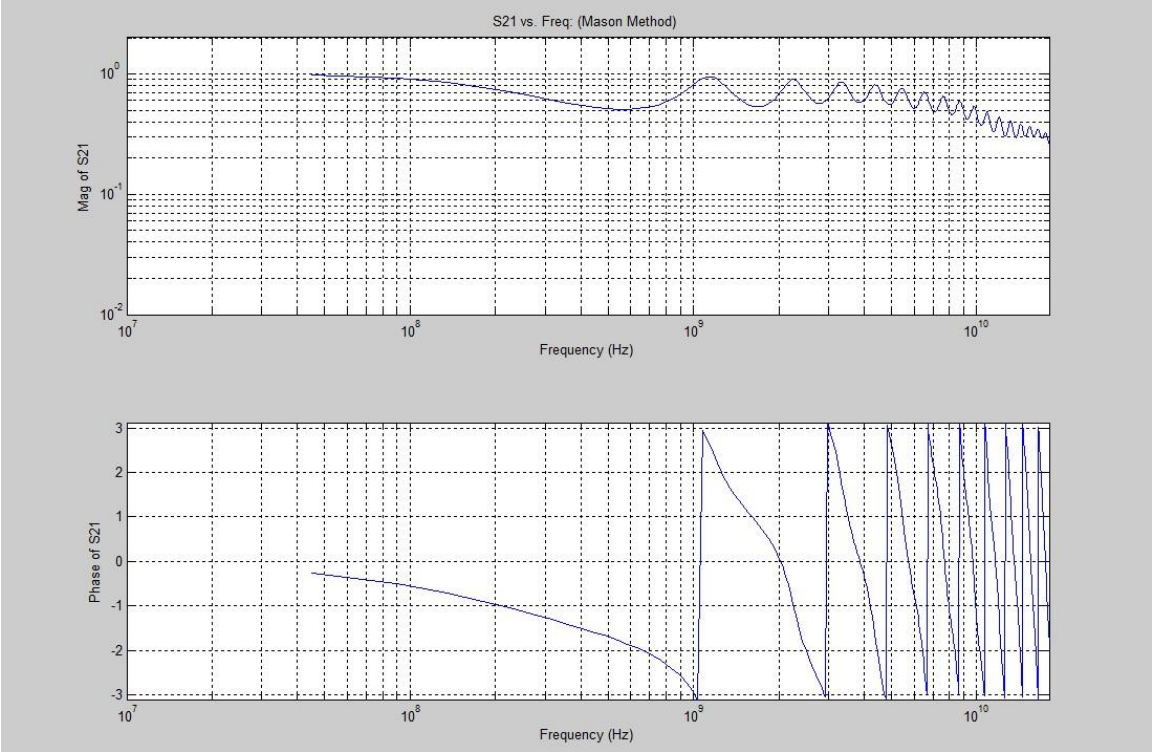


Figure 3.49: 2-Wire Probe: Dry Soil: FDT Prediction: 50Ω Termination: Mason Method: Parallel Model

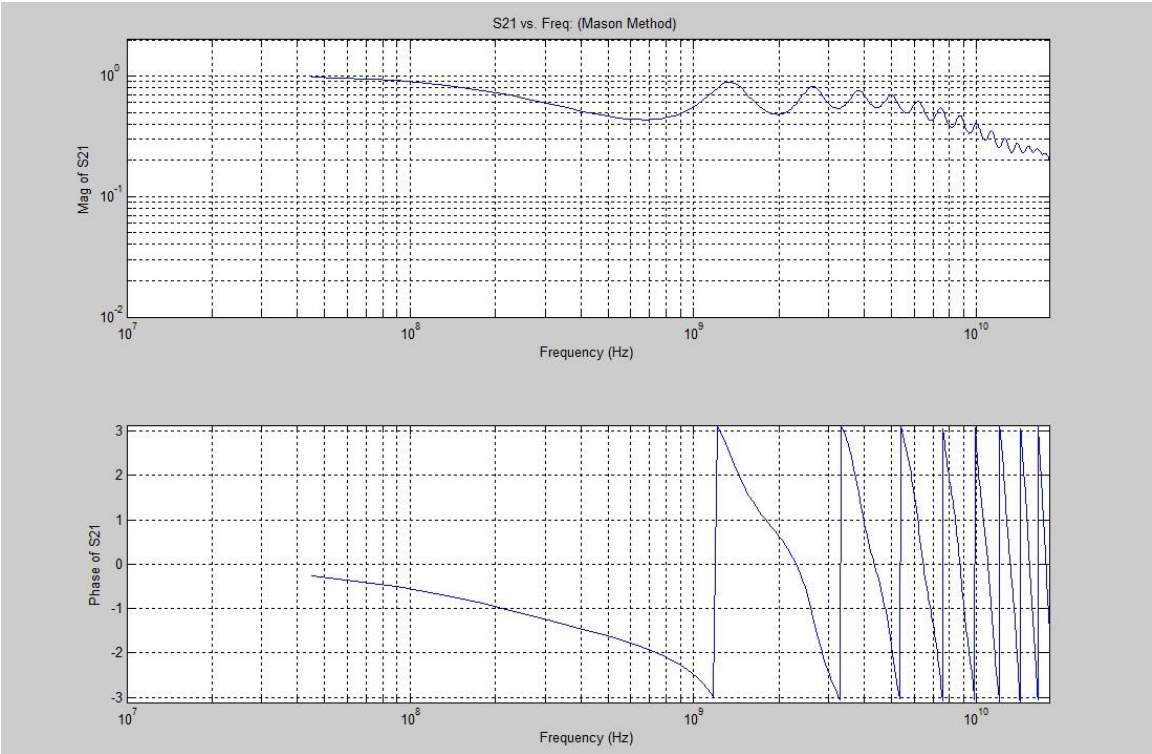


Figure 3.50: 2-Wire Probe: Dry Soil: FDT Prediction: 50Ω Termination: Mason Method: Series Model

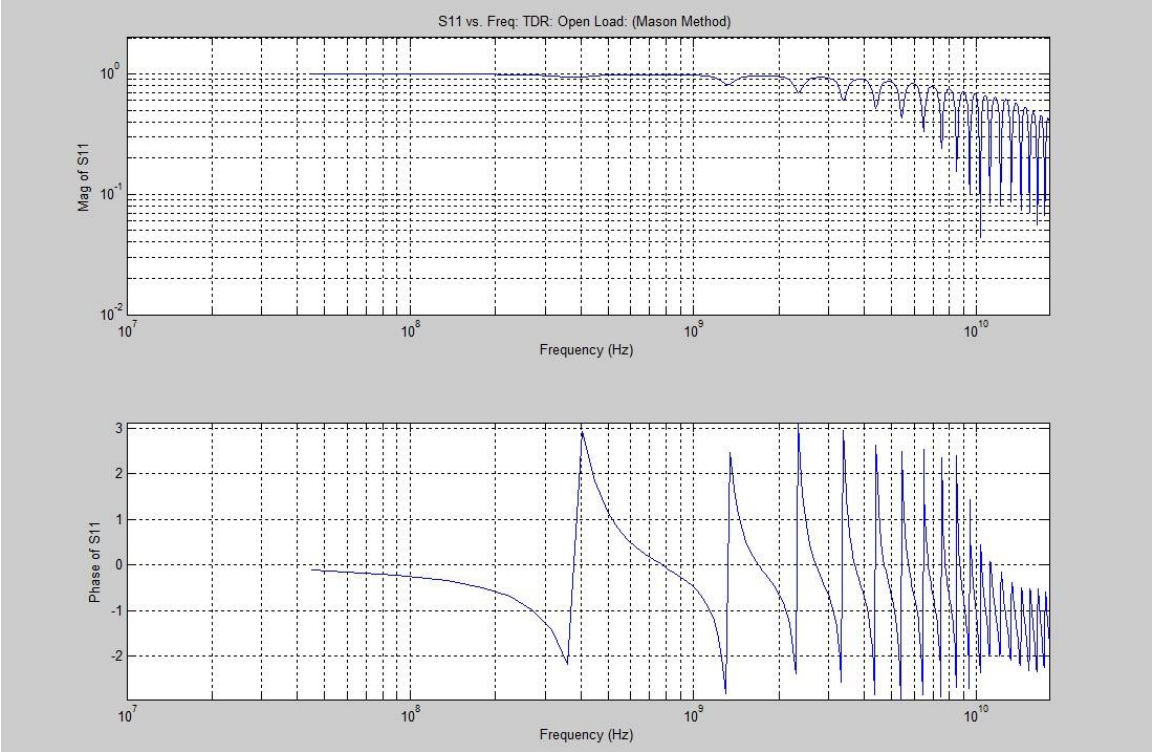


Figure 3.51: 2-Wire Probe: Dry Soil: FDR Prediction: Open Termination: Mason Method: Parallel Model

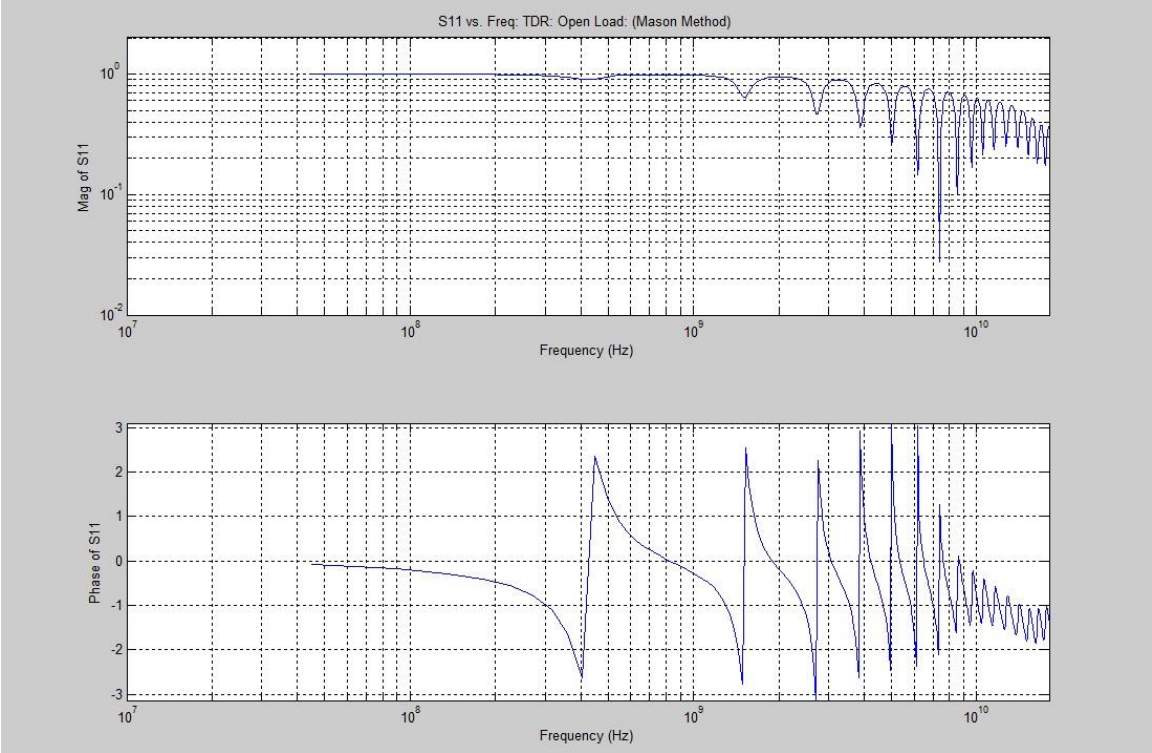


Figure 3.52: 2-Wire Probe: Dry Soil: FDR Prediction: Open Termination: Mason Method: Series Model

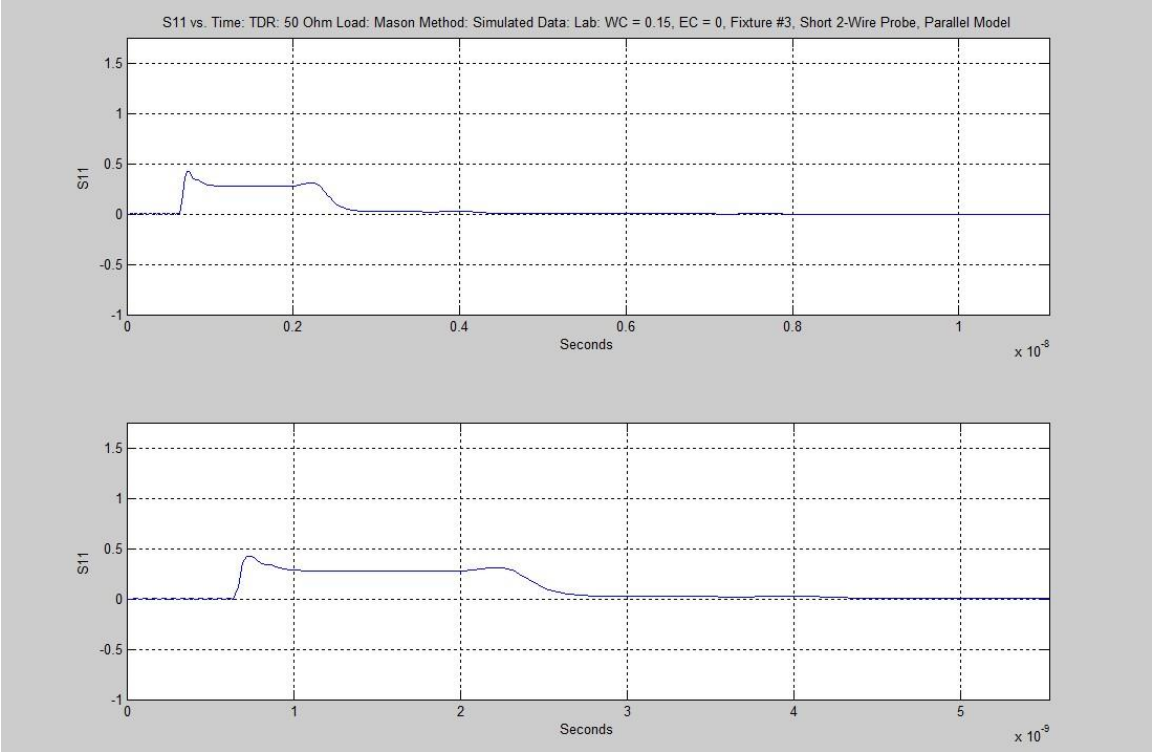


Figure 3.53: 2-Wire Probe: WC = 0.15: TDR Prediction: 50Ω Termination: Mason Method: Parallel Model

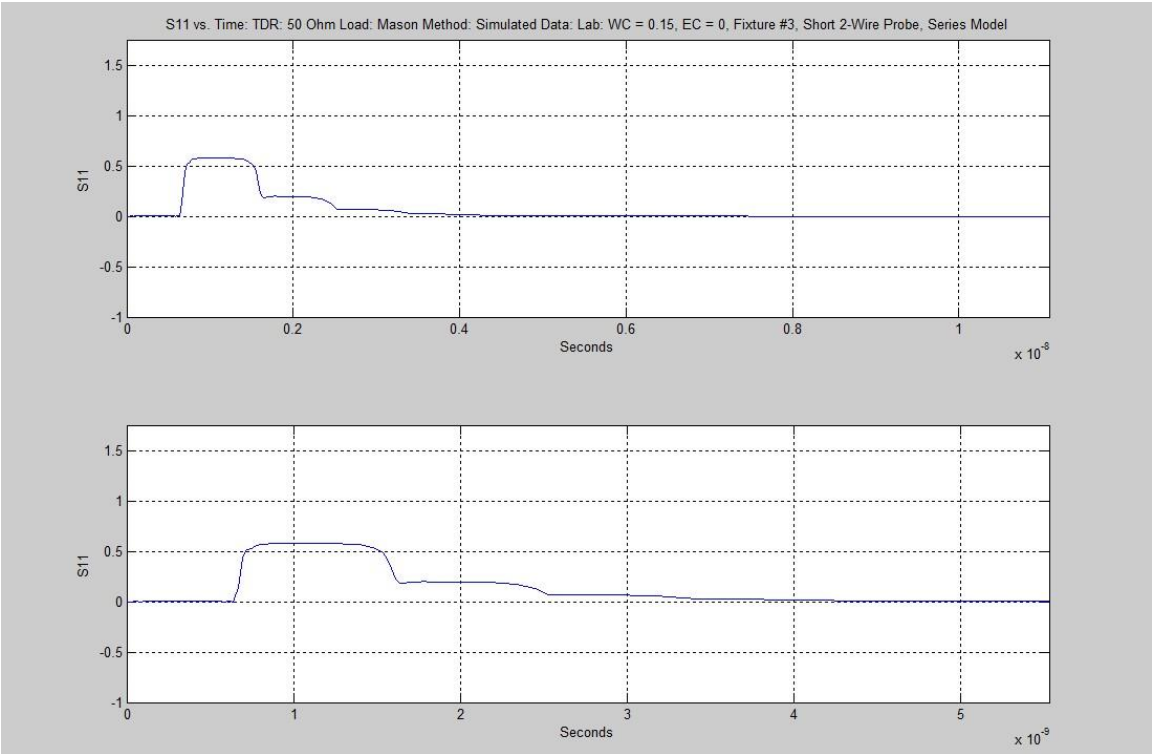


Figure 3.54: 2-Wire Probe: WC = 0.15: TDR Prediction: 50Ω Termination: Mason Method: Series Model

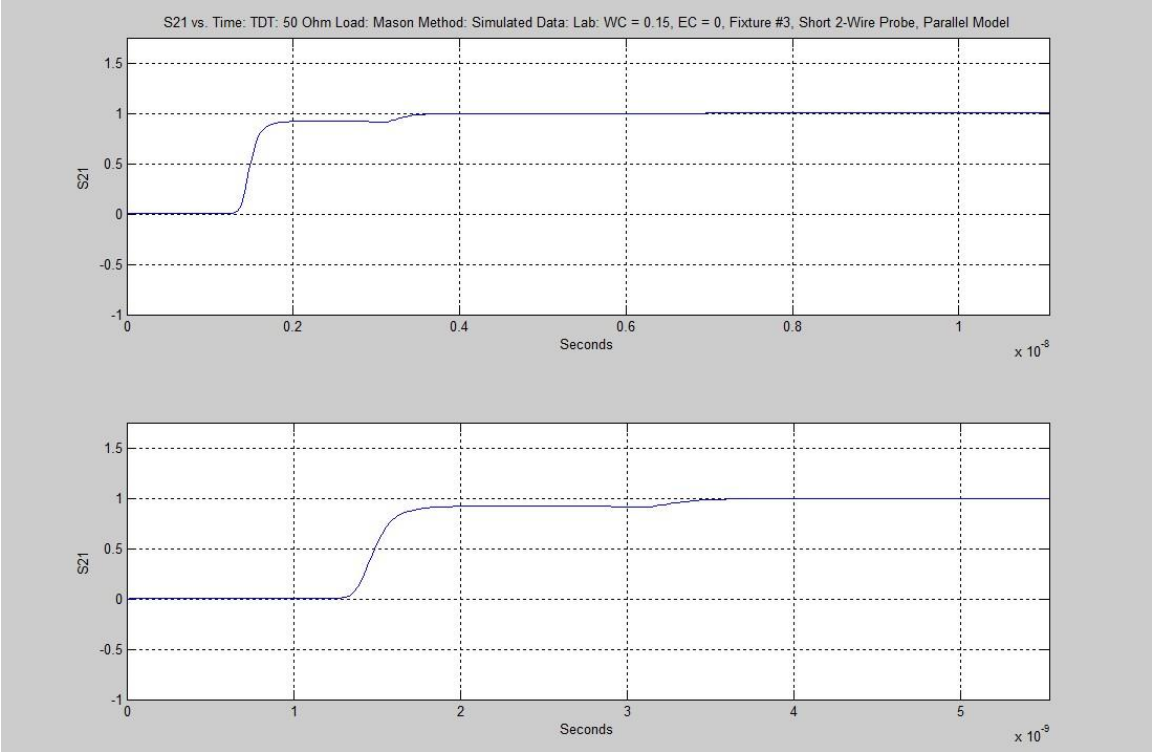


Figure 3.55: 2-Wire Probe: WC = 0.15: TDT Prediction: 50Ω Termination: Mason Method: Parallel Model

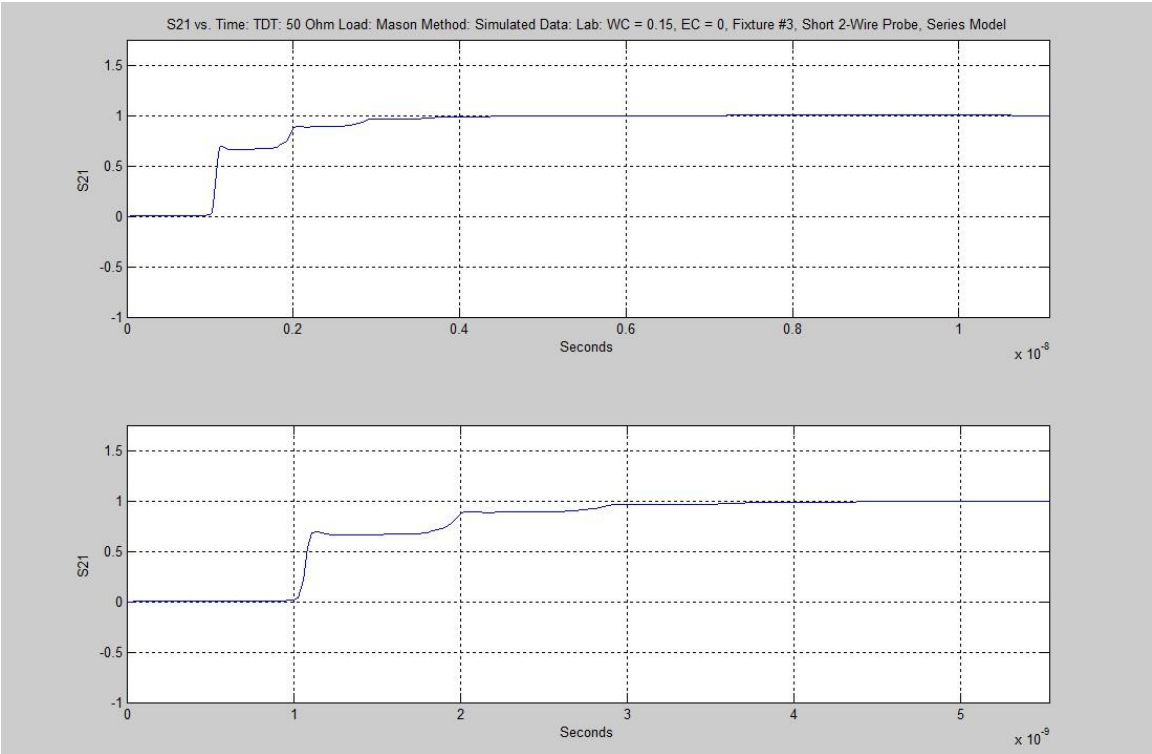


Figure 3.56: 2-Wire Probe: WC = 0.15: TDT Prediction: 50Ω Termination: Mason Method: Series Model

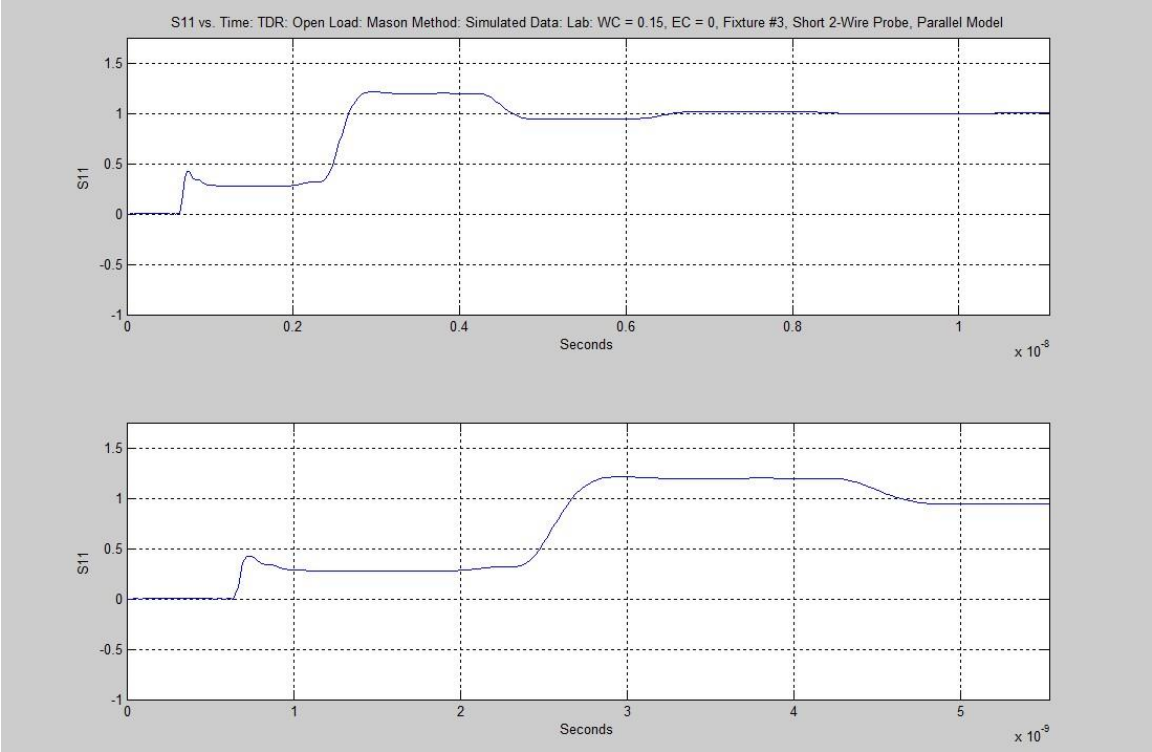


Figure 3.57: 2-Wire Probe: WC = 0.15: TDR Prediction: Open Term.: Mason Method: Parallel Model

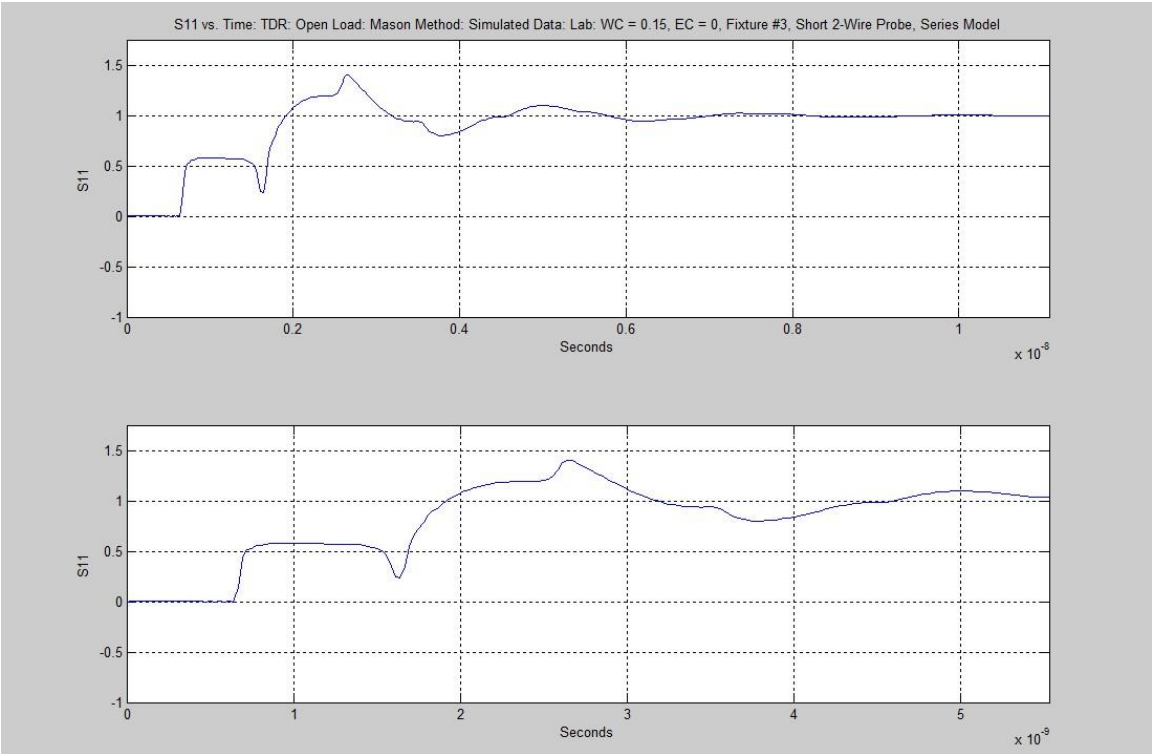


Figure 3.58: 2-Wire Probe: WC = 0.15: TDR Prediction: OpenTerm.: Mason Method: Series Model

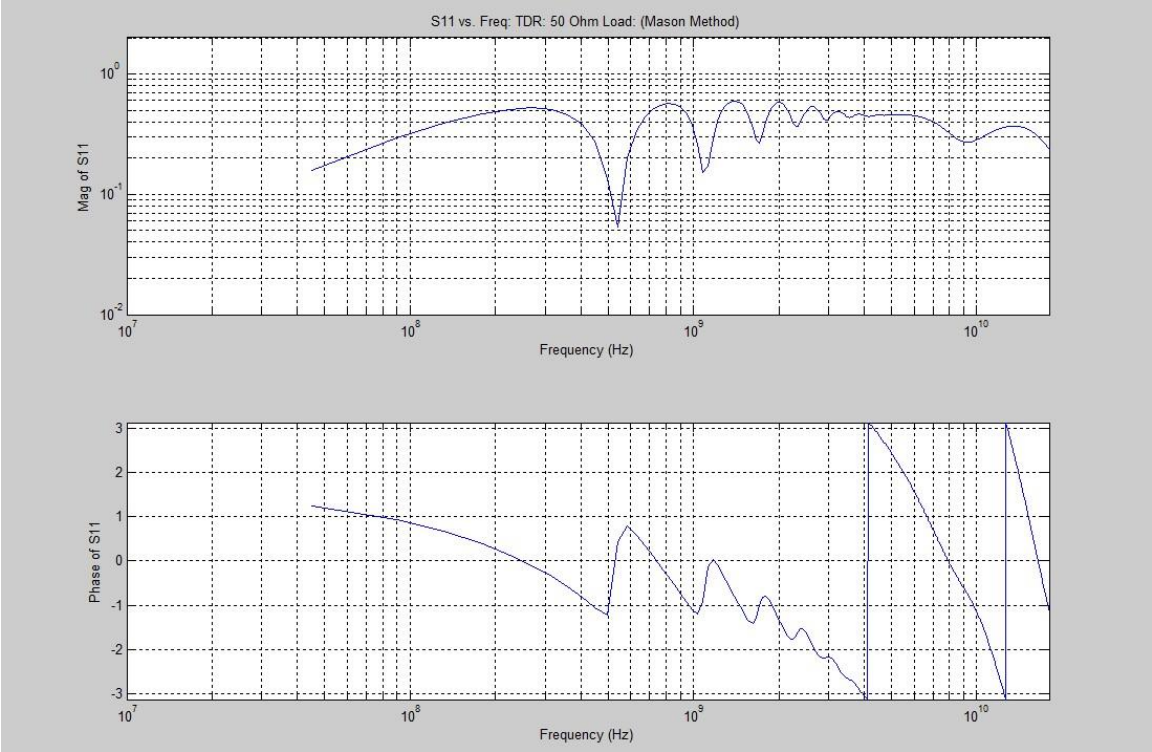


Figure 3.59: 2-Wire Probe: WC = 0.15: FDR Prediction: 50Ω Termination: Mason Method: Parallel Model

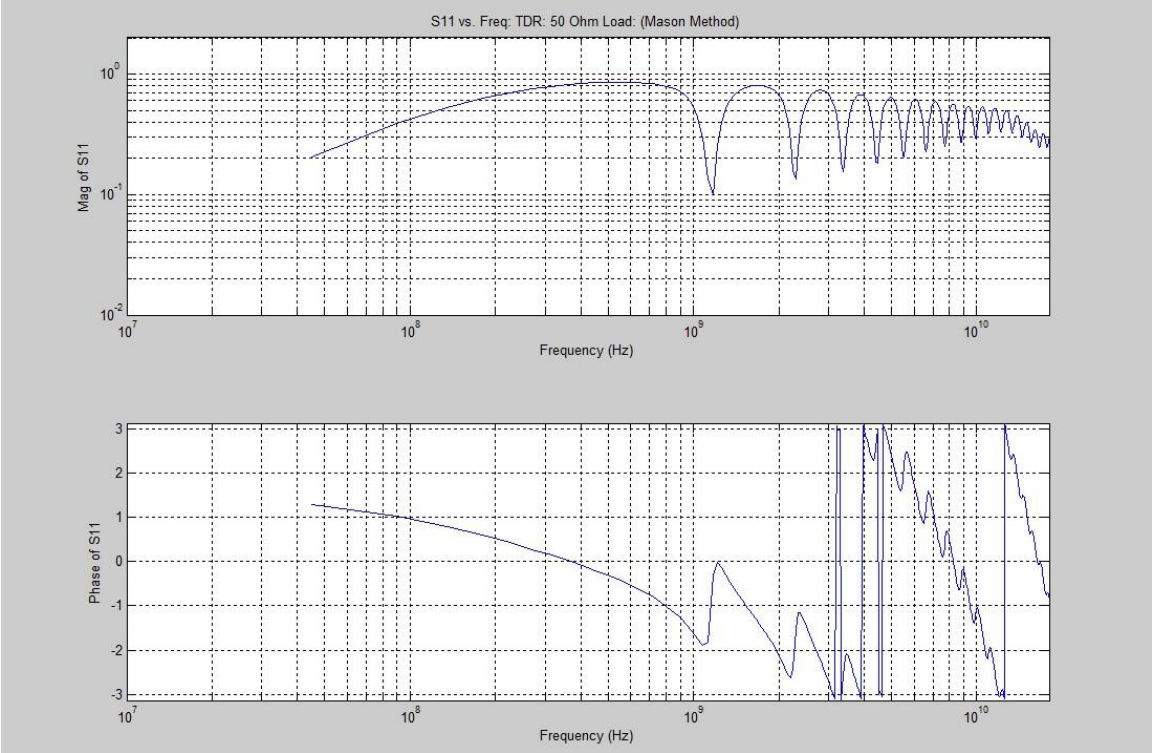


Figure 3.60: 2-Wire Probe: WC = 0.15: FDR Prediction: 50Ω Termination: Mason Method: Series Model

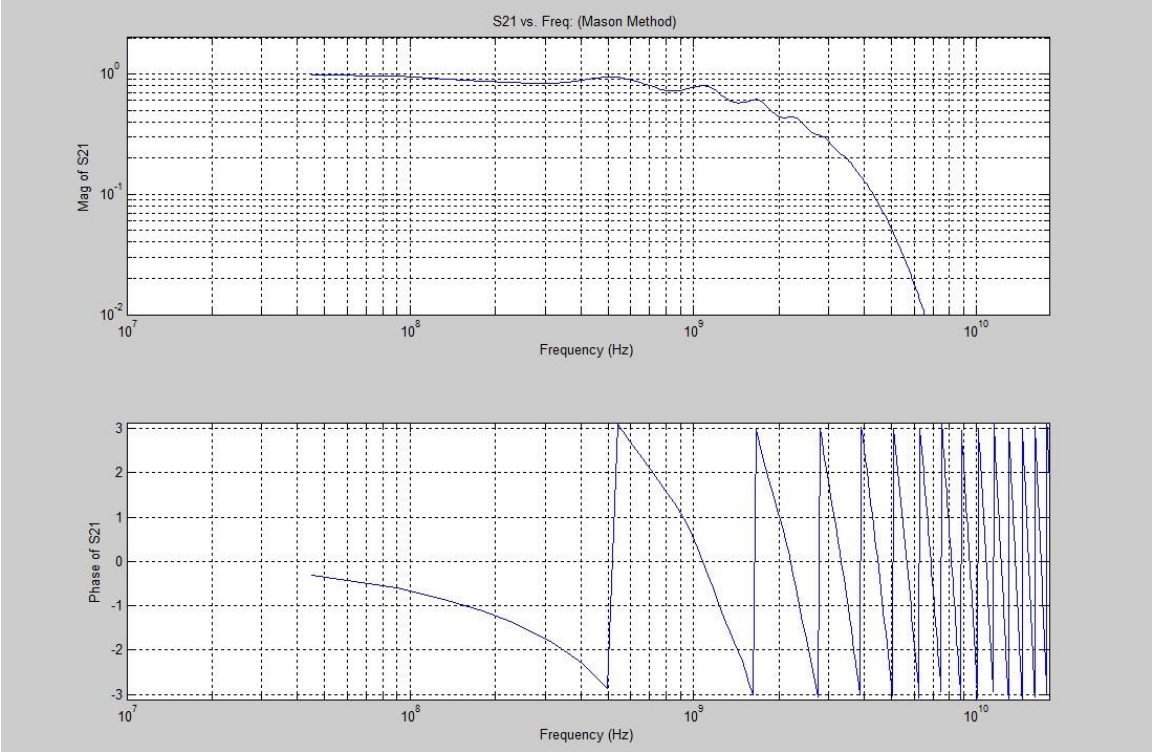


Figure 3.61: 2-Wire Probe: WC = 0.15: FDT Prediction: 50Ω Termination: Mason Method: Parallel Model

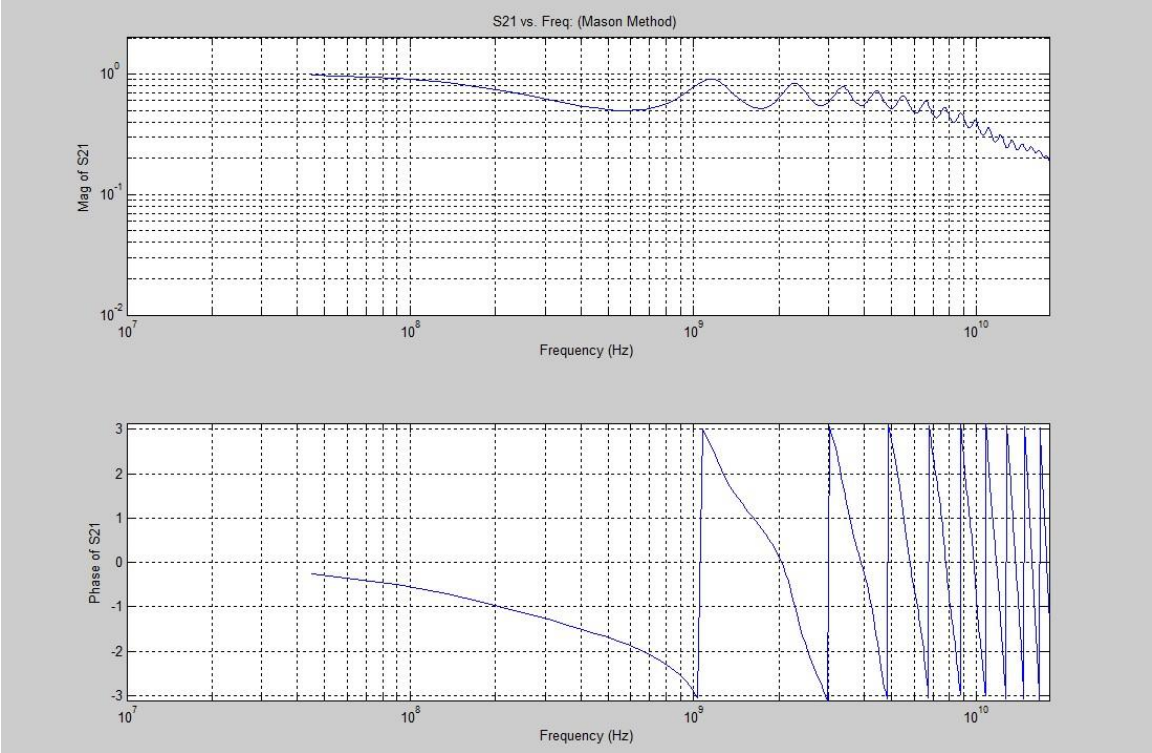


Figure 3.62: 2-Wire Probe: WC = 0.15: FDT Prediction: 50Ω Termination: Mason Method: Series Model

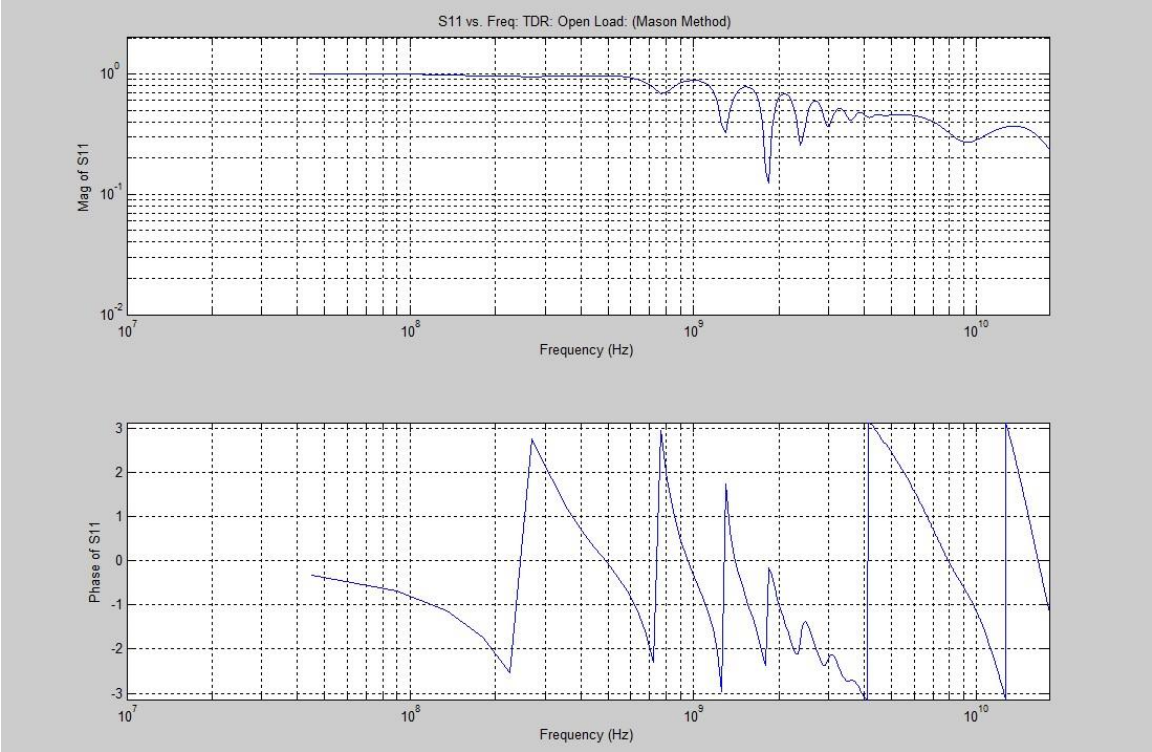


Figure 3.63: 2-Wire Probe: WC = 0.15: FDR Prediction: Open Term.: Mason Method: Parallel Model

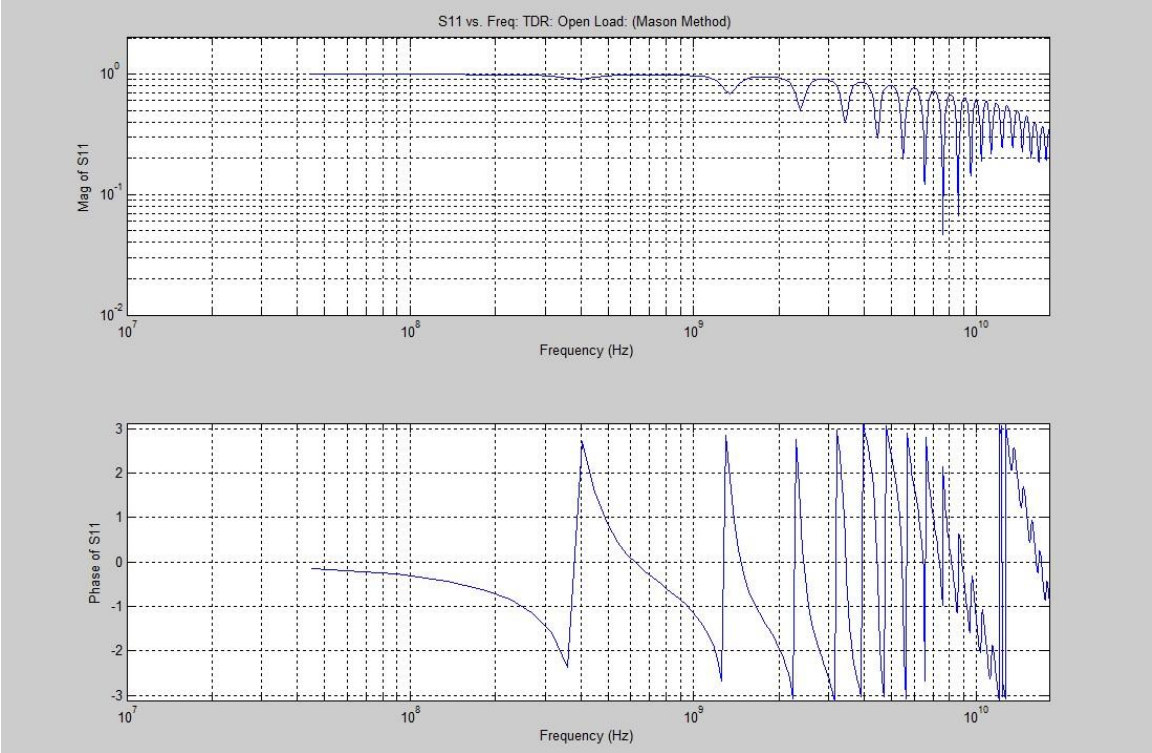


Figure 3.64: 2-Wire Probe: WC = 0.15: FDR Prediction: Open Term.: Mason Method: Series Model

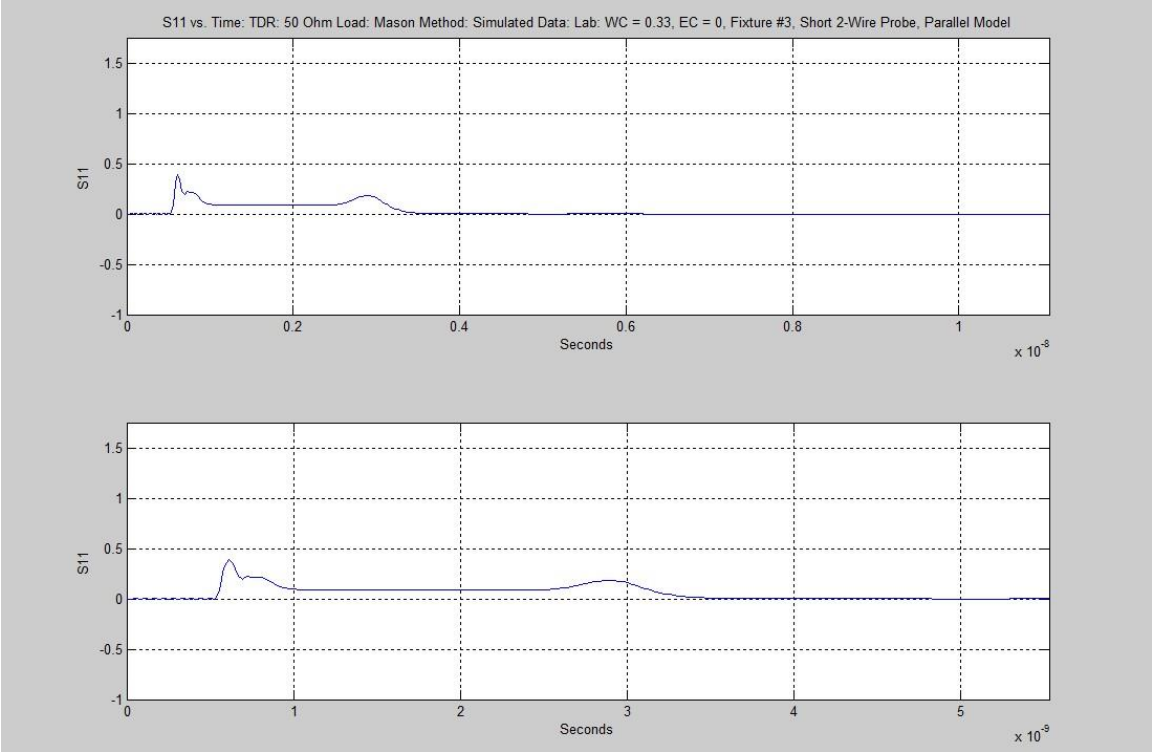


Figure 3.65: 2-Wire Probe: WC = 0.33: TDR Prediction: 50Ω Termination: Mason Method: Parallel Model

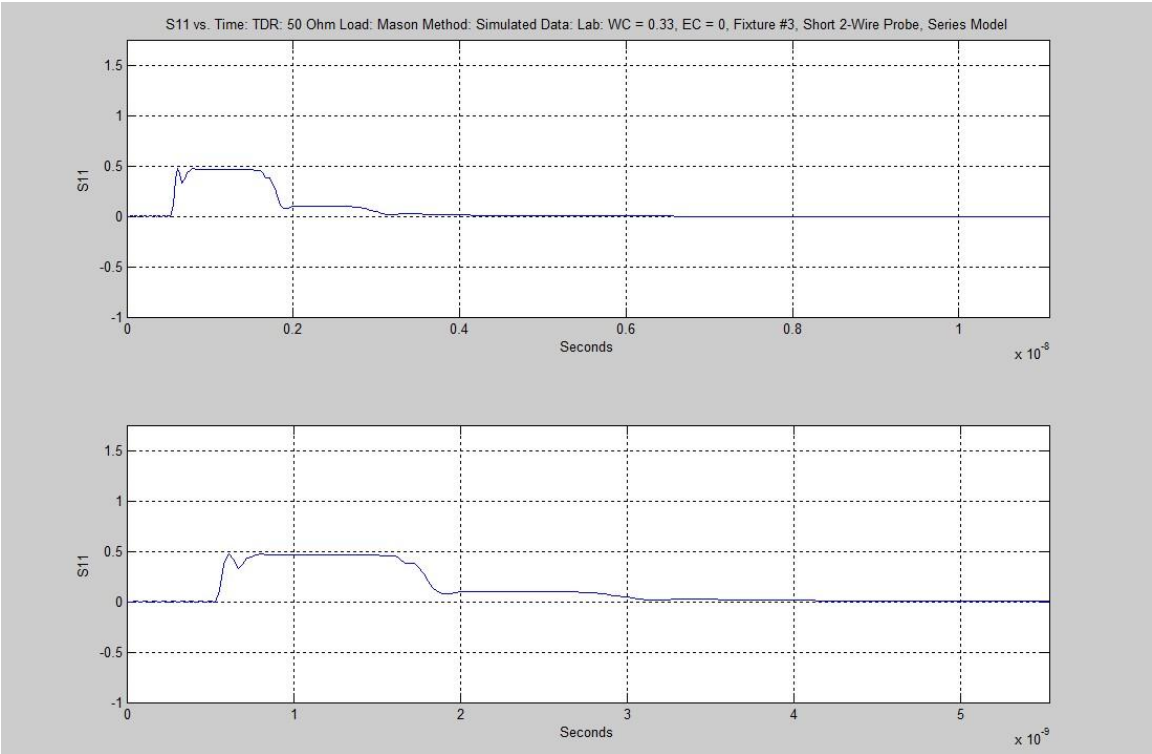


Figure 3.66: 2-Wire Probe: WC = 0.33: TDR Prediction: 50Ω Termination: Mason Method: Series Model

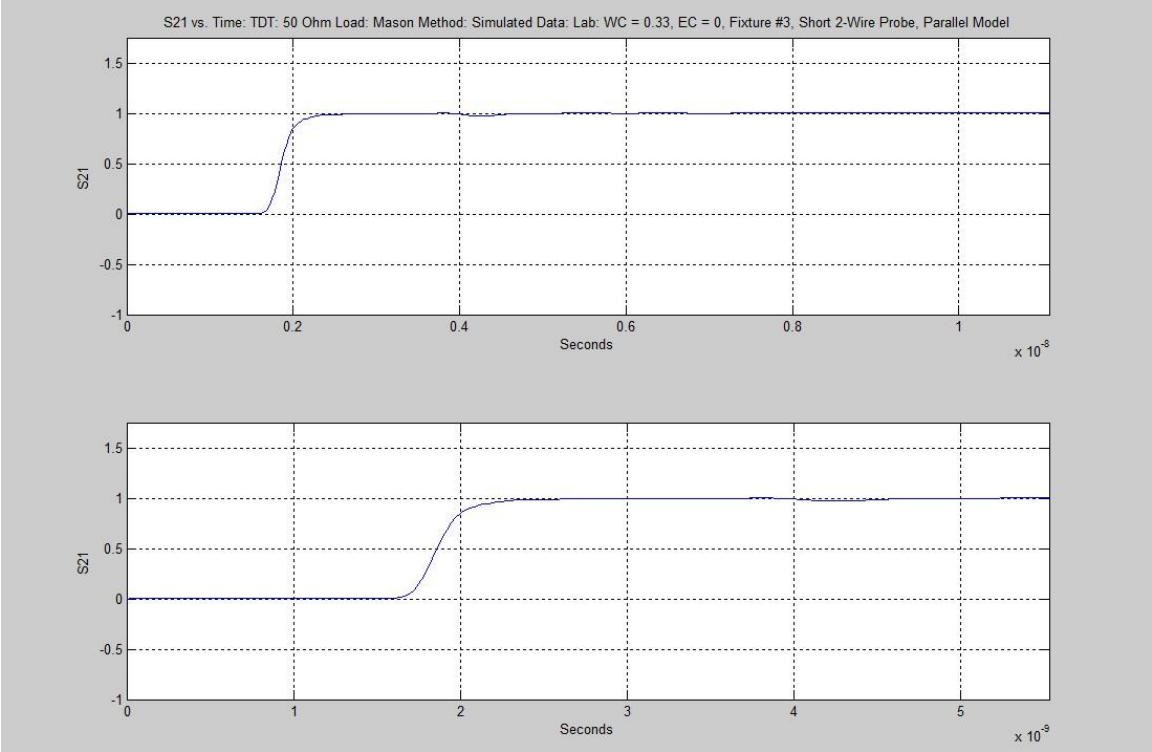


Figure 3.67: 2-Wire Probe: WC = 0.33: TDT Prediction: 50Ω Termination: Mason Method: Parallel Model

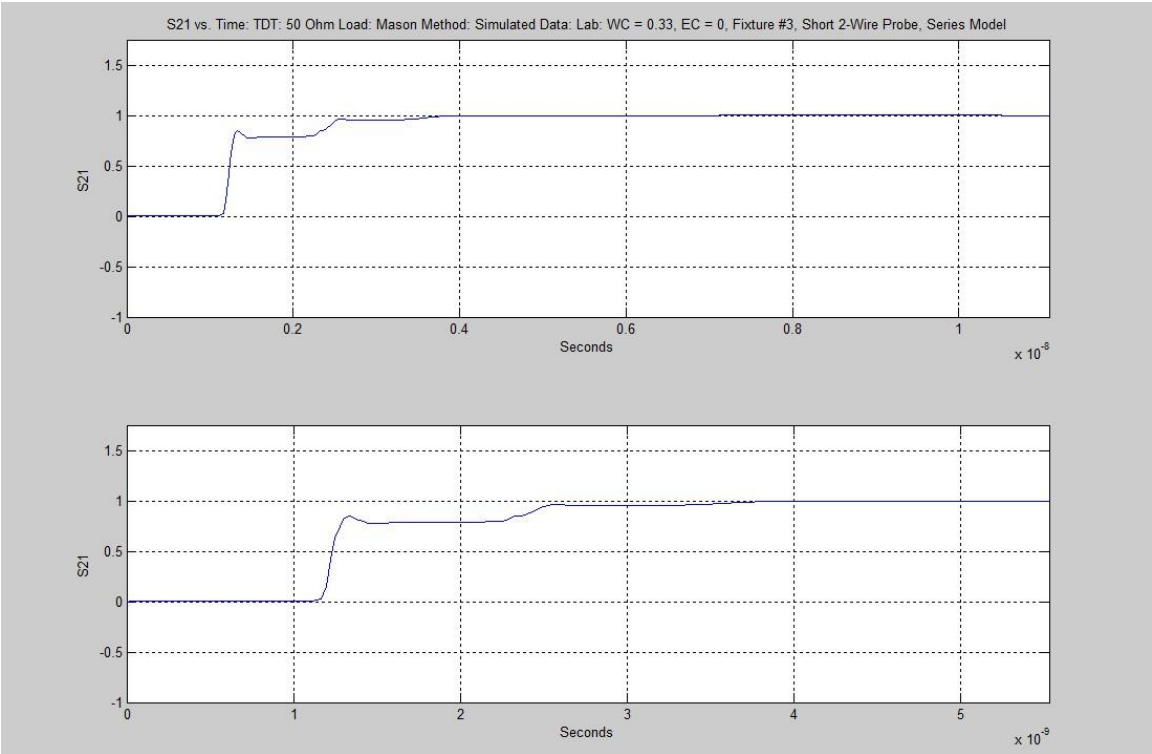


Figure 3.68: 2-Wire Probe: WC = 0.33: TDT Prediction: 50Ω Termination: Mason Method: Series Model

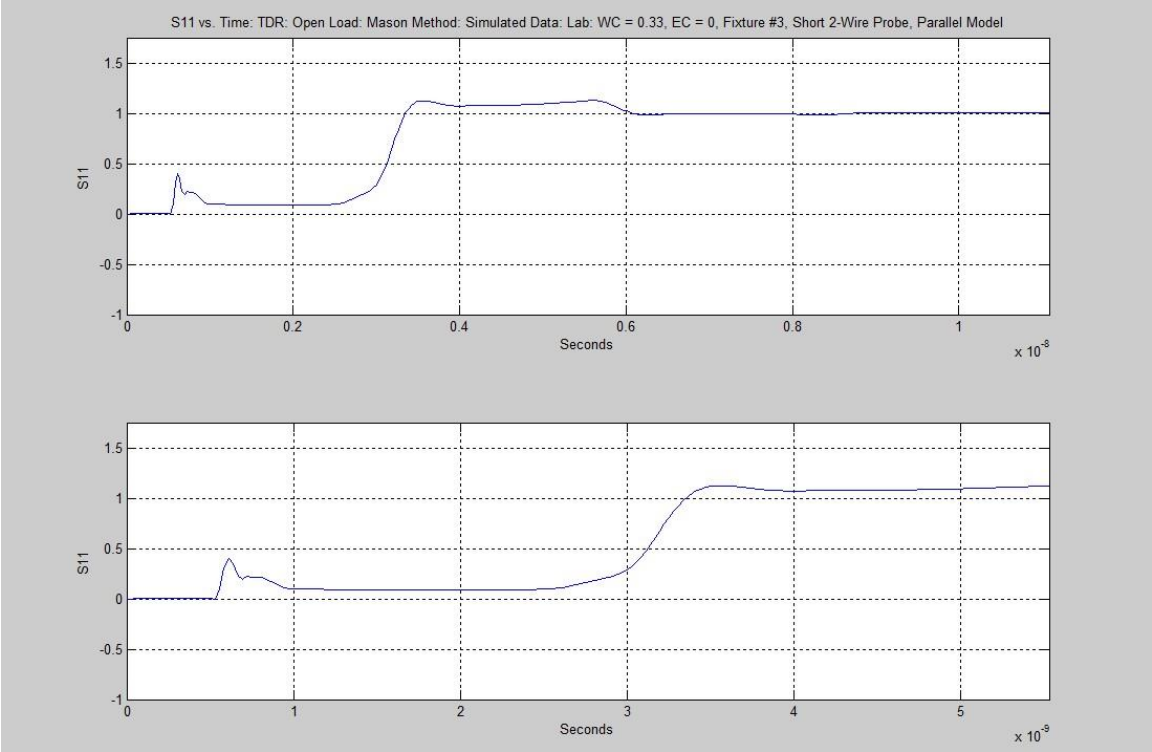


Figure 3.69: 2-Wire Probe: WC = 0.33: TDR Prediction: Open Term.: Mason Method: Parallel Model

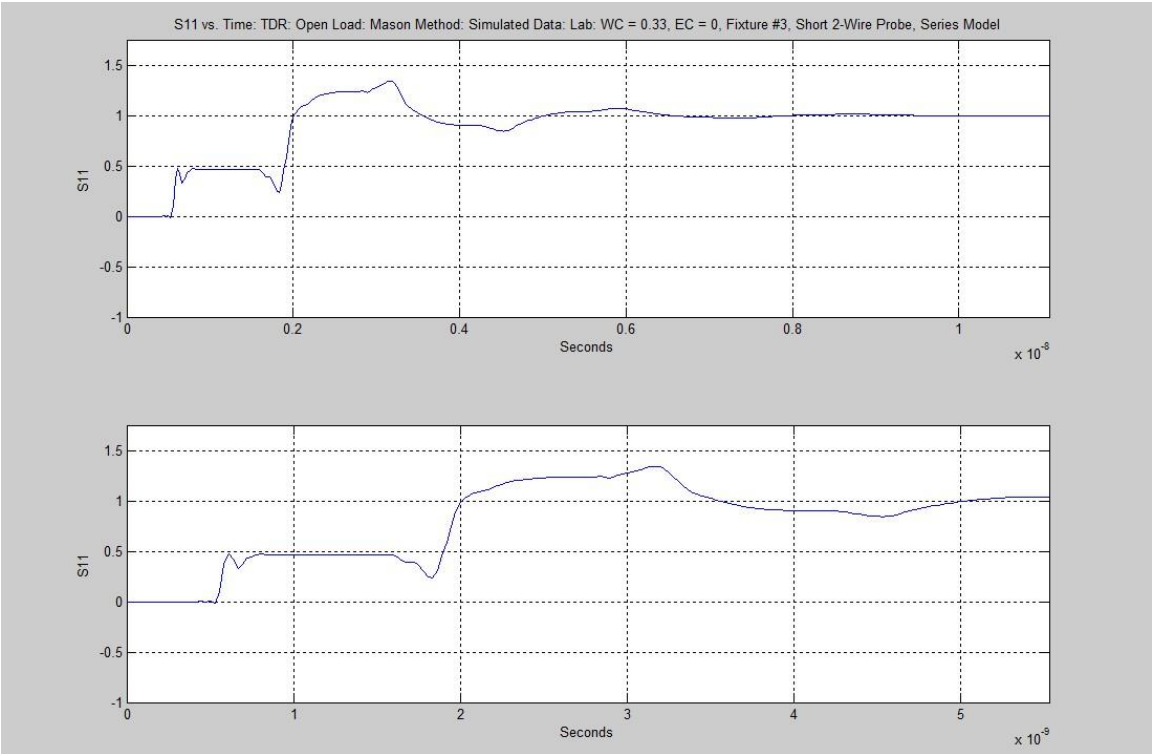


Figure 3.70: 2-Wire Probe: WC = 0.33: TDR Prediction: Open Term.: Mason Method: Series Model

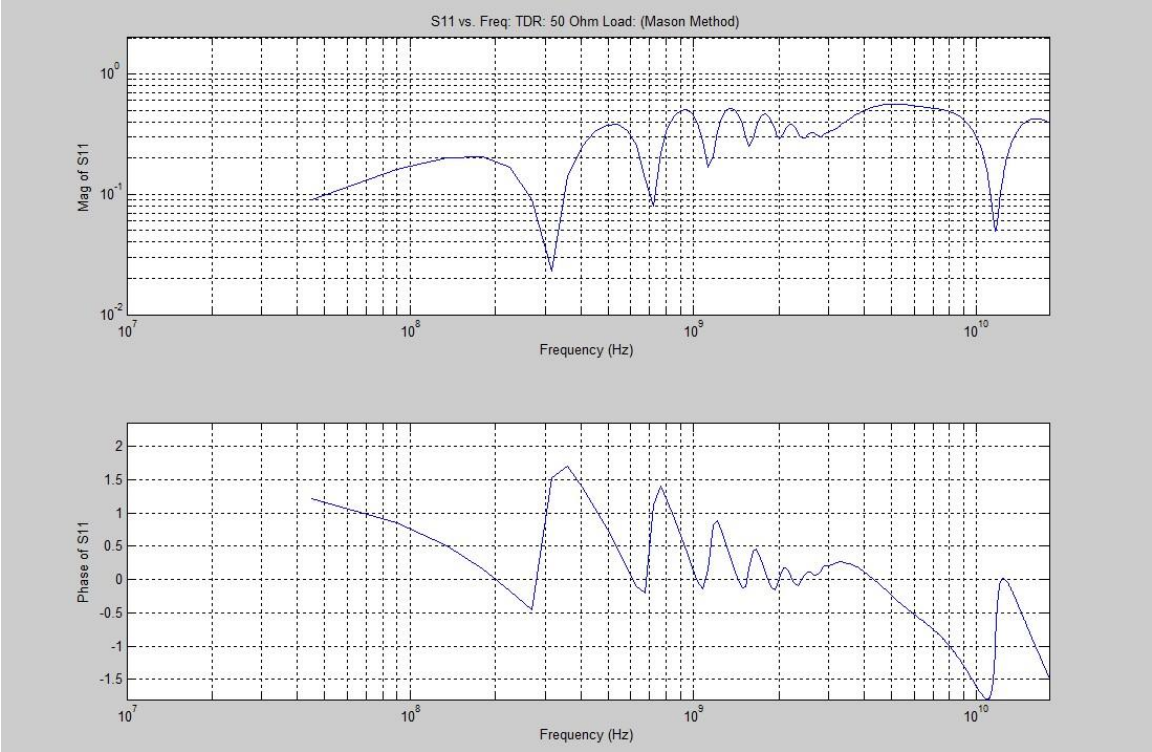


Figure 3.71: 2-Wire Probe: WC = 0.33: FDR Prediction: 50Ω Termination: Mason Method: Parallel Model

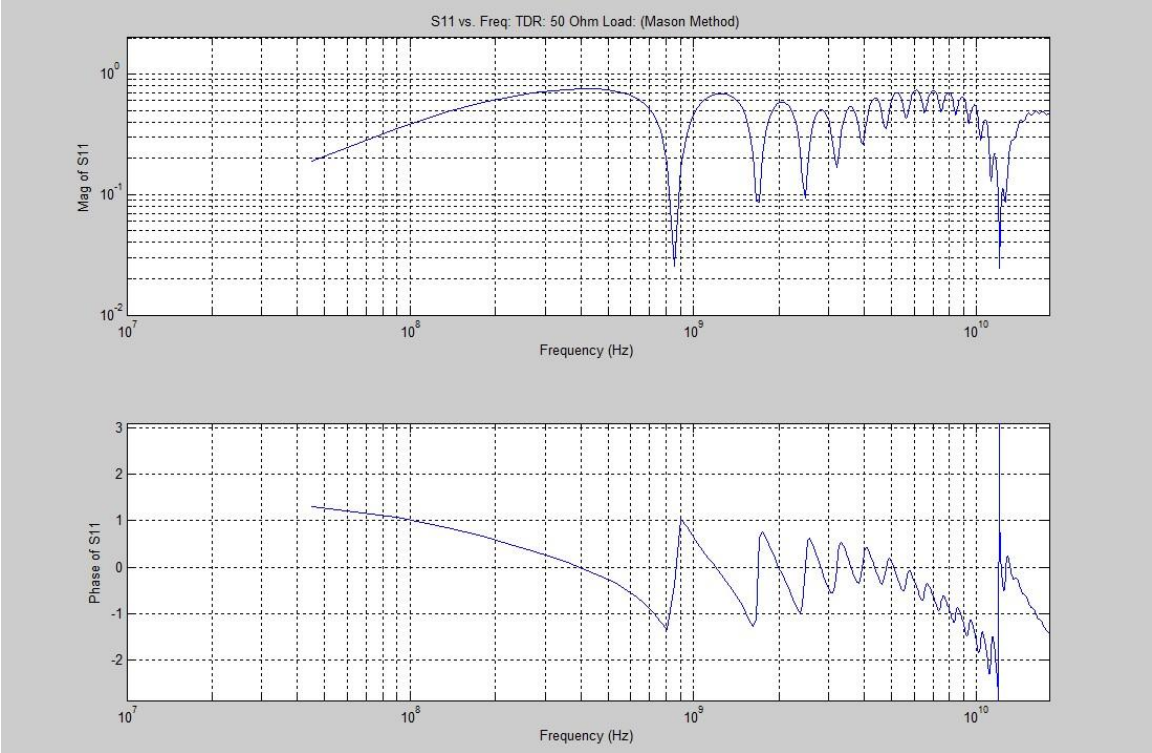


Figure 3.72: 2-Wire Probe: WC = 0.33: FDR Prediction: 50Ω Termination: Mason Method: Series Model

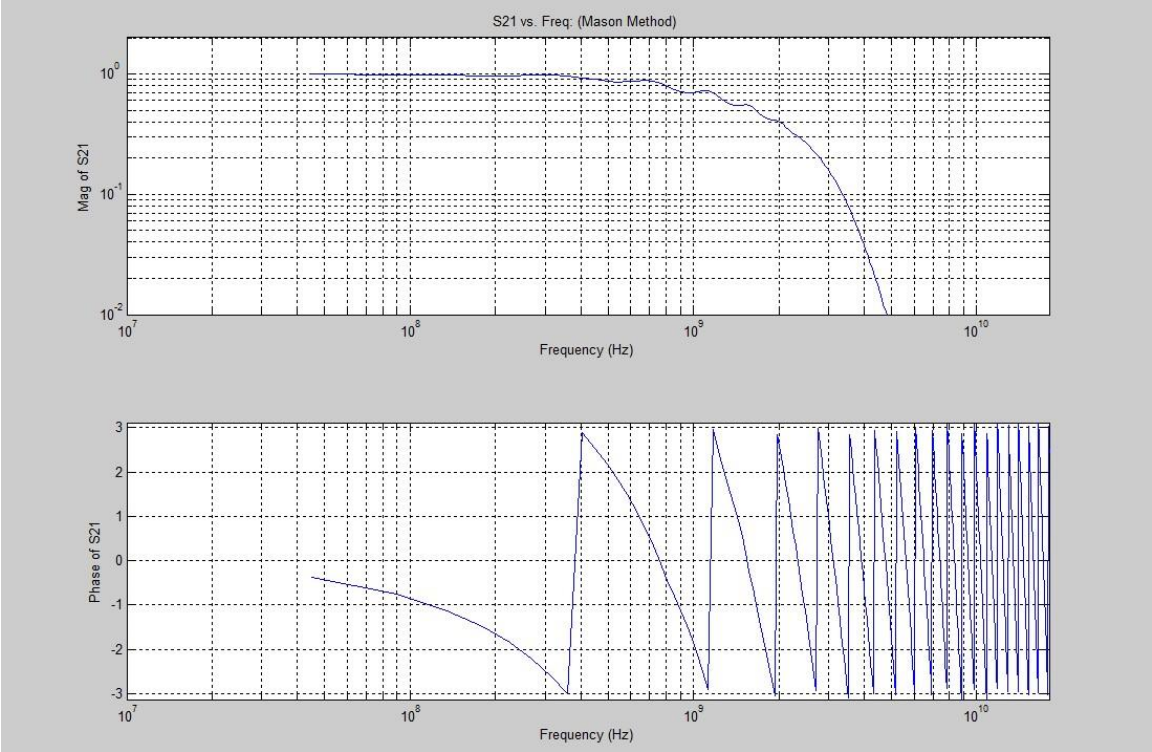


Figure 3.73: 2-Wire Probe: WC = 0.33: FDT Prediction: 50Ω Termination: Mason Method: Parallel Model

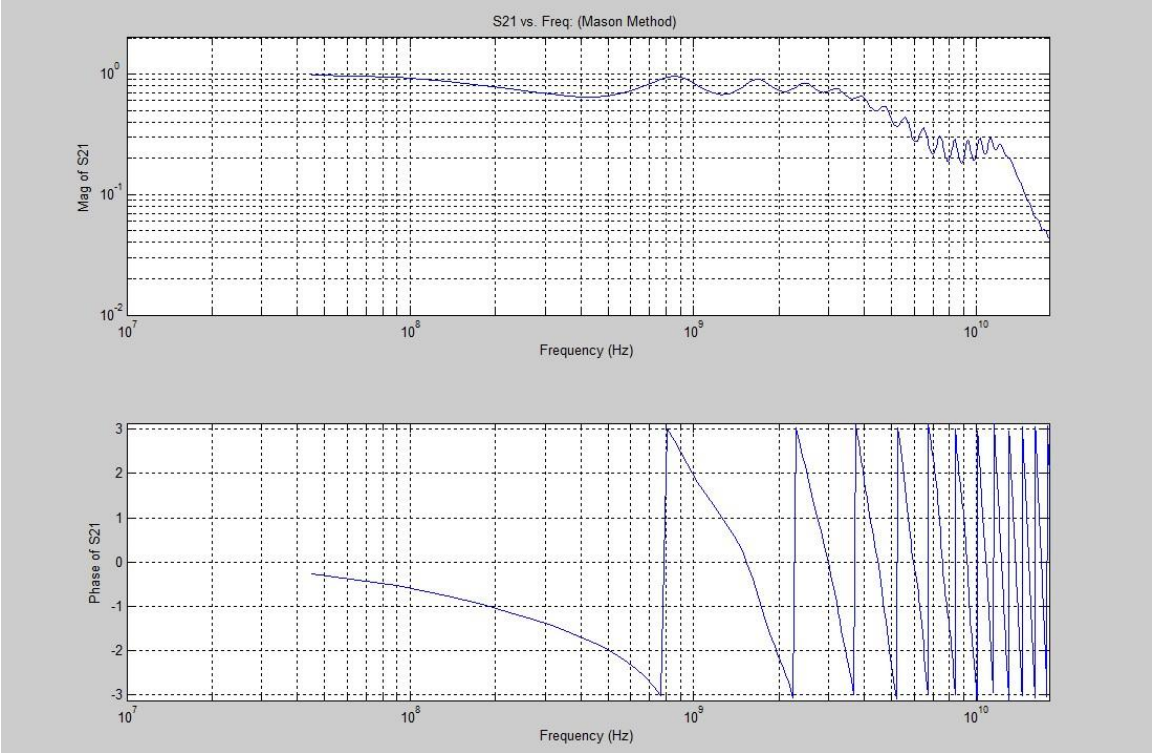


Figure 3.74: 2-Wire Probe: WC = 0.33: FDT Prediction: 50Ω Termination: Mason Method: Series Model

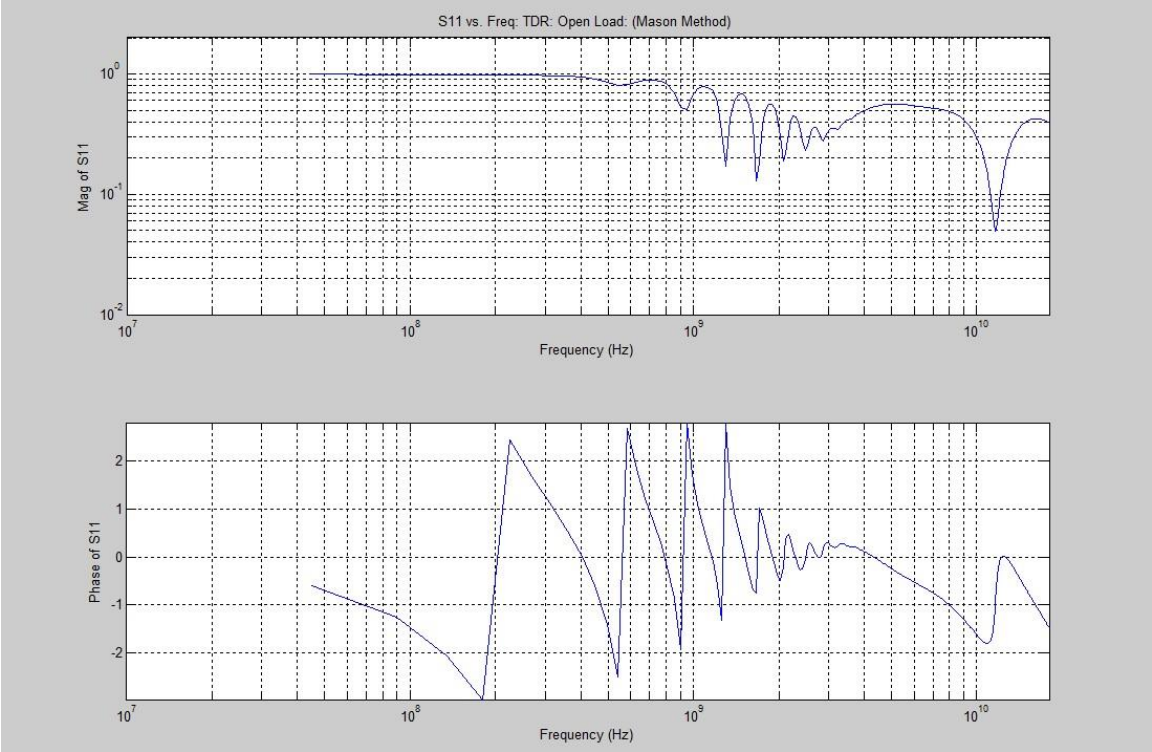


Figure 3.75: 2-Wire Probe: WC = 0.33: FDR Prediction: Open Term.: Mason Method: Parallel Model

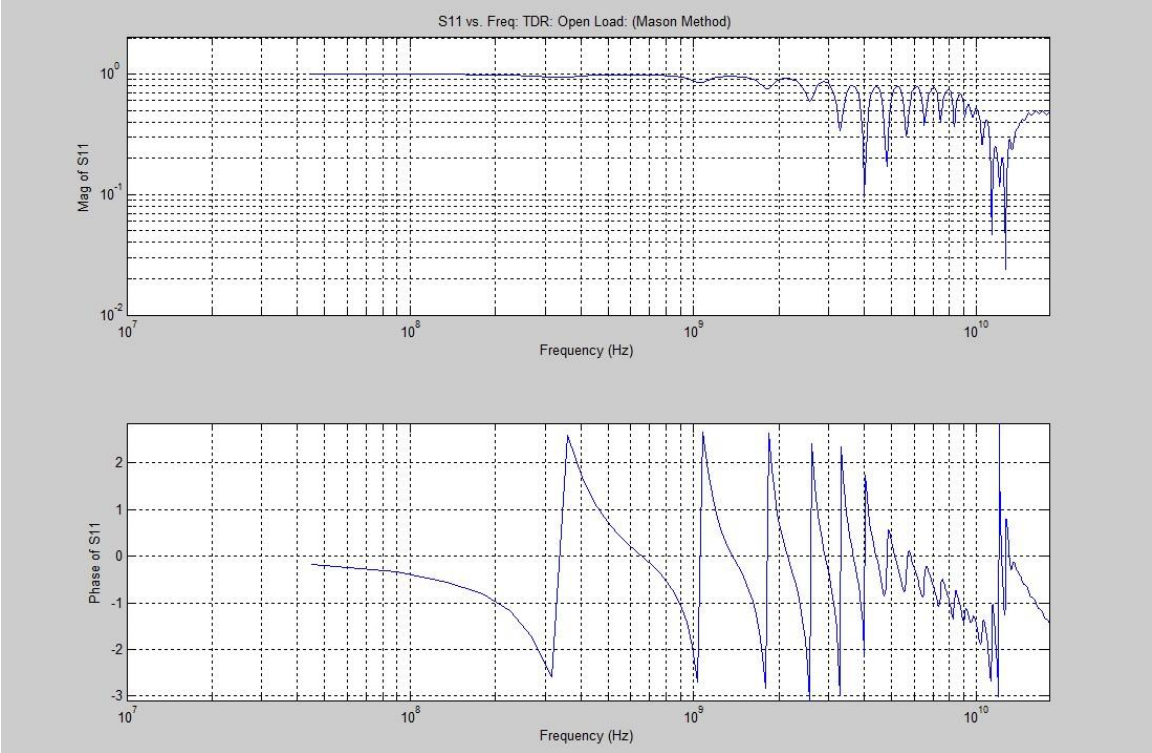


Figure 3.76: 2-Wire Probe: WC = 0.33: FDR Prediction: Open Term.: Mason Method: Series Model

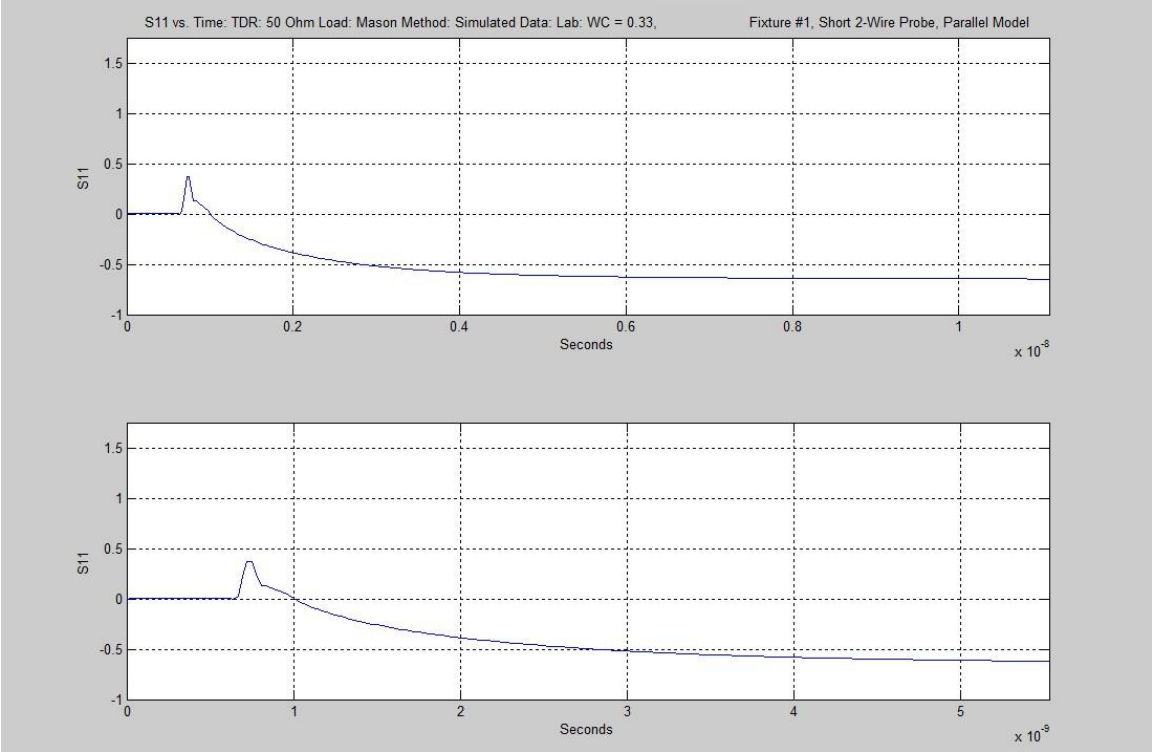


Figure 3.77: 2-Wire Probe: WC = 0.33: EC = 1.2 S/m: TDR Pred.: 50Ω Term.: Mason: Parallel Model

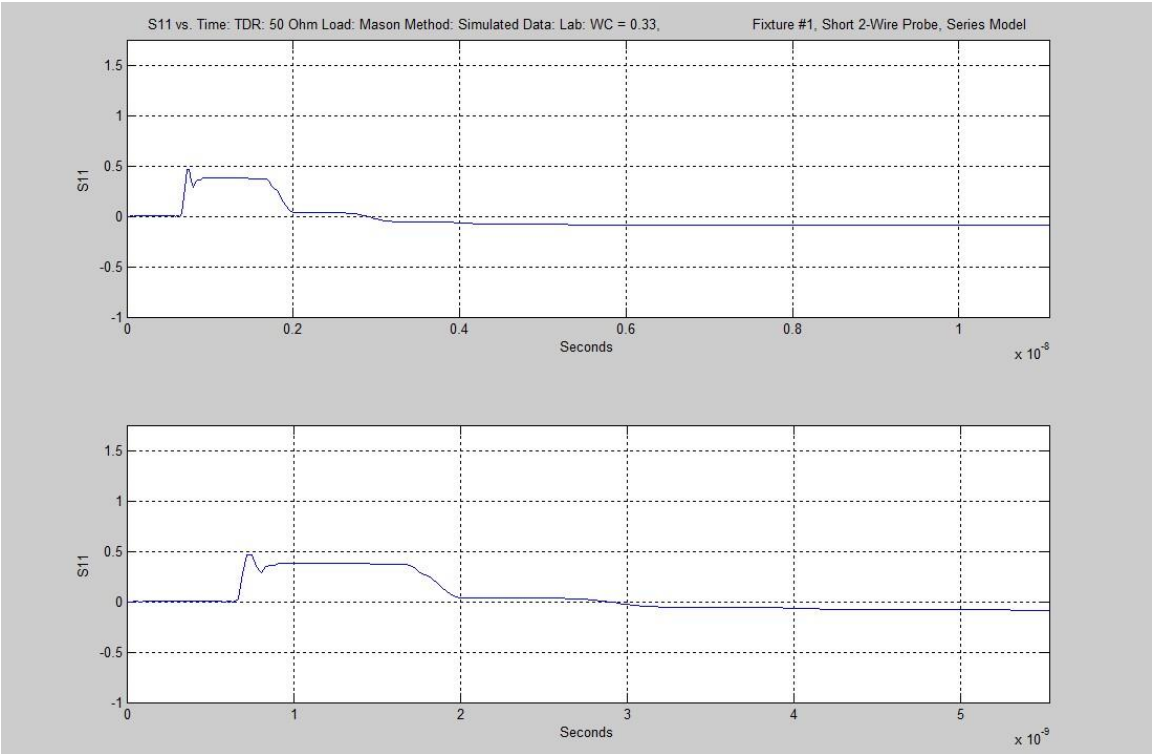


Figure 3.78: 2-Wire Probe: WC = 0.33: EC = 1.2 S/m: TDR Pred.: 50Ω Term.: Mason: Series Model

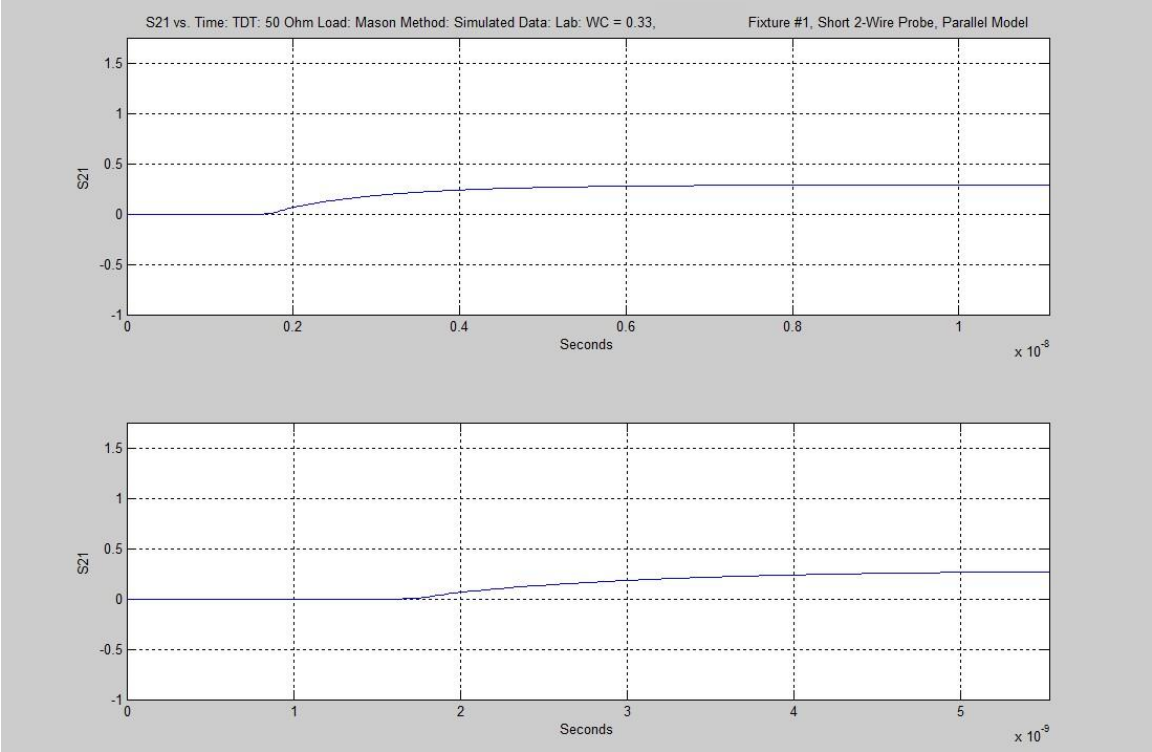


Figure 3.79: 2-Wire Probe: WC = 0.33: EC = 1.2 S/m: TDT Pred.: 50Ω Term.: Mason: Parallel Model

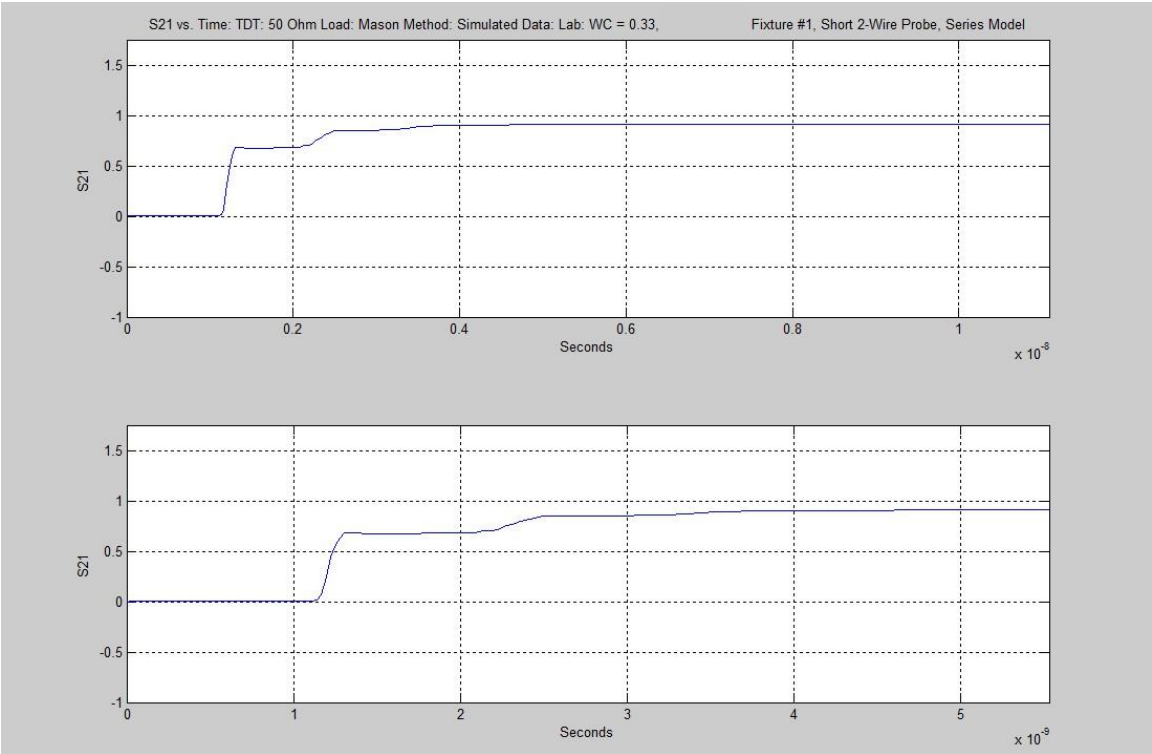


Figure 3.80: 2-Wire Probe: WC = 0.33: EC = 1.2 S/m: TDT Pred.: 50Ω Term.: Mason: Series Model

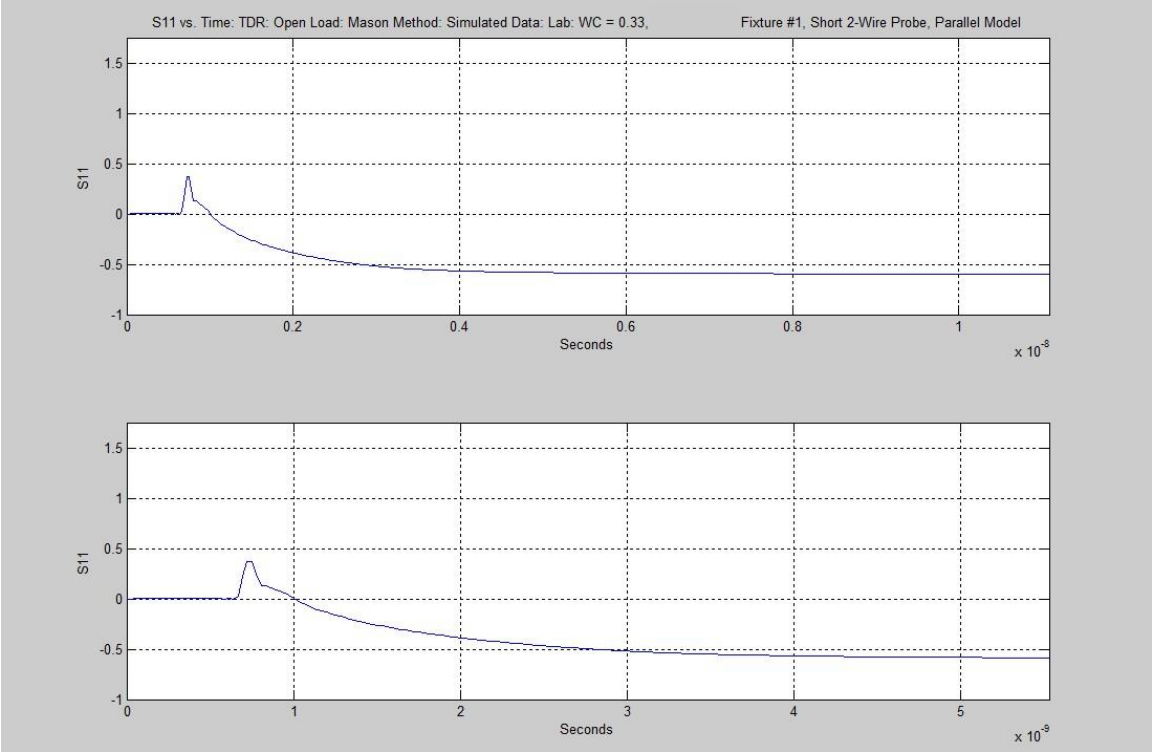


Figure 3.81: 2-Wire Probe: WC = 0.33: EC = 1.2 S/m: TDR Pred.: Open Term.: Mason: Parallel Model

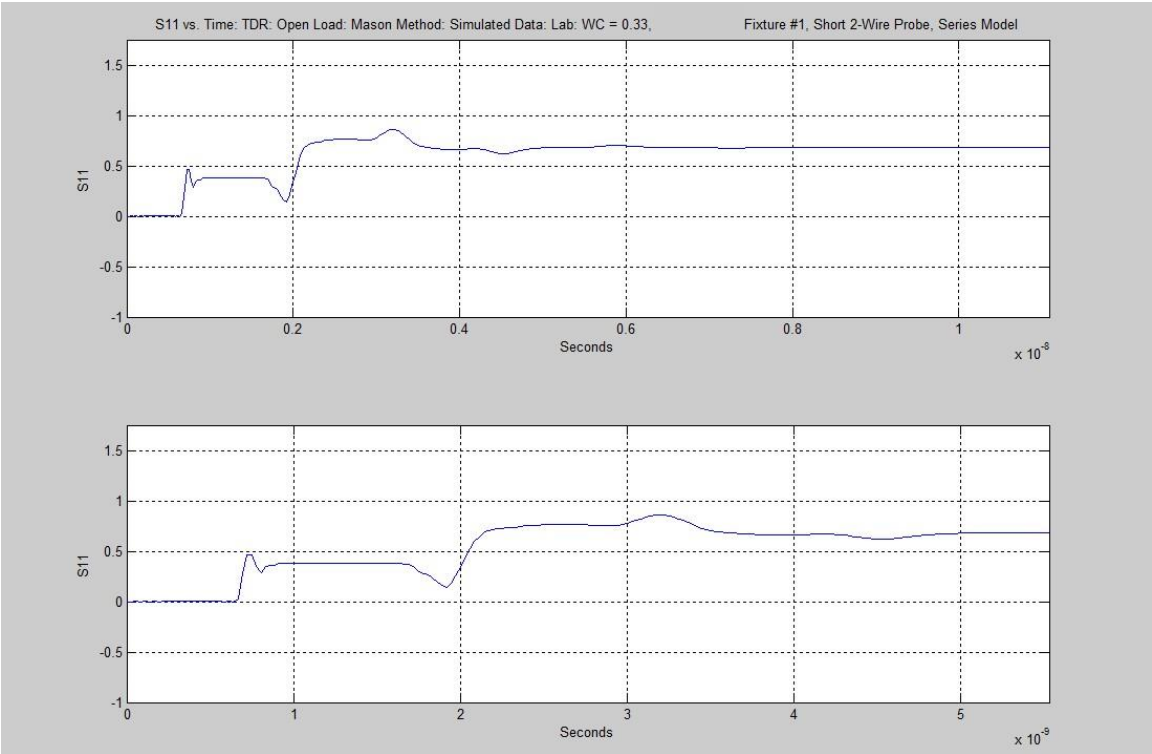


Figure 3.82: 2-Wire Probe: WC = 0.33: EC = 1.2 S/m: TDR Pred.: Open Term.: Mason: Series Model

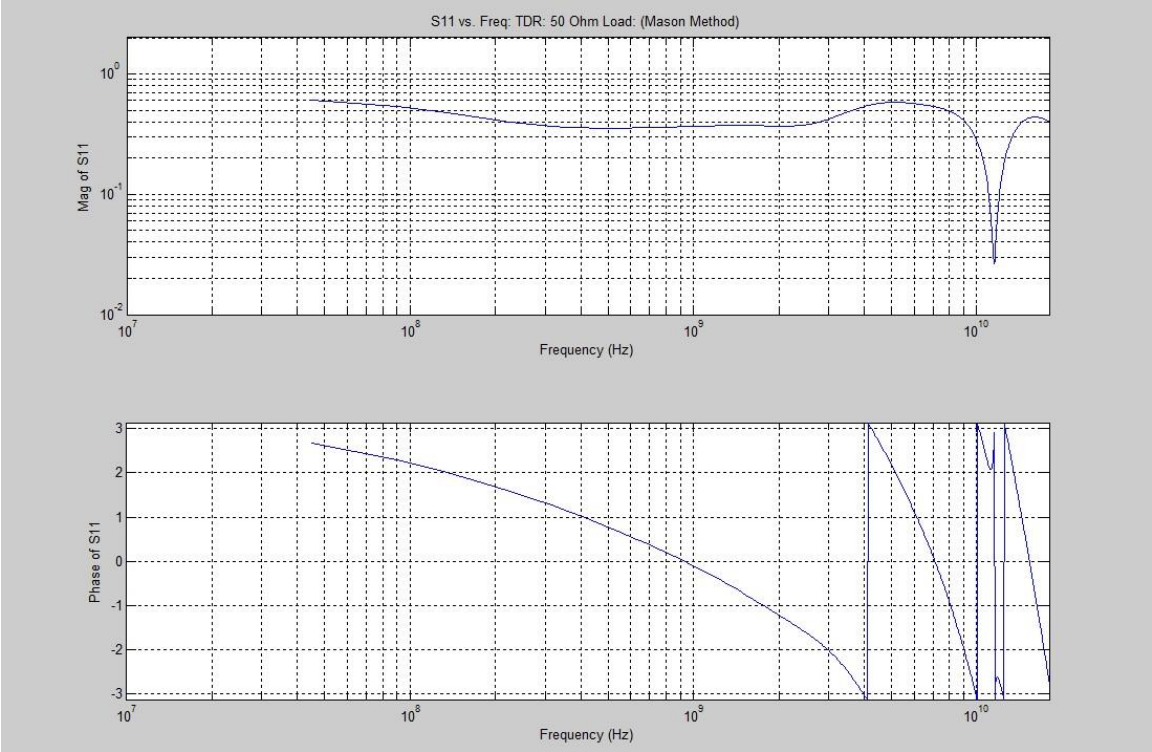


Figure 3.83: 2-Wire Probe: WC = 0.33: EC = 1.2 S/m: FDR Pred.: 50Ω Term.: Mason: Parallel Model

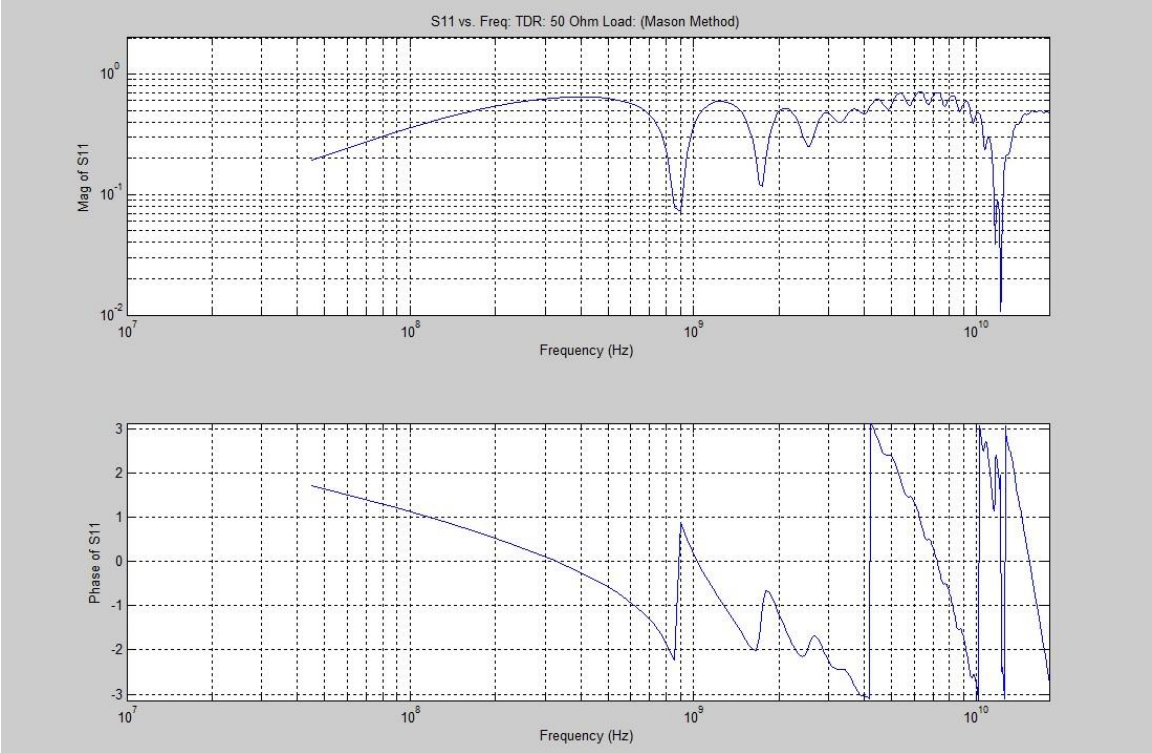


Figure 3.84: 2-Wire Probe: WC = 0.33: EC = 1.2 S/m: FDR Pred.: 50Ω Term.: Mason: Series Model

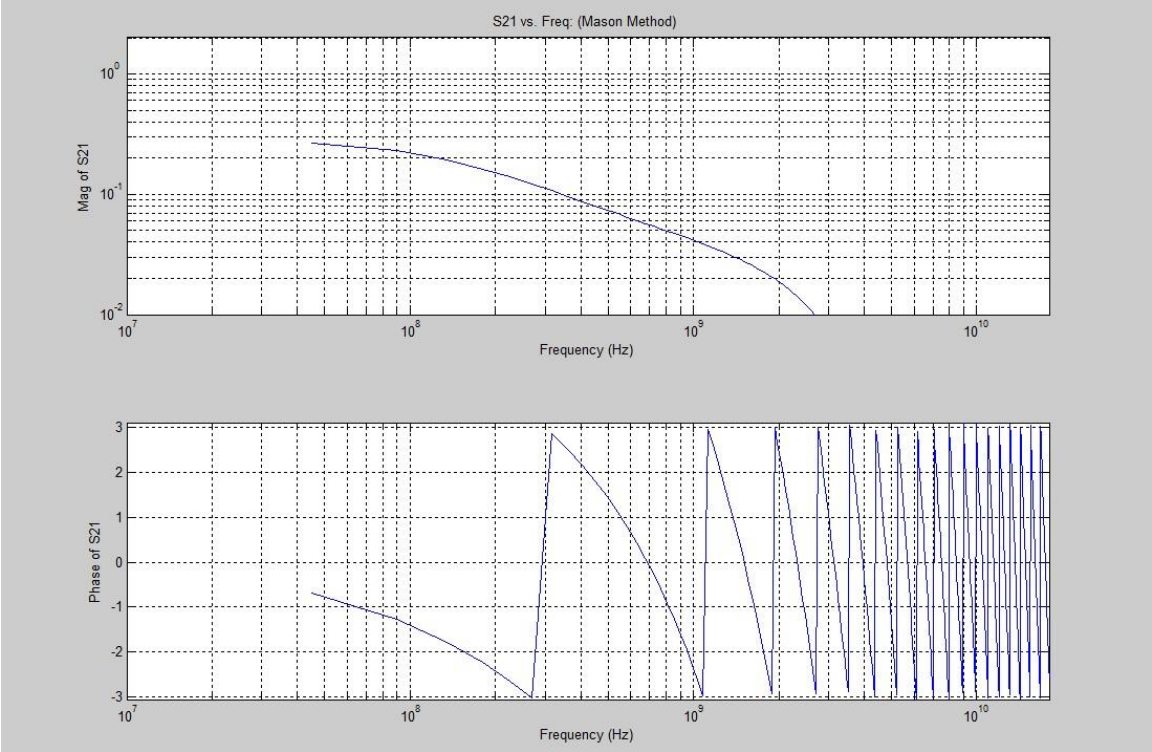


Figure 3.85: 2-Wire Probe: WC = 0.33: EC = 1.2 S/m: FDT Pred.: 50Ω Term.: Mason: Parallel Model

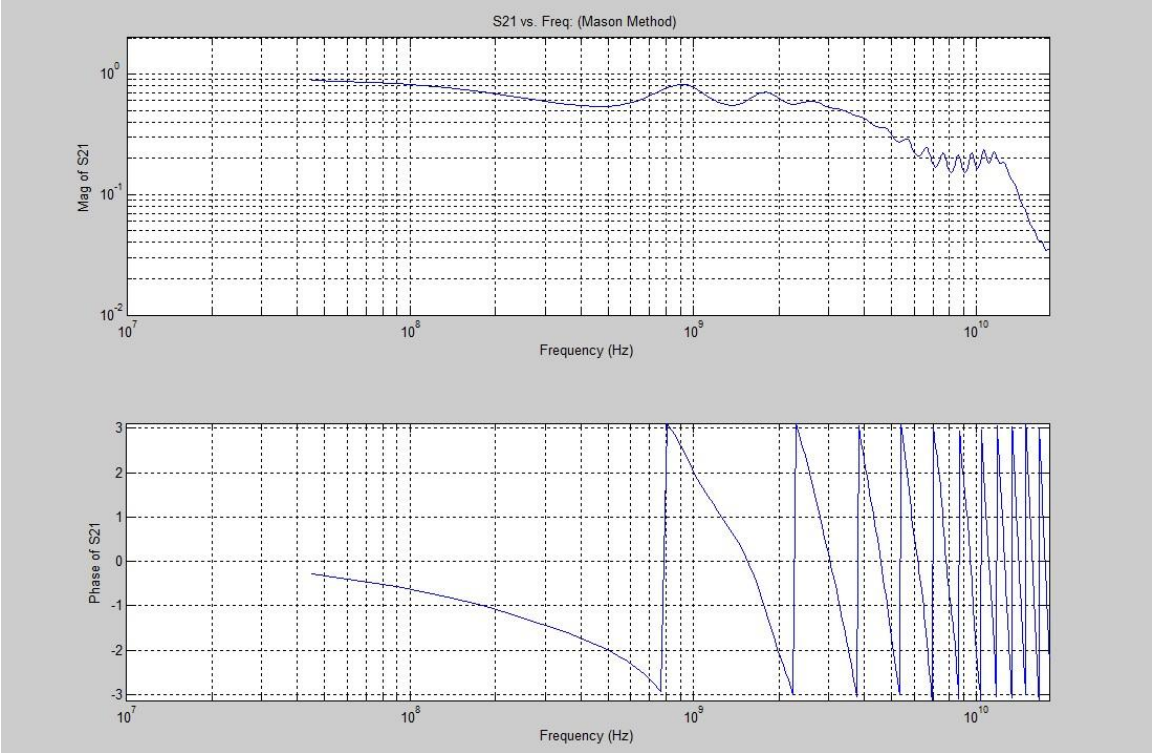


Figure 3.86: 2-Wire Probe: WC = 0.33: EC = 1.2 S/m: FDT Pred.: 50Ω Term.: Mason: Series Model

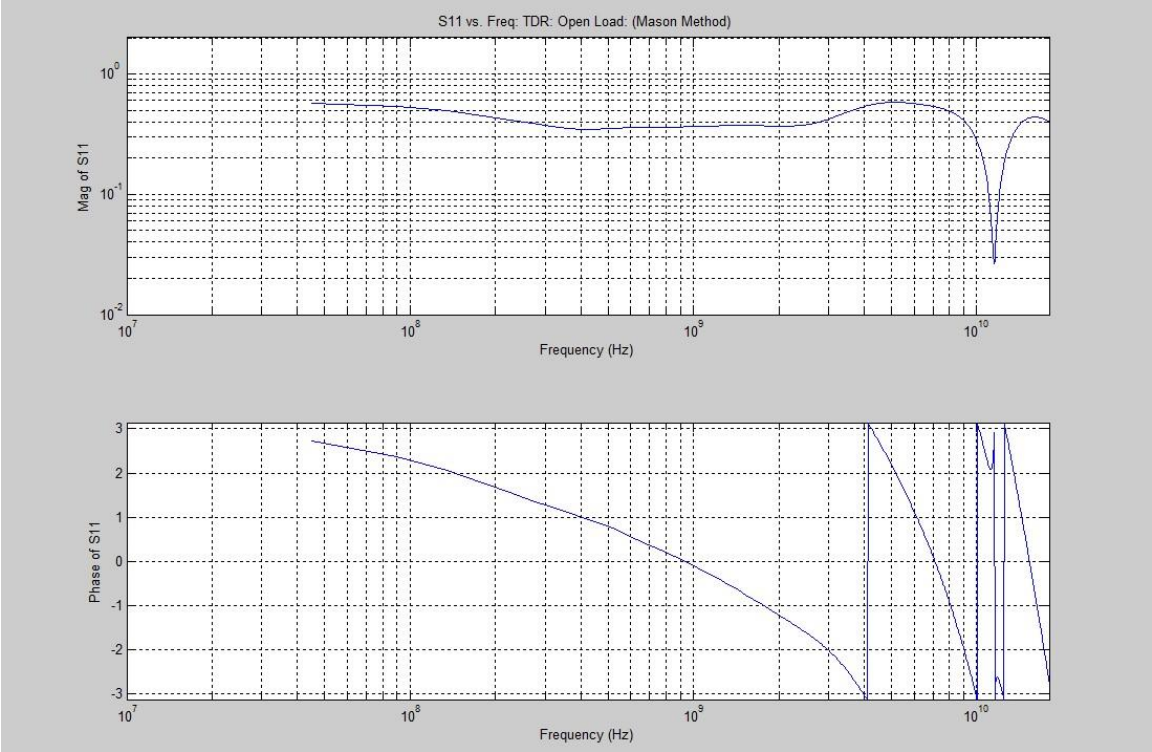


Figure 3.87: 2-Wire Probe: WC = 0.33: EC = 1.2 S/m: FDR Pred.: Open Term.: Mason: Parallel Model

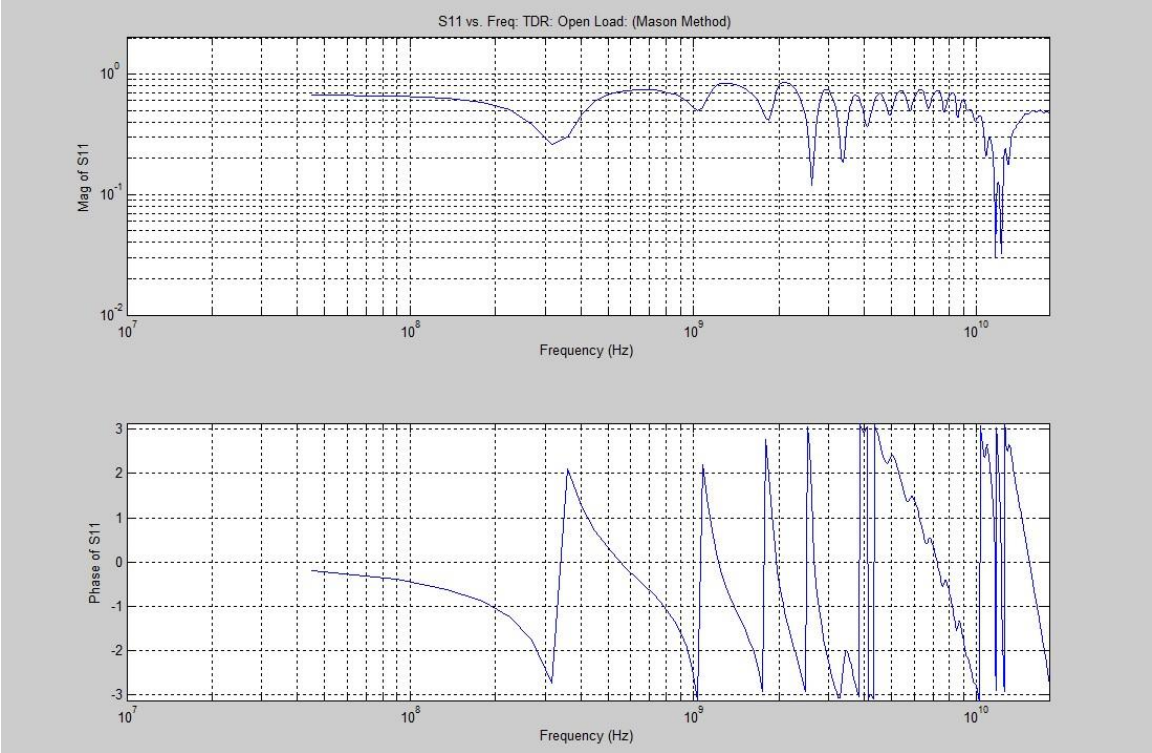


Figure 3.88: 2-Wire Probe: WC = 0.33: EC = 1.2 S/m: FDR Pred.: Open Term.: Mason: Series Model

# Chapter 4: Validation of Forward Prediction Models

## Overview:

Time Domain Reflectometry (TDR) and Time Domain Transmission (TDT) are popular tools for characterizing the electromagnetic propagation and impedance properties of various media and/or electromagnetic structures vs. position. This can be utilized to correlate to Volumetric Water Content and Electrical Conductivity as was shown in the Forward Prediction Models chapter. For low loss and low dispersion media these techniques are very effective as the phase velocity of the traveling waves is inversely related to the square root of the electric permittivity of the media and an abrupt change in impedance such as a fault in a cable can be located. However, in lossy dispersive geophysical and biological media such as soils, foods and wood, the interpretation of broadband limited dynamic range TDR and TDT waveforms is complex and presents limitations. In those media the phase velocity becomes a function of frequency (dispersion) as does the loss (attenuation) and finally the characteristic impedance and reflection coefficients at impedance boundaries. This can be overcome by utilization of high dynamic range swept narrowband frequency domain reflection and transmission measurements. These can be converted to the time domain to construct much higher quality TDR and TDT waveforms compared to direct Time Domain measurements. Changes in properties along a propagation path lead to localized time information visible in TDR and TDT waveforms. Therefore, information in both the time and frequency domains is important. The Forward Prediction Models of Chapter 3 have been developed for use in both the frequency and time domains for prediction of transmission and reflection waveforms in water content and electrical conductivity measurement systems. These models have also been integrated with cascaded transmission line models utilizing Scattering (S) Parameters and Transmission (T) Parameters for the modeling of transmission line probes in layered or heterogeneous media. This chapter presents the validation methods and chapter 5 presents the validation results for all of these models. The evaluation media included various soils over a wide range of volumetric water contents and electrical conductivities. In addition, specialized printed circuit boards were also utilized for the validation of cascaded transmission line models.

## Introduction:

Time Domain Reflectometry (TDR) and Time Domain Transmission (TDT) measurement techniques possess somewhat unique challenges in that they involve the utilization of broadband (wide frequency spectrum)and therefore relatively lower dynamic range (relatively higher noise floor) time domain information in the actual displayed measurement. It is therefore difficult to directly assess frequency dependent behavior as well as detect lower level reflected or transmitted signals in the presence of dispersive lossy media. However, utilization of narrowband (narrow frequency spectrum) and therefore relatively higher dynamic range (relatively lower noise floor) frequency domain information can overcome these challenges and lead to the correct interpretation of the waveforms in the presence of dispersive and lossy media such as soils. In addition, with High Speed Digital Signal Processing technologies available today it is now possible to conduct cost effective narrowband high dynamic range frequency domain measurements directly and convert back to the Time Domain. These are basically Frequency Domain Reflectometry (FDR) and Frequency Domain Transmission (FDT) measurements of which much higher quality TDR and TDT waveforms can be extracted from via Inverse Fast Fourier Transforms compared to what can be obtained by direct Time Domain TDR and TDT measurements. These FDR and FDT measurements are essentially equivalent to the swept Frequency Domain Vector Network Analyzer (VNA) measurements of S11 and S21 (Scattering Parameters) as described in the Appendix B. The result is much higher quality processed measurement data allowing for much more sophisticated models and waveform interpretation algorithms than were possible with classical wideband low dynamic range TDR/TDT systems. The frequency and time domains each have their advantages in displaying parameters and therefore having high quality processed data in both domains is very important. Therefore, modeling techniques must also be chosen to allow for good optimal utilization of both the time and frequency domains as is the case in the Forward Prediction Models presented in this dissertation.

This project investigated the feasibility of combining these state of the art signal processing technologies together with a set of newly developed physically based models to develop higher performance FDR, FDT, TDR and TDT water content and electrical conductivity measurement systems. The goal is to develop accurate measurement technologies even at high levels of electrical conductivity as well as in heterogeneous layered media. These systems make use of measurement algorithms that are based on physical models from the theory of

electromagnetics and transmission line network theory (scattering (S) parameters and transmission (T) parameters) as covered in the Forward Prediction Model chapter and appendices of this dissertation. These models rely less on the use of empirical relationships and have attempted to maximize the use of physically based models. These new algorithms make use of information in both the frequency and time domains and are dependent on these new state of the art signal processing measurement techniques that allow for cost effective narrow band high dynamic range direct swept frequency domain measurements that can then be converted into high quality time domain waveforms. The high frequency portion of the frequency domain information is key to being able to extract water content from the data when electrical conductivity is high as shown in the forward prediction model chapter for zone 3 frequencies. The medium frequency portion is important in determining water content at lower levels of conductivity (zone 2 frequencies) and finally the low frequency information is key to determining the electrical conductivity (zone 1 frequencies).

The objectives of the validation portion of this research project involved several steps as follows:

1.) Collection of Wide Band direct Time Domain TDR Data on Several Soil Types vs. Water Content and Electrical Conductivity. This was done both in the laboratory and in the field (the latter at different farm sites). Comparison to Forward Prediction Models Data was conducted.

2.) Collection of Narrowband High Dynamic Range direct Frequency Domain S-Parameters (reflection S11(FDR) and transmission S21(FDT)) utilizing a Vector Network Analyzer with specialized fixtures for measuring Soils with varying water contents and electrical conductivities. Generation of TDR and TDT waveforms from the Frequency Domain Data was conducted. Comparison to Forward Prediction Models Data was conducted.

3.) Collection of Narrowband High Dynamic Range direct Frequency Domain S-Parameters utilizing a Vector Network Analyzer with specialized circuit boards for emulating cascaded layered media of changing impedance. Generation of TDR and TDT waveforms from the Frequency Domain Data was conducted. Comparison to Forward Prediction Models Data was conducted.

For validation method #1, TDR data was obtained in the laboratory (for a sandy soil). In addition, TDR data was also obtained in the field over several soil types and conditions.These experiments utilized different types of direct time domain TDR measurement instrumentation (oscilloscopes) and TDR probes/fixtures over a wide range of water contents (WC) and electrical conductivities (EC) as described in the Methods section of this chapter.

For validation method #2, Narrowband High Dynamic Range Frequency Domain S-Parameter data (reflection S11 (FDR) and Transmission S21 (FDT)) was collected in a laboratory setting using a Vector Network Analyzer (VNA) together with specially constructed fixtures containing a sandy soil over wide ranges of WC and EC as described in the Methods Section.

For validation method #3, Narrowband High Dynamic Range Frequency Domain S-Parameter data (reflection S11 (FDR) and Transmission S21 (FDT)) was collected in a laboratory setting using a VNA together with specially constructed printed circuit boards with various non-uniform cascaded Transmission line traces/patterns (described in the Methods section).

The goals of these techniques was to validate the physically based Forward Prediction models and software algorithms developed and enhanced in Matlab and presented in chapter 3. For all four validation methods, simulation runs were conducted in Matlab using the Forward Prediction models and compared to the actual measured or simulated validation data in both the frequency and time domains using Fast Fourier Transform (FFT) and Inverse Fast Fourier Transform (IFFT) algorithms. These results are presented in this chapter.

The results of the validation testing on the Forward Prediction models/algorithms have shown that the electrical conductivity can be accurately determined over wide ranges of that parameter by using the low frequency information of the scattering network parameter S11. It was also found that for lower values of electric conductivity that the electric permittivity and dielectric constant information can be extracted at medium frequencies by looking at peaks in the effective dominant group delay plots vs. frequency (derivative of S11 phase with frequency). From these peak locations a lookup table based on the prediction models can be used to determine water content. In addition it was determined that if high dynamic range frequency domain methods are utilized, the permittivity, and therefore water content (which is a function of the

permittivity), can be extracted from plots of effective transmission line impedance vs. frequency as well as the overall transmission coefficient vs. frequency by using the medium to high frequency information of both S11 and S21 when the conductivity is high and using signal processing to remove the effects of the electrical conductivity (the latter again obtained from the low frequency portion of the spectrum).

It was found that the best fitting prediction models were based on weighted interpolations between two physically based opposite extreme boundary condition models that either assume that the physical constituents of air, solids and water are in series or in parallel when modeled as shunt components in the TDR or TDT transmission line probe. Finally, a new feature was added to the algorithm to be able to model water content and conductivity variations vs. depth along the probe by using advanced models from scattering S parameter network theory using Mason's non-touching loop rule for cascaded networks. These cascaded transmission line models were again validated with a special PCBA containing several different Non-Uniform Transmission line patterns including changes of impedance vs. position.

**Time vs. Frequency Resolution:**

There is a competing tradeoff on having high time resolution in the time domain (requiring higher frequencies in the frequency domain) and long time or high waveform record length in the time domain (requiring lower frequencies in the frequency domain). In fact a physical/theoretical limit on this comes from the Heisenberg Uncertainty Principle or relationship which indicates that one can’t simultaneously have infinite time resolution and infinite frequency resolution (analogous to the theoretical limits of not being able to simultaneously have infinite resolution on determining electron/wave position vs. infinite resolution on determining electron/wave energy/momentum from Quantum Mechanics). In addition, there is also a practical limit on this (reached far sooner than the theoretical limits predicted by Heisenberg) based on the competing tradeoffs of frequency resolution and bandwidth vs. tolerable measurement time in measurement instrumentation. Therefore, there is a computational tradeoff as to how fine of information one can utilize in the time domain vs. the frequency domain. However, state of the art waveform sampling and analog to digital conversion (ADC) hardware and corresponding digital signal processing (DSP) software technologies available today allow for pushing this tradeoff much further while still maintaining reasonable cost. Nevertheless there is still a

practical limitation as to how much simultaneous resolution can be obtained in the time and frequency domains. For example, in a soil with a TDR/TDT or FDR/FDT system, this becomes a constraint/tradeoff when trying to identify a changing property (such as water content) vs. position with high positional resolution while simultaneously trying to image that same soil over a large volume and/or long linear length.

There is another even more subtle tradeoff on this specific to Electrical Conductivity (EC) from the theory of electromagnetics in that it requires longer time (lower frequencies) to identify EC whereas it takes shorter or finer time resolution (higher frequencies) to identify changing electromagnetic properties vs. progressively finer positions along a probe. In fact as the EC increases and approaches infinity the electromagnetic wave propagation attenuates (loses amplitude) and retards (slows) and eventually disappears and stops all-together and can't penetrate the conductor (so the concept of high frequencies and fine positional resolution can't exist with very high EC). These attenuation and retardation effects are also frequency dependent (worsening with increasing frequency) leading to roll-off and dispersion or smearing/spreading of the sharp (high frequency) wavefronts required for fine positional resolution measurements. There may be EC changes along the length of a probe but due to the lower frequency physical mechanisms of EC (driven often by long time constant electrolytic and ion conduction physics in soils) together with the attenuation/dispersion effects on high frequencies it can be difficult if not impossible to isolate the contribution from localized positions along the probe relative to other positions when it comes to EC. Therefore, there is a practical limitation from physics as to how well electrical conductivity (EC) can be imaged vs. position. EC must generally be imaged as an average over a larger volume or length of a probe unless there is a localized area of high EC and all other areas along the probe have much lower EC. For a full discussion on this please refer to chapter 3 (covering the forward prediction models) as well as Appendix "A" (background on electromagnetic theory). These effects will also be shown in this chapter cover validation of the models.

In contrast Water Content (WC) correlates to Electric Permittivity (EP) as opposed to EC. EP also impacts the physics of wave propagation at all frequencies but in a different manner vs. EC. With EP the phase velocity of waves (even at high frequencies) is inversely proportional to the square root of EP (in the absence of any loss mechanisms). Therefore, with high EP (as is the case with water) there can be high frequency measurements obtained which also allows for

simultaneous imaging to finer positional resolutions. Therefore, it is very practical and feasible to obtain an image of WC vs. position along a probe when the loss/dispersion mechanisms are low to manageable. The utilization of Cascaded Transmission Line models along with S-Parameters and T-Parameters (Network Models) can be applied to this application as covered in chapter 3 (Forward Prediction Models) along with the appendices and also shown in this validation chapter. However, there is a limitation even with the use of EP if there is also the presence of loss and dispersion mechanisms (either EC or alternatively higher frequency dielectric loss mechanisms such as the Debye models for dielectric relaxation of water as covered in Chapter 3 and the appendices). Nevertheless it is more feasible to obtain an image of WC vs. position (for low to moderate loss/dispersion mechanisms) than it is to obtain an image of EC vs. position (for any value of EC) as will be shown in this dissertation. EC must be typically taken as an average over a longer length of probe. All of this will be a part of the validation discussion for the forward prediction models as presented in this chapter.

**Potential Inverse Modeling/Algorithm Techniques:**

Before moving on to the validation methods and validation results/discussion for the forward prediction models, a brief discussion/preview will be given on potential inverse modeling/algorithm techniques to extract WC and EC from actual potential TDR/TDT and/or FDR/FDT measurement systems using the forward prediction models and technologies presented in this dissertation. The full development of the inverse modeling/algorithm techniques represents a separate follow-on area of research currently underway by the author and will be presented in separate publications outside of this dissertation. However, several aspects of the inverse models and algorithms are covered in this dissertation and are important to the validation results of the forward prediction models. These include the ability to make some direct measurements from the TDR/TDT/FDR/FDT to extract some parameters to simplify the remainder of the inverse algorithms which will involve lookup tables and optimization algorithms. Some of the direct measurements which will be covered in more depth later in this chapter in the results section include the following: Utilization of Group Delay measurements (derivative of the phase of the reflection coefficient (S11) and transmission coefficient (S21) with respect to frequency to ascertain information about the overall effective electric permittivity which correlates to water content (looking at the medium to higher frequency portions of this data). In addition, looking at the low frequency portion of the effective input impedance will allow for making a good estimate of the overall electrical conductivity. By extracting these overall parameters it will allow for simplifying the balance of the inverse algorithms (especially for those cases where we are also interested in identifying individual profiles vs. position of the parameters). These aspects of the inverse models will be covered in more depth later in the context of the validation results. In addition, there are some important aspects of the potential inverse modeling/algorithm techniques that are relevant in the context of the time/frequency tradeoffs discussed above in this dissertation as well as with the overall validation of the forward prediction models covered in this chapter of this dissertation.

The primary goal of the inverse models and algorithms is to extract the desired target parameters (WC and EC) out of the various measurement signals (TDR/TDT and FDR/FDT measurements) utilizing a particular probe within a system under test. These target extracted parameters include overall WC and EC averages as well as a profile of WC vs. position (and on a

coarser scale a profile of EC vs. position to the extent possible – or possibly limited to just an overall average on EC depending on its value). Methods of inverse algorithms include direct extraction (mentioned above), lookup tables as well as various global and local optimization methods to fit the measured data to the forward prediction models.

In addition, to help address the competing tradeoffs of high time resolution vs. high frequency resolution three distinct modeling/transform techniques that use different approaches to handling the time/frequency modeling problem will also eventually be included in the inverse solving models/algorithms to assist in the computing efficiency and speed of the algorithms more so than the efficacy of the algorithms. These are given as follows:

1.) Classical Fourier Transform [134]:
    a. Infinite Frequency Resolution/Localization
    b. Zero (Absolute) Time Resolution/Localization

2.) Time Windowed Fourier Transform or Short Time Fourier Transform: (Example: Gabor Transform [135, 136]):
    a. Finite Fixed Scale Frequency Resolution/Localization
    b. Finite Fixed Scale Time Resolution/Localization

3.) Wavelet Transform: (Example: Haar Wavelets, Daubechies Wavelet Family, etc. [134, 137]):
    a. Finite but Variable Scale Frequency Resolution/Localization
    b. Finite but Variable Scale Time Resolution/Localization

However, again these additional techniques (Methods 2 and 3 above) focus on the computing efficiency and speed of the inverse algorithms and not so much the efficacy of the models/algorithms and so only method #1 (Classical Fourier Transform) is covered in this dissertation. The background theories of these other techniques are covered in the literature [134 - 137] and their application to the inverse models/algorithms will be covered in follow-on publications by the author.

The forward prediction models presented in chapter 3 of this dissertation are based on frequency domain and time domain representations where conversion between them is done by the Classical Fourier Transform and Classical Inverse Fourier Transform (#1 above). However, these forward prediction models will still be compatible with inverse modeling algorithms that utilize all three of the above methods. This will provide efficient computation on simultaneously taking advantage of both the narrowband frequency domain FDR/FDT and the wider band time domain TDR/TDT representations.

The forward prediction models presented in this dissertation are again based on classical Frequency Domain and Time Domain analysis per the Fourier and Inverse Fourier Transforms given as follows:

Classical Fourier Transform (Continuous Time Signals):

$$X(f) = \int_{-\infty}^{\infty} x(t) e^{-j2\pi ft}\, dt \;=\; \int_{-\infty}^{\infty} x(t) e^{-j\omega t}\, dt \qquad (4\text{-}1)$$

Classical Inverse Fourier Transform (Continuous Time Signals):

$$x(t) = \int_{-\infty}^{\infty} X(f) e^{j2\pi ft}\, df \;=\; \frac{1}{2\pi}\int_{-\infty}^{\infty} X(\omega) e^{j\omega t}\, d\omega \qquad (4\text{-}2)$$

Where f = Frequency (Hz)

$\omega = 2\pi f$ = Angular Frequency (Radians/Second)

t = Time (Seconds)

x(t) = Continuous-Time Signal

X(f) = Fourier Transform of x(t) at Frequency f

With TDR and TDT or alternatively FDR and FDT signals the measured and modeled time domain signals x(t) or frequency domain signals X(f) respectively are typically the result of the measured response of a stimulus signal and a system response function. Information about the system is what is of interest in the inverse algorithms. In electromagnetic measurements the system is often modeled with scattering parameters that can be modeled in either the time or frequency domains. In the time domain the overall signal x(t) can be represented as either a TDR or TDT response signal (tdr(t) or tdt(t)) each of which is the convolution of a particular stimulus signal a(t) with the system impulse response or function (reflection $h_r(t)$ or transmission $h_f(t)$) or

alternatively the particular scattering parameters (reflection coefficient s11(t) or transmission coefficient s21(t)). With the frequency domain it is simply the product of the measured frequency domain signal X(f) and the System Frequency Response H(f) and can utilize S-Parameters in the frequency domain (per Appendix B). These representations are shown as follows:

Time Domain Representation of particular response signals (TDR or TDT) (Continuous Form):

$$\text{TDR:} \quad x(t) = tdr(t) = a(t) * h_r(t) = \int_{\tau=0}^{t} a(t)h_r(t-\tau)d\tau = \int_{\tau=0}^{t} a(t)s_{11}(t-\tau)d\tau \tag{4-3}$$

$$\text{TDT:} \quad x(t) = tdt(t) = a(t) * h_f(t) = \int_{\tau=0}^{t} a(t)h_f(t-\tau)d\tau = \int_{\tau=0}^{t} a(t)s_{21}(t-\tau)d\tau \tag{4-4}$$

Frequency Domain Representations of FDR/FDT signals (Classical Fourier Transform):

$$\text{TDR:} \quad X(\omega) = FDR(\omega) = A(\omega)S11(\omega) = A(\omega)H_R(\omega) \tag{4-5}$$

$$\text{TDT:} \quad X(\omega) = FDT(\omega) = A(\omega)S21(\omega) = A(\omega)H_F(\omega) \tag{4-6}$$

The goal with whatever inverse modeling technique is utilized is to assess the system response to characterize the actual system including parametric information (such as WC and EC). With a classical Fourier transform on the measured time domain signals, the frequency domain representation of the system response can be simply obtained by dividing the Fourier Transform of the measured response by the Fourier Transform of the stimulus signal to obtain the Fourier Transform of the system response. However, this is the steady state response function whereas a transient response or short time decaying time information is lost in this type of analysis if the stimulus is non-repetitive such as a step. However, if a repetitive stimulus such as a square wave is utilized the transient responses such as occur with TDR and TDT signals can still be captured in the Classical Fourier Transform but at the cost of twice the information, as the stimulus waveform must be made repetitive and imaged or mirrored (resulting in two edges or replication of the TDR and TDT transient response images and thus 2x redundancy). This is

required to create finite energy at the frequencies of the information in the transient edges as the Fourier transform acts over infinite time. However, this can also be synthesized by combining multiple measured FDR and FDT signals over a wide range of narrowband measurements captured directly in the frequency domain. To take better advantage of these tradeoffs the other methods (WFT and Wavelets) will be utilized in the inverse algorithms being fully compatible with the forward prediction models of this dissertation.

**Determining Goodness of Fit:**

As part of the validation process of the forward prediction models (and also an important part of assessing the success of any inverse algorithm) a valid method of determining goodness of fit must be utilized to evaluate the effectiveness of the prediction models to agree with measured data. For the purposes of validation of the models in this dissertation the fitting evaluation was performed on the time domain signals (predicted and actual TDR signals) using evaluation parameters similar to those in linear regression.

The basic objective is to minimize the sum of squared errors between the predicted and actual TDR signal over the relevant length of the trace. The sum of squared errors of the modeled values relative to the actual values is defined as follows:

$$\text{Model Sum of Squared Errors} = \sum_{t = t_S}^{t_P/2} \left( S11_{Pred}(t) - S11_{Act}(t) \right)^2 \qquad (4\text{-}7)$$

where

$t_P$ = Period of waveform (square wave used instead of a step in prediction algorithm)

$t_S$ = Sampling interval or time increment in TDR waveform

and the other parameters in equation 4-7 are the predicted and actual values of the time domain S11 or TDR trace as a function of time.

Two different Goodness of Fit quantifying measures were utilized in this dissertation to assess how well equation 4-7 has been minimized. These are given as follows (termed Coefficient of Fit Methods A & B):

$$\text{Coefficient of Fit Method A} = 1 - \frac{\sum_{t=t_S}^{t_P/2} \left(S11_{Pred}(t) - S11_{Act}(t)\right)^2}{\sum_{t=t_S}^{t_P/2} \left(S11_{Act}(t) - S11_{ActMean}\right)^2} \qquad (4\text{-}8)$$

$$= 1 - \frac{ModelSumofSquaredErrors}{\sum_{t=t_S}^{t_P/2} \left(S11_{Act}(t) - S11_{ActMean}\right)^2}$$

$$\equiv R^2$$

$$\text{Coefficient of Fit Method B} = \frac{\sum_{t=t_S}^{t_P/2} \left(S11_{Pred}(t) - S11_{ActMean}\right)^2}{\sum_{t=t_S}^{t_P/2} \left(S11_{Act}(t) - S11_{ActMean}\right)^2} \qquad (4\text{-}9)$$

Equation 4-8 is by definition equal to the Coefficient of Determination $R^2$ in linear regression where a value of 1 would indicate a perfect fit (zero Sum of Squared Errors of the Model (Predicted) vs. Actual (Observed) Values). This is the primary quantifier utilized for assessing goodness of fit throughout this dissertation. Another alternative measure of the goodness of fit (Method B) that was also utilized in this dissertation is given by 4-9. It was derived through iterative trials and can be greater than or less than 1. A value of 1 in equation 4-9 is still the optimal goal and represents an approximate minimum of equation 4-7. It was observed that for Coefficient of Fit Method B values greater than 1 that the water content was overpredicted (transit time longer than actual) and for Coefficient of Fit Method B values less than 1 that the water content was underpredicted (transit time shorter than actual). It was therefore useful in determining direction of error. In contrast Coefficient of Fit Method A ($R^2$) given by 4-8 is

always less than or equal to 1 with 1 again indicating a perfect fit. Equations 4-7 through 4-9 were again used in the validation of the forward prediction models and are also valuable for the proposed inverse models in validating either lookup tables or optimization algorithms outcomes. Equations 4-7 through 4-9 were referenced in the data results section with values given for these goodness of fit parameters for all the various prediction model variations over full ranges of water content and electrical conductivity.

## Validation Methods:

The validation of the forward prediction models involved the following steps and associated collected databases:

1.) Wide Band direct Time Domain TDR Data:
    a. Lab Data: Sand Soil over wide ranges of WC and EC in a Controlled Experiment.
    b. Field Data: Several Soil Types at Different Farms with different ranges of WC and EC including Profiles vs. Depth.

2.) Narrowband High Dynamic Range direct Frequency Domain S-Parameters (FDR (S11, S22) and FDT (S12, S21) Data with Conversion to TDR / TDT Waveforms):
    a. Lab Data: Sand Soil over wide ranges of WC and EC in a Controlled Experiments.

3.) Narrowband High Dynamic Range direct Frequency Domain S-Parameters (FDR and FDT Data with Conversion to TDR / TDT Waveforms):
    a. Lab Data: Specialized circuit boards for emulating Cascaded Layered Media of changing Impedance vs. Position in a Controlled Experiment.

The following provides additional details on these validation objectives/methods and associated measurements that have been collected enabling databases to be developed for the validations of the forward prediction modeling techniques:

1.) Wide Band Direct Time Domain TDR Measurements:
   a. Laboratory Setup #1: Time Domain Reflectometry (TDR) Measurements Conducted on a Column of Soil Cells Designed to Emulate a Sandy Soil Profile with Varying WC & EC vs. Depth. Direct TDR Measurements were made using a Tektronix 11801D Oscilloscope with a TDR Option. Columns of Sand Soils of Different WC and EC Profiles were tested.

   b. Field Setup #1: Field TDR Measurements at Multiple Field Locations: Different Soil Types (Sand, Loam and Clay): Wide Ranges of WC and EC including some Profiles.

2.) Narrowband High Dynamic Range Direct Frequency Domain FDR (S11, S22) and FDT (S12, S21) Measurements:
   a. Laboratory Setup #2: 8510 Vector Network Analyzer (VNA) Frequency Domain Transmission FDT (S12,S21) and Reflection FDR (S11,S22) Measurements Using Individual Soil Cells with both Invasive and Non-Invasive Probes. TDR and TDT Waveforms were generated via Inverse Fast Fourier Transform Algorithms as well as via the Time Domain Option of VNA. Sand Soils of Different Volumetric Water Contents (WC) and Electrical Conductivity (EC) Values were tested.

3.) Narrowband High Dynamic Range direct Frequency Domain S-Parameters (FDR and FDT):
   a. Laboratory Setup #3: 8510 Vector Network Analyzer (VNA) Frequency Domain Transmission FDT (S12,S21) and Reflection FDR (S11,S22) Measurements using Specialized circuit boards for emulating Cascaded Layered Media of changing Impedance vs. Position (Characteristic Impedance Profiles) in a Controlled Experiment. These characteristic impedance profiles were emulated via non-uniformities in microstrip and stripline transmission lines of cascaded stepped impedance shifts on an RT Duroid 5880 substrate. Conversions to TDR and TDT Waveforms were also conducted.

## Laboratory Experiments #1: Time Domain Reflectometry

Figure 4.1 shows the lab setup (per #1a in the above validation methods) where a vertically layered column of 25 different individual soil cells (of two different heights depending on location within the column) was utilized. Experimental runs of open air, dry soil, saturated soil (distilled water), drained soil (distilled water), saturated soil (1M solution of NaCl in water), drained soil (with the 1M saline water solution), saturated soil (.02M solution of NaCl in water) and finally the drained conditions with the .02M solution of water were conducted on the 25 layers of rings in the vertical column. The soil type was a Unimin 40/50 mixture of sand. For the soil WC and EC experiments the column was initially filled to saturation at all levels (with either the distilled, 1M or 0.02M water) for the saturated experiments and then allowed to drain partially down into a flask as shown in figure 4.1a. This then allowed for a variable WC and EC profile vs. depth to develop where wetter WC values resided at the lower levels and drier WC values towards the top (as shown approximately by different shades of blue and gray in figures 1a and 1b). The actual WC profile approximately followed a curve based on the water characteristic curve of a sandy soil [51]. In this specific test setup there were parallel wire transmission lines inserted into each of the individual soil cells (shown in red in figure 4.1b) to allow for measuring the different levels of WC and EC vs. depth. Each of the transmission line probes were open circuited within the soil cell near the far end and terminated on their source end by an RF SMA connector for allowance of interface to a Tektronix 11801D high speed oscilloscope with a TDR measurement option. TDR waveforms were collected for all the cells for all the test cases of different WC and EC profiles. These were relatively higher (wide) bandwidth TDR measurements with spectral content to 18 GHz involving relatively short 7 cm TDR probes.

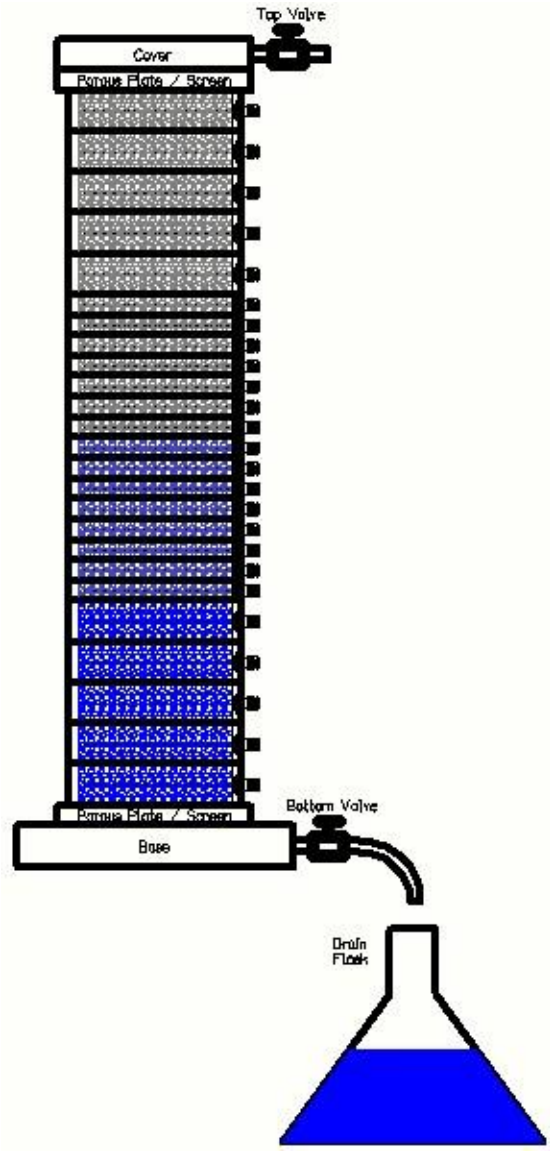


a.) Full Column with 25 Individual Soil Cells with Drain Flask to Allow for Variable Water Content vs. Vertical Position.

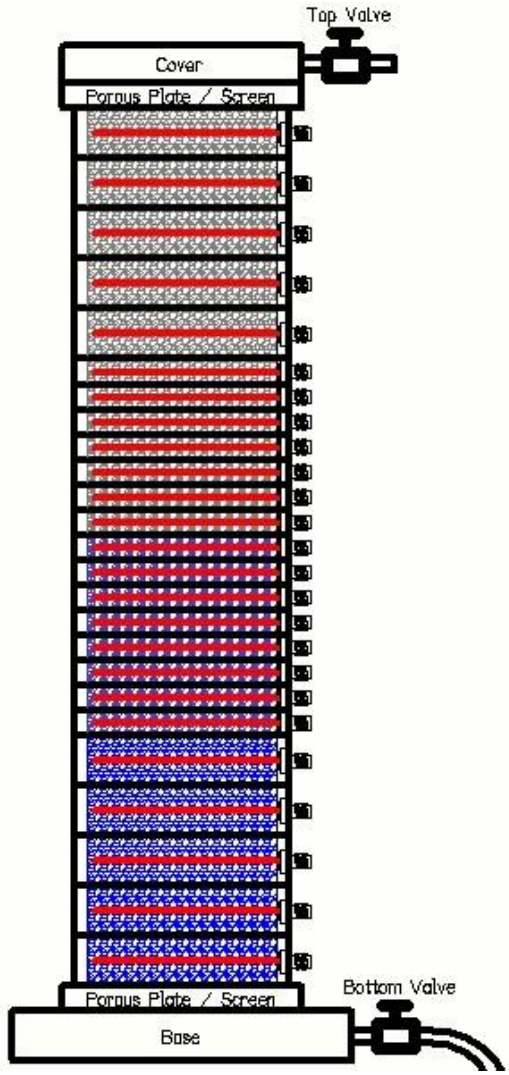


b.) Full Column with TDR Probes Shown in Red. The Probes Consist of Parallel Wire Transmission Lines with SMA Connectors.

Figure 4.1: Laboratory TDR Measurements Setup with Column of Soil Cells

## Field Experiments: Time Domain Reflectometry

An additional experimental setup (#1b in the validation methods) is shown in figure 4.2 and involved field experiments at various sites to emulate real-world conditions. The various test runs are tabulated in table 4.1. In each of the field test sites a Tektronix 1502B oscilloscope/cable tester (TDR/scope) was utilized along with a three wire TDR probe by Campbell Scientific (CS610). The probe was larger (30 cm length) and the measurements were still relatively wideband but lower bandwidth vs. the laboratory setup of #1a covered above. For these field experiments, with the 1502B, the maximum frequency range went up to approximately 2 GHz in terms of spectral content. However, that was still compatible with the tradeoff of measuring deeper along the longer probe (which is supported OK by sub-GHz frequencies). Soils of different types including sand, silt/loam and clay/loam (as tabulated in table 4.1) were measured at various WC and EC values. The sample count and verification methods for WC and EC are also tabulated in table 4.1. Time Domain (TDR) measurements were compiled and later post-processed with the techniques described in this dissertation.

**Table 4.1: Summary of Field Test Site Information**

| Location | Soil Type | Sample Count | WC and EC Verification Methods | Special Conditions |
|---|---|---|---|---|
| Monroe, OR Mint Farm | Clay Loam | 6 | Gravimetric Neutron Probe AC Resistance Bridge* | Poor Drainage Wetter Climate |
| Hermiston, OR Poplar Farm | Sand | 16 | Gravimetric Neutron Probe AC Resistance Bridge | Well Drained Arid Climate |
| Albany, OR High Salinity Irrigation | Silt Loam | 4 | Gravimetric AC Resistance Bridge | High Salinity |

*AC Resistance Bridge not as Effective for Clay Soils (with Charged Interfacial Mechanisms) due to low frequency operation of Bridge (inside the bandwidth of the electrolytic reactions and other charged interfacial mechanisms) and so only Order of Magnitude Approximations for EC Obtained for the Monroe Site.

These field datasets again involved TDR measurements on larger probes (30 cm) with wideband but relatively limited bandwidth spectral content (up to ~2 GHz maximum) compared to the setup of Validation Method #1a. Figure 4.2 is a drawing showing the setup.

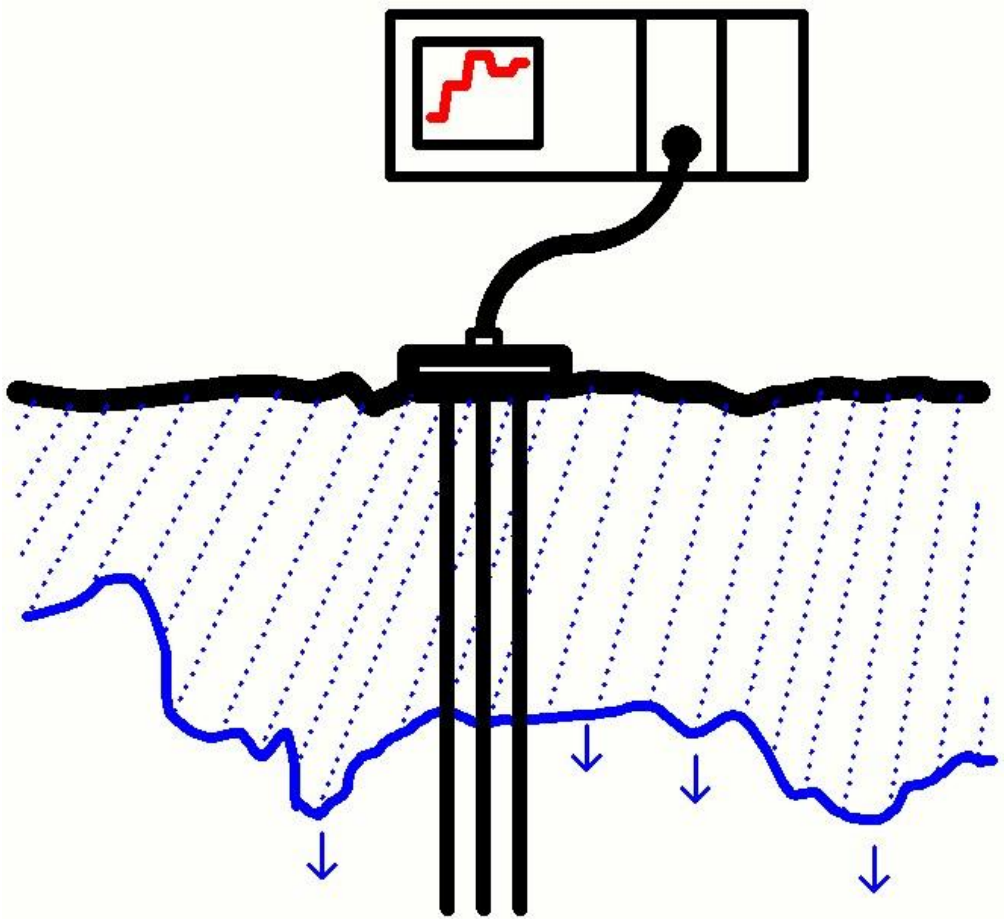

Figure 4.2: Field TDR Setup with Three Wire Probe (Showing Case of a Wetting Front after Irrigation)

## Laboratory Experiments #2: Frequency Domain & Time Domain Transmission and Reflection

The soil test cells/fixtures utilized for the validation method #2 are shown in figures 4.3a to 4.3d. There were two RT Duroid 5880 PCBA's mounted on the top and bottom of the soil cells and sealed to the cells via O-Rings and Covers. These two PCBA's each contained a parallel three conductor transmission line approximating a Coplanar Waveguide Transmission line on the RT Duroid dielectric substrate. The opposite surface of the transmission line was then affixed and exposed to the soil enclosed within the cell (either on the bottom or on the top of the cell) so that the propagation and impedance properties of the line was influenced by both the soil and the RT Duroid dielectric. Also contained in these soil cells was an invasive parallel wire transmission line through the center of the cells and oriented orthogonally to the PCBA transmission lines as shown in figure 4.3a. The total probe lengths within the cells were approximately 7.5 cm. On both ends of both of the Non-Invasive PCBA transmission lines as well as the invasive transmission lines there are RF SMA 50 Ohm connectors allowing for interface to the VNA. Forward and Reverse Frequency Domain Transmission FDT (S12 and S21) and Input and Output Frequency Domain Reflection FDR (S11 and S22) measurements with 50 Ohm ports on each end were made in the frequency domain up to 32 GHz using the HP8510 Vector Network Analyzer (VNA). In addition, a special reflection measurement was made with one port open circuited (S11 measurement only up to 18 GHz) again using the VNA. The Time Domain Option of the VNA was also utilized to develop Time Domain Reflectometry (TDR) waveforms for the open circuit measurement case. Finally, Inverse Fast Fourier Transform algorithms were utilized to generate the Time Domain TDR and Time Domain Transmission (TDT) waveforms for the 50 Ohm measurements (using Matlab).

The first datasets (soil cell per figures 4.3b and 4.3c) contained VNA frequency measurements up to 32 GHz for the 50 Ohm VNA transmission and reflection measurements (S21 and S11 with 50 Ohm terminated ports on both ends) and 18 GHz for the open circuited S11 measurements. The total probe lengths within the cells were approximately 7.5 cm.

Figure 4.3a: Soil Moisture Content Measurement Cell w/PCBA at Bottom and Parallel Wire Transmission Line through Center (Orthogonal to PCBA Coplanar Waveguide Transmission Line)

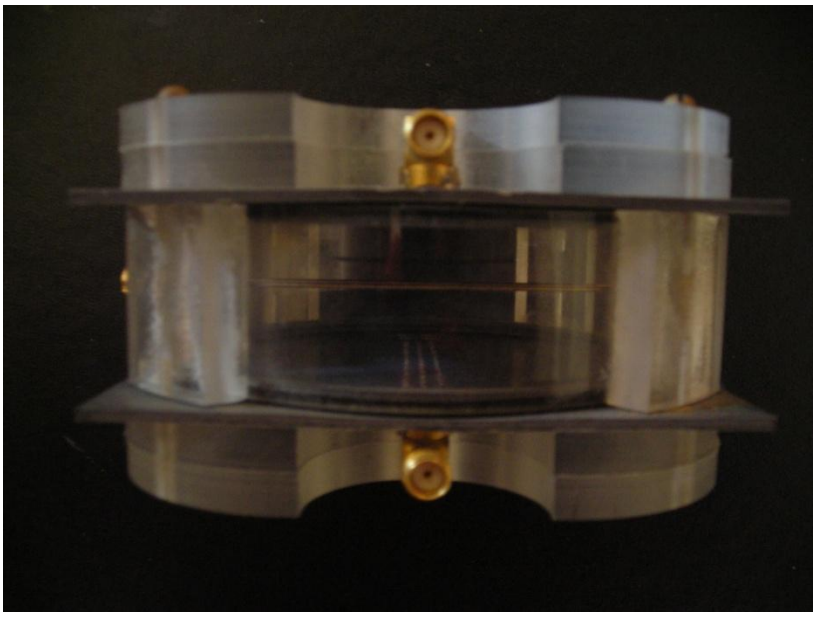

Figure 4.3b: Fully Enclosed Soil Moisture Measurement Cell (shown with just air enclosed). PCBA's located on both Top and Bottom w/Coplanar Transmission Lines. Parallel Wire Transmission Line through Center of Fixture (Orthogonal to PCBA Transmission Lines)

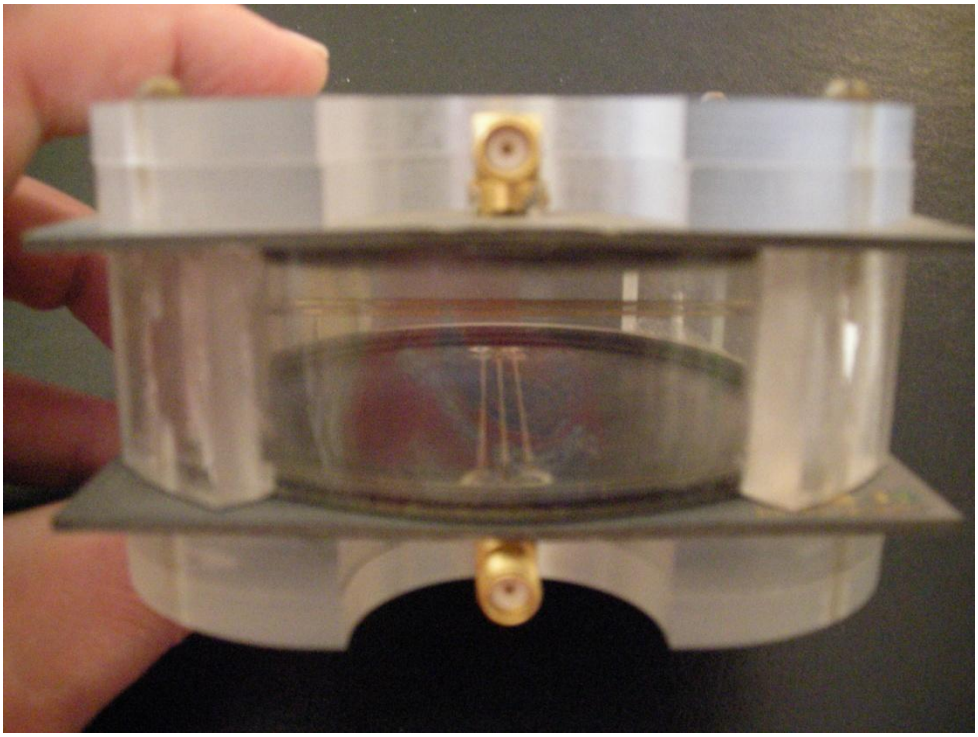

Figure 4.3c: Another View of Soil Moisture Measurement Cell (w/PCBA's)

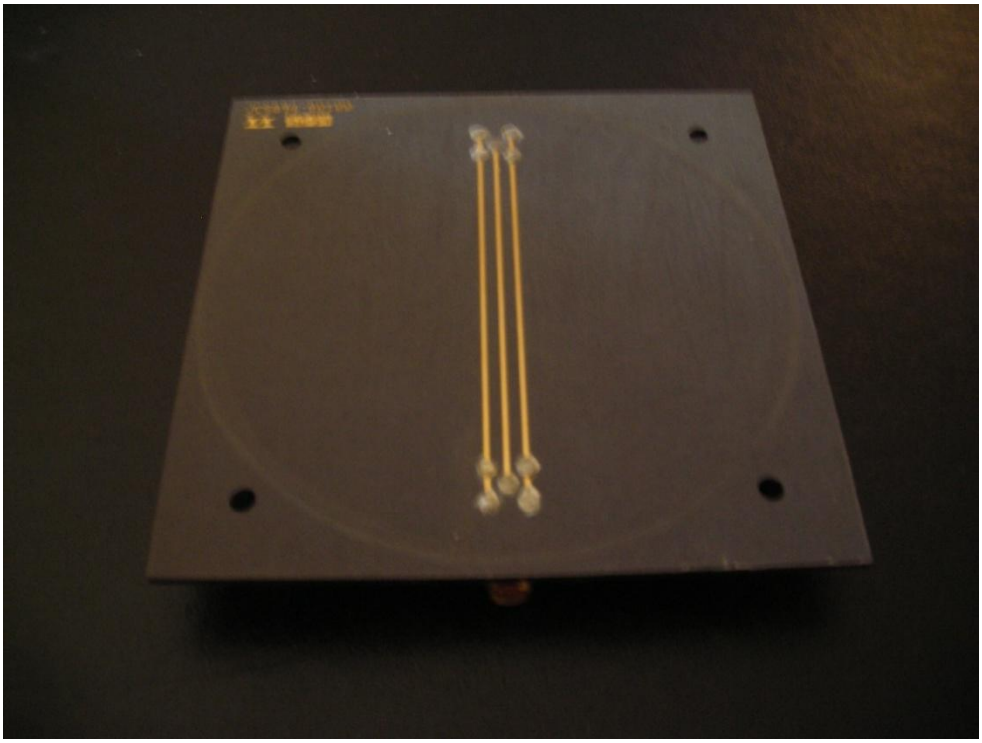

Figure 4.3d: RT Duroid 5880 PCBA with Coplanar Waveguide Transmission Line

## Laboratory Experiments #3: Frequency and Time Domain: Cascaded Transmission Lines

To evaluate the different modeling techniques on non-uniform transmission lines in the context of TDR and TDT signals various replicated test PCBA's were designed and constructed containing a variety of different cascaded transmission line types and patterns. These included both microstrip and stripline with different cascaded non-uniform sections of varying characteristic impedance as well as coplanar waveguide, edgewise coupled stripline and finally a couple of stub filter designs all on a 6 layer PCBA with RT-Duroid 5880 dielectric. One of these PCBA's is shown in figures 4.4a and 4.4b. Details of some of the transmission line patterns on the three signal layers (layers 1, 4 and 6) are also shown in figures 4.5a through 4.5c (the ground plane layers are on layers 2, 3 and 5 and aren't shown).

SMA right angle connectors were utilized on both ends of each transmission line under test (TLUT) and full 2-port Scattering (S) parameters in the frequency domain were measured for each TLUT using an 8510C vector network analyzer (VNA) over a frequency span from 45 MHz to 18.045 GHz (401 harmonically related points with 45 MHz frequency resolution). In addition the time domain response was also calculated and captured from the VNA for each S-Parameter using the time domain option available with the 8510C in both a 50 Ohm configuration (all four S-Parameter waveform responses in the time domain) and an open circuit termination configuration (S11 waveform response in the time domain only). The VNA time domain responses were also 401 points (generated via an Inverse Fourier Transform on the frequency domain S-Parameter data assuming also a step waveform stimulus). Finally, the time domain response for S11 (TDR) and S21 (TDT) were measured directly for each TLUT in a 50 Ohm context and S11 (TDR) also measured in an open circuit end termination context using a high speed Agilent 54750A oscilloscope with two 54754ATDR/TDT plug-in modules with 20 GHz bandwidth. These waveforms were all imported into Matlab and programs (m-files) were generated to allow for processing of the collected waveforms and comparing them to the forward prediction models.

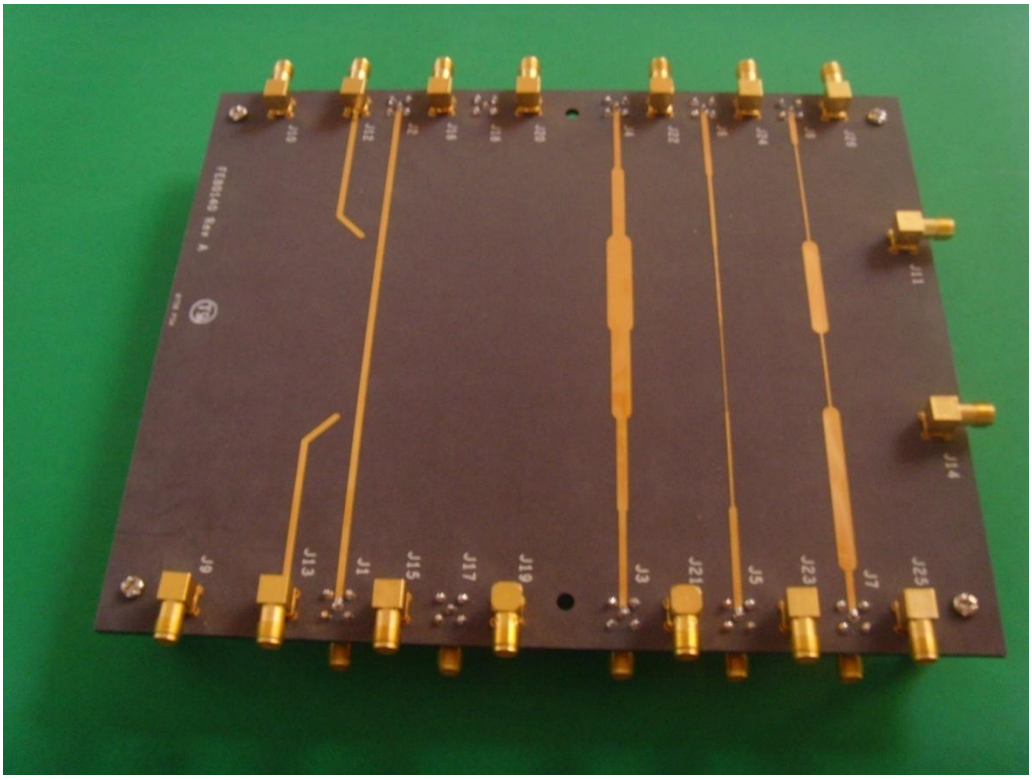


Figure 4.4a: Test PCBA (Top Layer): Microstrip Traces

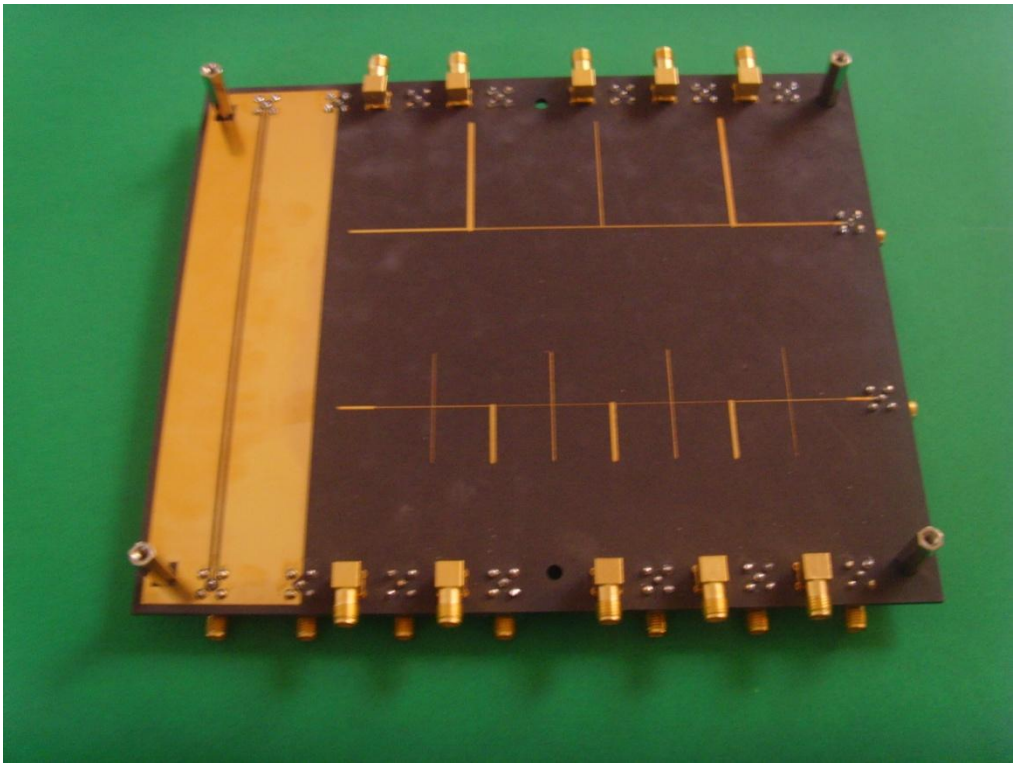

Figure 4.4b: Test PCBA (Bottom Layer): Coplanar Waveguide and Stub Filters

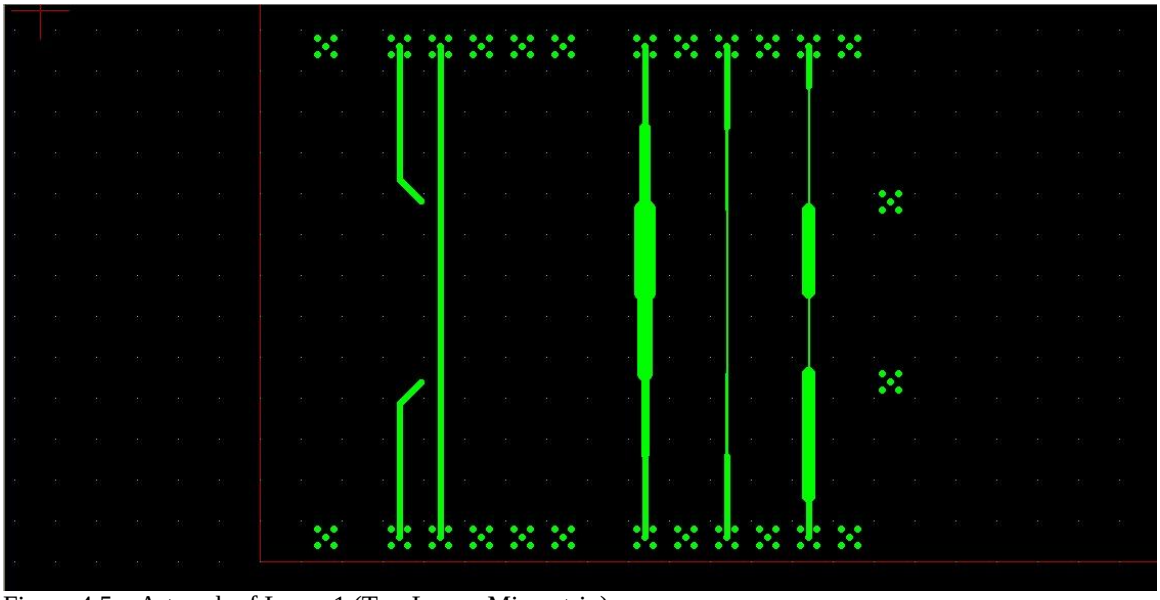

Figure 4.5a: Artwork of Layer 1 (Top Layer: Microstrip)

a. (Starting from the Left): Feeding Traces for Layer 6 Stub Filters
b. Microstrip: 50 Ohm Reference Transmission Line
c. Microstrip: Low Impedance Steps (< 50Ω): From Bottom End: 50, 38, 22, 17, 30, 50Ω
d. Microstrip: High Impedance Steps (> 50Ω): 50, 91, 133, 100, 75, 50Ω
e. Microstrip: Alternating High and Low Impedances: 50, 25, 100, 25, 100, 50Ω

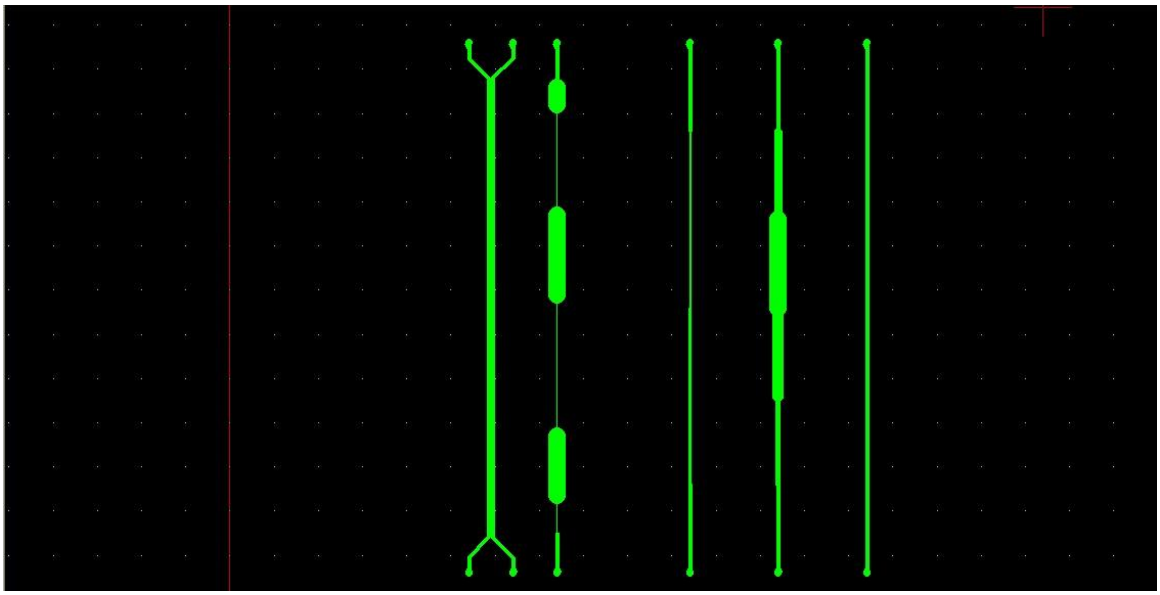

Figure 4.5b: Artwork of Layer 4 (Internal Layer: Stripline)

a.) Edgewise Coupled Stripline on Left (gap between traces not visible at this global view)
b.) Stripline: Alternating High and Low Impedances: 50, 115, 12.5, 115, 12.5, 115, 12.5, 50Ω
c.) Stripline: Non-Uniform Line: High Impedance Steps (> 50Ω): 50, 57, 64, 100, 75, 50Ω.
d.) Stripline: Non-Uniform Line: Low Impedance Steps (< 50Ω): 50, 37, 19, 12.5, 25, 50Ω.
e.) Stripline: 50Ω Reference Transmission Line

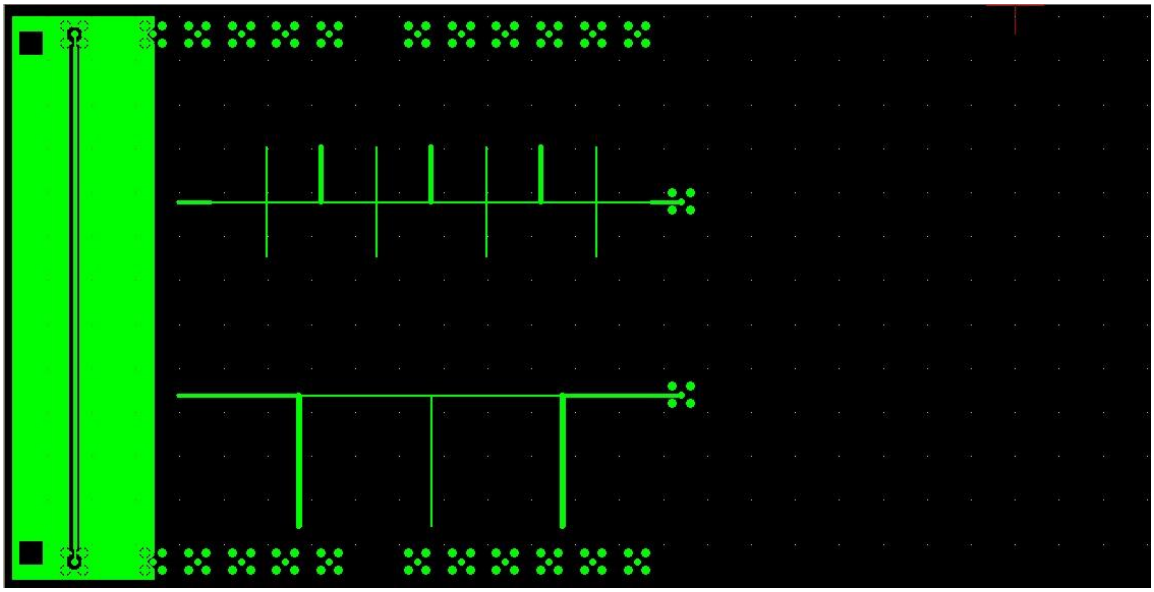

Figure 4.5c: Artwork of Bottom Layer (Layer 6):

a.) (On Left): Coplanar Waveguide: 111Ω
b.) Stub Filter #A (Lower Frequency Low Pass Filter): Bottom Filter in Figure
c.) Stub Filter #B (Higher Frequency Band Reject Filter): Top Filter in Figure

## Validation of Cascaded Transmission Line Models:

To model non-uniformities on transmission lines such as those shown in figures 4.4 and 4.5 for TDR, TDT, FDR and FDT systems, the line must be divided into smaller cascaded segments or finite elements. These models are described in detail in the forward prediction model chapter and in the appendices and only briefly reviewed again here before providing the validation results of those models later in this chapter. These cascaded segments or finite elements must be at a mesh scale to satisfy the assumptions of homogeneity at the individual element level while still allowing for heterogeneity or non-uniformity at the overall system or cascaded transmission line level. A successful measurement algorithm will then be able to individually de-convolve (time domain) or de-embed (frequency domain) various models for those internal elements based on external system boundary measurements to extract the relevant parameters and models for each individual internal element. The external system boundary measurements would be at the input of a cascaded transmission line for a TDR or FDR system and at both the input and output of a cascaded transmission line network for a TDT or FDT system.

A schematic representation of this type of cascaded transmission line partitioned into finite elements is shown in figure 4.6:

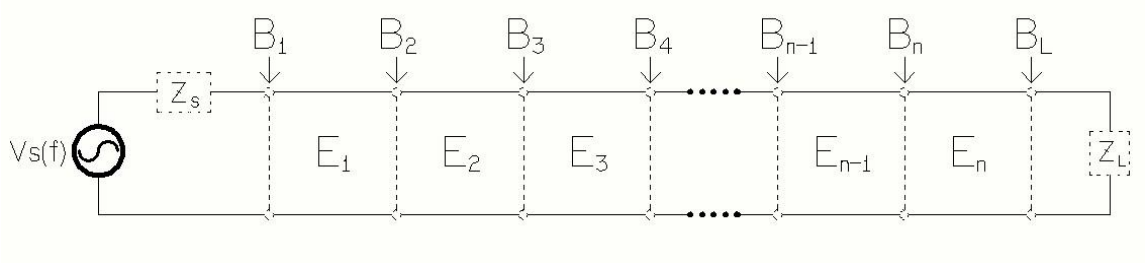


Figure 4.6: Finite Element Representation of a Cascaded Transmission Line

Where

$Vs(f)$ = Input AC Source (Broadband Multiple Frequency Source for TDR & TDT and Narrowband Higher Dynamic Range Single Frequency Source for FDR and FDT)

$Z_S$ = Source Impedance (Typically 50Ω for TDR/TDT/FDR/FDT Measurement Systems)

$Z_L$ = Load Impedance (Typically 50Ω for TDT/FDT and either 50Ω or Open Circuit Termination for TDR/FDR Systems)

$E_n$ = Element n (Homogeneous Electromagnetic Property Distributions across the Element)

$B_n$ = Boundary between Element "n" and Element "n-1"

Within the individual elements, models for the series Resistance per unit length (R), series Inductance per unit length (L), shunt Conductance per unit length (G) and shunt Capacitance per unit length (C) can then be developed for each element $E_n$. Such a model showing two sections or elements (n-1 and n) is shown in figure 4.7:

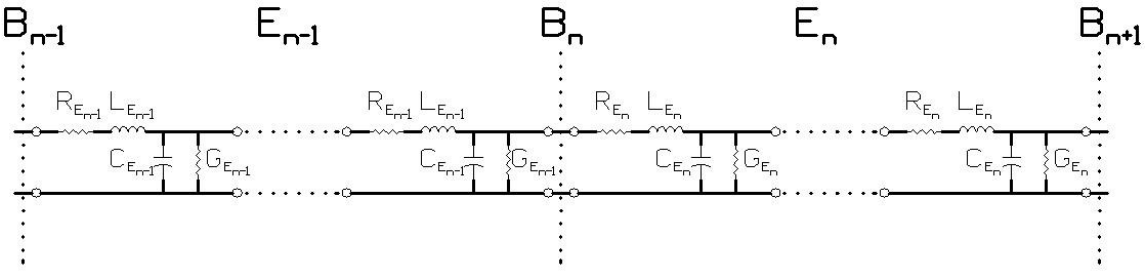


Figure 4.7: Distributed Transmission Line Model for Two Cascaded Sections

Identification of these models for each element in a non-uniform cascaded transmission line is the goal of the measurement interpretation algorithm. To accomplish this, models must also be developed for all the electromagnetic parameters for each finite element or cascaded subsection ($E_n$). This must be conducted at multiple levels within each element $E_n$ beginning with developing models for the base parameters ($\sigma_n$, $\varepsilon_n$', and $\varepsilon_n$") and then the transmission line distributed parameters ($R_n$, $L_n$, $G_n$, $C_n$) (figure 4.7) and finally the propagation and characteristic impedance expressions ($\gamma_n$, $Z_n$) all for each finite element $E_n$ and reflection coefficients ($\Gamma_n$) at each boundary $B_n$. This is illustrated further in figure 4.8:

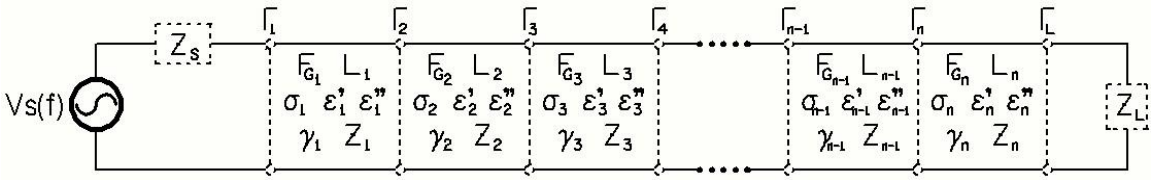


Figure 4.8: Cascaded Transmission Line Representation Showing Parameters of Each Element and Reflection Coefficients at each Boundary.

Where

$F_{Gn}$ = Probe Geometry Factor for Transmission Line Cascaded Element n.

$L_n$ = Length of Transmission Line Cascaded Element n.

$\sigma_n$ = Bulk Equivalent Electrical Conductivity of Cascaded Element n.

$\varepsilon_n$' = Bulk Equivalent Electric Permittivity Real (Storage) Term of Cascaded Element n.

$\varepsilon_n$" = Bulk Equivalent Electric Permittivity Imaginary (Loss) Term of Cascaded Element n.

$\gamma_n$ = Equivalent Propagation Constant for Transmission Line Cascaded Element n.

$Z_n$ = Equivalent Characteristic Impedance of Transmission Line Cascaded Element n.

$\Gamma_n$ = Reflection coefficient at the Boundary between Element n-1 and Element n.

Forward Prediction Models of these parameters in the specific context of Cascaded Transmission Lines were again developed and presented in the Forward Prediction Model Chapter as well as Appendix A and Appendix B.

These models can be further developed into cascaded network models involving Scattering (S) Parameters and Transmission (T) Parameters as described in Appendix B. There

are three alternative methods of determining the S parameters of such a complex cascaded network all of which are described in full detail in Appendix B but briefly reviewed here as well:

1.) Transmission (T) Parameter to Scattering (S) Parameter Conversions: Yields all Four S-Parameters: S11, S21, S12 & S22
2.) Mason's Non-Touching Loop Rule: Provides All Four S-Parameters: S11, S21, S12 & S22
3.) Nested Construction Method: Provides S11 & S22 Only

If properly implemented all these methods will lead to equivalent results (for the applicable parameters) and therefore can be utilized as a cross check on each other. Each has their advantages and disadvantages and all are therefore utilized in the forward prediction models in this research where they are most efficiently utilized. Each element and boundary in the cascaded transmission line models shown in figures 4.6 – 4.8 can be represented by either Scattering S-Parameters or Transmission T-Parameters. This is illustrated in figure 4.9 with full derivations for these parameters again found in Appendix B:

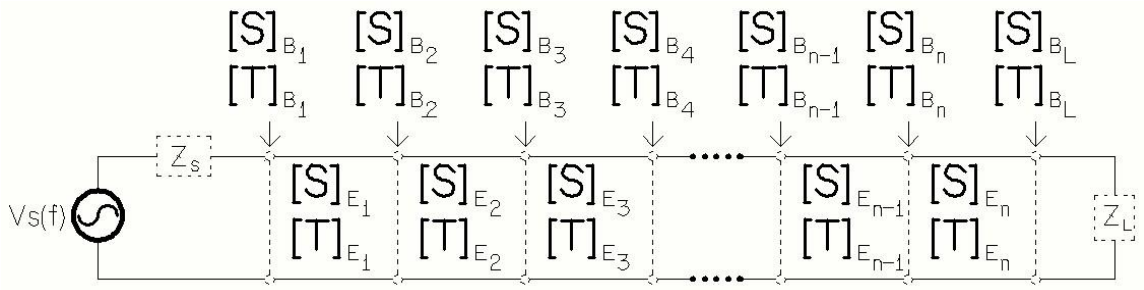


Figure 4.9: Cascaded Transmission Line Showing **S** and **T** Matrices for each boundary and element.

The goal of the inverse measurement algorithm is to solve for each of these sets of parameters for each boundary and element within the transmission line under test to assess information about the network. Measurements in either the time domain (TDR and TDT) and/or in the frequency domain (FDR and FDT) at the external boundaries (input and output) of a network under test across a broad frequency range provides the raw data of which a measurement algorithm must process and calculate the parameters of the internal elements and boundaries. Utilization of both the time domain and frequency domain as well as transmission and reflection information provides the greatest power to an algorithm for solving for these internal boundary and element parameters to fully characterize the system. This chapter will provide validation

results for those forward prediction models utilizing measured time domain (TDR and TDT) and frequency domain (FDR (S11 and S22) as well as FDT (S12 and S21)) information on the circuit board transmission line patterns shown in figures 4.4 and 4.5 and comparing them to the forward prediction model results for the same patterns. All three methods (T-Parameters, Mason's Non Touching Rule & Nested Construction) will be utilized as a cross check of each other on the results.

The author in companion research on the Inverse Algorithms is combining the above three techniques of Scattering (S) and/or Transmission (T) parameters in the classical Fourier Transform (Frequency Domain) realms together with the Wavelet transform [134 - 137] to assess information about the internal structure of the network containing non-uniform transmission lines with discontinuities in impedance as well as loss. That work will be presented in follow-on publications outside of this dissertation.

# Chapter 5: Results and Discussion

## Validation: Laboratory Methods #1:

The following sets of laboratory datasets were evaluated at the particular water content (WC) and electrical conductivity (EC) values:

Laboratory Setup #1: Column of 25 Rings per Figure 4.1
Soil Type: Sand: Unimin 40/50 Mixture: Porosity $\phi = 0.37$

Validation Datasets:

Open Air (Empty Rings with no Soil)
Dry Sand (WC = 0)
Saturated (WC = $\phi = 0.37$) Distilled Water: Low EC
Saturated (WC = $\phi = 0.37$) Moderately Saline Water (0.02M NaCl Solution): Medium EC
Saturated (WC = $\phi = 0.37$) Highly Saline Water (1M NaCl Solution): Higher EC
Drained ($0.03 < WC < 0.37$): Distilled Water: Low EC's
Drained ($0.03 < WC < 0.37$): Moderately Saline Water (0.02M NaCl Solution): Medium EC's
Drained ($0.02 < WC < 0.37$): Highly Saline Water (1M NaCl Solution): ($0.01 < EC < 1.9$S/m)

Measured Signals: Time Domain (Tektronix 11801D Oscilloscope): TDR: Open Circuit Termination

Multiple Time Resolutions & Time Windows (Various Record Lengths & Zooms):

Calculated Signals: Frequency Domain (via FFT): FDR (S11)

Forward Prediction Models/Simulated Signals: Time Domain (TDR) and Frequency Domain (FDR (S11))

Processed results for each actual data test case are given as follows:

Time Domain Plots of Waveforms (1-D Time Domain Plot)
Classical Fourier Transform: 1-D FFT Frequency Domain Plot

## Lab Data: Validation Method #1:

For Laboratory Validation Method #1, the laboratory experiments consisted of a vertical column of soil (Unimin sand 40/50 mix) that was segmented into 25 rings as shown earlier in figure 4.1. Each ring had its own short medium - high bandwidth TDR probe (2-wire probe driven by a 50-ohm coaxial cable via an SMA (3.5mm) connector). There were eight different test cases in the laboratory experiments:

1.) Open Air in the column.

2.) Column filled with dry sand.

3.) Column filled with sand saturated with distilled water.

4.) Column after having been allowed to drain partially resulting in a varying Water Content profile vs. height in the column (near saturation at bottom to near dry at the top).

5.) Column filled with sand saturated with saline water (1 Molar NaCl solution).

6.) Column with solution in number 5 after having been allowed to drain partially to achieve varying Water Content and Electrical Conductivity Profile vs. height in the column..

7.) Column filled with sand saturated with saline water (0.02 Molar NaCl solution).

8.) Column with solution in number 7 after having been allowed to drain partially to achieve varying Water Content and Electrical Conductivity profiles vs. height in the column.

A representative subset of results from the TDR measurements at different rings from experimental cases 1 to 6 will be summarized in this dissertation for laboratory validation method #1. This provides a good cross section of cases in terms of different water content and electrical conductivity values. For cases 1 to 4 the rings were numbered 1 - 25 starting from the bottom

ring. For cases 5 - 8 ring 3 was at the bottom and then rings 4 - 25 followed moving upward and then ring 1 was next to the top and ring 2 was on top.

The rings analyzed for each case are listed below:

Cases 1 - 3: Ring 1

Case 4: Rings 1, 6, 8, 10, 11, 12, 17, 25

Case 5: Ring 3

Case 6: Rings 3, 11, 12, 13, 14, 15, 16, 20, 2

The rings had the following inside dimensions for all 8 cases:

| | | | |
|---|---|---|---|
| Rings 1 - 5, 21 - 25: | 7.62 cm inside diameter | x | 2 cm height |
| Rings 6 - 20: | 7.62 cm inside diameter | x | 1 cm height |

For the mix of sand used the air filled porosity was theoretically determined to be .3446 but was experimentally determined to actually be .37 (probably due to an imperfect packing of the sand).

Table 5.1 lists the results of the lab experiments for validation method #1 and provides comparisons with the simulation models using two of the specified simulation models as a subset of the several forward prediction models presented in this dissertation. The two chosen models were the Parallel Model and the Weighted Rectangular Mean Model the latter of which interpolates between the two Theoretical limits of the Parallel and Serial Models as presented in the Forward Prediction Model chapter. These were arrived at out of the larger list of available models via testing showing the best fit as quantified by the Goodness of Fit parameter (Coefficient of Fit Method #A or $R^2$) and given as follows:

**Table 5.1. Laboratory Testing Results: Validation Laboratory Method #1: Column of Rings: All Cases Open Termination at End of Probe**

| Case # | Ring # | Air-Filled Porosity | Actual Water Content | Algor. Water Content | Actual Elec. Cond. | Algor. Elec. Cond. | Simulation. Model | Series Coef. | Par. Coef. | Coef. of Fit Method B | Coef of Fit: Method A $R^2$ |
|---|---|---|---|---|---|---|---|---|---|---|---|
| 1 | 1 | 1.00 | 0 | 0 | 0 | 0 | Parallel | 0 | 1 | 1.017 | 0.907 |
| 2 | 1 | 0.37 | 0 | 0 | 0 | 0 | Parallel | 0 | 1 | 1.062 | 0.936 |
| 3 | 1 | 0.37 | .37 | .37 | 0 | 0 | Parallel | 0 | 1 | 0.956 | 0.982 |
| 4 | 1 | 0.37 | .37 | .37 | 0 | 0 | Parallel | 0 | 1 | 0.949 | 0.985 |
| 4 | 6 | 0.37 | .29 | .29 | 0 | 0 | Rectangular Mean | 4 | 1 | 0.956 | 0.977 |
| 4 | 8 | 0.37 | .24 | .24 | 0 | 0 | Rectangular Mean | 5 | 1 | 0.967 | 0.979 |
| 4 | 10 | 0.37 | .18 | .18 | 0 | 0 | Rectangular Mean | 4 | 1 | 0.963 | 0.981 |
| 4 | 11 | 0.37 | .13 | .13 | 0 | 0 | Rectangular Mean | 2.4 | 1 | 0.962 | 0.981 |
| 4 | 12 | 0.37 | .096 | .10 | 0 | 0 | Rectangular Mean | 1.8 | 1 | 0.959 | 0.973 |
| 4 | 17 | 0.37 | .053 | .05 | 0 | 0 | Rectangular Mean | 0.25 | 1 | 0.950 | 0.973 |
| 4 | 25 | 0.37 | .033 | .03 | 0 | 0 | Rectangular Mean | 0.1 | 1 | 1.052 | 0.977 |
| 6 | 3 | 0.37 | .33 | .33 | 1.735 | 1.73 | Parallel | 0 | 1 | 0.830 | 0.980 |
| 6 | 3 | 0.37 | .33 | .33 | 1.735 | 2.227 | Rectangular Mean | 0.33 | 1 | 1.089 | 0.952 |
| 6 | 11 | 0.37 | .31 | .31 | 0.891 | 1.137 | Rectangular Mean | 3 | 1 | 0.750 | 0.957 |
| 6 | 12 | 0.37 | .28 | .28 | 0.461 | 0.589 | Rectangular Mean | 4 | 1 | 0.930 | 0.985 |
| 6 | 13 | 0.37 | .25 | .25 | 0.409 | 0.420 | Rectangular Mean | 5 | 1 | 0.775 | 0.932 |
| 6 | 14 | 0.37 | .18 | .18 | 0.225 | 0.246 | Rectangular Mean | 3 | 1 | 1.147 | 0.882 |
| 6 | 15 | 0.37 | .14 | .14 | 0.157 | 0.169 | Rectangular Mean | 2.8 | 1 | 0.860 | 0.884 |
| 6 | 17 | 0.37 | .10 | .10 | 0.097 | 0.105 | Rectangular Mean | 2.2 | 1 | 0.712 | 0.938 |
| 6 | 20 | 0.37 | .063 | .06 | 0.049 | 0.054 | Rectangular Mean | 1 | 1 | 0.825 | 0.966 |
| 6 | 2 | 0.37 | .014 | .01 | 0.016 | 0.017 | Parallel | 0 | 1 | 0..936 | 0.977 |

It was found from the data as well as determined theoretically (as described in depth in the Forward Prediction Model Chapter) that the electromagnetic parameters influencing wave phase velocity and impedance behave as though the medium is made up of a mix of two opposite theoretically based extreme types of composite sub-structures as follows:

1.) Series Model: Where the 3 phases of water, air and solids behave as though they are in series between the two guiding conductors of a transmission line.

2.) Parallel Model: Where the 3 phases of water, air and solids behave as though they are in parallel between the two guiding conductors of a transmission line.

In this project several different interpolation models were therefore explored and developed to model values of propagation factors and impedance between the theoretical boundaries (see Forward Prediction Model Chapter). It was found that the weighted rectangular mean interpolation model reliably had the best fit and in some cases (typically at very wet and very dry conditions) the parallel model was actually the best fit. Therefore, the results of those two models are included in table 5.1 and in other sections of this validation chapter. However, all of the interpolation models behaved in a similar fashion with similar trends. Each model required weighting constants to bias towards the series or parallel model based on experimental results. The results from table 5.1 (validation method #1) and confirmed in the additional validation methods of this chapter showed that the parallel model represented a good fit at very low water contents (including dry soil and open air) as well as at very high water contents. At intermediate water contents interpolation between the parallel and series models was the best fit as shown by the interpolation coefficients of the weighted rectangular mean model in table 5.1.

Actual plots of both time domain and frequency domain comparisons between actual data and the model simulation runs (forward prediction models) are compiled in appendix D with a few representative plots given in this chapter further below. Plots of TDR waveforms in the time domain and S11 in the frequency domain are included in Appendix D for each of the test cases in Table 5.1 comparing actual data to predictions from the forward prediction models. Plots of Group Delay and Effective Port Impedance are also included in this chapter to illustrate key points of the proposed inverse algorithms.

The actual values of electrical conductivity in Table 5.1 were determined by using an HP4194 impedance analyzer to give a low frequency impedance vs. frequency plot with the same short TDR transmission line probe used as the electrodes for the conductivity measurement. The HP4194 analyzer had built in features to extract the resistance components from the capacitance and then geometry calibration factors were used to determine electrical conductivity from the HP4194 measured resistance values. The frequency range of this measurement was from 100Hz to 40 MHz and the resistance value was chosen in a flat portion of the curve generally around 10 kHz. The TDR inverse model algorithm used the low frequency information of S11(acquired via an FFT on the measured 11801D TDR traces) to determine the conductivity and there was good tracking with the independent measurement of conductivity (HP4194 values) but there was a consistent error or bias on the high side due likely to a geometry calibration error on the thin wire electrodes. The long time information (after TDR traces settles out) and the low frequency S11 information were found to be very accurately modeled by the prediction algorithm and are key to the accurate determination of bulk electrical conductivity. Therefore the algorithm shows great promise and feasibility in determining electrical conductivity.

The actual values of water content were determined for each ring in laboratory validation method 1 (including all of those in Table 5.1) via gravimetric analysis. In terms of determining water content with the TDR algorithm (as an inverse algorithm using the forward prediction models), different procedures were used depending on the level of electrical conductivity. As part of the proposed and preliminary tested inverse model/algorithm, for low levels of electrical conductivity, plots of dominant effective group delay of S11 (derivative of phase with respect to frequency as given in (B-35) in Appendix B) were generated (figures 5.1 – 5.10) and the frequencies where peaks occurred were used in conjunction with a lookup table to determine water content. For higher levels of conductivity, plots of transmission line effective input impedance were generated per equation (B-38) in Appendix B (figures 5.11 – 5.19) and the low frequency information was utilized to extract EC per (B-37) in Appendix B. In addition, the medium to higher frequency information of S11 and effective impedance can be used in conjunction with a lookup table to determine water content (where there is sufficient dynamic range – preferably with a direct frequency domain S11 measurement as opposed to an FFT on a TDR waveform). The slope of the impedance vs. frequency (low to medium frequency transition) as well as the level at peaks (medium to high frequency) can both be used to extract

information that is dominantly dependent on the electric permittivity and therefore the water content (again where there is sufficient dynamic range such as with direct Frequency Domain measurements). However, it was also found that using TDR alone (reflection measurement alone) is potentially inconclusive in determining bulk water content down the probe length due to significant attenuation of the returning signal. Therefore, TDR by itself using the input impedance method appears to only be effective for extracting water content information near the input of the probe (i.e. near the surface of the soil) when EC is very high. However, as will be shown in laboratory validation method #2 when combining with a transmission measurement (Time Domain Transmission (TDT) or Frequency Domain Transmission (FDT or S21) especially if obtained via higher dymanic range direct frequency domain measurements, the ability to identify water content along the length of the probe under conditions of higher EC becomes much more feasible.

Agreement between the prediction algorithm and actual data was generally very good as shown in the $R^2$ values in Table 5.1 but it was found that the model series/parallel weighting factors had to be adjusted to give a slight bias towards the series model in intermediate water contents and a strong bias towards the parallel model at both extremes of water content (very wet and very dry). At wetter water contents there was a high frequency limit to the group delay plots due to loss of the reflected signal from the end of the probe (second reflection) due to the dielectric losses of water. As conductivity rises there also arises a low frequency limit to the group delay plots as well and so above a certain level of conductivity the group delay approach can no longer be used to determine water content (essentially because the reflected signal at the end of the probe (2nd reflection) is attenuated below detectable levels). For low levels of conductivity it was concluded that it is technically feasible for the algorithm to accurately determine water content via the lookup tables based on the locations of group delay peaks in S11 vs. frequency (as shown in figures 5.1 – 5.19).

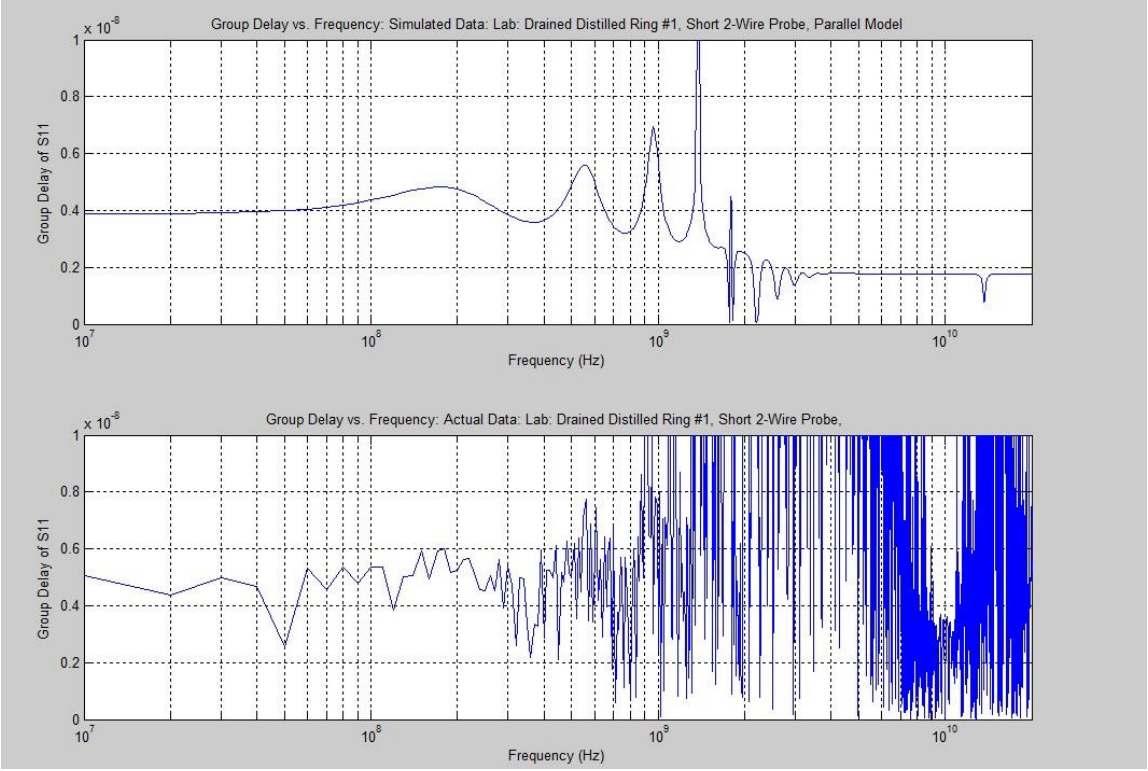


Figure 5.1: Laboratory Validation Set #1: Group Delay vs. Frequency: WC = 0.37, EC ~= 0

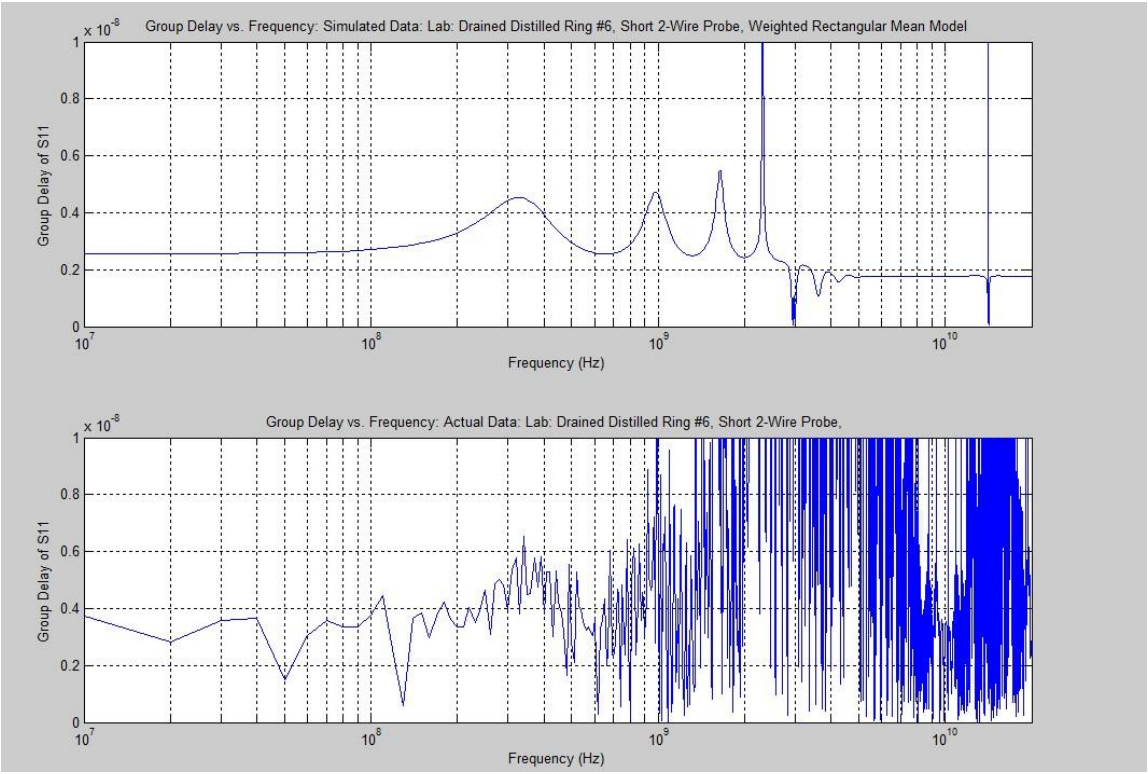


Figure 5.2: Laboratory Validation Set #1: Group Delay vs. Frequency: WC = 0.29, EC ~= 0

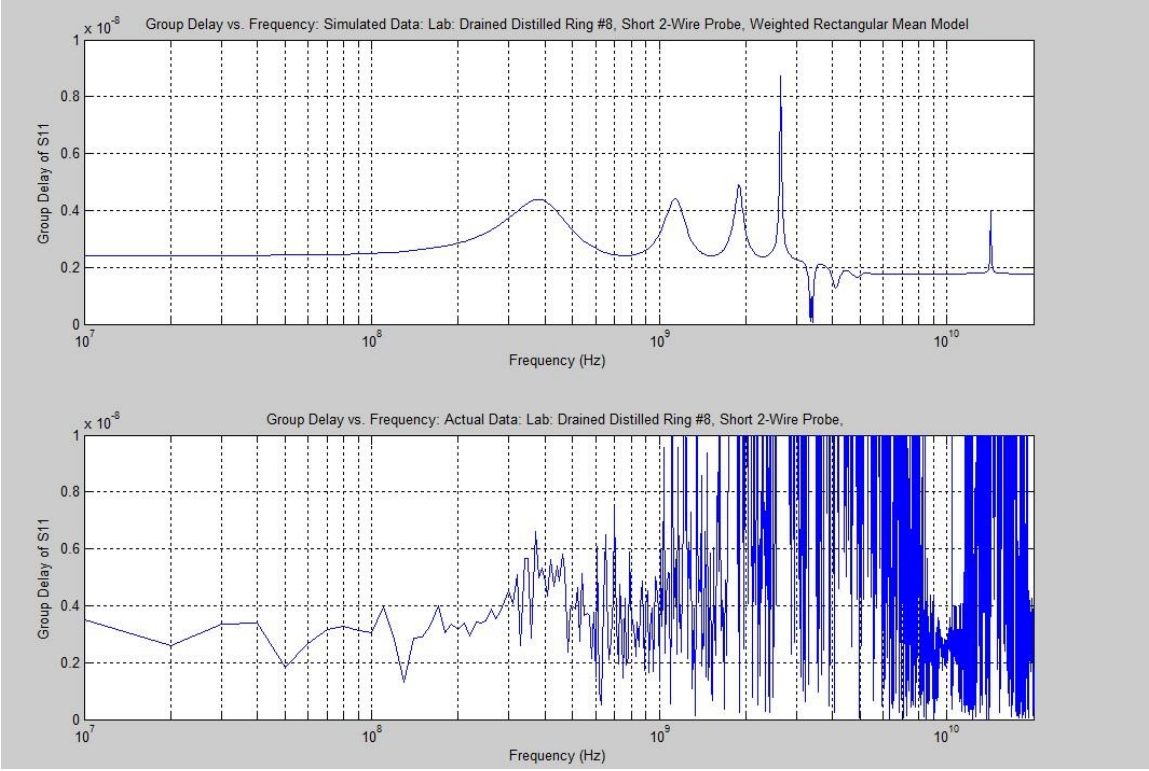


Figure 5.3: Laboratory Validation Set #1: Group Delay vs. Frequency: WC = 0.24, EC ~= 0

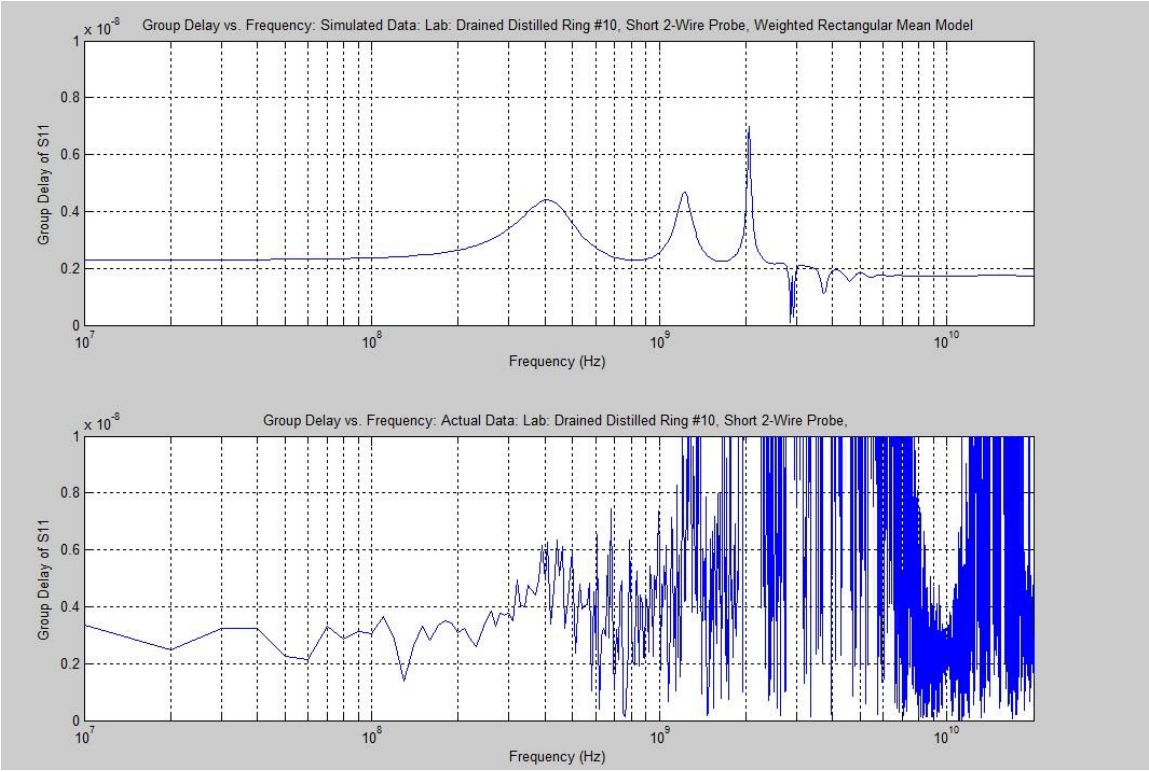


Figure 5.4: Laboratory Validation Set #1: Group Delay vs. Frequency: WC = 0.18, EC ~= 0

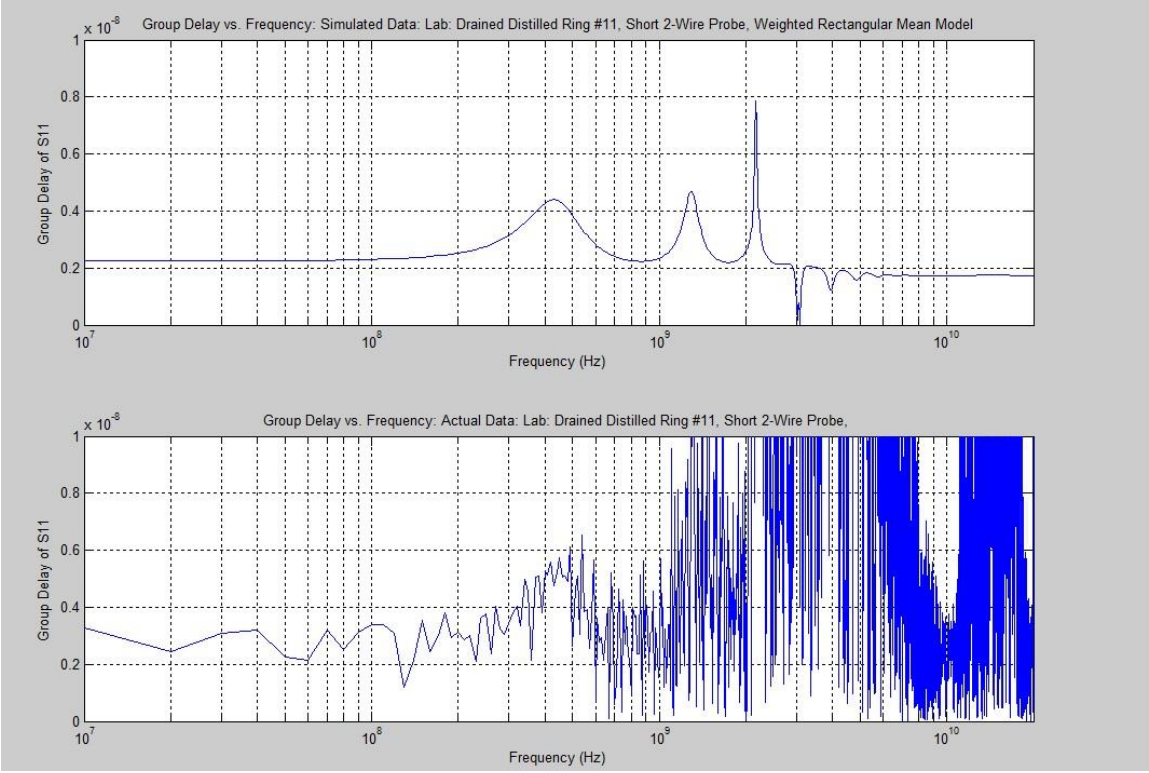


Figure 5.5: Laboratory Validation Set #1: Group Delay vs. Frequency: WC = 0.13, EC ~= 0

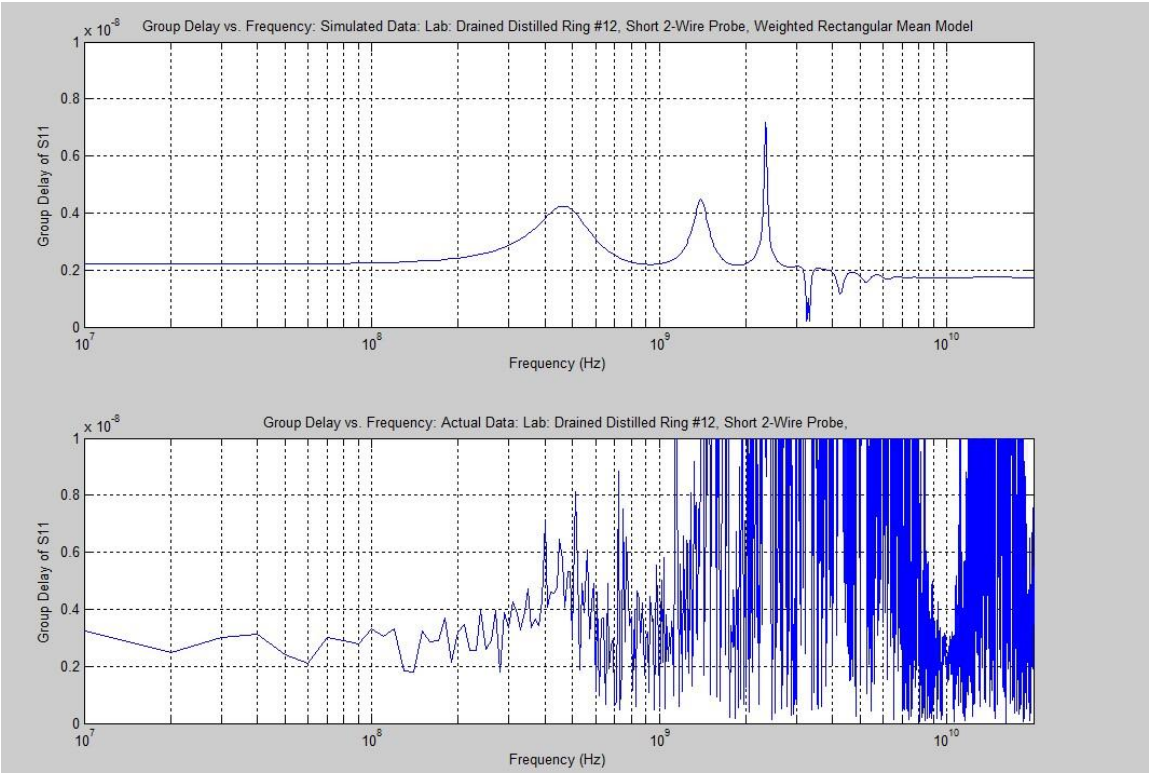


Figure 5.6: Laboratory Validation Set #1: Group Delay vs. Frequency: WC = 0.10, EC ~= 0

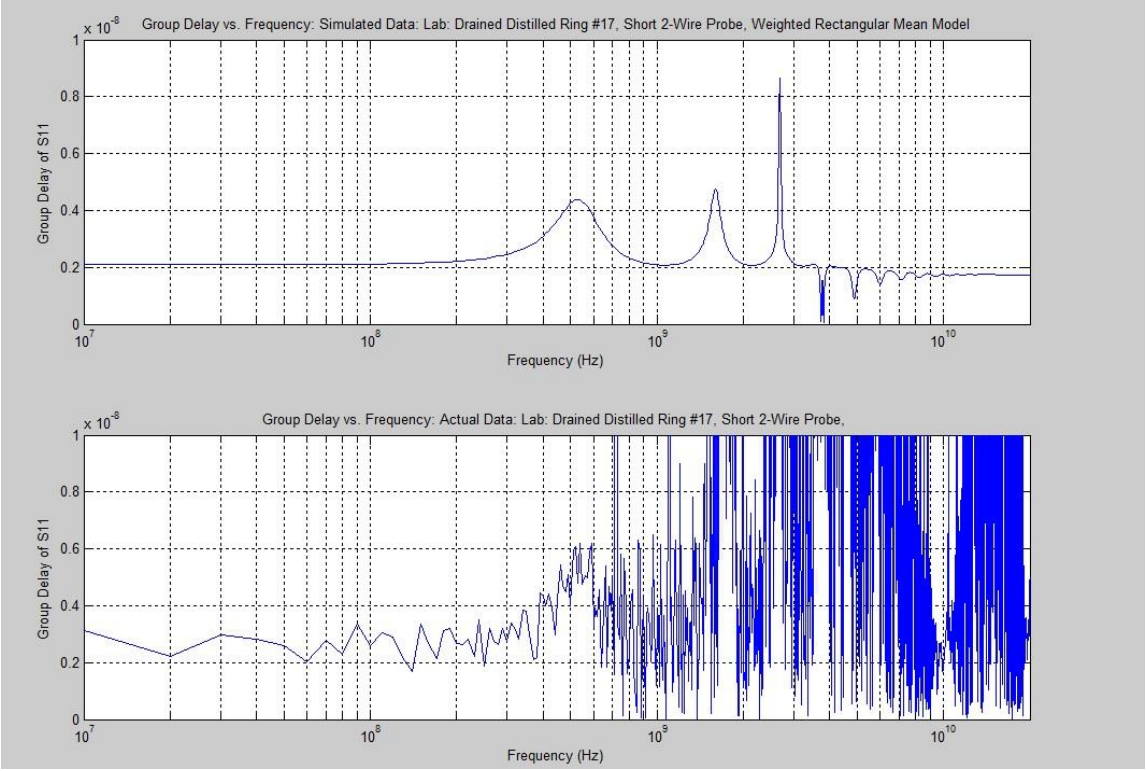


Figure 5.7: Laboratory Validation Set #1: Group Delay vs. Frequency: WC = 0.05, EC ~= 0

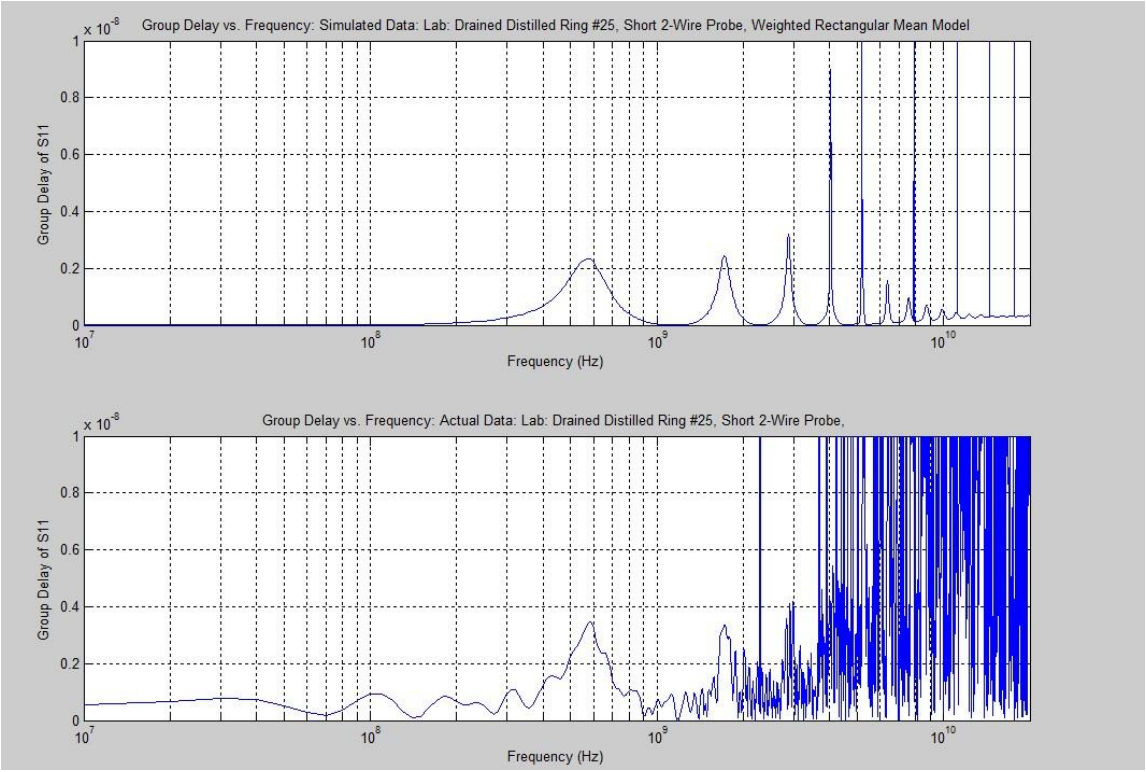


Figure 5.8: Laboratory Validation Set #1: Group Delay vs. Frequency: WC = 0.03, EC ~= 0

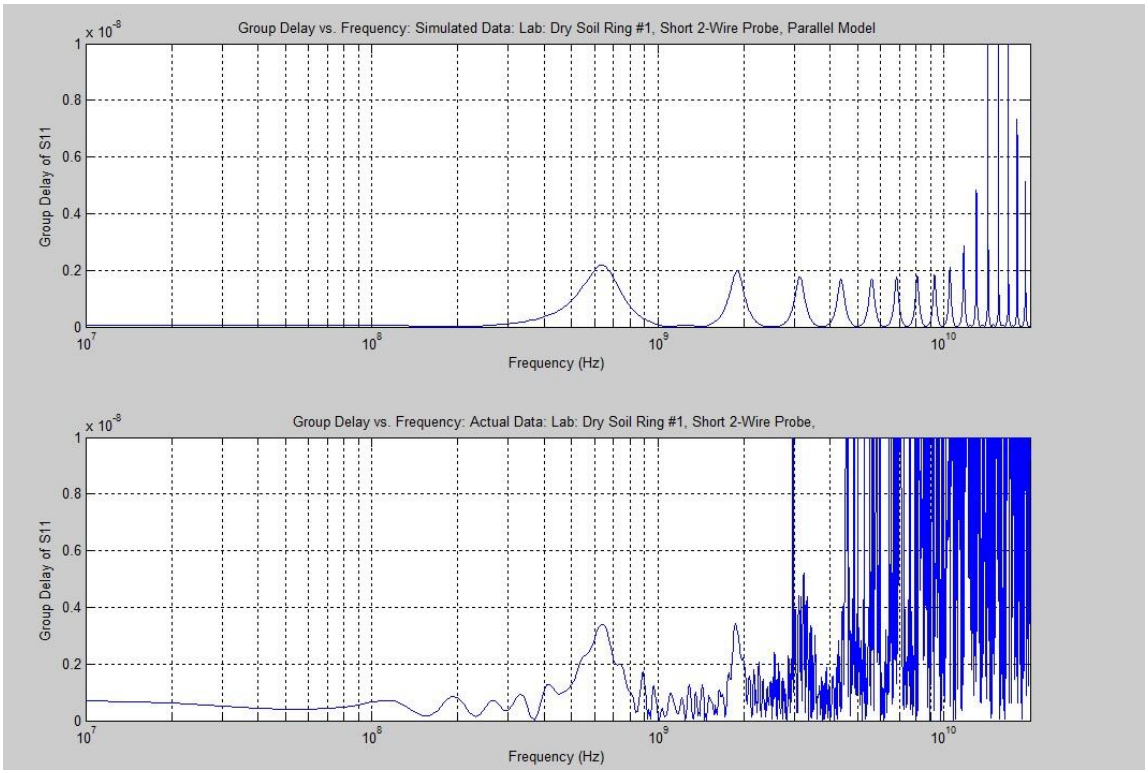


Figure 5.9: Laboratory Validation Set #1: Group Delay vs. Frequency: WC = 0 (Dry Soil), EC ~= 0

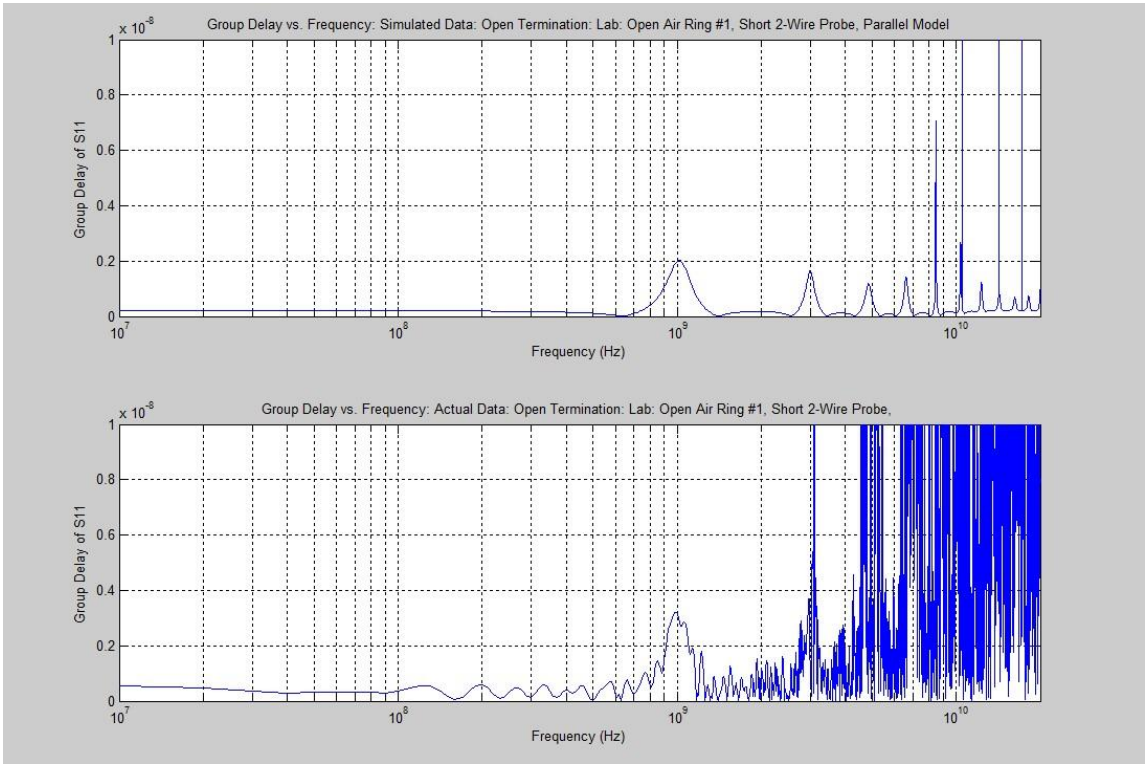


Figure 5.10: Laboratory Validation Set #1: Group Delay vs. Frequency: Open Air (Empty Fixture)

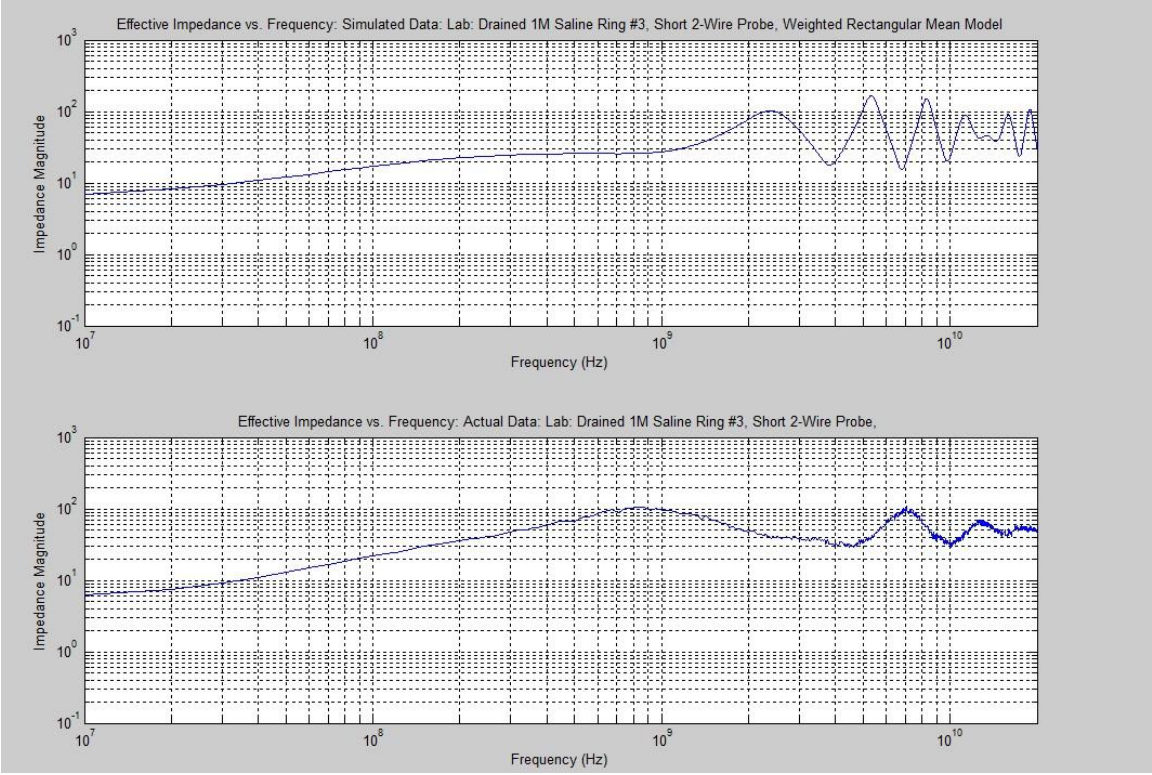


Figure 5.11: Laboratory Validation Set #1: Impedance vs. Frequency: WC = 0.33, EC ~= 1.74 S/m

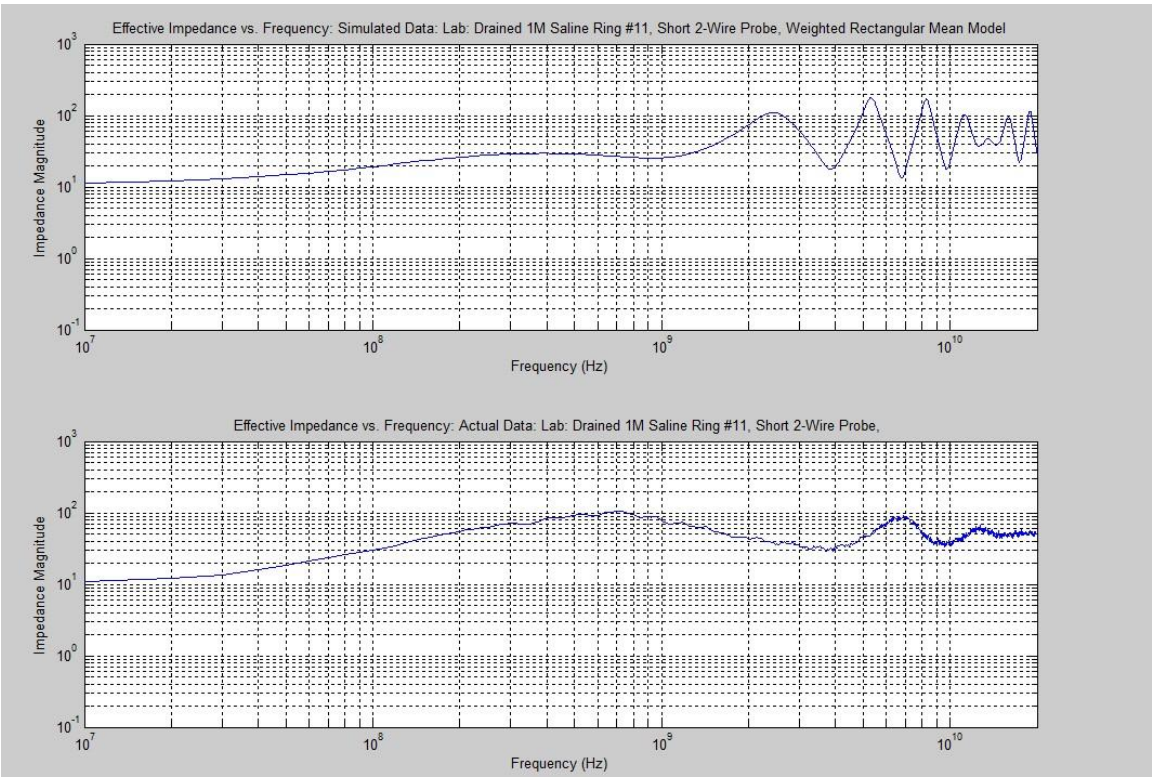


Figure 5.12: Laboratory Validation Set #1: Impedance vs. Frequency: WC = 0.31, EC ~= 0.89 S/m

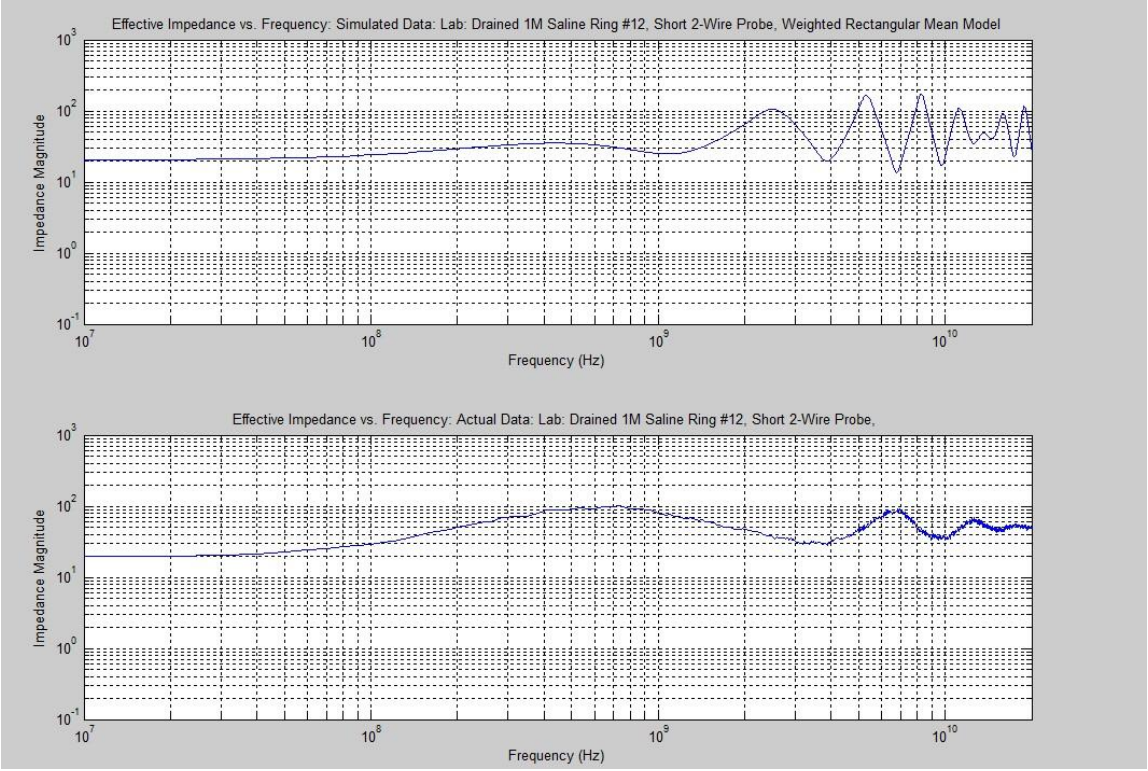


Figure 5.13: Laboratory Validation Set #1: Impedance vs. Frequency: WC = 0.28, EC ~= 0.46 S/m

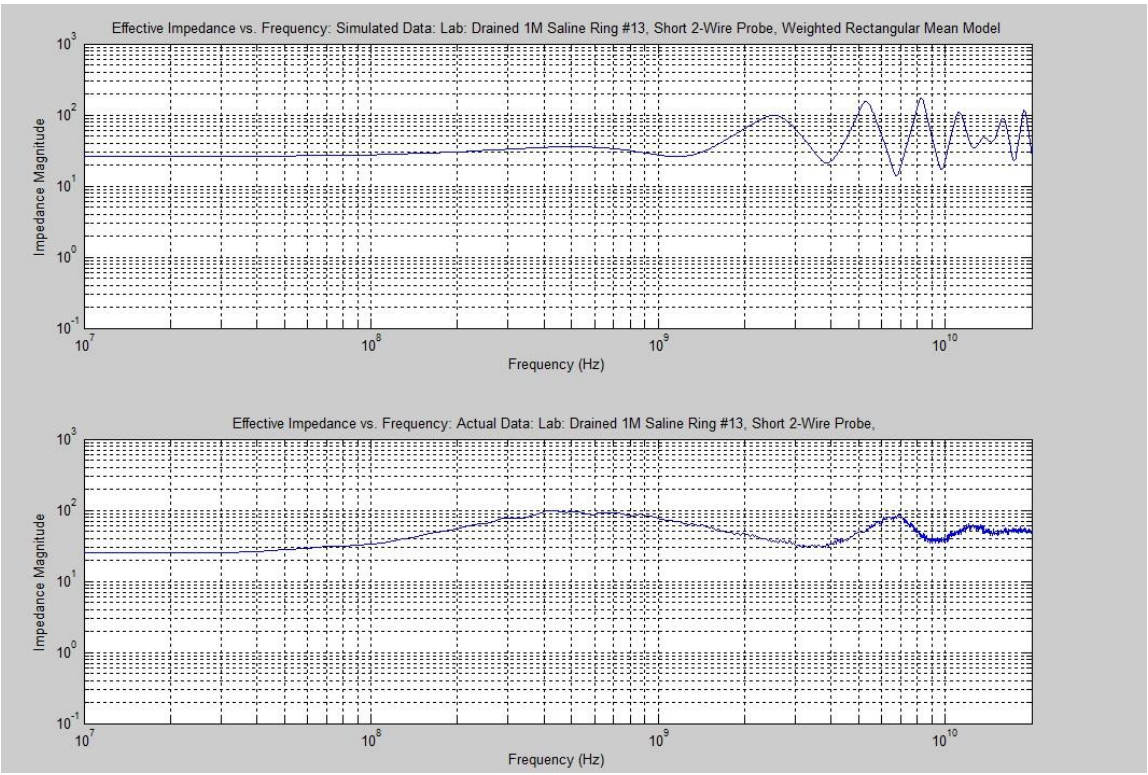


Figure 5.14: Laboratory Validation Set #1: Impedance vs. Frequency: WC = 0.25, EC ~= 0.41 S/m

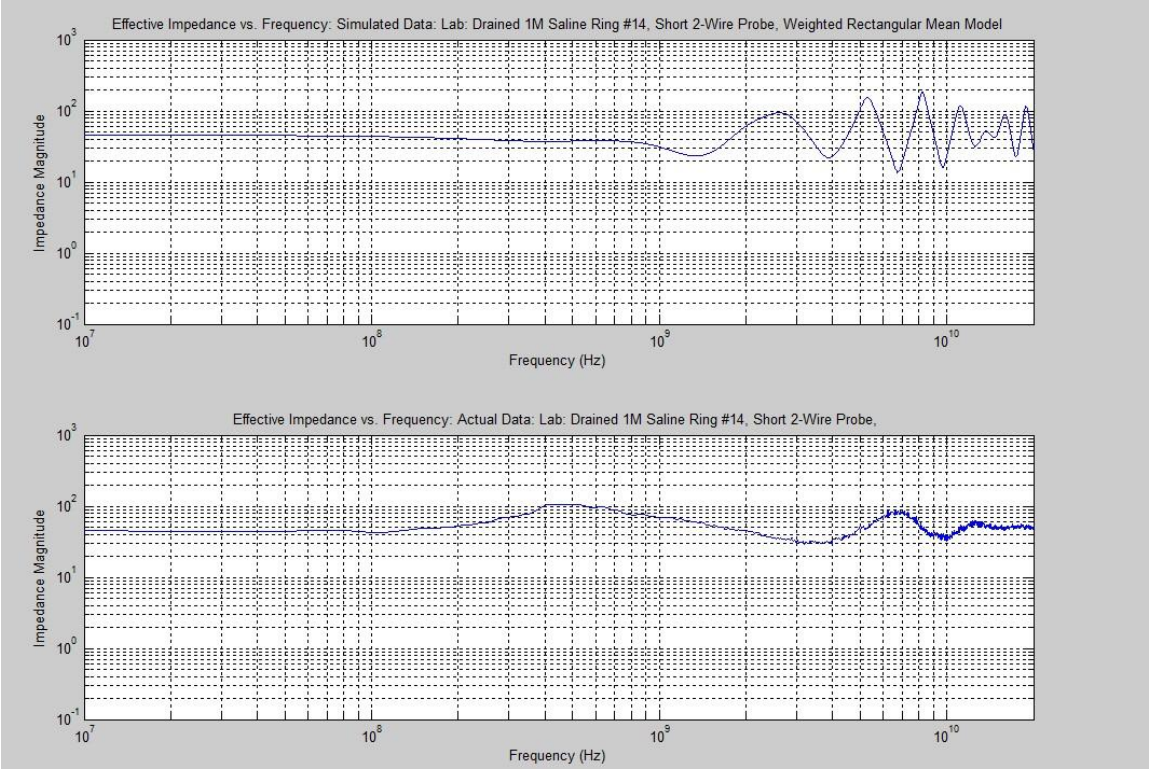


Figure 5.15: Laboratory Validation Set #1: Impedance vs. Frequency: WC = 0.18, EC ~= 0.23 S/m

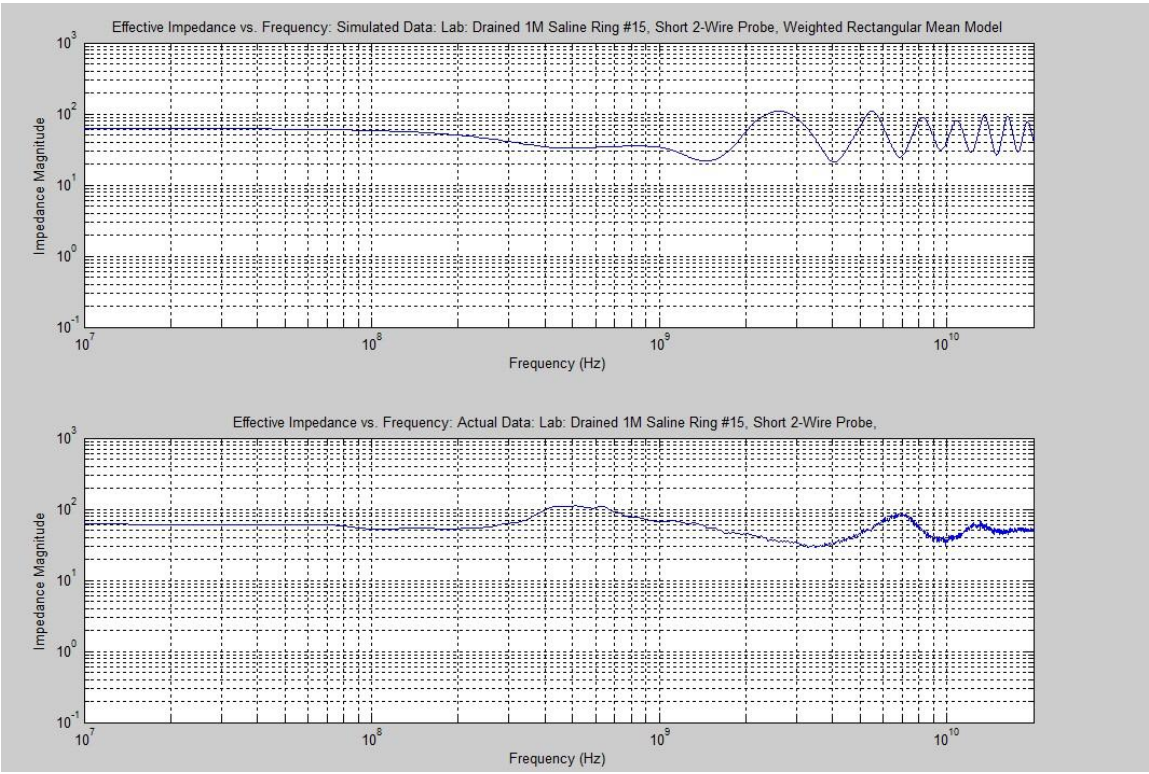


Figure 5.16: Laboratory Validation Set #1: Impedance vs. Frequency: WC = 0.14, EC ~= 0.16 S/m

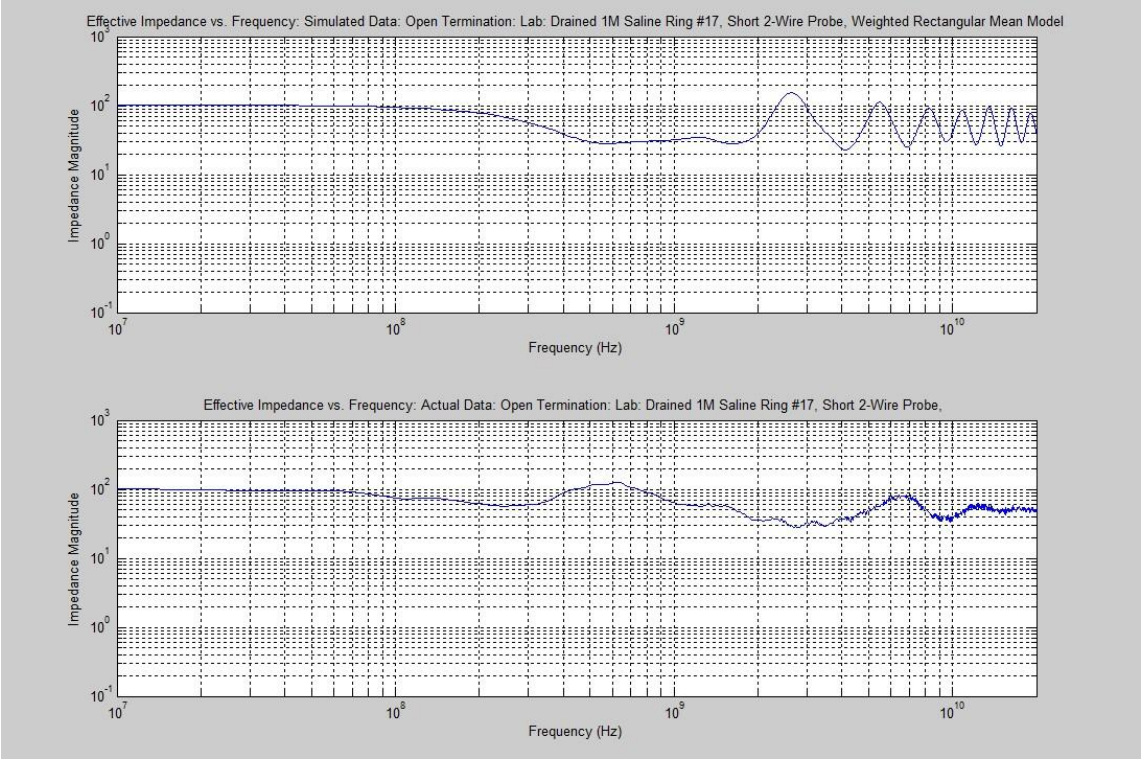


Figure 5.17: Laboratory Validation Set #1: Impedance vs. Frequency: WC = 0.10, EC ~= 0.10 S/m

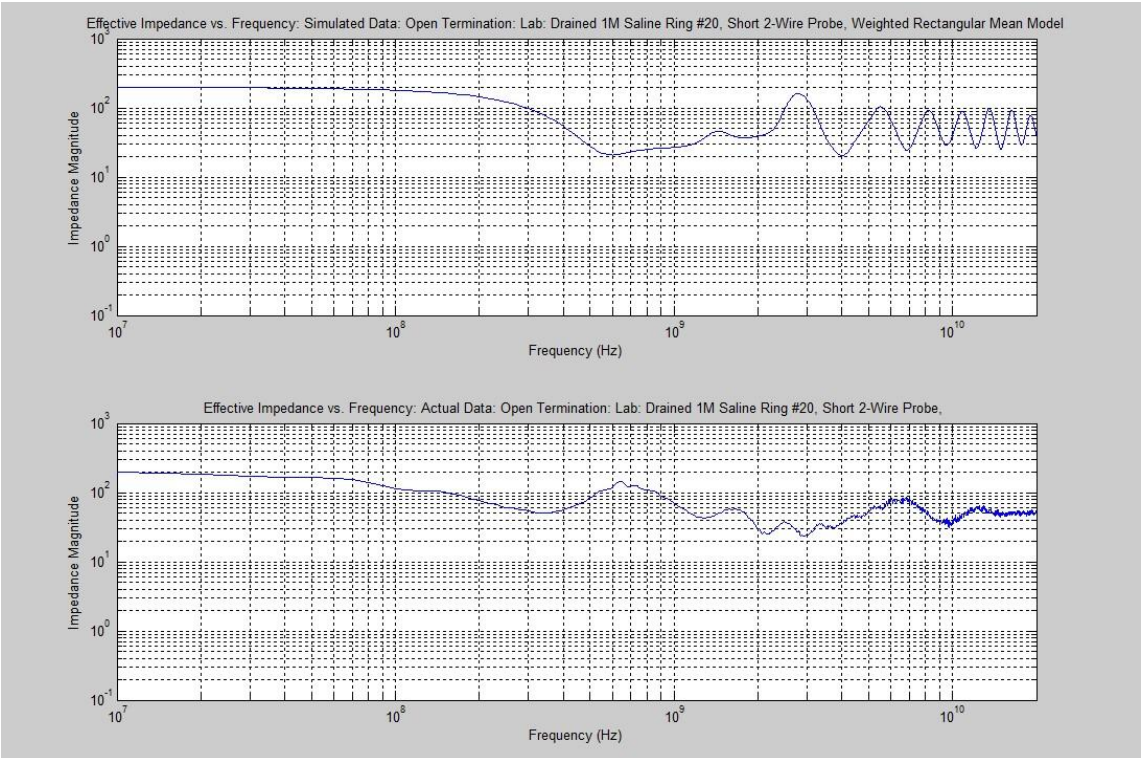


Figure 5.18: Laboratory Validation Set #1: Impedance vs. Frequency: WC = 0.06, EC ~= 0.05 S/m

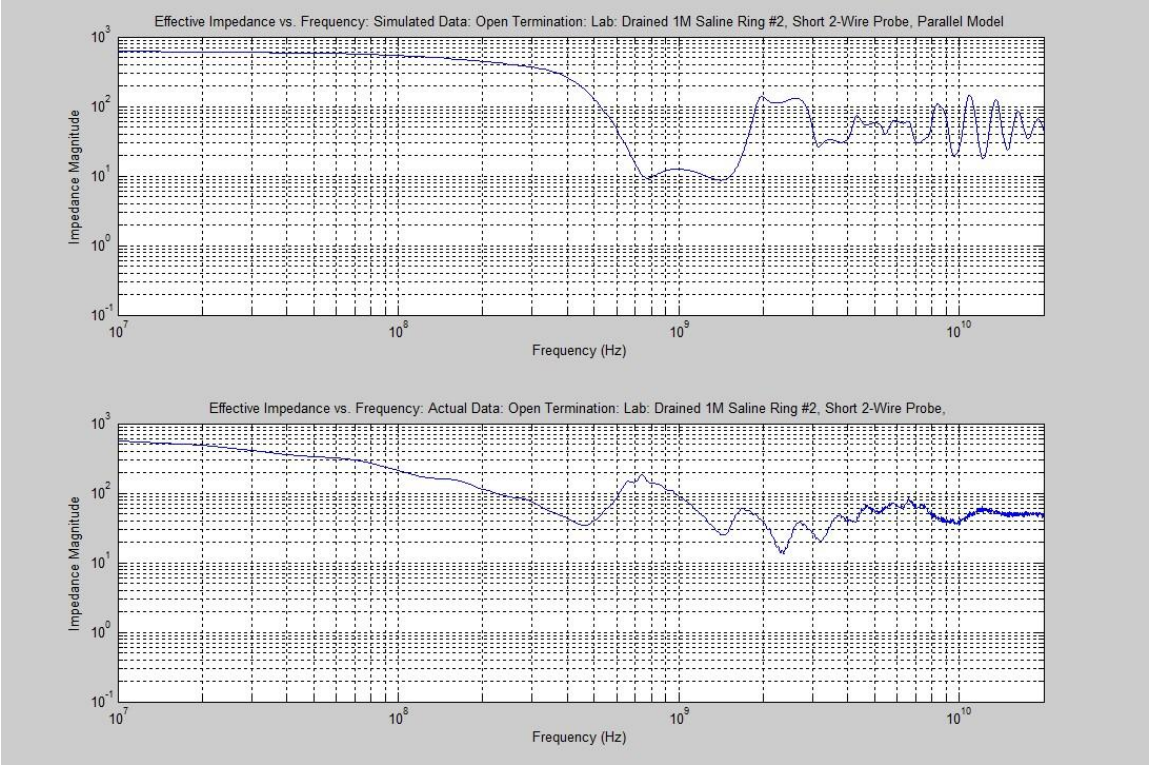


Figure 5.19: Laboratory Validation Set #1: Impedance vs. Frequency: WC = 0.01, EC ~= 0.02 S/m

It was also found that there were other medium to higher frequency losses associated with cables (some attenuation between the test fixture and the 11801D scope) as well as the two wire TDR probe (likely radiation at drier or lower water contents and at abrupt probe transitions-especially at the input where there is harsh transition between a coaxial connector and a two wire probe leading to higher order propagation modes for a short distance) that were not completely modeled by the algorithm. This led to modest errors in the level of S11 between the first and second reflections as well as the rise times (time domain) and at medium to high frequencies (frequency domain). These errors effected the level of the signal more than the phase or delay and so for low water contents the algorithm still accurately determined water content (dependent on timing or group delay) but at high values of electrical conductivity there was a modest amount of increased error as the level of S11 is more critical (determination of impedance) to measuring water content. Sensitivity to changes in water content in the impedance values was still very good though and the principal investigator believes that if a better hardware package can be developed to minimize coaxial cable losses (by eliminating the cable) and improve the bandwidth of the TDR probe (short multiconductor probe that emulates a coaxial pattern that constrains the wave to TEM modes up to at least 10 GHz and requires the least amount of interface hardware (connectors/baluns) with the shortest electrical length possible, then this portion of the algorithm can be made to be feasible in a TDR/TDT measurement system to extract water content when electrical conductivity is high. **For a TDR only measurement the key to extracting water content when the electrical conductivity is high is to use the S11 first reflection information at high enough frequencies to be able to extract the permittivity from the impedance from which water content can be determined via a lookup table based on the prediction models. However, as will be shown in the section covering Validation method #2, combining TDR with TDT along with high dynamic range narrowband FDR and FDT measurements provide the greatest power in extracting WC when EC is high.** The following figures show several additional aspects of the findings from Validation laboratory method #1 and how they behave relative to the theoretical limits of the Parallel and Series Models.

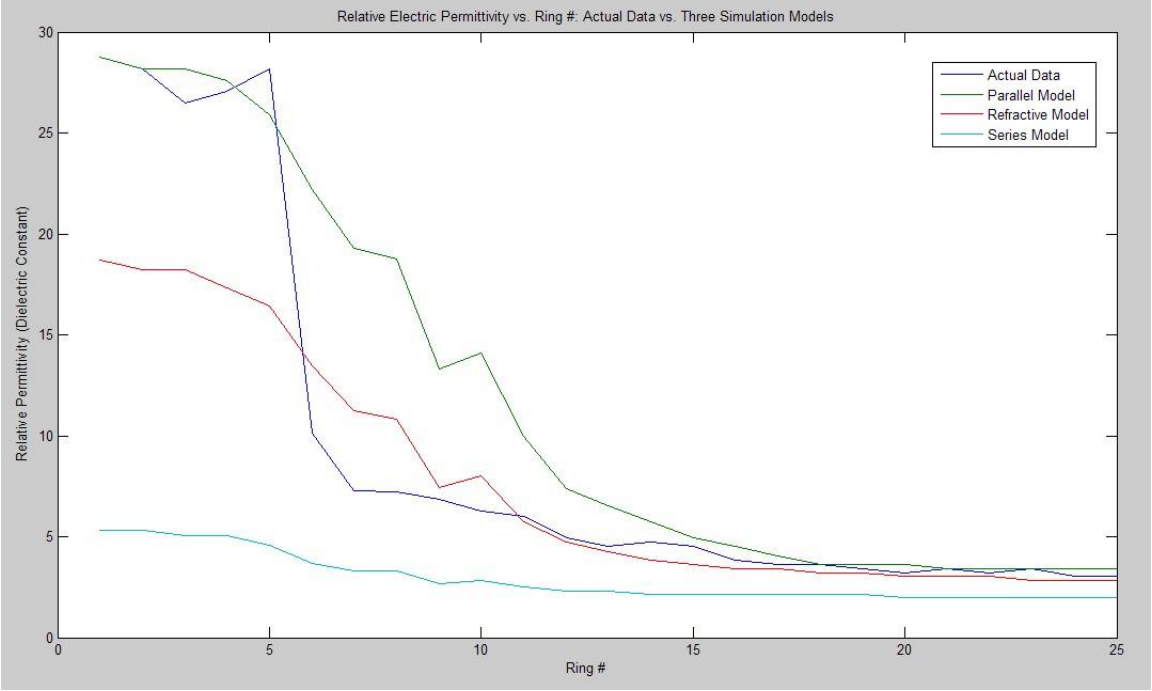


Figure 5.20: Equivalent Relative Electric Permittivity vs. Ring Number (Actual Data: Table 5.1: Case #4)

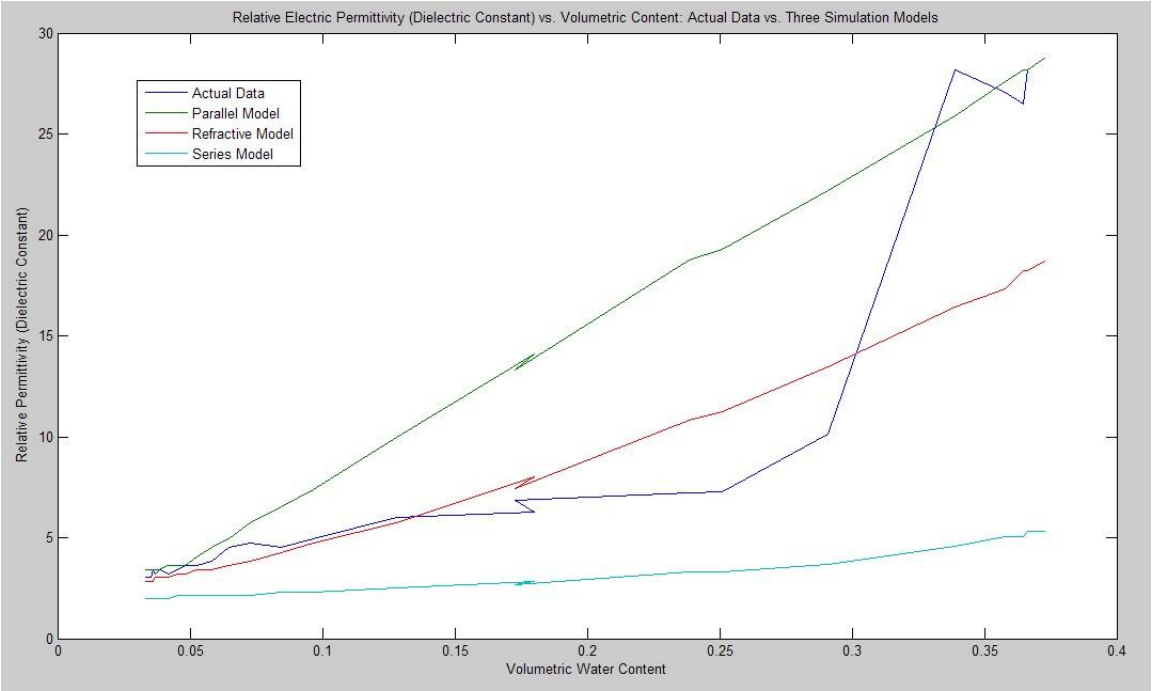


Figure 5.21: Equivalent Relative Electric Permittivity vs. WC (Actual Data: Table 5.1: Case #4)

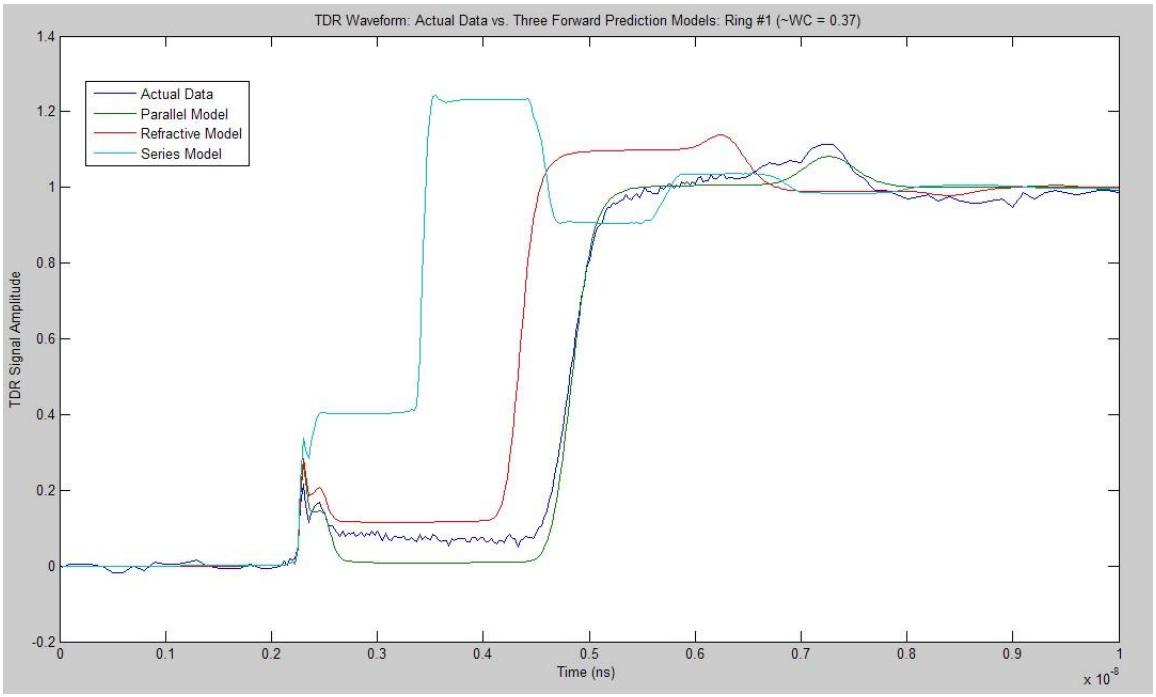


Figure 5.22: TDR Waveform relative to Different Model Types: WC = 0.37 (Table 5.1: Case #4)

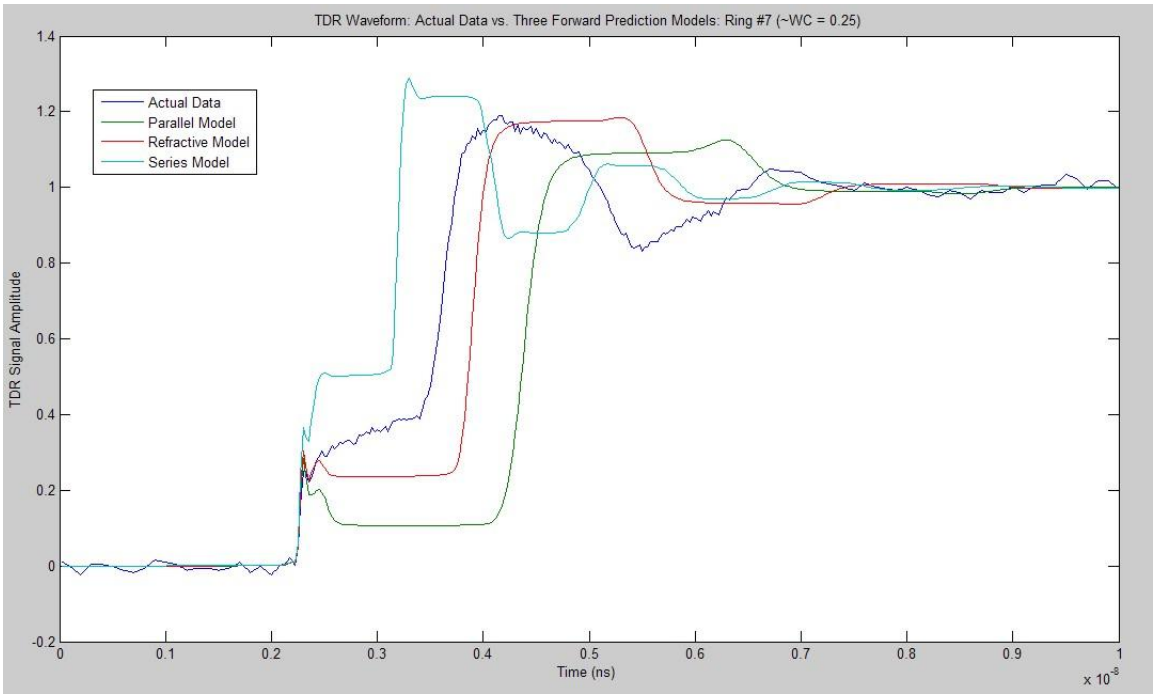


Figure 5.23: TDR Waveform relative to Different Model Types: WC = 0.25 (Table 5.1: Case #4)

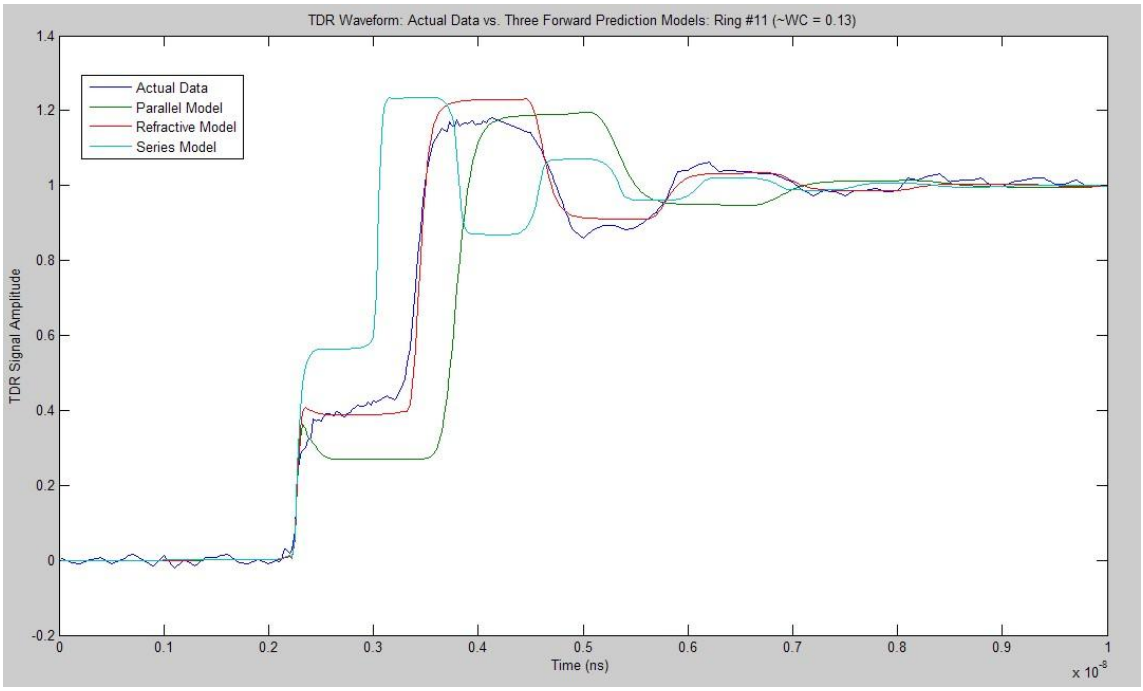


Figure 5.24: TDR Waveform relative to Different Model Types: WC = 0.13 (Table 5.1: Case #4)

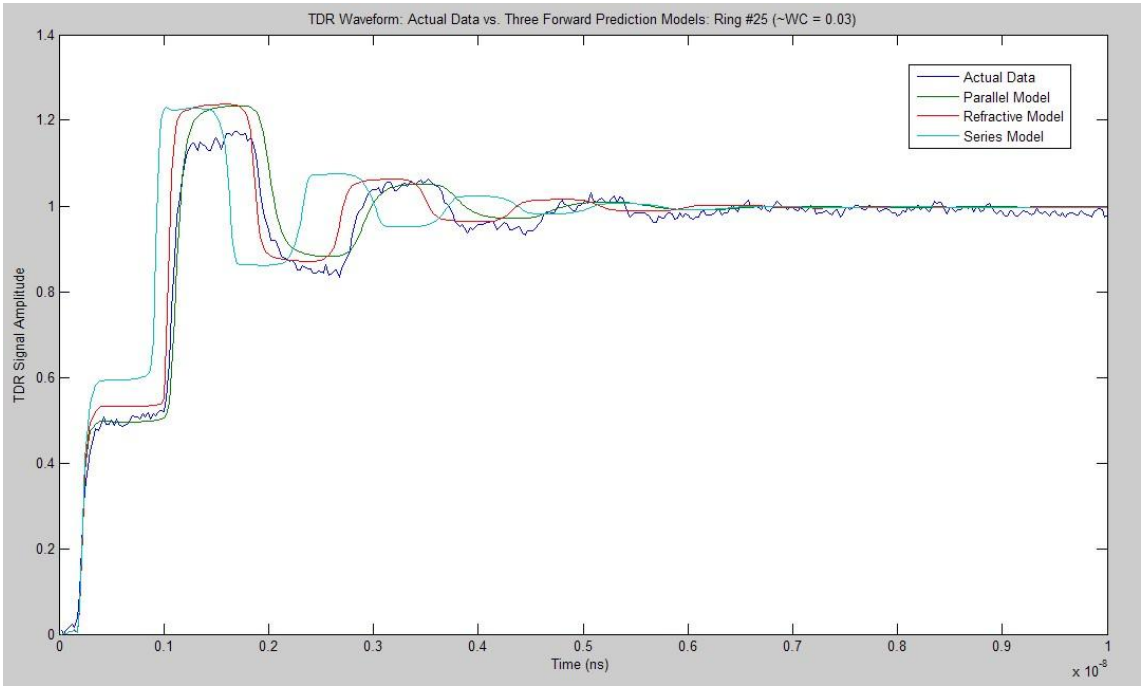


Figure 5.25: TDR Waveform relative to Different Model Types: WC = 0.03 (Table 5.1: Case #4)

As can be seen from figures 5.20 – 5.25 the data can be closely approximated by the parallel model at the extremes of water contents (very wet and very dry) and then falls between those limits at intermediate water contents (with the Cascade Model offering a good approximate fit over various ranges). The Weighted Rectangular Mean model is the general purpose model utilized in the algorithms to adjust fit to different locations between the limits of the Parallel and Series model as shown in Table 5.1 and later in the other validation methods of this chapter.

The next few figures (5.26 – 5.28) utilize some additional techniques that can be employed by the proposed inverse models (in addition to those earlier presented via group delay (low EC's) and input impedance (higher EC's)), The following methods utilize slope measurements of various aspects of the TDR waveforms utilizing different noise thresholds. These methods are only applicable when the second reflection is visible (lower EC's).

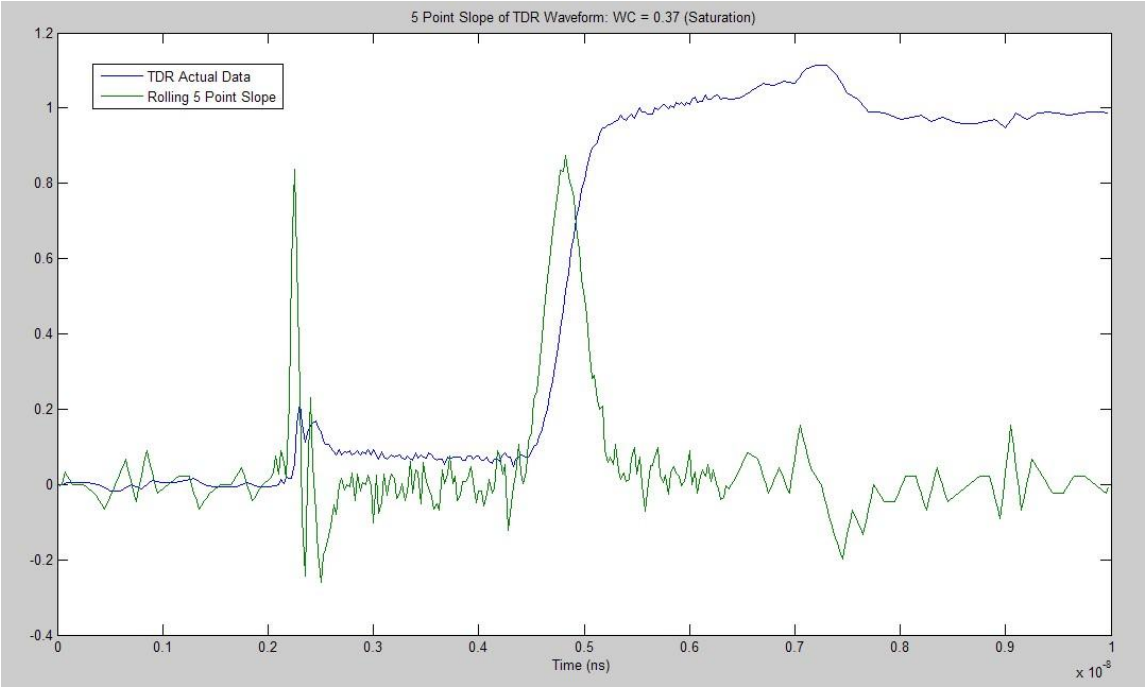


Figure 5.26: Slope Measurement of TDR Waveform: WC = 0.37: Lower Noise Threshold

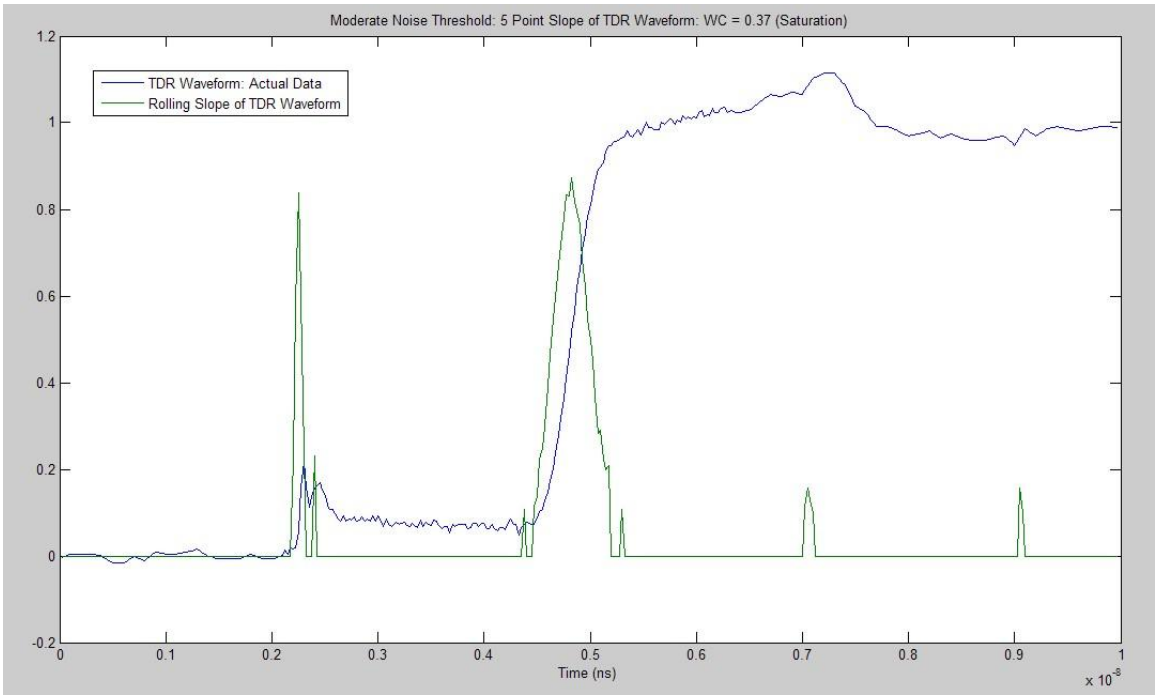


Figure 5.27: Slope Measurement of TDR Waveform: WC = 0.37: Moderate Noise Threshold

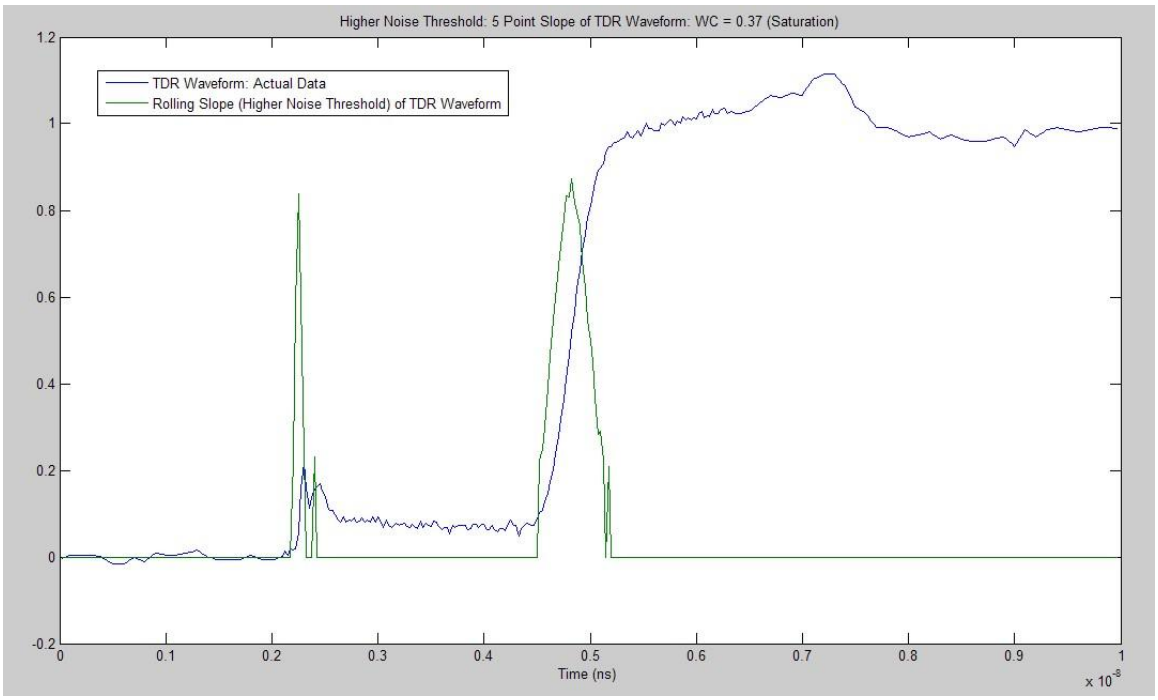


Figure 5.28: Slope Measurement of TDR Waveform: WC = 0.37: Higher Noise Threshold

## Validation Method #1b: Field Experiments:

TDR traces were also collected at three different field test sites to get a representation of real world type TDR signals and measurement conditions. The three locations along with the soil types and conditions and the number of samples or test sites at each location are summarized below in table 5.2.

**Table 5.2. Summary of Field Test Site Information**

| Location | Soil Type | Sample Count | Verification Methods | Special Conditions |
|---|---|---|---|---|
| Monroe, OR Mint Farm | Clay Loam | 6 | Gravimetric Neutron Probe AC Resistance Bridge* | Poor Drainage Wetter Climate |
| Hermiston, OR Poplar Farm | Sand | 16 | Gravimetric Neutron Probe AC Resistance Bridge | Well Drained Arid Climate |
| Albany, OR High Salinity Irrigation | Silt Loam | 4 | Gravimetric AC Resistance Bridge | High Salinity |

*AC Resistance Bridge not as Effective for Clay Soils (with Charged Interfacial Mechanisms) and so only Order of Magnitude Approximations for EC Obtained for the Monroe Site.

In each of the field test sites the TDR instrument used was the Tektronix 1502B cable tester and the TDR probe was a three wire probe by Campbell Scientific (CS610) of 30cm length.

The Monroe, OR farm is located in the southern portion of the Willamette Valley of Western Oregon and consisted of a medium to heavy textured clay loam soil. This farm is a mint farm and the irrigation method was a side roll wheel line. The irrigation interval averaged around 7 days and TDR measurements were obtained in several locations, with variations on how recently the ground had been watered. Water content was calibrated via gravimetric samples taken at two depths at close proximity to each TDR measurement site. At six of the locations a Neutron probe was also used for water content calibration. Only very approximate order of magnitude Electrical conductivity estimates were obtained for this site as the AC resistance half bridge is less effective for measuring electrical resistance in charged soils such as clays due to the low frequency operation of the AC Bridge being within the bandwidth of electrolytic and other charged interface mechanisms.

The Hermiston, OR farm is located in the Eastern Columbia River basin in Northeastern Oregon and consisted of a well draining sandy soil. This farm is a poplar farm owned and operated by the Potlatch Company. The irrigation method was a drip irrigation system. The irrigation interval consisted of water applications each day. Water content was again calibrated via gravimetric analysis (this time at three depths) at all test sites and via neutron probe at a number of sites as well. Electrical conductivity verified via an AC resistance half bridge back at the lab with a two wire probe before the gravimetric analysis was performed.

The Albany, OR farm is located in the central portion of the Willamette Valley in Western Oregon. This farm is also a poplar farm and is located on ground owned by the Oremet Corporation and is irrigated via wastewater/reclaimed water from the company leading to high salinity conditions. Water content calibrations via gravimetric analysis and electrical conductivity verifications via an AC resistance half bridge on soil cores were obtained (although with special care due to the high salinity reclaimed irrigation water). This site was used to show what a field TDR trace looks like in a highly saline environment. An example of this type of waveform in very saline conditions from the Albany site is given as follows in figures 5.29 and 5.30 (both time and frequency domains).

Water content and electrical conductivity were also estimated from the TDR trace for each site using the new algorithms based on the forward prediction models. Example TDR waveforms (Time Domain) along with their FFT's (Frequency Domain) from each of the sites (Albany, Hermiston and Monroe) are shown in figures 5.29 -5.34. Overall comparisons to the forward prediction models for all three of these locations across all of their test sites are also summarized in Tables 5.3 to 5.5. In addition, several additional figures are also given in Appendix D showing comparisons between actual data and simulated/predicted data (the latter from the forward prediction models). The findings from these field validation experiments are summarized later in this section of this chapter.

**Table 5.3: Field Testing Results: Validation Field Method #1: Field TDR Data: Hermiston, OR: 3-Wire Probe: Open Termination at End**

| Location | Soil Type | Site # | Air-Filled Porosity | Actual Water Content | Algor. Water Content | Actual Elec. Cond. | Algor. Elec. Cond. | Simulation. Model | Series Coef. | Parallel Coef. | Coef.of Fit Method B | Coef of Fit: Method A $R^2$ |
|---|---|---|---|---|---|---|---|---|---|---|---|---|
| Hermiston | Air | Open Air | 1 | 0 | 0 | 0 | 0 | Parallel | 0 | 1 | 0.944 | 0.979 |
| Hermiston | Sand | 1a | 0.445 | 0.055 | 0.055 | 0.0011 | 0.0023 | Rect. Mean | 0.8 | 1 | 0.969 | 0.973 |
| Hermiston | Sand | 1b | 0.432 | 0.062 | 0.062 | 0.0017 | 0.0026 | Rect. Mean | 0.8 | 1 | 0.969 | 0.973 |
| Hermiston | Sand | 1c | 0.419 | 0.068 | 0.068 | 0.0023 | 0.0034 | Rect. Mean | 0.8 | 1 | 0.969 | 0.973 |
| Hermiston | Sand | 2a | 0.479 | 0.085 | 0.085 | 0.0045 | 0.0049 | Rect. Mean | 2 | 1 | 0.894 | 0.965 |
| Hermiston | Sand | 2b | 0.453 | 0.078 | 0.078 | 0.0030 | 0.0041 | Rect. Mean | 2 | 1 | 0.894 | 0.965 |
| Hermiston | Sand | 2c | 0.426 | 0.070 | 0.070 | 0.0017 | 0.0029 | Rect. Mean | 2 | 1 | 0.894 | 0.965 |
| Hermiston | Sand | 4 | 0.435 | 0.064 | 0.064 | 0.0012 | 0.0037 | Rect. Mean | 1.3 | 1 | 0.839 | 0.935 |
| Hermiston | Sand | 6 | 0.435 | 0.077 | 0.077 | 0.0018 | 0.0026 | Rect. Mean | 1.8 | 1 | 1.041 | 0.958 |
| Hermiston | Sand | 7 | 0.435 | 0.070 | 0.070 | 0.0015 | 0.0019 | Rect. Mean | 2.5 | 1 | 0.933 | 0.963 |
| Hermiston | Sand | 10 | 0.435 | 0.075 | 0.075 | 0.0017 | 0.0025 | Rect. Mean | 2.4 | 1 | 1.036 | 0.954 |
| Hermiston | Sand | 12a | 0.555 | 0.160 | 0.160 | 0.0144 | 0.0084 | Rect. Mean | 2 | 1 | 0.839 | 0.949 |
| Hermiston | Sand | 12b | 0.445 | 0.137 | 0.137 | 0.0112 | 0.0072 | Rect. Mean | 2 | 1 | 0.839 | 0.949 |
| Hermiston | Sand | 12c | 0.426 | 0.072 | 0.072 | 0.0039 | 0.0029 | Rect. Mean | 2 | 1 | 0.839 | 0.949 |
| Hermiston | Sand | 13a | 0.502 | 0.119 | 0.119 | 0.0057 | 0.0041 | Rect. Mean | 2.2 | 1 | 0.914 | 0.955 |
| Hermiston | Sand | 13b | 0.426 | 0.084 | 0.084 | 0.0055 | 0.0037 | Rect. Mean | 2.2 | 1 | 0.914 | 0.955 |
| Hermiston | Sand | 13c | 0.392 | 0.105 | 0.105 | 0.0066 | 0.0043 | Rect. Mean | 2.2 | 1 | 0.914 | 0.955 |
| Hermiston | Sand | 14a | 0.502 | 0.058 | 0.058 | 0.0009 | 0.0018 | Rect. Mean | 1.2 | 1 | 0.920 | 0.955 |
| Hermiston | Sand | 14b | 0.445 | 0.061 | 0.061 | 0.0011 | 0.0019 | Rect. Mean | 1.2 | 1 | 0.920 | 0.955 |
| Hermiston | Sand | 14c | 0.415 | 0.072 | 0.072 | 0.0037 | 0.0035 | Rect. Mean | 1.2 | 1 | 0.920 | 0.955 |
| Hermiston | Sand | 15a | 0.445 | 0.047 | 0.047 | 0.0013 | 0.0012 | Rect. Mean | 1.2 | 1 | 1.039 | 0.962 |
| Hermiston | Sand | 15b | 0.423 | 0.074 | 0.074 | 0.0049 | 0.0018 | Rect. Mean | 1.2 | 1 | 1.039 | 0.962 |
| Hermiston | Sand | 15c | 0.415 | 0.082 | 0.082 | 0.0076 | 0.0029 | Rect. Mean | 1.2 | 1 | 1.039 | 0.962 |
| Hermiston | Sand | 16a | 0.483 | 0.023 | 0.023 | 0.0000 | 0.0006 | Rect. Mean | 0.15 | 1 | 0.851 | 0.952 |
| Hermiston | Sand | 16b | 0.445 | 0.065 | 0.065 | 0.0013 | 0.0021 | Rect. Mean | 0.15 | 1 | 0.851 | 0.952 |
| Hermiston | Sand | 16c | 0.430 | 0.071 | 0.071 | 0.0029 | 0.0038 | Rect. Mean | 0.15 | 1 | 0.851 | 0.952 |
| Hermiston | Sand | 17a | 0.513 | 0.142 | 0.142 | 0.0080 | 0.0069 | Rect. Mean | 0.7 | 1 | 1.064 | 0.913 |
| Hermiston | Sand | 17b | 0.415 | 0.128 | 0.128 | 0.0075 | 0.0085 | Rect. Mean | 0.7 | 1 | 1.064 | 0.913 |
| Hermiston | Sand | 17c | 0.392 | 0.090 | 0.090 | 0.0028 | 0.0032 | Rect. Mean | 0.7 | 1 | 1.064 | 0.913 |
| Hermiston | Sand | 18a | 0.438 | 0.079 | 0.079 | 0.0022 | 0.0040 | Rect. Mean | 1.5 | 1 | 0.864 | 0.935 |
| Hermiston | Sand | 18b | 0.434 | 0.077 | 0.077 | 0.0011 | 0.0032 | Rect. Mean | 1.5 | 1 | 0.864 | 0.935 |
| Hermiston | Sand | 18c | 0.381 | 0.084 | 0.084 | 0.0021 | 0.0040 | Rect. Mean | 1.5 | 1 | 0.864 | 0.935 |

**Table 5.4: Field Testing Results: Validation Field Method #1: Field TDR Data: Albany, OR: 3-Wire Probe: Open Termination at End**

| Location | Soil Type | Site # | Air-Filled Porosity | Actual Water Content | Algor. Water Content | Actual Elec. Cond. S/m | Algor. Elec. Cond. S/m | Simulation Model | Series Coef. | Parallel Coef. | Coef.of Fit Method B | Coef of Fit: Method A $R^2$ |
|---|---|---|---|---|---|---|---|---|---|---|---|---|
| Albany | Silt Loam | 1a | 0.470 | 0.385 | 0.385 | 0.114 | 0.077 | Parallel | 0 | 1 | 1.148 | 0.974 |
| Albany | Silt Loam | 1b | 0.469 | 0.370 | 0.370 | 0.125 | 0.082 | Parallel | 0 | 1 | 1.148 | 0.974 |
| Albany | Silt Loam | 1c | 0.501 | 0.370 | 0.370 | 0.109 | 0.073 | Parallel | 0 | 1 | 1.148 | 0.974 |
| Albany | Silt Loam | 2a | 0.459 | 0.396 | 0.396 | 0.094 | 0.057 | Parallel | 0 | 1 | 0.986 | 0.947 |
| Albany | Silt Loam | 2b | 0.513 | 0.371 | 0.371 | 0.075 | 0.049 | Parallel | 0 | 1 | 0.986 | 0.947 |
| Albany | Silt Loam | 2c | 0.484 | 0.428 | 0.428 | 0.098 | 0.060 | Parallel | 0 | 1 | 0.986 | 0.947 |
| Albany | Silt Loam | 3a | 0.531 | 0.421 | 0.421 | 0.084 | 0.052 | Parallel | 0 | 1 | 0.983 | 0.967 |
| Albany | Silt Loam | 3b | 0.489 | 0.411 | 0.411 | 0.123 | 0.067 | Parallel | 0 | 1 | 0.983 | 0.967 |
| Albany | Silt Loam | 3c | 0.489 | 0.427 | 0.427 | 0.131 | 0.081 | Parallel | 0 | 1 | 0.983 | 0.967 |
| Albany | Silt Loam | 4a | 0.474 | 0.379 | 0.379 | 0.183 | 0.084 | Parallel | 0 | 1 | 0.966 | 0.952 |
| Albany | Silt Loam | 4b | 0.516 | 0.371 | 0.371 | 0.105 | 0.060 | Parallel | 0 | 1 | 0.966 | 0.952 |
| Albany | Silt Loam | 4c | 0.486 | 0.392 | 0.392 | 0.066 | 0.031 | Parallel | 0 | 1 | 0.966 | 0.952 |

**Table 5.5: Field Testing Results: Validation Field Method #1: Field TDR Data: Monroe, OR: 3-Wire Probe: Open Termination at End**

| Location | Soil Type | Site # | Air-Filled Porosity | Actual Water Content | Algor. Water Content | Actual Elec. Cond. S/m | Algor. Elec. Cond. S/m | Simulation Model | Series Coef. | Parallel Coef. | Coef.of Fit Method B | Coef of Fit: Method A $R^2$ |
|---|---|---|---|---|---|---|---|---|---|---|---|---|
| Monroe | Air | Open Air | 1 | 0 | 0 | 0 | 0 | Parallel | 0 | 1 | 0.942 | 0.981 |
| Monroe | Clay Loam | 1a | 0.497 | 0.330 | 0.330 | 0.01* | 0.034 | Rect. Mean | 0.15 | 1 | 0.996 | 0.929 |
| Monroe | Clay Loam | 1b | 0.470 | 0.365 | 0.365 | 0.01* | 0.034 | Rect. Mean | 0.15 | 1 | 0.996 | 0.929 |
| Monroe | Clay Loam | 1c | 0.465 | 0.380 | 0.380 | 0.01* | 0.034 | Rect. Mean | 0.15 | 1 | 0.996 | 0.929 |
| Monroe | Clay Loam | 2a | 0.497 | 0.330 | 0.330 | 0.01* | 0.019 | Rect. Mean | 1 | 1 | 0.982 | 0.857 |
| Monroe | Clay Loam | 2b | 0.470 | 0.365 | 0.365 | 0.01* | 0.019 | Rect. Mean | 1 | 1 | 0.982 | 0.857 |
| Monroe | Clay Loam | 2c | 0.465 | 0.380 | 0.380 | 0.01* | 0.019 | Rect. Mean | 1 | 1 | 0.982 | 0.857 |
| Monroe | Clay Loam | 3a | 0.494 | 0.320 | 0.320 | 0.01* | 0.021 | Rect. Mean | 1 | 1 | 0.937 | 0.846 |
| Monroe | Clay Loam | 3b | 0.468 | 0.360 | 0.360 | 0.01* | 0.022 | Rect. Mean | 1 | 1 | 0.937 | 0.846 |
| Monroe | Clay Loam | 3c | 0.460 | 0.380 | 0.380 | 0.01* | 0.022 | Rect. Mean | 1 | 1 | 0.937 | 0.846 |
| Monroe | Clay Loam | 4a | 0.464 | 0.320 | 0.320 | 0.01* | 0.024 | Rect. Mean | 1.2 | 1 | 0.720 | 0.862 |
| Monroe | Clay Loam | 4b | 0.479 | 0.340 | 0.340 | 0.01* | 0.024 | Rect. Mean | 1.2 | 1 | 0.720 | 0.862 |
| Monroe | Clay Loam | 4c | 0.479 | 0.360 | 0.360 | 0.01* | 0.024 | Rect. Mean | 1.2 | 1 | 0.720 | 0.862 |
| Monroe | Clay Loam | 5a | 0.487 | 0.390 | 0.390 | 0.01* | 0.038 | Parallel | 0 | 1 | 1.235 | 0.865 |
| Monroe | Clay Loam | 5b | 0.453 | 0.380 | 0.380 | 0.01* | 0.038 | Parallel | 0 | 1 | 1.235 | 0.865 |
| Monroe | Clay Loam | 5c | 0.445 | 0.370 | 0.370 | 0.01* | 0.038 | Parallel | 0 | 1 | 1.235 | 0.865 |
| Monroe | Clay Loam | 6a | 0.540 | 0.230 | 0.230 | 0.01* | 0.023 | Rect. Mean | 1 | 1 | 0.599 | 0.826 |
| Monroe | Clay Loam | 6b | 0.445 | 0.340 | 0.340 | 0.01* | 0.024 | Rect. Mean | 1 | 1 | 0.599 | 0.826 |
| Monroe | Clay Loam | 6c | 0.438 | 0.360 | 0.360 | 0.01* | 0.024 | Rect. Mean | 1 | 1 | 0.599 | 0.826 |
| Monroe | Clay Loam | 7a | 0.517 | 0.370 | 0.370 | 0.01* | 0.033 | Rect. Mean | 0.15 | 1 | 1.027 | 0.863 |
| Monroe | Clay Loam | 7b | 0.494 | 0.400 | 0.400 | 0.01* | 0.033 | Rect. Mean | 0.15 | 1 | 1.027 | 0.863 |
| Monroe | Clay Loam | 7c | 0.487 | 0.420 | 0.420 | 0.01* | 0.033 | Rect. Mean | 0.15 | 1 | 1.027 | 0.863 |
| Monroe | Clay Loam | 8a | 0.479 | 0.350 | 0.350 | 0.01* | 0.024 | Rect. Mean | 0.6 | 1 | 0.958 | 0.879 |
| Monroe | Clay Loam | 8b | 0.483 | 0.370 | 0.370 | 0.01* | 0.024 | Rect. Mean | 0.6 | 1 | 0.958 | 0.879 |
| Monroe | Clay Loam | 8c | 0.483 | 0.390 | 0.390 | 0.01* | 0.024 | Rect. Mean | 0.6 | 1 | 0.958 | 0.879 |
| Monroe | Clay Loam | 9a | 0.497 | 0.330 | 0.330 | 0.01* | 0.033 | Rect. Mean | 0.5 | 1 | 0.836 | 0.878 |
| Monroe | Clay Loam | 9b | 0.470 | 0.365 | 0.365 | 0.01* | 0.033 | Rect. Mean | 0.5 | 1 | 0.836 | 0.878 |
| Monroe | Clay Loam | 9c | 0.465 | 0.380 | 0.380 | 0.01* | 0.033 | Rect. Mean | 0.5 | 1 | 0.8356 | 0.878 |

*Order of Magnitude Approximation only. AC Resistance Bridge less Effective for Measuring EC in Clay Soils.

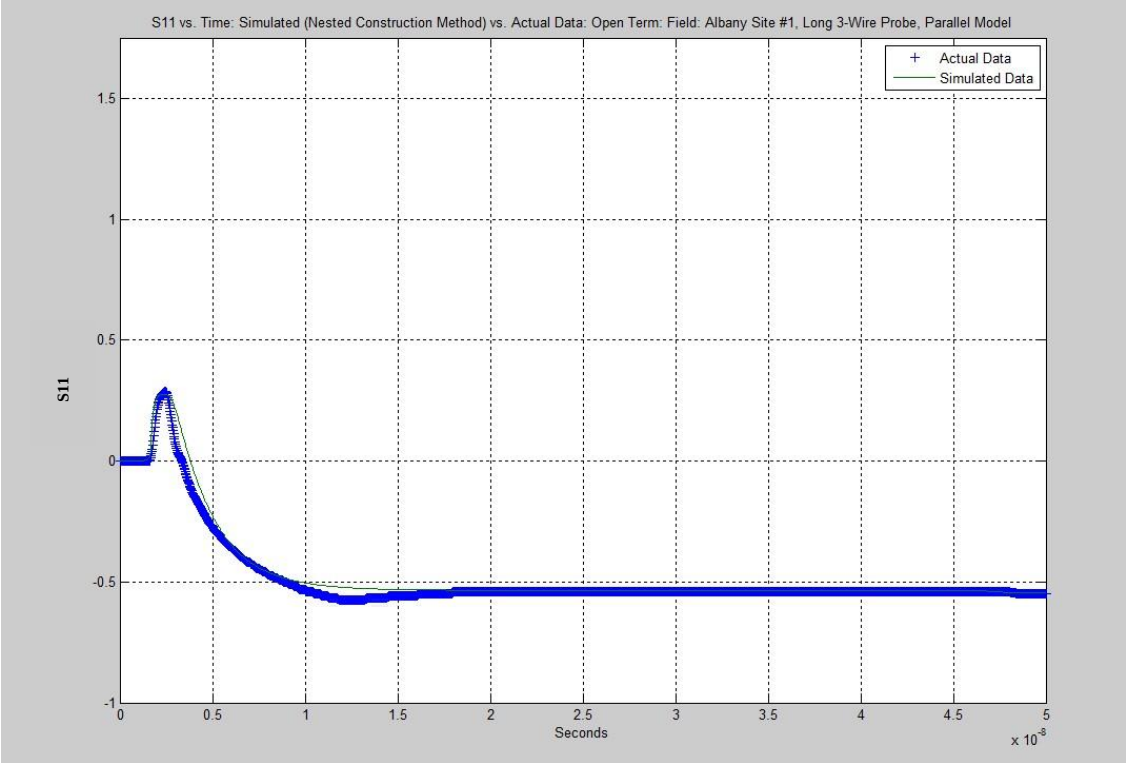


Figure 5.29: Example of TDR Waveform in very Saline Conditions: Field: Albany: Site #1: Sim. vs. Actual

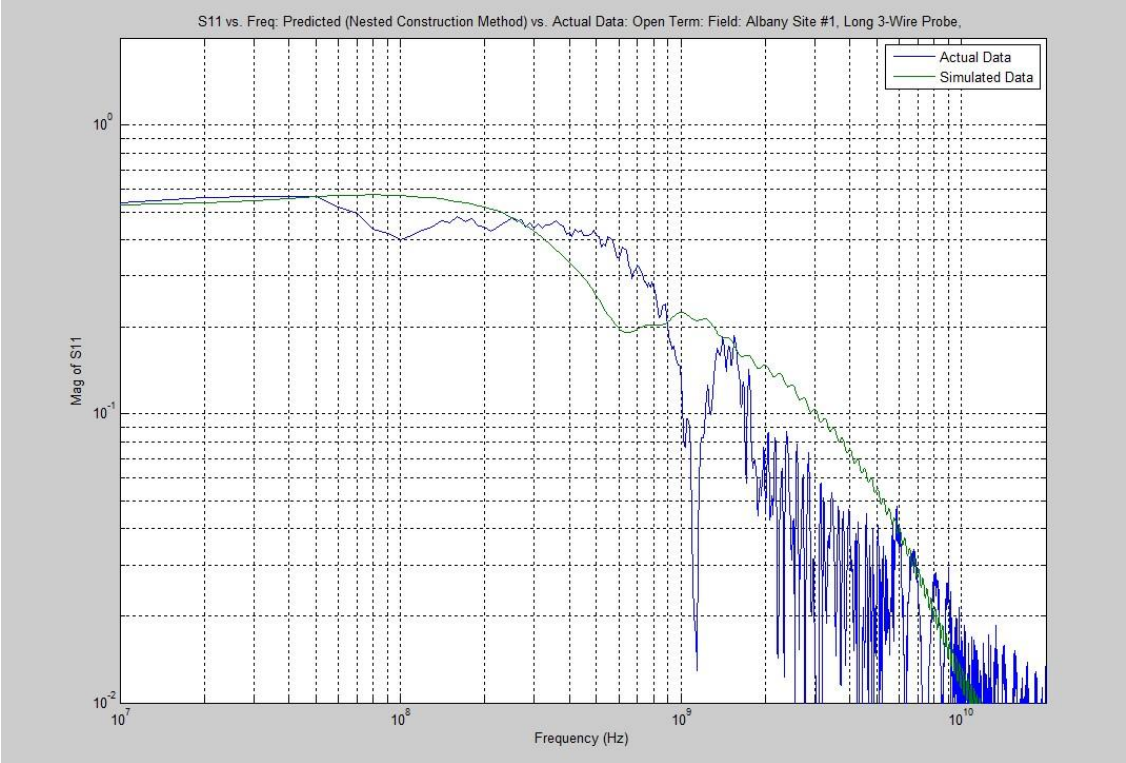


Figure 5.30: Example of an FDR Spectrum in very Saline Conditions: Field: Albany Site #1: Simulated vs. Actual

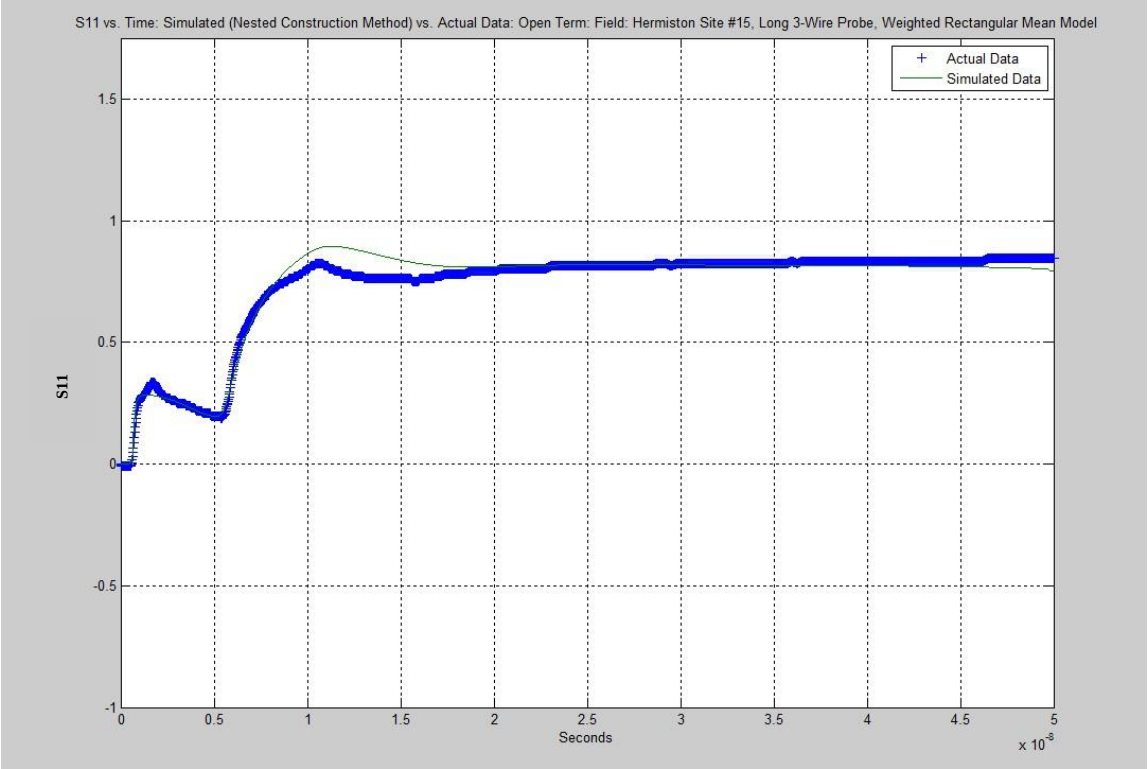


Figure 5.31: Example of TDR Waveform: Sllght WC increase vs. Depth: Field: Hermiston: Site #15: Simulated vs. Actual

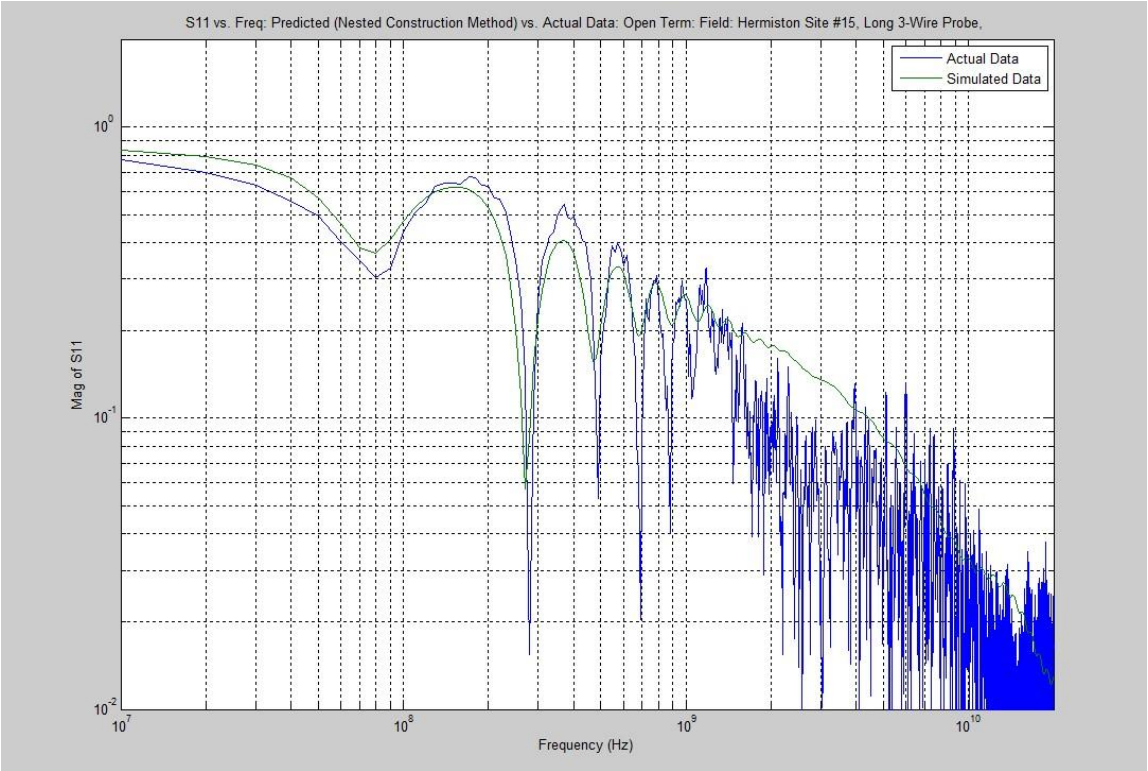


Figure 5.32: Example of FDR Spectrum: Field Data: Hermiston: Site #15: Simulated vs. Actual

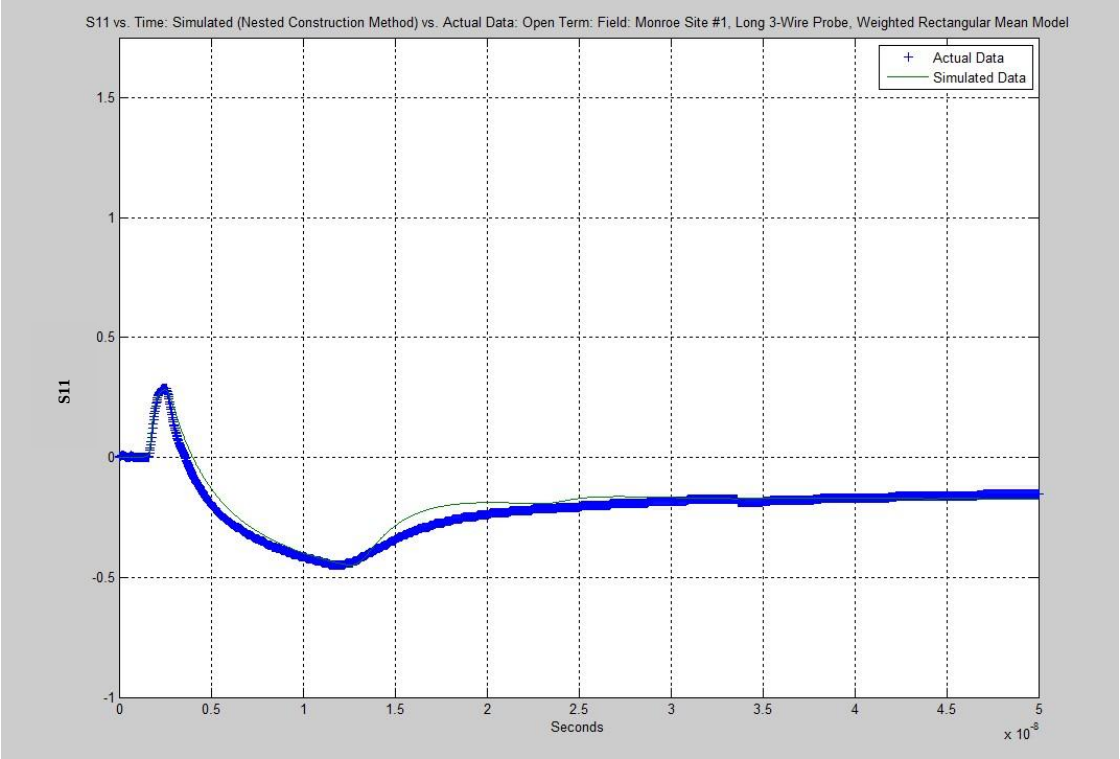


Figure 5.33: Example of TDR Waveform in Moderate Saline Conditions & with Varying WC Profile with Depth: Field: Monroe: Site #1

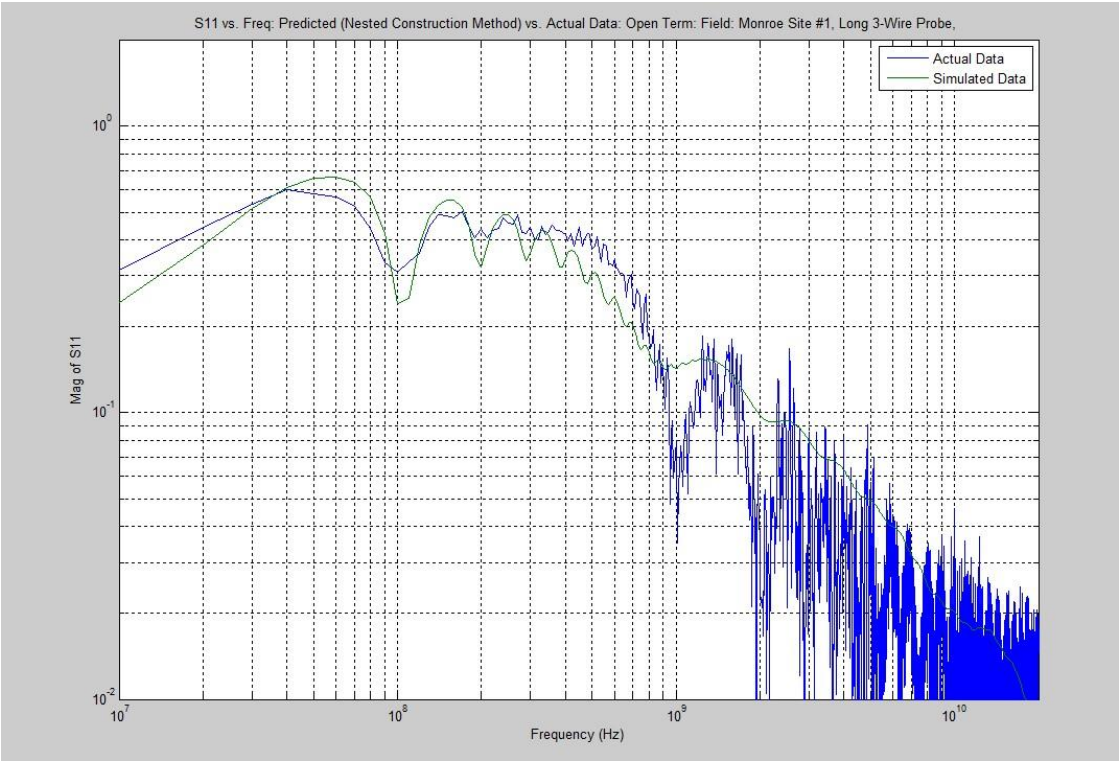


Figure 5.34: Example of FDR Spectrum: Field Data: Monroe: Site #1: Simualted vs. Actual

All three sets of field measurement data were compiled in Microsoft Excel and then transferred to Matlab (Mathworks corp.) where an FFT was performed on each data set and the forward prediction models based algorithms run to determine water content and electrical conductivity. The new revised algorithm also has the capability of separating out moisture content vs. depth along the probe using advanced scattering S parameter models based on Mason's non-touching loop rule (further covered in validation method #3 later in this chapter) to extract impedance vs. position along the probe (in this case of these field measurements dividing the probe into 11 segments). This was important for the field data as the water content varied modestly along the length of the probe (although a significant portion of the droop in the waveform is also due to electrical conductivity related loss mechanisms and other loss mechanisms which was found to mask a lot of the WC variations). The FFT on the data allows for the separation of water content from electrical conductivity even in the presence of high salinity by looking at the data at both low frequencies (for determining conductivity) and high frequencies (for determining water content) as was described in the lab results section and in more detail in the forward prediction model chapter. However, in this field data that appears to be limited to the overall bulk average WC with the fine variations of WC vs. position effectively masked by the loss terms due to EC. But the bulk overall WC can still be extracted via review of the frequency domain information (especially for the Hermiston data where the group delay method of identifying overall WC is still viable – see plots in Appendix D).

The field data did appear to show larger errors on EC measurements vs. the higher accuracy found in the lab data. However, some of that may have been due to the difficulty of obtaining an accurate independent measurement of EC on the extracted field soil samples (and no accurate independent EC validation data could be obtained for the clay loam soil at the Monroe site) due to the low frequency operation of the AC Resistance Half Bridge (which operates inside the bandwidth of charged interfacial mechanisms as well as electrolytic reactions). In contrast the HP4194A Impedance analyzer utilized for the laboratory calibrations of EC could perform the measurements up at 10 kHz outside the bandwidths of those mechanisms. The field based TDR system probably was more accurate than the independent methods used to measure EC due to these above stated reasons and also due to to the TDR system causing less disturbance to the soil vs. the extracted soil samples/cores. But again the lab data (where EC could be measured

independently in situ in the fixtures with a high dynamic range impedance analyzer at higher frequencies) there was very good agreement between simulated and actual EC.

A sampling of the results of the field data compared to the forward prediction models are shown in Appendix D. A sampling of data from each of the field sites is shown. For each site the plot of S11 vs. frequency is shown for both the actual data and a fitted simulated run of the forward prediction algorithm. In addition a plot of impedance vs. frequency is given for both the actual data and simulation predictions. Similarly a plot of group delay vs. frequency for both actual data and a fitted simulation run are shown and finally a comparison of the actual data and fitted simulation runs are shown in the time domain. Summary reports for each field test case were given above in tables 5.3 – 5.5. The results of the actual data and fitted simulation run for parameters such as water content vs. depth, bulk overall electrical conductivity, the various methods of coefficient of fit and other parameters are given in those tables. A significant finding from the field data was that the loss terms due mainly to electrical conductivity for the most part swamped out the actual field data waveforms in terms of being able to extract the fine variations of WC vs. position. However, overall bulk WC can still be extracted (especially with the group delay method for the Hermiston data).

Appendix D gives some additional plots where a portion of the loss terms (due to EC are artificially removed) which reveals the WC profiles vs. depth (an artificial exercise involving the simulation plots only and not visible in the actual data). However, with the actual data, the fine variation of water content with depth appears to be masked by the other loss terms associated with EC (effectively a low pass filter). High frequency information is required to identify the fine changes with position of WC. Any significant amount of EC appears to swamp out that high frequency information (the type of information that is visible in validation method #3 utilizing test PCBA's of very low loss). Validation method #3 shows that variations of impedance vs. position can be simulated and determined via the forward prediction based algorithms to a reasonable level of accuracy at this time to at least show that the development of this type of algorithm is feasible. However, in actual soils where losses are often high a method must be developed to remove (via signal processing software) the loss terms due to electrical conductivity to then reveal the remaining higher frequency WC driven terms. To accomplish this is part of ongoing research by the author and also requires a high dynamic range swept narrowband frequency domain reflection and transmission measurement system (essentially a Vector Network

Analyzer). State of the art digital signal processing hardware/software is bringing the costs of such a system down to being feasible for wider spread use. However, as was also the case in the lab data the electrical conductivity can be determined with good precision using the low frequency information or long time levels. The overall bulk average WC can also still be measured (it is only the fine WC variations that appear to be swamped). Again there was some modest error in the level of the TDR trace at medium to high frequencies (which is important for extracting water content when the conductivity is high) but the timing of the trace was fairly accurate (important for determining overall water content when the conductivity is low to moderate) and the low frequency level was very accurate (important for obtaining electrical conductivity). Again more work is needed to improve on modeling loss mechanisms at medium to high frequencies and improvement is needed in the hardware as well to minimize those losses. Both of these enhancements/improvements are now possible with state of the art software assisted radio technology allowing for the creation of a high dynamic range vector network analyzer type of measurement for FDR and FDT at very reasonable costs. This will be further investigated in follow-on research.

The conclusions from the field testing are therefore similar to those from the lab testing with the following added conclusions:

4.) In real world field conditions the water content often varies with depth. The enhanced version of this developed algorithm shows the potential of being a feasible tool in extracting water content vs. depth or length along the probe with great precision by using the impedance values vs. position along the length of the probe (obtainable from the time domain trace in combination with the frequency domain information). However, for a reflection only based method such as TDR or FDR this algorithm would only be feasible in lower levels of conductivity as a reflected signal from the probe end is required to ascertain information about what happens along the probe and high frequency information is required to show fine but sometimes abrubt variations of impedance vs. position (for WC profiles). Since this portion of the algorithm (determining water content vs. depth) depends on both the level of S11 as well as the timing, it is a prerequisite for feasibility to develop a higher bandwidth TDR hardware measurement system as well as improve the software algorithm's ability to model (and effectively remove via signal processing) all medium to high frequency loss mechanisms that remain. To best achieve this also requires a high

dynamic range Frequency Domain Transmssion (FDT or S21) measurement. This is the subject of ongoing research by the author.

Again based on these conclusions as well as those from the lab results section along with what will be shown in validation method #3, feasibility of the combination of this developed software forward prediction model and proposed inverse algorithm along with the proposed higher bandwidth higher dynamic range FDR/FDT hardware solution has been demonstrated. Again, it is recommended that both a reflection and transmission based system be employed to take full advantage of these algorithms. Enhancements and further validations will continue in follow-on research.

Plots of Field Data:

Appendix D contains a sampling of plots obtainable from the developed measurement algorithm. The plots included are listed as follows obtained for all three locations (Hermiston, Albany and Monroe):

1.) Time Domain Comparisons between Actual Data and the Forward Prediction Models.
2.) Frequency Domain Comparisons between Actual Data and the Forward Prediction Models.
3.) Group Delay vs. Frequency comparisons between Actual Data and the Forward Prediction Models.
4.) Impedance vs. Frequency comparisons between Actual Data and the Forward Predictionn Models.

### Validation Method #2: Laboratory Setup #2: FDR/FDT Measurements

Laboratory Setup #2: FDR (S11, S22), FDT (S12, S21), TDR, TDT: Soil Fixtures per Figure 4.3: The following test conditions were conducted during Validation Method #2 involving higher dynamic range Vector Network Analyzer (VNA) measurements of all S-Parameters (Reflection and Transmission):

Laboratory Setup #2: (Sandy Soil)

WC = 0 (Dry Soil)
WC = 0.01
WC = 0.02
WC = 0.05
WC = 0.10
WC = 0.15
WC = 0.20
WC = 0.25
WC = 0.30
WC = 0.33 (Nearly Saturated Soil: Porosity ~0.35): Distilled Water
WC = 0.33, EC~= 1.2 S/M (High EC)
WC = 0.33, EC~= 0.65 S/M (Moderately High EC)
WC = 0.33, EC~= 0.2 S/M (Moderate EC)
WC = 0.33, EC~= 0.067 S/M (Low to Moderate EC)

The following Measurements were obtained:

Time Domain: TDR and TDT: 50 Ohm Ports.
Frequency Domain: FDR and FDT: 50 Ohm Ports
Time Domain: TDR: Open Circuit Termination on Opposite End of Fixture
Frequency Domain: FDR: Open Circuit Termination on Opposite End of Fixture

The non-saline 50 Ohm measurements were replicated in two different datasets of these particular fixtures and measurement techniques over two separate years. The saline measurements along with the open circuit termination measurements were only conducted in the second dataset associated with this validation method. The overall results are summarized in tables 5.6 and 5.7.

**Table 5.6. Laboratory Testing Results: Validation Method #2: DataSet #1 (50 Ohm Termination Only)**

| Fixture # | Air-Filled Porosity | Actual Water Content | Algor. Water Content | Actual Elec. Cond. | Algor. Elec. Cond. | Simulation. Model | Series Coef. | Par. Coef. | Coef. Of Fit Method B | Coef of Fit: Method A $R^2$ |
|---|---|---|---|---|---|---|---|---|---|---|
| 1 | 1 | 0 | 0 | 0 | 0 | Parallel | 0 | 1 | 1.027 | 0.985 |
| 1 | 0.35 | 0 | 0 | 0 | 0 | Parallel | 0 | 1 | 1.035 | 0.971 |
| 1 | 0.35 | 0.05 | 0.05 | 0 | 0 | Parallel | 0 | 1 | 1.002 | 0.958 |
| 1 | 0.35 | 0.10 | 0.10 | 0 | 0 | Rectangular Mean | 0.75 | 1 | 0.969 | 0.960 |
| 1 | 0.35 | 0.15 | 0.15 | 0 | 0 | Rectangular Mean | 1.8 | 1 | 0.935 | 0.954 |
| 1 | 0.35 | 0.20 | 0.20 | 0 | 0 | Rectangular Mean | 1.35 | 1 | 0.891 | 0.938 |
| 1 | 0.35 | 0.25 | 0.25 | 0 | 0 | Rectangular Mean | 1.05 | 1 | 0.923 | 0.892 |
| 1 | 0.35 | 0.33 | 0.33 | 0 | 0 | Rectangular Mean | 0.75 | 1 | 0.960 | 0.632 |

**Table 5.7. Laboratory Testing Results: Validation Method #2: DataSet #2 (50 Ohm and Open Termination Test Cases)**

| Fixture # | Air-Filled Porosity | Actual Water Content | Algor. Water Content | Actual Elec. Cond. | Algor. Elec. Cond. | Simulation. Model | Series Coef. | Par. Coef. | 50Ω Term COF Method B | 50Ω Term COF Method A $R^2$ | Open Term COF Method A $R^2$ | Open Term COF Method B |
|---|---|---|---|---|---|---|---|---|---|---|---|---|
| 3 | 1 | 0 | 0 | 0 | 0 | Parallel | 0 | 1 | 1.006 | 0.961 | 0.883 | 1.025 |
| 3 | 0.35 | 0 | 0 | 0 | 0 | Parallel | 0 | 1 | 1.001 | 0.962 | 0.809 | 0.980 |
| 3 | 0.35 | 0 | 0 | 0 | 0 | Parallel | 0 | 1 | 1.004 | 0.943 | 0.858 | 1.002 |
| 3 | 0.35 | 0.01 | 0.01 | 0 | 0 | Parallel | 0 | 1 | 1.014 | 0.926 | 0.852 | 0.979 |
| 3 | 0.35 | 0.02 | 0.02 | 0 | 0 | Parallel | 0 | 1 | * | * | 0.874 | 1.012 |
| 3 | 0.35 | 0.05 | 0.05 | 0 | 0 | Parallel | 0 | 1 | 1.144 | 0.865 | 0.881 | 1.024 |
| 3 | 0.35 | 0.10 | 0.10 | 0 | 0 | Rect. Mean | 0.75 | 1 | 0.891 | 0.959 | 0.914 | 1.055 |
| 3 | 0.35 | 0.15 | 0.15 | 0 | 0 | Rect. Mean | 1.25 | 1 | * | * | 0.934 | 1.055 |
| 3 | 0.35 | 0.20 | 0.20 | 0 | 0 | Rect. Mean | 1.25 | 1 | 1.003 | 0.808 | 0.938 | 1.111 |
| 3 | 0.35 | 0.25 | 0.25 | 0 | 0 | Rect. Mean | 1.15 | 1 | 1.05* | 0.670* | 0.933 | 1.147 |
| 3 | 0.35 | 0.33 | 0.33 | 0 | 0 | Rect. Mean | 0.75 | 1 | 0.67 | 0.831 | 0.926 | 1.066 |
| 3 | 0.35 | 0.33 | 0.33** | 0 | 0 | Rect. Mean | 0.75 | 1 | 0.645 | 0.842 | 0.925 | 1.068 |
| 3 | 0.35 | 0.33 | 0.33 | 0.067 | 0.049 | Rect. Mean | 0.75 | 1 | 0.855 | 0.813 | 0.913 | 1.099 |
| 3 | 0.35 | 0.33 | 0.33 | 0.2 | 0.15 | Rect. Mean | 0.75 | 1 | 1.005 | 0.905 | 0.699 | 1.567 |
| 3 | 0.35 | 0.33 | 0.33 | 0.65 | 0.55 | Parallel | 0 | 1 | 1.091 | 0.970 | 0.846 | 1.424 |
| 3 | 0.35 | 0.33 | 0.33 | 1.2 | 1.32 | Parallel | 0 | 1 | 1.090 | 0.982 | 0.983 | 1.345 |

* These noted 50 Ohm Actual TDR Datasets were Low Amplitude (Out of Calibration)

** This run had an Antenna/Probe Resonance Added to the Simulation Models

As can be seen from these tables there is a similar trend to the earlier (Validation #1) laboratory results where the extremes of low water content and high water content tend to lean towards the parallel model and intermediate water contents tend to lie somewhere between the parallel and series models (although not quite as prominent with these runs). There was some modest error in measuring/simulating EC but the trends were still very similar to the results from validation laboratory method #1. A full set of plots from these runs covering time and frequency domain are given in Appendix D. A sampling of them are also given as follows in this chapter:

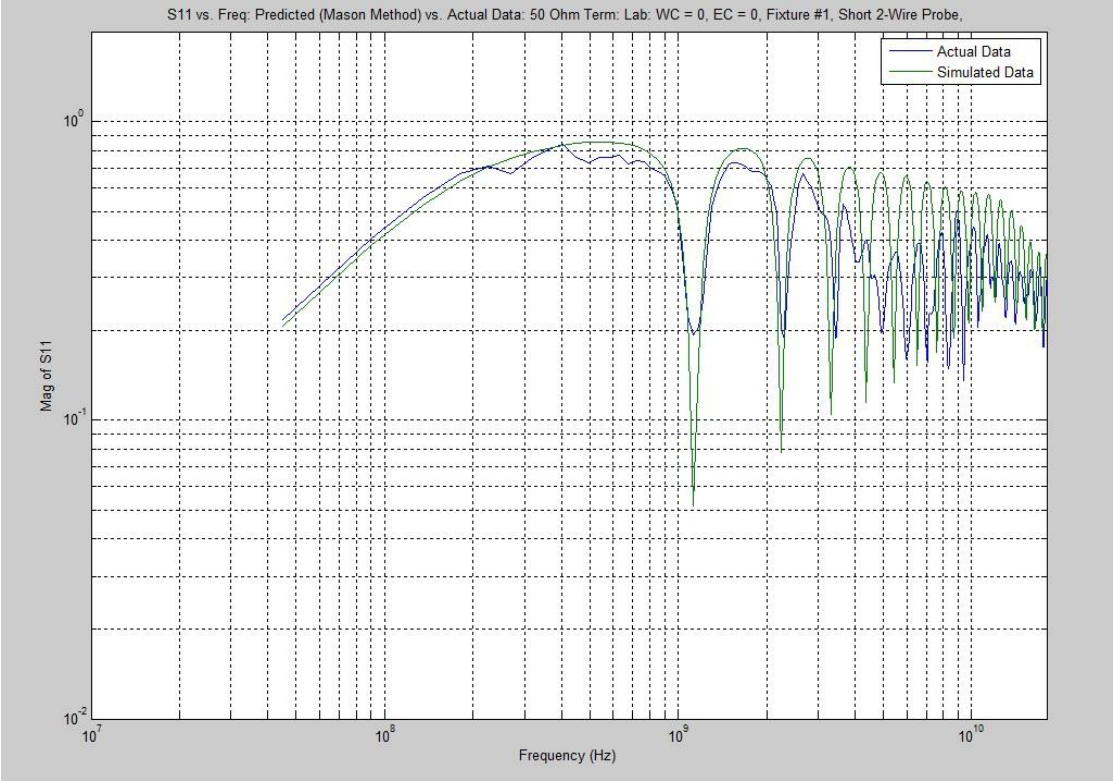


Figure 5.35: Laboratory Validation Method #2: FDR: S11: 50Ω Term.: Dry Soil: WC = 0, EC = 0 S/m

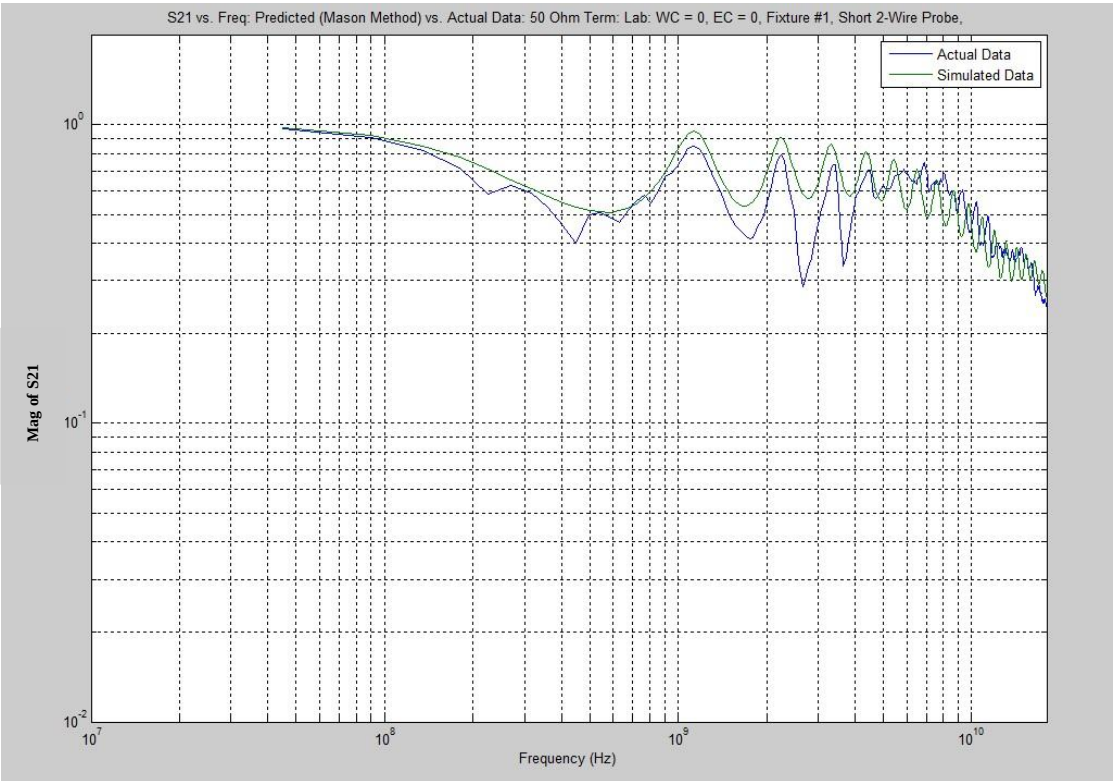


Figure 5.36: Laboratory Validation Method #2: FDT: S21: 50Ω Term.: Dry Soil: WC = 0, EC = 0 S/m

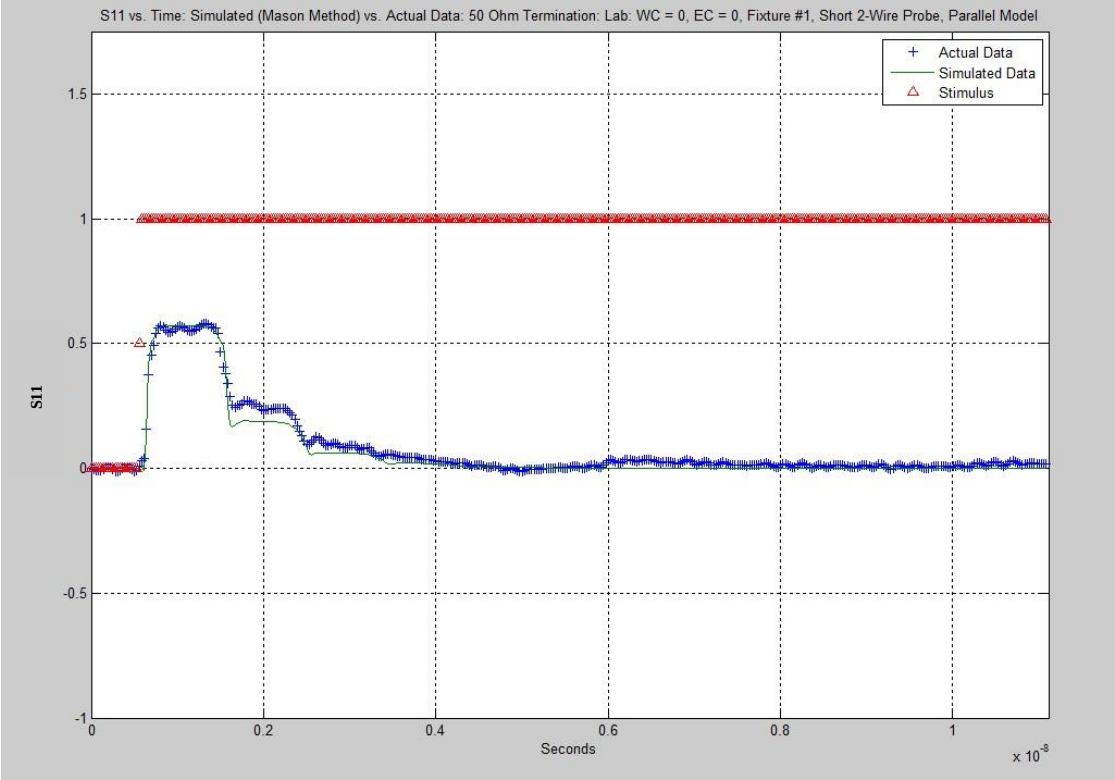


Figure 5.37: Laboratory Validation Method #2: TDR: S11: 50Ω Term.: Dry Soil: WC = 0, EC = 0 S/m

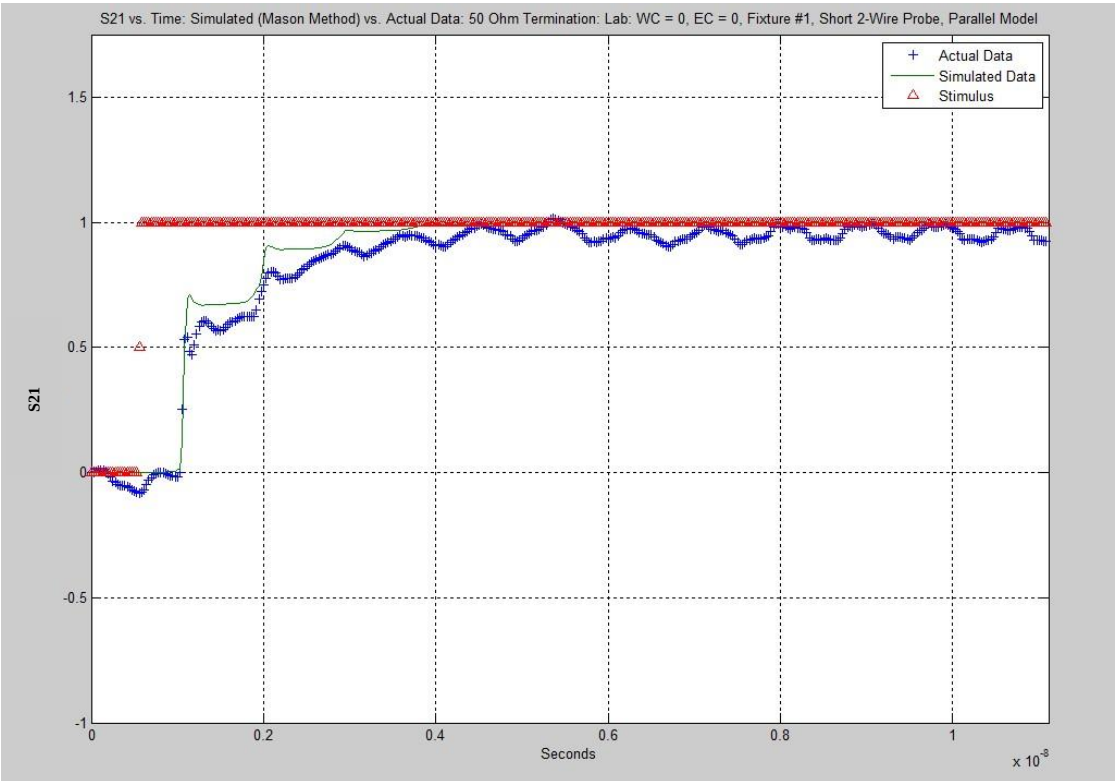


Figure 5.38: Laboratory Validation Method #2: TDT: S21: 50Ω Term.: Dry Soil: WC = 0, EC = 0 S/m

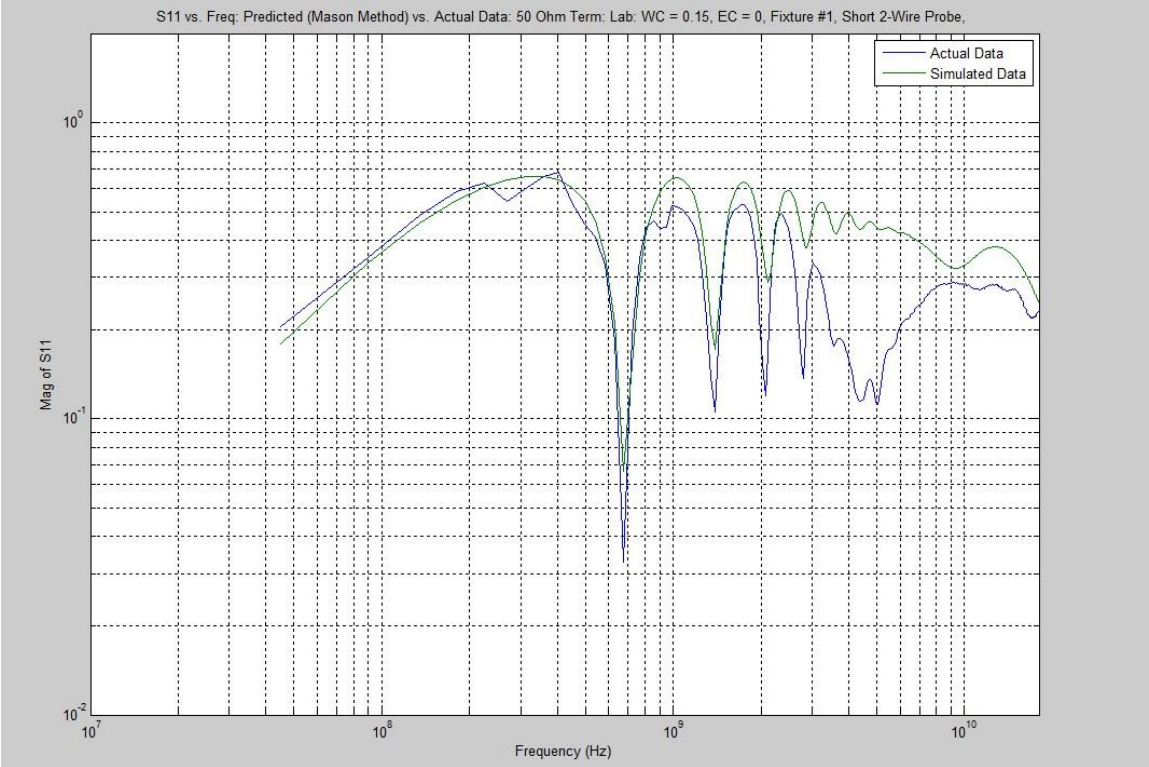


Figure 5.39: Laboratory Validation Method #2: FDR: S11: 50Ω Term.: WC = 0.15, EC = 0 S/m

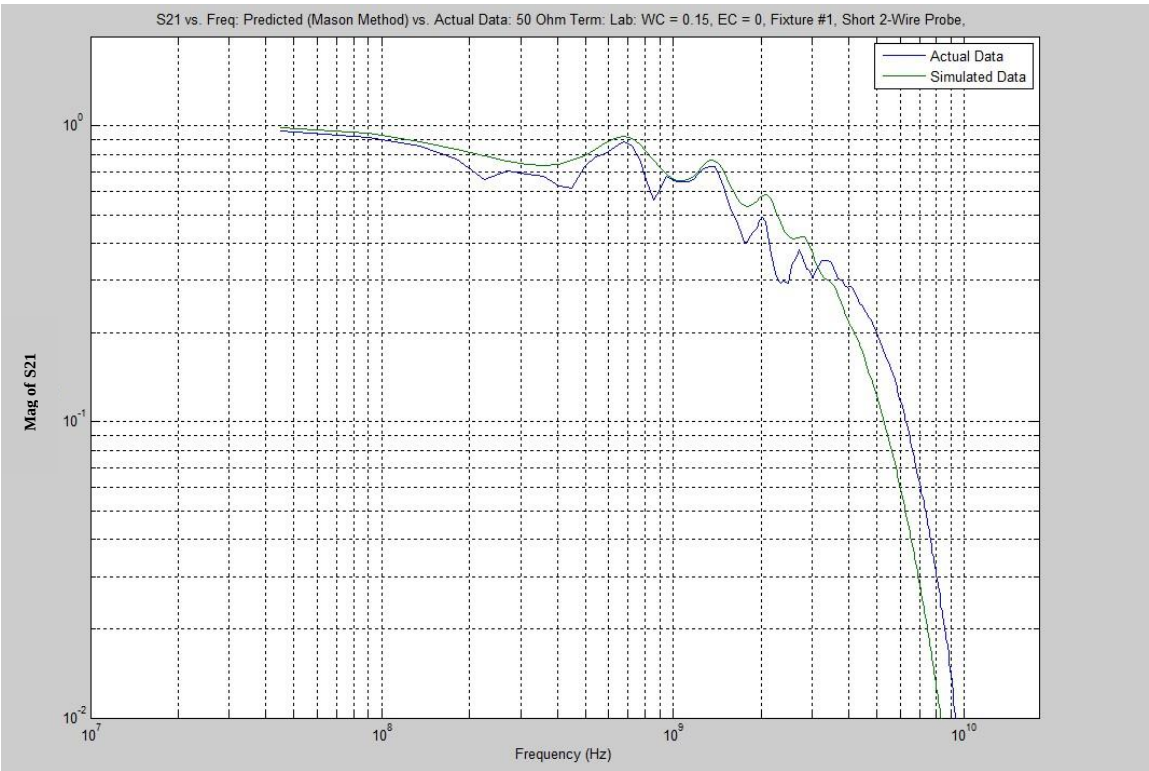


Figure 5.40: Laboratory Validation Method #2: FDT: S21: 50Ω Term.: WC = 0.15, EC = 0 S/m

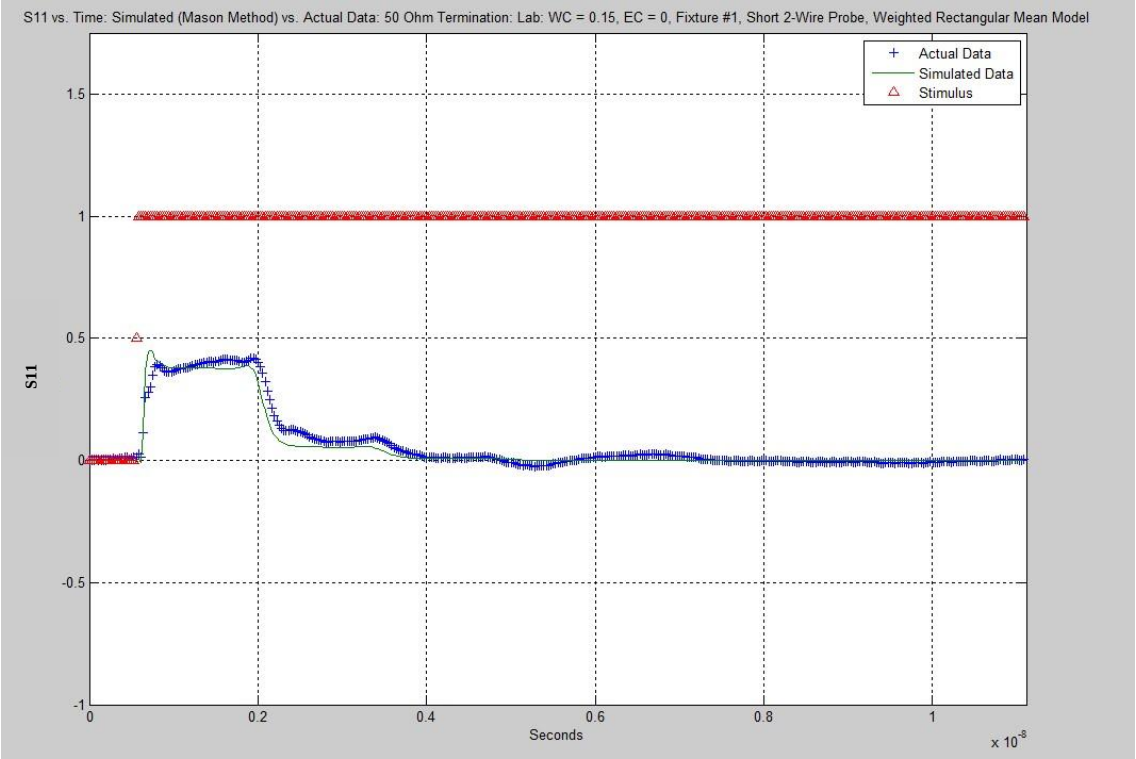


Figure 5.41: Laboratory Validation Method #2: TDR: S11: 50Ω Term.: WC = 0.15, EC = 0 S/m

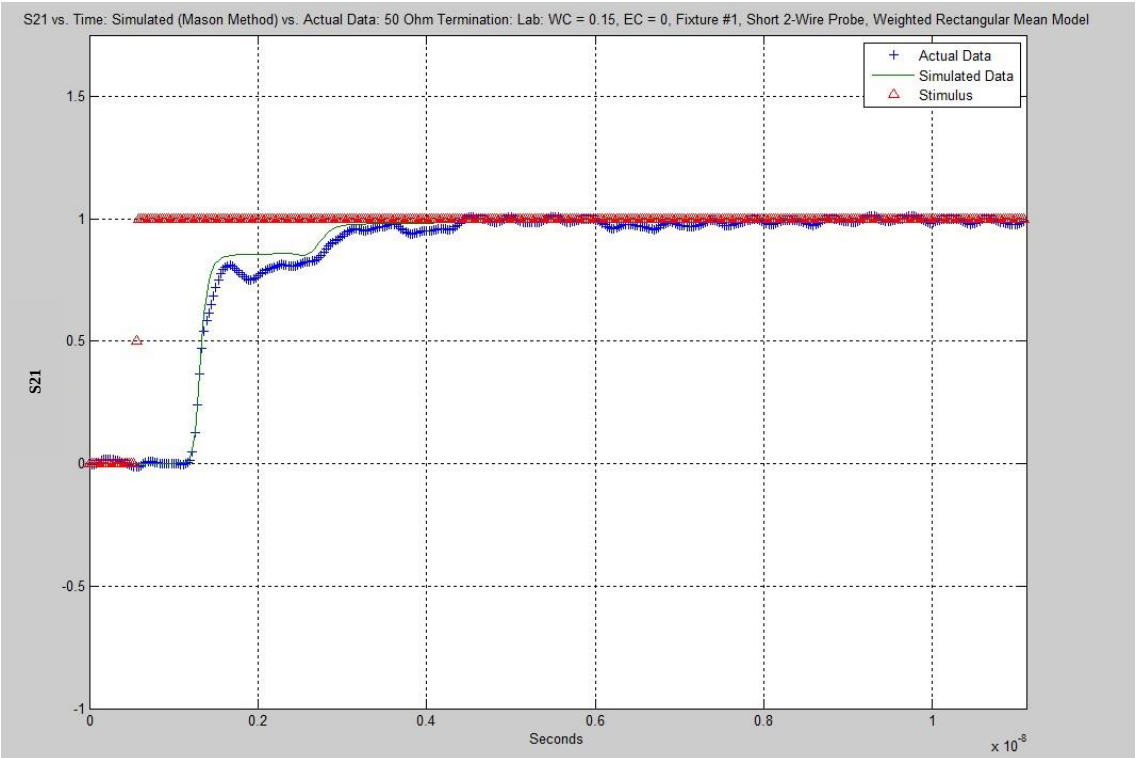


Figure 5.42: Laboratory Validation Method #2: TDT: S21: 50Ω Term.: WC = 0.15, EC = 0 S/m

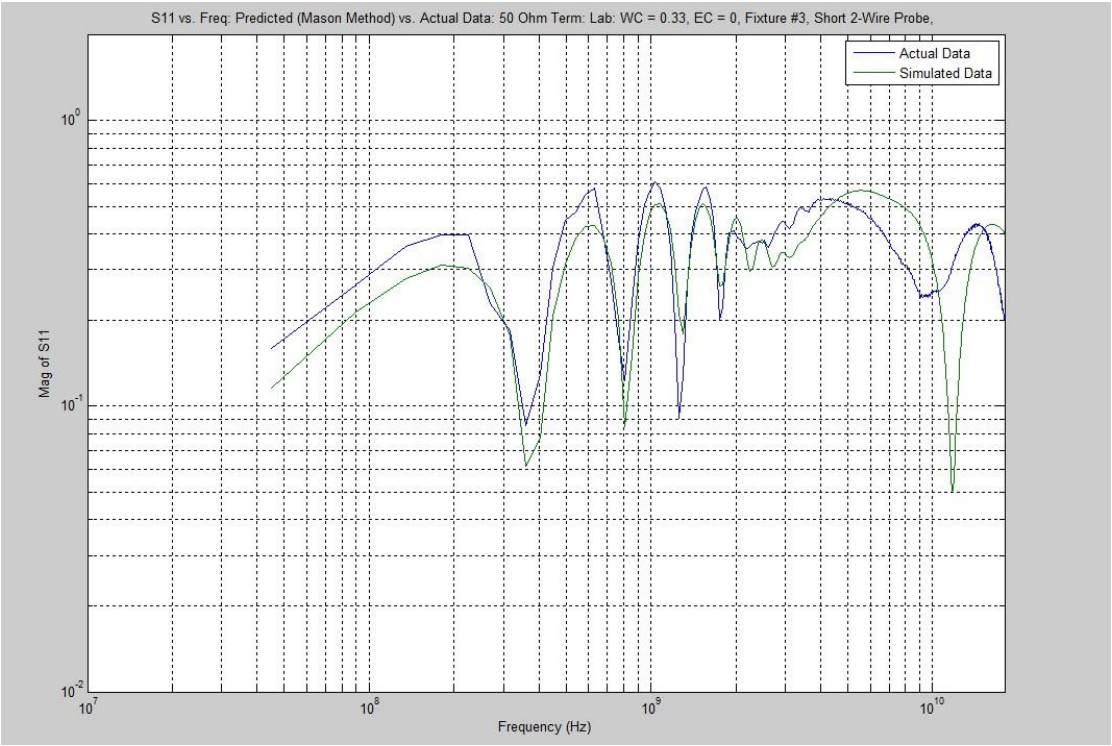


Figure 5.43: Laboratory Validation Method #2: FDR: S11: 50Ω Term.: WC = 0.33, EC = 0 S/m

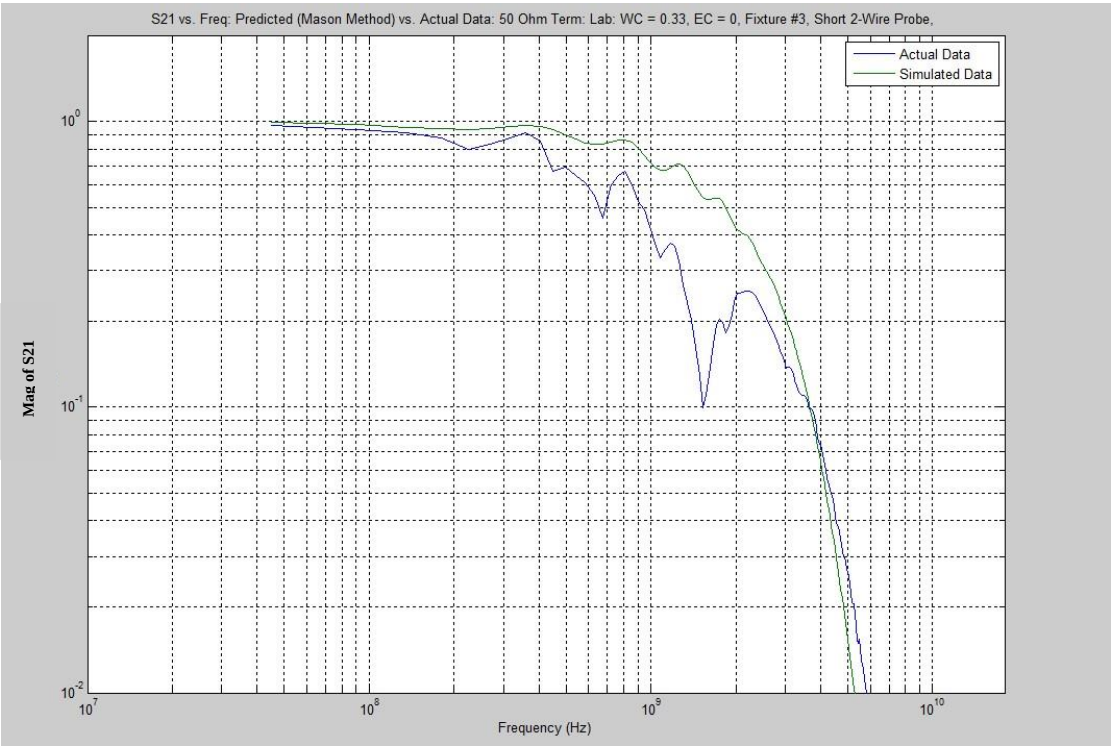


Figure 5.44: Laboratory Validation Method #2: FDT: S21: 50Ω Term.: WC = 0.33, EC = 0 S/m

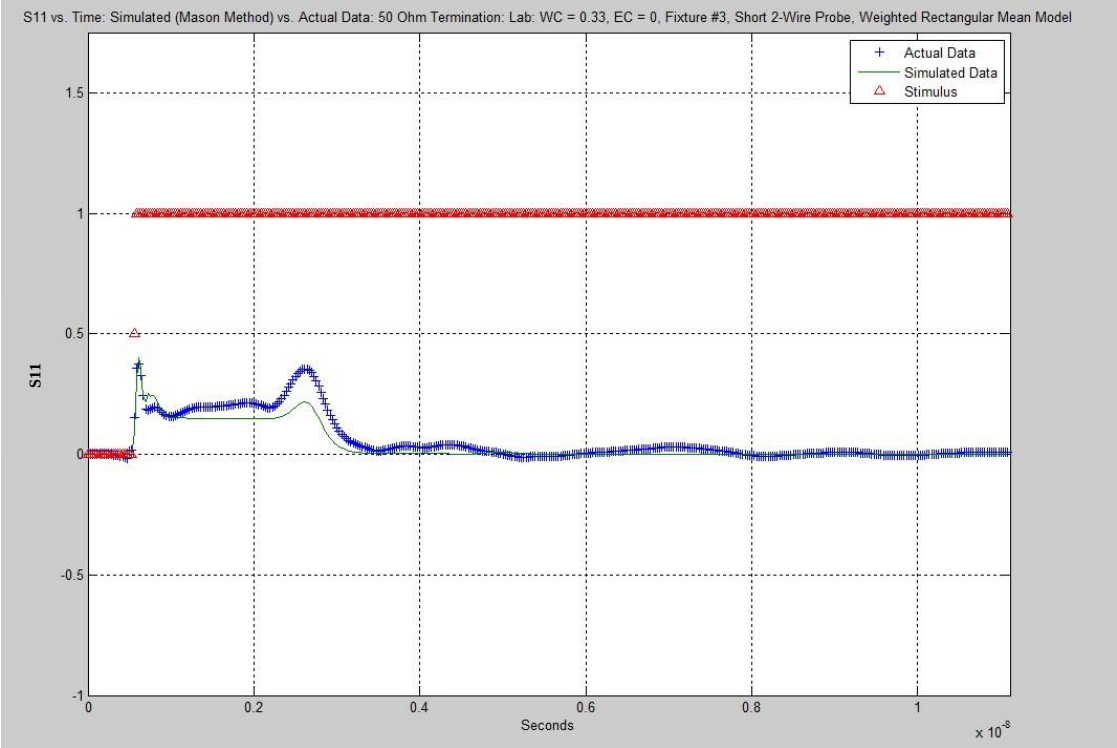


Figure 5.45: Laboratory Validation Method #2: TDR: S11: 50Ω Term.: WC = 0.33, EC = 0 S/m

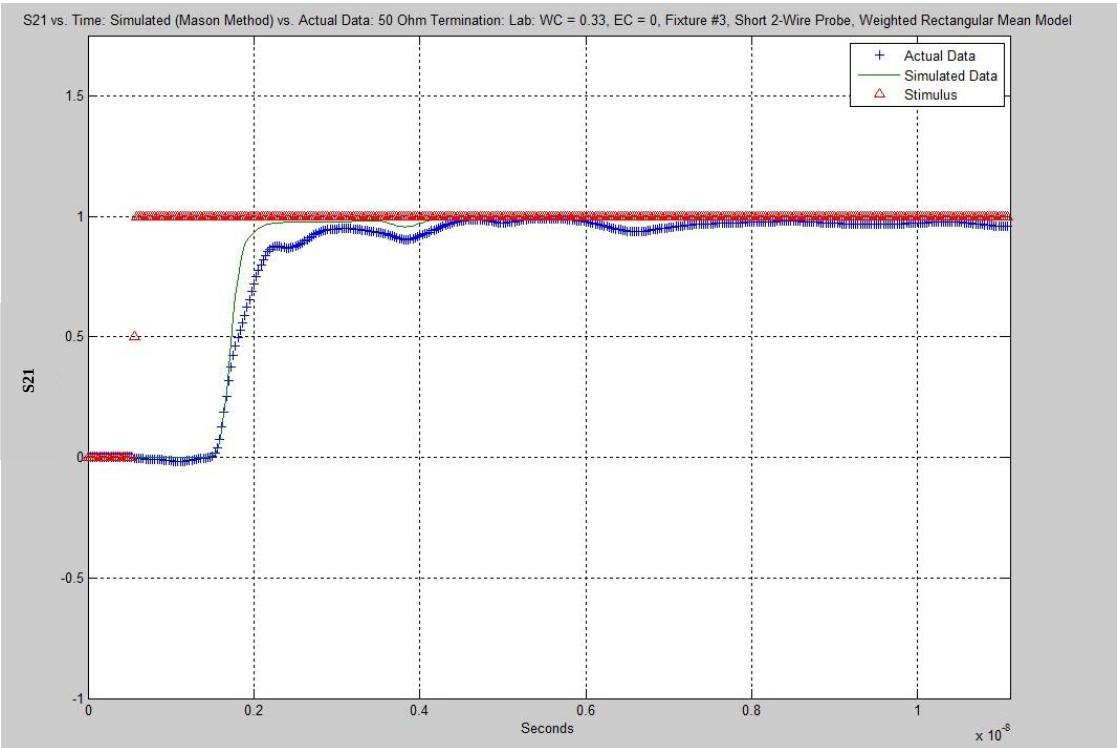


Figure 5.46: Laboratory Validation Method #2: TDT: S21: 50Ω Term.: WC = 0.33, EC = 0 S/m

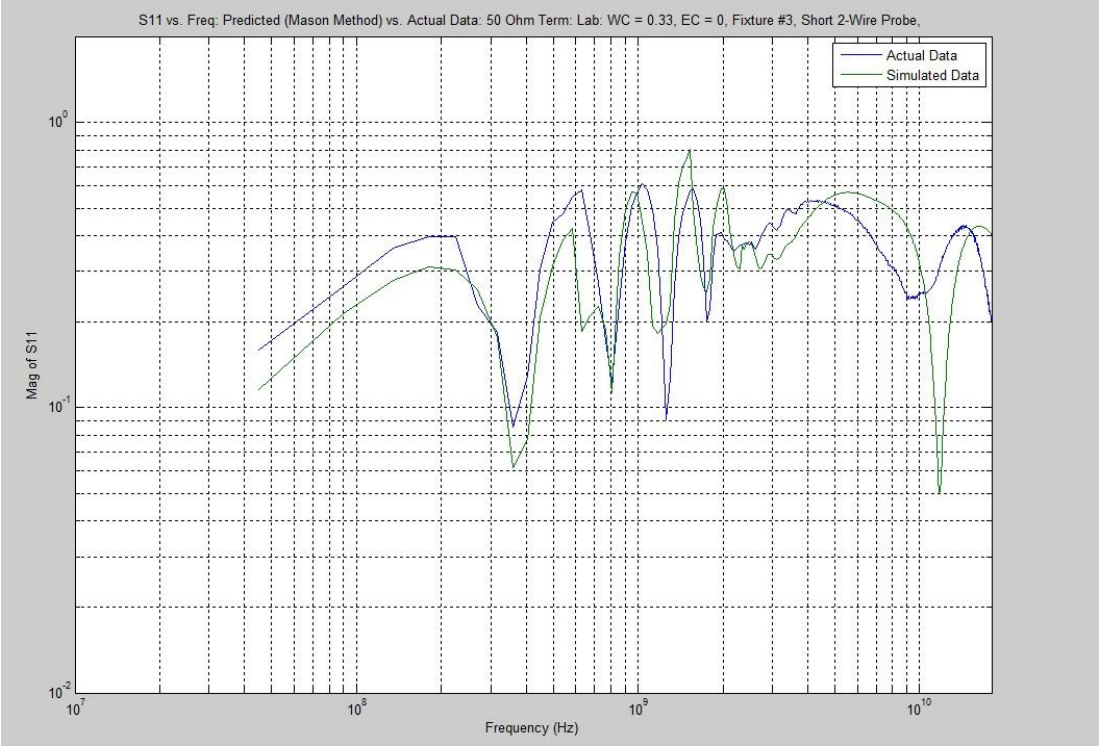


Figure 5.47: Laboratory Validation Method #2: FDR: S11: 50Ω Term.: WC = 0.33, EC = 0 S/m: Extra Probe Resonance Modeled

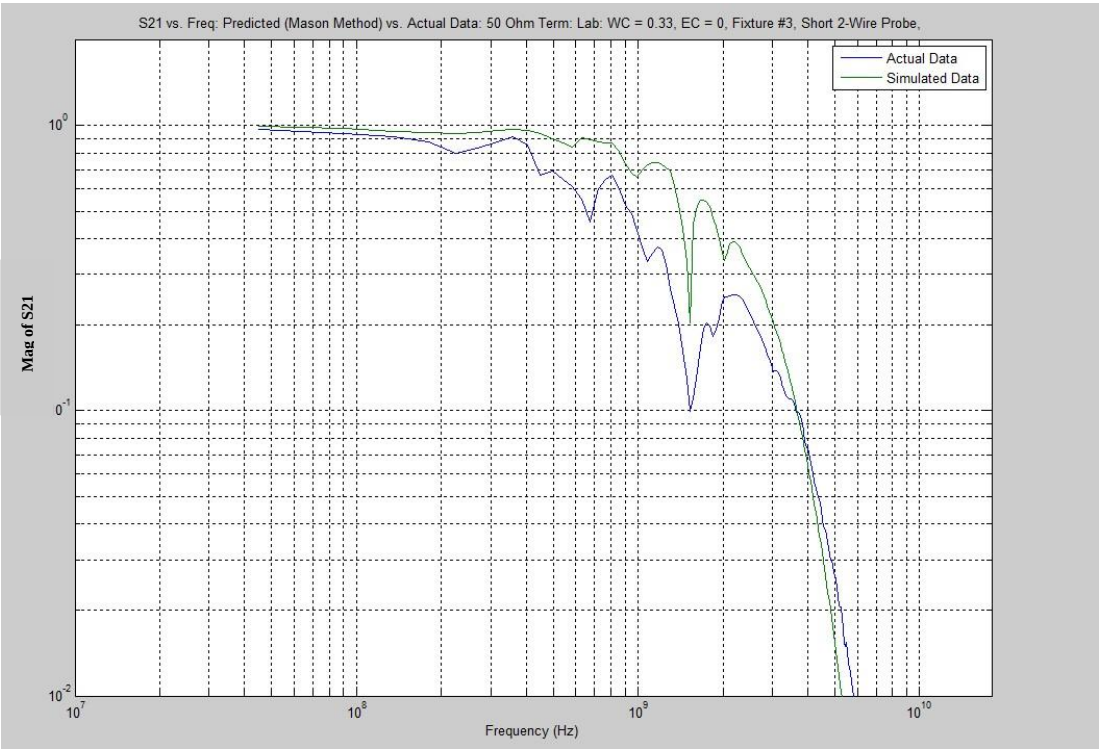


Figure 5.48: Laboratory Validation Method #2: FDT: S21: 50Ω Term.: WC = 0.33, EC = 0 S/m: Extra Probe Resonance Modeled

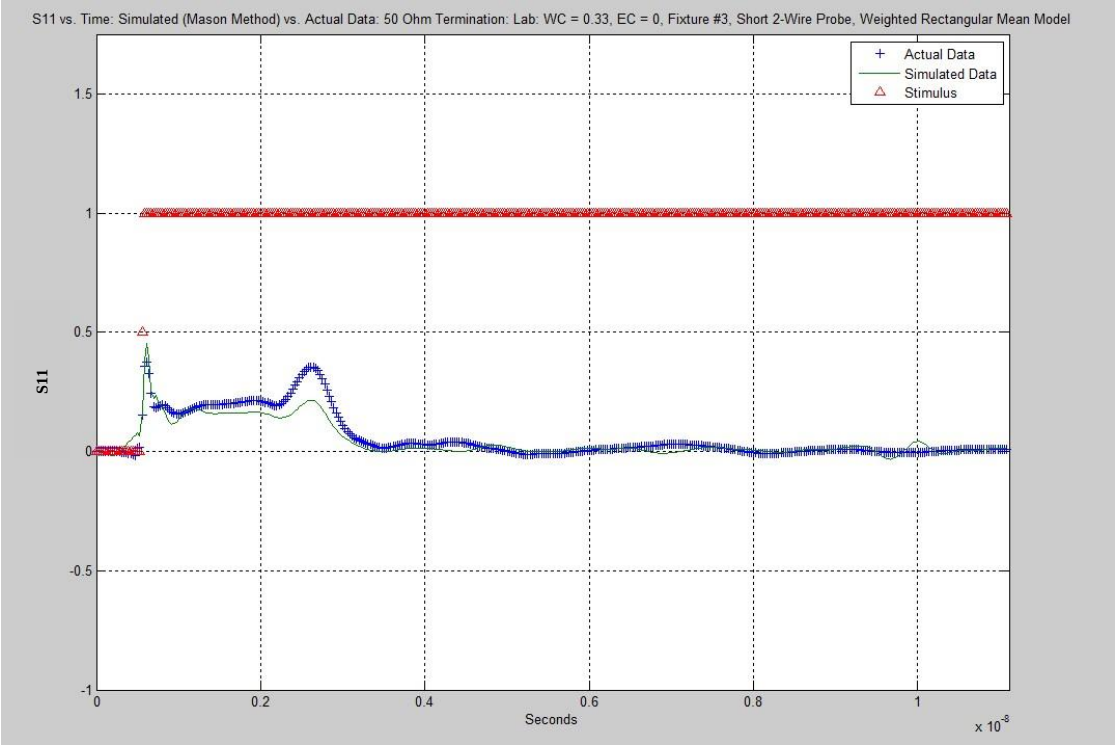


Figure 5.49: Laboratory Validation Method #2: TDR: S11: 50Ω Term.: WC = 0.33, EC = 0 S/m: Extra Probe Resonance Modeled

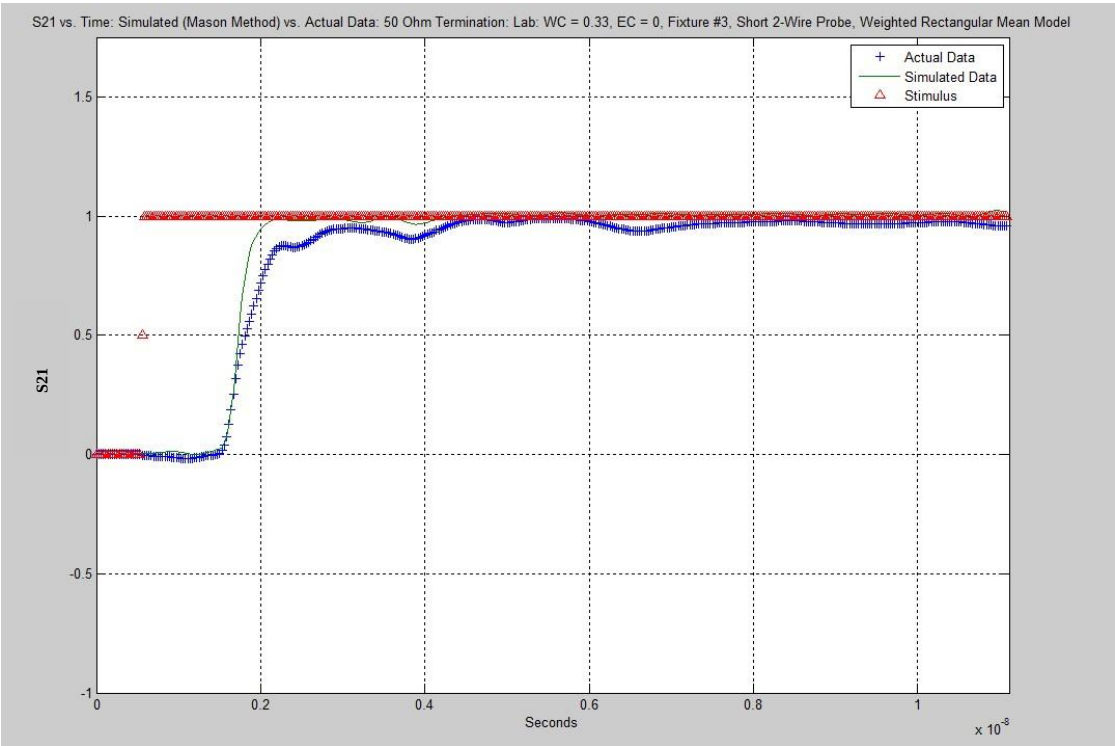


Figure 5.50: Laboratory Validation Method #2: TDT: S21: 50Ω Term.: WC = 0.33, EC = 0 S/m: Extra Probe Resonance Modeled

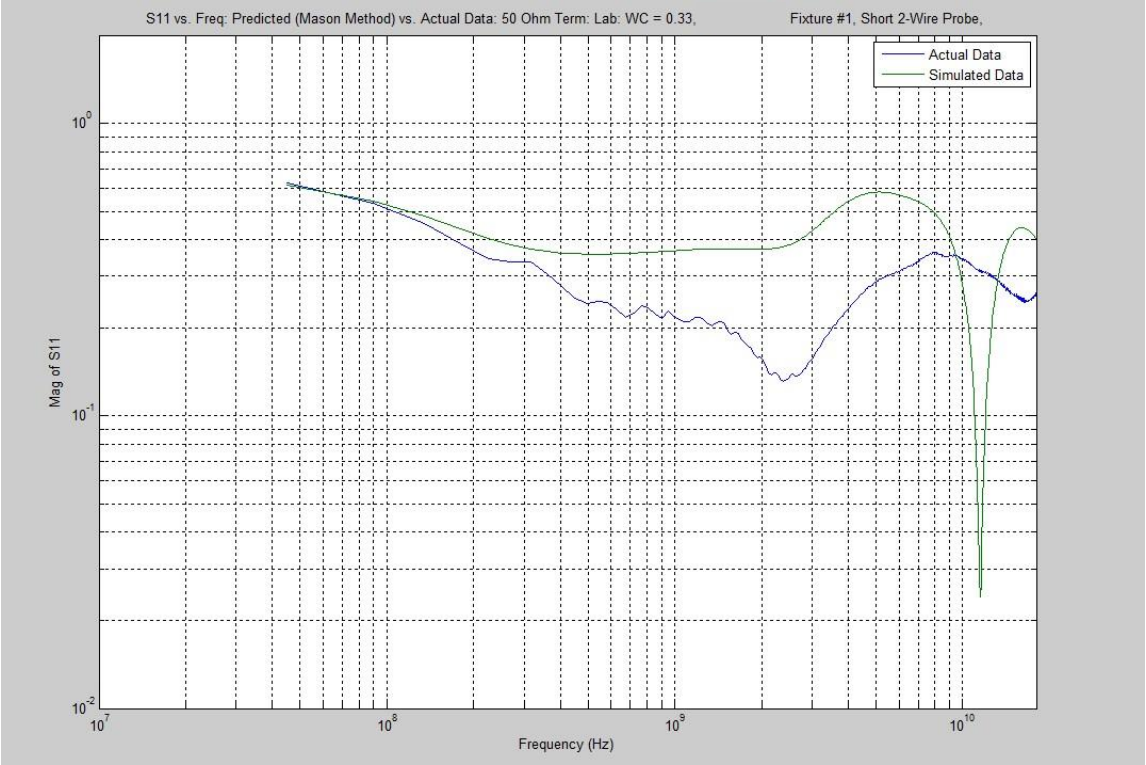


Figure 5.51: Laboratory Validation Method #2: FDR: S11: 50Ω Term.: WC = 0.33, EC = 1.2 S/m

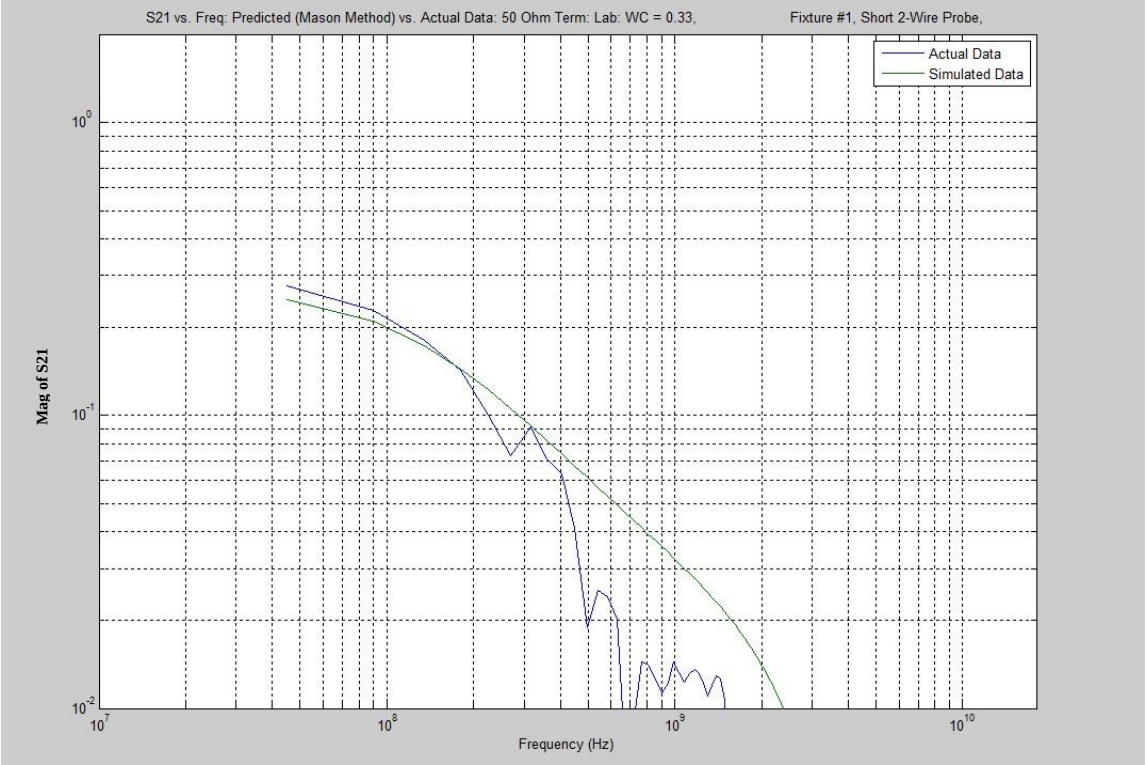


Figure 5.52: Laboratory Validation Method #2: FDT: S21: 50Ω Term.: WC = 0.33, EC = 1.2 S/m

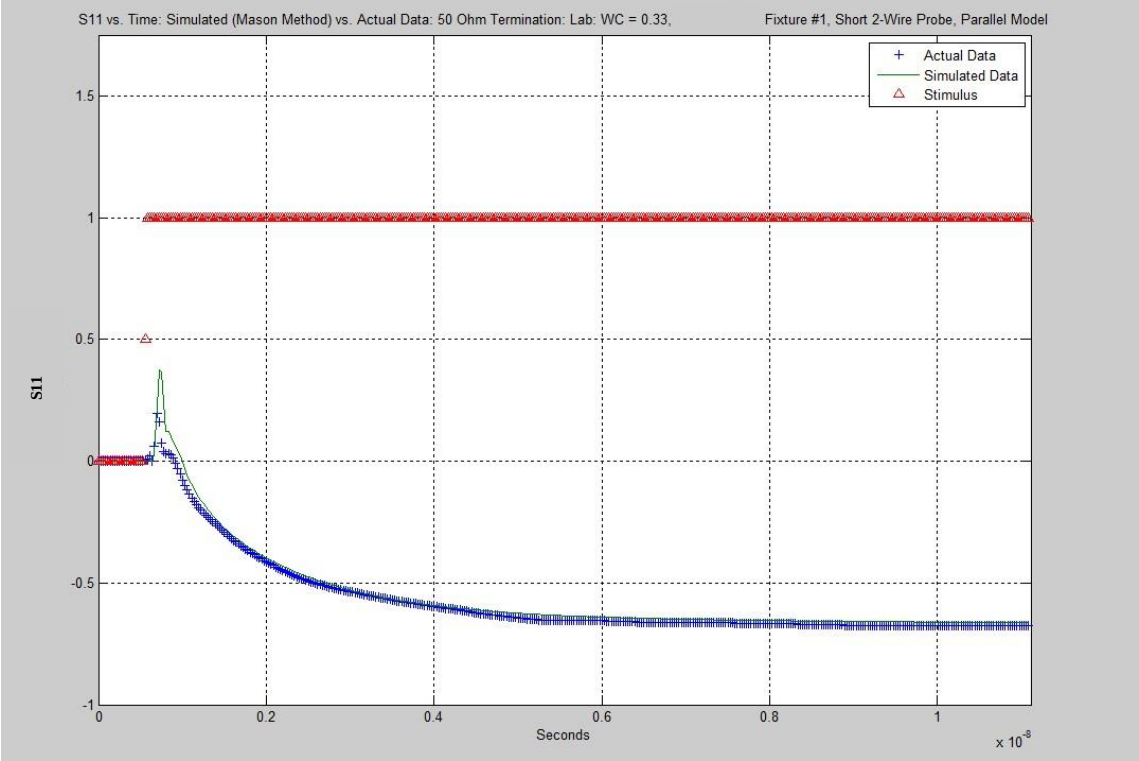


Figure 5.53: Laboratory Validation Method #2: TDR: S11: 50Ω Term.: WC = 0.33, EC = 1.2 S/m

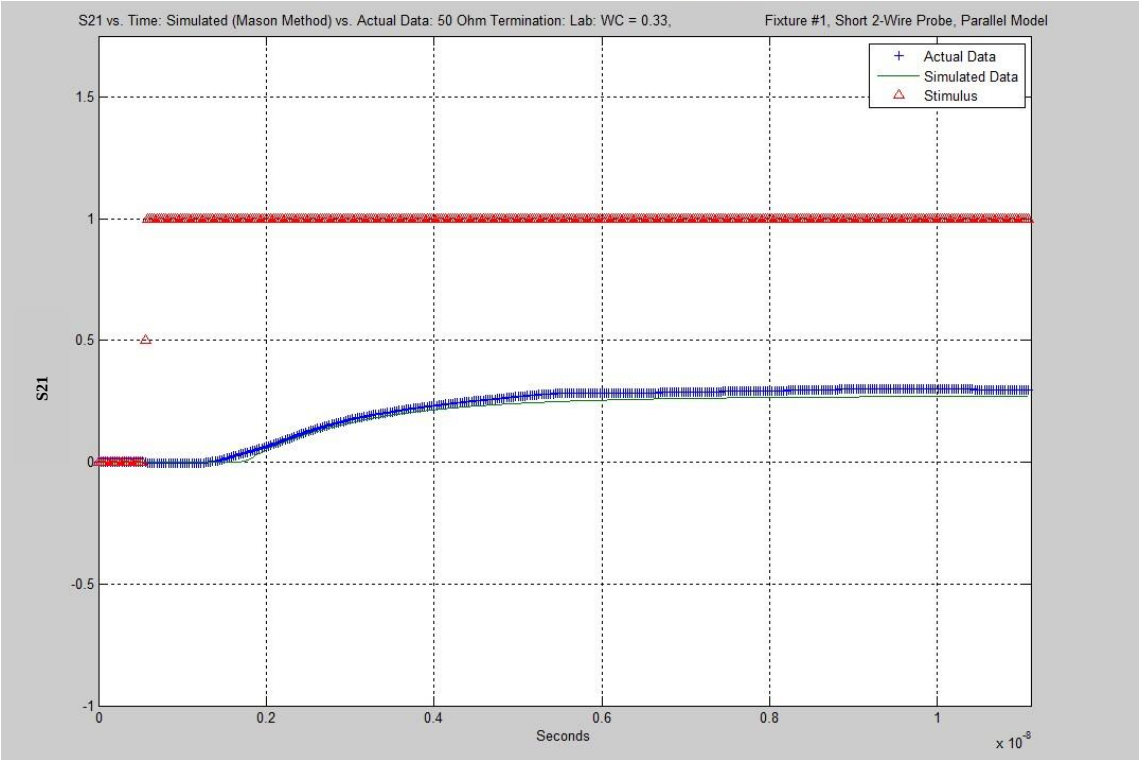


Figure 5.54: Laboratory Validation Method #2: TDT: S21: 50Ω Term.: WC = 0.33, EC = 1.2 S/m

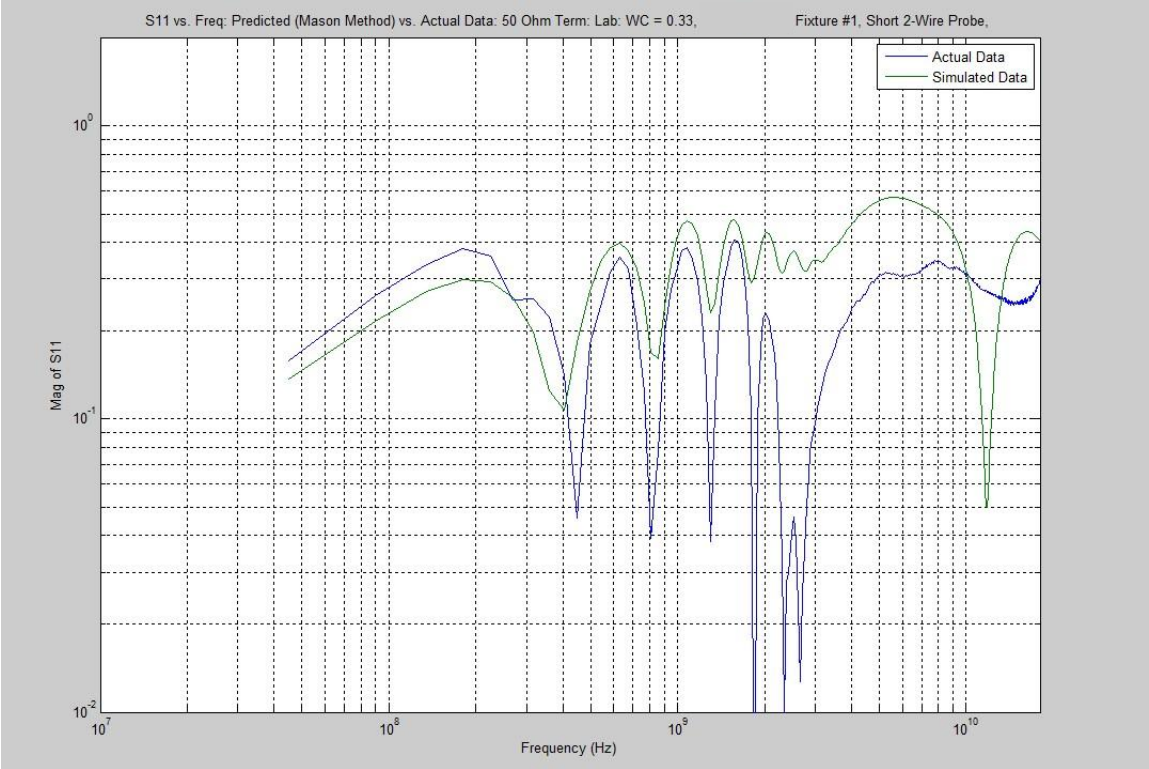


Figure 5.55: Laboratory Validation Method #2: FDR: S11: 50Ω Term.: WC = 0.33, EC = 0.067 S/m

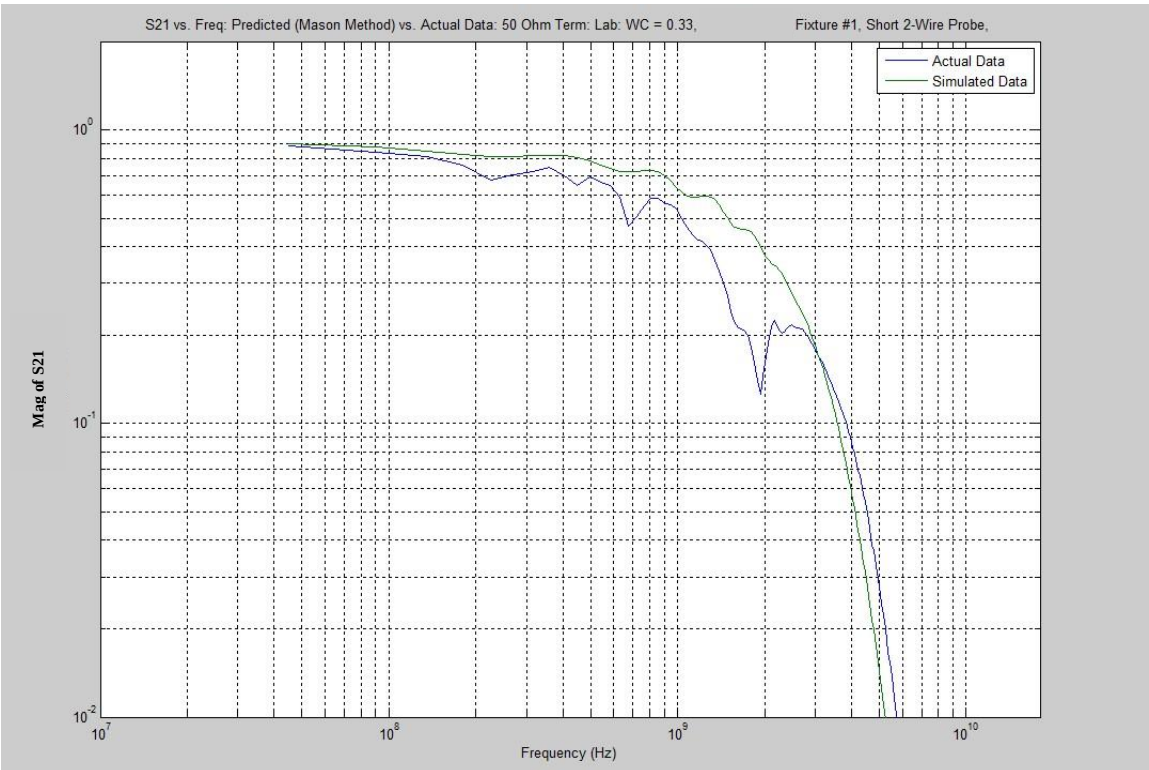


Figure 5.56: Laboratory Validation Method #2: FDT: S21: 50Ω Term.: WC = 0.33, EC = 0.067 S/m

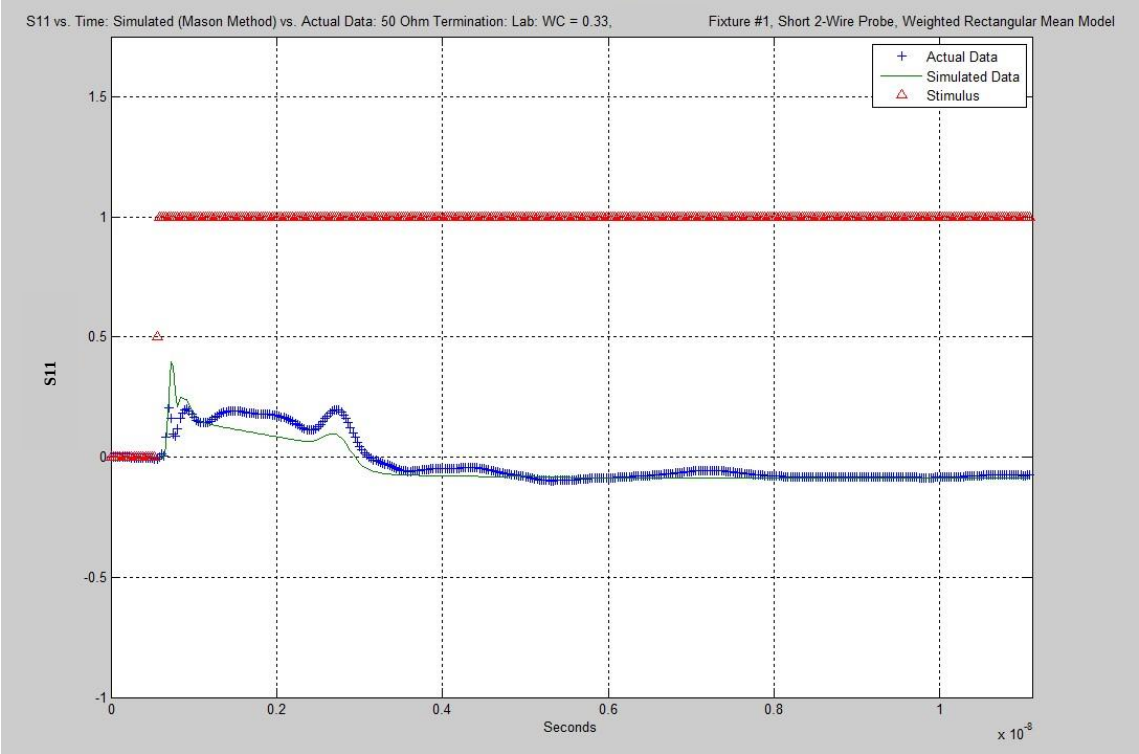


Figure 5.57: Laboratory Validation Method #2: TDR: S11: 50Ω Term.: WC = 0.33, EC = 0.067 S/m

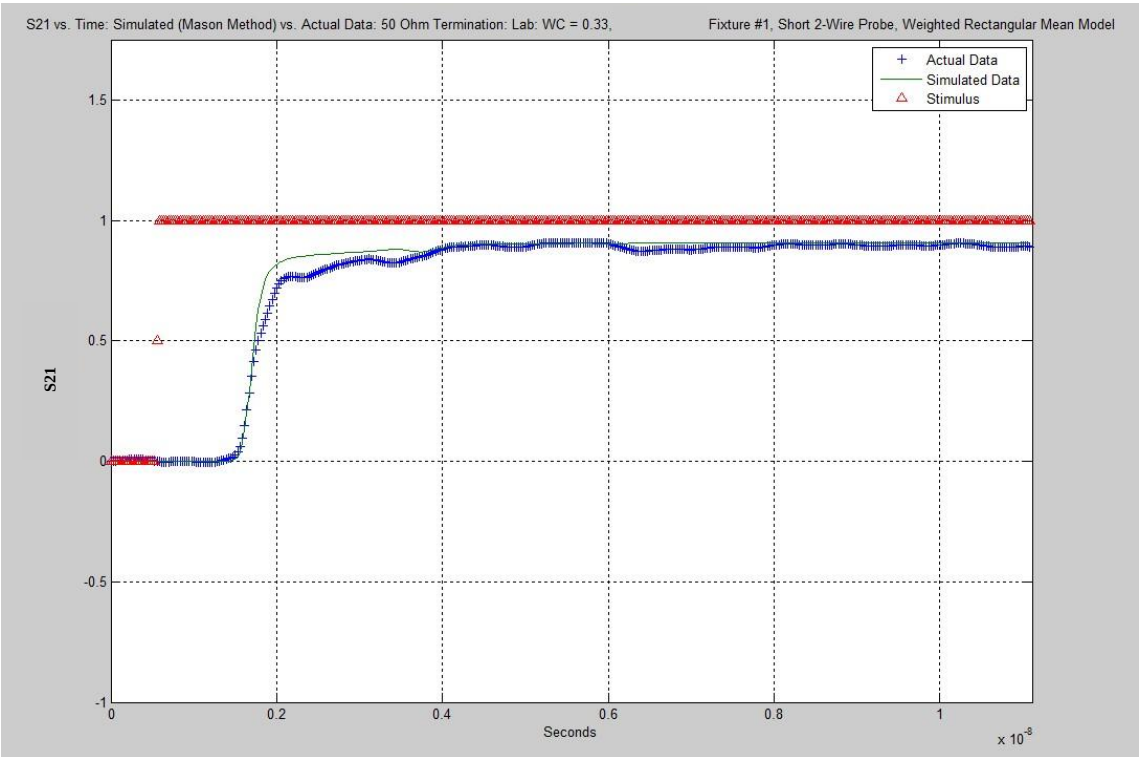


Figure 5.58: Laboratory Validation Method #2: TDT: S21: 50Ω Term.: WC = 0.33, EC = 0.067 S/m

These figures help validate the forward prediction models against several different cases of WC and EC. In addition, figure 5.44 showed a phenomena that appeared to be specific to the fixtures associated with Laboratory Validation Method #2 (the TDT fixtures of figure 4.3). There appears to be a resonance of the probe itself (full wave antenna type resonance in 3D) that results in a null of the transmission S21 and an elevated peak of the reflection S11 terms. Figure 5.48 represents an addition to the forward prediction models to account for this term. The existence of this resonance was validated using 3D finite element method (FEM) simulation software provided by COMSOL Multiphysics. Those results are given in the following figures:

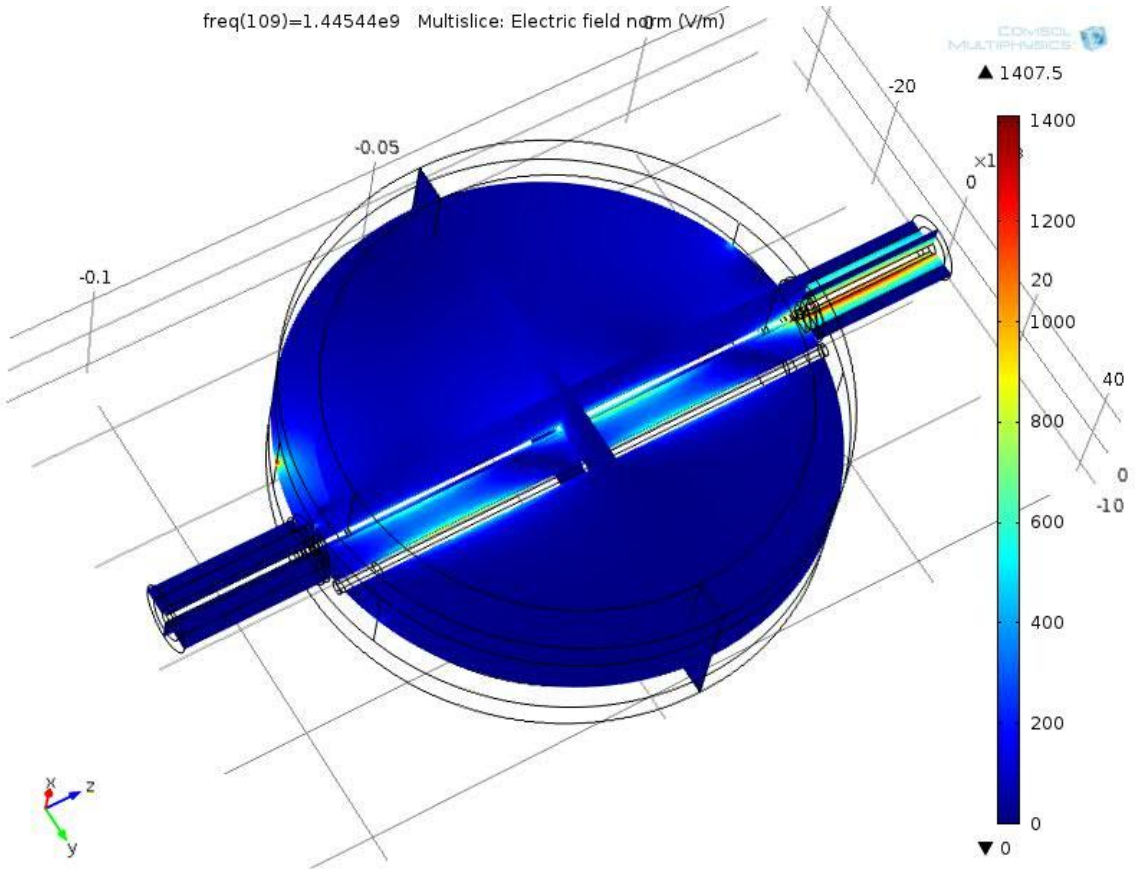


Figure 5.59: Full Wave Resonance of Fixture Two Wire Probe Resulting in Null at Output Port

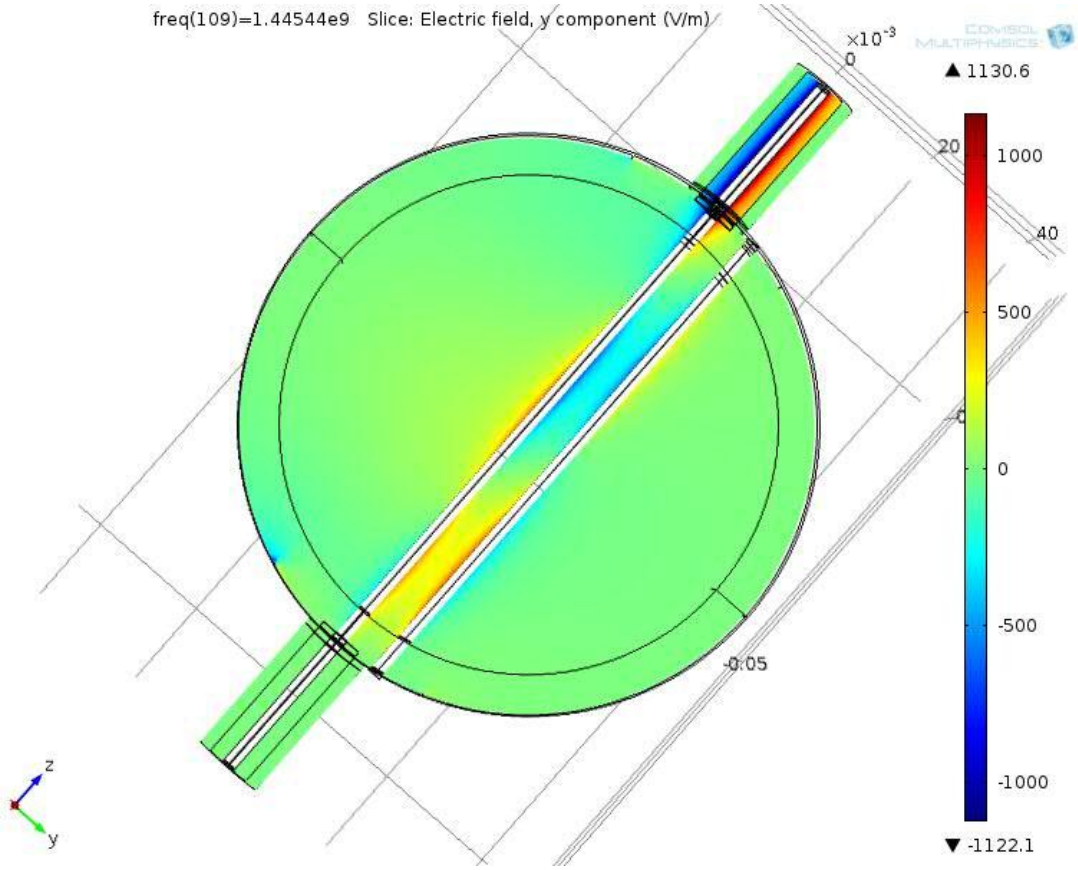


Figure 5.60: Electric Field Ey Term (Between Conductors and Outside of them) Showing also Zone of Influence of Surrounding Media (Very Limited).

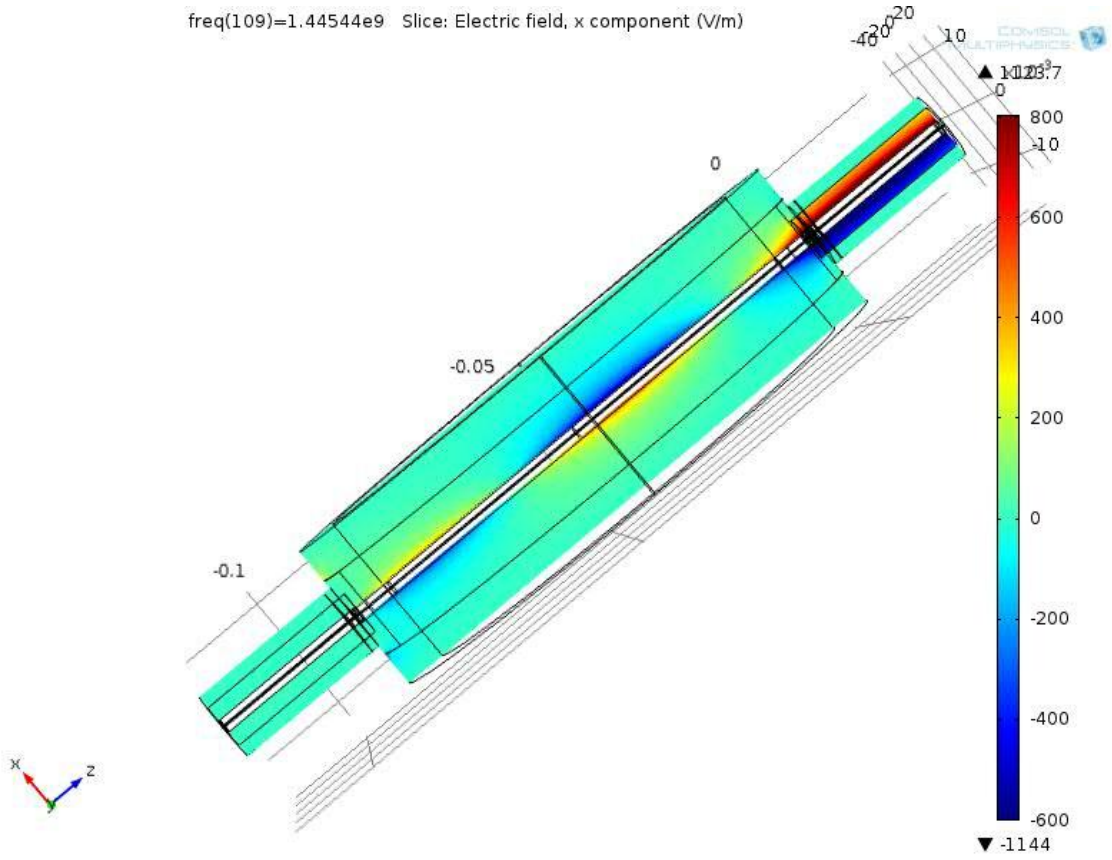


Figure 5.61: Electric Field Ex Term (Orthogonal to Plane Between Conductors): Antenna Type Resonance

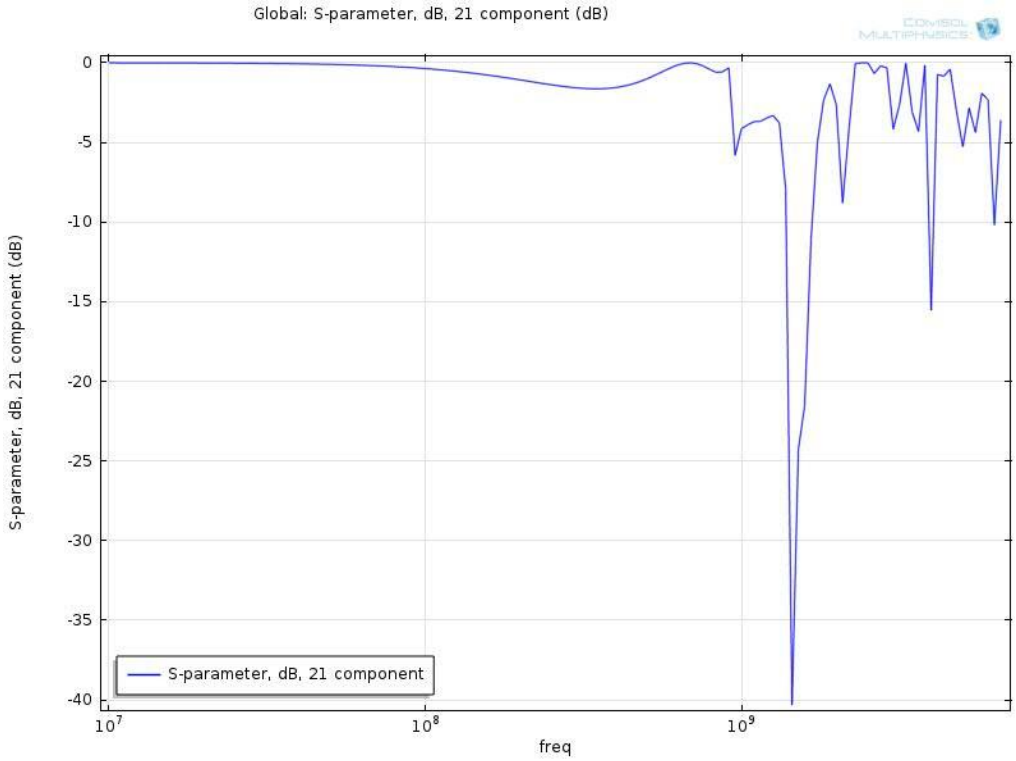


Figure 5.62: S21 vs. Frequency (Fixed Lossless Dielectric Constant of 7) Showing Probe Resonance (Null)

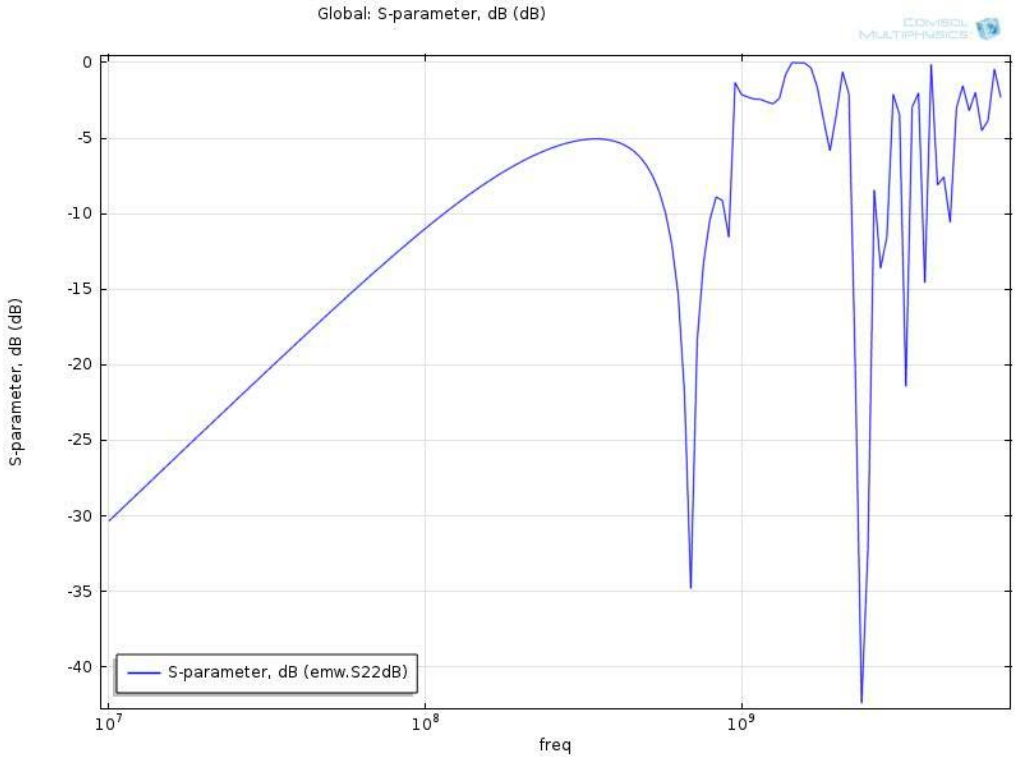


Figure 5.63: S11 vs. Frequency (Fixed Lossless Dielectric Constant of 7) Showing Probe Resonance (Peak in S11)

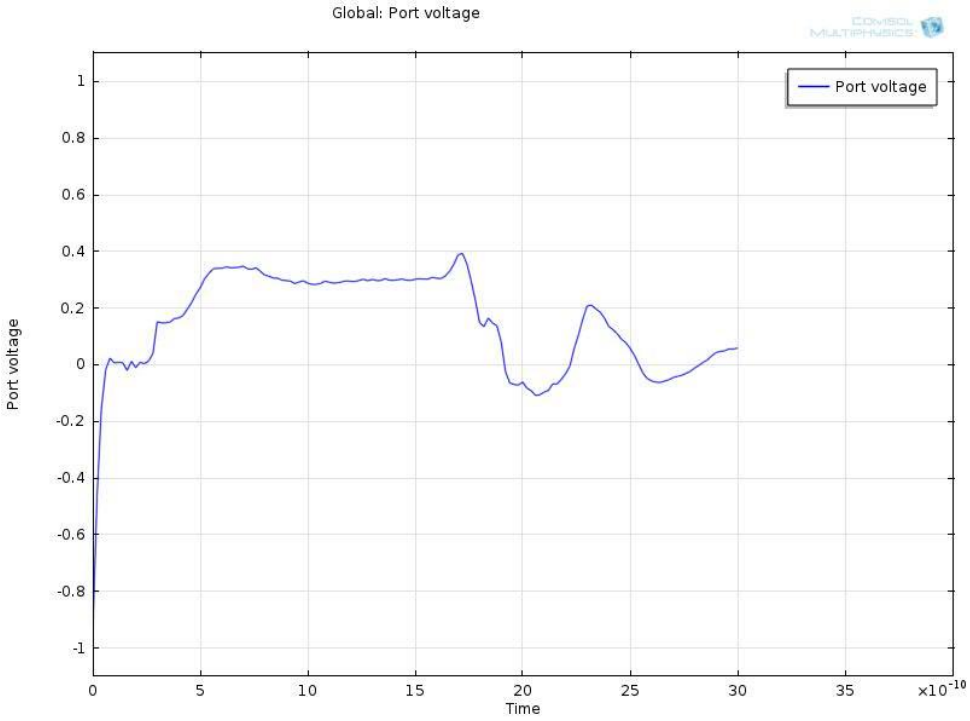


Figure 5.64: TDR Waveform (COMSOL FEM Simulation): 50 Ohm Termination: er = 7 (lossless) but with Probe Resonance (causing some extra ringing).

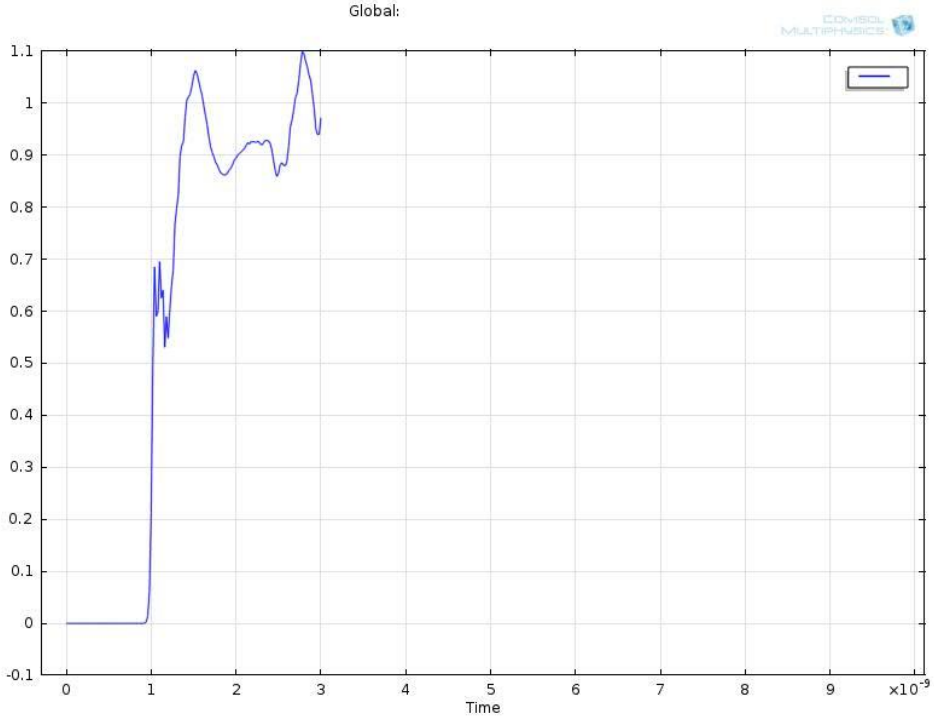


Figure 5.65: TDT Waveform (COMSOL FEM Simulation): 50 Ohm Termination: er = 7 (lossless) but with Probe Resonance (again causing some extra ringing).

The actual resonance is damped partially due to lossy soil in the Lab fixtures for validation method #2 but is still present as seen in figures 5.44 and 5.48.

The conclusions of the testing for Validation Methods #1 and #2 are given as follows:

1.) It is technically feasible for the developed software inverse algorithm to accurately determine bulk electrical conductivity via direct calculation using the low frequency information of S11 and proper probe geometry calibration values.

2.) It is technically feasible for the developed software inverse algorithm to accurately determine water content at low levels of electrical conductivity using lookup tables based on the frequency location of peaks in the effective dominant group delay (derivative of S11 phase with frequency) plots vs. frequency.

3.) It is not yet fully technically feasible to determine water content accurately with existing broadband low dynamic range TDR hardware when the conductivity is high even with this developed algorithm. To address this requires a higher dynamic range and higher bandwidth hardware approach which extends the bandwidth of the probe and measurement system up to at least 10 GHz by eliminating the cable and improving the probe and interface design. In addition, the utilizion of both transmission and reflection low noise swept narrowband (high dynamic range) measurements and further optimizing the software algorithm to better model any remaining losses accurately up to 10 GHz are required. The proposed approach is to utilize state of the art technology allowing for cost effective high dynamic range Vector Network Analyzer FDR (S11) and FDT (S21) measurement systems to address these needs. Then it will likely be feasible to determine water content even in high values of electrical conductivity by looking at frequency domain reflection and transmission measurements as well as impedance plots vs. frequency all at medium to high frequencies and using lookup tables and optimization fitting algorithms to determine water content based on the forward prediction models.

4.) Modeling Cascaded changes or profiles of WC vs. position is feasible although there are some limitations due to the potential for uniqueness of solutions violations. The feasibility of the cascaded models will be addressed in more detail in validation method #3 next.

## Validation Method #3: Cascaded Transmission Lines: Laboratory Results:

The focus of validation method #3 was to validate the cascaded transmission line models utilized by the forward prediction models. These included both S-Parameter and T-Parameter based models as described in Appendix B and briefly earlier in this chapter as well. The intent here is to show performance for TDR, TDT, FDR and FDT applications with all three methods of generating cascaded transmission line S-Parameter models as follows:

1.) Nested Construction Method
2.) Mason's Non-Touching Loop Rule
3.) Transmission (T) Parameter Cascade Modeling and Conversions to S-Parameters

The setup utilized was shown in figures 4.4 and 4.5 earlier in the methods section (and again below in figure 5.66) involving a multilayer Test PCBA of several different types of transmission line patterns as described in the methods section.

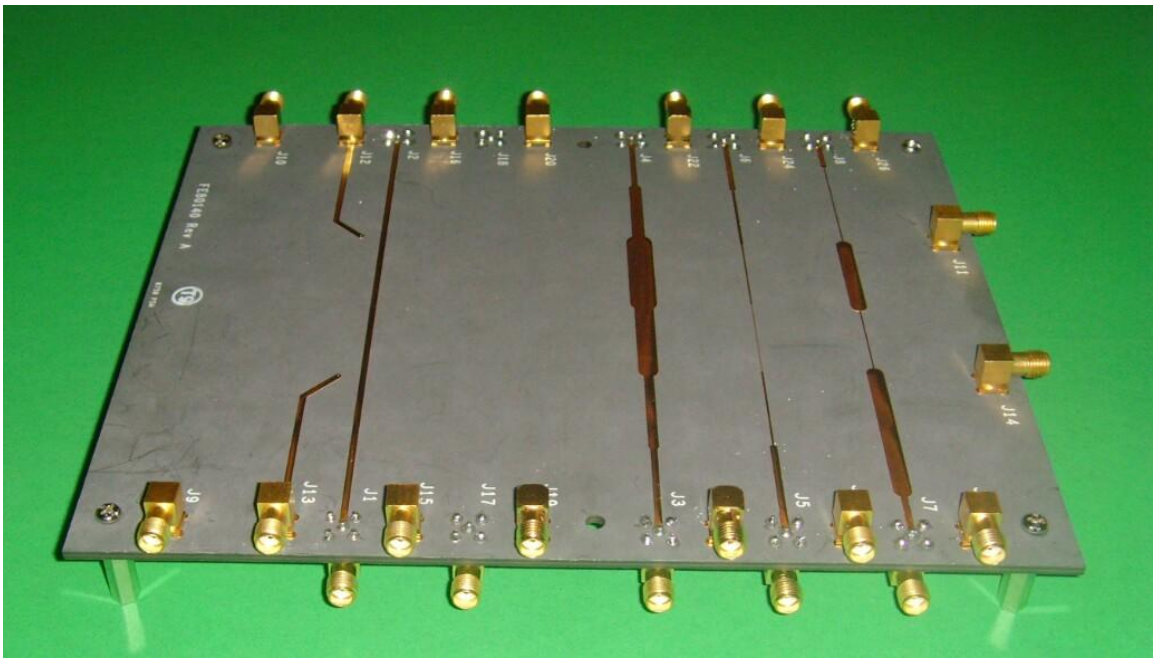


Figure 5.66: Test PCBA for Cascaded Transmission Line Validations of the Forward Prediction Models

**Validation Method #3: Results and Discussion:**

From the test PCBA's the following representative examples of non-uniform transmission lines (all of 6" or 15cm total length) were chosen for presentation in this dissertation to illustrate the various cascaded transmission line modeling techniques. These are listed as follows along with the approximate theoretical (baseband) characteristic impedance steps (as calculated by a program supplied by the Rogers Corporation (MWI.exe) [139] and validated in MATLAB [138] using formulas from the literature [12-13]):

1.) Coplanar Waveguide: 117 Ohms (Figures 4.4 and 4.5) (Note: Actual Measured = 111 Ohms)
2.) Microstrip: High Impedance Steps: 50, 91, 133, 100, 75, 50 Ohms (Figures 4.4 and 4.5)
3.) Stripline: Low Impedance Steps: 50, 37, 19, 12.5, 25, 50 Ohms (Figure 4.5)
4.) Microstrip: Alternating Low and High Impedance Steps: 50, 25, 100, 25, 100, 50 Ohms (Figures 4.4 and 4.5)

In all cases there are comparisons of the three cascaded transmission line modeling methods (Nested Construction, Mason's Non-Touching Loop Rule and Transmission (T) Parameters). Both Time Domain (TDR, TDT) and Frequency Domain (FDR, FDT) plots are given. These results are presented in the next several figures:

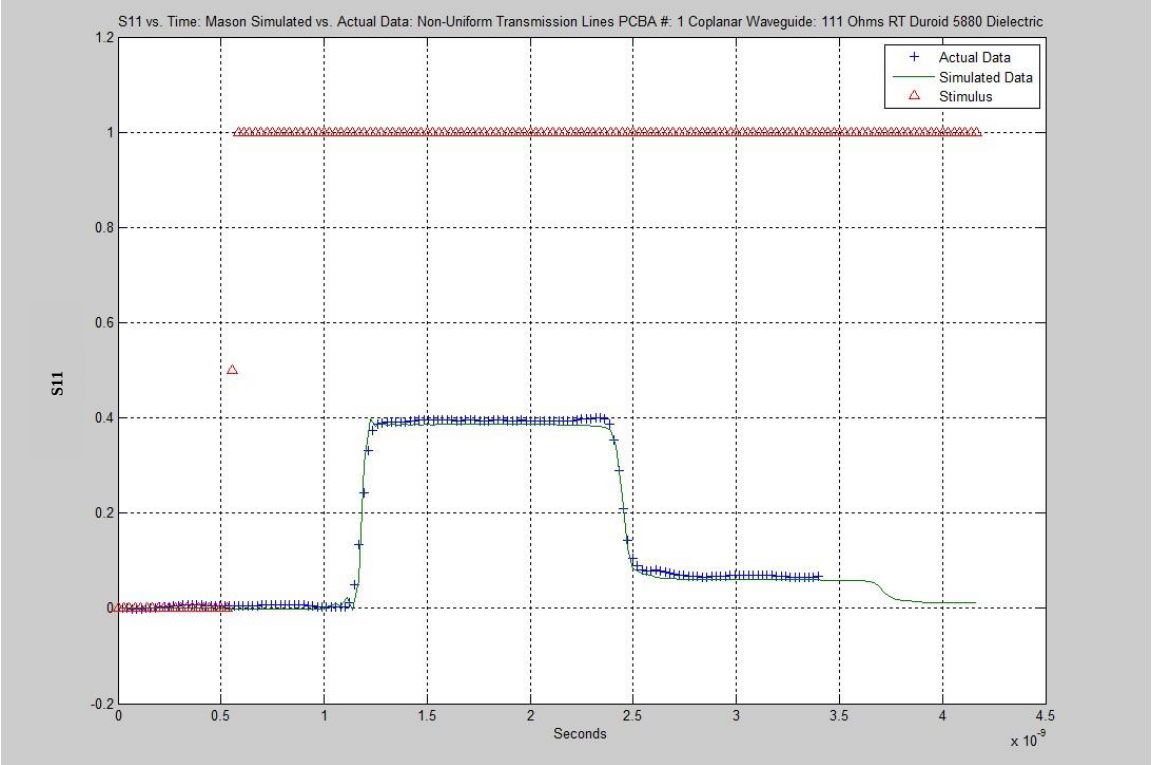


Figure 5.67: Coplanar Waveguide TDR: Simulated (Mason Method) vs. Actual

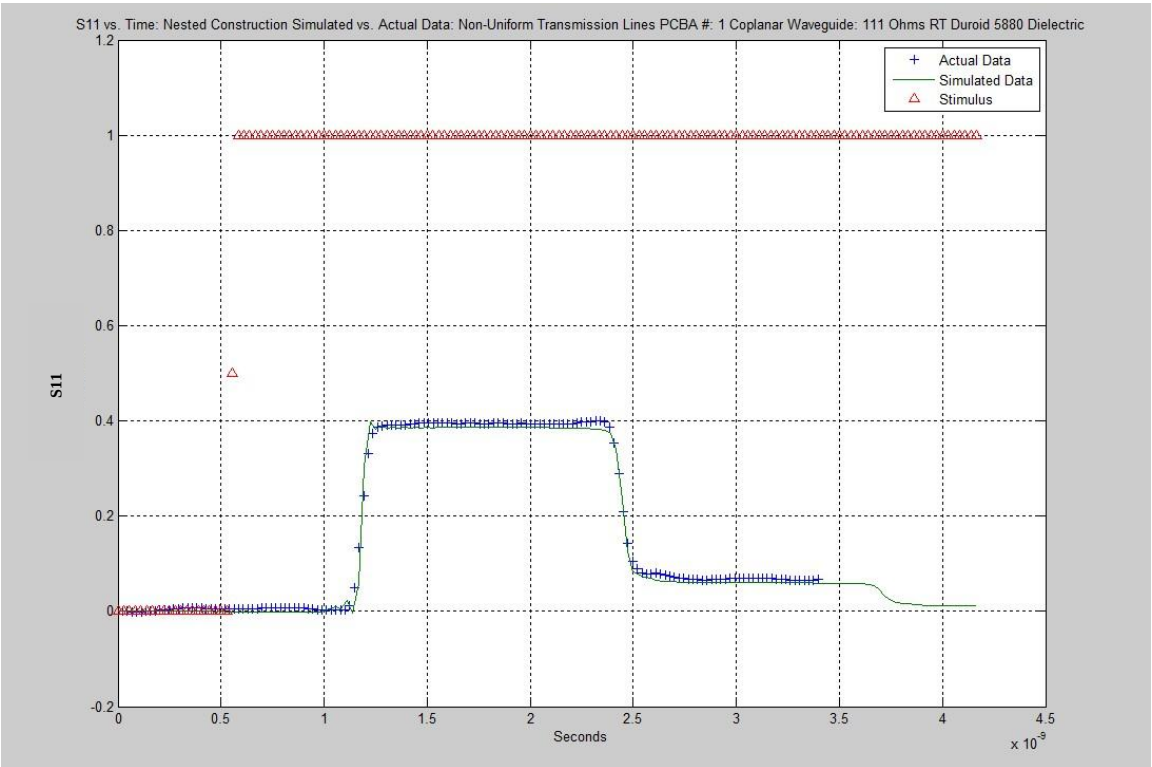


Figure 5.68: Coplanar Waveguide TDR: Simulated (Nested Construction Method) vs. Actual

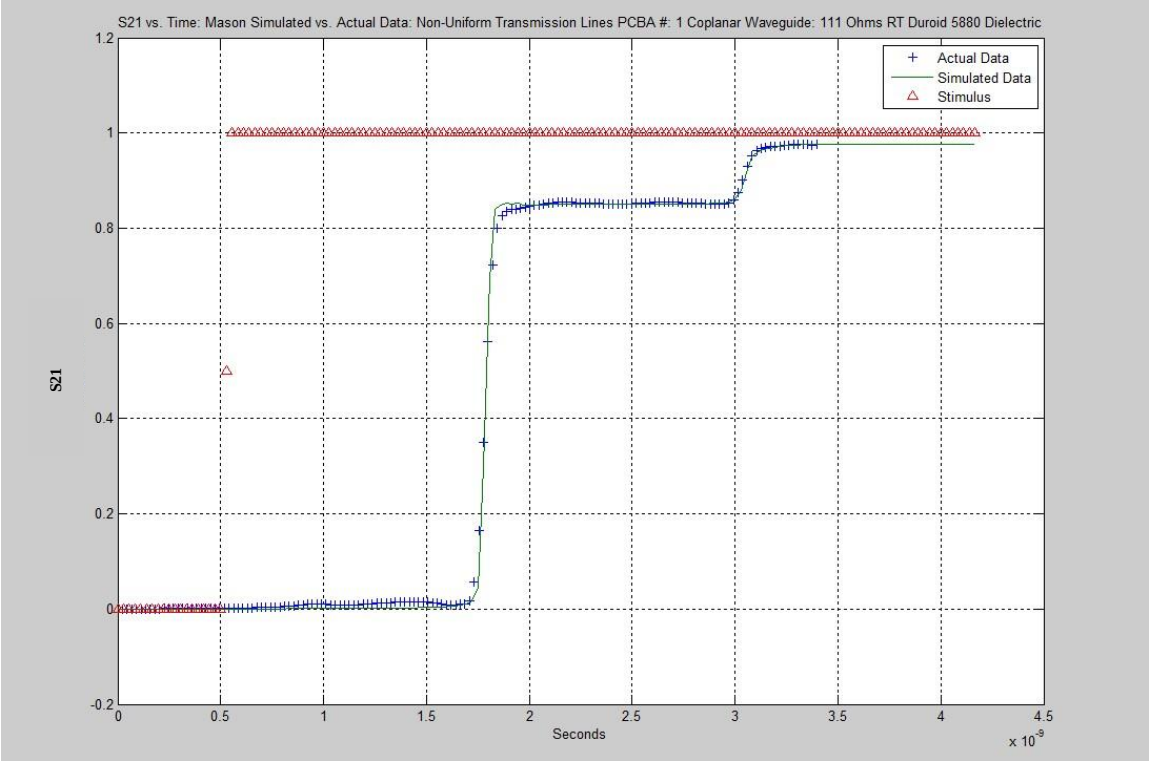


Figure 5.69: Coplanar Waveguide TDT: Simulated (Mason Method) vs. Actual

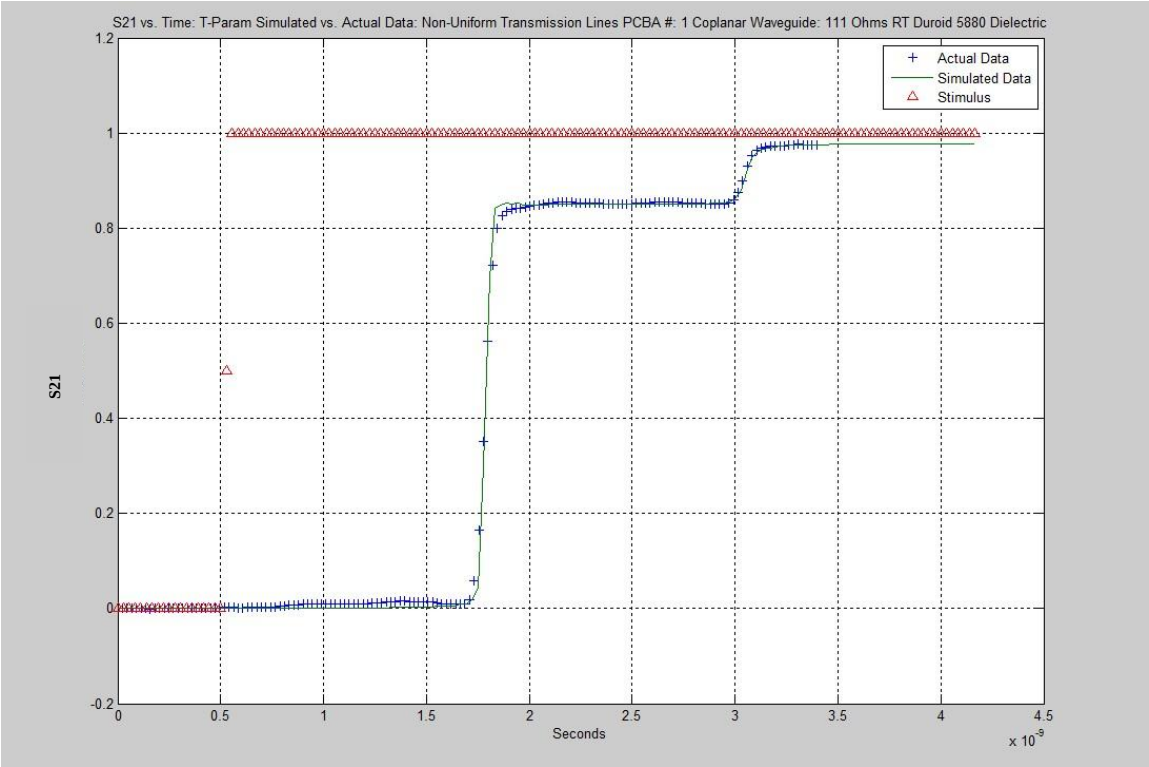


Figure 5.70: Coplanar Waveguide TDT: Simulated (T-Parameter Method) vs. Actual

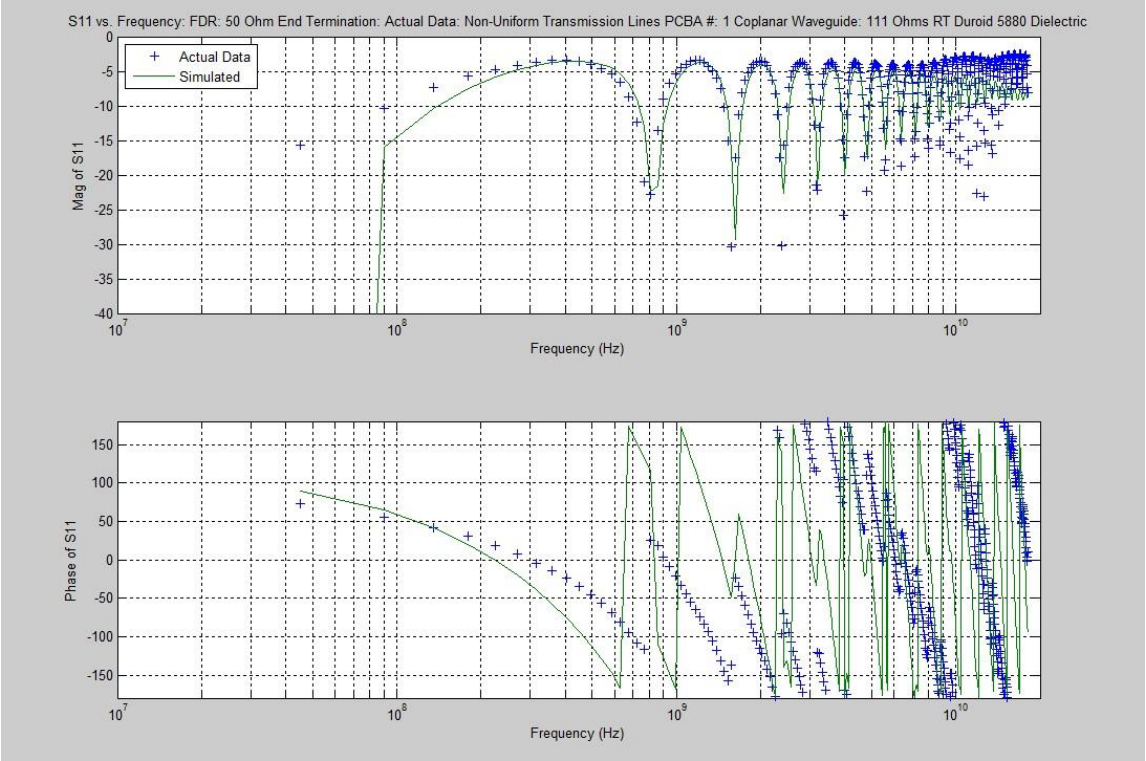


Figure 5.71: Coplanar Waveguide FDR: S11: Simulated (Mason Method) vs. Actual

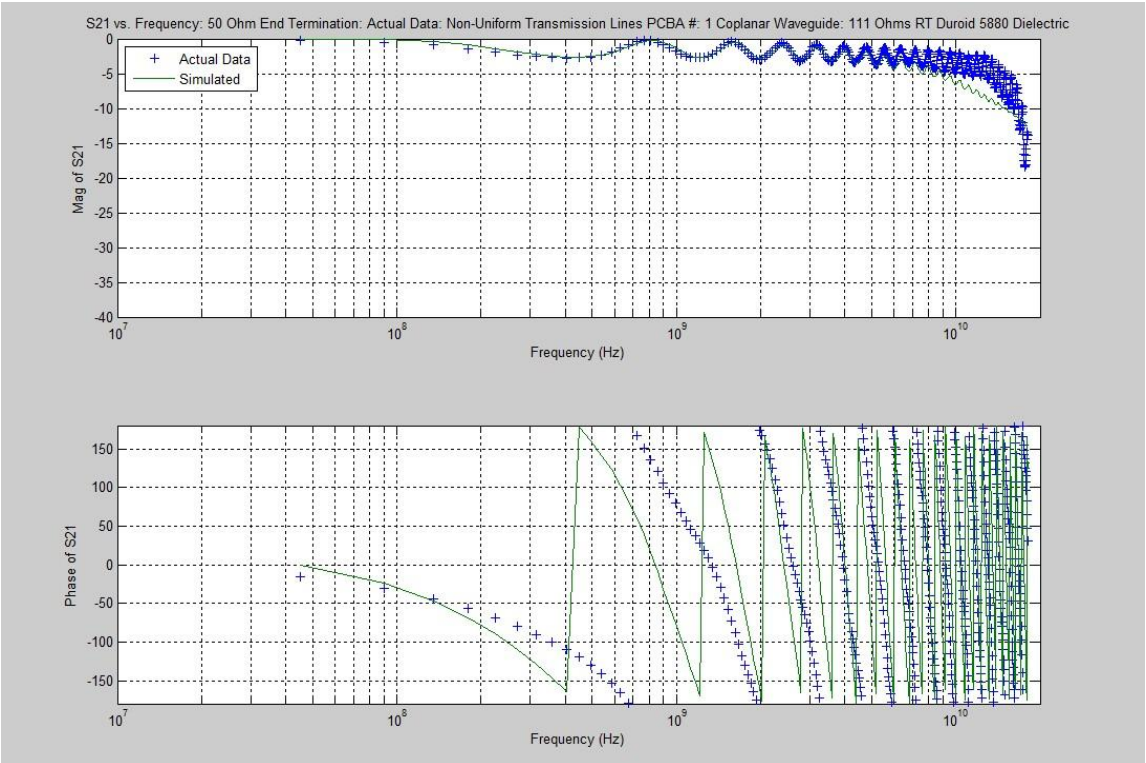


Figure 5.72: Coplanar Waveguide FDT: S21: Simulated (Mason Method) vs. Actual

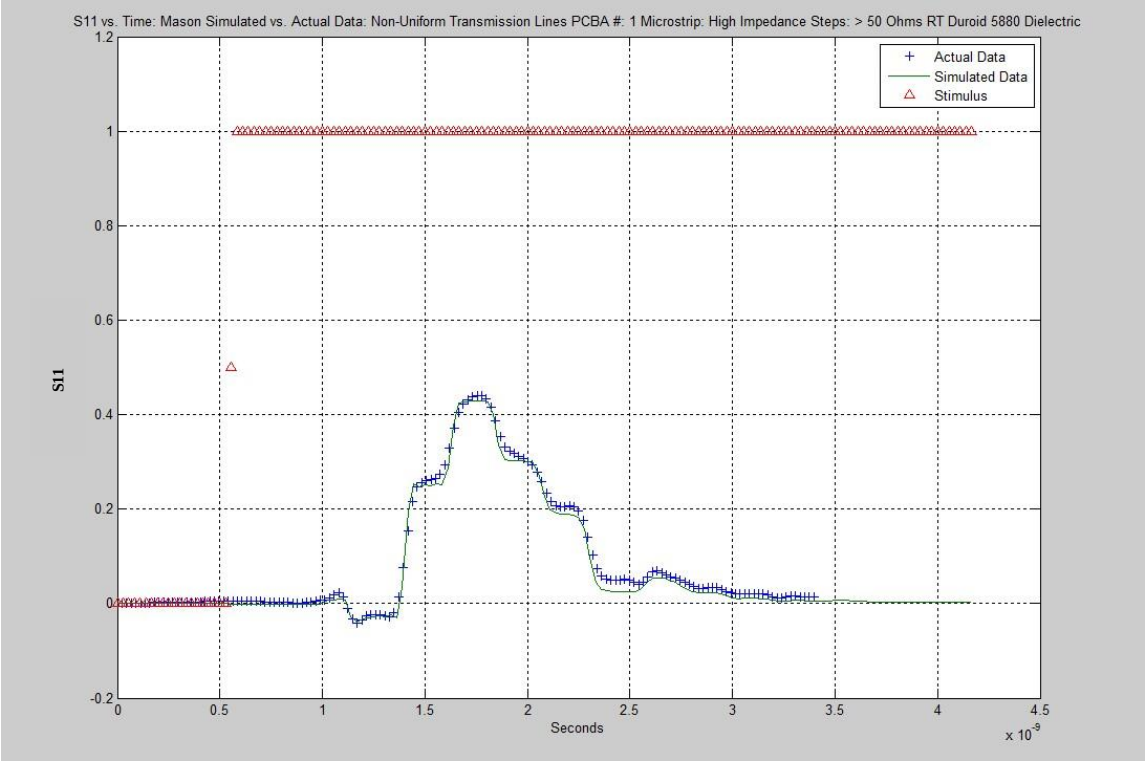


Figure 5.73: Microstrip High Impedance Steps TDR: S11: Simulated (Mason Method) vs. Actual

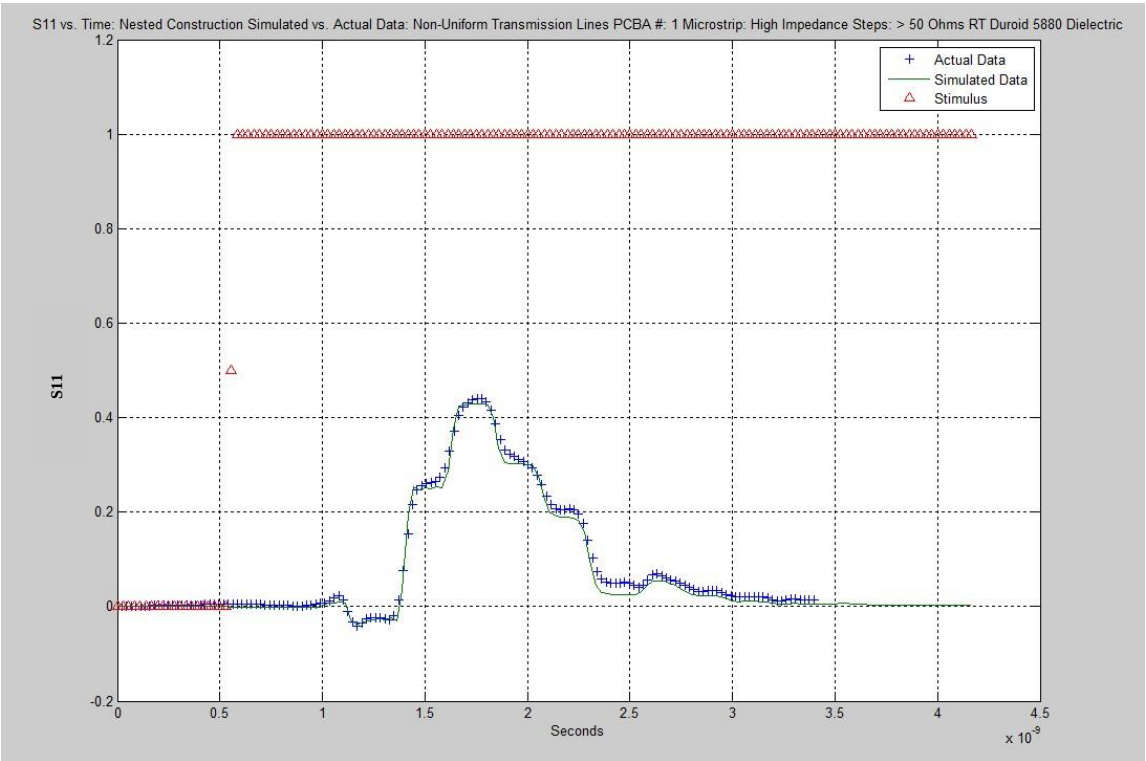


Figure 5.74: Microstrip High Impedance Steps TDR: S11: Simulated (Nested Construction Method) vs. Actual

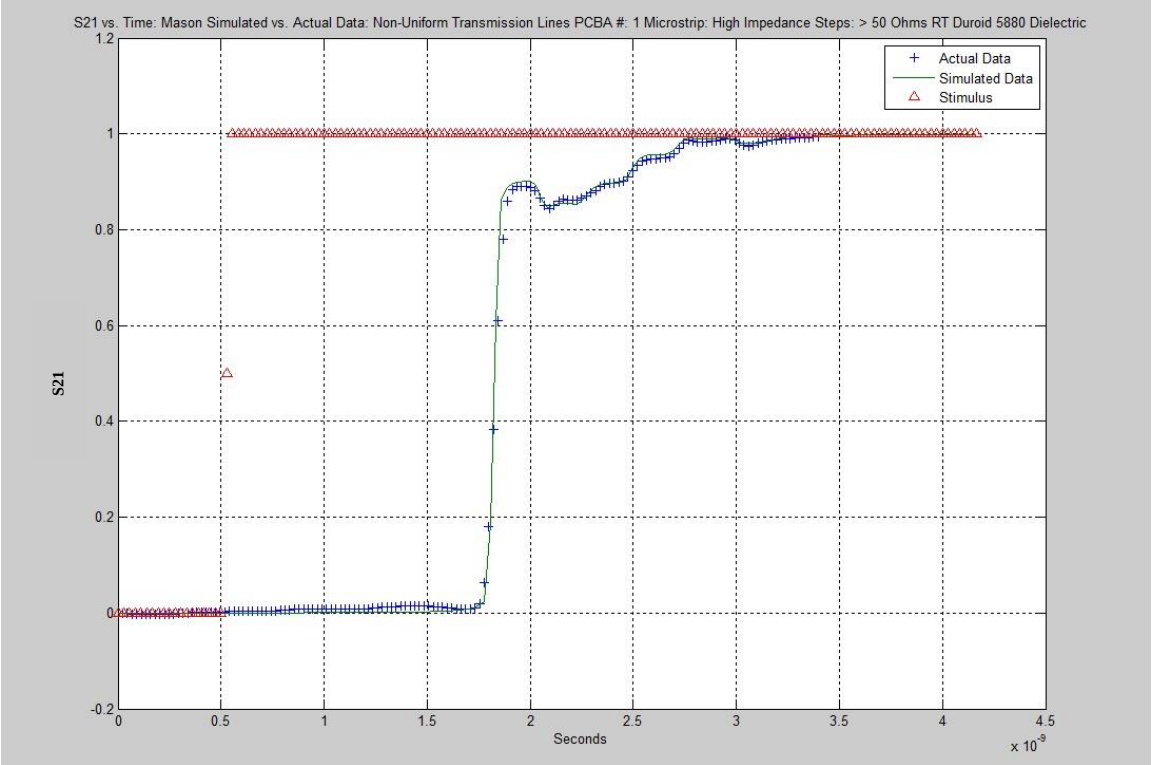


Figure 5.75: Microstrip High Impedance Steps TDT: S21: Simulated (Mason Method) vs. Actual

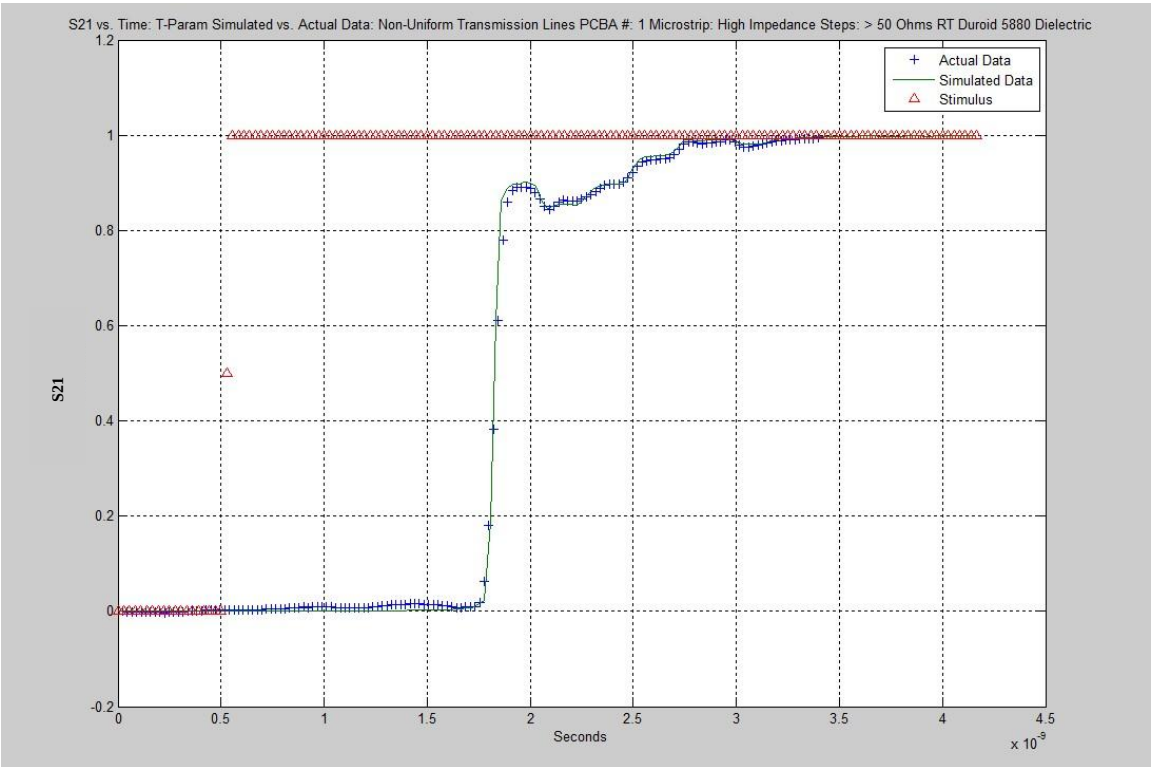


Figure 5.76: Microstrip High Impedance Steps TDT: S21: Simulated (T Parameters Method) vs. Actual

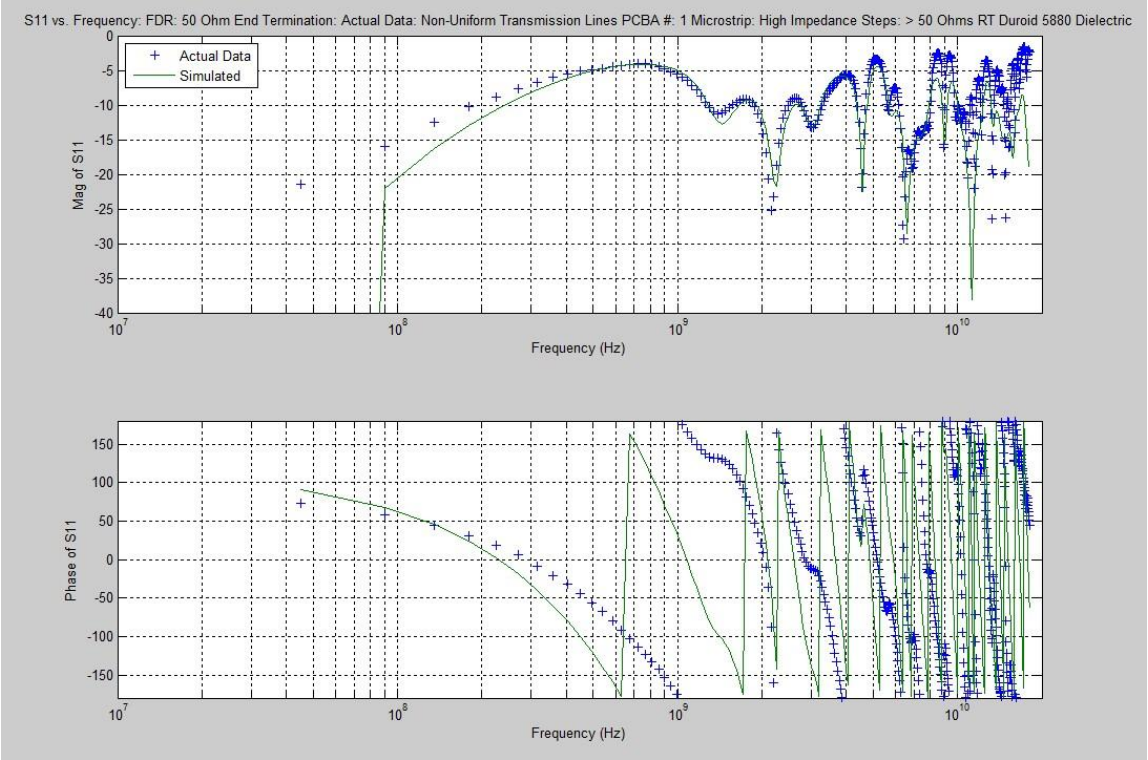


Figure 5.77: Microstrip High Impedance Steps FDR: S11: Simulated (Mason Method) vs. Actual

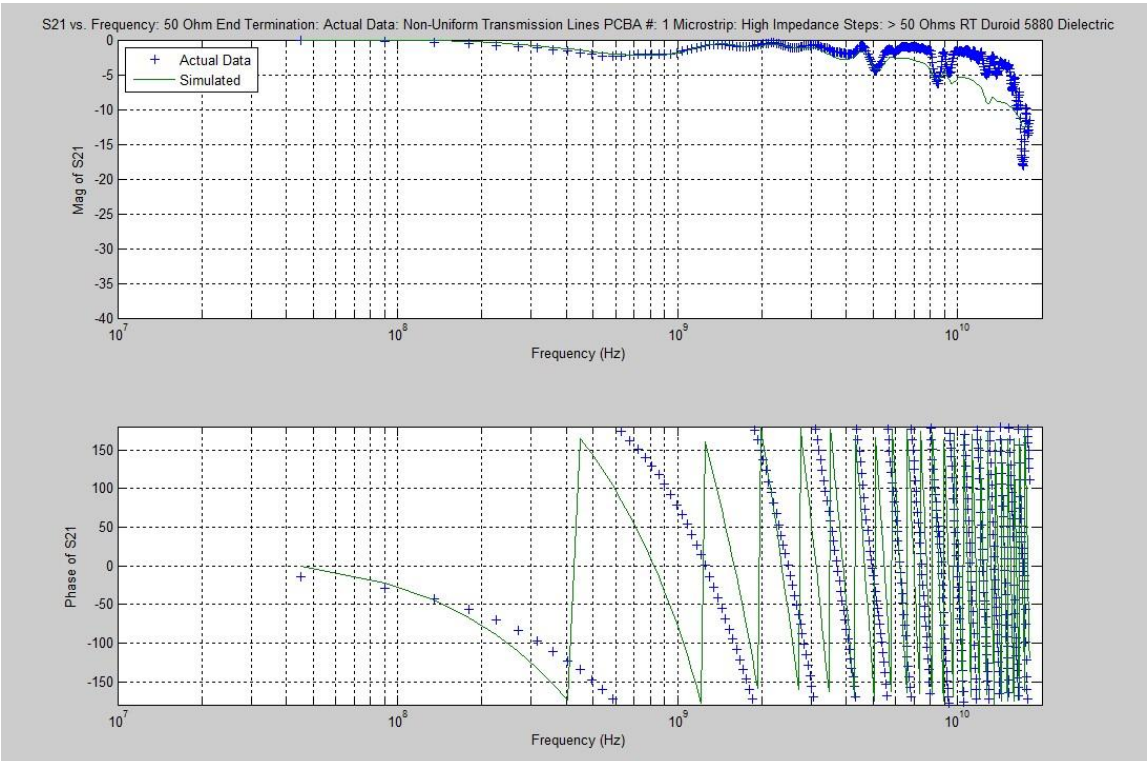


Figure 5.78: Microstrip High Impedance Steps FDT: S21: Simulated (Mason Method) vs. Actual

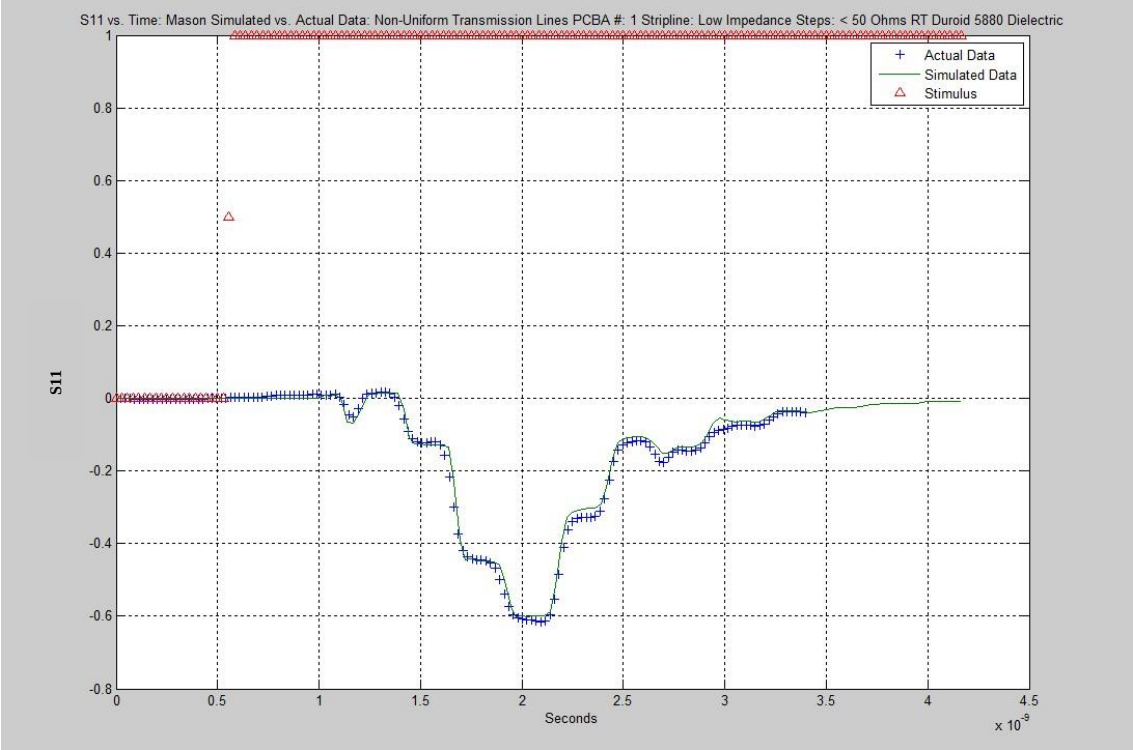


Figure 5.79: Stripline Low Impedance Steps TDR: S11: Simulated (Mason Method) vs. Actual

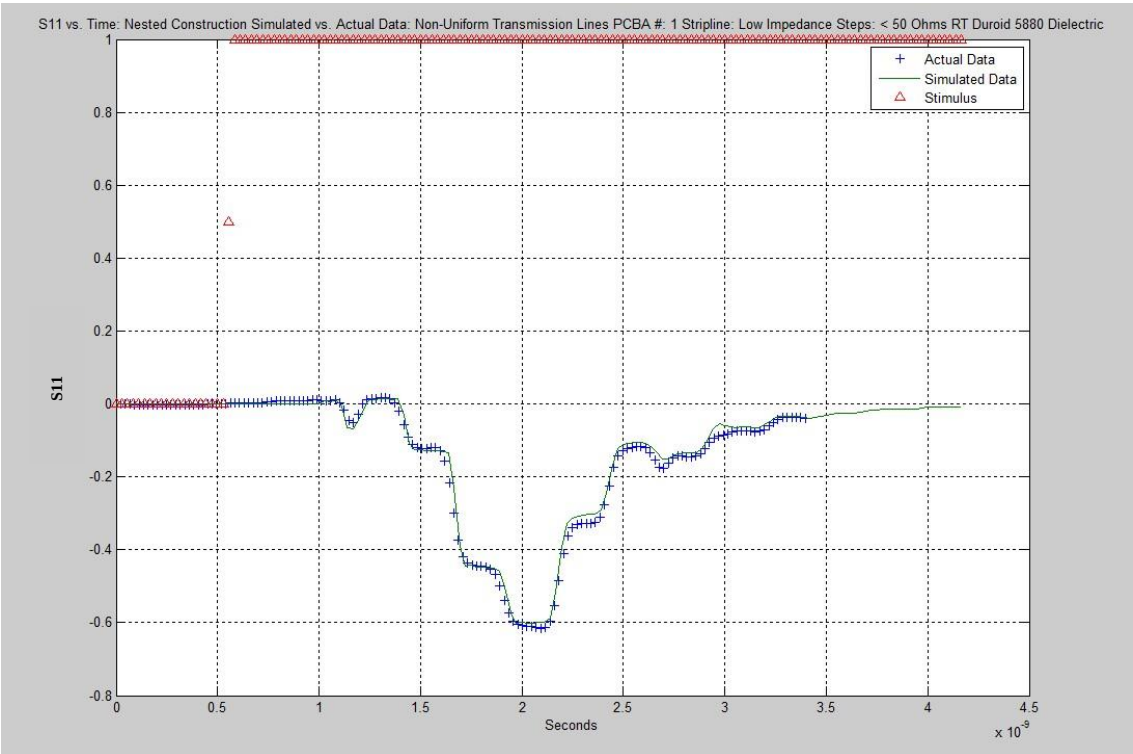


Figure 5.80: Stripline Low Impedance Steps TDR: S11: Simulated (Nested Construction Method) vs. Actual

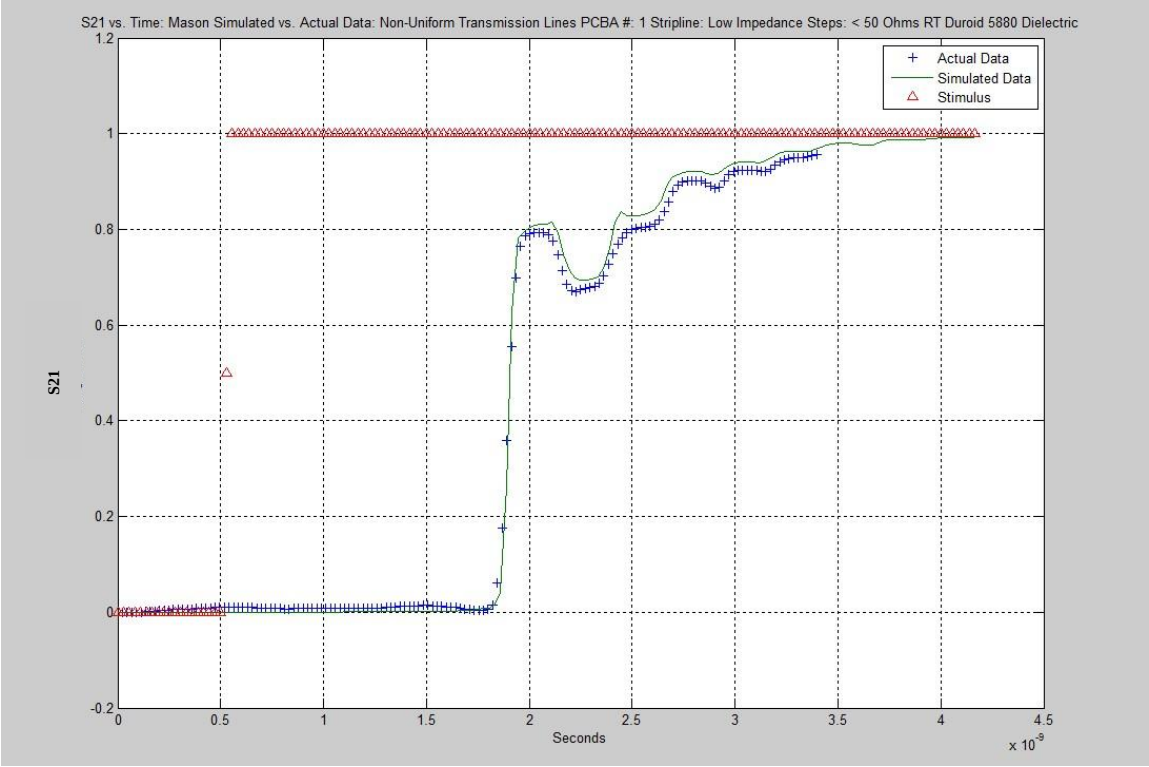


Figure 5.81: Stripline Low Impedance Steps TDT: S21: Simulated (Mason Method) vs. Actual

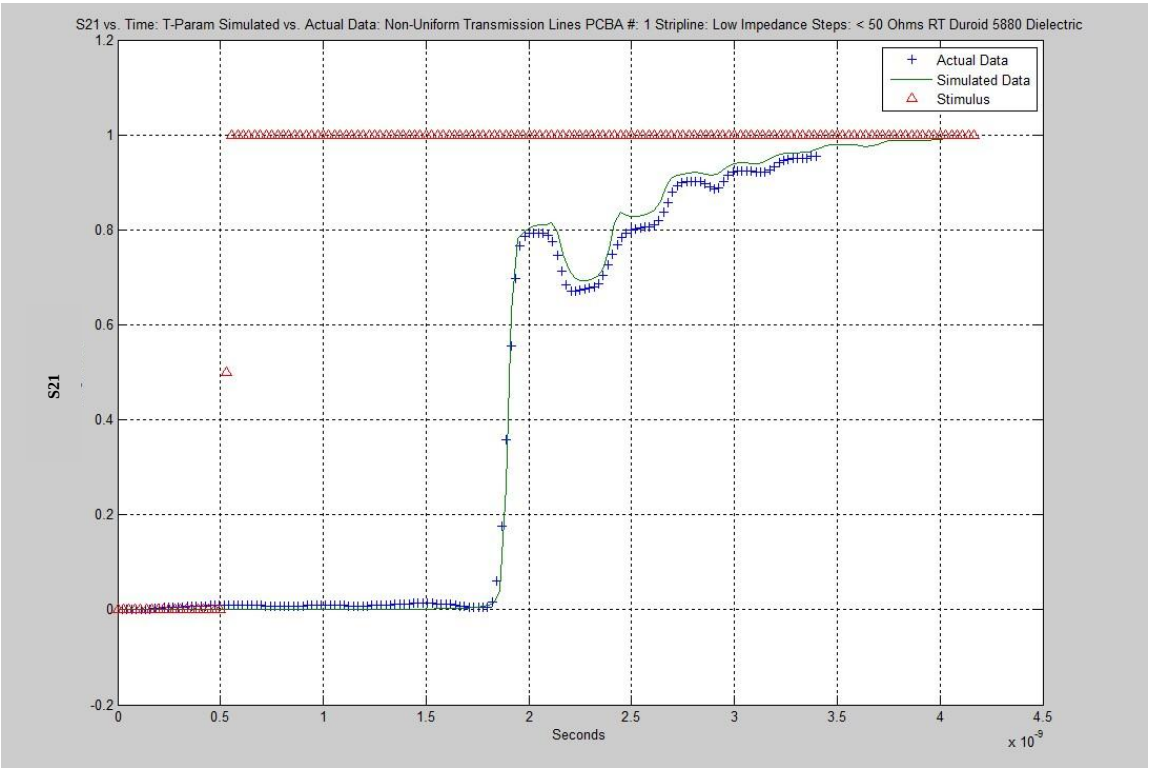


Figure 5.82: Stripline Low Impedance Steps TDT: S21: Simulated (T Parameters Method) vs. Actual

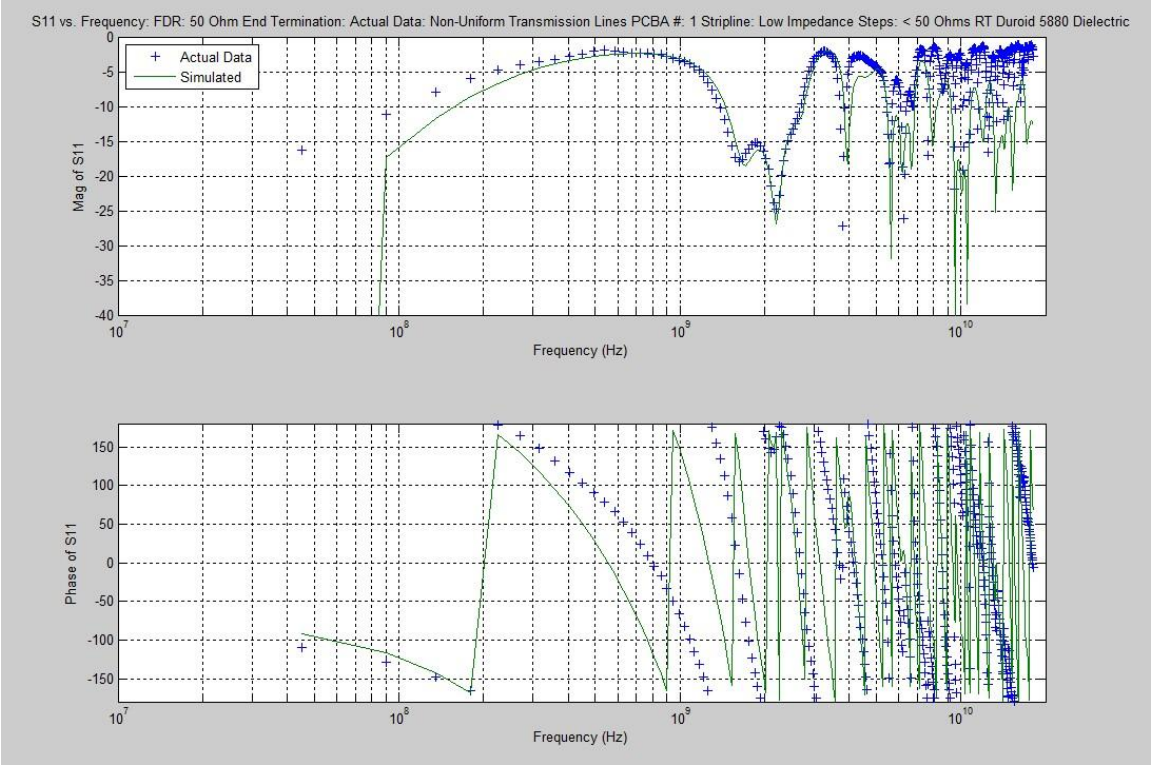


Figure 5.83: Stripline Low Impedance Steps FDR: S11: Simulated (Mason Method) vs. Actual

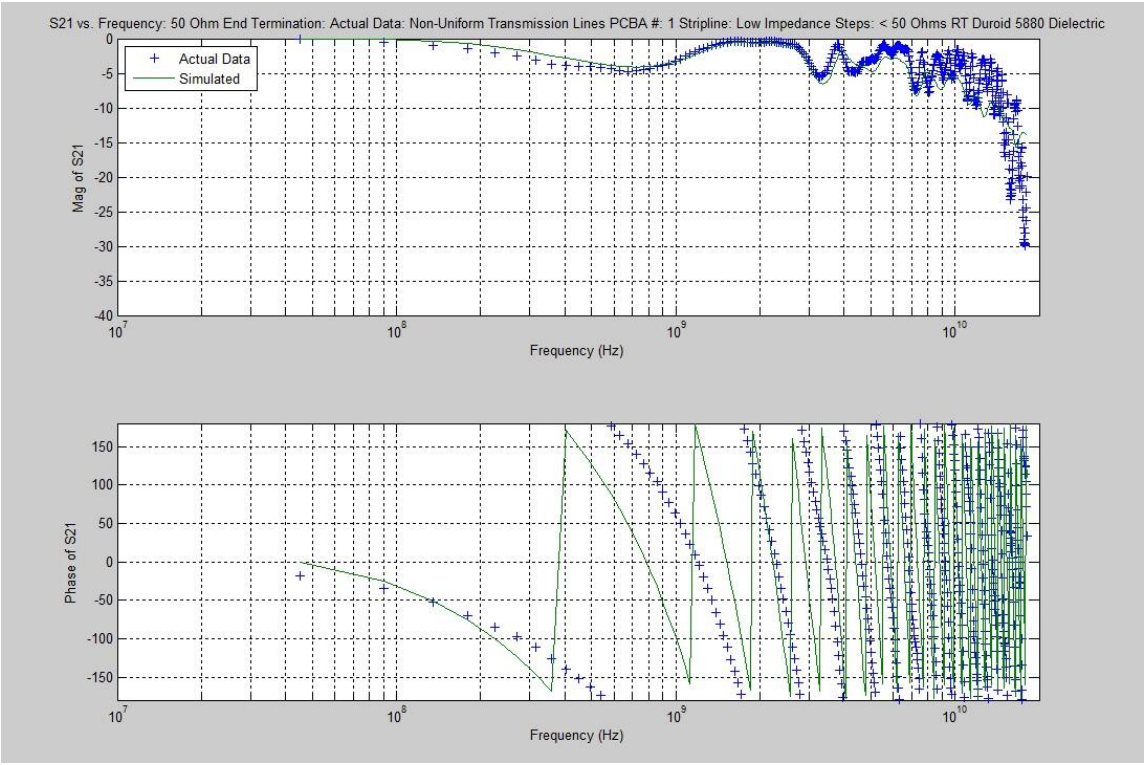


Figure 5.84: Stripline Low Impedance Steps FDT: S21: Simulated (Mason Method) vs. Actual

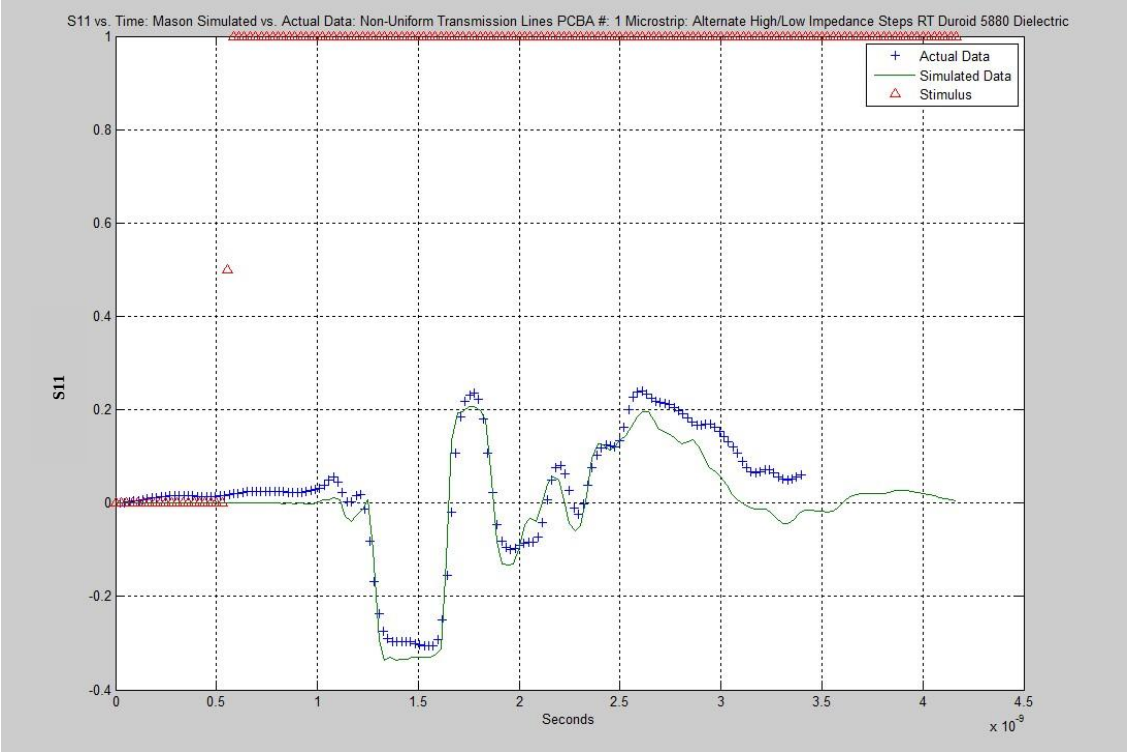


Figure 5.85: Microstrip Alternating High/Low Impedance Steps TDR: S11: Simulated (Mason Method) vs. Actual

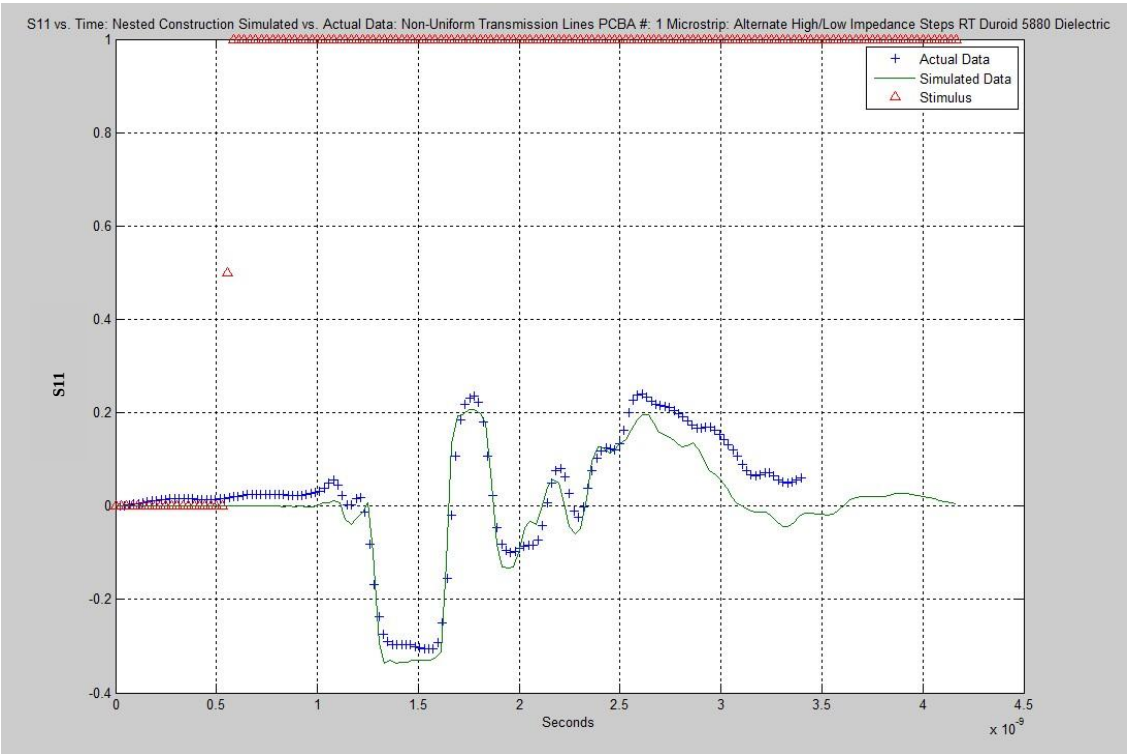


Figure 5.86: Microstrip Alternating High/Low Impedance Steps TDR: S11: Simulated (Nested Construction Method) vs. Actual

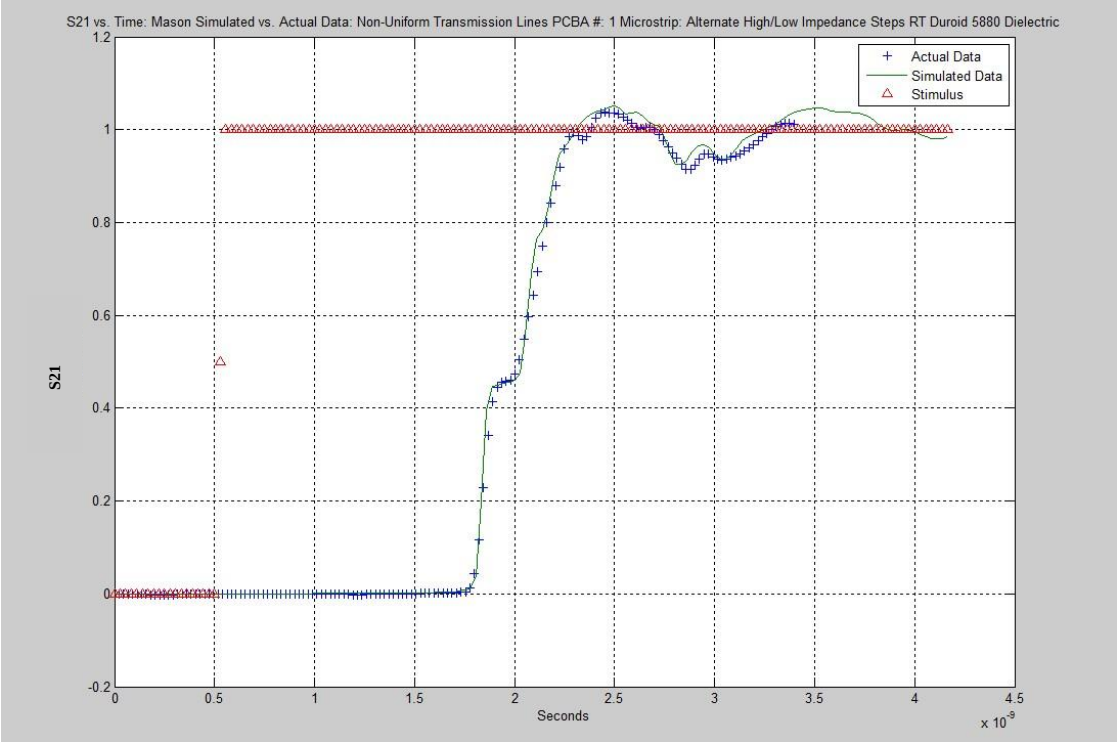


Figure 5.87: Microstrip Alternating High/Low Impedance Steps TDT: S21: Simulated (Mason Method) vs. Actual

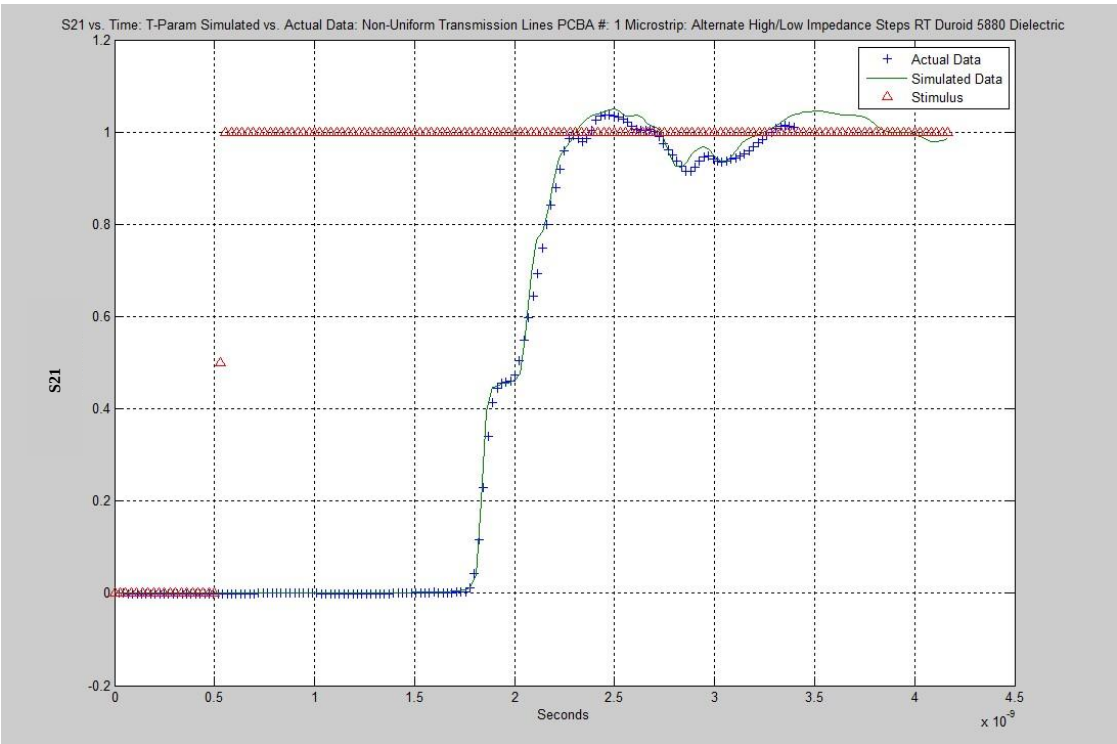


Figure 5.88: Microstrip Alternating High/Low Impedance Steps TDT: S21: Simulated (T-Parameters Method) vs. Actual

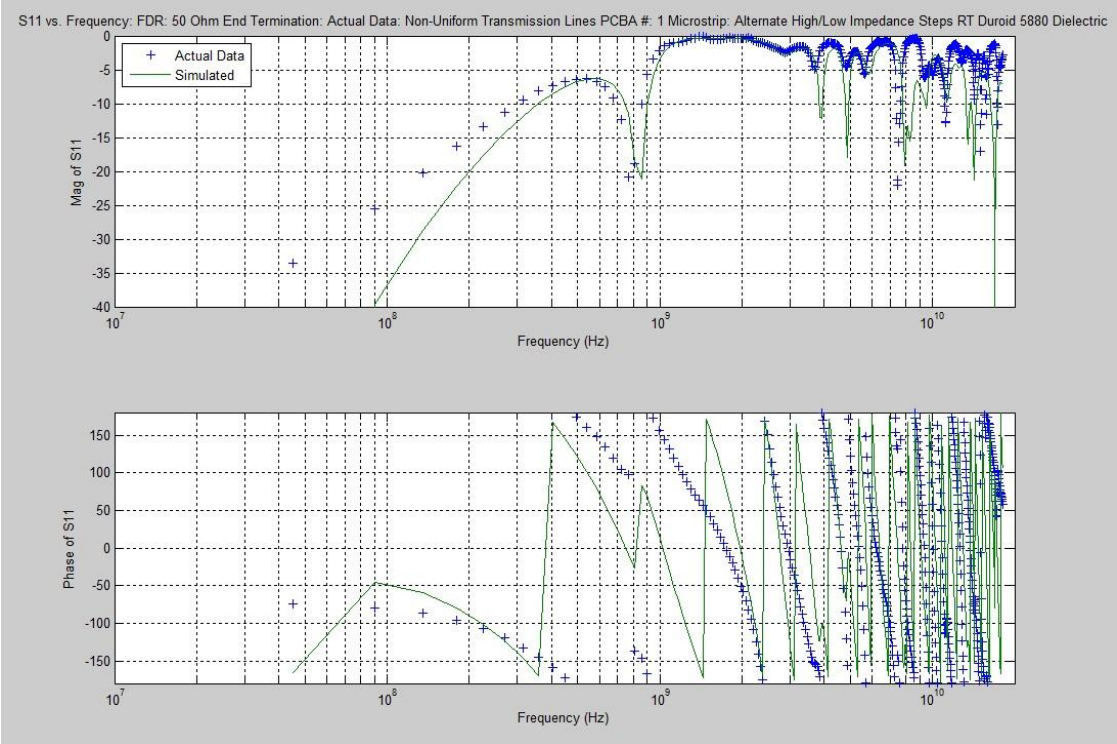


Figure 5.89: Microstrip Alternating High/Low Impedance Steps FDR: S11: Simulated (Mason Method) vs. Actual

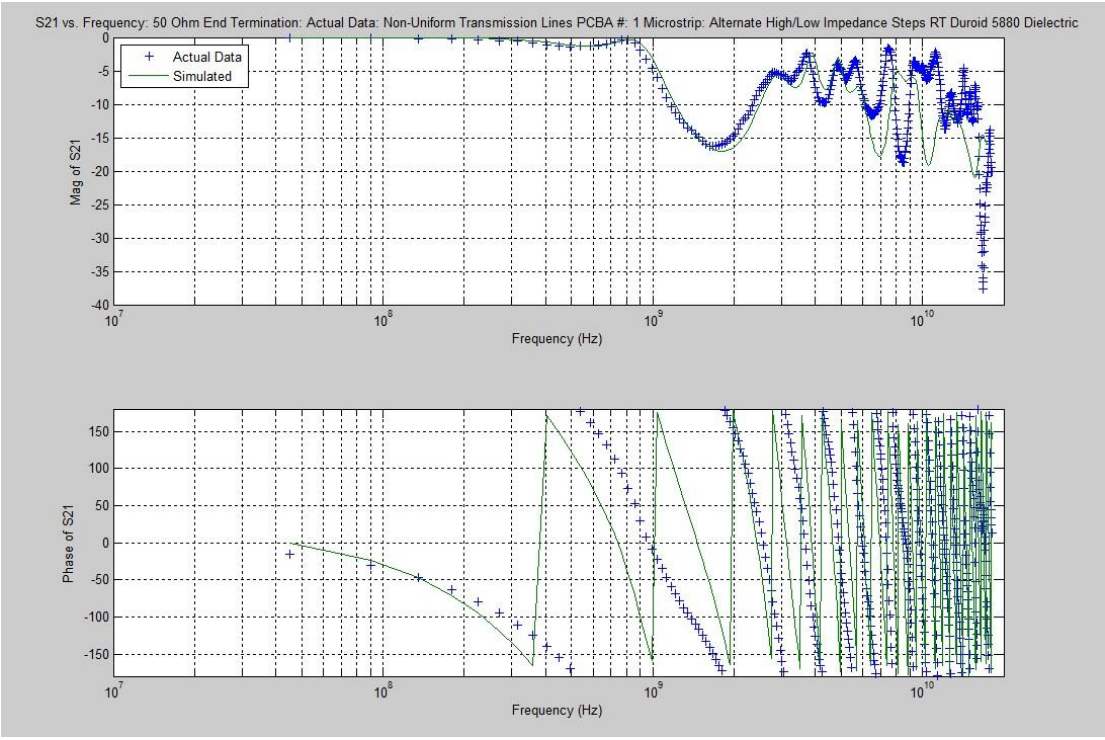


Figure 5.90: Microstrip Alternating High/Low Impedance Steps FDT: S21: Simulated (Mason Method) vs. Actual

The performance of the forward prediction models agree very well with actual data for all of these cases. For the Coplanar Waveguide (CPW) case the calculated impedance from the fitted model was determined to be 111 Ohms and it was found that the effective relative electric permittivity or dielectric constant was 1.75. These compare reasonably well although not exactly with theoretical calculations of 117 Ohms for the characteristic impedance and relative permittivity of 1.6 based on models in the literature (assuming a dielectric constant of 2.2 for RT Duroid and a coplanar waveguide geometry). The slight error could be due to slight variations in the board material and construction. Some modest loss was also incorporated into the models for the permittivity above 5 GHz.

The results in figures 5.67 – 5.90 resulted in the following additional findings:

1.) Dielectric Loss must be accounted for and was incorporated in terms of the imaginary component of permittivity rising to 10% of real component of permittivity above 5 GHz (loss tangent = 0.1) but at a much lower level (1% of permittivity or loss tangent = 0.01) significantly below 5 GHz. Series Losses have not been incorporated yet but could be a factor in the very thinnest and highest impedance traces (those models will be incorporated in follow-on research).

2.) The fitted models in some cases were slightly off from the theoretically predicted values. This could be accounted for by a slight variation in the PCBA stack-up formulation

3.) The fitted models of all three cascaded transmission line modeling techniques (Nested Construction, Mason's Non-Touching Loop Rule and the Transmission (T) Parameters methods) all agreed with each other with no detectable differences.

4.) Although in these test cases the models were shown to agree very well with the data it was also found through additional simulations that it is possible to confound a cascaded transmission line model in terms of not having uniqueness of solutions. This can be addressed by having different types of probe geometries with signature boundaries already built in to help add resolution. All four S-Parameters in a two port measurement (transmission/reflection) setup will also help mitigate for uniqueness of solutions issues. This will be the subject of follow-on research.

Additional Findings:

1.) 3D Zone of Influence of Propagating Electromagnetic Waves: For Lossy Soils this is shown to be very limited in all orthogonal axes about a transmission line probe. As previously known, lower frequencies penetrate further but also have less resolution. However, the proposed algorithms rely on the use of both lower and higher frequency components. There is therefore a direct tradeoff on precision on profiling WC vs. volumetric zone of influence.

2.) Uniqueness of Solutions: The simulations show that it is possible to provide identical or often nearly identical waveforms in a cascaded transmission line arising from different profiles. A simple parallel conductor uniform line by itself will not be sufficient to address this. It is therefore proposed that a couple of companion probes be utilized (one with a more uniform geometry and a second one with a non-uniform geometry) together with both reflection and transmission measurements as two separate but integrated 2-Port networks. This will be the subject of follow-on research.

3.) Sensitivity Analysis: The algorithms have been shown via companion FEM simulations to have much better “relative” sensitivity analysis or relative resolution vs. “absolute” accuracy (the latter due to confounding elements such as temperature and other temporal and spatial variables). Therefore, trending changes in profiles vs. time (such as the propagation of a wetting front) will be one of the better applications for these algorithms requiring less site specific calibration. However, significant site specific calibration will be required to obtain good “absolute” accuracy performance.

# Chapter 6: Conclusions

## Overall Findings:

It was found from examination of the laboratory data that the all of the interpolation models presented in the Forward Prediction Model chapter can be made to accurately model the electromagnetic propagation constant vs. frequency for changing water content and electrical conductivity if the weighting factors are set up along the following biasing trends:

All Conductivities:

Very Low Water Contents (WC< 0.05): Strong Weighting towards Parallel Model

Low-Medium Water Contents (0.05 < WC < 0.15): Equal Weighting of Series & Parallel Model (Modeled well by interpolation models as well as the Cascade Model in these ranges)

Medium Water Contents (0.15 < WC < 0.30): Slight to Moderate Weighting towards Series Model: (Requires Interpolation Models in these ranges)

High Water Contents (WC > 0.30): Strong Weighting towards Parallel Model

In general the forward prediction interpolation models with the above weighting trends were found to be the best fitting models to actual data. For the sub-case of high electrical conductivities the simpler cascade model (from which classical equations such as the index of refraction equation used in existing TDR systems can be derived) was still found to be an acceptable fit but it was a poorer fit in medium to higher water contents with lower conductivity. Therefore, the basis of the presented models and associated inverse algorithms will be these interpolation models since good fit is required for all values of electrical conductivity and water content.

Incorporating the above biasing or weighting trends into the interpolation algorithms is an additional aspect of this research and one example is given below for the geometric mean model where the weighting parameters have been made functions of the water content and air content.

Enhanced Geometric Mean Model with Weighting Functions Incorporated:

In this case the weighting constant "a" is set up in the geometric mean model as follows to give more weighting to the parallel model at higher water contents and progressively more equal billing to the series model as water content is reduced:

$$\gamma_{\text{Geometric}} = \sqrt{\gamma_L^{\left(((\phi-\theta)/\theta)+.15\right)}\gamma_U^{\left((\theta/\phi)+.85\right)}} \qquad (6\text{-}1)$$

This model is still not complete and is only valid for water contents between 0.05 and 0.15 and above 0.30. It does not give enough bias to the series model at medium water contents and not enough to the parallel model at very low water contents. A higher order function is required for the weighting parameters to accurately reflect the necessary biasing trends shown in the tables of results given above. The model in equation 6-1 is just shown to show the direction that is being followed in this research. Similar weighting functions could be incorporated into the other interpolation models that are functions of the water and air contents (functions of water content and porosity). Site specific calibration of these interpolation models will be required for each soil type. In the measurement algorithm in its present state, the lookup table for water content was generated with the rectangular mean model with manually entered best fit weighting parameters as shown in tables 5.1, 5.3 - 5.7 of the lab and field results sections.

Once the propagation constant is determined from the proper model, then physically based equations from the theory of electromagnetics (Appendix A) could be used to calculate the phase velocity, intrinsic impedance and characteristic impedance respectively of the composite medium for each of the different models by plugging the propagation constant into the proper location in those equations. All of these expressions would form the basis for the S-parameter models which model the cascaded segments of the TDR transmission line. Each segment on the transmission line would have its own expression for propagation constant and characteristic impedance which are functions of frequency. Each segment would also have a corresponding

physical length. Boundaries between these segments can be modeled by reflection coefficients and transmission coefficients as described in Appendix B covering S-parameter network theory.

Sensitivity Analysis:

The results figures from the Validation chapters and Appendix D show that very fine sensitivity to changes in WC (0.01 to 0.02) can be detected. In addition, fairly fine sensitivities to changes in EC can also be detected but overall accuracy is coarser than the resolution (so trending is a good option). The field data showed that when conductivity is significant it is no longer feasible to extract WC profiles vs. position as the high frequency data required for that is significantly attenuated. However, overall bulk WC can still be estimated especially if a transmission measurement is also utilized.

Uniqueness of Solutions:

It has been determined through the field validation data as well as separate simulation work that there will always be uniqueness of solution challenges with these algorithms.

## Other Soil Types:

Clay Soils:

The controlled laboratory experiments for this phase I project were limited to a sand soil. Field data was collected in clay/loam soils but only over a limited range of water contents and electrical conductivities. Therefore additional follow-on research is planned for other types of soil.

The main difference between the clay soil and sandy soil is the fact that the porosity and therefore saturation water content is much higher than that in a sandy soil. Therefore there is a larger range in the transit times for TDR waveforms as water content is varied from a dry soil to saturated soil. The same effects of attenuation, dispersion and frequency dependent reflections occur in the clay soil as were found in the sandy soil data and properly modeled in the algorithm. Some of the more apparent differences between a sandy soil and clay soil are bound water effects at negatively charged clay complexes at low water contents and swelling soils (increasing porosity) at higher water contents (especially in the presence of $Na^+$ ions with a clay such as smectite). Both of these effects can be indirectly accounted for in the models by making the porosity a variable (swelling soils) as well as assigning a fourth phase (bound water) to the composite mixing model as has been done in the forward prediction models. Typically the bound water will have a much lower dielectric constant than free water due to its attraction to the negatively charged clay complexes (i.e. hydrogen side of the polar water molecule) which prevents the free rotation of the polar water molecules to line up with an externally applied electric field. A gradual progression through a semi-bound water zone of progressively increased dielectric constant and relaxation frequency then occurs when moving away from the charged interfaces. These types of models are in the forward prediction models and were presented in the chapter covering those prediction models. In this paper it is assumed that water contents less than 0.05 act as a dry soil (assumption of the bound water having a lower dielectric constant that is near to the dielectric constant of the soil solids) and is accounted for by simply adjusting down the porosity by .05 in the model and assuming that it is impossible to really have a water content equal to 0 in a clay soil. The present algorithm assumes that the soil is non-swelling but could easily be enhanced to account for that by making porosity a function of the water content (leading

to a very complex and possibly non-feasible measurement algorithm due to the large number of variables and spacial variability in the soil).

Silty/Loam Soils:

These soils would behave similar to sand only that their particle size distributions are wider leading to a more even distribution of possible stable water contents. In the sandy soil it is difficult to maintain a stable water content just below saturation due to the sharp transition on the water characteristic curve.

Soils with Organic Matter Fractions:

These soils would exhibit characteristics similar to the clay soils in that they can contain negatively charged sites (hydroxide groups) along their outer fringes. Extremely high water contents (.7 - .8) are possible with a largely organic soil and so that would have to be accounted for in the algorithm. Again porosity would potentially be a function of water content further complicating the algorithm.

Spatial Variability in the Field:

At the present time the model assumes a relatively simple homogeneous mix of the subconstituents of water, air and solids. As more field data is collected it will likely be concluded that some stochastic modeling may need to occur to properly bias the interpolation models and account for heterogeneity in the soil. The weighting constants in those models would then become stochastic variables based on probability density functions and distribution functions that give occurrence intervals of soil subconstituents modeled best by either the series model limit or parallel model limit. There is a limit to what can be modeled in a real world soil situation and still achieve a reasonable convergence on a measurement. At the present time the algorithm is still dependent on a site specific field calibration at least one known water content and would need to be recalibrated if the soil properties changed over time (e.g. change in bulk density or porosity by extensive plowing, etc.).

Soil/Water Temperature:

It is a known fact that the dielectric constant and electrical conductivity are both functions of temperature in any medium and so eventually this algorithm will need to account for temperature in determining water content accurately (especially in places like the desert southwest). This will again be investigated and developed in follow-on research.

## Remaining Limitations with the Software Algorithm/Model:

The earlier versions of the simulation model did not fully account for all the higher frequency loss mechanisms associated with a two wire probe. In close examination of comparisons between actual data and the simulation model predictions it is observed that there is additional medium frequency and high frequency loss mechanisms (> 200 MHz) that needed to be accounted for in the models. A strong resonance of the probe itself above 1 GHz was observed in the data and validated by FEM simulations. Accounting for this resonance has now been added into the latest versions of the models. The models agree very well with the low to medium frequency performance of the actual data and up to very high frequencies when modeling controlled structures such as RF PCBA's. Some of the high frequency losses are more notable in low water content conditions and dry soil and open air calibrations. This points to the potential of radiative losses that are more prevalent in the absence of other loss mechanisms that would d-Q a radiation resonance. A balanced twin lead cable/probe is known to have radiation losses at frequencies above 200 MHz at imperfections in the cable (e.g. boundary between coax and twin lead and termination at end of the twin lead probe). The models have been enhanced to account better for these losses in follow-on research. What must be part of that process is the experimentation with other types of probes to increase the bandwidth of the probe up into the 10 GHz region to be compatible with the high bandwidth requirements of the algorithm for extracting water content when the electrical conductivity is high.

**Remaining Limitations with Hardware:**

The hardware must consist of a high bandwidth TDR probe system that has the shortest electrical length possible in the interface connector as well as a probe geometry that is compatible with high frequency operation (up to 10 GHz). This necessitates a multiconductor probe that emulates a coaxial cable that has a minimizes radiation and other resonances at high frequencies, minimizes high frequency distorting reflections between the connector and the probe, insures TEM propagation up to 10 GHz as well as minimizes other loss mechanisms at high frequencies associated with the probe. The TDR sampling front end must have a sampling frequency of at least 20 GHz and preferably higher. With today's technology it is proposed that a hardware solution consisting of high dynamic range swept narrowband network analyzers connect the sampling front end directly to the probe without a cable to achieve these goals of higher bandwidth operation to be compatible with the algorithm.

Technical Feasibility Criteria #1:

| Measurement Goal | Measurable Item | Extractable Item that Correlates to Desired Parameter |
|---|---|---|
| Electrical Conductivity | TDR Trace | Low Frequency Values of S-Parameter: S11 |
| Water Content (Low EC) | TDR Trace | Group Delay vs. Frequency Peaks (Medium Freq.) |
| Water Content (High EC) | TDR Trace | Effective Impedance vs. Frequency (Higher Freq.) |
| Water Content vs. Depth | TDR Trace | Effective Impedance vs. Position and Frequency |

Technical Feasibility Criteria #2:

The experimental results show that there is good sensitivity of each of the above extractable items to variations in the corresponding desired measurement parameter. Water content variations of .01 can be detected and electrical conductivity variations of .01 dS/m can be detected in the controlled laboratory experiments by careful examinations of all portions of the frequency domain data of S11. The key to whether a successful measurement can occur to that level of precision or resolution in the field will depend on the variations of other parameters in the soil which may dominate over low level changes of water content and electrical conductivity. More data must be collected over wider ranges of field conditions to make that determination. The conclusion is that the measurement algorithm contains adequate sensitivity to changes in water content and EC in the soil except in the case of water content measurements in conditions of very high conductivity where the sensitivity has been masked by other more larger variations due to bandwidth limitations of the existing TDR hardware and interfacing connector effects. This will be addressed by follow-on research. Again, relative resolution or sensitivity is stronger than absolute accuracy (due to the presence of confounding variables) and hence a trending algorithm tracking relative changes of WC and EC vs. time and position offers great potential in the application of these algorithms.

Technical Feasibility Criteria #3:

In terms of measurement accuracy there again is good performance for electrical conductivity over a large range of values of that parameter in the laboratory data. There was a repeatable error of 12% to 16% (with a couple of larger exceptions) on the high side of the actual data in the laboratory data (for validation method #1) which is probably due to probe calibration error and therefore could be corrected for. With that correction in place the measurement accuracy improves to better than 5% with the algorithm in its present state with much room for improvement still ahead in future research. But again, relative trending may be a greater application for the technology vs. absolute accuracy. The field data appeared to show larger errors on EC measurements but some of that may have been due to the difficulty of obtainin an accurate independent measurement of EC on the extracted soil samples. The field based TDR system probably was more accurate than the independent methods used to measure EC as the latter disturbed the soil samples. But the lab data (where EC could be measured independently in situ in the fixtures) there was very good agreement between simulated and actual EC (especially upon removing the fixed upward bias error).

In terms of water content measurement accuracy there is very high precision possible (<2% error) with the group delay method when the conductivity is low and the soil calibration is properly set up. On the other hand when the electrical conductivity is high the level of water content measurement accuracy drops drastically to unacceptable levels (> 10% error and worse) due to the bandwidth limitations of the existing TDR hardware systems (scope + cable + interface + probe). The only way that this algorithm can be feasible in accurately determining water content when the salinity is high is to use it with a TDR or preferably a high dynamic range FDR hardware system that has an overall bandwidth approaching 10 GHz including connector effects that are invisible until well above that frequency. This type of hardware technology is now becoming cost effective with high speed electronics and it is now therefore a feasible goal to modify the rest of the hardware to accommodate that by developing a cableless fixture with a multiconductor probe to emulate the higher bandwidth field containing capabilities of a coaxial cable. This approach will be discussed as a development goal for follow-on research.

Technical Feasibility Criteria #4:

The calibration required at this time for the algorithm includes a one time factory open air calibration to enter the probe dependent factors and then a one time field calibration at each measurement location with one known water content and bulk density measurement to calibrate for the particular soil. This is comparable to or less than existing calibration requirements for water content measurements and is especially less than that required for methods that rely exclusively on regression models. As the follow-on research proceeds the database of soil calibration data will increase and values of the particular weighting constants or functions will be perfected for most soil types to help reduce the amount of field calibration required.

Technical Feasibility Criteria #5:

At the present time the measurement speed is around a couple of seconds for a lower precision measurement (401 samples in time) and around 10 - 15 seconds for a higher precision measurement (2001 samples in time and covering 5 times as much frequency spectrum) but there is also a lot of unnecessary overhead in the algorithm (plotting routines, etc.). Therefore the conclusion is that measurement speed goals can be met by this algorithm that are acceptable to end users.

## General Conclusions

Based on the above criteria and the test results from both the laboratory and field experimental cases and on the comparisons to various aspects of the prediction algorithm the following conclusions can be drawn on the technical feasibility of using this algorithm to obtain water content and electrical conductivity accurately over wide ranges of those parameters:

1.) Electrical Conductivity:

Technical feasibility has been demonstrated by the algorithm for the whole range of values found in the field by controlled laboratory experiments (0 – 1.7 S/m in the lab experiments).

2.) Water Content (Low EC):

Technical feasibility has been demonstrated by the algorithm for the whole range of values found in a sandy soil by controlled laboratory experiments (0 - .37 in the lab experiments). In addition the field measurements show that the algorithm show promise in tracking the water content for other soil types for low to medium conductivities.

3.) Water Content (High EC):

Technical feasibility has not yet been demonstrated due to bandwidth limitations of existing field based TDR measurement hardware and due to the fact that the model does not yet fully account for all those excessive medium to high frequency losses nor can it extract water content dependent impedance from the more dominant connector impedance at high frequencies (above 1 GHz). This will be solved by developing a new field TDR hardware system which has a much higher bandwidth (no cable + improved high BW probe) and contains simpler interface hardware pushing connector effects in S11 to frequencies well above 10 GHz. In addition, A high dynamic range FDR/FDT Vector Network Analysis reflection/transmission measurement system is proposed.

4.) Water Content vs. Depth (Low EC):

Technical feasibility has been partially demonstrated in that water content variations vs. depth can be modeled accurately by the simulation model, but the same high bandwidth hardware requirements exist for this feature as exist for number 3 above and so the development of that high bandwidth TDR hardware system will make this feature also a feasible reality. The ability to measure water content vs. depth along the probe is one of the more powerful features of this algorithm along with number 3 above and so the need for the high bandwidth TDR hardware is a high priority and will be the focus of follow-on research.

## Conclusion on overall feasibility:

Based on the above conclusions for both technical and commercial feasibility, it is the general conclusion of this author that this algorithm is a feasible tool in making accurate high resolution water content and electrical conductivity measurements over wide ranges of those parameters assuming that a companion field TDR/TDT or high dynamic range FDR/FDT hardware solution can be developed to improve the bandwidth of the field TDR hardware and probe system to frequencies up to 10 GHz to take advantage of the power of the algorithm. This will again be the focus of continued ongoing research.

## Commercial Applications:

The test results and algorithm development have shown that it is technically feasible to develop a measurement system to determine water content and electrical conductivity over wide ranges of those parameters if improvements are made in the field TDR measurement hardware to increase its bandwidth up to 10 GHz and improvements are made in the software algorithm to better model any medium to high frequency losses that effect the portion of the spectrum that is important for determining water content. Therefore, a new hardware approach based on high dynamic range FDR/FDT instrumentation is proposed which makes use of a short high resolution high bandwidth probe connected directly (without a cable) to a high bandwidth TDR and/or FDR/FDT front end module which digitizes the data and transmits it via telemetry to a central base station computer which contains the processing power of the algorithm. Several TDR probes at various locations in a farm field could be networked to a single base station which lowers the overall cost of measurement for this system. This approach, when used together with the software algorithm, not only allows for the high frequency operation but is also key to the commercial feasibility of this product as there would be markets available to electronics instrumentation manufacturers as well as various end-users (in the agriculture industry) in this new approach to measuring water content and electrical conductivity. These enhancements in both hardware and software will lead to a powerful new TDR/TDT/FDR/FDT based water content and electrical conductivity measurement tool.

**Summary of Key Items of Algorithm:**

Software Algorithm:

1.) The use of frequency domain information and scattering S parameters to extract extra information from a Time Domain Reflectometry (TDR) or Time Domain Transmission (TDT) waveform (using FFT's on the time domain waveform) or directly from a Frequency Domain Reflectometry (FDR) or Frequency Domain Transmission (FDT) system to aid in the determination of water content and electrical conductivity over the relevant ranges of those parameters found in field conditions. The low frequency information is used to determine electrical conductivity and the medium to high frequency range is used to determine water content (see forward prediction model chapter and validation sections earlier in this chapter). The electrical conductivity is calculated directly from the low frequency information of the scattering parameter S11 (reflected signal divided by the incident signal). The water content is determined by lookup tables using either 2.) or 3.) below depending on the level of electrical conductivity.

2.) The use of effective group delay vs. frequency plots (derivative of phase with respect to angular frequency in S11) to accurately determine water content at lower levels of electrical conductivity. The peaks in those plots correspond to quarter wave null resonances on the TDR transmission line probe of which can be used along with the length of the probe to accurately determine wave velocity which correlates to water content at high enough frequencies where the dielectric constant dominates over the electrical conductivity. The lower the conductivity the wider range of frequencies that can be used to look for these peaks in group delay. In this inverse algorithm a lookup table is used with these peaks in group delay to determine water content. As a cross checking procedure the effective actual delay vs. frequency (phase divided by angular frequency in S11) can also be used but the group delay gives the most sensitivity to quarter wave nulls due to the rapid change in phase (peaks in group delay) at those nulls. The use of group delay vs. frequency information is only meaningful when the reflected signal from the end of the TDR probe is not attenuated to the point where it is not the dominant contributor to phase in S11 in the frequency range of interest. Therefore this approach is limited to regions of low to medium conductivity and 3.) below must be used when the conductivity is high.

3.) The use of impedance vs. frequency plots (obtainable from S11) to determine water content at higher levels of electrical conductivity where reflected signals from the end of the probe are attenuated below detectable levels. In these conditions the group delay plots from 2.) are not useable as the phase of S11 does not relate to the transit time of a pulse down and back a TDR probe as the reflected signal is attenuated below detectable levels. The impedance in this case comes from the first reflection data of a TDR signal. The higher the conductivity the higher the frequency that must be looked at to determine water content (again high enough frequency where the permittivity dominates over the conductivity effects). The water content is determined by lookup tables using the impedance data at high enough frequencies (frequency chosen based on the calculated value of electrical conductivity from 1.)).

4.) The use of Mason's non-touching loop rule together with the Nested Construction method and T-Parameters methods in combination with the scattering S parameters to model the TDR transmission line probe as a series of cascaded elements to help determine water content vs. depth in a soil or vs. length along the probe. This procedure uses both the frequency and time domain information from a TDR/TDT and/or FDR/FDT signal and looks at the impedance vs. length along the probe to extract water content. This procedure can only be used at lower water contents as the reflected signal from the probe end must be detectable to be able to determine information about the impedance and eventually water content along the length of the probe.

Hardware:

5.) The design of a high bandwidth cableless TDR/TDT and/or FDR/FDT measurement system to be compatible with the high bandwidth requirements of the measurement algorithm (for extracting water content when the electrical conductivity is high: items 1 and 3 above). For the case of a TDR implementation, the output circuit of the TDR system would have the shortest and simplest interface possible between the step waveform generator and the TDR probe (connectors and cable/PC board length) to insure the highest bandwidth possible to extract water content information when the electric conductivity is high. The product would look something like the following (shown with a 3 wire probe):

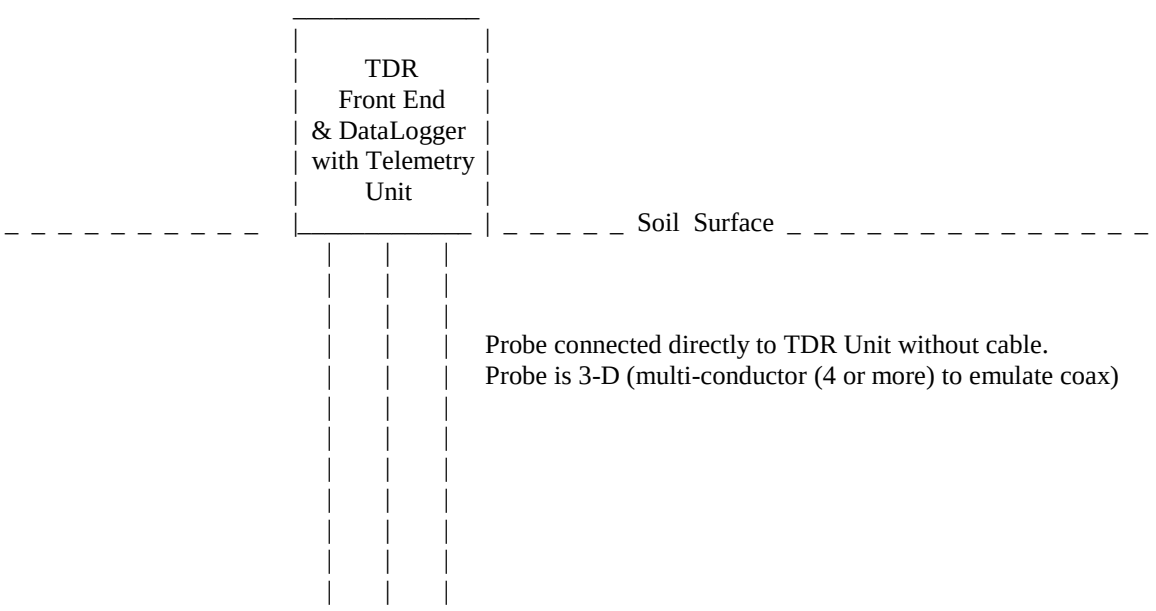


Figure 6.1: Compact Cableless TDR System

6.) The design of a high bandwidth TDR/TDT and/or FDR/FDTprobe (10 GHz) to be compatible with the high bandwidth requirements of the measurement algorithm (items 1 and 3 above). This would be a multiconductor probe that would have a minimal amount of radiation losses (emulate a coaxial cable and insure TEM propagation to 10 GHz) and would also be short with low series resistance and series inductance. This short high bandwidth probe would also give higher resolution in measuring water content vs. length along the probe (see item 4 above). 3.5mm SMA

interface hardware would be used in the TDR circuit module (item 5) to interface to this probe with a minimal distortion of the reflected signal up to the higher bandwidths.

7.) The use of a built in battery powered data acquisition system/telemetry system to log and transmit periodically the measured TDR/TDT/FDR/FDT data back to a base station for processing. A wake up circuit would keep the data acquisition circuit asleep and powered down except during a measurement interval and would keep the telemetry transmitter asleep and powered down except for an even less frequent transmission interval (perhaps once every 100 or 1000 measurement intervals). This would allow for low powered battery backup operation and for keeping the higher cost overhead of the algorithm back in a centralized base station computer thus reducing the cost of measurement for a large field by having the field probes consist of a small compact circuit/probe with a minimal amount of processing power.

The author (Ben Flugstad) plans to pursue all of the above enhancements during follow-on research and eventual development. The above enhancements give the potential of developing a powerful water content and electrical conductivity measurement tool that is of value to several potential markets including agriculture, water resources related industries, the food industry, scientific researchers and many more.

# Appendix A: Background Theory for Forward Prediction Model:

## Electromagnetic Wave Propagation Models:

### A.) Non-Bounded Uniform Plane Waves in a Lossy Homogeneous Medium

The general electromagnetic wave equations in physics are shown in (A-1) to (A-4) in both the time and frequency domains:

$$\nabla^2 \mathbf{E} = \mu \frac{\partial}{\partial t}[\sigma \mathbf{E} + \varepsilon \frac{\partial \mathbf{E}}{\partial t}] \quad \text{(A-1)}$$

$$\nabla^2 \mathbf{E} = j\omega\mu(\sigma + j\omega\varepsilon)\mathbf{E} = \gamma^2 \mathbf{E} \quad \text{(A-2)}$$

$$\nabla^2 \mathbf{H} = \mu \frac{\partial}{\partial t}[\sigma \mathbf{H} + \varepsilon \frac{\partial \mathbf{H}}{\partial t}] \quad \text{(A-3)}$$

$$\nabla^2 \mathbf{H} = j\omega\mu(\sigma + j\omega\varepsilon)\mathbf{H} = \gamma^2 \mathbf{H} \quad \text{(A-4)}$$

where $\omega = 2\pi f =$ angular frequency in radians / second.

$f =$ frequency in hertz or cycles / second.

$\varepsilon =$ Electric permittivity (Farads/meter)

$\mu =$ Magnetic permeability (Henries/meter)

$\sigma =$ Electrical Conductivity (Siemans/meter)

$H =$ Magnetic Field Intensity (Amps/meter)

$E =$ Electric Field Intensity (Volts/meter)

The general solutions to (A-1) and (A-3) are given in (A-5) and (A-6), for uniform plane waves propagating in the positive and negative z-direction away from an infinite current plane. They are both sine waves in time and space, but with amplitudes orthogonal in space which are both orthogonal to the propagation direction of the sine wave. These solutions are given as follows based on [12-17]:

$$\mathbf{E}_x(z,t) = [Ae^{-\alpha z}\cos(\omega t - \beta z + \vartheta) + Be^{\alpha z}\cos(\omega t + \beta z + \varphi)] \quad \text{(A-5)}$$

$$\mathbf{H}_y(z,t) = [\frac{A}{|\eta|}e^{-\alpha z}\cos(\omega t - \beta z + \vartheta - \xi) - \frac{B}{|\eta|}e^{\alpha z}\cos(\omega t + \beta z + \varphi - \xi)] \quad \text{(A-6)}$$

$\vartheta$, $\varphi$, and $\xi$ are additional phase shift terms of the positive and negative traveling waves and between the magnetic and electric field terms and are assumed equal to zero in this dissertation.

Equations A-5 and A-6 show propagating waves in both the positive and negative z-directions with electric and magnetic field components oriented in the x and y directions respectively. The waves attenuate over distance z in an exponential manner with the decay constant equal to $\alpha$.

Equations A-5 and A-6 are time domain solutions. In the frequency domain the solutions (to A-2 and A-4) are shown by equations A-7 and A-8 (positive z terms only and neglecting additional phase shifts):

$$E(z,\omega) = Ae^{-\gamma z} \qquad \text{(A-7)}$$

$$H(z,\omega) = \frac{A}{\eta} e^{-\gamma z} \qquad \text{(A-8)}$$

where $\gamma$ is the overall propagation constant and is given as follows:

$$\gamma = \sqrt{j\,\omega\mu(\sigma + j\,\omega\varepsilon)} = \sqrt{j\,\omega\mu(\sigma + \omega\varepsilon'' + j\,\omega\varepsilon')} \equiv \alpha + j\beta$$

$$= j\omega\sqrt{\mu\varepsilon'\left[1 - j\left[\frac{\sigma + \omega\varepsilon''}{\omega\varepsilon'}\right]\right]} \qquad \text{(A-9)}$$

where $\frac{\sigma + \omega\varepsilon''}{\omega\varepsilon'}$ = Loss Tangent (A-10)

and where

$\alpha$ = attenuation constant (Nepers/meter)

$\beta$ = phase constant (radians/meter).

The electric permittivity ε can be complex, as seen in (A-9) and (A-10) and defined by equations A-11to A-13 (where $j = \sqrt{-1}$), due to high frequency loss mechanisms not accounted for in DC conductivity such as the ability of a medium to absorb energy due to the self resonance of polar molecules such as water at microwave frequencies.

$$\varepsilon = \varepsilon' - j\varepsilon'' = \varepsilon_r'\varepsilon_0 - j\varepsilon_r''\varepsilon_0 = \varepsilon_r^*\varepsilon_0 \qquad \text{(A-11)}$$

where
$\varepsilon'$ = real or energy storage term of electric permittivity
$\varepsilon''$ = imaginary or energy loss term of electric permittivity
$\varepsilon_r'$ = real or energy storage term of dielectric constant
$\varepsilon_r''$ = imaginary or energy loss term of dielectric constant
$\varepsilon_r^*$ = overall complex dielectric constant

A widely used mathematical model for the complex electric permittivity when dielectric/polar relaxation mechanisms are present is the Cole-Cole model (neglecting dc conductivity) and is shown as follows [33-35]:

$$\varepsilon_r^* = \left[ \varepsilon_\infty + \frac{\varepsilon_s - \varepsilon_\infty}{1 + j\omega\tau^{(1-\kappa)}} \right] \qquad \text{(A-12)}$$

where

$\varepsilon_s$ = Low frequency dielectric constant
$\varepsilon_\infty$ = High frequency dielectric constant
$\tau$ = Relaxation time of the polar water molecule $H_2O$.
κ = A Parameter to account for spread in the resonance and is between 0 and 1.

For special cases where the spread parameter κ equals zero the model (A-12) reduces to the classical Debye relaxation model [36]. The Debye relaxation model is shown as follows for both the real (energy storage) and imaginary (energy loss) components of the permittivity.

$$\varepsilon' = \varepsilon_0 \left[ \varepsilon_\infty + \frac{\varepsilon_s - \varepsilon_\infty}{1 + \omega^2 \tau^2} \right] \quad \text{(A-13)}$$

$$\varepsilon'' = \frac{\omega \varepsilon_0 \tau (\varepsilon_s - \varepsilon_\infty)}{1 + \omega^2 \tau^2} \quad \text{(A-14)}$$

An example of the use of these models showing the frequency dependence on the permittivity components is shown as follows in figure A.1 for water with a Debye relaxation resonance near 17 GHz.

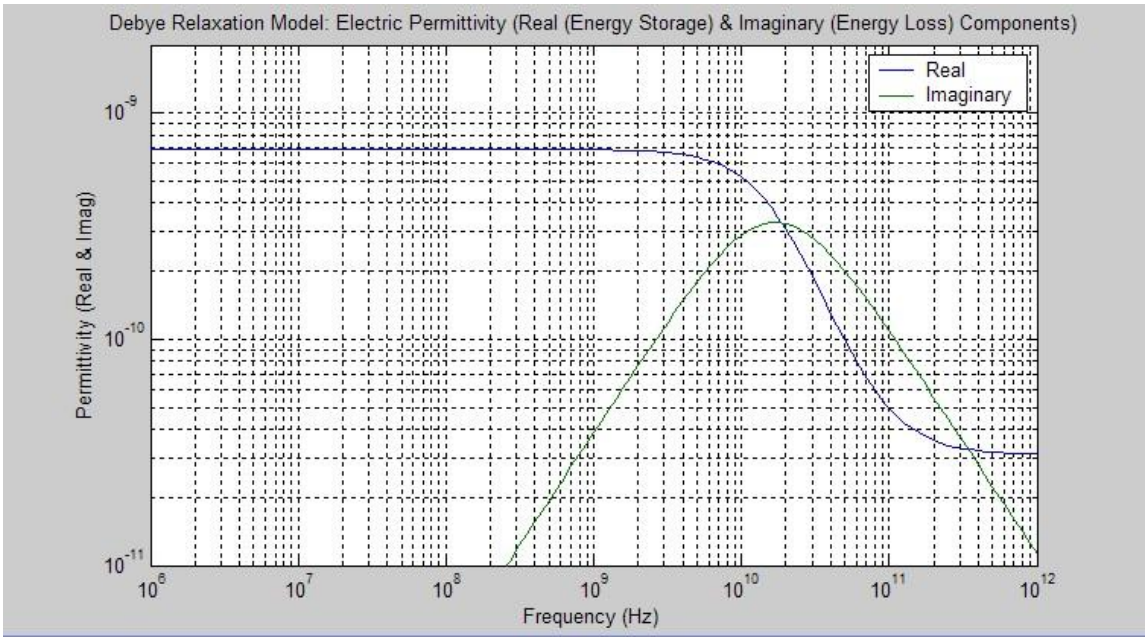


Figure A.1: Real (ε') and Imaginary (ε") Components of Permittivity vs. Frequency for Free Water with a Debye Relaxation Resonance at 17 GHz.

When a composite medium containing multiple relaxation times exist then the more general model can be represented as a summation of Debye terms (again assuming the spread parameter κ equals zero) as given by (A-15) (loss term only) [Metaxas et al., 1983]:

$$\varepsilon'' = \sum_{\tau = \tau_0}^{\tau_n} g(\tau) \left( \frac{\omega \tau}{1 + \omega^2 \tau^2} \right) \Delta\tau \quad \text{(A-15)}$$

Where $g(\tau)$ is the fraction of orientation polarization processes in each interval $\Delta\tau$. This summation assumes a linear combination of polarizations or Debye resonances. More complex mathematical models also exist for multiple Debye resonances if linearity is not assumed and for complex composite dielectric materials with varying geometrical arrangements of the constituents [Neelakanta, 1995]. The forward prediction models presented in this dissertation have the capability of modeling several multiple Debye Relaxation expressions and such a methodology is employed to model the combination of bound, semi-bound and free water. As is shown in the forward prediction model chapter the presence of bound and semi-bound water near charged interfaces such as are present with clay and organic matter can lead to multiple Debye relaxation terms with relaxation resonances spanning a wide range (10 MHz – 17 GHz) with the lower end of the range for fully bound water and the high end of the range for fully free water with a stochastic transition in between the ranges (modeled as semi-bound water).

The models shown in (A-12) – (A-15) can be employed in equation A-10 to obtain the loss tangent and subsequently into equations A-9, A-16 to A-19 and A-22 to A-24 for the other electromagnetic parameters. For (free) water (A-13) and (A-14) are often employed as models for the permittivity components. With those models (assuming a Debye relaxation resonance near 17 GHz) it can be readily shown that the wave propagation parameters and characteristic impedance become very complex especially above 1 GHz where the loss component of permittivity becomes more significant due to the dielectric relaxation phenomena (figure A.1). Therefore very high bandwidth TDR systems run into limitations at the high end of frequency due to the dispersion and attenuation due to the dielectric loss mechanisms of water.

In reviewing (A-9) the parameters $\alpha$ (attenuation constant) and $\beta$ (phase constant) are given as follows:

$$\alpha = \omega \sqrt{\frac{\mu \varepsilon'}{2}\left(\sqrt{1 + \left(\frac{\sigma + \omega\varepsilon''}{\omega\varepsilon'}\right)^2} - 1\right)} \tag{A-16}$$

$$\beta = \omega \sqrt{\frac{\mu \varepsilon'}{2}\left(\sqrt{1 + \left(\frac{\sigma + \omega\varepsilon''}{\omega\varepsilon'}\right)^2} + 1\right)} \tag{A-17}$$

The waves propagate at a velocity $v_p$ (phase velocity) given by:

$$v_p = \frac{\omega}{\beta} = \frac{1}{\sqrt{\frac{\mu\varepsilon'}{2}\left(\sqrt{1+\left(\frac{\sigma+\omega\varepsilon''}{\omega\varepsilon'}\right)^2}+1\right)}} \quad \text{(A-18)}$$

$\eta$ is the intrinsic impedance and is given by:

$$\eta = \sqrt{\frac{j\omega\mu}{\sigma+\omega\varepsilon''+j\omega\varepsilon'}} = \sqrt{\frac{\mu/\varepsilon'}{1-j\left[\frac{\sigma+\omega\varepsilon''}{\omega\varepsilon'}\right]}} \quad \text{(A-19)}$$

## B.) Guided Waves in a Lossy Homogeneous Medium: Transmission Lines:

Equations (A-5 to A-19) apply to the simplified case of uniform plane waves through a media of particular electromagnetic properties. However, TDR and TDT systems fall under the category of guided or bounded electromagnetic wave propagation technologies and more specifically transmission lines where two or more conductors are used to "guide" the waves in a particular direction or path [12-17].

Wave propagation in a transmission line can still take on many of the propagation characteristics of uniform plane waves propagating in the positive and negative "X" directions (or axis of the transmission line). Under certain assumptions about the geometry of the probe and the frequency content of the signal, the electric and magnetic fields can still be considered to be orthogonal to each other in the Y and Z planes with propagation in the X axis (the axis of the transmission line) as shown in figure A.2 (for standing waves as a result of waves propagating in both the positive and negative X direction). This assumption is termed the Transverse Electric Magnetic (TEM) propagation mode. The forward prediction models in this dissertation assume TEM propagation models.

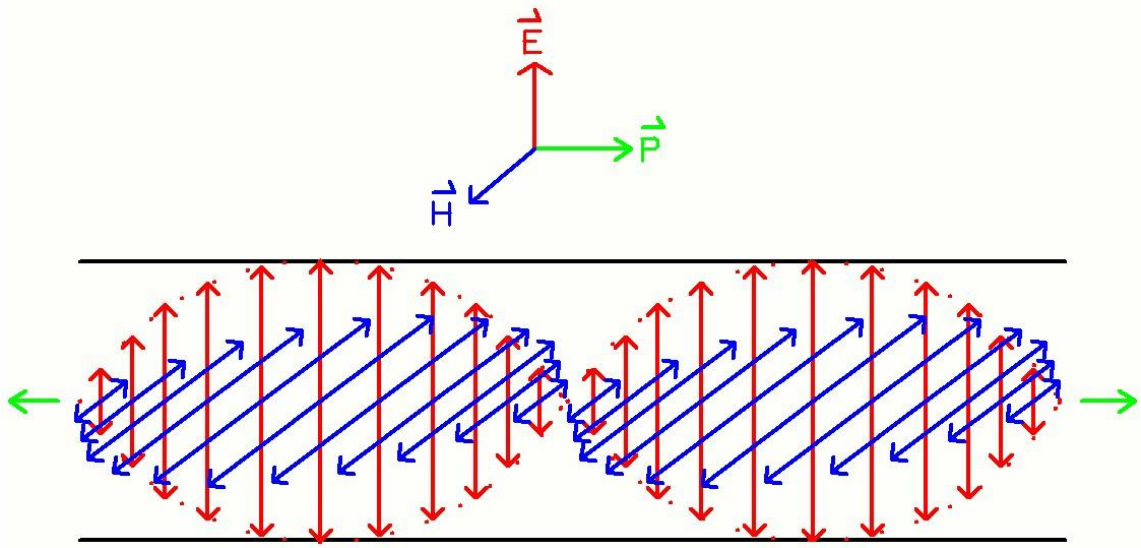


Figure A.2: TEM Wave Propagation Representation in a Parallel Conductor Transmission Line

Where

| | | |
|---|---|---|
| E | = | Electric Field Intensity |
| H | = | Magnetic Field Intensity |
| P | = | Poynting Vector or Direction of Wave (& Energy/Power) Propagation |

A transmission line is modeled with distributed elements for impedance as the waves are propagating down the line and do not see the impedance of the entire path simultaneously (if the wavelengths are short compared to the geometry of the probe (i.e. Zone 3 frequencies for a TDR / TDT system as described in the forward prediction model chapter)). A general representation for the distributed impedance elements per unit length along a particular length of transmission line is shown in the following figure:

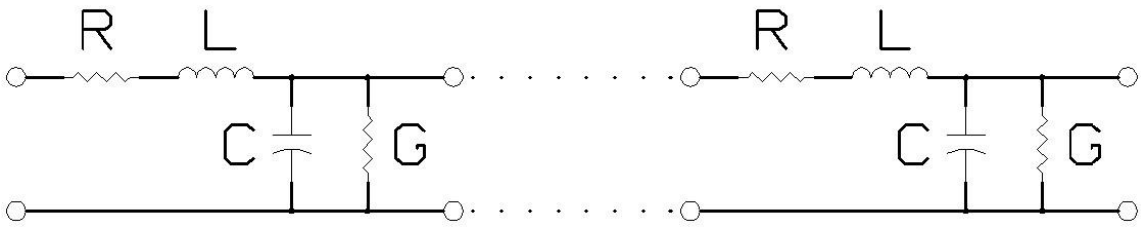


Figure A.3: Distributed Model for a Transmission Line

Where

R = Series Resistance per unit length of the Transmission Line

L = Series Inductance per unit Length of the Transmission Line

G = Shunt Conductance per unit Length of the Transmission Line

C = Shunt Capacitance per unit Length of the Transmission Line

In figure A.3 each distributed section (or R, L, G and C per unit length) represents some finite incremental length dx of the transmission line where the length dx is short compared to a wavelength but the overall length of the line is long compared to a wavelength (zone 3 frequencies in a TDR / TDT system). Figure A.3 also represents a case where the transmission line is homogeneous over the particular length that is being modeled so that R, L, C and G remain constant over that entire length in question. As will be shown later in this section in soils that assumption can only hold for limited lengths and hence the partitioning of the transmission line into cascaded sections or finite elements as shown earlier in figure 3.1 of the forward prediction model chapter and figures B.5 – B.14 in Appendix B.

Based on the above distributed model in figure A.3 the general expression for the propagation constant of a transmission line is given as follows:

$$\gamma = \sqrt{(R + j\omega L)(G + j\omega C)} \tag{A-20}$$

Similarly, the characteristic impedance for a transmission line is given as follows:

$$Z = \sqrt{\frac{R + j\omega L}{G + j\omega C}} \tag{A-21}$$

For the special case of a transmission line where the series loss term R (due typically to skin effect resistivity losses of the transmission line conductors themselves) can be neglected but the shunt losses (due to the medium) are still significant then it can be shown that (A-21) can be expressed as follows:

$$Z = \sqrt{\frac{j\omega L}{G + j\omega C}} = \sqrt{\frac{(j\omega\mu)(F_G)}{(\sigma + \omega\varepsilon'' + j\omega\varepsilon')/(F_G)}} = F_G \sqrt{\frac{\mu/\varepsilon'}{1 - j\left[\frac{\sigma + \omega\varepsilon''}{\omega\varepsilon'}\right]}} = F_G\eta \tag{A-22}$$

Where

$F_G$ = function of the geometrical parameters of the transmission line per unit length

In similar fashion it can be shown that if R = 0 the propagation constant γ in (A-20) reduces to the uniform plane wave expression for γ shown in (A-9) by the following relations:

$$\gamma = \sqrt{(j\omega L)(G + j\omega C)} = \sqrt{((j\omega\mu)(F_G))\frac{(\sigma + \omega\varepsilon'' + j\omega\varepsilon')}{F_G}} = \sqrt{j\omega\mu(\sigma + \omega\varepsilon'' + j\omega\varepsilon'}$$

$$\gamma = j\omega\sqrt{\mu\varepsilon'\left[1 - j\left[\frac{\sigma + \omega\varepsilon''}{\varepsilon'}\right]\right]} \qquad \text{(A-23)}$$

For a parallel wire transmission line (figure 3.3 in the forward prediction model chapter along with figure A.2 above in this appendix), the characteristic impedance is given as follows:

$$Z = \frac{1}{\pi}\text{Cosh}^{-1}\left(\frac{s}{d}\right)\sqrt{\frac{j\omega\mu}{\sigma + \omega\varepsilon'' + j\omega\varepsilon'}} = \frac{1}{\pi}\text{Cosh}^{-1}\left(\frac{s}{d}\right)\sqrt{\frac{\mu/\varepsilon'}{1 - j\left[\frac{\sigma + \omega\varepsilon''}{\varepsilon'}\right]}} = \frac{1}{\pi}\text{Cosh}^{-1}\left(\frac{s}{d}\right)\eta$$

(A-24)

Where

s = spacing between the conductors

d = diameter of the conductors

Comparing (A-22) to (A-24) gives the following relation for the geometrical factor:

$$F_G = \frac{1}{\pi}\text{Cosh}^{-1}\left(\frac{s}{d}\right)$$

(A-25)

Using (A-25) along with (A-22) and assuming R is significant the following values for R, G, L and C can be derived [12]:

$$C = \frac{\pi \varepsilon '}{\text{Cosh}^{-1}\left(\frac{s}{d}\right)} \tag{A-26}$$

$$L = \left(\frac{\mu}{\pi}\right) Cosh^{-1}\left(\frac{s}{d}\right) \tag{A-27}$$

$$G = \frac{\pi(\sigma + \omega\varepsilon '')}{\text{Cosh}^{-1}\left(\frac{s}{d}\right)} \tag{A-28}$$

$$R = \left(\frac{2\,R_s}{\pi\,d}\right)\left[\frac{\frac{s}{d}}{\sqrt{(s/d)^2 - 1}}\right] \tag{A-29}$$

Where Rs = the skin effect surface resistivity of the metal wire and is given by equation A-30:

$$R_s = \sqrt{\frac{\omega \mu_c}{2\,\sigma_c}} \tag{A-30}$$

Plugging these equations into equations A-20 and A-21 we get the following general expression for total propagation constant $\gamma_T$ and total characteristic impedance $Z_T$ accounting for all loss mechanisms:

$$\gamma_T = \sqrt{\left(\frac{2\,R_s}{\pi\,d}\left[\frac{\frac{s}{d}}{\sqrt{\left(\frac{s}{d}\right)^2 - 1}}\right] + \frac{j\omega\mu\,\text{Cosh}^{-1}\left(\frac{s}{d}\right)}{\pi}\right)\left(\frac{\pi(\sigma + \omega\varepsilon '')}{\text{Cosh}^{-1}\left(\frac{s}{d}\right)} + \frac{j\omega\pi\varepsilon '}{\text{Cosh}^{-1}\left(\frac{s}{d}\right)}\right)} \tag{A-31}$$

$$Z_T = \sqrt{\left( \frac{2R_s}{\pi d}\left[ \frac{\frac{s}{d}}{\sqrt{\left(\frac{s}{d}\right)^2 - 1}} \right] + \frac{j\omega\mu \,\mathrm{Cosh}^{-1}\left(\frac{s}{d}\right)}{\pi} \right) \Bigg/ \left( \frac{\pi\left(\sigma + \omega\varepsilon''\right)}{\mathrm{Cosh}^{-1}\left(\frac{s}{d}\right)} + \frac{j\omega\pi\varepsilon'}{\mathrm{Cosh}^{-1}\left(\frac{s}{d}\right)} \right)} \quad \text{(A-32)}$$

For gold plated or other high quality conductors the skin effect surface resistivity Rs can often be neglected below 20 GHz (where most TDR systems operate at) and it can be shown that equation A-31 reduces to the same expression as that for the propagation constant for uniform plane waves as given in equation A-9 and repeated in equation A-23. Similarly, equation A-32 reduces to that given in equations A-22 and A-24 when the series resistivity loss terms are neglected. However, the general equations (A-31) and (A-32) including the series loss component for the parallel wire transmission line propagation constant and characteristic impedance terms are included in the forward prediction model developed in MATLAB and presented in this dissertation as one example of a transmission line geometry. For other transmission line geometries there would be other equations or models developed as $F_G$ would be different. Another example of a popular transmission line geometry for TDR and TDT systems is a 3 wire (coplanar) transmission line probe (figure 3.4 in the forward prediction model chapter). Coplanar 3-wire probes have gained popularity as they better approximate the “unbalanced” transmission line of a feeding system (such as a coaxial cable) and hence do not require a “balun” at the interface and don’t have as large of an impedance discontinuity at the first reflection. A “balun” is a balanced (e.g. parallel line) to unbalanced (e.g. coaxial line) transformer that also can provide some limited impedance matching capability (for the case of a 4:1 balun). However, baluns are problematic as they are typically of some limited bandwidth (far narrower than the frequency range of a TDR/TDT signal) and also represent one additional cascaded element that must be de-embedded (frequency domain) or de-convolved (time domain) in a measurement algorithm. Finally the impedance matching capability of a balun is again limited in bandwidth as well as only applicable for a narrow range of water contents (as the characteristic impedance of a parallel wire line varies over a wide range with the typical ranges of water contents in a soil). Therefore a balun is of little value in a soil TDR/TDT system and causes more problems than any benefits it could provide. The forward prediction models in this dissertation were evaluated with both two wire (balanced) and three wire coplanar (unbalanced) probes (neither of which utilized baluns). Other mutli-conductor probes (up to 7 conductors) have been used in the field.

A common expression found in equations A-9, A-16 to A-19 and A-22 to A-24 is again the loss tangent defined earlier in (A-10). The loss tangent is important in that when it is greater than one the loss terms are dominating and when it is less than one the dielectric or storage terms are dominating in terms of influencing the electromagnetic propagation and impedance functions.

# Appendix B: Scattering (S) Parameter Theory & Cascaded Transmission Line Models:

A common modeling technique used by both electromagnetic and non-electromagnetic scattering algorithms involves the utilization of Scattering (S) Parameters and Transmission (T) parameters (background theory developed in [1] through [18] and summarized in this appendix). The underlying theory for S-parameters and T-Parameters has its roots in classical linear matrix algebra and scattering particle physics dating back to the later $19^{th}$ century and early $20^{th}$ century. One of the earliest references to the application of S-parameters to an engineering problem is in the work by Campbell and Foster (1920) [1] in applying these techniques to the modeling of networks associated with telephone substation and switching/repeater circuits. However, the widespread utilization of S-parameters and T-Parameters in the context of modeling engineering problems did not occur until the post World War II period with the pioneering modeling work at the Massachusetts Institute of Technology (MIT) beginning with the work of Montgomery et al (1948) [2]. This continued on into the next decade with the early pioneering work on signal flow graphs by Dr. Samuel .J. Mason also of MIT with his two landmark publications in 1953 [3] and 1956 [4] where his theory on modeling cascaded networks ("Mason's Non-Touching Loop Rule) was presented. That same year (1956) also saw several publications on S-parameters in a special issue of the Transactions of International Radio Engineers (IRE) Journal devoted to this topic including [5] and [6]. A good review of the use of signal flow graphs together with S-parameters was presented by Hunton in 1960 [7]. The practical use of S-Parameters in actual measurements was made possible with the invention and release of the first commercially available network analyzer (Hewlett Packard 8410) in the later 1960's corresponding with the 1967 HP Journal Article: "S-Parameter Theory and Application" [8] and referenced in [9] ,[10] and [11]. Scattering (S) parameter and Transmission (T) Parameter modeling can be applied to all branches of science where scattering phenomena exist and are even used in non-science disciplines. The background theory for S-Parameters and T-Parameters is summarized in this appendix and applied to the TDR and TDT measurement methods involving cascaded transmission line probes. The techniques are also applicable to general cascaded domain techniques such as GPR and Remote Sensing.

Scattering parameters allow for the convenient handling and modeling of a complex array of reflected and transmitted signals of multiple ports to model the scattering phenomena associated with complex systems. This representation can be modeled as a set of simultaneous matrix equations shown as follows for an n-port structure or scattering body [10]:

$$\begin{bmatrix} b_1 \\ b_2 \\ . \\ . \\ b_n \end{bmatrix} = \begin{bmatrix} S_{11} & S_{12} & . & . & S_{1n} \\ S_{21} & S_{22} & . & . & S_{2n} \\ . & . & . & . & . \\ . & . & . & . & . \\ S_{n1} & S_{n2} & . & . & S_{nn} \end{bmatrix} \begin{bmatrix} a_1 \\ a_2 \\ . \\ . \\ a_n \end{bmatrix} \tag{B-1}$$

Where

$$\frac{b_i}{a_k} = S_{ik} \Big|_{a_j = 0 \quad \text{for } j \neq k} \tag{B-2}$$

for the specific case when the contributions from stimuli "a" from all non-k ports is zero. This specific case allows for representing the contribution to scattered response signal $b_i$ exiting port "i" from the specific stimulus $a_k$ at port "k" and related by the scattering coefficient or S-parameter $S_{ik}$. In the context of electromagnetic wave propagation systems by convention the signal flow graph terms ("a" and "b" terms) are related to incident and reflected voltage terms via the following relations [12, 13]:

$$a_k = \frac{V_k^+}{\sqrt{Z_k}} \tag{B-3}$$

$$b_i = \frac{V_i^-}{\sqrt{Z_i}} \tag{B-4}$$

Where

$V_k^+$ = Voltage of the wave incident at port k.

$V_i^-$ = Voltage of the scattered response wave at port i.

$Z_k$ = Characteristic Impedance at port k.

$Z_i$ = Characteristic Impedance at port i.

The general relation for S-Parameters about various ports for an n-port structure with differing characteristic impedances for each port is therefore given as follows [13]:

$$\frac{b_i}{a_k} = S_{ik} = \frac{V_i^- \sqrt{Z_k}}{V_k^+ \sqrt{Z_i}} \Bigg|_{a_j = 0 \quad \text{for } j \neq k} \tag{B-5}$$

Again, this is defined for the cases where all non-k stimuli (i.e. all non-k "a" terms and therefore all non-k incident voltage terms) are zero (i.e. those other ports are "matched" in terms of impedance so that no signals return into those ports from subsequent reflections). These expressions show that the "a" and "b" terms making up the S-parameters are voltage terms normalized to the square root of impedance and are therefore analogous to square root of power terms (henceforth called "normalized signal flow" terms). The S-Parameters are ratios of these various normalized signal flow terms and therefore ratios of the square roots of the corresponding scattered power flows.

The representation given in (B-1) shows the general case where the scattered response signals are actually functions of stimuli from all multiple "n" ports. Both reflected signals and transmitted signals about a scattering interface or complex set of multiple scattering interfaces via multiple ports can be modeled with this representation. Scattering Parameters can be represented in either the time domain or frequency domain and there are situations where one or the other domains is preferable and other situations where switching back and forth and using both domains is of value. This latter approach is utilized in the forward prediction models presented in this dissertation.

There are different levels to scattering models that all must be addressed. If it is assumed that a particular medium is made up of several boundaries or impedance discontinuities then reflections will occur at those boundaries and some portion of the signal power will return back towards the source and the remaining portion of the signal power will transmit on through the medium. There can be multiple subsequent boundaries throughout the medium between any two given ports resulting in several sub-segments of different properties throughout the medium between those ports. Complex superposition (convolution) in the time domain of multiple reflected and transmitted signals due to each of these boundaries occurs to make up the total set

of scattered signals. All of this makes up the scattering profile which can be modeled by the scattering (S-Parameter) matrix as shown in general fashion in (B-1).

At the lowest level the parameters associated with each sub-segment or region within a medium (between significant boundaries) must be modeled or determined. The modeling of these individual segments can be complicated if there are multiple varying parameters such as electrical conductivity (ohmic) and electric permittivity (dielectric) parameters together with geometrical variations (of the segment or particular probe or guided structure if present). At the higher level the signal response of each of these segments is then convolved into a total scattering model or matrix leading to potentially very complex modeling problems if several distinct segments or zones exist within a medium.

Although the representation in (B-1) is for the general n-port case the forward prediction models presented in this dissertation have been initially developed and validated with 2-port structures associated with transmission line modeling. However, the principles associated with the models have direct application to multiple port devices and future research will extend the use of the models to those applications.

**S-Parameters of 2-Port Networks:**

For the specific case of transmission lines including the sub-case of TDR and TDT systems the systems are modeled as two port networks. The Scattering or S-parameters are defined as follows for a 2-port network:

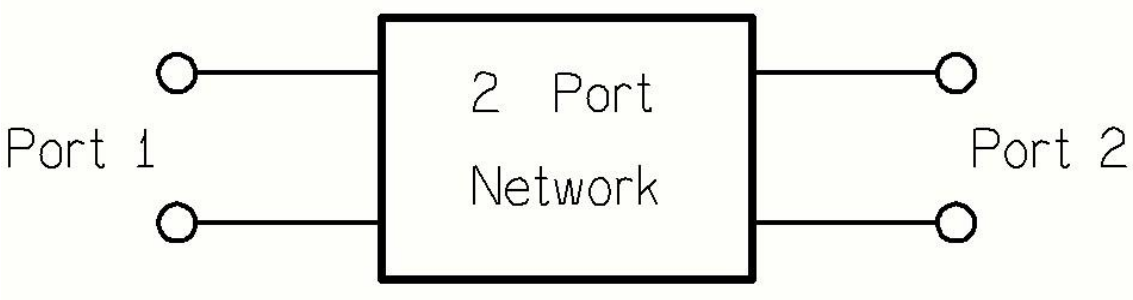


Figure B.1: Two Port Network for S-Parameter Definitions

Scattering Coefficients (S-Parameters) of a Two Port Network:

$$S11 = \frac{\text{Net Reflected Normalized Signal Flow at port 1 (b1)}}{\text{Incident Normalized Signal Flow at port 1 (a1)}} \quad \text{(with port 2 matched)} \qquad \text{(B-6)}$$

$$S21 = \frac{\text{Net Transmitted Normalized Signal Flow to port 2 (b2)}}{\text{Incident Normalized Signal Flow at port 1 (a1)}} \quad \text{(with port 2 matched)} \qquad \text{(B-7)}$$

$$S12 = \frac{\text{Net Transmitted Normalized Signal Flow to port 1 (b1)}}{\text{Incident Normalized Signal Flow at port 2 (a2)}} \quad \text{(with port 1 matched)} \qquad \text{(B-8)}$$

$$S22 = \frac{\text{Net Reflected Normalized Signal Flow at port 2 (b2)}}{\text{Incident Normalized Signal Flow at port 2 (a2)}} \quad \text{(with port 1 matched)} \qquad \text{(B-9)}$$

The two port network could be a series of cascaded two port networks in which only the last stage (input stage or output stage) is matched to satisfy the above definitions. There could be several internal stages that are not matched leading to multiple reflections that add or subtract to form a composite reflected and transmitted signal. This is why the term “net” is in all the above definitions. The topic of cascaded networks will be discussed later in this section.

A common two-port electromagnetic wave propagation structure that can be modeled with S-Parameters includes a transmission line with impedance discontinuities illustrated as follows for a single discontinuity at boundary $B_2$.

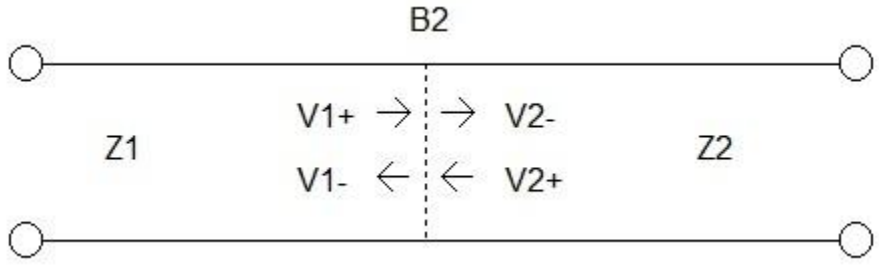


Figure B.2: Impedance Discontinuity on a Transmission Line

The boundary between the two impedances can be further modeled with the following signal flow graph [3], [4]:

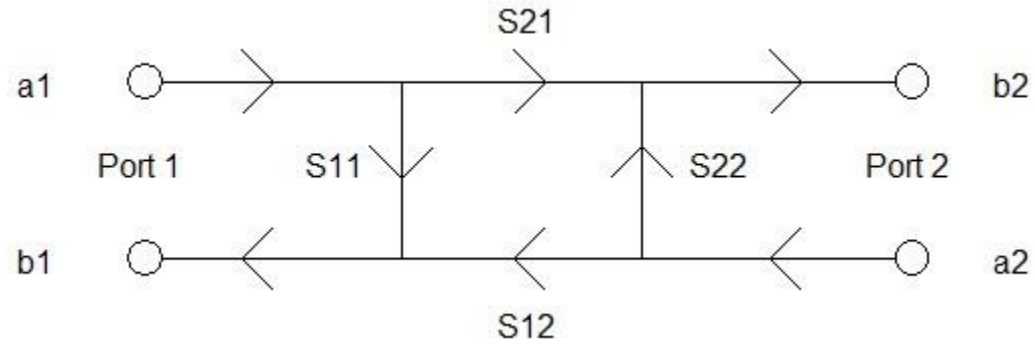


Figure B.3: Signal Flow Graph for Impedance Discontinuity Boundary

Z1 and Z2 are the characteristic impedances of the transmission lines at port 1 and port 2 respectively and the Vn+ and Vn- terms are the incoming and outgoing voltage terms for port n

(or in this case ports 1 and 2). By convention the normalized signal flow graph terms ("a" and "b" terms) are related to the voltage terms via the following relations [12], [13]:

$$a_1 = \frac{V_1^+}{\sqrt{Z_1}} \qquad \text{(B-10a)} \qquad\qquad a_2 = \frac{V_2^+}{\sqrt{Z_2}} \qquad \text{(B-10b)}$$

$$b_1 = \frac{V_1^-}{\sqrt{Z_1}} \qquad \text{(B-10c)} \qquad\qquad b_2 = \frac{V_2^-}{\sqrt{Z_2}} \qquad \text{(B-10d)}$$

Therefore for the case of this simple impedance boundary and utilizing equations (B-1 to B-10) the S-parameters are given as follows (assuming the opposite port is matched to the impedance beyond it – e.g. $a_2 = 0$ when determining S-Parameters associated with $a_1$ and vice versa).

$$S11 = \frac{b_1}{a_1} = \Gamma_1 = \frac{Z_2 - Z_1}{Z_2 + Z_1} = \text{Input Reflection Coefficient} \qquad \text{(B-11)}$$

$$S21 = \frac{b_2}{a_1} = \sqrt{\frac{Z_1}{Z_2}}\left(1+\Gamma_1\right) = \text{Forward Transmission Coefficient} \qquad \text{(B-12)}$$

$$S12 = \frac{b_1}{a_2} = \sqrt{\frac{Z_2}{Z_1}}\left(1+\Gamma_2\right) = \sqrt{\frac{Z_2}{Z_1}}\left(1-\Gamma_1\right) = \text{Reverse Transmission Coefficient} \qquad \text{(B-13)}$$

$$S22 = \frac{b_2}{a_2} = \Gamma_2 = \frac{Z_1 - Z_2}{Z_1 + Z_2} = -\Gamma_1 = \text{Output Reflection Coefficient} \qquad \text{(B-14)}$$

Note that the "a" and "b" terms and therefore the S-parameters are all again normalized to the square root of impedance. Therefore the S-Parameters can be interpreted as ratios of the square root of the power of the respective signal flows at each port. For the special case where the impedances are equivalent at each port the S-Parameters would simplify to the point where they are equivalent to voltage ratios. Within a given port (e.g. S11) the S-Parameters are always equivalent to voltage ratios (as the square root of impedance terms drop out in the ratios).

Therefore reflection and transmission terms across lossless boundaries $B_n$ associated with impedance discontinuities (as shown in figure 3.1 (Forward Prediction Models Chapter) along with figures B.2 and B.3) can be modeled via S-Parameters. In addition, propagation delay and loss terms for the propagating waves can be modeled into the paths between the boundaries on these networks as well (modeled as individual propagation elements $E_n$ in a cascaded transmission line per figure B.5). The simplified 2-port structure from figures B.2 and B.3 can be expanded to include a propagation term (accounting for electrical length and loss) associated with section 2 or element $E_2$ (per the conventions of figure B.5) (w/impedance = $Z_2$). If we assume that there is a subsequent load connected to Port 2 with an equivalent scattering parameter and reflection coefficient looking into that load ($S_L = \Gamma_L$) then the signal flow model of figure B.3 can be modified as shown in figure B.4:

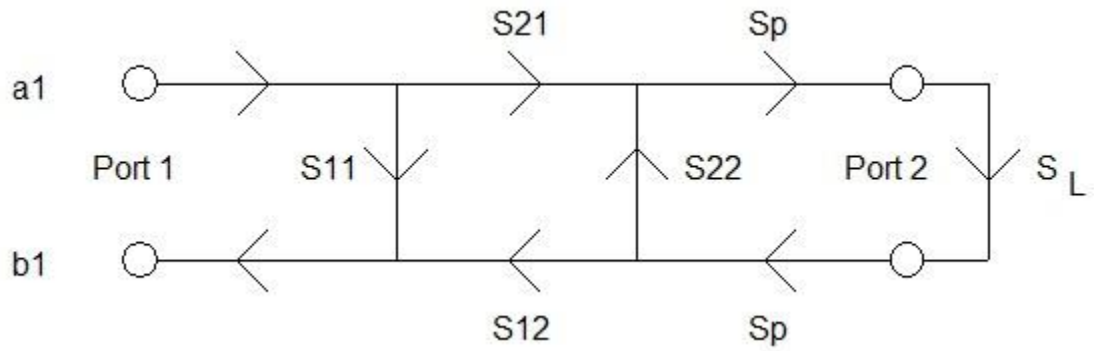


Figure B.4: Signal Flow Graph with Propagation Parameters and Load Termination Added

Where $S_L$ is the S-Parameter associated with the reflection coefficient (equivalent to $\Gamma_L$) looking into the load from the output of port 2 and Sp is an additional forward transmission S-Parameter coefficient to account for the propagation parameters of delay and loss (within section 2 or element $E_2$). Sp is defined as follows (in the frequency domain):

$$S_p = e^{-\gamma_2 L_2} = e^{-(\alpha_2 + j\beta_2)L_2} \qquad \text{(B-15)}$$

Where $\gamma_2$ is the propagation constant from electromagnetic wave propagation theory ([12-18] and given also in appendix A) for section 2 or element $E_2$. $L_2$ is the physical length of section 2 or element $E_2$ of the network. From the theory of electromagnetics [12-18] the propagation

constant (in general) can be shown to be that given by (A-23) in Appendix A for a lossy network in the frequency domain (neglecting the series R term) or more generally by (A-31) in Appendix A accounting for all loss terms for the specific case of a parallel wire transmission line. For the case of composite media within the particular element the propagation constant would make use of one of the composite mixing or stochastic interpolation models for propagation constant based on (3-7 to 3-16, 3-24, 3-25, 3-32 to 3-35, 3-42, 3-46, 3-50, 3-52, 3-56 or 3-62) presented in the Forward Prediction Model chapter of this dissertation. Similarly the characteristic impedance values for sections or elements 1 and 2 given in equations (B-11) to (B-14) can be shown to be that given by (A-22) or (A-24) in Appendix A for a lossy network in the frequency domain (again neglecting the series R term) or more generally by (A-32) in Appendix A again accounting for all loss terms for the specific case of a parallel wire transmission line. Finally models for the characteristic impedance can be derived from the composite mixing models based on (3-7 to 3-16) and (3-17 to 3-67) presented in the Forward Prediction Model chapter of this dissertation and plugging the appropriate parameter models for the permittivity terms and conductivity into (A-32) from Appendix A for a parallel wire transmission line or other similar equations for other geometries of transmission lines. All of these models are included in the forward prediction models presented in this dissertation.

The overall expression (in the frequency domain) for the effective overall reflection coefficient or overall scattering function looking into port 1 (considering the unmatched termination at port 2 and the propagation terms in section 2) can then be shown to be the following [8 – 11 and 13] using Mason's non-touching loop rule (derivation shown in cascaded transmission line section of this Appendix):

$$S11\_Input = S11 + \frac{(S21)(S12)S_L(S_p)^2}{1-(S22)S_L(S_p)^2} = \Gamma_1 + \frac{\left(1-\Gamma_1^2\right)\Gamma_L e^{-j2\gamma_2 L_2}}{1+\Gamma_1\Gamma_L e^{-j2\gamma_2 L_2}} = \frac{\Gamma_1 + \Gamma_L e^{-j2\gamma_2 L_2}}{1+\Gamma_1\Gamma_L e^{-j2\gamma_2 L_2}} \quad \text{(B-16)}$$

Where $\Gamma_1$ = S11 = Input Reflection Coefficient at Boundary of Section 1 and 2.

The specific S-Parameters that go into this equation can then be developed using equations (A-7 to A-32) from Appendix A and (3-3 to 3-16) from the Forward Prediction Model Chapter together with (3-17 to 3-67) from the forward prediction model chapter and plugging that

information back into equations (B-11 to B-14). It is readily seen that a large number of variables are already contributing to this expression for even this simplified network. These expressions will get very complex if composite media of mixtures of various constituents make up each section (involving equations (3-17 to 3-67) from the forward prediction model chapter). All of this is accounted for in the forward prediction models presented in this dissertation.

## S-Parameters of Cascaded Networks:

Often in real world systems such as those found in TDR and TDT time domain measurement systems or Vector Network Analyzer (VNA) frequency domain measurement systems the transmission line is realistically a series of cascaded transmission lines of different impedance and propagation properties within each sub-segment. A general representation of such a network is shown in figure B.5:

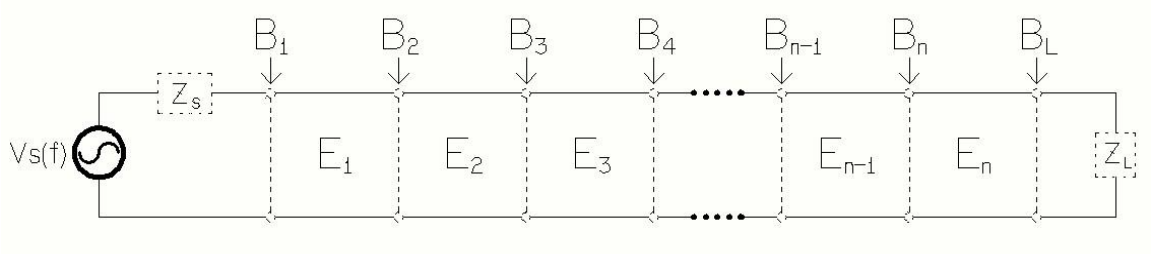


Figure B.5: Cascaded Transmission Line Representation Showing Individual Elements and Boundaries

Where

$E_n$ = Transmission Line Cascaded Element n.

$B_n$ = Boundary at Input of Element n or between Element n-1 and Element n.

Vs(f) = Broadband RF/Microwave Voltage Source as a function of Frequency (f).

$Z_S$ = Source Impedance (Often near 50 Ohms for TDR/TDT or VNA Equipment)

$Z_L$ = Load Impedance (Open Circuit for TDR and typically 50 Ohms for TDT or VNA)

For a TDR system the load will typically be an open circuit although could just as well be a short circuit. With TDR signals would only be measured at the input based on the superposition of the incident and overall equivalent reflected signals (from all the individual element boundaries within). For a TDT system or alternatively a Vector Network Analyzer (VNA) system the load impedance will typically be near 50 Ohms and signals will be measured at both the input and output of the network. For all these systems the source impedance is typically near 50 Ohms. Each element can be further broken down per figure B.6:

Each of the individual cascaded elements in the transmission line can in turn be represented by both the geometrical (probe) parameters and electromagnetic parameters as described in Appendix A along with the Forward Prediction Model chapter and shown graphically as follows:

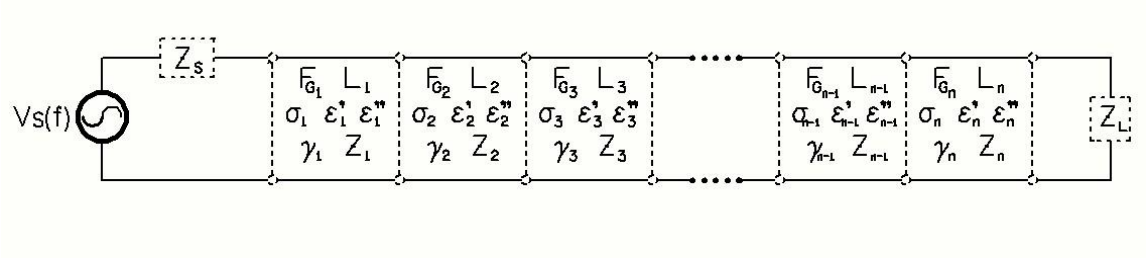


Figure B.6: Cascaded Transmission Line Representation Showing Parameters of Each Element

Where

$F_{Gn}$ = Probe Geometry Factor for Transmission Line Cascaded Element n.

$L_n$ = Length of Transmission Line Cascaded Element n.

$\sigma_n$ = Bulk Equivalent Electrical Conductivity of Cascaded Element n.

$\varepsilon_n'$ = Bulk Equivalent Electric Permittivity Real (Storage) Term of Cascaded Element n.

$\varepsilon_n''$ = Bulk Equivalent Electric Permittivity Imaginary (Loss) Term of Cascaded Element n.

$\gamma_n$ = Equivalent Propagation Constant for Transmission Line Cascaded Element n.

$Z_n$ = Equivalent Characteristic Impedance of Transmission Line Cascaded Element n.

The boundaries between each individual elements lead to reflection coefficients due to the difference in impedance as given by equations (3-5) (Forward Prediction Model Chapter) and (B-11). This is illustrated in figure B.7:

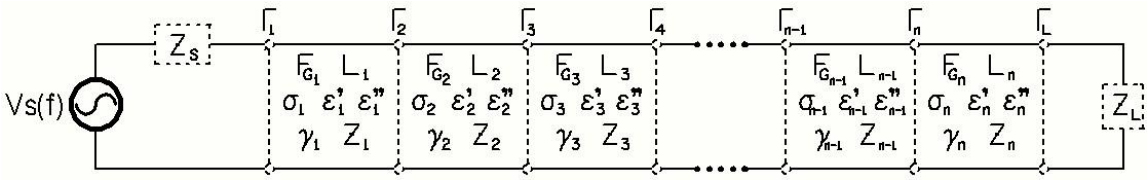


Figure B.7: Cascaded Transmission Line Showing Boundaries with Individual Reflection Coefficients

Where

$\Gamma_n$ = Reflection coefficient at the Boundary between Element n-1 and Element n.

Three alternative methods of deriving the S parameters of complex cascaded network are presented:

1.) Transmission (T) Parameter to Scattering (S) Parameter Conversions
2.) Mason's Non-Touching Loop Rule
3.) Nested Construction Method (S11 or S22 only)

All these methods will lead to equivalent results (where they can be employed) and each has their advantages and disadvantages. All of these methods are implemented in the forward prediction models in places where they are most efficiently utilized. Each of these methods are now described:

## 1.) Transmission (T) Parameters:

One method of modeling networks of multiple cascaded networks involves the use of transmission (T) parameters [11]. In analogous fashion to S-parameters a set of matrix equations can be developed for T-Parameters as shown in (B-17) for a simple two port network (where the "a" and "b" normalized signal flow terms are as previously defined):

$$\begin{bmatrix} a_1 \\ b_1 \end{bmatrix} = \begin{bmatrix} T_{11} & T_{12} \\ T_{21} & T_{22} \end{bmatrix} \begin{bmatrix} a_2 \\ b_2 \end{bmatrix} \tag{B-17}$$

The T-Parameters of multiple cascaded sections can simply be multiplied together to get a T-Matrix representation of the entire network which is a simpler process than that which utilizes S-Parameters directly. Converting between T-Parameters and S-Parameters is straight forward and shown as follows [11].

$$\begin{bmatrix} T_{11} & T_{12} \\ T_{21} & T_{22} \end{bmatrix} = \begin{bmatrix} -\dfrac{S_{11}S_{22} - S_{21}S_{12}}{S21} & \dfrac{S_{11}}{S_{21}} \\ -\dfrac{S_{22}}{S_{21}} & \dfrac{1}{S_{21}} \end{bmatrix} \tag{B-18}$$

$$\begin{bmatrix} S_{11} & S_{12} \\ S_{21} & S_{22} \end{bmatrix} = \begin{bmatrix} \dfrac{T_{12}}{T_{22}} & \dfrac{T_{11}T_{22} - T_{21}T_{12}}{T_{22}} \\ \dfrac{1}{T_{22}} & -\dfrac{T_{21}}{T_{22}} \end{bmatrix} \tag{B-19}$$

Each element and boundary in the cascaded transmission line models shown in figures B.5 to B.7 can be represented by either S-Parameters or T-Parameters. This is illustrated in figure B.8:

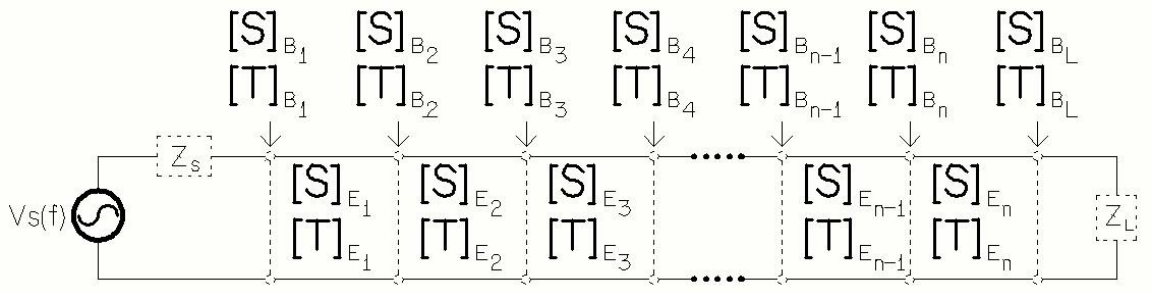


Figure B.8: Cascaded Transmission Line Showing **S** and **T** Matrices for Each Element & Boundary

Figures B.9 – B.14 give signal flow graphical representations for cascaded TDT and TDR systems:

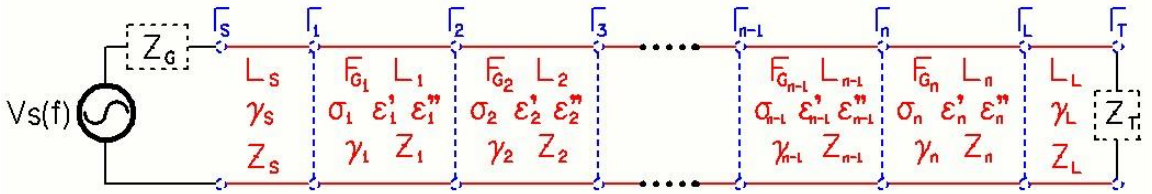


Figure B.9: TDT Transmission Line Separated into Elements (red) and Boundaries (blue)

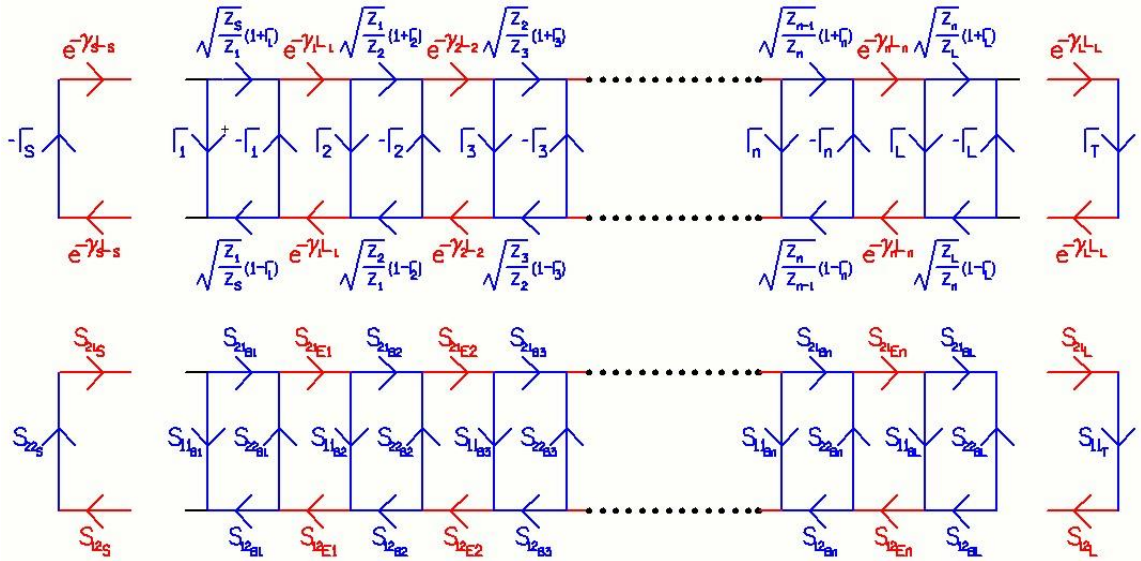

Figure B.10: TDT Signal Flow Graph and S-Parameters for Each Element (Red) and Boundary (Blue)

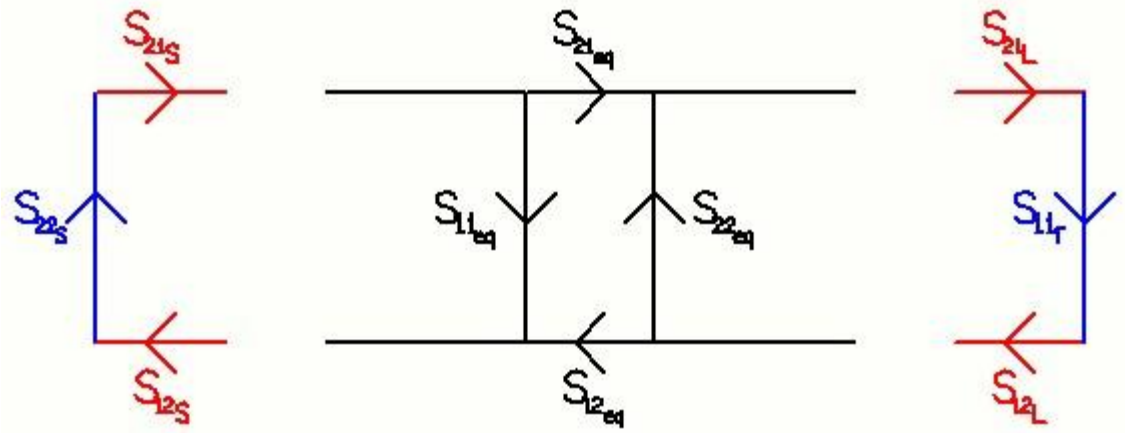

Figure B.11: Equivalent Overall S-Parameter Model for Cascaded Transmission Line for TDT System

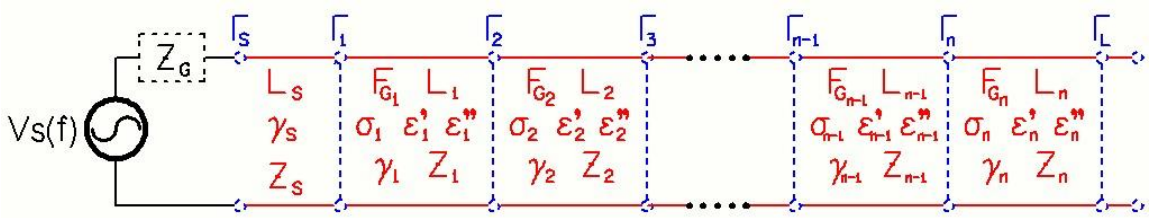


Figure B.12: TDR Transmission Line Separated into Elements (red) and Boundaries (blue)

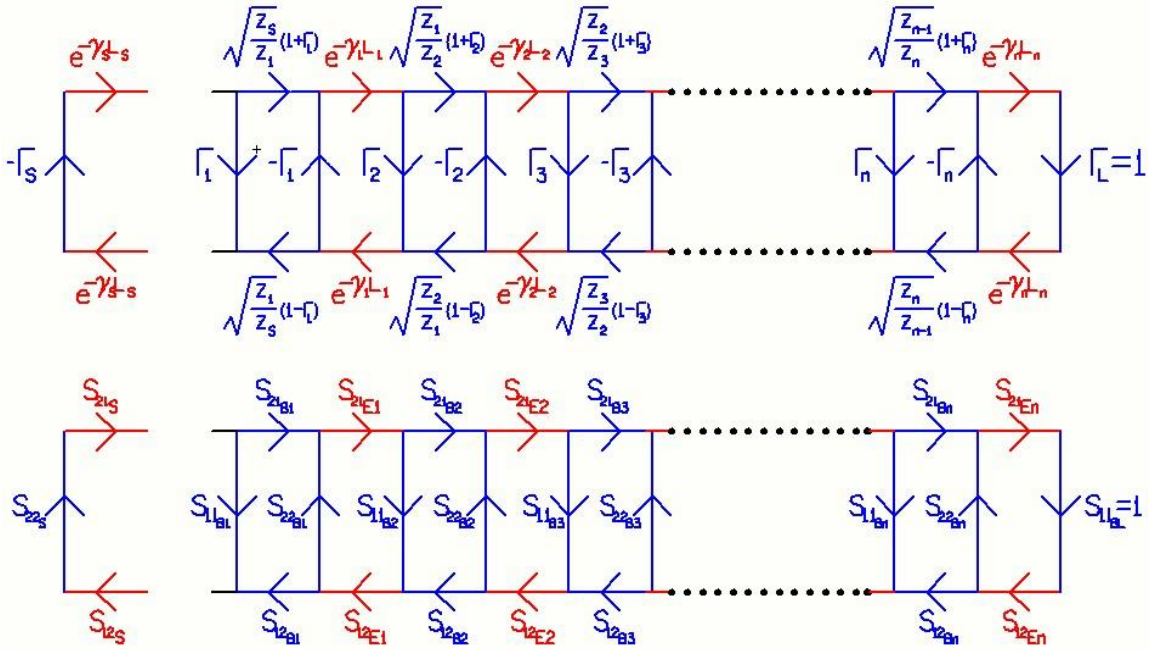


Figure B.13: TDR Signal Flow Graph and S-Parameters for Each Element (Red) and Boundary (Blue)

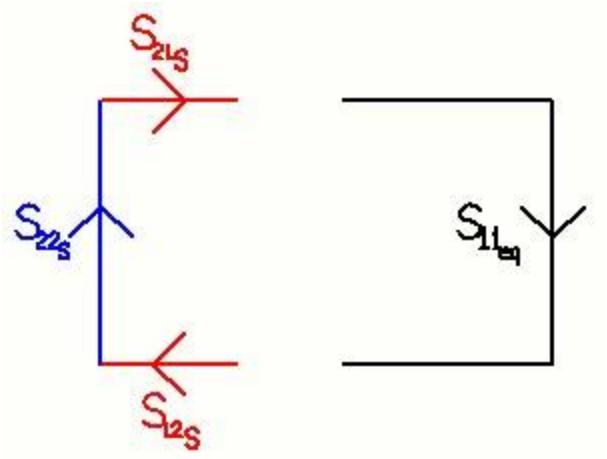


Figure B.14: Equivalent Overall S-Parameter Model for Cascaded Transmission Line for TDR System

In figures B.9 – B.14 the "blue" represents boundaries $B_n$ and the "red" represents elements $E_n$ in terms of how the S-Parameter signal flow graphs are generated for the overall cascaded network or transmission line. The forward prediction models in this dissertation use both Mason's Non-Touching Loop Rule (described next) as well as switching between S-Parameters and T-Parameters (described above) as alternative tools to simplify the overall signal flow graphs of figures B.10 and B.13 to give the simplified equivalent networks of figures B.11 and B.14 respectively. Mason's non-touching loop rule is more computationally intensive than the conversions between S-Parameters and T-Parameters and subsequent T-Matrix calculations. Both give essentially equivalent results for most network problems although the Mason method tends to have less sensitivity to propagated errors (and hence is slightly more accurate but at the cost of more computational power).

**2.) Mason's Non-Touching Loop Rule:**

Mason's non-touching loop rule is a network modeling simplification tool first introduced in the early pioneering work on signal flow graphs by Dr. Samuel .J. Mason of MIT with his two landmark publications in 1953 [3] and 1956 [4] where his theory on modeling cascaded networks ("Mason's Non-Touching Loop Rule) was presented. The full derivation for Mason's non-touching loop rule will be left to the cited literature and only the key concepts presented here to illustrate the procedures.

The goal is to simplify the signal flow graphs of the cascaded networks of TDT (figure B.10) and TDR (figure B.13) systems to arrive at the equivalent simplified networks of figures B.10 and B.14 respectively. In reviewing figures B.10 and B.13 one can envision many different nested continuous "loops" where a signal can propagate through and return to the source via many different paths. The loops are defined at different orders as follows:

First Order Loops: A first order loop is any continuous loop path that can be traced within the networks of figures B.10 and B.13. An example of two different first order loops in figure B.10 is shown as follows in figure B.15 (paths highlighted in green and violet):

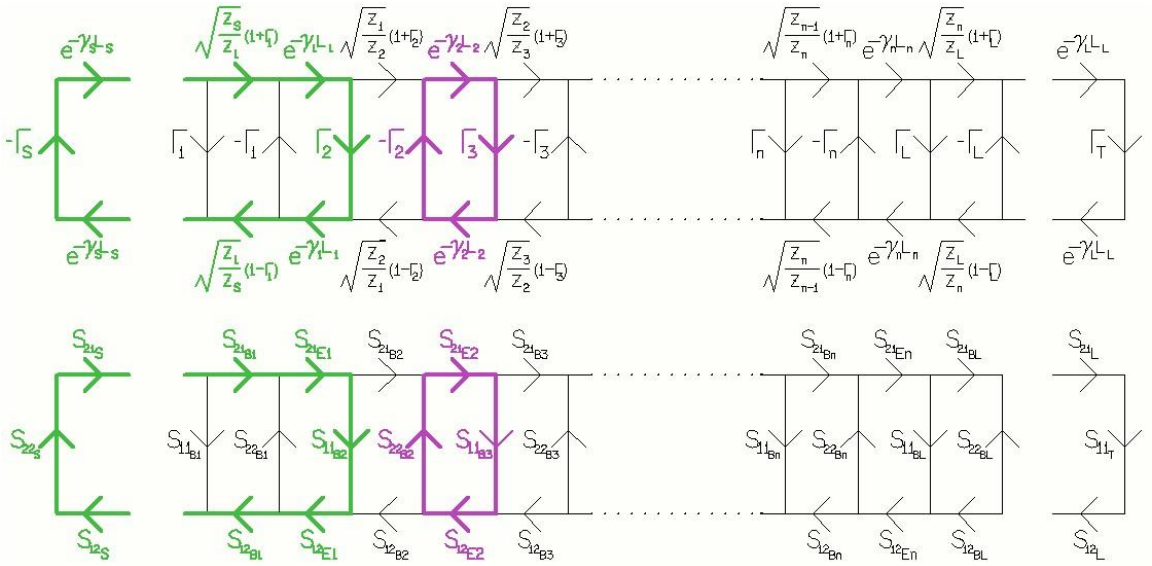

Figure B.15: Example of Two Different First Order Loops for Mason's Non-Touching Loop Rule

As can be seen from figure B.15 the loops can be small and local or can be larger and stretch across several boundaries and elements. Loops can also be traced that overlap or "touch" other loops. An example of this is the largest first order loop in the above network which is simply tracing the entire path through the network through the load termination and then back to the source. That first order loop touches all other first order loops. Identification of these first order loops as well as which other loops they touch and which other loops they don't touch (they always touch a subset of the other loops) is a major component of Mason's Non-Touching Loop rule in the derivation of the overall equivalent S-Parameters of the network as shown in a moment. The loop expression for a particular loop is then the multiplication of all of the S-Parameters around that particular loop.

Second Order Loops: A second order loop is then defined as the product of the loop expressions of any two non-touching loops.

$m^{th}$ Order Loops: In general an $m^{th}$ order loop is the product of the loop expressions of any m non-touching first order loops.

The expression for the S-Parameter from node "y" to node "z" in a cascaded transmission line network is then derived as follows from Mason's Non-Touching Loop Rule:

$S_{yz}$ =

$$\frac{P_1(1-\sum L_1^1+\sum L_2^1-\sum L_3^1+\ldots+(-1)^n\sum L_n^1)+\ldots+P_k(1-\sum L_1^k+\sum L_2^k-\sum L_3^k+\ldots+(-1)^j\sum L_j^k)}{1-\sum L_1+\sum L_2-\sum L_3+\ldots+(-1)^m\sum L_m} \quad \text{(B-20)}$$

Where

$S_{yz}$ = Equivalent Scattering (S) Parameter from node "y" to node "z"

$P_k$ = $k^{th}$ different direct path from node "y" to node "z".

$\sum L_j^k$ = Sum of all $j^{th}$ order loops not touching path k.

$\sum L_m$ = Sum of all $m^{th}$ order loops where an $m^{th}$ order loop is a product of any m non-touching first order loops.

$\sum L_1$ = Sum of all $1^{st}$ order loops where a first order loop is any continuous loop path in the signal flow graph for a particular network.

A simple example of the application of Mason's Non-Touching Loop rule was illustrated by using the earlier example shown in figure B.4 to derive (B-16). In figure B.4 $S_L$ is the S-Parameter associated with the reflection coefficient (equivalent to $\Gamma_L$) looking into the load from the output of port 2 and Sp is an additional forward transmission S-Parameter coefficient to account for propagation parameters of delay and loss (within section 2 or element $E_2$ using our conventions for cascaded transmission line elements) and is defined as follows (in the frequency domain):

$$S_p = e^{-\gamma_2 L_2} = e^{-(\alpha_2 + j\beta_2)L_2} \quad \text{(B-21)}$$

Where $\gamma_2$ is the propagation constant from electromagnetic wave propagation theory [12-18] for section 2 and $L_2$ is the electrical length of section 2 of the network.

The expression for the overall reflection coefficient looking into port 1 can be developed as follows from Mason's Non-Touching loop rule:

$S_{yz} = S_{11\_Overall}$ (B-22)

$\Rightarrow$ y = z (or the ending node is the same as the source node)

$P_1 = S11 = \Gamma_1$ (B-23)

$$P_2 = (S21)(S_p)S_L(S_p)(S12) = (S21)(S12)S_L(S_P)^2 = (1-\Gamma_1^2)\Gamma_L e^{-2\gamma_2 L_2} \quad \text{(B-24)}$$

First Order Loops (only one):

$$L_1 = (S22)(S_P)S_L(S_P) = (S22)(S_L)(S_P)^2 = (-\Gamma_1)(\Gamma_L)e^{-2\gamma_2 L_2} \quad \text{(B-25)}$$

Plugging these values into (B-20) results in the following expression for the overall S11 looking into the input of the network:

$$S_{11\_Overall} = \frac{P_1(1-L_1)+P_2}{1-L_1} = \frac{\Gamma_1(1+\Gamma_1\Gamma_L e^{-2\gamma_2 L_2})+(1-\Gamma_1^2)\Gamma_L e^{-2\gamma_2 L_2}}{1+\Gamma_1\Gamma_L e^{-2\gamma_2 L_2}} = \frac{\Gamma_1+\Gamma_L e^{-2\gamma_2 L_2}}{1+\Gamma_1\Gamma_L e^{-2\gamma_2 L_2}} \quad \text{(B-26)}$$

Close examination shows the equivalency with (B-16).

### 3.) Nested Construction Method

A third and simplified modeling approach (computationally more efficient than the full application of Mason's algorithms as well as the T to S parameter conversions) was developed specific to the development of overall S11 models (and also applicable to S22 models). This simplified algorithm makes use of cascading/nesting the S-parameter expressions derived by a simplified implementation of Mason's non-touching loop rule applied to only two adjacent stages at a time beginning at the load end and working back towards the source end (for deriving S11). Each successive cascaded section (moving back towards the source) is incorporated by using the expression for effective S11 looking into that particular section as the load S11 for the preceding stage. The signal flow graphic which represents these stages (whether looking in at the load end

or source end of the network or somewhere in between looking towards the right end or towards the load end of the network) is shown in figure B.16 (for the case of S11 derivation). It is based on the individual S-parameters for the boundary $B_n$ at that stage (stage n: $S21_n$, $S12_n$, $S11_n$, and $S22_n$) as well as the propagation term for the element $E_n$ for that stage ($e^{-j\gamma_n L_n}$) and finally the equivalent expression for S11 ($S11\_{}_{N+1}$) for all the combined stages to the right of section n (i.e., n+1 on up to the load section). A very simplified application of Mason's Non-Touching loop rule is applied to the network in the right of figure B.16 to derive the expression in the left of figure B.16 ($S11\_{}_{N}$).

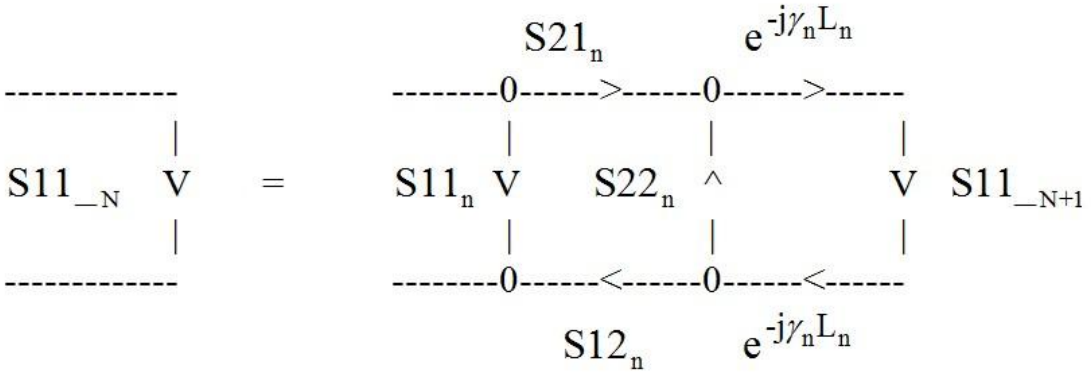


Figure B.16: Building Block for Overall S-Parameter (S11) Model Construction

The building block S11 expression that forms the basis for this algorithm is then derived in (B-27):

$$S11\__N = S11_n + \frac{S21_n S12_n S11\__{N+1} e^{-j2\gamma_n L_n}}{1 - S22_n S11\__{N+1} e^{-j2\gamma_n L_n}} = \Gamma_n + \frac{\left(1-\Gamma_n^2\right) S11\__{N+1} e^{-j2\gamma_n L_n}}{1 + \Gamma_n S11\__{N+1} e^{-j2\gamma_n L_n}} \qquad \text{(B-27)}$$

where the right most expression above is derived based on the fact that the S-parameters for each boundary $B_n$ can be expressed in terms of the individual reflection and transmission components for each boundary as derived from (B-11 to B-15). Beginning with the right most section (or load end) in the overall network the reflection coefficient at the load end ($\Gamma_{Load}$) can be plugged into the expression for $S11\__{N+1}$ and then (B-27) calculated for $S11\__N$. This derived $S11\__N$ can then be placed back into (B-27) again for the next section moving to the left (n-1 section) to give

an expression for $S11\_{N-1}$. This process can be continued unto the left end or source end of the overall network to give a complete expression for overall S11 looking into the source end of the network. This process can also be applied to the derivation of S22 by reversing the direction of the procedure. This approach is a computationally efficient method to derive S11 or S22 for either a TDR or TDT system and has also been utilized for the forward prediction models. The result is a general expression (again in the frequency domain) for the overall S11 looking into a multiple cascaded section transmission line at its' input or source end. In summary, the effective overall input reflection coefficient or scattering function $S11\_N$ looking into section "n" can be derived from the S-Parameters of section n along with the overall input reflection coefficient $S11\_N+1$ looking into the section that follows (n+1). A further simplification of (B-27) is given as follows:

$$S11\_N = S11_n + \frac{S21_n S12_n S11\_N+1 e^{-j2\gamma_n L_n}}{1 - S22_n S11\_N+1 e^{-j2\gamma_n L_n}} = \Gamma_n + \frac{\left(1-\Gamma_n^2\right) S11\_N+1 e^{-j2\gamma_n L_n}}{1+\Gamma_n S11\_N+1 e^{-j2\gamma_n L_n}} \quad \text{(B-28)}$$

$$\text{Or} \qquad S11\_N = \frac{\Gamma_n + S11\_N+1 e^{-j2\gamma_n L_n}}{1+\Gamma_n S11\_N+1 e^{-j2\gamma_n L_n}}$$

This expression (B-28) can be used to build recursively the overall input reflection coefficient or scattering function (S11_Input) in the frequency domain at the input of an overall transmission line with multiple cascaded sections. This approach is termed the "nested construction method" and is also employed by the forward prediction models were applicable (specific to S11 or S22).

## Application to TDR and TDT Systems:

The above three methods can be applied to TDR and TDT systems as described in this section. Assume that a test fixture or device under test contains a transmission line similar to that modeled in figure B.17. Each cascaded section of this transmission line would have a characteristic impedance value (either defined by (A-32) in Appendix A for a parallel wire transmission line or alternative but similar equation for other transmission line geometries such as a coaxial connector). This transmission line would also have different wave propagation

parameters ($\alpha$ and $\beta$) for each cascaded section as defined by equations (A-16) and (A-17) in Appendix A and derived from the real and imaginary components of either (A-31) in Appendix A or equivalent expression for other transmission line geometries.

An example of a simple cascaded transmission line is a test fixture with imperfect connectors as follows:

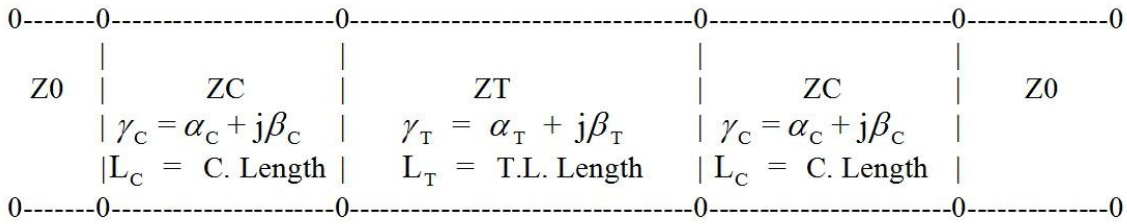


Figure B.17: Transmission Line with imperfect connectors attached to cable with impedance = Z0:

Where

ZT = Characteristic Impedance of Transmission Line

ZC = Characteristic Impedance of Connectors

Z0 = Characteristic Impedance of Coaxial Cable or Driving Line.

and

$\gamma_C = \alpha_C + j\beta_C$ = Overall Propagation Constant for the connectors (See Appendix A).

$\gamma_T = \alpha_T + j\beta_T$ = Overall Propagation Constant for the transmission line (See Appendix A).

and

$\Gamma_C$ = Reflection coefficient between driving cable and connector.

$\Gamma_T$ = Reflection coefficient between connector and transmission line.

$L_C$ = Connector length

$L_T$ = D.U.T. Transmission line length

It can be shown by the above presented methods (Transmission matrix generation and/or Mason's non-touching loop rule and/or nested construction method (S11 or S22 only)) that the S parameter functions are given by (B-29) for TDR and (B-30 to B-31) for TDT systems respectively.

TDR System: For the case of an open circuit termination at the far end of the symmetrical transmission line of figure B.17 (with non-ideal connectors at both ends) the expression for S11 becomes that as follows:

Open circuit termination at far end of transmission line (i.e. TDR Probe):

$$S11 = \frac{e^{-2\gamma_T L_T}\left(e^{-2\gamma_C L_C} + \Gamma_c\Gamma_T\right)\left(e^{-2\gamma_C L_C} - \Gamma_T\right) + \left(-\Gamma_T e^{-2\gamma_C L_C} + 1\right)\left(\Gamma_T e^{-2\gamma_C L_C} + \Gamma_C\right)}{e^{-2\gamma_T L_T}\left(\Gamma_C e^{-2\gamma_C L_C} + \Gamma_T\right)\left(e^{-2\gamma_C L_C} - \Gamma_T\right) + \left(\Gamma_C\Gamma_T e^{-2\gamma_C L_C} + 1\right)\left(-\Gamma_T e^{-2\gamma_C L_C} + 1\right)} \quad \text{(B-29)}$$

TDT System: The S-Parameters for a TDT system with non-ideal connectors and 50 ohm termination on each end are given as follows:

$$S11 = \frac{-e^{-2\gamma_T L_T}\left(e^{-2\gamma_C L_C} + \Gamma_c\Gamma_T\right)\left(\Gamma_C e^{-2\gamma_C L_C} + \Gamma_T\right) + \left(\Gamma_C\Gamma_T e^{-2\gamma_C L_C} + 1\right)\left(\Gamma_T e^{-2\gamma_C L_C} + \Gamma_C\right)}{-e^{-2\gamma_T L_T}\left(\Gamma_C e^{-2\gamma_C L_C} + \Gamma_T\right)^2 + \left(\Gamma_C\Gamma_T e^{-2\gamma_C L_C} + 1\right)^2} \quad \text{(B-30)}$$

$$= S22$$

$$S21 = S12 = \frac{e^{-\gamma_T L_T} e^{-2\gamma_C L_C}\left(1-\Gamma_C^2\right)\left(1-\Gamma_T^2\right)}{-e^{-2\gamma_T L_T}\left(\Gamma_C e^{-2\gamma_C L_C} + \Gamma_T\right)^2 + \left(\Gamma_C\Gamma_T e^{-2\gamma_C L_C} + 1\right)^2} \quad \text{(B-31)}$$

where

$\gamma_C = \alpha_C + j\beta_C =$ Overall Propagation Constant for the connectors.

$\gamma_T = \alpha_T + j\beta_T =$ Overall Propagation Constant for the transmission line.

as defined by (A-31) (Appendix A) or similar equation for other geometries.

and

$\Gamma_C =$ Reflection coefficient between driving cable (50 ohms) and connector.

$\Gamma_T =$ Reflection coefficient between connector and transmission line D.U.T.

as defined by (A-32 – Appendix A), (3-5 – Forward Prediction Model Chapter) and (B-11).

$L_C =$ Connector length

$L_T =$ D.U.T. Transmission line length

General purpose S-parameter models to account for additional multiple cascaded stages (figures B.5 – B.14) can be developed from Mason's Non-Touching Loop Rule, the T-Matrix method or the Nested Construction Method. This can also include non-symmetrical networks (e.g. a TDR probe with a connector on one end and an open termination without a connector on the other end or alternatively a TDT system with 50 Ohm terminations on both ends but with non-symmetrical elements along the line). An example of a non-symmetrical network included in the forward prediction models is shown in figure B.18:

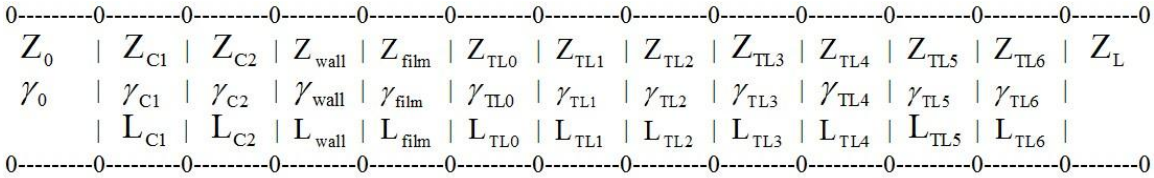


Figure B.18: Model of a Cascaded Transmission Line with Imperfect Connectors & Multiple Sections

The network model of figure B.18 was applied to a cascaded transmission line TDR test fixture involving a coaxial SMA bulkhead connector protruding a plastic wall of a cylindrical column followed by a parallel wire transmission line inserted into a test soil on the other side of the wall (inside of the column). In this specific case $Z_L$ = Open Circuit (or approximating an open circuit with a very high impedance termination). This model was developed specific to one of the lab setups where a column of rings was constructed where each ring contained soil of different water contents. A parallel wire transmission line was inserted into each ring and terminated in an open circuit near the far end of the ring. Note: many other different partitioning models were also developed in this dissertation including those for TDT systems and larger number of cascaded sections.

For the TDR model in figure B.18, starting from left to right the source impedance and propagation constant (cable) is designated by the suffix "0". The input SMA bulkhead connector is divided up into two stages designated by the suffixes "1" and "2". The ring wall is modeled by the suffix: "wall". A thin film layer is modeled at the beginning of the TDR transmission line and is designated by the suffix: "film". This thin film can represent either a water film or air film depending on the overall water content of the fixture. The actual TDR transmission line within a test soil is divided up into seven subsections to account for water content variations along the

length of the probe (important especially for the field measurements). These seven subsections are designated by the suffixes “0” through “6”. Finally the load impedance is designated by the suffix “L”.

Again, other cascaded models have also been developed for the other probe fixtures (including models for TDT systems involving both parallel wire transmission lines as well as PCBA based non-invasive transmission lines). Additional models were developed specific to the field probe structure (a longer 3-wire probe which consists of an interface module at its input (containing connectors and a balun-type structure) between the cable and the TDR transmission line probe). All of these fixtures and models are described and validated in the validation mthods and results/discussion chapters of this dissertation covering validation methods and validation results. The models can be extended to much larger numbers of cascaded elements approaching a finite element method (FEM) type of simulation with a direct tradeoff on computational time or measurement speed with measurement resolution.

For each cascaded model type, the computer algorithm (using Mason’s Non-Touching Loop Rule or alternatively T-Matrix multiplications and conversions or alternatively the nested construction method where applicable) develops the composite overall expression for all the S-Parameters to account for all these cascaded stages. The models make use the models developed for the individual reflection coefficients ($S11_{B_n}$ and $S22_{B_n}$) and individual transmission coefficients ($S21_{B_n}$ and $S12_{B_n}$) at each boundary $B_n$ as given by equations (B-11 to B-15) applied to each boundary $B_n$. In addition, the models also make use of the transmission coefficients ($S21_{E_n}$ and $S12_{E_n}$) developed for each element $E_n$ to account for the propagation phase shift and loss terms for each element (given by $e^{-\gamma_n L_n}$). For a TDR system the load impedance is typically taken as an open circuit but in the forward prediction models a fringe impedance load can be substituted for the load impedance that properly accounts for finite load impedances at high frequencies and high salinities. For TDT systems the load impedance is set to 50 Ohms to represent the terminating impedances of the measurement instrumentation.

Several different models for predicting S11 and S21 have been developed for TDR and TDT systems as part of the forward prediction models utilizing Mason’s Non-Touching Loop

Rule or alternatively the T-Matrix multiplications and conversions to S-Parameters or alternatively the Nested Construction Method (S11 or S22 only). These were developed to model several different lab and field TDR and TDT setups of which the models were validated against.

The three different approaches for handling cascaded transmission line modeling (Mason's Non-Touching Loop rule, T-S parameter conversions and the Nested Construction Method) are all used as the basis of the algorithms used in this research. They allow for accounting for connector variations and also water content and electrical conductivity variations along the length of the probe allowing for the measurement of those parameters vs. depth in a soil. Knowledge of all of the physical electromagnetic parameters that make up the S-Parameters at each section along with the termination impedance at the last section would be required (either via A-priori knowledge or via simulations based on the derivations) to develop the overall forward prediction models. They would first be derived using equations (3-7to 3-16) for the individual constituent models and then utilizing (3-17) to (3-67) to derive the overall composite models for the composite permittivity, conductivity, propagation constant and characteristic impedance functions. The propagation constant and characteristic impedance values are then utilized with (3-5) and (B-11 to B-15) to derive the S-Parameters for each boundary $B_n$ and element $E_n$ for each cascaded section. Again the above is a frequency domain representation that can be developed from the scattering parameters of each cascaded section. The frequency domain representation of the actual total response function at the input ($R(\omega)$) can be found by conducting an FFT on a particular specific stimulus signal x(t) (typically a step waveform with fast risetime) to give $X(\omega)$ and then multiplying it by the overall scattering function looking into the input or S11_Input($\omega$) to give the following expression:

A.) Frequency Domain:

$$R(\omega) = X(\omega)S11\_Input(\omega) = X(\omega)H(\omega) \quad \text{(B-32)}$$

Where $H(\omega)$ is interpreted as the overall transfer function of the system or alternatively the FFT of the overall impulse response of the system h(t). An Inverse Fast Fourier Transform (IFFT) can be conducted on $R(\omega)$ to give the response function or total response signal in the time domain r(t) which can also be interpreted as the convolution of x(t) with h(t) or the time domain representation of the scatter function $s_{11\_Input}(t)$ shown as follows (for a causal system beginning at time t = 0).

B.) Time Domain:

$$r(t) = x(t) \otimes h(t) = \int_{\tau=0}^{t} x(t)h(t-\tau)d\tau = \int_{\tau=0}^{t} x(t)s_{11\_Input}(t-\tau)d\tau \quad \text{(B-33)}$$

Or alternatively the discretized time domain form of the convolution is given as follows:

$$r(n) = x(n) \otimes h(n) = \sum_{m=0}^{n} x(n)h(n-m) = \sum_{m=0}^{n} x(n)s_{11\_Input}(n-m) \quad \text{(B-34)}$$

There are specific inverse scattering modeling problems that are better suited to the frequency domain and others that are better suited to the time domain and still others that are best solved using both the frequency and time domain representations or information. If there is frequency dependence of any of the network parameters (causing phenomena such as loss and dispersion) then often the frequency domain representation is best suited. If the system is lossless and non-dispersive (no frequency dependence) then often the time domain is best suited. Some inverse problems are more intuitive to solve in the time domain or alternatively the frequency domain as will often be seen in the problems covered in this review. The usual case is that the response signal or scattered signal is the measured or known entity and the goal is to perform signal processing on that measured information to ascertain information or properties about the network (including each of its sub-elements or sections) through either a de-convolution process in the time domain or alternatively various de-embedding processes in the frequency domain (both resulting in equivalent results).

As can be seen these expressions are functions of the parameters: $\alpha$ (attenuation constant), $\beta$ (propagation constant), $\Gamma$ (reflection coefficient) and L (probe or transmission line length or connector length) for each of the cascaded stages and boundaries (i.e. connectors, device under test transmission line, etc.). The S-parameters are therefore ultimately functions of frequency as well as the basic parameters $\varepsilon$ (electric permittivity), $\mu$ (magnetic permeability), $\sigma$ (electrical conductivity) and finally probe geometry. The electric permittivity $\varepsilon$ is itself a complex function of frequency and other parameters and has a different behavior depending on whether the water is fully free, semi-bound or fully bound as described in the forward prediction chapter. The electrical conductivity $\sigma$ is considered a DC variable and is not treated as a function of frequency in these models. The magnetic permeability $\mu$ is considered a constant and equal to that of free space (1.26E-6 Henries/meter). These models from the theories of electromagnetics and S-parameters along with FFT (fast Fourier transform) and IFFT (inverse FFT) algorithms (to switch back in forth between the time and frequency domains) form the basis of the TDR and TDT soil water content and electrical conductivity measurement prediction model and measurement algorithm presented in this dissertation.

The forward prediction model utilizes new models for handling complex composite media with mixtures of various constituents (as described in the forward prediction model chapter) that make up the various sections in the network and using both S-Parameters and T-Parameters. In addition a new set of techniques/algorithms for solving the inverse scattering problems for such networks has been developed and is presented in introductory fashion in this dissertation and will be covered in full detail in follow-on research and publications.

With the forward prediction models the above equations and modeling techniques can be used to develop either S-Parameters and/or T-Parameters for an entire network based on knowledge of the electromagnetic parameters or properties of each section within the network. However, in the solving of the inverse scattering problem the reverse path must be followed. The elements inside the network are considered as unknowns and often the only piece of information is the measured external scattered signal exiting the input port (for the case of the transmission line for the above example). Or more generally if there are multiple ports (i.e. more complex structures) the measured scattered signals at each port must be utilized to ascertain information about the internal parameters or properties of the medium. Varying amounts of a-priori

knowledge about the medium itself can sometimes be utilized if available to supplement the information from the measured external scattered signals to help reduce the number of variables or unknowns and simplify the inverse scattering problem. An example of this would be knowledge in advance that the system or medium is not lossy (i.e. the loss tangent of each sub-section or the entire medium is zero). Another example might be knowledge that the entire medium is homogeneous with no cascaded boundaries or sub-sections of changing properties. This type of information can be very useful if available to simplify the inverse scattering problem. However geophysical and biological media are rarely that simple. The inverse algorithms are presented in introductory fashion in this dissertation and will be covered in full detail in follow-on research and publications.

As was alluded to briefly earlier, the algorithm also makes use of Mason's non-touching loop rule and other cascaded transmission line modeling techniques to model the TDR or TDT probe as a cascaded series of small transmission lines each with their individual values of electrical permittivity $\varepsilon$, magnetic permeability $\mu$ and electrical conductivity $\sigma$. In addition the algorithm has the ability to assign a different physical length to each of the segments as well as a different value of porosity to each segment. This allows for the modeling of variations of electrical conductivity and water content vs. depth along the probe length (a key feature for real world field measurements where water content variations vs. depth are the norm).

The algorithm for determining water content vs. depth for low conductivity systems also makes use of the time domain information and not just the frequency domain information as the impedance vs. depth is the basis of this signature algorithm and so levels of S11 vs. time between the first and second reflections are the key. Moisture content vs. depth can not be obtained with this enhanced portion of the algorithm when the electrical conductivity is sufficiently high to attenuate the reflected signal below detectable levels. Therefore this special enhancement feature is constrained to those regions where $\sigma_{bulk}$ is below around 1 dS/m (this will vary depending on a lot of factors). This cascaded transmission line approach presented in this dissertation essentially falls under the category of finite element methods with a grid ranging from 11 to 15 subsections (each with a boundary $B_n$ and element $E_n$) depending on the specific model (the TDT models involved extra sections to model connectors on both ends of the fixture). However, the models are compatible with other grid resolutions.

Modeling with S-parameters is key as in an actual TDR measurement system the Fast Fourier Transform (FFT) of actual measured TDR or TDT time domain data yields frequency domain information from which the S-parameters can be derived. Therefore there is an opportunity to compare models which can be derived to data in a similar form that can be measured which creates the opportunity for a measurement system which can extract useful parameters such as electrical conductivity $\sigma$ and volumetric water content $\theta$ . As was presented in the discussion on inverse models in this dissertation as well as shown in equations B- and B-, the electrical conductivity $\sigma$ can be calculated directly from the low frequency information in the measured S-parameter data. The volumetric water content can then be determined by either a look-up table of electromagnetic parameter information (extractable from the S-parameter data at frequencies above where the loss tangent (equation A-10) crosses below one) or alternatively by an optimization procedure (or by both methods together) to fit actual measured data to different forward prediction model waveforms and subsequently extract the desired parameters of water content and electrical conductivity. Several Examples of waveforms generated by simulations with the forward prediction models including those with different cascaded sections are given in this dissertation.

## Group Delay for Determining Bulk Water Content for Lower EC's

One additional parameter that is utilized to ascertain information about the dispersion in a medium for fairly simple networks (single or small numbers of cascaded sections) is the group delay. A group delay vector can be determined by generating a vector whose values are equal to the incremental change in phase angle (of S11 for a TDR system or alternatively S21 for a TDT system) divided by the incremental change in frequency (or frequency step in the vector) to approximate the derivative or slope of phase with frequency in S11 as given by equation B-35:

$$D_g = \frac{\partial \phi}{\partial \omega} \approx \frac{\left(\angle\left(S11(i)\right) - \angle\left(S11(i-1)\right)\right)}{\Delta\omega} \quad \text{(B-35)}$$

where:

$D_g$ = Effective Group Delay of S11 (seconds)

$\phi$ = Phase of S11 (radians)

$\Delta\omega$ = Step change in angular frequency (radians/sec)

$\angle$ S11(i) = Phase of the i'th component of S11 (radians)

As a cross check the actual delay can also be determined using the phase velocity (similar to equation A-18 in Appendix A but for the reflected signal to incident signal ratio S11) as given in equation B-36:

$$D_a = \frac{2L_P}{\omega/\phi} = \left(\frac{2L_P}{\omega}\right)\left(\angle S11(i)\right) \quad \text{(B-36)}$$

where:

$D_a$ = Actual effective delay of S11 (seconds)

$L_P$ = The total length of the TDR probe (m).

Peaks in (B-35) correspond to half wave null resonances in S11 (probe length = quarter wavelength) (for low conductivity conditions) and so can be used to determine the electrical permittivity and water content when the conductivity is low enough and/or the frequency is high enough to make those peaks detectable. A lookup table can be used to match these group delay peak locations (half wave null resonances in S11) to water content (using also the bulk electrical conductivity as a pointer). The algorithm has a built in calibration feature to account for connector lengths, etc. Examples of group delay plots for a fully dry soil and a fully wet soil are given in figure B.19.

**Effective Impedance for Identifying Bulk Electrical Conductivity:**

It has been shown in this dissertation that the low frequency information of S11 provides direct information on the DC electrical resistance from which the bulk electrical conductivity can be calculated. Once the S11 frequency domain vector has been obtained by either directly measuring S11 (Frequency Domain FDR system) or alternatively performing an FFT on the normalized TDR trace and dividing the result by the FFT of a square wave or step wave then the bulk electrical conductivity $\sigma_{bulk}$ can be directly calculated from the low frequency values in the vector and by the geometry factors of the probe. The equation to determine bulk electrical conductivity is given as follows for a two wire probe similar to what was used in laboratory validation methods #1 and #2:

$$\sigma_{bulk} = \left(\frac{1 - S11(1)}{1 + S11(1)}\right)\left(\frac{1}{Z_0}\right)\left(\frac{1}{\pi L_P}\right)\left(\cosh^{-1}\left(\frac{s}{d}\right)\right) \qquad \text{(B-37)}$$

where:

S11(1) = The dc or lowest frequency value in the S11 frequency domain vector.

$Z_0$ = The characteristic impedance of the driving cable or output impedance of generator (50Ω).

$L_P$ = The total length of the TDR probe (m).

s = The spacing between conductors in the 2 wire probe (m).

d = The diameter of the conductors in the 2 wire probe (m).

Equation B-37 is valid when the frequency is low enough so that the electrical length of the probe is insignificant so that the entire probe can be modeled as a lumped element impedance. Also the frequency must be low enough so that the electrical conductivity effects dominate over the effects of the loss component of the dielectric constant. Therefore the logical choice is to use the dc component or lowest frequency value in the S11 frequency domain vector. Equation B-37 then gives the value for one of the measurement objectives of the TDR/FDR measurement system (bulk electrical conductivity or $\sigma_{bulk}$). No lookup table is required to determine the bulk electrical conductivity as it can be calculated directly from the S11 frequency domain data using equation

B-37. A more general direct measurement derivable from B-37 and actually representing what is directly measured with real hardware is the Effective input impedance $Z_{Eff}$ given by B-38

$$Z_{Eff} = \left( \frac{1 + S11(1)}{1 - S11(1)} \right) (Z_0) \qquad \text{(B-38)}$$

Once the bulk electrical conductivity is determined ($\sigma_{bulk}$) then it can be used as a pointer to determine the proper algorithm steps to determine volumetric water content θ (or the other objective or targeted measurement parameter of the TDR/FDR/TDT/FDT measurement system). If the electrical conductivity is lower (perhaps less than 0.01 S/m in very approximate fashion – not a fixed limit or threshold as other variables impact this) then the Group Delay method per equation B-35 above can be used to determine overall bulk water content θ. For higher EC's where the peaks become undetectable in the group delay plot from equation B-35 then the medium to higher frequency information from the impedance data from equation B-38 together with the medium to higher frequency information in both S11 and S21 (via high dynamic range FDR/FDT methods) can be used to determine water content. Digital signal processing can be utilized to remove the effects of electrical conductivity to reveal the impacts from water content (impacting electric permittivity) for the case where high dynamic range frequency domain measurements are utilized (FDR/FDT) where all the relevant reflected and transmitted information even after attenuation is still above the noise floor at all frequencies.

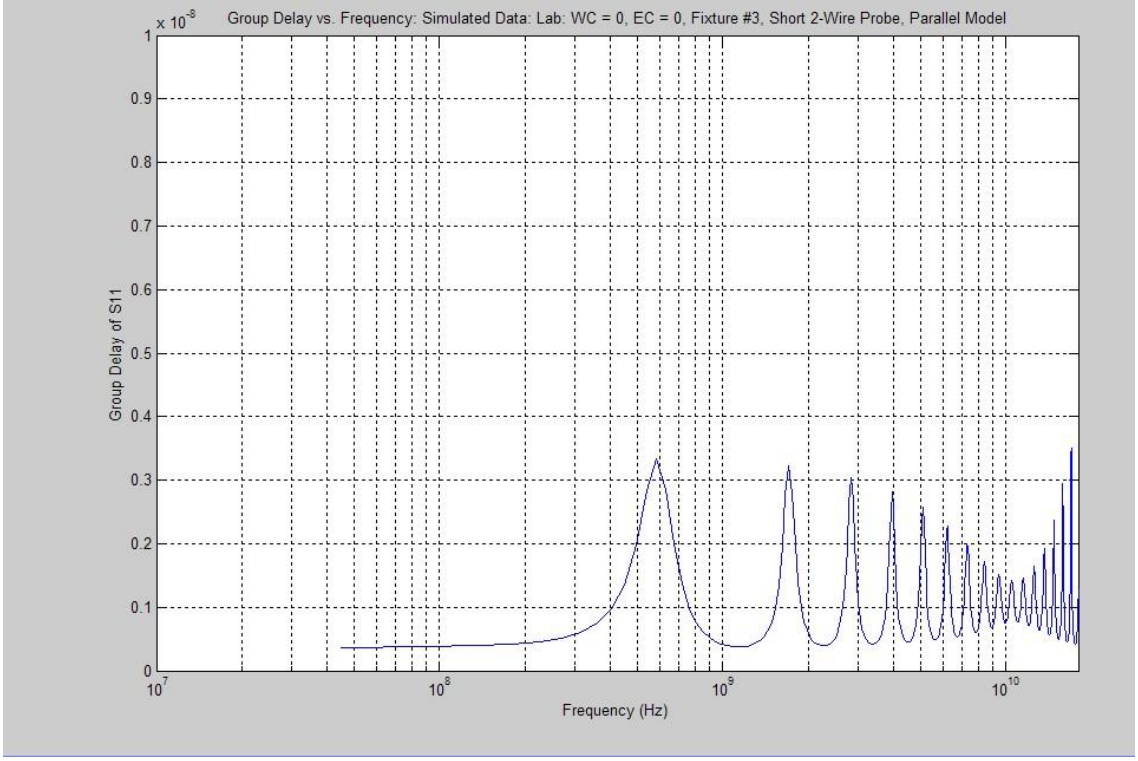


Figure B.19a: Group Delay Plot for a Dry Soil

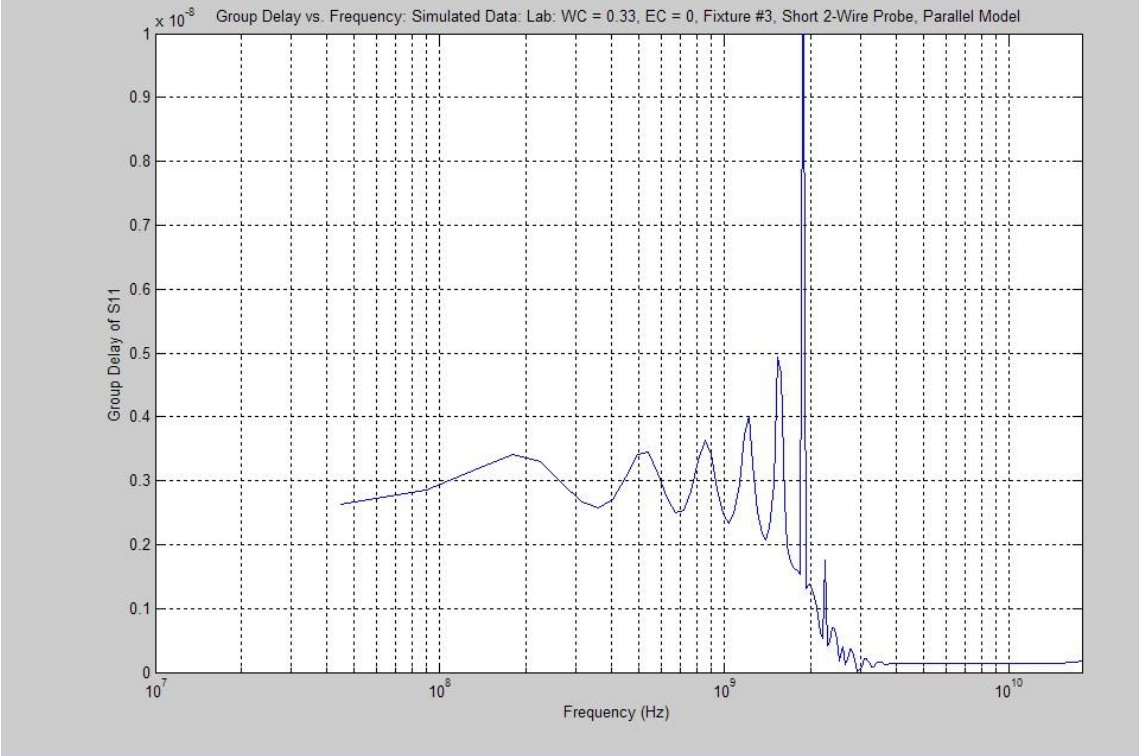


Figure B.19b: Group Delay Plot for a Wet Soil

**Determining Goodness of Fit:**

A valid method of determining goodness of fit is required to evaluate the effectiveness of the prediction algorithm to agree with measured data. The fitting evaluation was performed on the time domain signals (predicted and actual TDR signals) using evaluation parameters similar to those in linear regression. The basic objective is to minimize the sum of squared errors between the predicted and actual TDR signal over the relevant length of the trace. The sum of squared errors is defined as follows:

$$\text{Sum of Squared Errors} = \sum_{t = t_S}^{t_P / 2} \left( S11_{Pred}(t) - S11_{Act}(t) \right)^2 \qquad \text{(B-39)}$$

where

$t_P$ = Period of waveform (square wave used instead of a step in prediction algorithm)

$t_S$ = Sampling interval or time increment in TDR waveform

and the other parameters in (B-39) are the predicted and actual values of the time domain S11 or TDR trace as a function of time.

Two different Goodness of Fit quantifying measures were utilized in this Dissertation to assess how well equation B-39 has been minimized. These are given as follows (termed Coefficient of Fit Methods A & B):

$$\text{Coefficient of Fit Method A} = 1 - \frac{\sum_{t=t_S}^{t_P/2} \left(S11_{Pred}(t) - S11_{Act}(t)\right)^2}{\sum_{t=t_S}^{t_P/2} \left(S11_{Act}(t) - S11_{ActMean}\right)^2} \qquad \text{(B-40)}$$

$$= 1 - \frac{ModelSumofSquaredErrors}{\sum_{t=t_S}^{t_P/2} \left(S11_{Act}(t) - S11_{ActMean}\right)^2}$$

$$\equiv \quad R^2$$

$$\text{Coefficient of Fit Method B} = \frac{\sum_{t=t_S}^{t_P/2} \left(S11_{Pred}(t) - S11_{ActMean}\right)^2}{\sum_{t=t_S}^{t_P/2} \left(S11_{Act}(t) - S11_{ActMean}\right)^2} \qquad \text{(B-41)}$$

Equation B-40 is by definition equal to the Coefficient of Determination $R^2$ in linear regression where a value of 1 would indicate a perfect fit (zero Sum of Squared Errors of the Model (Predicted) vs. Actual (Observed) Values). This is the primary quantifier utilized for assessing goodness of fit throughout this Dissertation. Another alternative measure of the goodness of fit (Method B) that was also utilized in this Dissertation is given by B-41. It was derived through iterative trials and can be greater than or less than 1. A value of 1 in equation B-41 is still the optimal goal and represents an approximate minimum of equation B-39. It was observed that for Coefficient of Fit Method B values greater than 1 that the water content was overpredicted (transit time longer than actual) and for Coefficient of Fit Method B values less than 1 that the water content was underpredicted (transit time shorter than actual). It was therefore useful in determining direction of error. In contrast Coefficient of Fit Method A ($R^2$) given by B-40 is always less than or equal to 1 with 1 again indicating a perfect fit. Equations B-39 through B-41 were again used in the validation of the forward prediction models and are also valuable for the

proposed inverse models in validating either lookup tables or optimization algorithms outcomes. Equations B-39 through B-41 were referenced in the data results section with values given for these goodness of fit parameters for all the various prediction model variations over full ranges of water content and electrical conductivity.

# Appendix C: Supplement to Literature Review of Existing Dielectric Mixing and Propagation Constant Mixing Models:

Before developing the new dielectric mixing and propagation constant mixing models presented in this dissertation a very brief summary of the most popular existing models in literature is provided. The full comprehensive coverage on this is provided in the literature review chapter and so only a very brief summary is provided here.

## Refractive Dielectric Mixing / Cascaded Propagation Constant Models:

There are several levels of complexity in modeling a composite heterogeneous soil as just described. One of the simplest methods would be to assume that the soil across the entire length of a TDR / TDT probe is made up of volume spaces each composed entirely of a particular sub-constituent in the soil (e.g. solids, water, air, organic material, etc.). For purposes of illustrating this model we will assume initially that the soil is divided up into volumetric fractions of solids, air and water. The model will be extended in a moment to include bound water and organic matter constituents but we will start with the three major constituents of free water, solids and air. In general the models could easily be extended to include other fractions as well (e.g. different types of solids, liquids and gases) but for the moment we will assume the three dominant sub-constituents of a single solid phase and then water and air.

In developing expressions for the propagation constant and characteristic impedance for the composite medium there are again several levels of complexity. The simplest form of the model would assume that the electromagnetic propagation and impedance parameters are affected by the major sub-constituents as if they are in cascade or the wave passes through them in succession within a medium. This cascade form of the model is shown in equations (C-1 to C-5) for the propagation constant, phase velocity, intrinsic impedance and ultimately characteristic impedance functions of the composite medium.

Cascade Model:

$$\gamma_T = \gamma_s(1-\phi) + \gamma_W(\theta) + \gamma_A(\phi-\theta) = \alpha_T + j\beta_T \qquad \text{(C-1)}$$

$$\gamma_T = \frac{\gamma_s L_S + \gamma_W L_W + \gamma_A L_A}{L_T} \quad \text{(C-2)}$$

$$V_{P_T} = \frac{\omega}{\beta_T} \quad \text{(C-3)}$$

Where $\gamma_T$ = Overall Propagation Constant of Soil Mix (3 phases)

$\gamma_s$ = Overall Propagation Constant in Soil Solids

$\gamma_W$ = Overall Propagation Constant in Water

$\gamma_A$ = Overall Propagation Constant in Air

$\phi$ = Soil Porosity

$\theta$ = Soil Volumetric Water Content

$\alpha_T$ = Overall Attenuation Constant of Soil Mix (3 phases)

$\beta_T$ = Overall Phase Constant of Soil Mix (3 phases)

$V_{P_T}$ = Phase Velocity in Soil Mix (3 phases)

$L_W$ = Length of the Cascaded Element Containing only Water

$L_A$ = Length of the Cascaded Element Containing only Air

$L_S$ = Length of the Cascaded Element Containing only Solids

$L_T$ = Total Length of the Line

The overall propagation constants for the individual phases can be calculated using equations A-9 to A-31 in Appendix A for the water component and equation A-9 of Appendix A for the solid and air components, entering the proper values for permittivity, permeability and conductivity.

Intrinsic impedance and characteristic impedance of the transmission line in the composite mix (soil with solids, water and air) can also be determined as follows:

$$\eta_T = \frac{j\omega\mu}{\gamma_T} \quad \text{(C-4)}$$

$$Z_T = F_G \eta_T = \left(\frac{1}{\pi}\right) \text{Cosh}^{-1}\left(\frac{s}{d}\right) \eta_T \qquad \text{(C-5)}$$

where

$\eta_T$ = The intrinsic impedance in the overall composite mix

and $Z_T$ = The characteristic impedance for the special case of a parallel wire transmission line in the overall composite mix (assuming series resistivity losses are neglected).

Equations C-4 and C-5 can be used to derive the forward propagation term as follows (for a line of length $L_T$):

$$e^{-\gamma_T L_T} = e^{-\gamma_w(\theta) L_T} e^{-\gamma_A(\phi-\theta) L_T} e^{-\gamma_S(1-\phi) L_T} = e^{-\gamma_w L_w} e^{-\gamma_A L_A} e^{-\gamma_S L_S} \qquad \text{(C-6)}$$

Close inspection of (C-6) shows that this expression is equivalent to cascading three sections together (one with solely water, one with air and one with the solids). This then gives an overall propagation constant for the entire line as if one single medium was present.

In reality there is not a situation where the water, solids and air fractions are segregated into successive cascaded sections and so (C-1) and (C-2) have only limited value for a mixing model for those three fractions (as will be discussed more in a moment). However, the cascade model does have promise and application to the level 1 and level 2 macroscopic heterogeneity problems (referencing the Forward Prediction Model chapter) where large layers of different properties may be present in a soil (i.e. different soil types, veins or a wetting front (i.e. saturated zone followed by a drier zone)). In that context this model would therefore be a technique to use together with zone 3a frequencies (covered in the forward prediction model chapter) to approximate the entire probe as a composite mix of these fractions of heterogeneity with a single effective overall propagation constant term $\gamma_T$. A general expression of the cascaded model can be shown as follows:

$$\gamma_T = \frac{\gamma_1 L_1 + \gamma_2 L_2 + .... + \gamma_n L_n}{L_T} \quad \text{(C-7)}$$

Where

$$\sum_i L_i = L_T \quad \text{(C-8)}$$

The Cascade model is a superset of simpler models such as the index of refraction model used in existing TDR systems. The index of refraction model can be derived from (C-1) if the electrical conductivity and complex permittivity are both assumed equal to zero by utilizing (C-3) and plugging the value of $V_{P_T}$ into (3-2) in the forward prediction model chapter.

It is shown in the validation chapter that this cascade form of the model is a good fit to actual data for only limited cases. The best fits occur when there are coarse cascaded sections of heterogeneity in a soil such as large layers or veins of different properties that the waves successively pass through and the cascade mixing model is applied (different weighted propagation constants for each cascaded constituent). For homogeneous soils there were a few limited zones where this model was actually found to have a reasonable fit to actual data. These include lower water contents (< .15) when the electrical conductivity is low and a reasonably good fit for all water contents when the electrical conductivity is high. Unfortunately it is not a good fit for medium to high water contents when the electrical conductivity is low and so more powerful models needed to be developed which are presented in the forward prediction model chapter (after showing the cascade model). Again, in general the Cascade Model is not expected to be a good fit for smaller constituents where all the constituents act on the same portion of the wave simultaneously.

## Refractive Dielectric Mixing Model:

The cascade model can also be shown to be equivalent to the refractive dielectric mixing model that is often cited in recent literature for soil water content measurements. For

simplification purposes if we rewrite equation A-9 from Appendix A neglecting all loss terms the expression reduces to the following:

$$\gamma = j\omega\sqrt{\mu\varepsilon} = j\beta \quad \text{(C-9)}$$

Then for the cases of these three cascaded components (C-1), (C-2) and (C-9) can be rewritten as follows:

$$\gamma_T = \gamma_s(1-\phi) + \gamma_W(\theta) + \gamma_A(\phi-\theta) = j\omega\sqrt{\mu}\,(\sqrt{\varepsilon_s}(1-\phi) + \sqrt{\varepsilon_w}(\theta) + \sqrt{\varepsilon_A}(\phi-\theta)) \quad \text{(C-10)}$$

$$\gamma_T = j\omega\sqrt{\mu}(\sqrt{\varepsilon_T}) = j\omega\sqrt{\mu}\,(\frac{\sqrt{\varepsilon_s}L_S + \sqrt{\varepsilon_w}L_w + \sqrt{\varepsilon_A}L_A}{L_T}) \quad \text{(C-11)}$$

This reduces to the following form equivalent to the refractive dielectric mixing models found in the literature:

$$\sqrt{\varepsilon_T} = \frac{\sqrt{\varepsilon_s}L_S + \sqrt{\varepsilon_w}L_w + \sqrt{\varepsilon_A}L_A}{L_T} \quad \text{(C-12)}$$

The general form can then be given as follows for "n" heterogeneous cascaded coarse sections (using (C-7) and (C-8)) from the cascade model:

$$\sqrt{\varepsilon_T} = \frac{\sqrt{\varepsilon_1}L_1 + \sqrt{\varepsilon_2}L_2 + .... + \sqrt{\varepsilon_n}L_n}{L_T} \quad \text{(C-13)}$$

Schaap et al. [52] analyzed the performance of TDR soil water content measurements in layered media of multiple layers of different thicknesses and properties and even orientations (both parallel and orthogonal layer orientations relative to the probe). They assessed the influences of these layers to the overall TDR measurement as if the layered media was one composite block (i.e. there was no attempt to de-convolve or identify the specific layers individually from the TDR measurement). Their findings included that if there are a small

number of larger sections of which the probe penetrates that the effective overall permittivity of the composite dielectric mixture follows a classical relation referred to as refractive averaging and given by the following equation (for two sections):

Refractive Averaging Model:
$$\varepsilon_{eff} = \left( \frac{L_1\sqrt{\varepsilon_1} + L_2\sqrt{\varepsilon_2}}{L_{Tot}} \right)^2 \qquad \text{(C-14)}$$

Where
$\varepsilon_{eff}$ = Effective Overall Permittivity of the Composite Mixture
$\varepsilon_1$ = Permittivity of Medium in Section 1
$\varepsilon_2$ = Permittivity of Medium in Section 2
$L_1$ = Length of Probe in Section 1
$L_2$ = Length of Probe in Section 2
$L_{Tot}$ = Total Length of the Probe = $L_1 + L_2$

Close inspection of (C-14) shows its equivalence in form to the general refractive dielectric mixing models of (C-12) and (C-13).

As a further finding of the above it was found that a “thick” layer is defined as a layer that is greater than one quarter of a wavelength of the frequency of measurement. Therefore the refractive mixing model is frequency dependent and the spectrum of the TDR signal would need to be closely evaluated. Higher frequencies would lead to smaller/thinner limits of the thicknesses above which would satisfy the above relation.

## Arithmetic Mean Model:

It was also found in their study that if there were a large number of closely spaced thin layers and the layers were thinner than a quarter wavelength of the frequency of measurement that the mixing model switched to following a simple arithmetic mean model as follows:

Arithmetic Mean Model:
$$\varepsilon_{eff} = \frac{\varepsilon_1 L_1 + \varepsilon_2 L_2}{L_{Tot}} \qquad \text{(C-15)}$$

This arithmetic mean model will be shown later in this section to be equivalent to the parallel model theoretical bound in lumped element micro-constituent dielectric mixing models. The arithmetic mean (parallel) model was also found in the datasets for this dissertation to be a close fit in some circumstances but not others which will all be spelled out in the validation chapter.

Another finding from [52] was that if layers were oriented parallel to the probe that the resulting overall permittivity tended to follow the arithmetic mean (further validating the "equivalence" of the arithmetic mean to the "parallel" model). Finally it was found in [52] that for broadband methods such as TDR that the mixing models tended to follow one or the other mixing models (which would imply that the layering is either predominately large compared to a quarter wavelength or small compared to a quarter wavelength to the majority of the frequency components or spectrum in the TDR pulse). However for narrowband single frequency measurements much more frequency dependence was shown. An intuitive explanation for this is that zone 3b frequencies (presented in the Forward Prediction Model chapter) will follow the refractive mixing model and zone 1, 2 and up through zone 3a frequencies would follow the arithmetic mean (parallel) model if the findings from [52] were universal. More discussion on this is provided in the forward prediction model chapter and the chapters to follow in this dissertation including showing the circumstances where each of these models can be applied. The forward prediction model utilizes variants of these models as well as new models all presented in that chapter of this dissertation.

Robinson et al. [53] conducted a simulation on layered soil dielectrics and found again that for thicker layer dimensions that the refractive mixing model of (C-12) to (C-14) can be followed (but again only if the dimensions of the layer are large compared to a quarter wavelength of the highest significant frequency component in the TDR pulse (i.e. zone 3b frequencies)) confirming the results from [52].

**Other Dielectric / Propagation Constant Mixing Models:**

Other recent supporting studies using models essentially equivalent to the refractive mixing model include Martinez et al [85] who characterized and modeled the dielectric constant values of various Geologic materials to aid in the calibration and inverse measurement algorithms for a GPR system. They modeled three different rock types with variable mineralogy, porosity and saturation. They reviewed and evaluated different types of dielectric mixing models and chose the "Time-Propagation" mixing model shown as follows:

Time Propagation (Refractive) Mixing Model: $$\varepsilon_r = \left[\sum \mathrm{V_i} \left(\varepsilon_n\right)^{0.5}\right]^2 \qquad \text{(C-16)}$$

This expression comes from a more classical "Power Law" mixing model (Lichtenecker-Rother equation cited by the authors in [85] , [97], [99]:

Generalized Power Law Mixing Model: $$\varepsilon_r = \left[\sum \mathrm{V_i} \left(\varepsilon_n\right)^{\alpha}\right]^{1/\alpha} \qquad \text{(C-17)}$$

Therefore for the refractive mixing model the empirical parameter α is set to 0.5.

Mironov et al [95] applied the generalized refractive mixing dielectric model (GRMDM) (equations C-12 to C-14) to a soil containing also a humus component (organic matter). They found that this model could be utilized for organic matter constituents and adapted the model accordingly. In a follow-up paper Mironov et al. [96] presented an updated version of the generalized refractive mixing dielectric model with a number of the improvements that had been incorporated specific to soils (e.g. the above reference [95] for organic matter and reference [91] for frozen water and other bound water mechanisms (e.g. clay), and other recent adaptations including accounting for Debye and Cole/Cole models for dielectric loss). The updated generalized refractive mixing dielectric model is given as follows where the square root of the overall permittivity (accounting for all terms including loss terms) is defined as the complex refractive index (CRI) or n* and given as follows:

Complex Refractive Index n*:

$$n^* = \sqrt{\varepsilon_T} = 1 + (\sqrt{\varepsilon_{Solids}} - 1)W_{Solids} + \sqrt{\varepsilon_{Air}}W_{Air} + \sqrt{\varepsilon_{B\_Water}}W_{B\_Water} + \sqrt{\varepsilon_{F\_Water}}W_{F\_Water}$$

$$n^* = n + j\kappa \tag{C-18}$$

Where

n = Refractive Index (real/energy storage terms)

κ = Normalized Attenuation Coefficient (imaginary/loss terms)

The "W" terms represent the respective volumetric fractions of the various constituents for solids, air, bound water (B_Water) and free water (F_Water) and the permittivity terms are for those respective constituents and all are given by complex values (note the forward prediction models presented in this dissertation introduced the extra zone of semi-bound water as earlier described and not covered in the literature). For the case of the solids fraction the volumetric fraction can be further defined as follows:

$$W_{Solids} = \frac{\rho_d}{\rho_m} \tag{C-19}$$

Equation C-19 therefore relates the solids fraction to the ratio of the bulk density of the dry soil to the specific density of the soil solids. The solid components of mineral constituents (standard minerals and swelling clays) as well as organic constituents are modeled under this formula for the solids. In addition, the real and imaginary terms of the permittivity can be modeled in to equation C-18 (as a function of frequency) based on the following relations:

$$n = \sqrt{\frac{\left(\sqrt{(\varepsilon')^2 + (\varepsilon'')^2}\right) + \varepsilon'}{2}} \tag{C-20}$$

$$\kappa = \sqrt{\frac{\left(\sqrt{(\varepsilon')^2 + (\varepsilon'')^2}\right) - \varepsilon'}{2}} \tag{C-21}$$

(C-20) and (C-21) can be derived for a particular medium by utilizing (A-9) to (A-19) in Appendix A. (C-20) can be obtained by dividing (A-18) (phase constant) by the special case of (A-9) for free space. (C-21) can be obtained by dividing (A-17) (attenuation constant) by the special case of (A-9) (again for free space). In both of these cases the conductivity is either embedded into the loss component of permittivity (by dividing by angular frequency) or alternatively set to zero.

Mironov et al. [116] – [119] has since provided enhanced versions of these GRMDM and other models including the development of the Mineralogy-based soil dielectric model (MBSDM) that can account for multiple frequency dependent relaxation models.

Again, the refractive mixing models have limited ranges of applicability (where the dimensions of the constituents are large compared to the wavelengths at which the mixing models are being applied). Therefore, there is need for new dielectric mixing models as developed and presented in the forward prediction model chapter of this dissertation.

# Appendix D: Examples of TDR/TDT/FDR/FDT Plots: Actual Measurement Data and Simulations

Examples of Time Domain Reflectometry (TDR) and Time Domain Transmission (TDT) waveforms along with Frequency Domain Reflectometry (FDR) and Frequency Domain Transmission (FDT) spectra are given in this Appendix. These figures are in support of and referenced by the earlier chapters in this Dissertation.

Figures D.1- D.4 give actual measurements of sandy soils in the lab with different WC and EC values. Examples given are for a dry soil (WC < 0.05), a wet (saturated) soil (WC = 0.34) and an intermediate condition (WC = 0.20). Also shown in the figures is an example of a saline soil with high EC. The TDT measurements utilized a different fixture setup (Laboratory Validation Method #2 as described in chapter 4) vs. the TDR measurements (Laboratory Validation Method #1 as decribed in chapter 4) with a slightly longer probe but close enough to illustrate the differences of TDT vs. TDR measurements for these initial examples. The key observations to show with these initial plots are the sensitivity of the waveform transit time (time between first and second reflections) to the changing values of WC. A higher WC results in a higher value of electric permittivity which in turns slows down the propagating wave which results in a longer transit time. In addition, when salinity is high the second reflection can be swamped out due to attenuation which can complicate the extraction of WC from the measurement. New methods of how to overcome that are presented in this Dissertation. Also given are examples of the frequency domain representation of the equivalent S-parameters (S11 and S22). S-Parameters are described in depth in Appendix B including techniques for modeling cascaded domains of a medium.

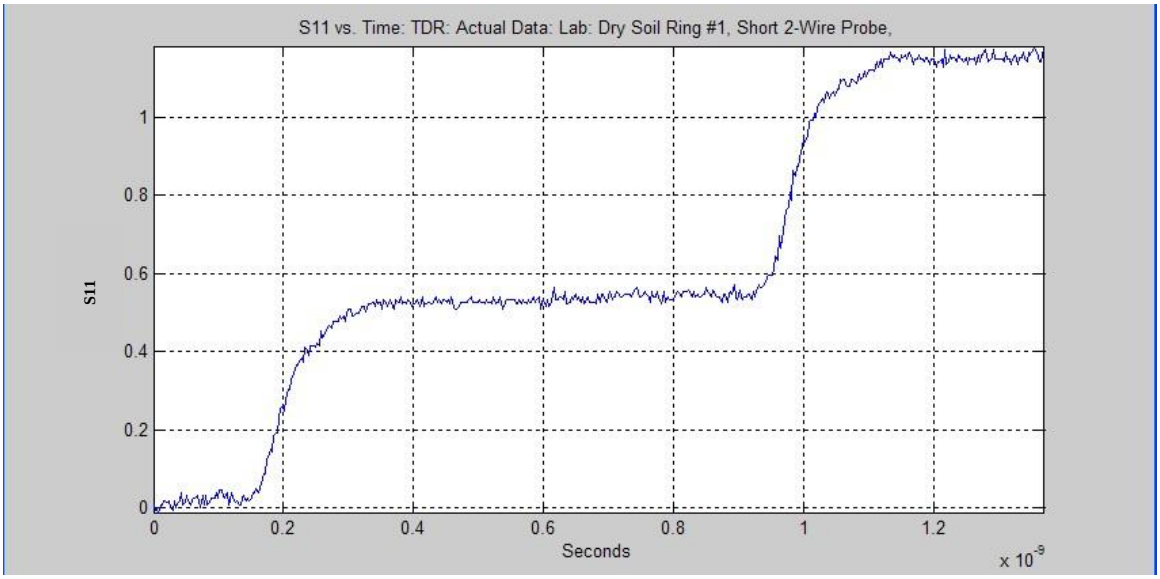


Figure D.1a: TDR Waveform for a Dry Soil (Laboratory Validation Method #1): Shorter Time Scale

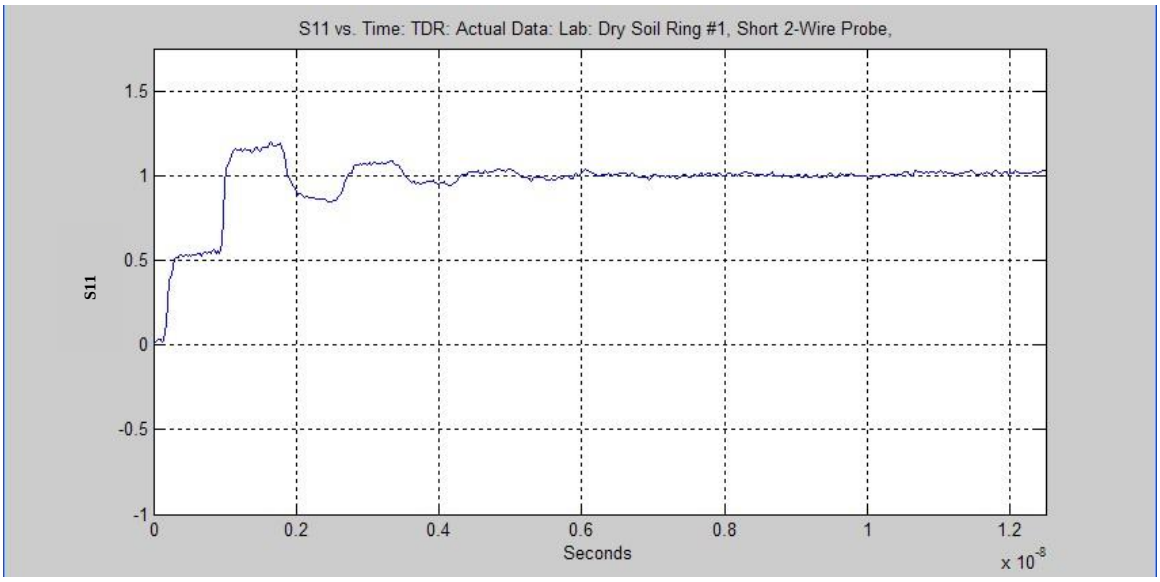


Figure D.1b: TDR Waveform for a Dry Soil (Laboratory Validation Method #1): Longer Time Scale

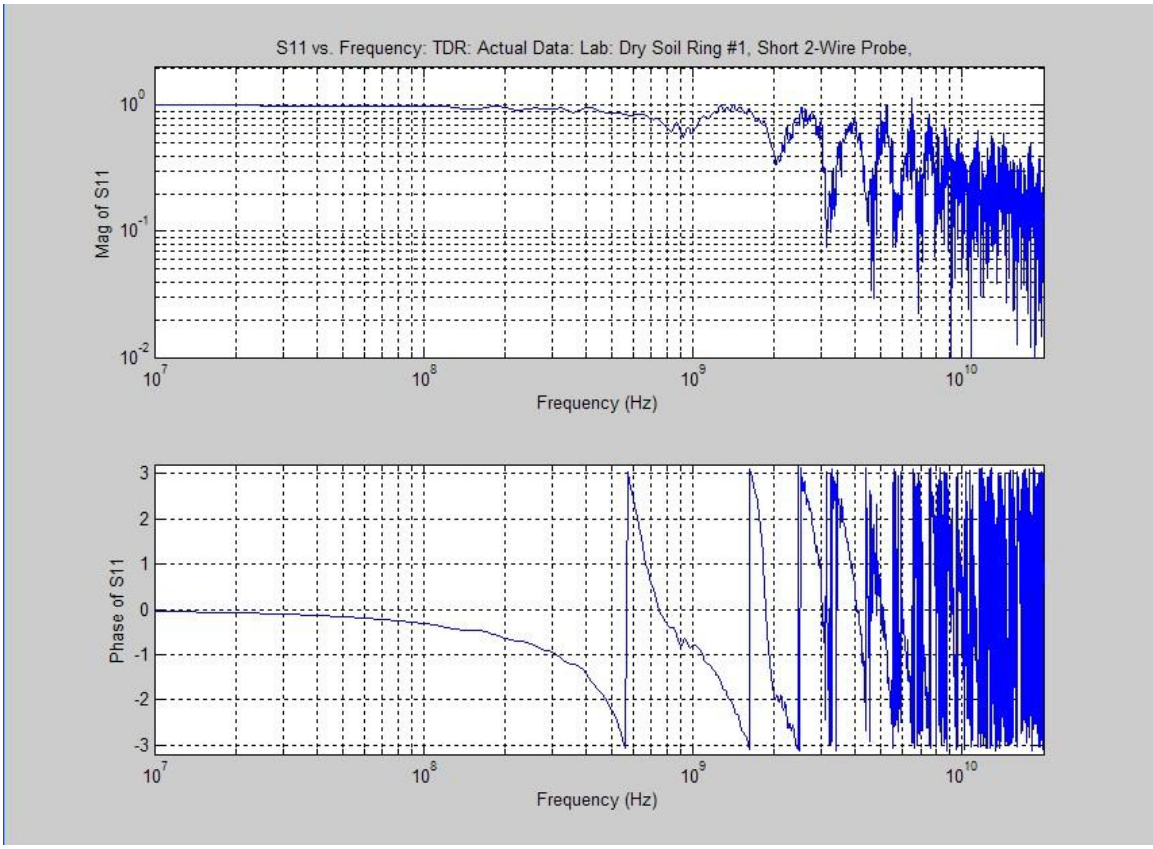


Figure D.1c: Frequency Domain Representation of S11 for a TDR Setup (Dry Soil – Laboratory Validation Method #1)

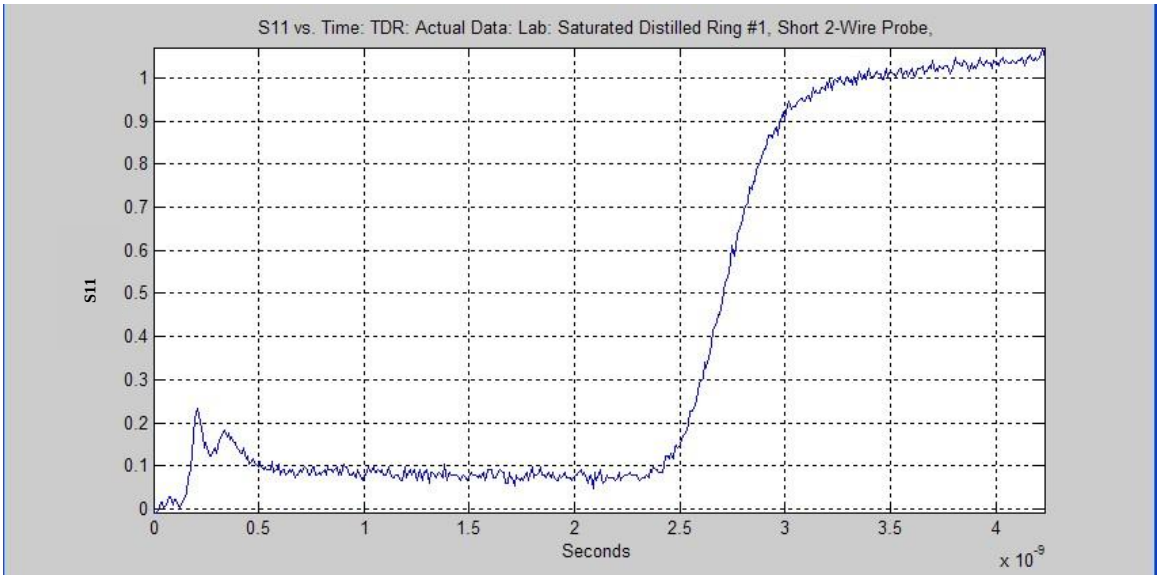


Figure D.2a: TDR Waveform for a Wet Soil (Laboratory Validation Method #1): Shorter Time Scale

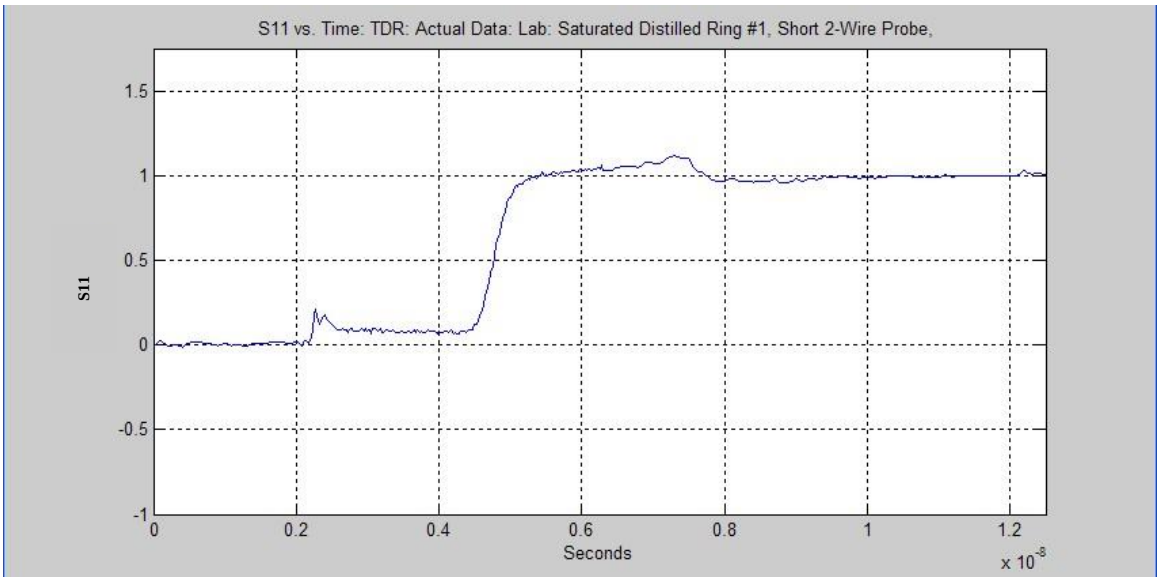


Figure D.2b: TDR Waveform for a Wet Soil (Laboratory Validation Method #1): Longer Time Scale

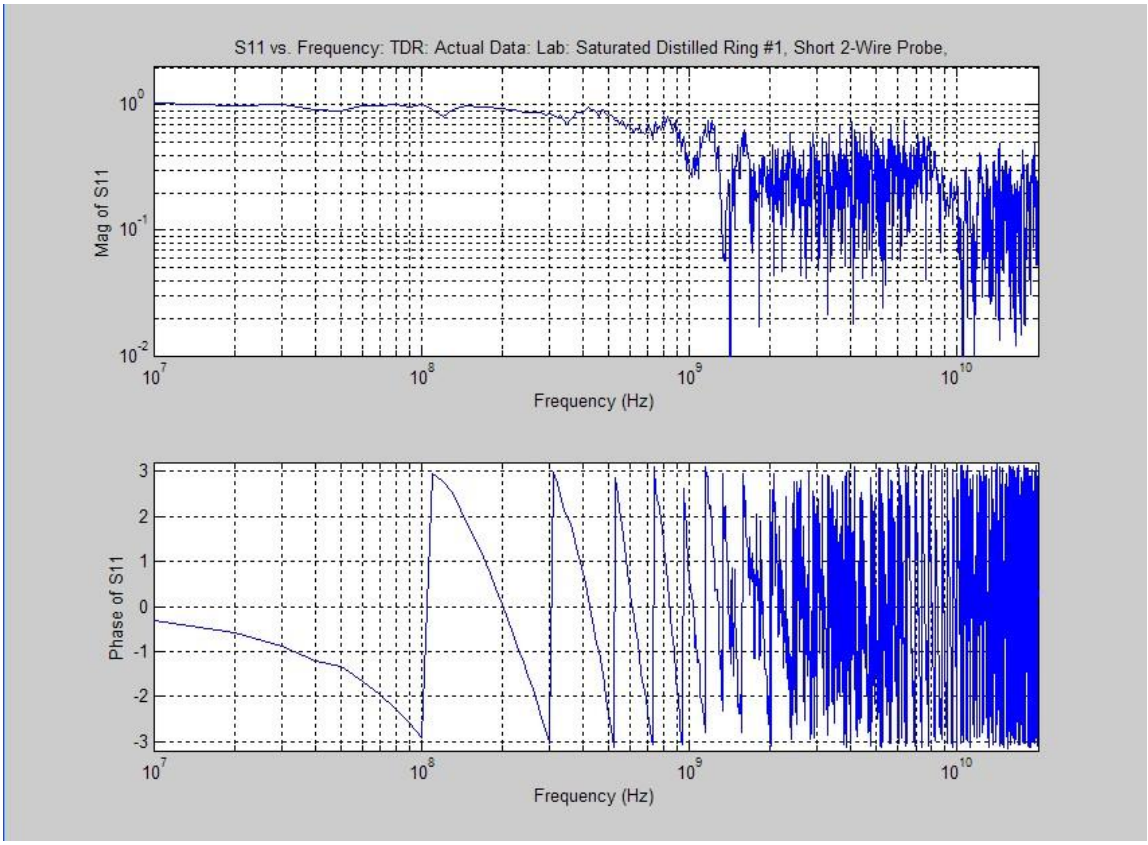


Figure D.2c: Frequency Domain Representation of S11 for a TDR Setup (Wet Soil – Laboratory Validation Method #1)

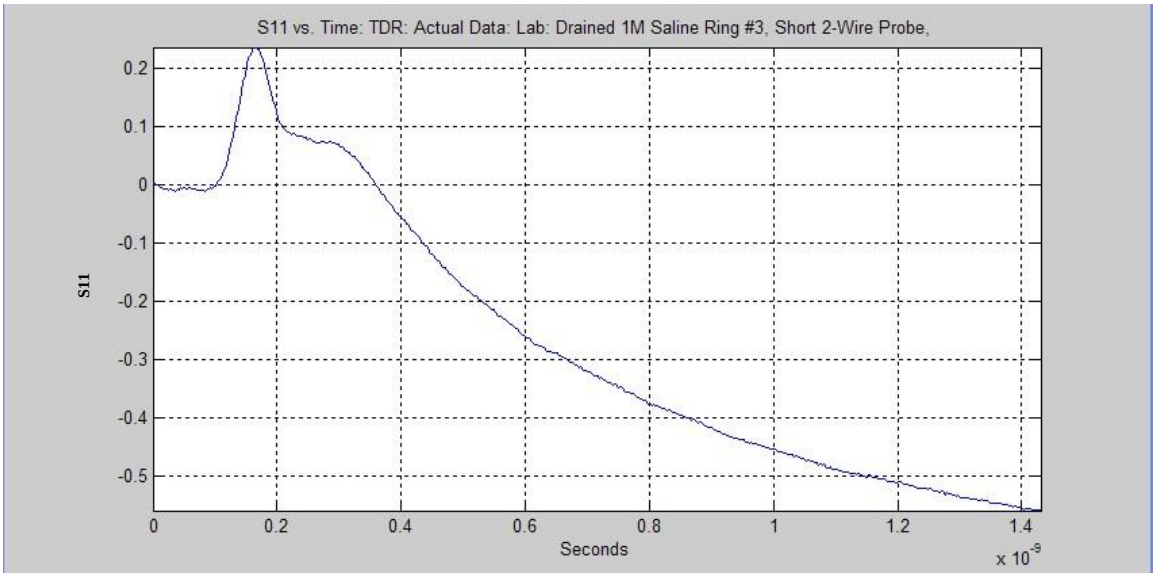


Figure D.3a: TDR Waveform for a Wet Saline Soil (Laboratory Validation Method #1): Shorter Time Scale

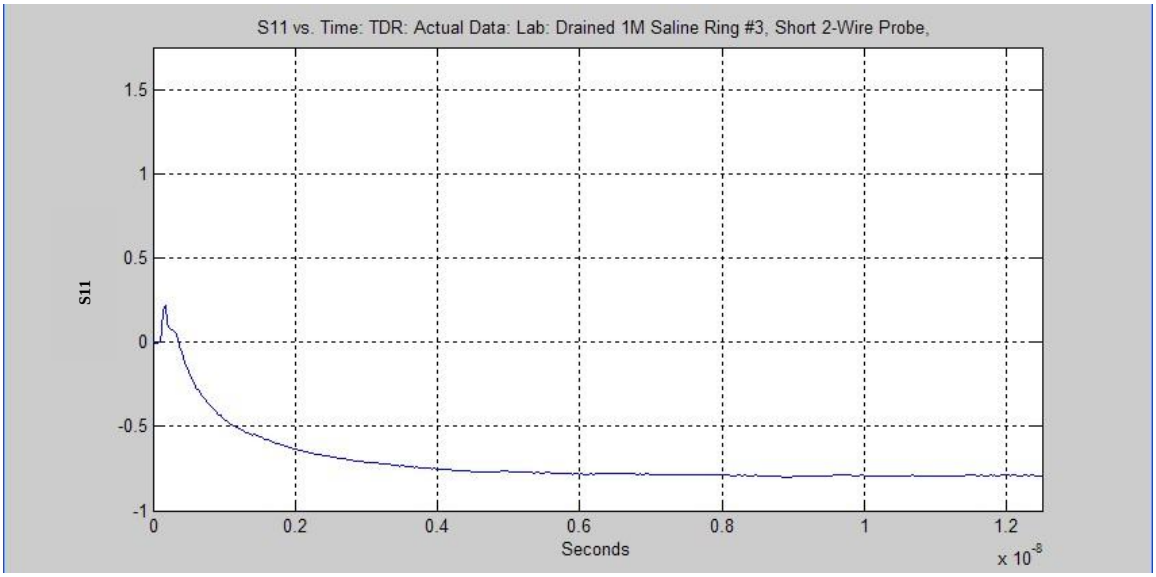


Figure D.3b: TDR Waveform for a Wet Saline Soil (Laboratory Validation Method #1): Longer Time Scale

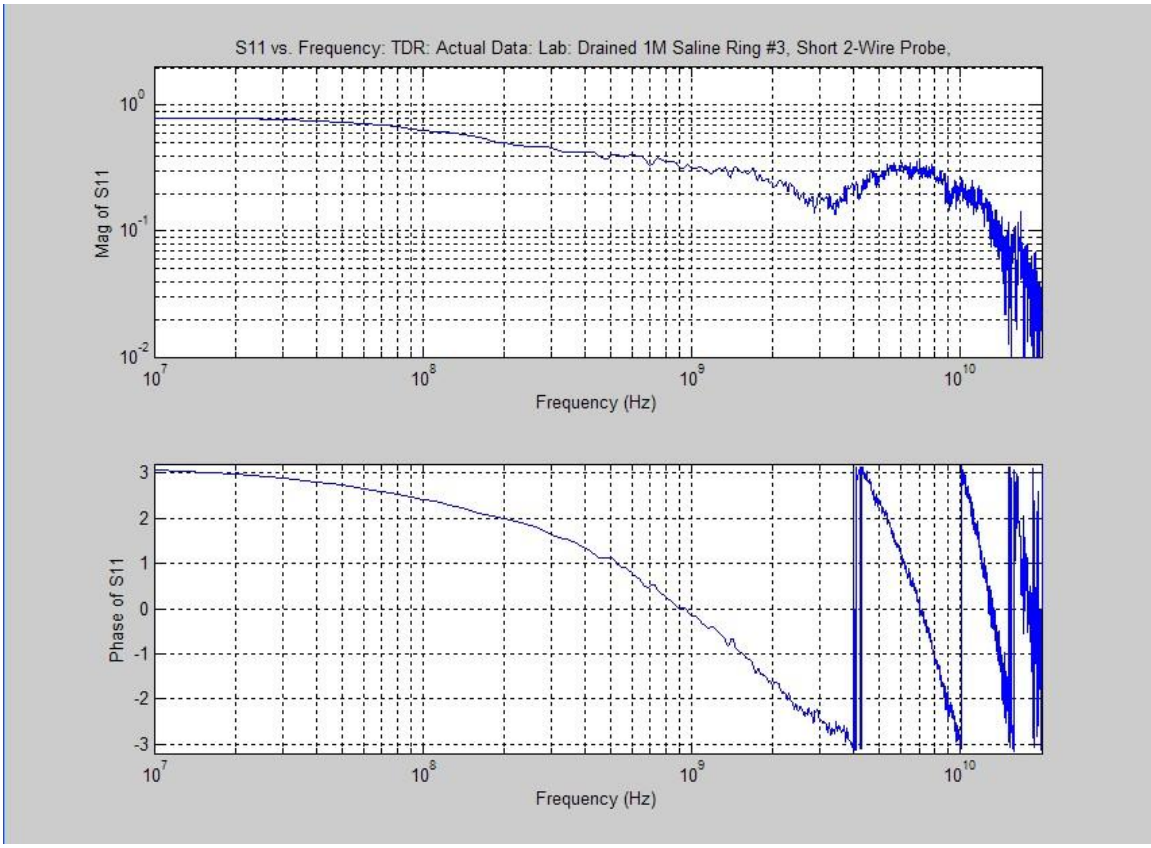


Figure D.3c: Frequency Domain Representation of S11 for a TDR Setup (Wet Saline Soil – Laboratory Validation Method #1)

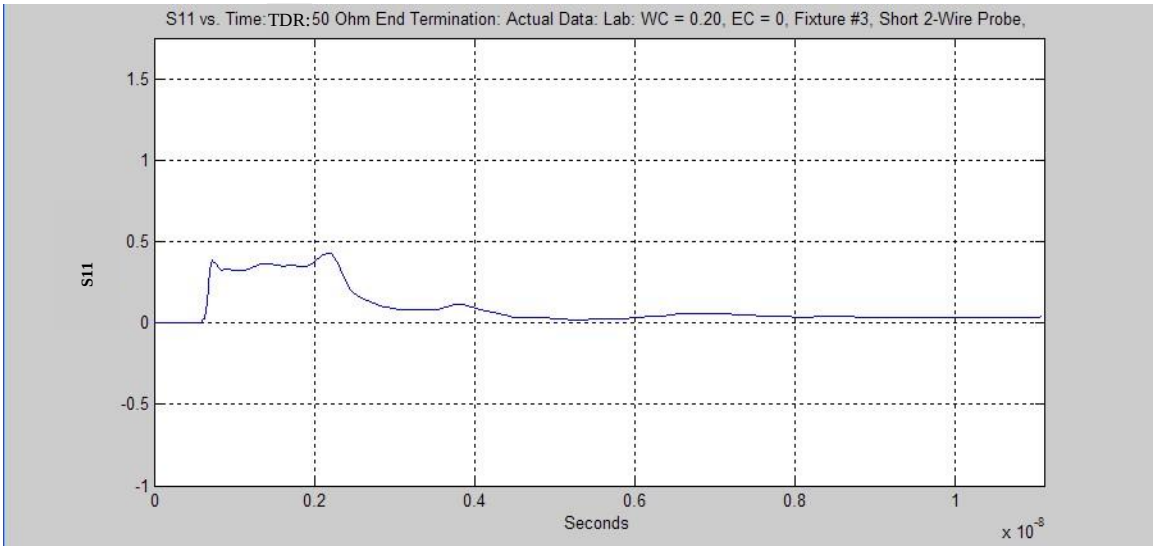


Figure D.4a: TDR Reflection Waveform (S11) with a 50Ω End Termination for an Intermediate WC Soil (Laboratory Validation Method #2)

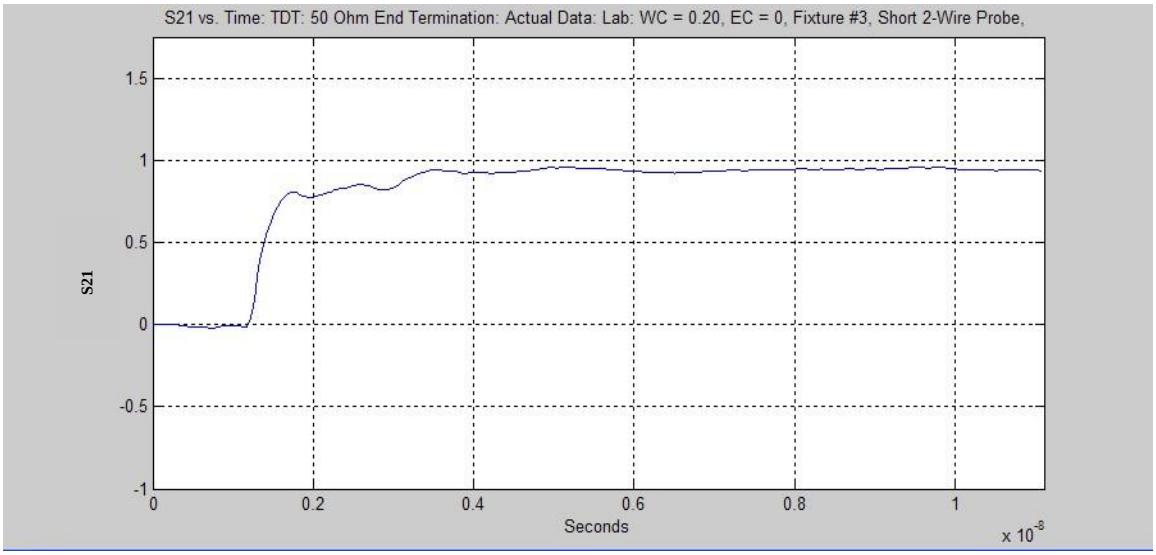


Figure D.4b: TDT Transmission Waveform (S21) for an Intermediate WC Soil (Laboratory Validation Method #2)

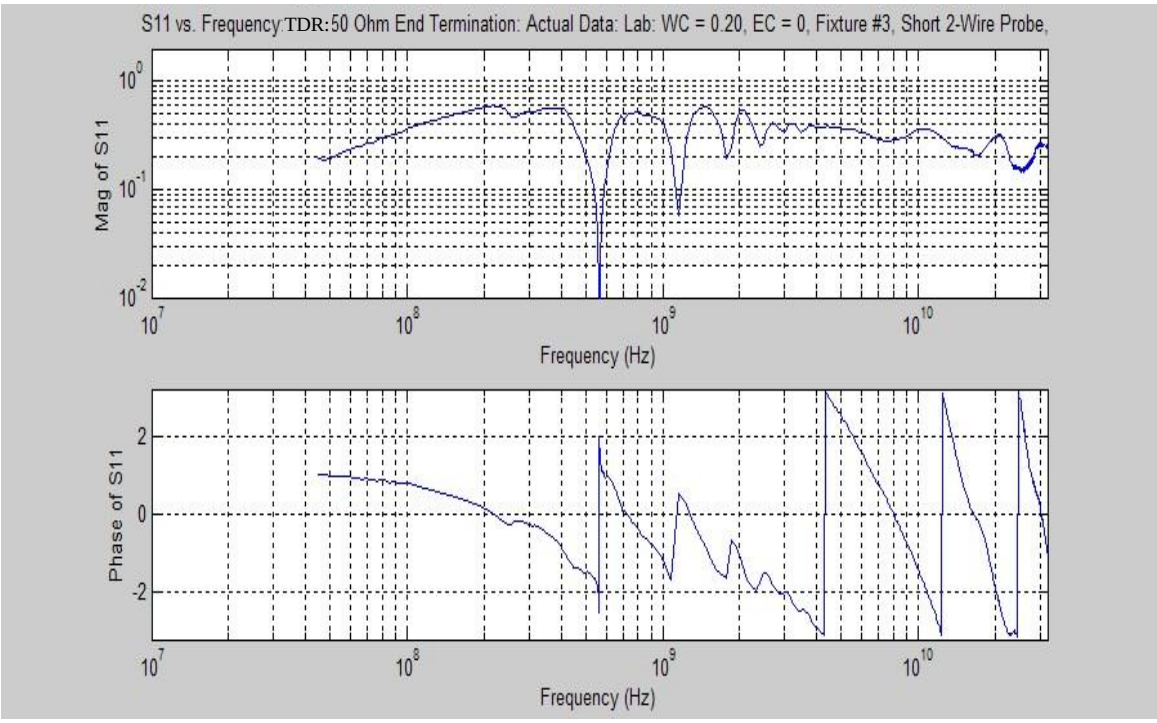


Figure D.4c: TDR Frequency Domain Representation (S11) with a 50 Ohm End Termination for an intermediate WC Soil (Laboratory Validation Method #2)

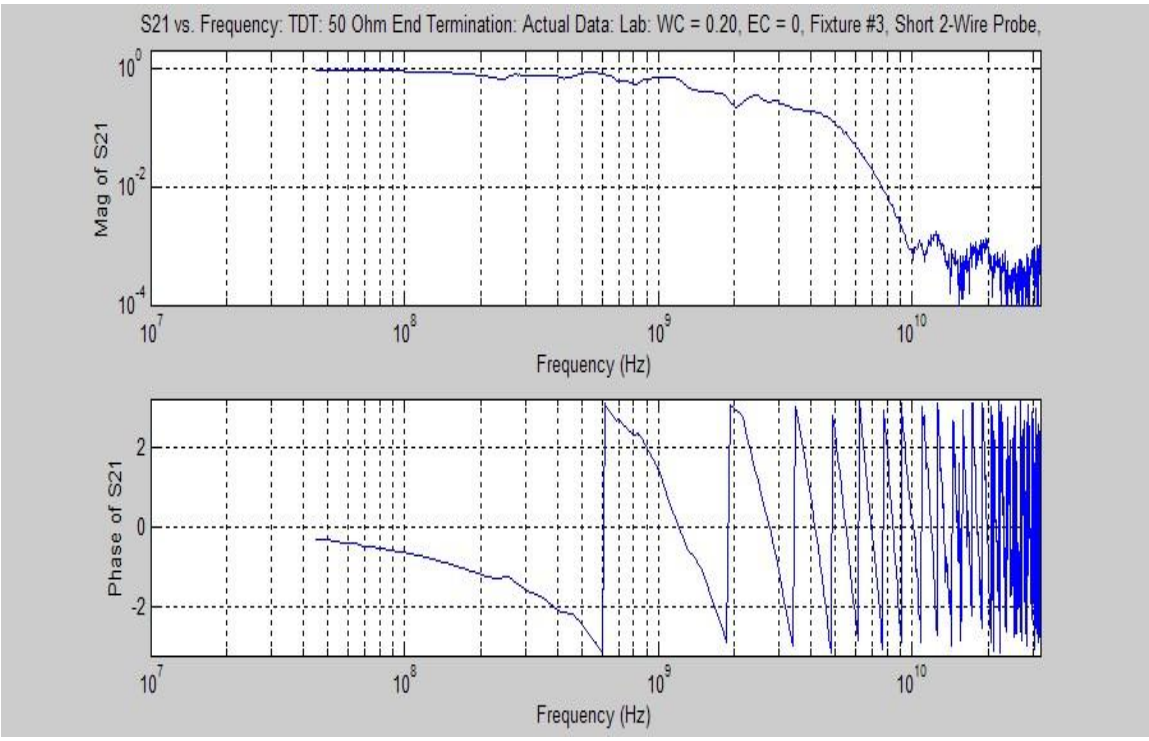


Figure D.4d: TDT Frequency Domain Representation (S21) for an intermediate WC Soil (Laboratory Test)

The TDT waveforms (figure D.4) were again generated with a different fixture and lab setup (Laboratory Validation Method #2) vs. the TDR waveforms (figures 1 -3) (from Laboratory Validation Method #1) resulting in a slightly longer probe length but close enough to still illustrate the points. With the TDT setup (Laboratory Validation Method #2 as described in Chapter 4) the load termination is 50 ohms (the input impedance of the measurement receiver – a vector network analyzer (VNA) or alternatively a high frequency scope). However, in the TDR setup (Laboratory Validation Method #1 as described in Chapter 4) the output is open circuited. These plots give an initial snapshot of the amount of information available in both the time and frequency domains with both TDR and TDT signals. The forward prediction models utilize both the time and frequency domains as well as TDR and TDT models as described in chapter 3. Full information on the actual data and comparisons to the forward prediction models is given in chapters 4 and 5 covering validation methods and results as well as later in this appendix. The above plots were for sandy soils and are again just an initial snapshot of representative waveforms and spectra.

The remaining figures in this appendix show additional validation comparisons between the forward prediction model simulations and the actual data (in support of and referenced by chapters 4 and 5 covering the forward prediction model validation methods and results):

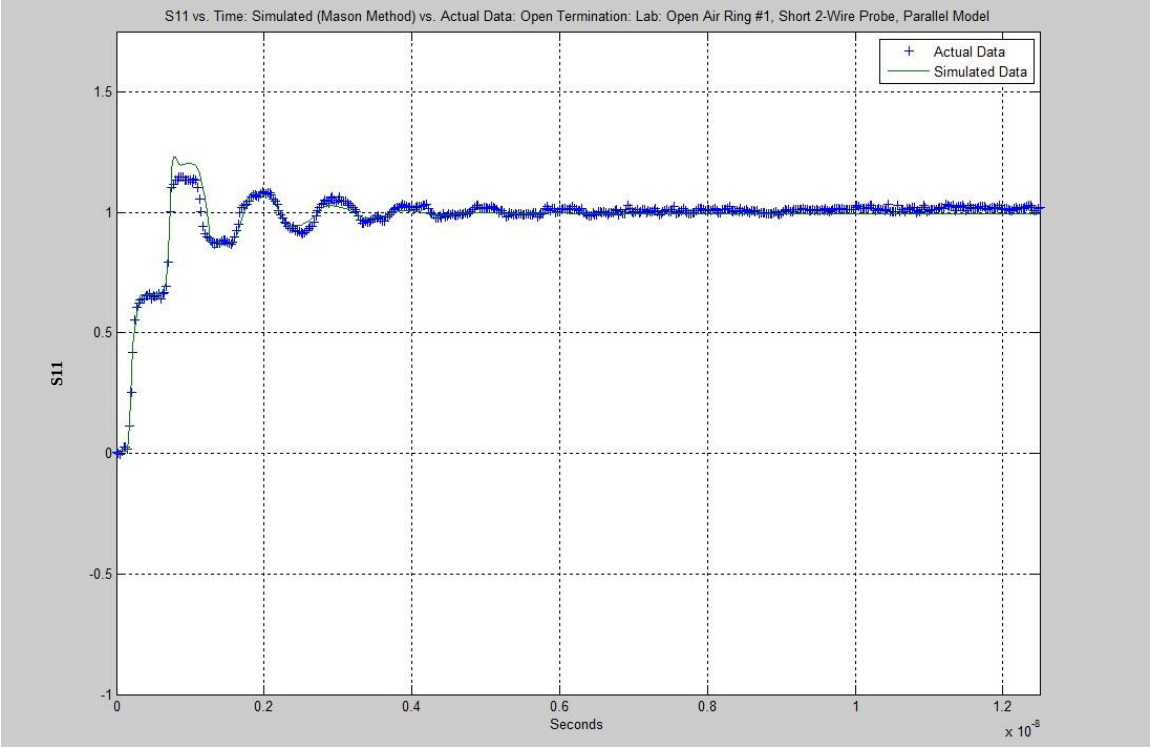


Figure D.5a: Lab Validation Method #1: TDR Waveform: Open Air Calibration: Simulated vs. Actual

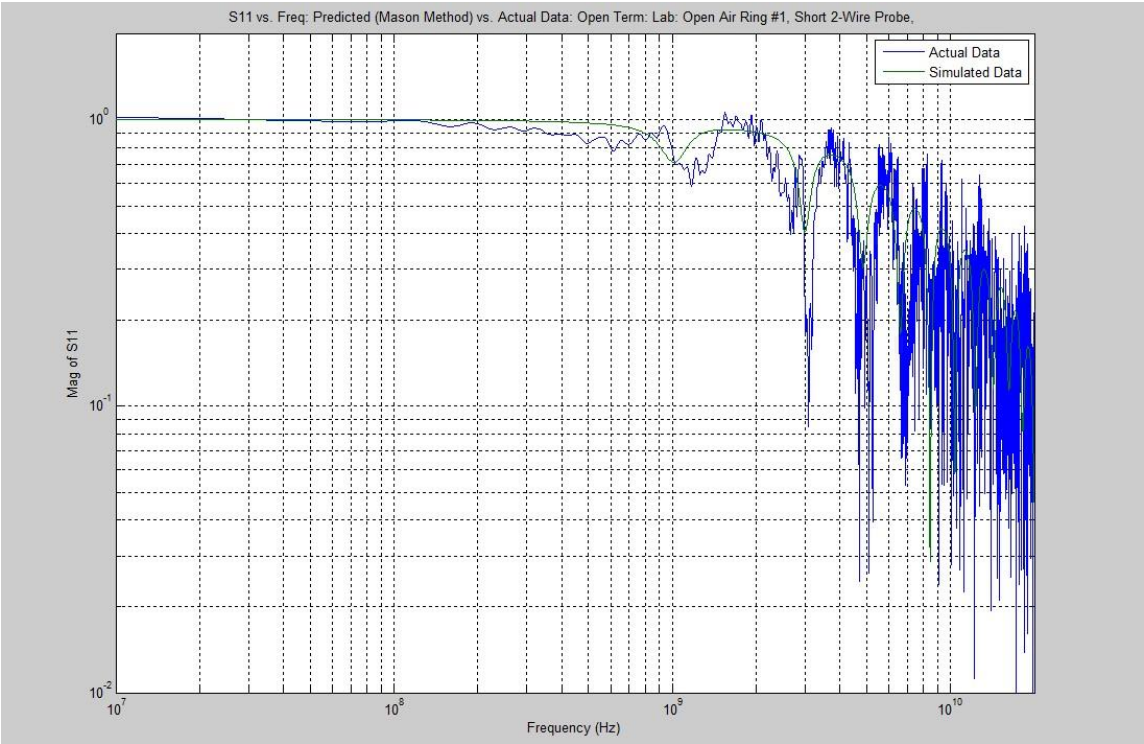


Figure D.5b: Lab Validation Method #1: Frequency Domain Spectrum: Open Air: Simulated vs. Actual

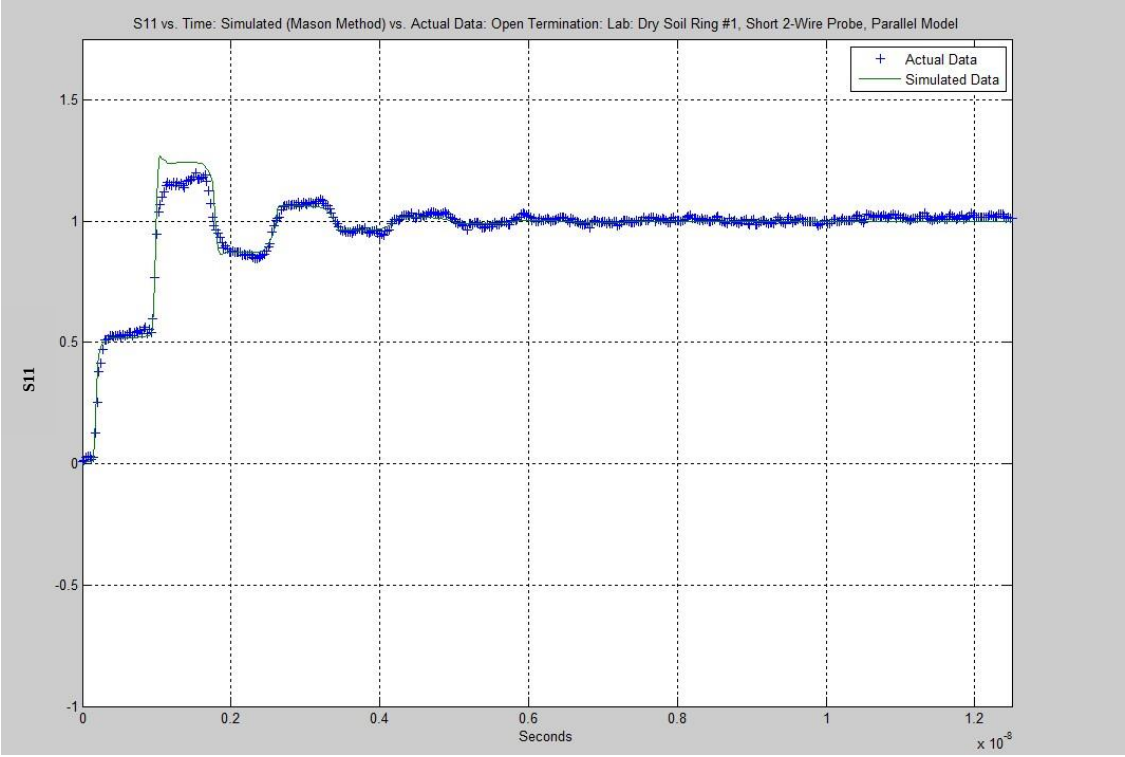


Figure D.6a: Lab Validation Method #1: TDR Waveform: Dry Soil Calibration: Simulated vs. Actual

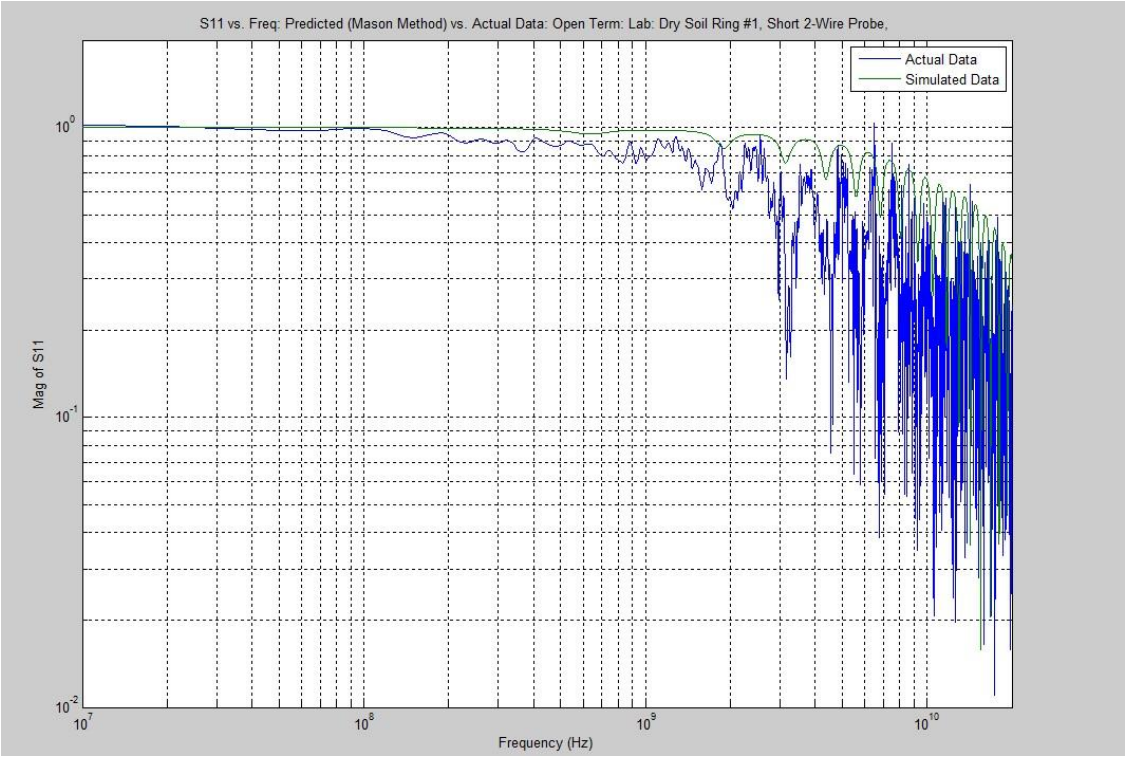


Figure D.6b: Lab Validation Method #1: Frequency Domain Spectrum: Dry Soil: Simulated vs. Actual

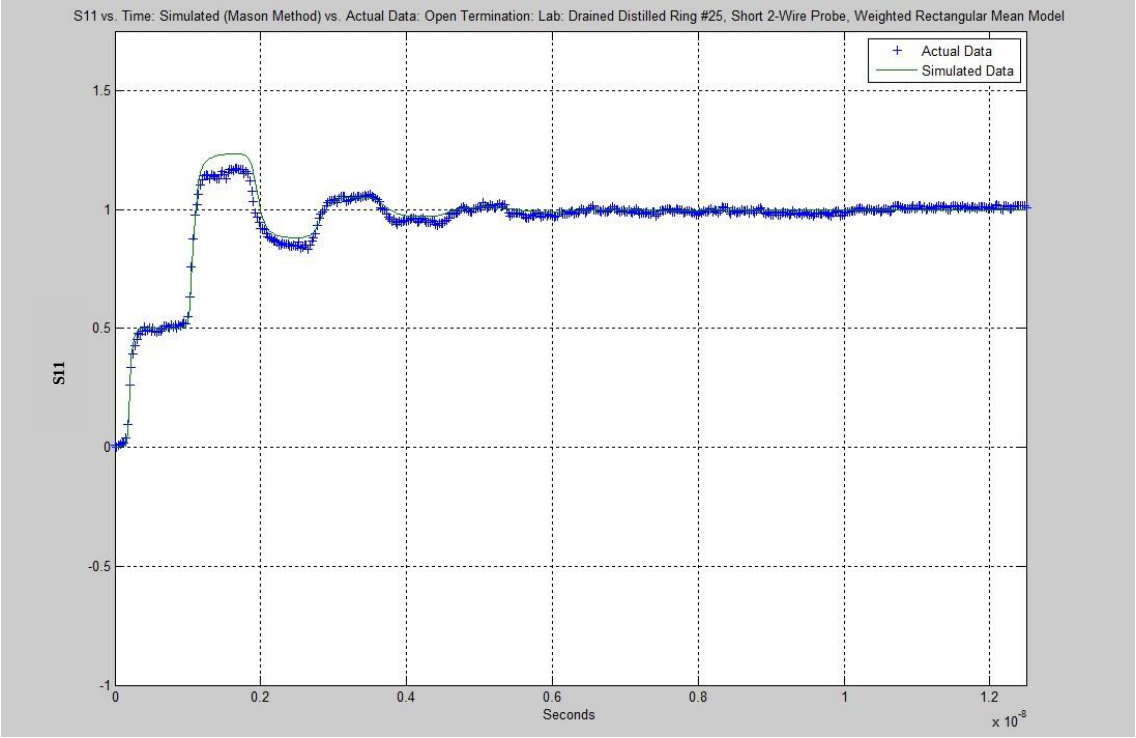


Figure D.7a: Lab Validation Method #1: TDR Waveform: WC = 0.03: Simulated vs. Actual

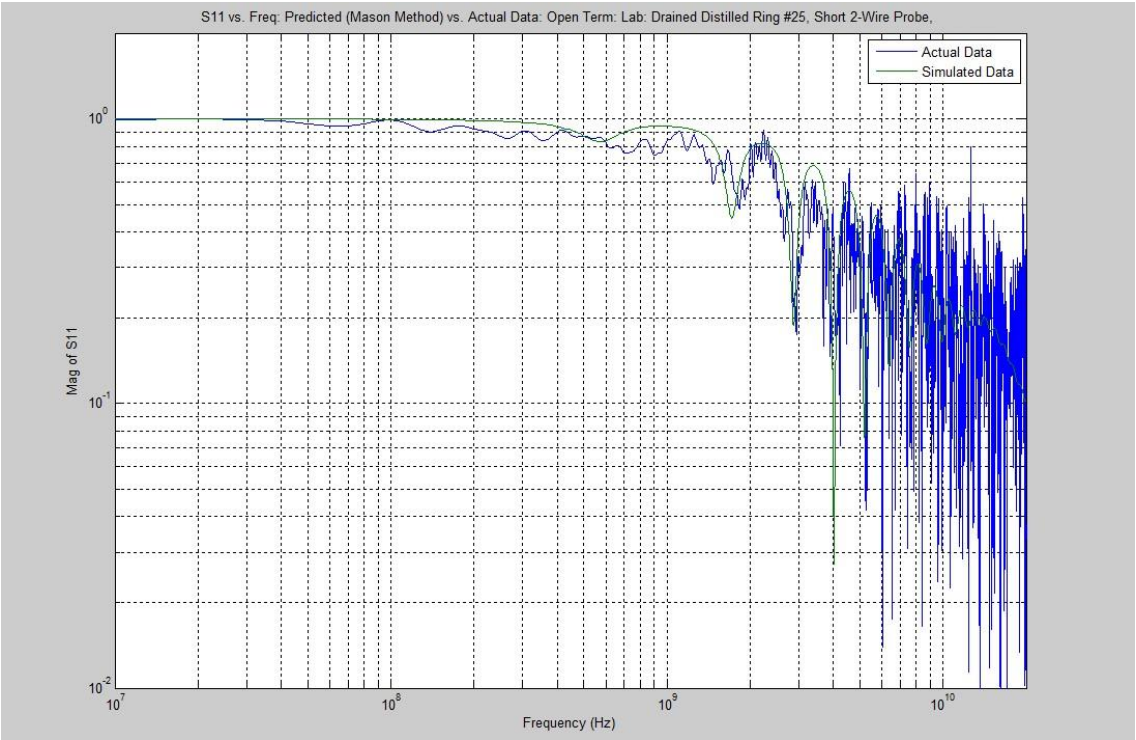


Figure D.7b: Lab Validation Method #1: Frequency Domain Spectrum: WC = 0.03: Simulated vs. Actual

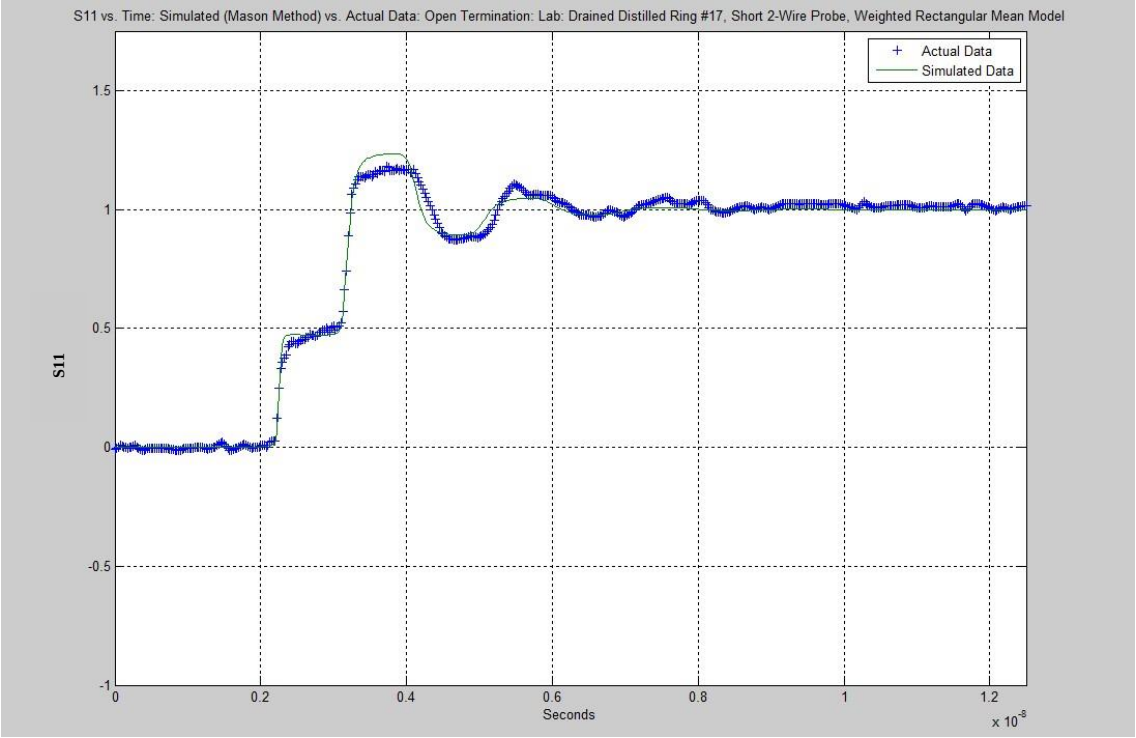


Figure D.8a: Lab Validation Method #1: TDR Waveform: WC = 0.05: Simulated vs. Actual

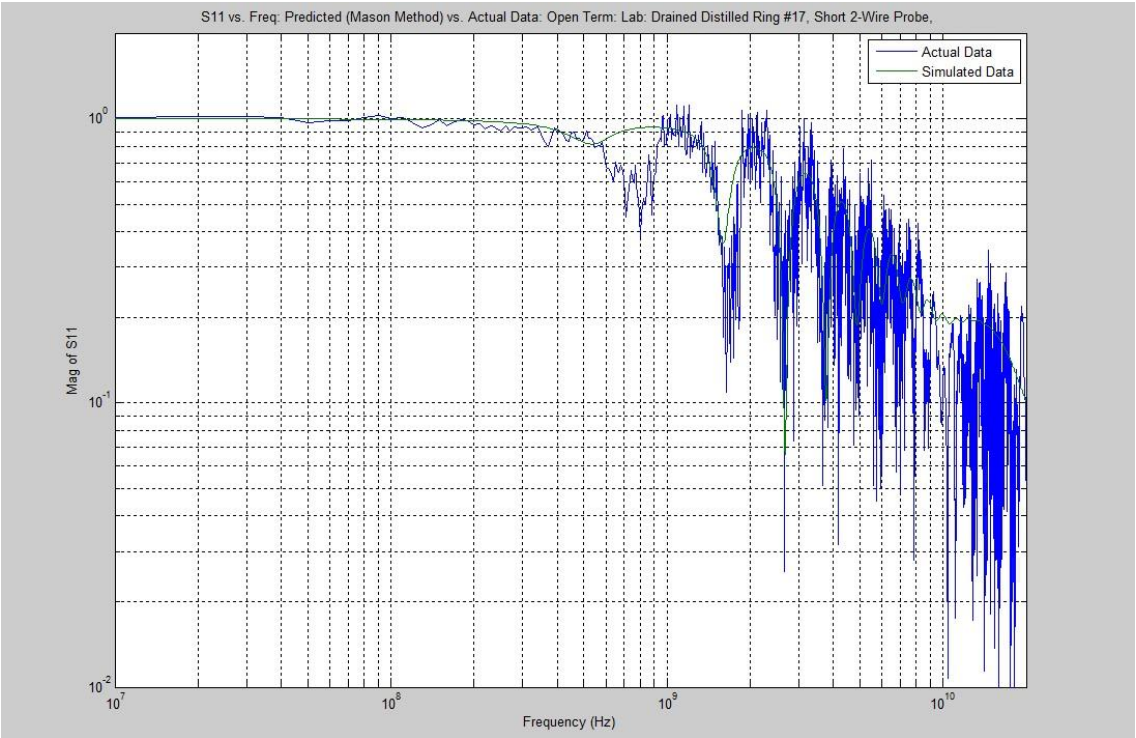


Figure D.8b: Lab Validation Method #1: Frequency Domain Spectrum: WC = 0.05: Simulated vs. Actual

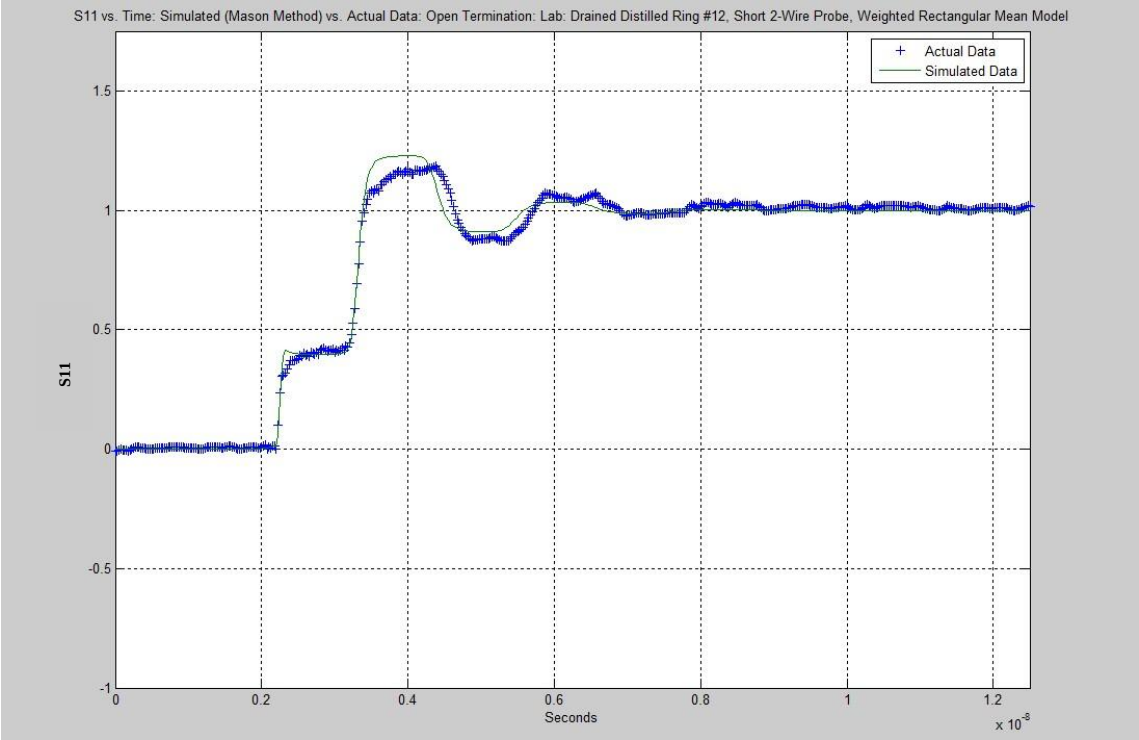


Figure D.9a: Lab Validation Method #1: TDR Waveform: WC = 0.10: Simulated vs. Actual

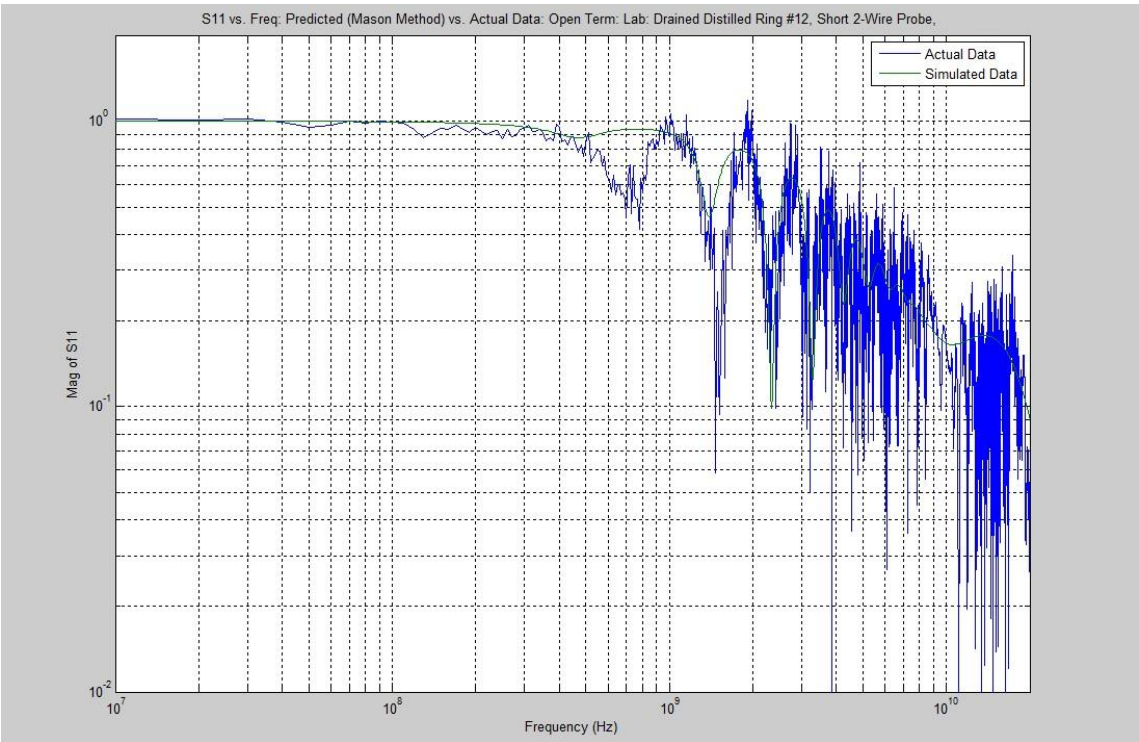


Figure D.9b: Lab Validation Method #1: Frequency Domain Spectrum: WC = 0.10: Simulated vs. Actual

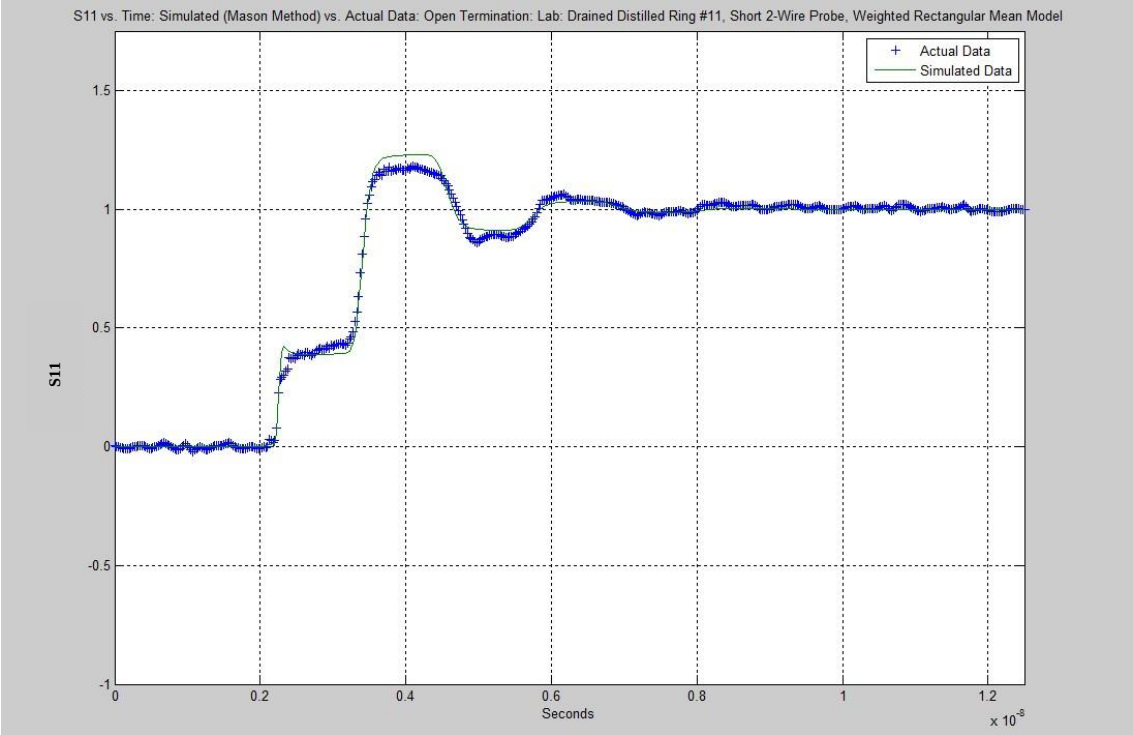


Figure D.10a: Lab Validation Method #1: TDR Waveform: WC = 0.13: Simulated vs. Actual

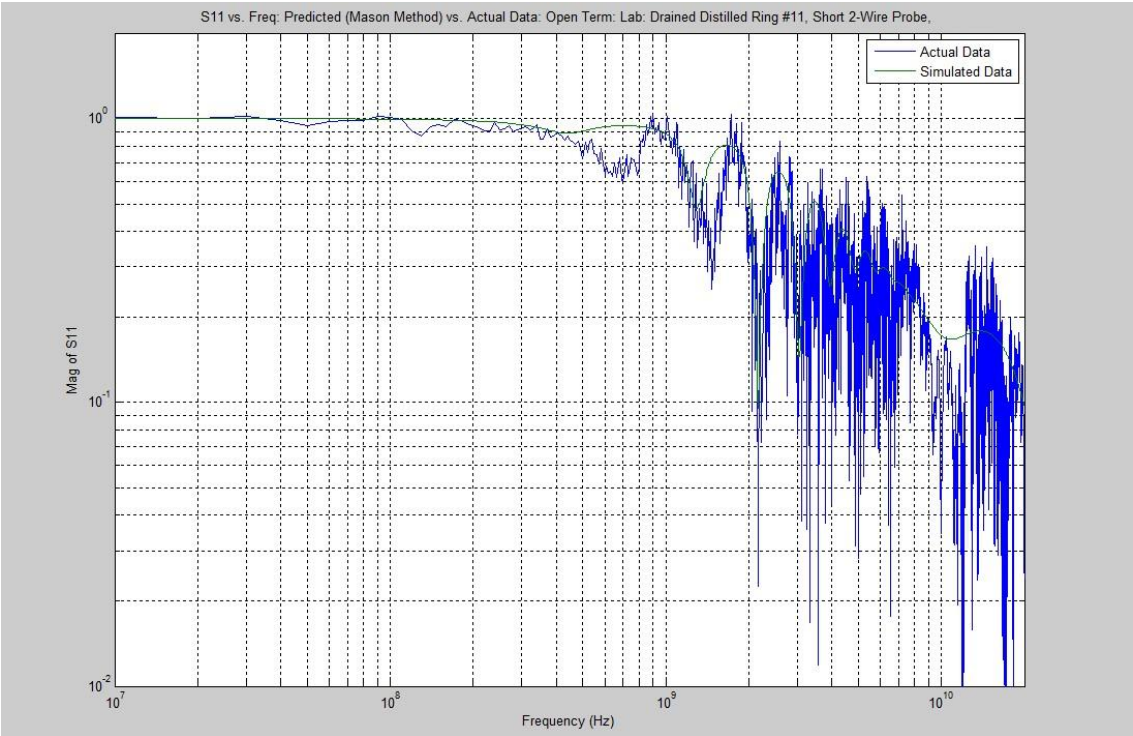


Figure D.10b: Lab Validation Method #1: Frequency Domain Spectrum: WC = 0.13: Simulated vs. Actual

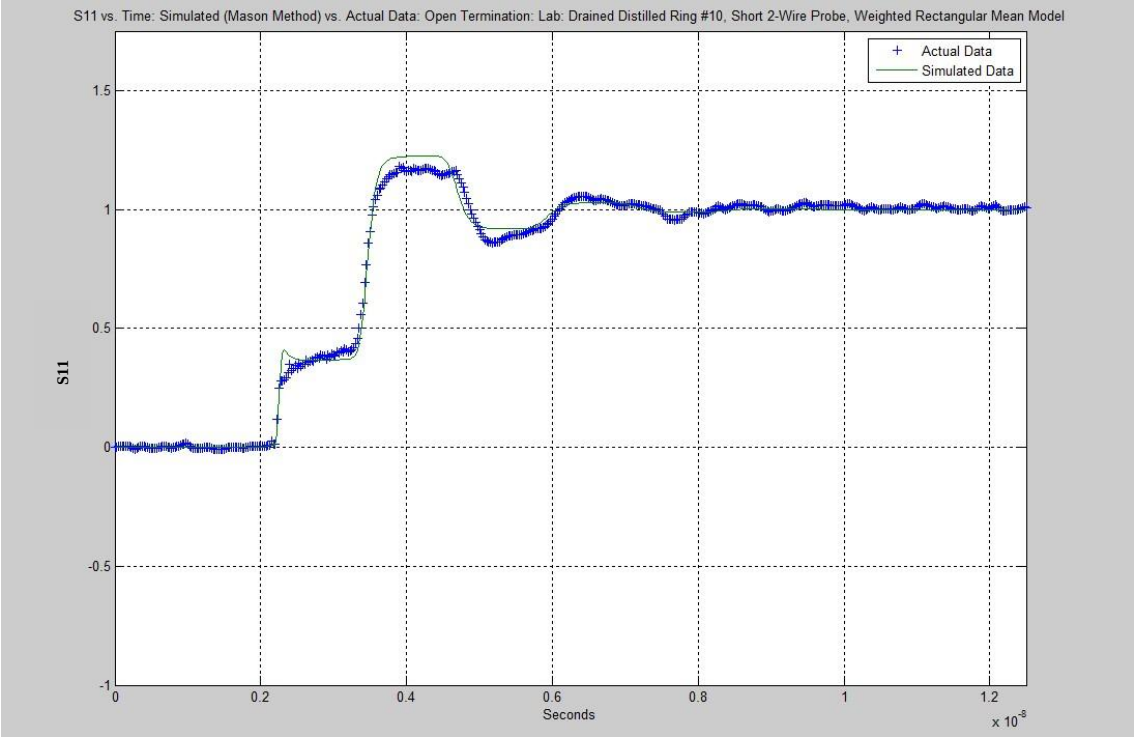


Figure D.11a: Lab Validation Method #1: TDR Waveform: WC = 0.18: Simulated vs. Actual

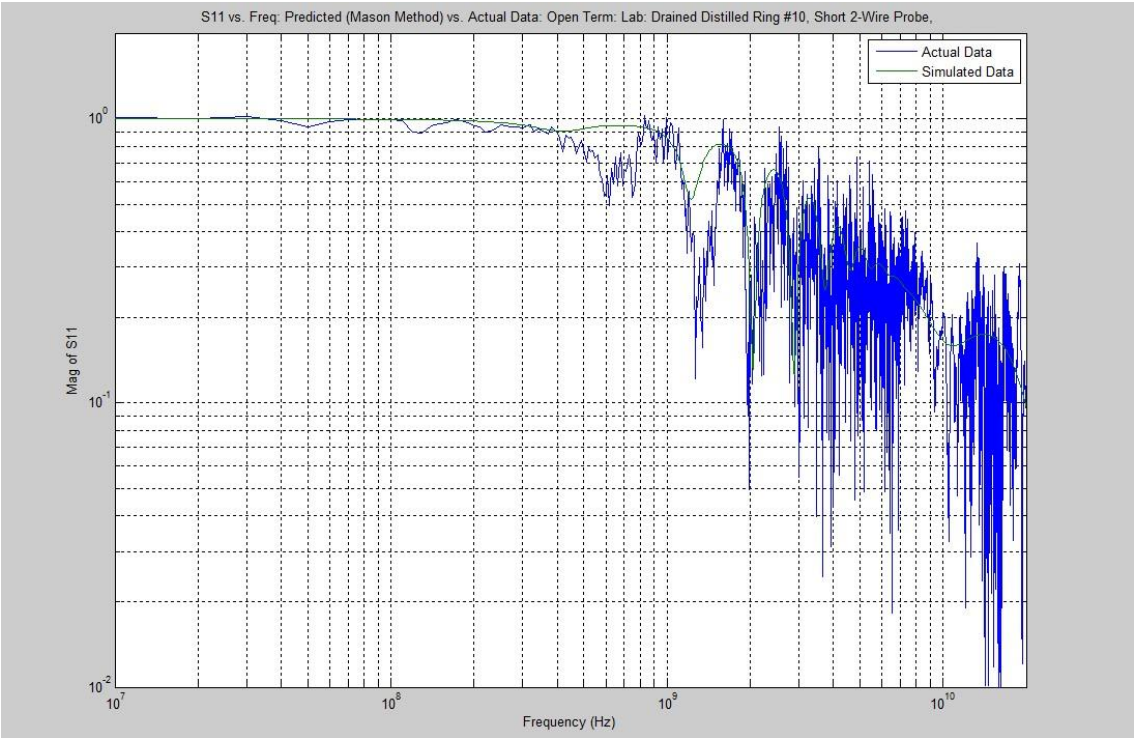


Figure D.11b: Lab Validation Method #1: Frequency Domain Spectrum: WC = 0.18: Simulated vs. Actual

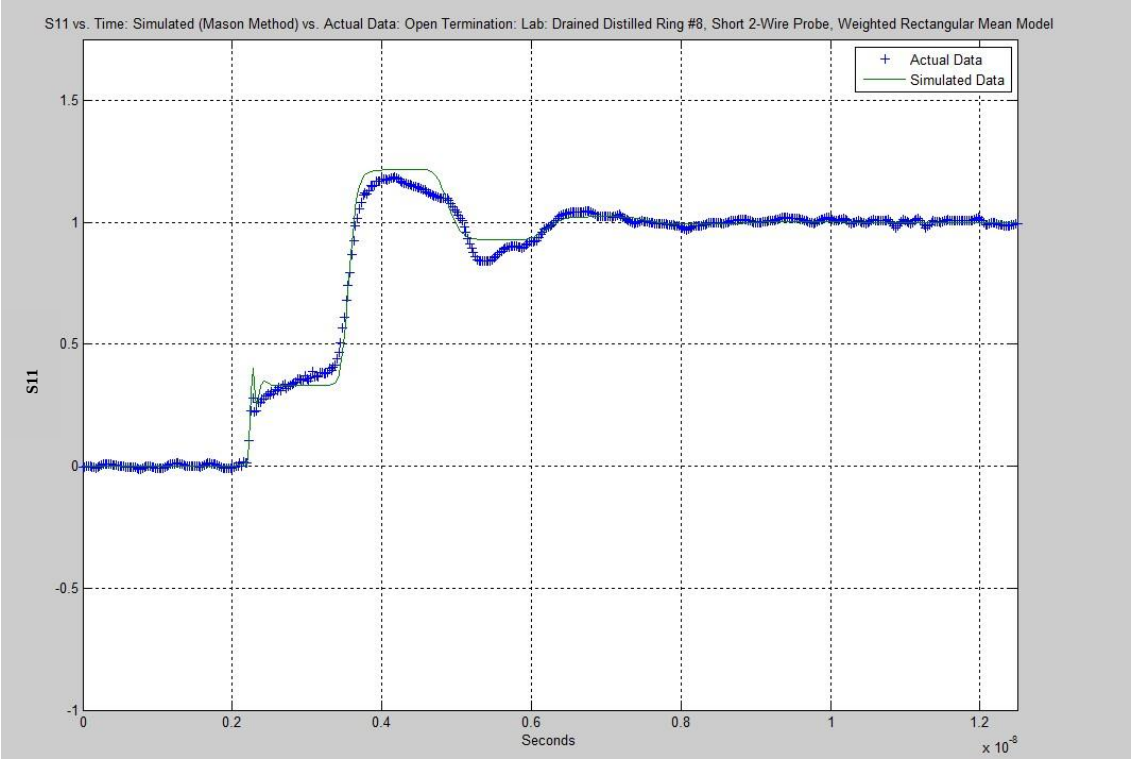


Figure D.12a: Lab Validation Method #1: TDR Waveform: WC = 0.24: Simulated vs. Actual

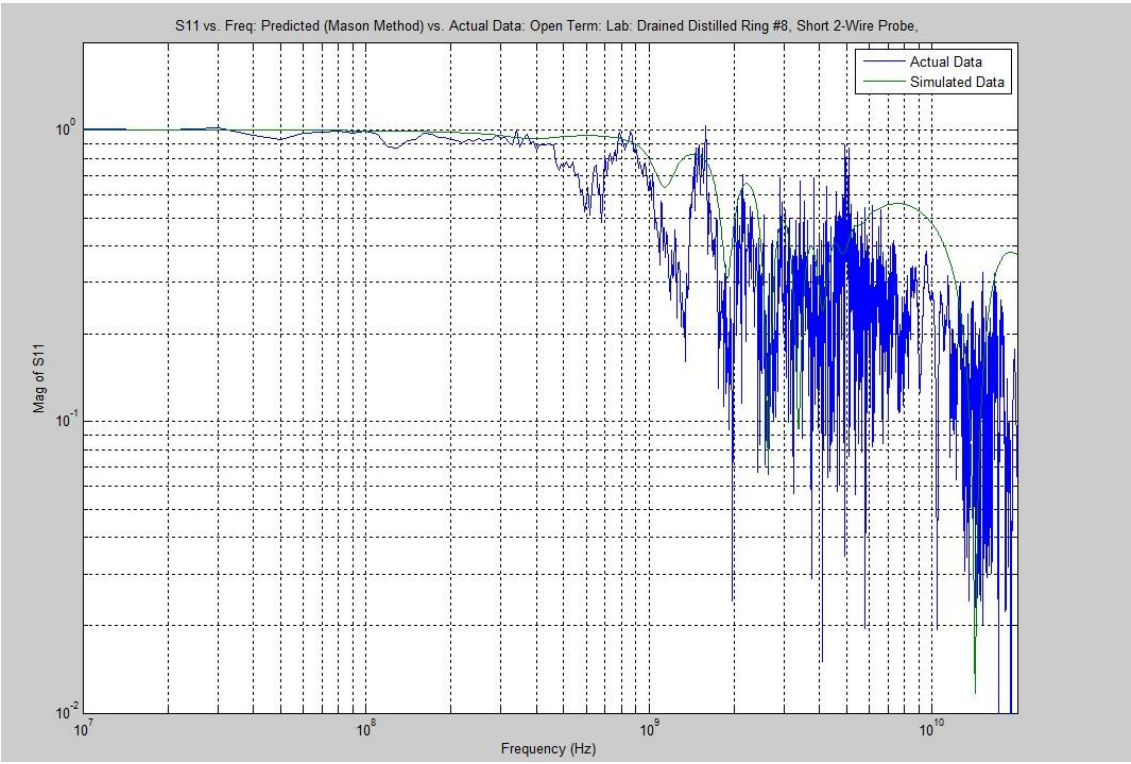


Figure D.12b: Lab Validation Method #1: Frequency Domain Spectrum: WC = 0.24: Simulated vs. Actual

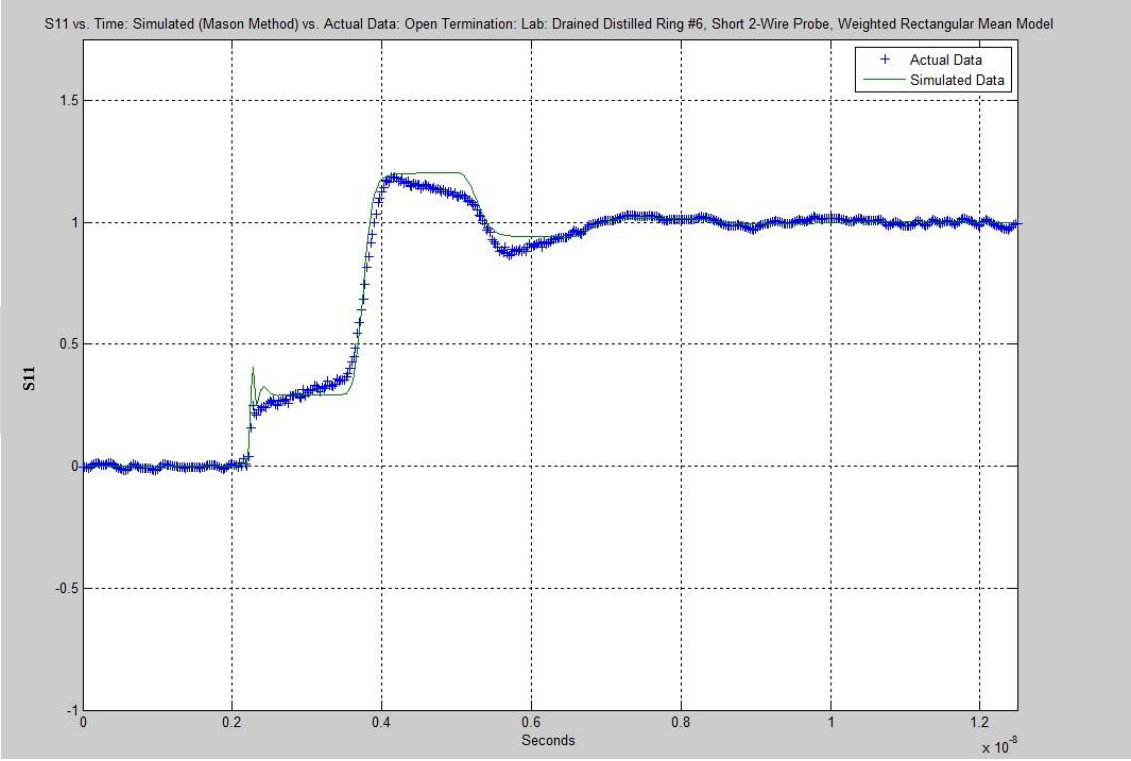


Figure D.13a: Lab Validation Method #1: TDR Waveform: WC = 0.29: Simulated vs. Actual

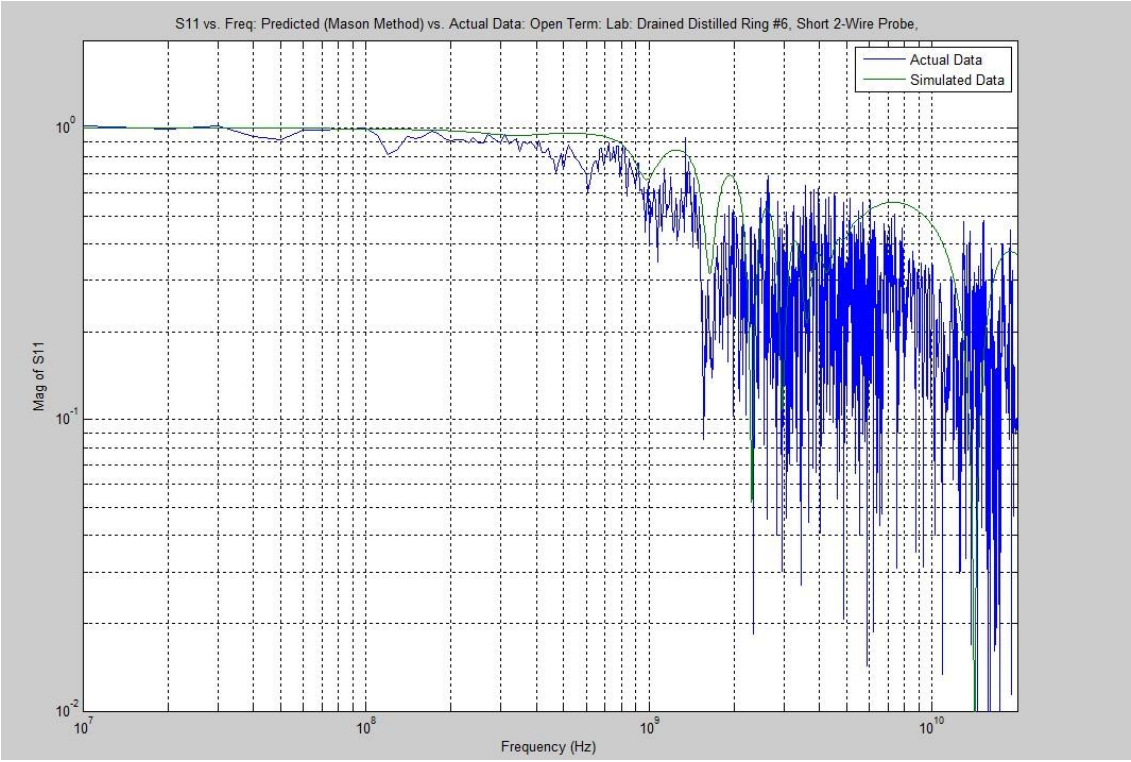


Figure D.13b: Lab Validation Method #1: Frequency Domain Spectrum: WC = 0.29: Simulated vs. Actual

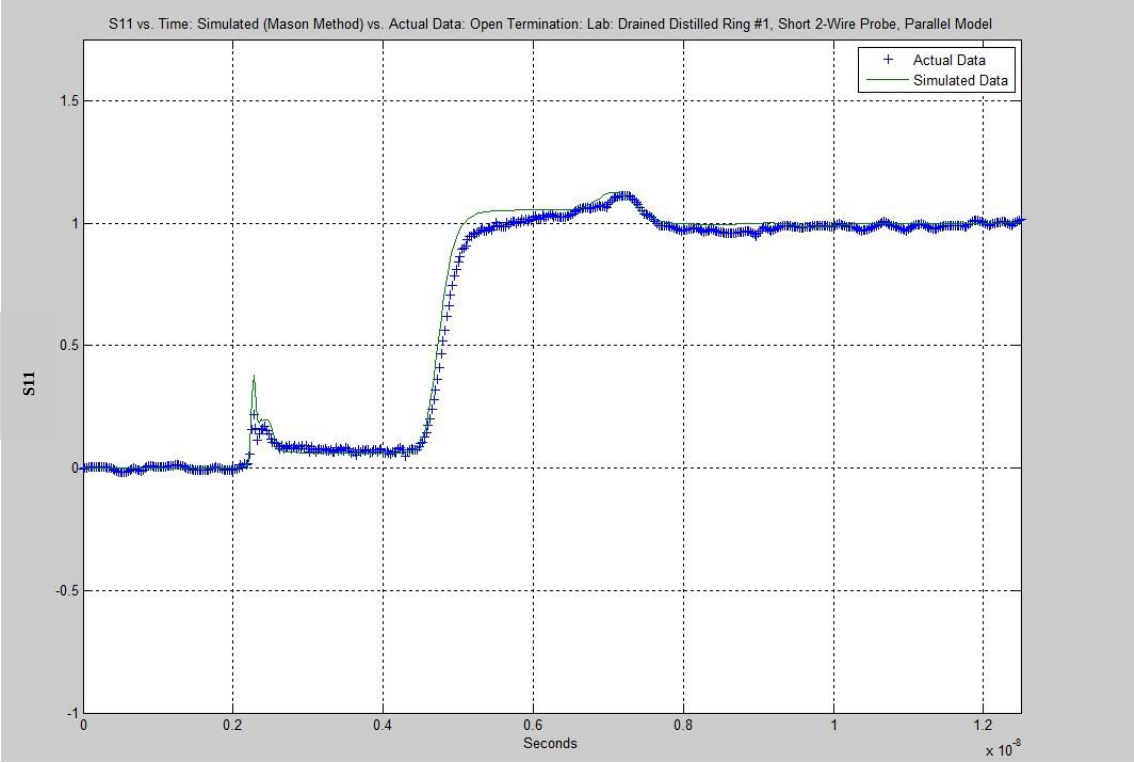


Figure D.14a: Lab Validation Method #1: TDR Waveform: WC = 0.37 (Saturated): Simulated vs. Actual

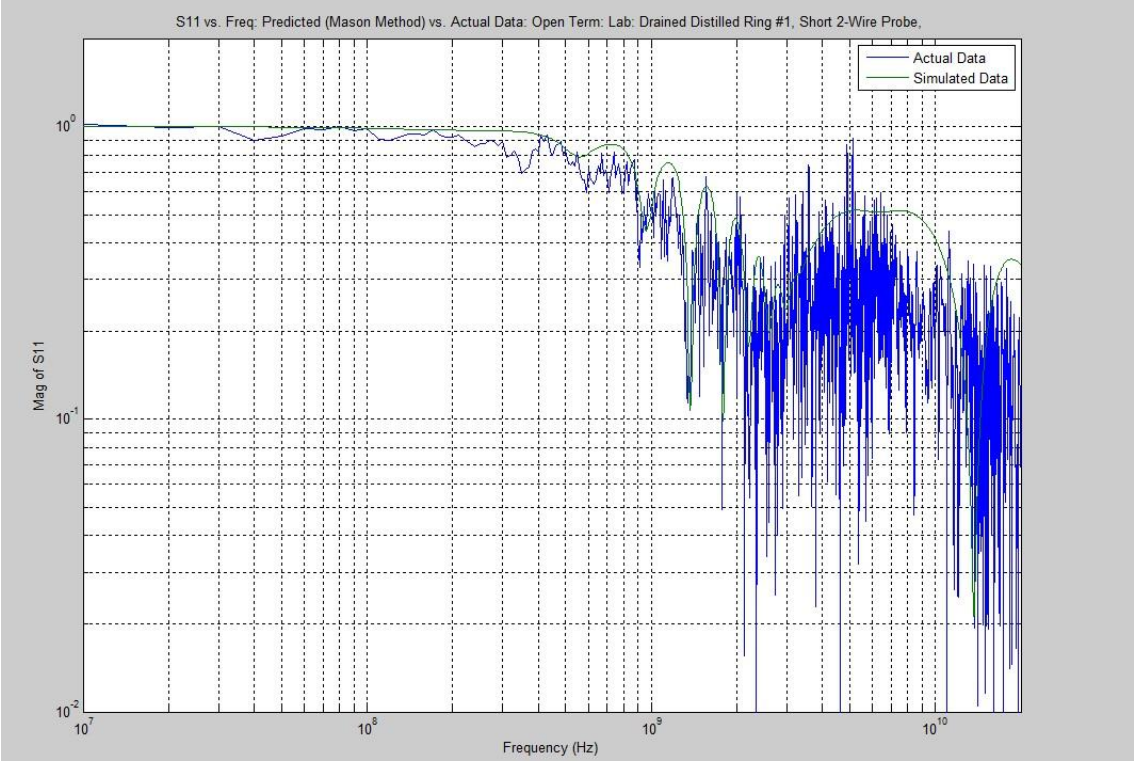


Figure D.14b: Lab Validation Method #1: Frequency Domain Spectrum: WC = 0.37: Simulated vs. Actual

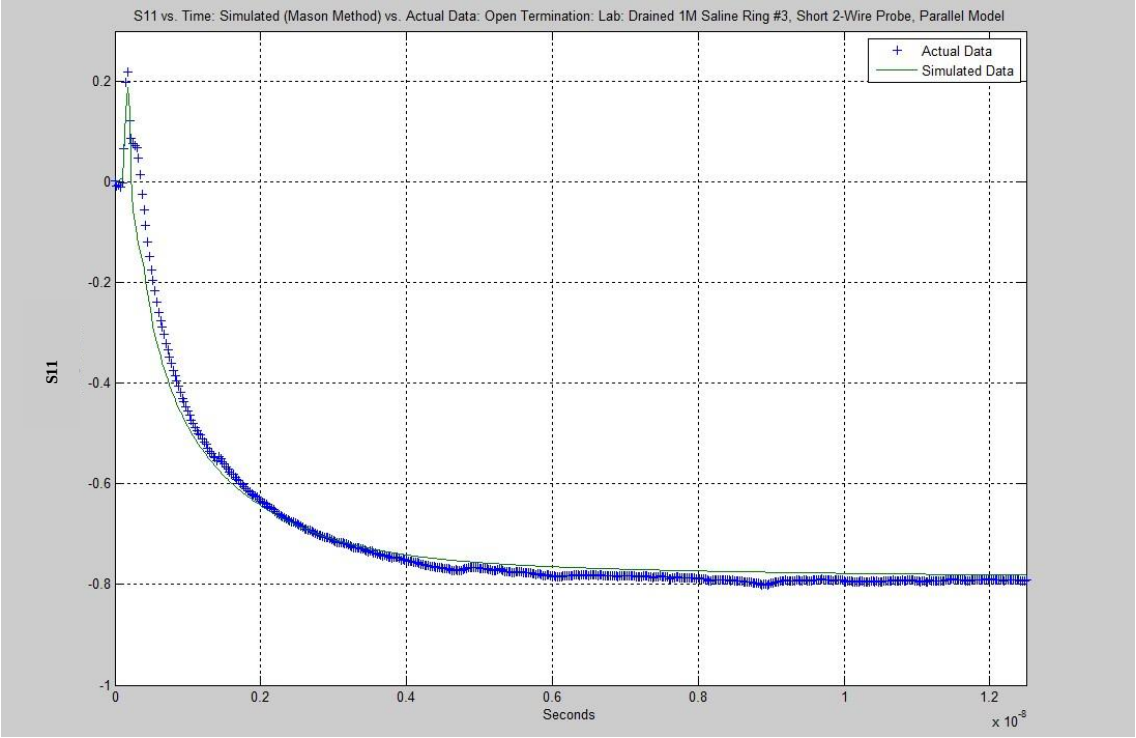


Figure D.15a: Lab Validation Method #1: TDR Waveform: WC = 0.33, EC = 1.7 S/m: Simulated vs. Actual

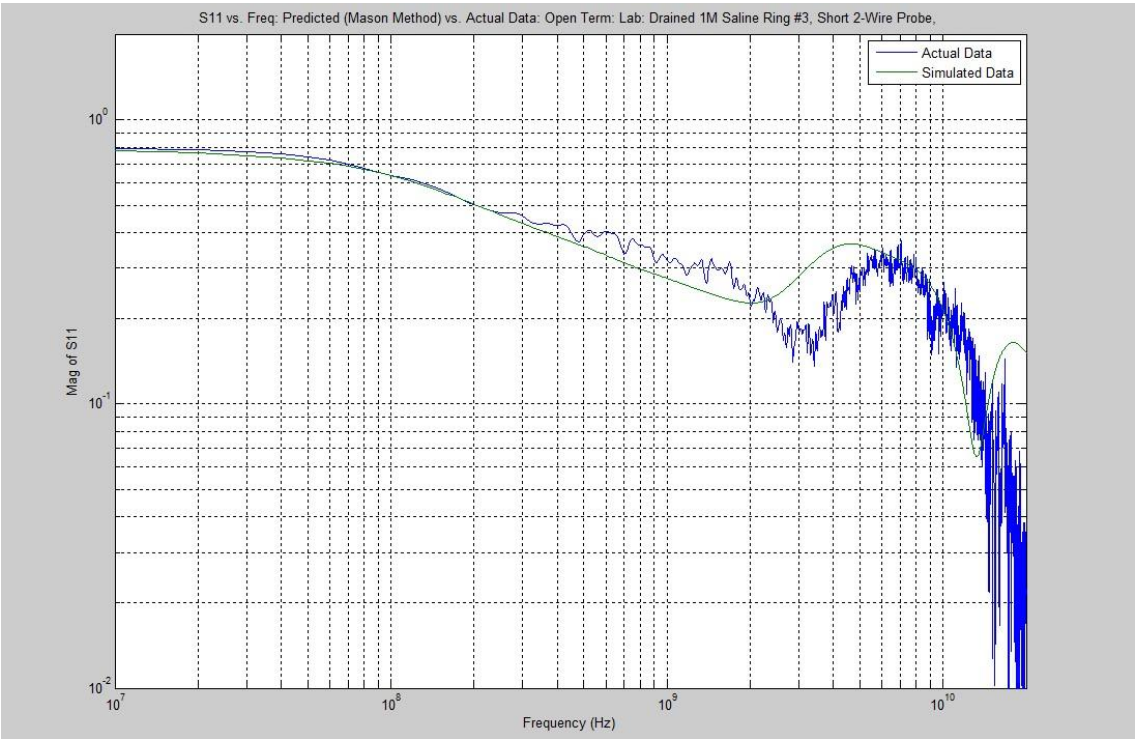


Figure D.15b: Lab Validation Method #1: Frequency Domain Spectrum: WC = 0.33, EC = 1.7 S/m: Simulated vs. Actual

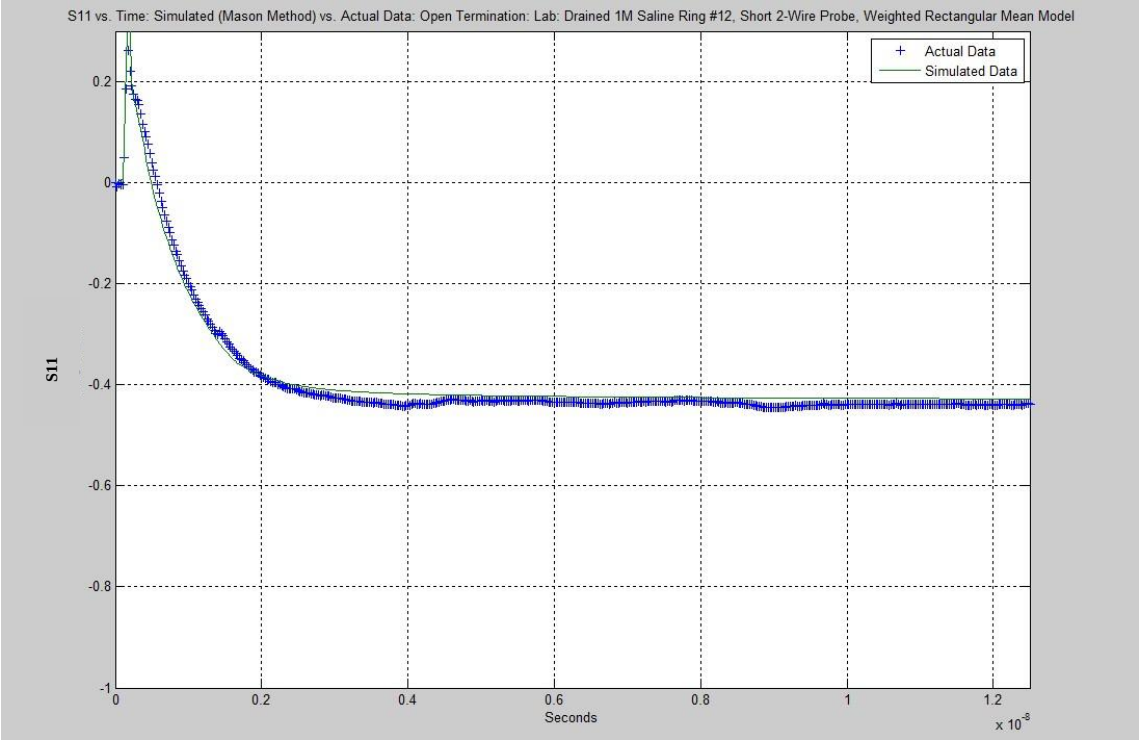


Figure D.16a: Lab Validation Method #1: TDR Waveform: WC = 0.28, EC = 0.46 S/m: Simulated vs. Actual

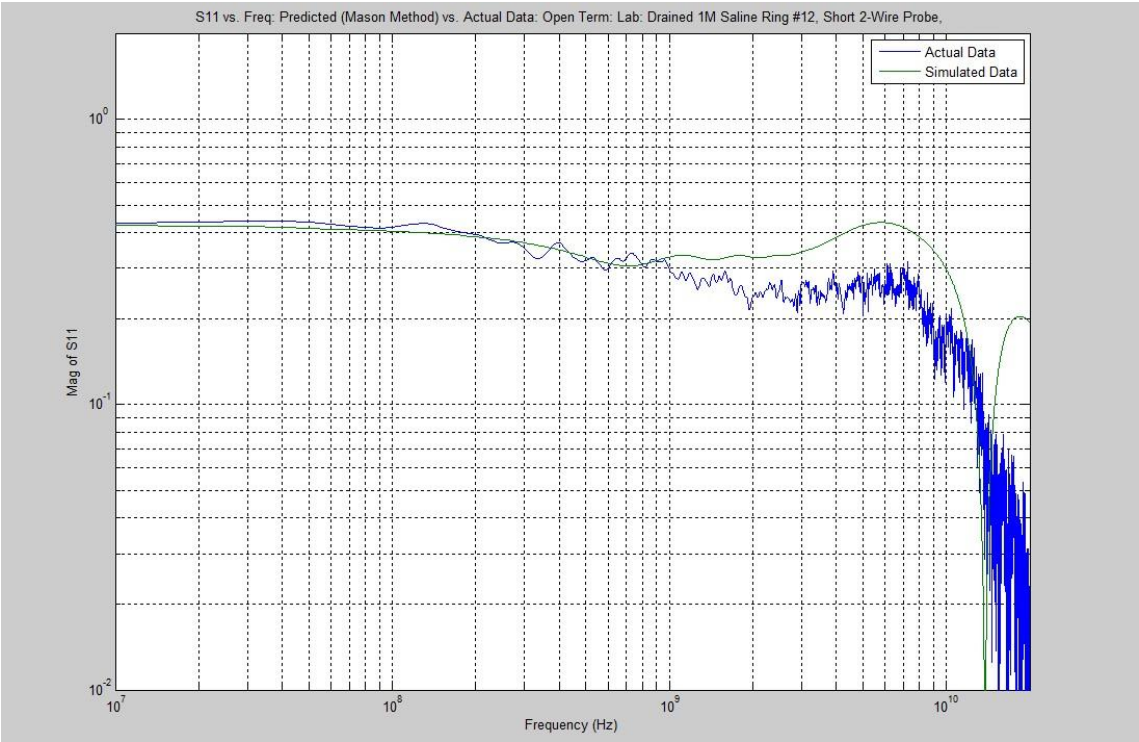


Figure D.16b: Lab Validation Method #1: Frequency Domain Spectrum: WC = 0.28, EC = 0.46 S/m: Simulated vs. Actual

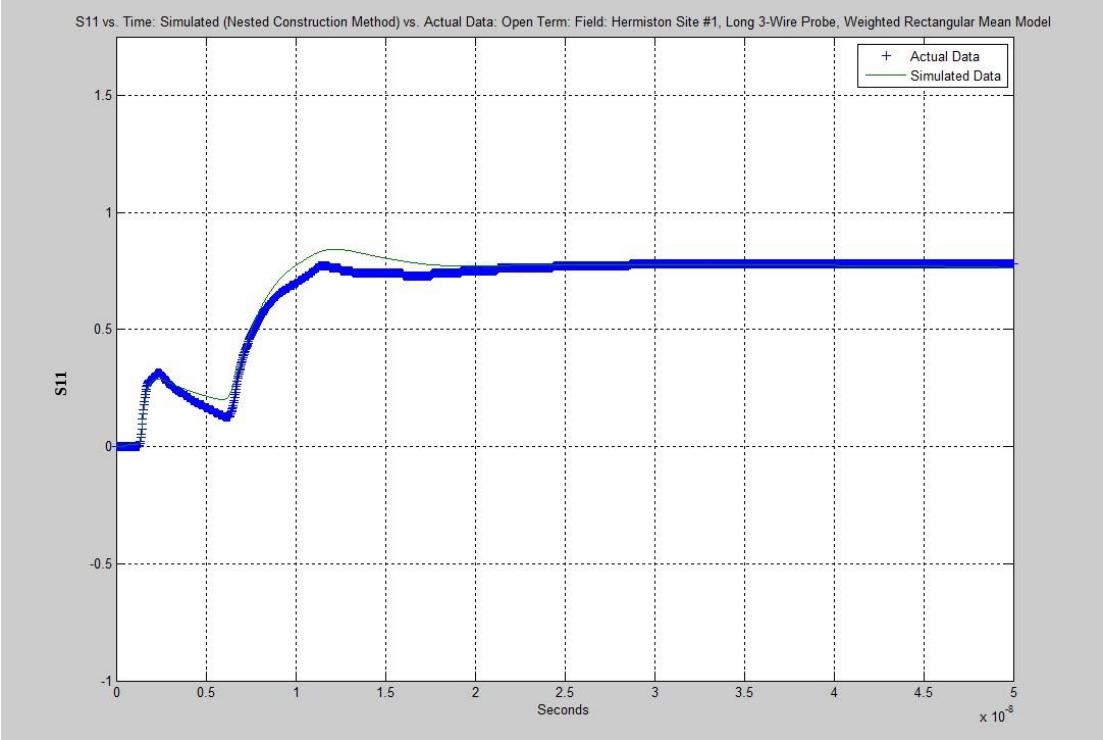


Figure D.17a: Field Validation Data: Hermiston/Potlatch Site #1 (See Table 5.3): TDR: Simulated vs. Actual

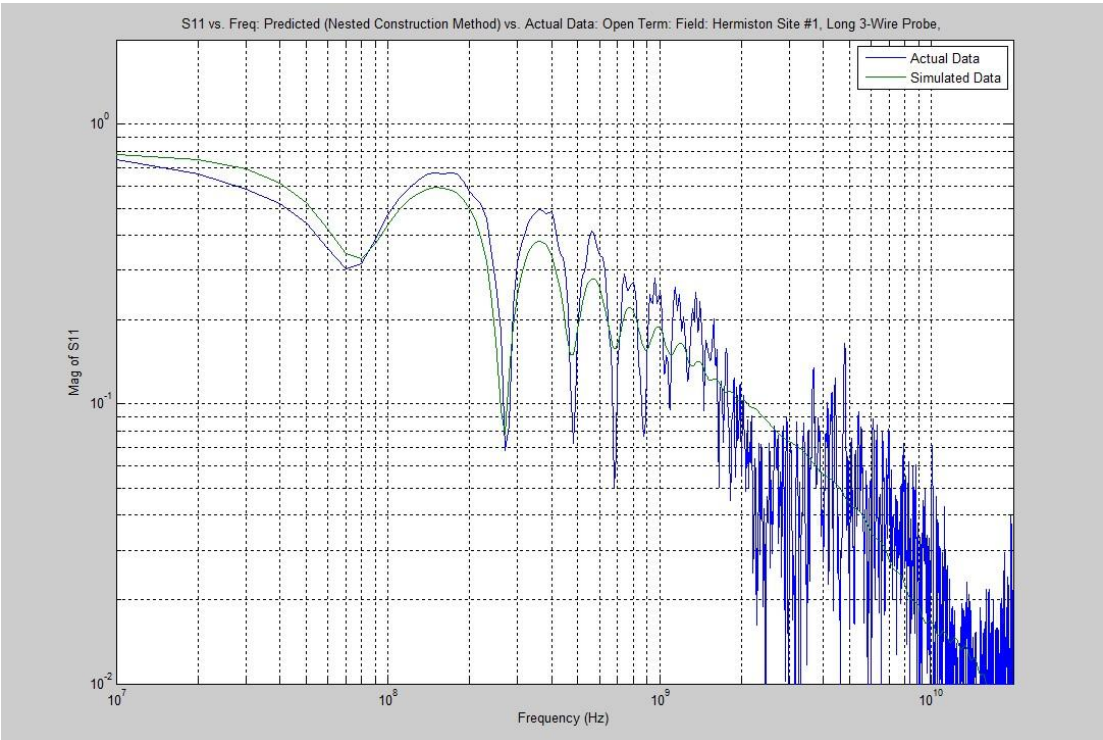


Figure D.17b: Field Validation Data: Hermiston/Potlatch Site #1 (See Table 5.3): FDR: Simulated vs. Actual

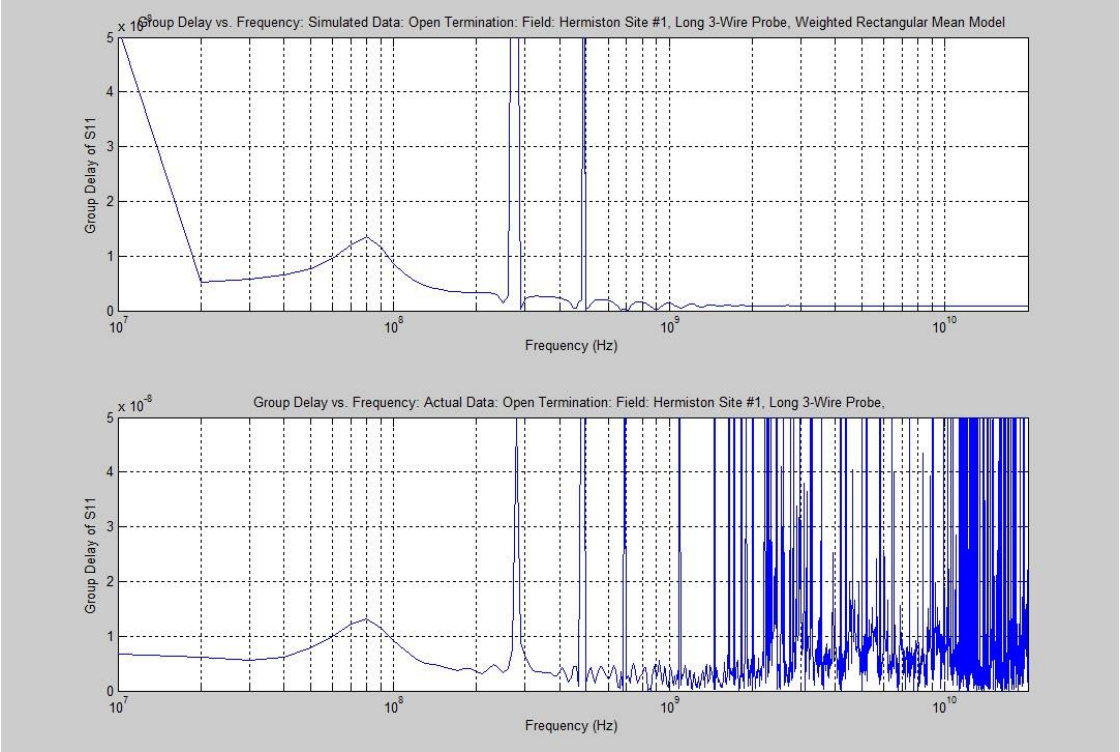


Figure D.17c: Field Validation Data: Hermiston/Potlatch Site #1 (See Table 5.3): Group Delay: Simulated vs. Actual

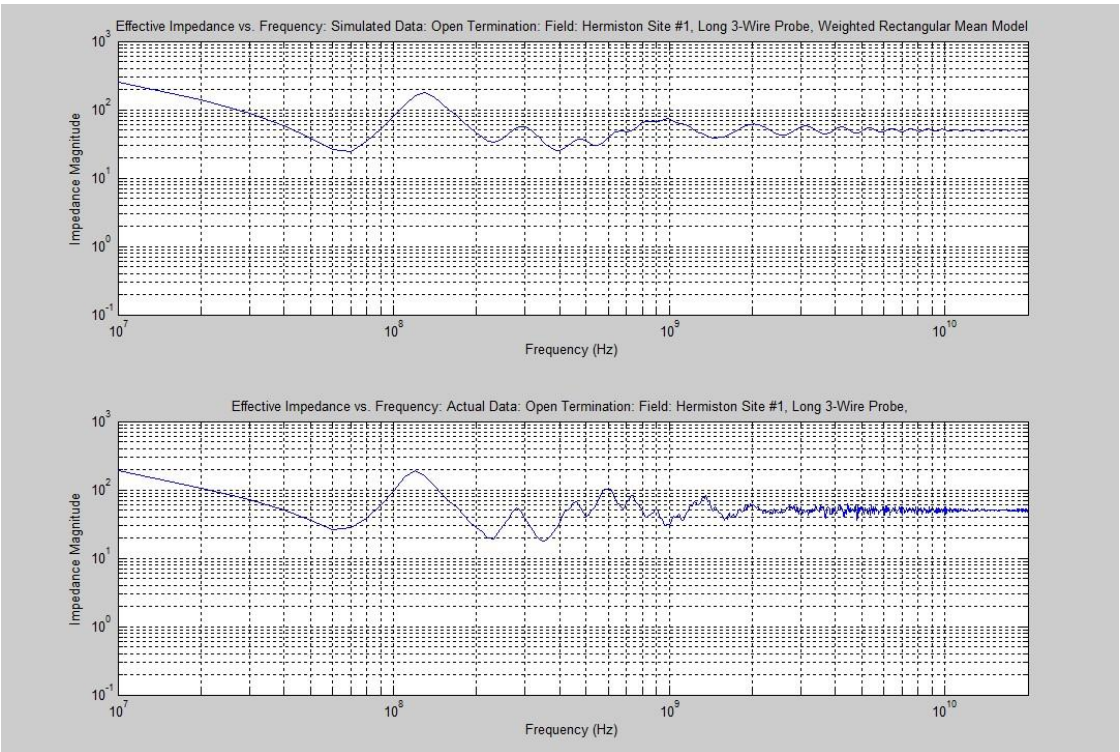


Figure D.17d: Field Validation Data: Hermiston/Potlatch Site #1 (See Table 5.3): Impedance: Simulated vs. Actual

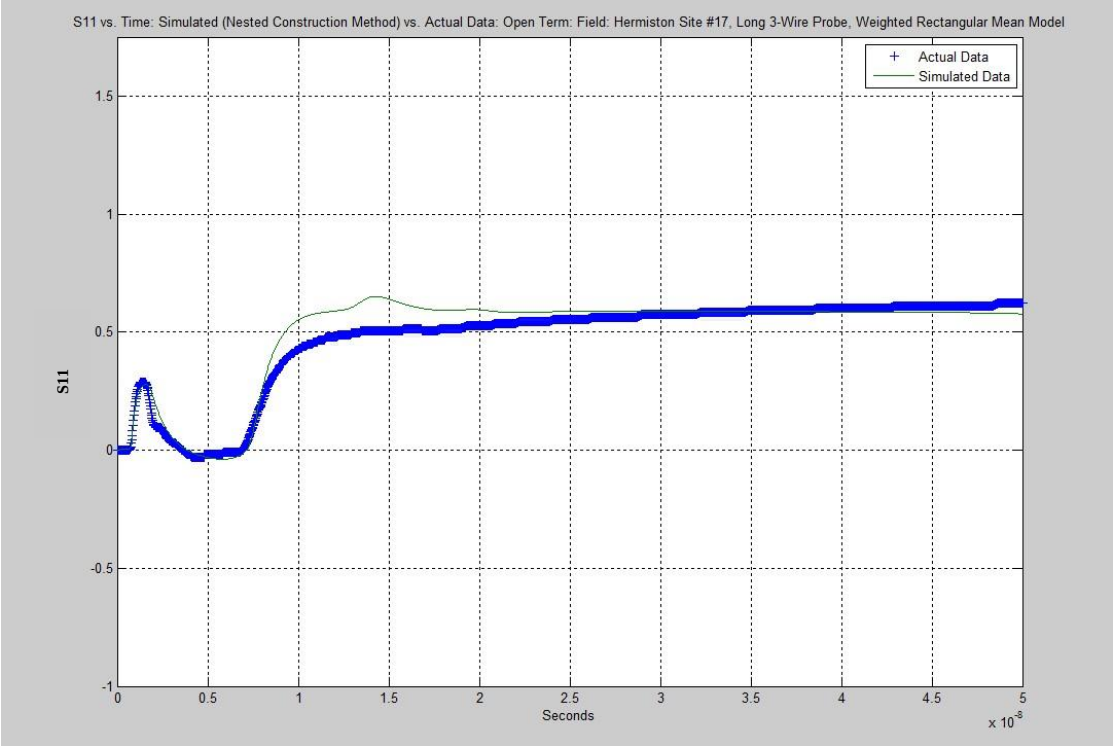


Figure D.18a: Field Validation Data: Hermiston/Potlatch Site #17 (See Table 5.3): TDR: Simulated vs. Actual

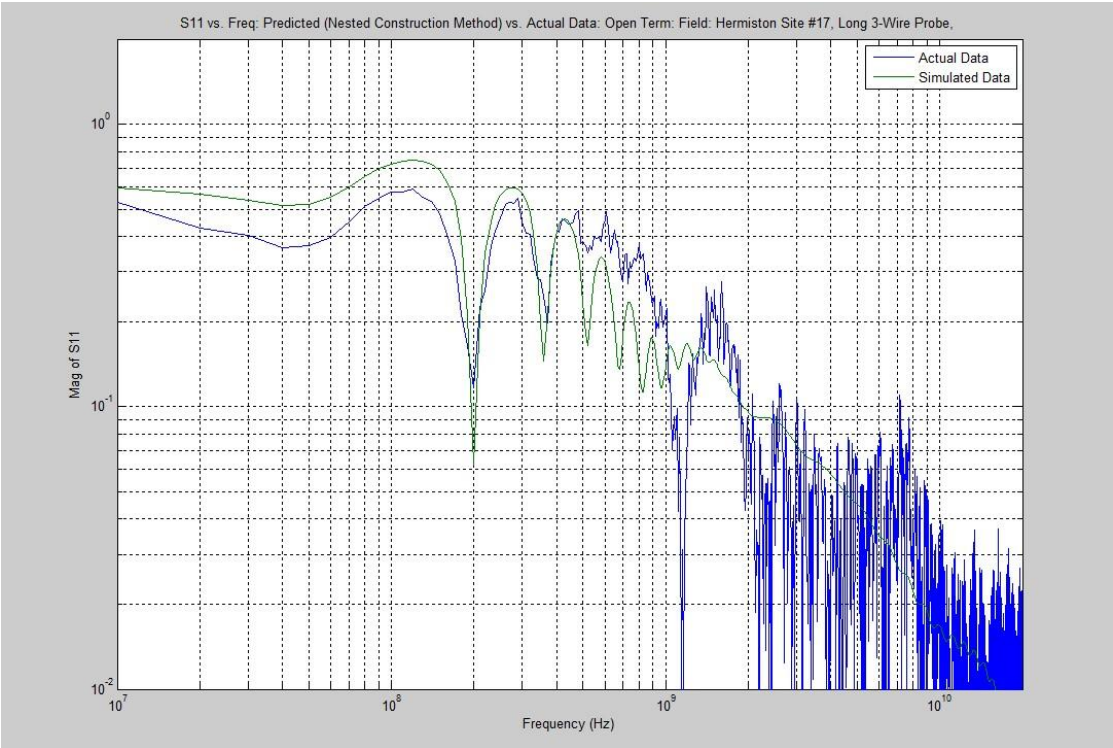


Figure D.18b: Field Validation Data: Hermiston/Potlatch Site #17 (See Table 5.3): FDR: Simulated vs. Actual

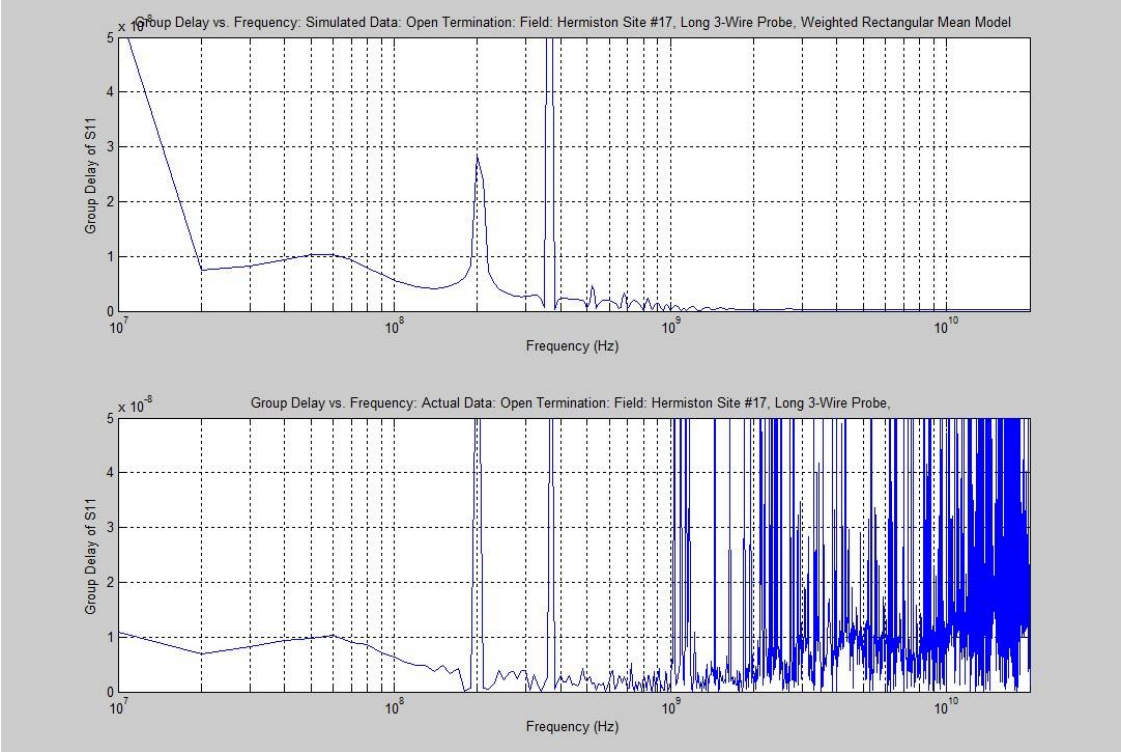


Figure D.18c: Field Validation Data: Hermiston/Potlatch Site #17 (See Table 5.3): Group Delay: Simulated vs. Actual

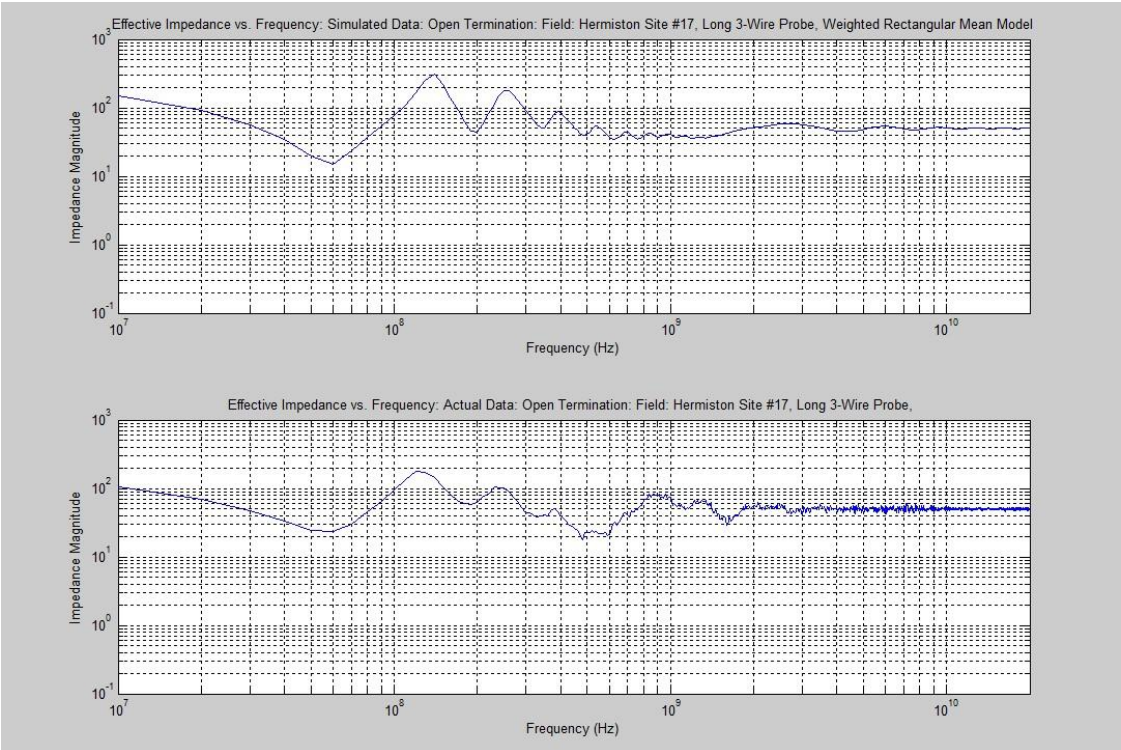


Figure D.18d: Field Validation Data: Hermiston/Potlatch Site #17 (See Table 5.3): Impedance: Simulated vs. Actual

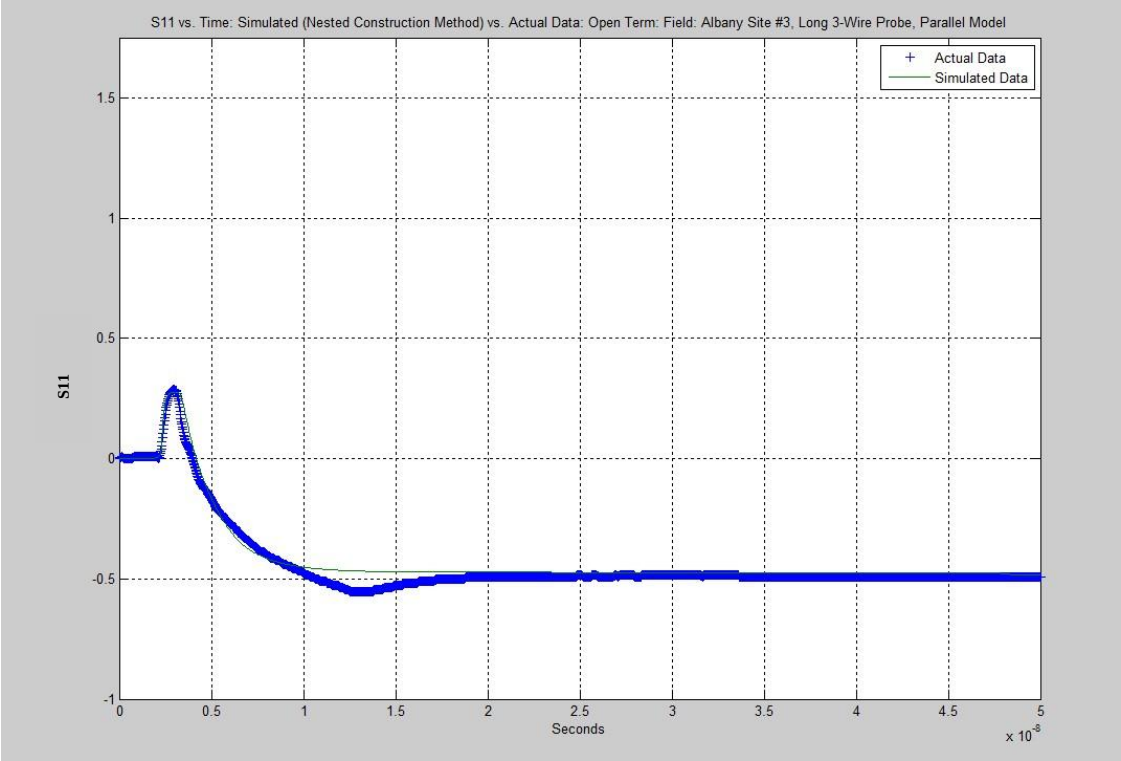


Figure D.19a: Field Validation Data: Albany Site #3 (See Table 5.4): TDR: Simulated vs. Actual

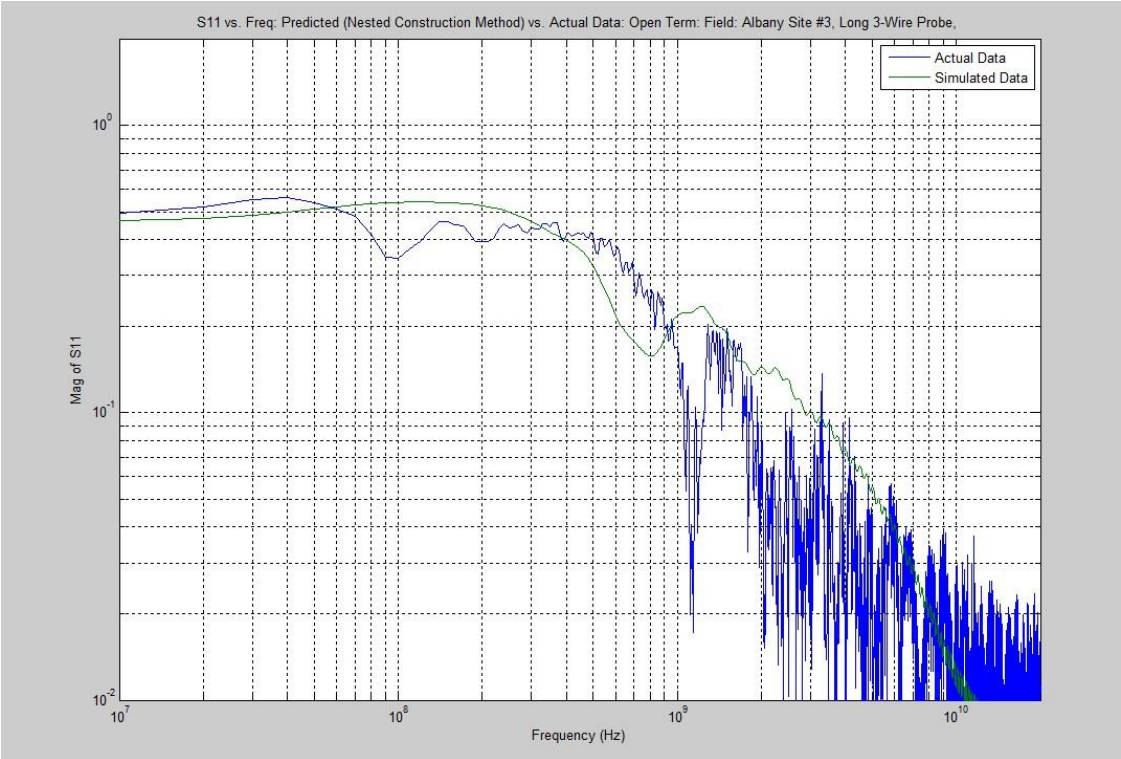


Figure D.19b: Field Validation Data: Albany Site #3 (See Table 5.4): FDR: Simulated vs. Actual

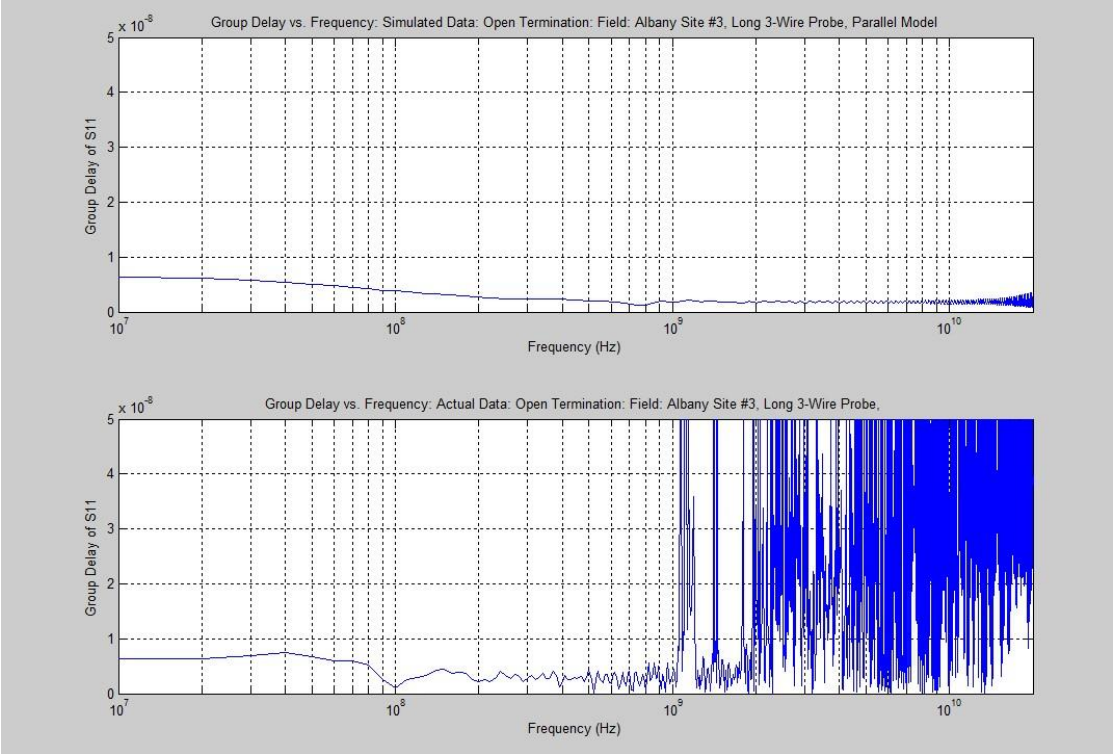


Figure D.19c: Field Validation Data: Albany Site #3 (See Table 5.4): Group Delay: Simulated vs. Actual

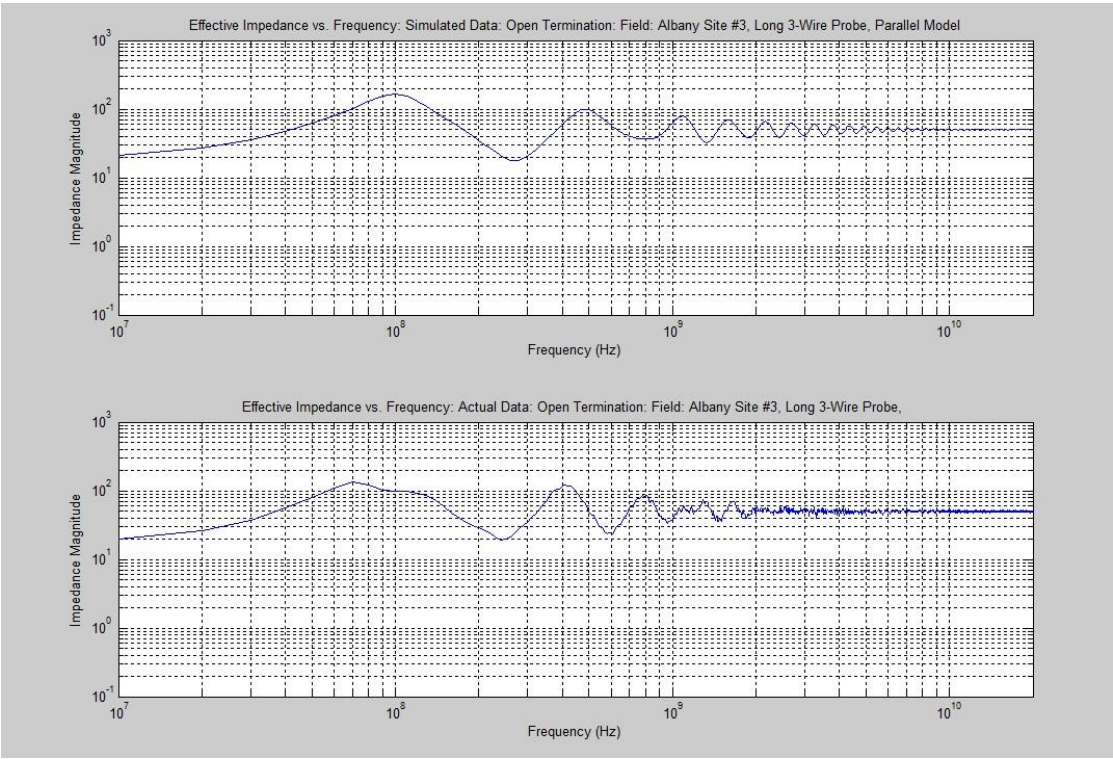


Figure D.19d: Field Validation Data: Albany Site #3 (See Table 5.4): Impedance: Simulated vs. Actual

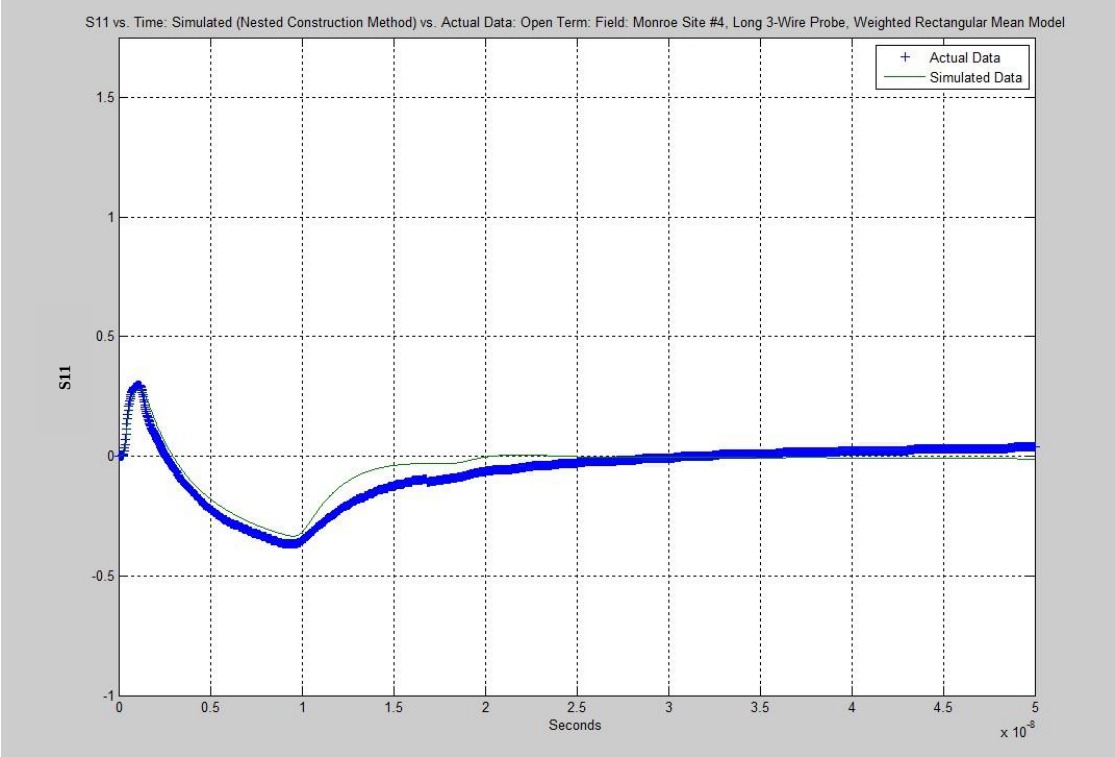


Figure D.20a: Field Validation Data: Monroe Site #4 (See Table 5.5): TDR: Simulated vs. Actual

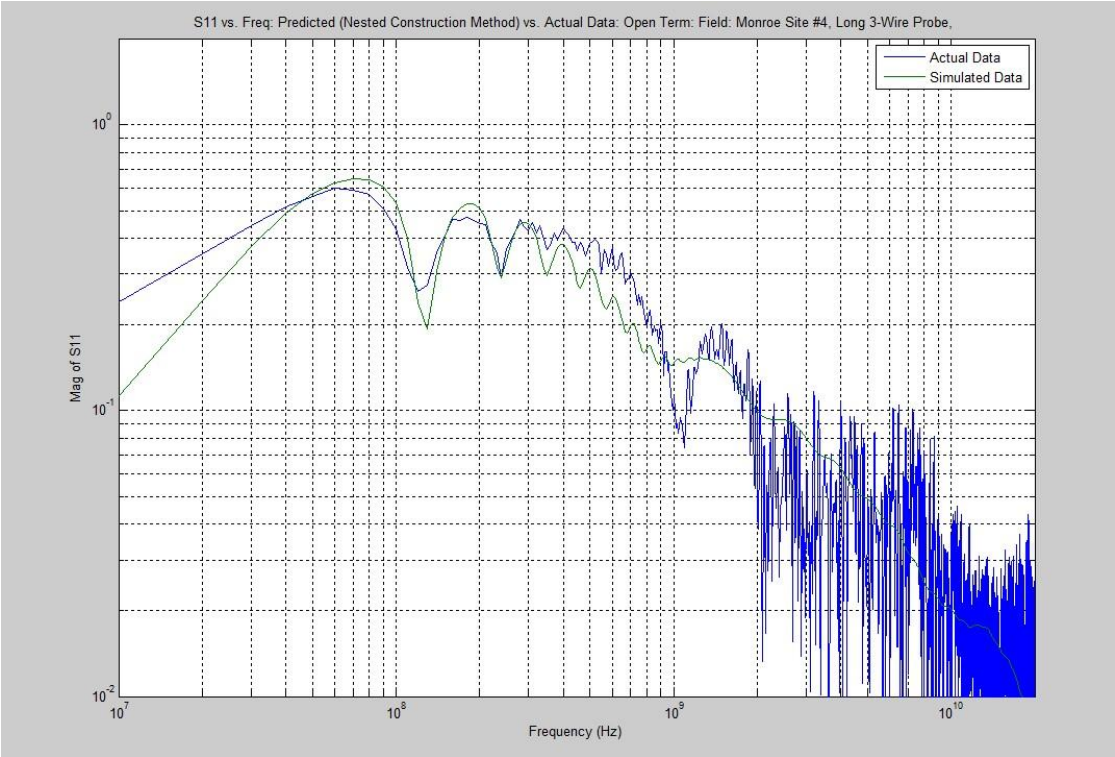


Figure D.20b: Field Validation Data: Monroe Site #4 (See Table 5.5): FDR: Simulated vs. Actual

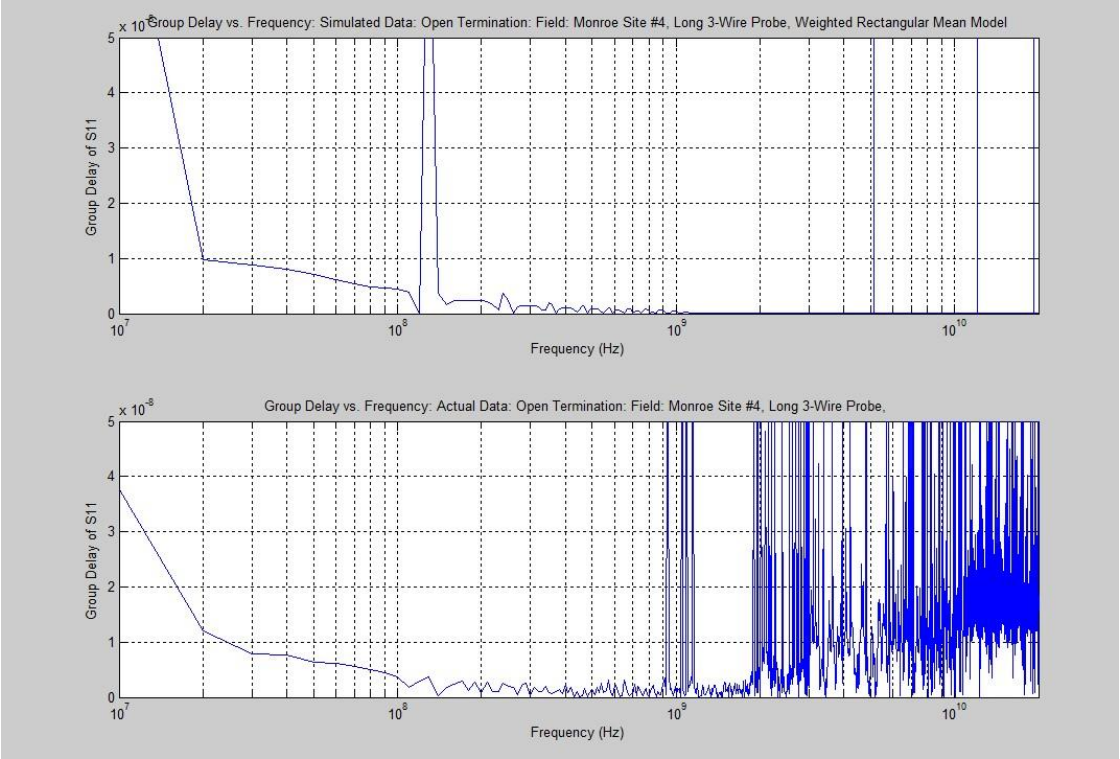


Figure D.20c: Field Validation Data: Monroe Site #4 (See Table 5.5): Group Delay: Simulated vs. Actual

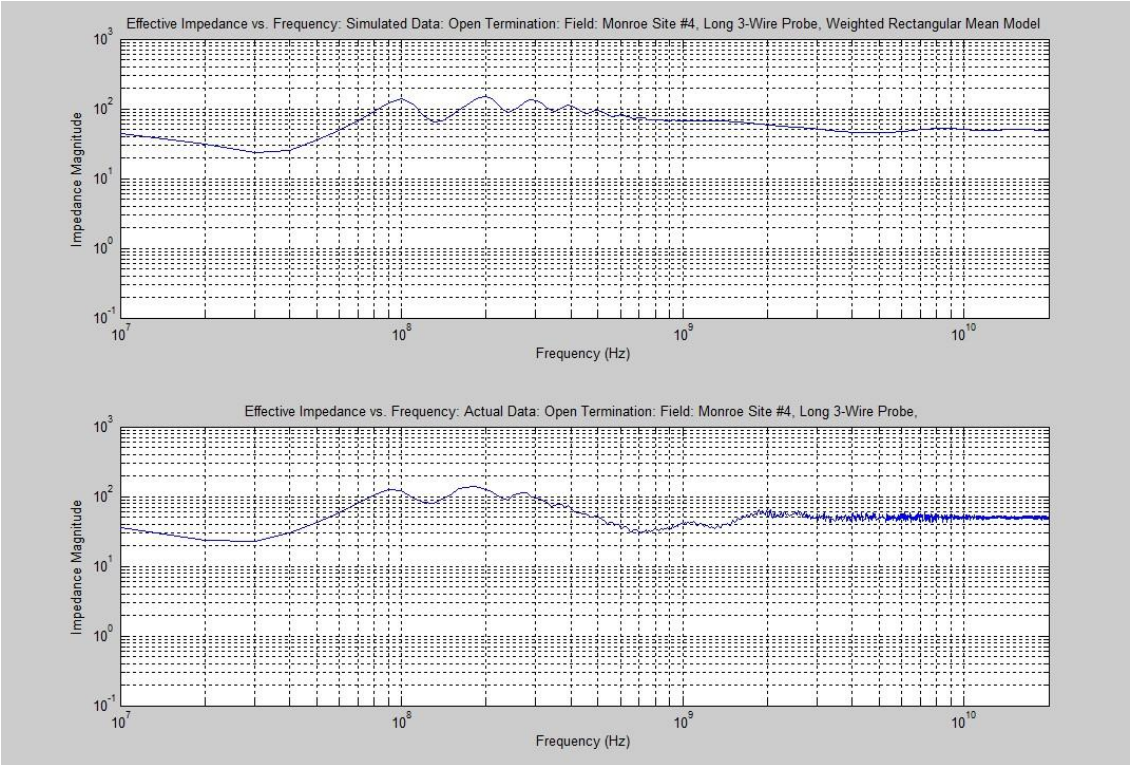


Figure D.20d: Field Validation Data: Monroe Site #4 (See Table 5.5): Impedance: Simulated vs. Actual

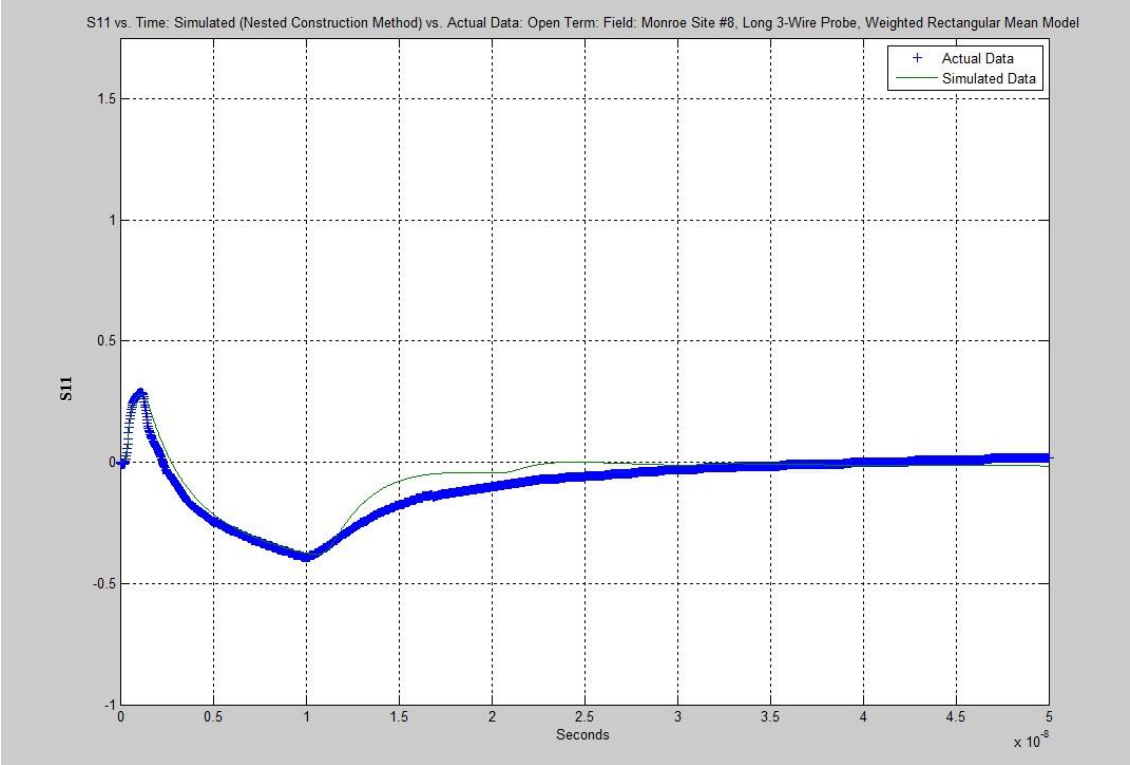


Figure D.21a: Field Validation Data: Monroe Site #8 (See Table 5.5): TDR: Simulated vs. Actual

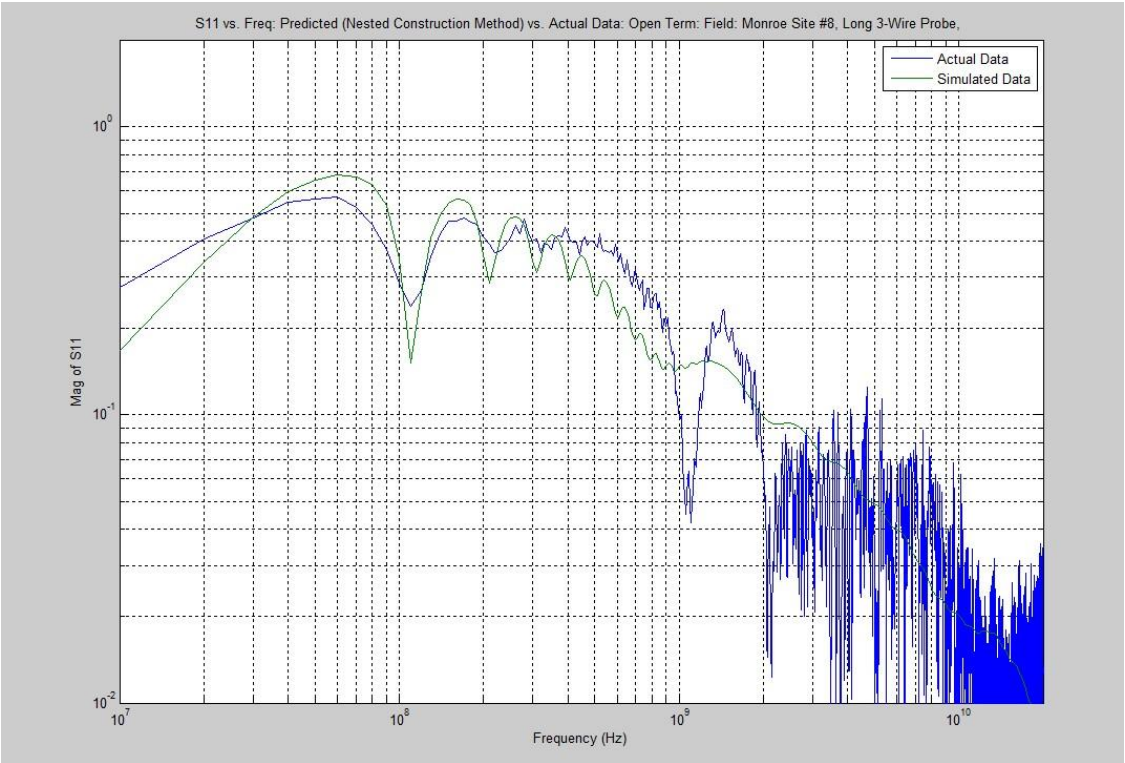


Figure D.21b: Field Validation Data: Monroe Site #8 (See Table 5.5): FDR: Simulated vs. Actual

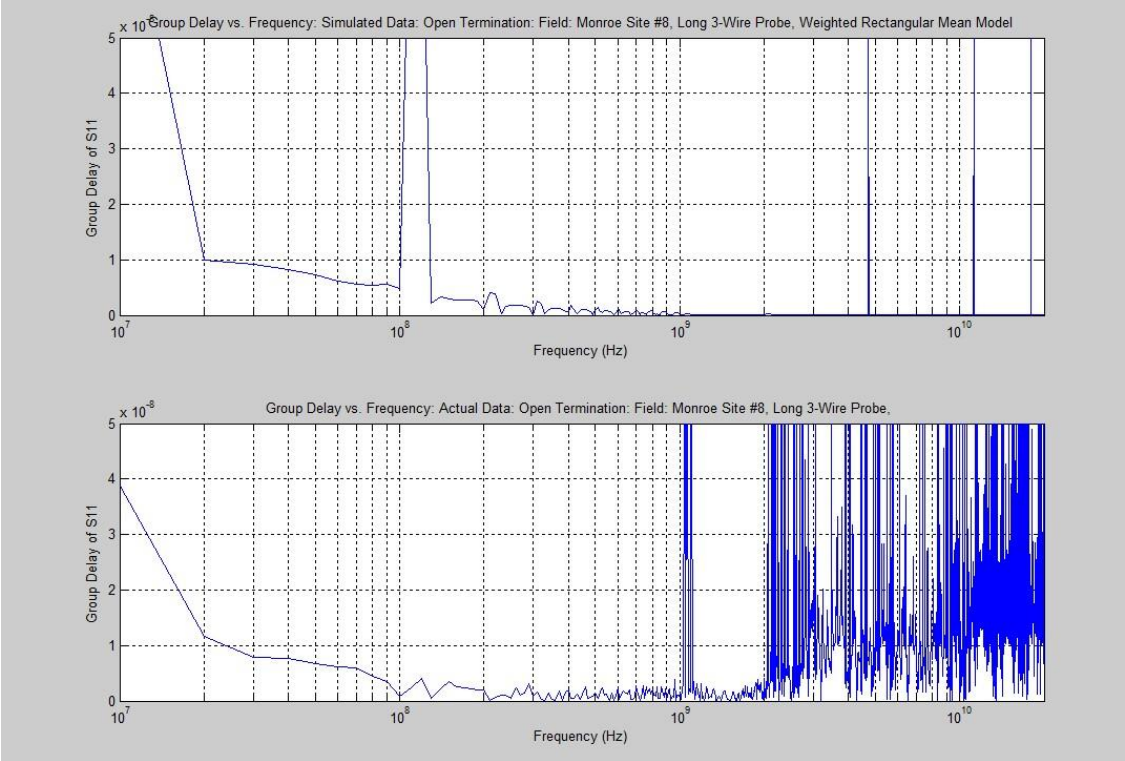


Figure D.21c: Field Validation Data: Monroe Site #8 (See Table 5.5): Group Delay: Simulated vs. Actual

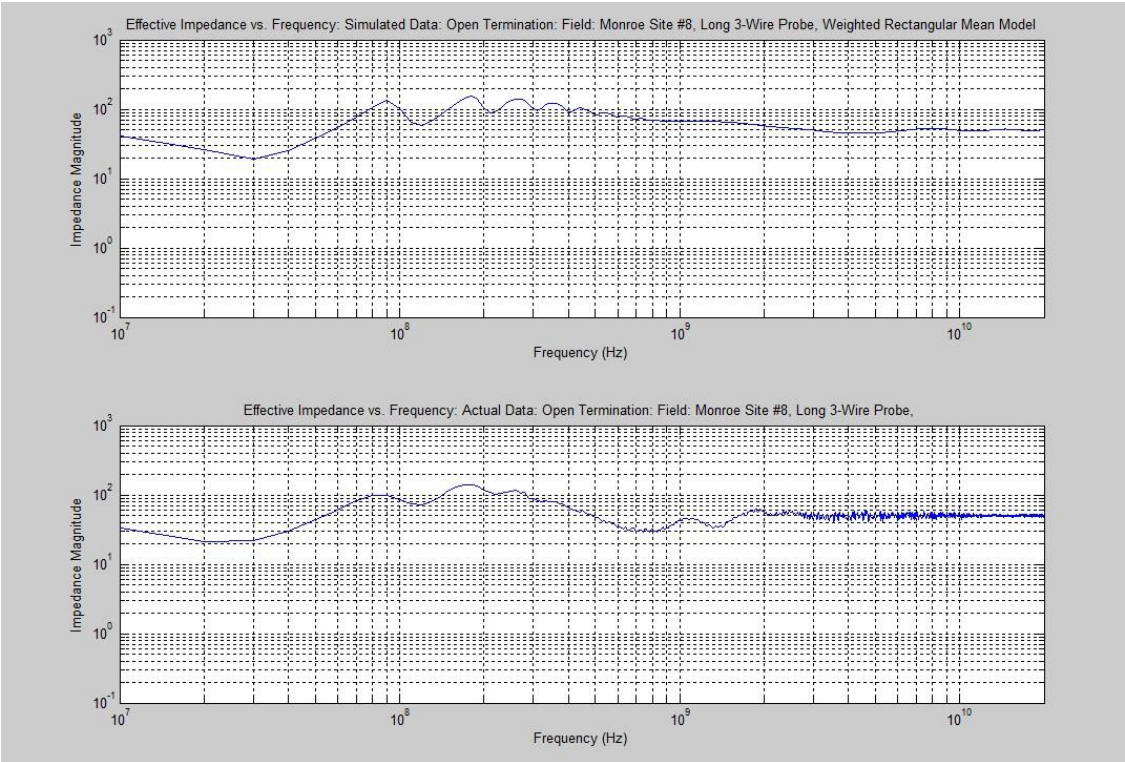


Figure D.21d: Field Validation Data: Monroe Site #8 (See Table 5.5): Impedance: Simulated vs. Actual